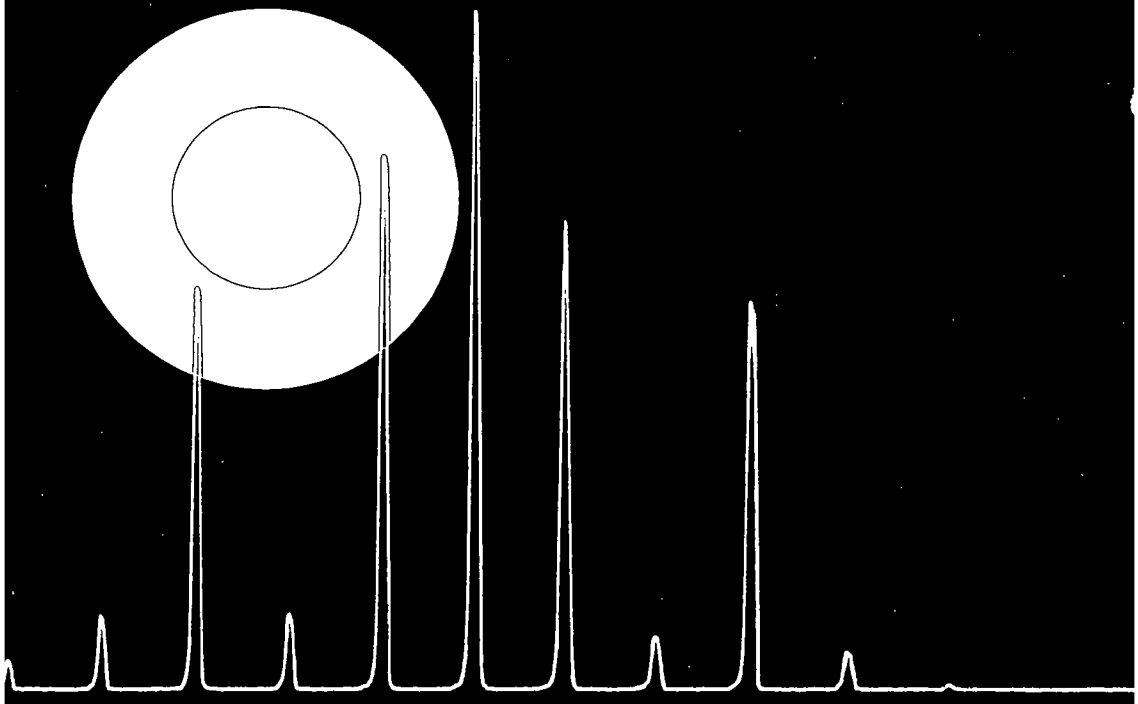

Nineteenth Annual Conference on Mass Spectrometry and Allied Topics

Nineteenth Annual Conference on Mass Spectrometry and Allied Topics

May 2-7, 1971
Atlanta, Georgia

Arranged by the
American Society for Mass Spectrometry
in cooperation with ASTM Committee E-14

Table of Contents

1. Introduction---------- 3

2. Proceedings of the Nineteenth Annual Conference---------- 5

3. Author Index---------- 359

4. Committees of ASMS and Subcommittees of ASTM E-14---------- 363

5. Committee and Subcommittee Reports---------- 364

6. ASMS Nominating Proceedures---------- 380

7. Benefits of Membership in ASMS---------- 381

8. Information Available to ASMS Members---------- 382

Introduction

This volume is a collection of papers presented at the Nineteenth Annual Conference on Mass Spectrometry and Allied Topics, held in Atlanta, Georgia, May 2-7, 1971. It is intended that this volume be distributed only to members of ASMS, and registrants of the Conference, and therefore should not be considered as a publication.

It is suggested that any future reference to individual reports be cited in the form: author(s), presented at the Nineteenth Annual Conference on Mass Spectrometry and Allied Topics, Atlanta, Georgia, May 2-7, 1971.

F. H. Field, Program Chairman

Arranged by the American Society for Mass Spectrometry (ASMS), in cooperation with ASTM Committee E-14.

ASMS

President: R. E. HONIG, RCA Laboratories, Princeton, New Jersey 08540

Vice-President (Program): F. E. FIELD, Rockefeller University, New York, New York 10021

Vice-President (Arrangements): G. L. KEARNS, AEI Scientific Apparatus, Inc., 500 Executive Blvd., Cross Westchester Executive Park, Elmsford, New York 10523

Vice-President (Data & Standards): H. R. HARLESS, Union Carbide Technical Center, S. Charleston, West Virginia 25303

Secretary: F. E. SAALFELD, Naval Research Laboratories, Washington, D. C. 20390

Treasurer: H. D. COOK, Westinghouse Bettis Atomic Power Laboratories, Box 79, West Mifflin, Pennsylvania 15122

Past President: J. L. FRANKLIN, Department of Chemistry, Rice University, Houston, Texas 77001

Directors-at-Large:

A. G. SHARKEY, U. S. Bureau of Mines, 4800 Forbes Avenue, Pittsburgh, Pennsylvania, 15213

A. L. WAHRHAFTIG, Department of Chemistry, University of Utah, Salt Lake City, Utah 84112

ASTM COMMITTEE E-14

Chairman: H. R. HARLESS, Union Carbide Technical Center, South Charleston, West Virginia 25303

Vice-Chairman: H. E. LUMPKIN, Esso Research & Engineering Co., P. O. Box 4255, Baytown, Texas 77520

Secretary-Treasurer: W. F. KUHN, Philip Morris, Inc., Richmond, Virginia 23206

To VERNON DIBELER and JOHN HERRON:

THANKS FOR A JOB WELL DONE!

The members of the Board of Directors of ASMS would like to call to the attention of the ASMS membership the outstanding contributions to our Society by two members,

Dr. V. H. Dibeler

and

Dr. J. T. Herron,

both of the National Bureau of Standards, who have handled the details of the publication of our Proceedings for the past 11 years. The services of these gentlemen has contributed much to the success of the ASTM E-14 and ASMS meetings. On behalf of the Society, the Board of Directors would like to express its gratitude to Drs. Dibeler and Herron for their outstanding service.

F. E. Saalfeld
Secretary

Paper No. Page No.

Ion Energetics

A1. Rotational Effects on the Formation of CH_3^+ from CH_4 in the Threshold Region.
H. M. Rosenstock, K. E. McCulloh, V. H. Dibeler, and J. A. Walker---------- 14

A2. Photoionization-Mass Spectrometric Study of Formaldehyde H_2CO, HDCO, D_2CO.
Paul M. Guyon, William A. Chupka, and Joseph Berkowitz

A3. Photoionization Studies of Some Diatomic Interhalogens.
V. H. Dibeler, J. A. Walker, and K. E. McCulloh---------- 15

A4 Photoelectron Spectroscopy of High Temperature Vapors with a Cylindrical mirror Analyzer.
J. Berkowitz and R. Spohr

A5. Cyclic and Acyclic C_3H_3 and C_3H_4 Neutrals and Cations.
F. P. Lossing---------- 16

A6. Accurate Threshold Potentials with a Quadrupole Mass Spectrometer.
Thomas C. Ahlert---------- 17

A7. Using Model Ionization Efficiency Curves to Evaluate the Methods for Determining Appearance Potentials.
J. L. Occolowitz and B. Cerimele---------- 24

A8. Enthalpies of Formation of Some Structural Isomers of $C_2H_5O^+$ and $C_2H_6N^+$ Ions.
B. H. Solka and M. E. Russell

A9. Reformulation of the Quasi-Equilibrium Theory of Ionic Fragmentation.
Cornelius E. Klots---------- 25

A10. Energy Deposition Functions in Mass Spectrometry.
G. G. Meisels, C. T. Chen, B. G. Giessner, and R. H. Emmel-------- 27

Mass Spectra of Organic Compounds

B1. Dynamic Stereochemistry - A Structural Proge for Fragmenting Electron Impacted Ions.
Mark M. Green and John G. McGrew

B2. Stereochemical Requirements for Intramolecular Rearrangements in Trimethylsilyl and Trimethylsilylphosphate Derivatives.
D. J. Harvey, M. G. Horning, and P. Vouros---------- 32

B3. Interaction of a Silyl Center with Distant Phenyl Groups in Organo-silicon Compounds.
William P. Weber---------- 33

B4. Mass Spectra of Aryl Dimethyl Phosphates.
Don C. DeJongh and Martha L. Gay---------- 35

B5. Hydrogen Exchange in a Six-Membered Ring Transition State: Evidence for a Stepwise McLafferty Rearrangement.
P. Vouros, P. R. Briggs, and T. W. Shannon---------- 36

B6. The Internuclear Distance Through Which Bifunctional Interaction Can Occur in an Ion Radical.
C. C. Fenselau and C. H. Robinson---------- 37

*Invited Paper

Paper No. Page No.

B7. Determination of Fragmentation Pathways of [[(1-ethyl-3-methyl-5-pyrazolyl)-amino] methylene] malonic acid, diethyl ester by High-resolution Mass Spectrometry and Metastable Ion Defocusing.
Phillip T. Funke and Allen I. Cohen---------- 38

B8. Ionization-Dissociation Processes in Carbodiimides and Ureas from Mass Spectral and Ion Kinetic Energy Studies.
William A. Laurie and Morton E. Wacks

B9. Mass Spectroscopy of the Dicyanomethylene Derivatives of Long Chain Molecules.
J. Throck Watson, B. J. Sweetman, and R. E. Wolff---------- 42

B10. The Mass Spectra of p-Methylphenylthiaalkanes.
Norman G. Foster and Robert W. Higgins---------- 44

B11. Photoionization and Electron Impact Studies on Linear Olefins and Their Stereochemical Derivatives.
Bruce M. Johnson and James W. Taylor---------- 45

B12. Energy Partition in Organic Ions.
R. Graham Cooks, Keith Jennings, and Stephen Jones---------- 46

Various Ionization Techniques

C0.* Spectra and Structures of Molecular Ions.
G. Herzberg

C2. Catalytic Reactions Occurring on the Walls of an Ion Source.
Richard F. Herzog

C3. *Field-Ionization Mass Spectrometry of Organosilicon Compounds.*
J. E. Coutant and R. J. Robinson---------- 48

C4. Computer Model of a Field Ion Source.
J.-Peter Pfeifer, A. M. Falick, and A. L. Burlingame---------- 52

C5. The Emission of Polyatomic Ions during Heavy Ion Bombardment of Metals.
Friedrich G. Rudenauer

Mass Spectra of Organic Compounds (concluded);

Information and Data Processing

D1. Utilization of the Pre-ionization Loss of Hydrogen to Characterize Geometrical Isomers in Selected Cyclic Systems.
S. Osman, C. J. Dooley, and T. A. Foglia

D2. Mass Spectral Evidence for the Conversion of Benzenephosphonic Acid to Its Cyclic, Trimeric Anhydride and of Benzenephosphonous Acid to Phenylphosphine.
Richard H. Wiley---------- 57

D3. Mass Spectral Information. A Report from the Mass Spectrometry Data Centre.
R. G. Ridley and W. M. Scott---------- 58

D4. Computer Recognition of Metastable Ions.
A. M. Duffield, W. E. Reynolds, D. A. Anderson, R. A. Stillman, Jr., and C. A. Carroll---------- 63

D5. Further Aspects of the Naive Analysis of Structure.
D. H. Robertson and R. I. Reed---------- 68

D6. Computer Analysis of Mass Spectral Information.
Kain-Sze Kwok, R. Venkataraghavan, and F. W. McLafferty---------- 70

D7. Computer Techniques for Identifying Low Resolution Mass Spectra.
Stanley Grotch---------- 72

Paper No. Page No.

D8. Investigation Into Intensity Measurements with Automated Data Acquisition Systems.
W. J. McMurray and S. R. Lipsky---------- 74

Symposium: Fundamental Aspects of Mass Spectrometry

E0.* Change of Coupling in the Theory of Electron and Photon-Induced Processes.
U. Fano

E1.* Ionization of He by Electron Impact: Measurements of the Triple Differential Cross Section.
H. Ehrhardt, K. H. Hesselbacher, K. Jung, and K. Willmann--------- 75

E2.* Measurement and Interpretation of Ionization Potentials of Molecules.
Burkhard Brehm---------- 78

Information and Data Processing (concluded), Mass Spectra of Biological Compounds

F1. A Multipurpose Computer Interface for High Resolution Mass Spectrometry.
R. P. Page and A. V. Nowak---------- 84

F2. The Application of a GC-MS-Computer System and Various Interpretative Programs to Problems in Natural Products Chemistry.
James. E. Biller, Harry S. Hertz, and K. Biemann---------- 85

F3. A Combined High and Low Resolution Data System for GC-MS Applications.
P. Powers and M. J. Wallington---------- 88

F4. A Time-Shared Computer System for the Mass Spectrometry Laboratory.
R. N. Stillwell, J. G. Leferink, N. R. Earle, and L. S. Washco---- 93

F5. Mass Spectrometric Characterization of Aminocyclitol Antibiotics.
Kenneth L. Rinehart, Jr., Phillip Schaefer, J. Carter Cook, Carl P. Schaffner, and Allan Kershner---------- 94

F6. A Gas Chromatographic-Mass Spectrometric Investigation of the Alkaloids Found in Single Seeds of Ormosia paraensis and O. tovarensis.
Woodfin V. Ligon, Jr., and Kenneth L. Rinehart, Jr.---------- 95

F7. Gas Chrometography and Mass Spectrometry of the Erythrina Alkaloids and Their Trimethylsilyl Derivatives.
David S. Millington and Kenneth L. Rinehart, Jr.---------- 96

F8. The Mass Spectra of Trimethylsilyl Derivatives of Some 6-acid Substituted Pteridines.
Jim Serum, Pat Haug, Toshiyuki Urushibara, and Hugh S. Forrest---- 97

Symposium: Fundamental Aspects of Mass Spectrometry. (concluded)

G1.* Infrared and Ultraviolet Spectroscopic Studies of Molecular Ions Trapped in Inert Solid Matrices.
Dolphus E. Milligan and Marilyn E. Jacox---------- 100

G2.* Thermochemical Properties Obtained by Ion Cyclotron Resonance.
J. L. Beauchamp

G3.* Measurement of Rate Constants and Their Dependence on Ion Kinetic Energy by Ion Cyclotron Resonance.
Jean H. Futrell---------- 105

G4.* ICR Analysis of Primary Processes.
Jay M. S. Henis

Mass Spectra of Biological Compounds

Paper No. Page No.

H1. Instrumentation and Techniques for Screening Physiological Fluids for Trace Metabolites.
John Roboz, Laszlo Sarkozi, Alexander Ruhig, and Ferenc Hutterer-- 106

H2. Uses of Mass Spectrometry in Toxicology.
H. M. Fales, N. Law, G. W. A. Milne, and V. Aandahl

H3. Applications of Mass Spectrometry to Clinical Problems. Utilization of a GC-MS-Small Computer System for Metabolite Identification.
Sanford P. Markey and James R, Plattner---------- 108

H4. Analysis of Mixtures of Amino Acid and Peptide Derivatives by Micromolecular Distillation in a Mass Spectrometer.
R. D. Grigsby, J. S. Bird, and K. E. Bird---------- 110

H5. The Quantitative Sequential Degradation of Proteolytic Peptide Mixtures Using Mass Spectrometry.
R. E. Lovins, T. Fairwell, C. Cabaniss, and T. Sun---------- 116

H6. The Use of Chemical Ionization Mass Spectrometry in Biomedical Problems.
G. W. A. Milne and H. M. Fales---------- 117

H7. Chemical Ionization Studies of Biologically Significant Molecules.
Helene Sage, William Gray, Leonard Wojcik, and Jean Futrell

H8. Mass Spectral Structural Elucidation Techniques for Biological Materials.
Piet A. Leclercq, Patricia A. White, and Dominic M. Desiderio----- 118

H9. Mass Spectral Studies of Natural Products. Cardenolides and Bufadienolides.
Peter Brown, Yoshiaki Kamano, and George R. Pettit---------- 123

H10. Application of an Isotope MS20 Mass Spectrometer in Clinical Research for the Measurement of ^{15}N and Heavy Water.
D. Halliday, L. E. Moore, and G. J. Chew---------- 124

H11. Determination of Trace Elements in Biologicals Using Spark Source Mass Spectrometry with Electrical Detection.
George H. Morrison and Bruce N. Colby

Symposium: Mass Spectra of Organo-Metallic and Inorganic Compounds

I1.* The Mass Spectra, Energy Relationships and Fragmentation Mechanisms of Metallocenes.
H. J. Svec, G. A. Junk, and G. D. Flesch---------- 127

I2.* Mass Spectral Studies of Substituted Metal Carbonyl Compounds.
F. E. Saalfeld, M. V. McDowell, and J. J. DeCorpo---------- 133

I3.* Fragmentation Processes in Selected Metal Complexes.
Robert W. Kiser and Robert E. Fraas

I4.* Some Unusual Features in the Mass Spectra of Metal Carbonyl Derivatives.
R. B. King

I5. Mass Spectra of Organometallic Perfluoroaromatic Heterocycles.
Gilbert F. Lanthier and Jack M. Miller

Chemical Ionization; Negative Ions

J1. Deuterium Labelling as a Mechanistic Probe in Chemical Ionization Mass Spectrometry.
Catherine Fenselau, J. H. Duncan, and H. M. Fales---------- 134

J2. Chemical Ionization Mass Spectra of Pesticides.
Noel Einolf, John Michnowicz, and Burnaby Munson---------- 135

Paper No. Page No.

J3. Applications of Chemical Ionization Mass Spectrometry.
G. P. Arsenault and J. J. Dolhun---------- 137

J4. Negative Chemical Ionization Mass Spectrometry.
Ralph C. Dougherty, John Dalton, and David Roberts---------- 140

J5. Applications of Chemical Ionization Mass Spectrometry.
Rodger L. Foltz---------- 142

J6. The Application of Chemical Ionization Mass Spectrometry to the Identification of Drugs in Body Fluids.
David P. Beggs, Ralph C. Dougherty, and William H. Johnston------ 146

J7. Chemical Ionization Mass Spectrometry. XV. Polytertiary Alklamines.
T. A. Whitney, L. P. Klemann, and F. H. Field

J8. Isotope Effect in the Formation of HS^- and DS^- by Electron Impact on H_2S, HDS, and D_2s.
Florence Fiquet-Fayard and Jean-Pierre Ziesel---------- 149

J9. Formation of O^- from N_2O at Temperatures Above 2000 K.
J. M. Madson, J. H. Mullen, and L. N. Medgyesi-Mitschang---------- 151

J10. Reactions of Some Solvated Alkoxy Anions.
E. G. Jones and T. O. Tiernan---------- 156

J11. Some Negative Ion Reactions with Water.
John F. Paulson---------- 158

Mass Spectra of Organo-Metallic and Inorganic Compounds; Metastable Ions

K1. Electron Impact Fragmentation Mechanisms of Some Haloruthenocenes.
Arun K. Bhattacharya and Lee D. Smithson---------- 159

K2. Pyrolysis Studies and Molecular Beam Mass Spectra of 1,2-Dimethoxytatramethyldisilane; 1,1,2,2-Tetramethoxydimethyldisilane and Hexamethoxydisilane.
Sara J. Steck, John L. Margrave, and Ronald P. Steiger---------- 162

K3. Positive and Negative Ion Mass Spectra of Some Organomercurials.
Stuart C. Cohen---------- 163

K4. Mass Spectra of Organometallic Acetylenes of Group IV and V Elements.
M. L. Blazinet, W. G. Yeomans, and C. Merritt, Jr.---------- 165

K5. Chemical Ionization Mass Spectrometry of Selected Boron Hydrides.
Jerone J. Solomon and Richard F. Porter

K6. Charge Localization in Doubly Charged Ions.
Kai-Li Ting and Henry M. Fales

K7. Study of Metastable Decompositions of Doubly-Charged Ions by Ion Kinetic Energy Spectroscopy (IKES).
Theodor Ast, John H. Beynon, and Richard M. Caprioli---------- 169

K8. Energy Release in Metastable Transitions of Retro-Diels-Alder Reactions.
Thomas A. Elwood, John H. Beynon, and Peter W. Rabideau---------- 173

K9. Direct Analysis of Daughter Ions Arising from Metastable Decompositions.
K. H. Maurer, C. Brunnee, G. Kappus, K. Habfast, U. Schroder, and P. Schulze

K10. Further Results on Metastable Ions Using the Metastable Ion Detector.
N. R. Daly, A. McCormick, and R. E. Powell

K11. Metastable Transitions in the Mass Spectrum of Deuterated Ethylenes.
Irene Baumel, Robert Hagemann, and Rene Botter---------- 174

Paper No. Page No.

Negative Ions; High Temperature

Mass Spectrometry

L1. Electron Attachment.
F. C. Fehsenfeld

L2. Proton-Transfer Reactions of Negative Ions with Methane and Methyl Compounds.
A. di Domenico and J. L. Franklin---------- 179

L3. Negative Ion-Molecule Reactions in Nonmetal Fluorides.
Thomas C. Rhyne and John G. Dillard---------- 180

L4. Fragmentation of Small Inorganic Molecules.
Fred E. Stafford---------- 182

L5. Relative Stabilities of Gaseous Molecules of Transition Metal Compounds from Mass Spectrometric Studies of Temperature Dependence of High Temperature Equilibria.
Gary D. Blue

L6. Dissociation Energies of the Molecules Tb_2, Ho_2, Lu_2, TbAu, HoAg, HoAu and LuAu.
K. A. Gingerich, D. L. Cocke, H. C. Finkbeiner, and R. J. Seyse--- 186

L7. Mass Spectrometric Identification of Gaseous InGaO, $InGaO_2$, and GaAlO.
Fred J. Kohl and Carl A. Stearns---------- 191

L8. Vaporization of the Group IVA Metal Carbides.
Carl A. Stearns and Fred J. Kohl---------- 192

L9. Vapor Composition and Chemical Reactions of Laser Vaporized Carbon.
R. T. Meyer, A. W. Lynch, and J. M. Freese---------- 193

L10. Negative Ion Production from Carbon Allotropes.
Wayne Stuckey and A. G. Whitaker---------- 194

L11. Mass Spectrometric Vaporization of Ilmenite.
J. S. Ogden, C. A. Alexander, and W. M. Pardue---------- 196

Ion-Molecule Reactions

M0.* Dynamics of Ion-Molecule Reactions.
Richard Wolfgang

M1. Ion-Dipole Capture Cross Sections at Low Ion and Rotational Energies; Comparison of Reaction and Capture Cross Sections; Vibrational Effects.
John V. Dugan, Jr., and Bruce Canright, Jr.---------- 197

M2. Reactions of Molecules in Highly Excited Rydberg States Produced by Photon Absorption.
William A. Chupka and Joseph Berkowitz---------- 198

M3. Reaction of NO^+ with Water in a Photoionization Mass Spectrometer.
M. J. McAdams and L. I. Bone---------- 199

M4. Ion-Molecule Reactions in Disilane.
T-Y. Yu, V. Kempter, and F. W. Lampe

M5. Ion-Molecule Reactions Involving Alkyl Siliconium and Related Alkyl Metal Ions.
Paul Vouros, D. J. Harvey, and M. G. Horning---------- 202

M6. Intermolecular Hydrogen Transfer Reactions in the Mass Spectra of Dialkyl Malonates.
Mary H. Wilson and James A. McCloskey---------- 203

M7. Chemical Ionization: Arrival Time Distributions of Reactant Ions.
G. Sroka, C. Chang, and G. G. Meisels---------- 205

Paper No. Page No.

M8. Chemical Ionization Mass Spectrometry. XVI. Reactions of Tertiary Alkyl Acetates with Isobutane.
W. A. Laurie and F. H. Field

Instrumentation

N1. Direct Coupling of a Gas Chromatograph to a Mass Spectrometer.
Pat Haug, James Serum, and William Updegrove---------- 210

N2. Analysis of Steroid Hormones by a New Direct GC/MS Interface.
H. M. McNair, C. R. Dibbs, L. H. Aung, D. C. Damoth, and
A. J. Luchte---------- 212

N3. New Techniques in Gas Chromatography - Mass Spectrometry.
J. R. Chapman, T. O. Merren, and H. J. Limming---------- 218

N4. Combined Molecular Beam - Mass Spectrometer for Analyzing Transient Intermediates in Gaseous Reactions.
Myron Kaufman and Charles Kolb---------- 222

N5. A Combined Gas Chromatograph-Vapor Phase Pyrolysis-Mass Spectrometric Analysis System.
C. Merritt, Jr., C. DiPietro, and M. L. Bazinet---------- 224

N6. A Computer Controlled Gas Chromatograph-Mass Spectrometer System.
Aron Kuppermann

N7. An Automated Quadrupole Mass Spectrometer for High Temperature Effusion Studies.
Margaret A. Frisch---------- 227

N8. Computer Determinations of Quadrupole Mass Spectrometer Performance Characteristics in Cylindrical Coordinates.
M. Mosharrafa---------- 229

Ion-Molecule Reactions

O1. A Low Energy Study of Symmetric and Asymmetric Charge Transfer.
David L. Smith and Jean H. Futrell---------- 230

O2. Charge Transfer Spectra of C_4H_8 Isomers.
T. O. Tiernan and L. P. Hills---------- 234

O3. Cermak Type Studies of Charge Exchange in a Pulsed Electron Impact Source.
P. M. Hierl, J. L. Franklin, and D. K. Sen Sharma---------- 239

O4. Single Ion Impact Mass Spectra of Peptide Derivatives.
Robert J. Beuhler and Lewis Friedman---------- 240

O5. Energy Spectra of Ions Produced by Collision Between Hydrocarbon Ions and Neutral Molecules.
Eisuke Mitani, Hitoshi Tsuyama, and Michiyasu Itoh

O6. Determination of the Abundance of Excited States in O^+ Ion Beams Produced by Electron Impact on O_2, CO_2, N_2O, and H_2O.
B. M. Hughes and T. O. Tiernan---------- 241

O7. Association and Switching Reactions.
F. C. Fehsenfeld

Instrumentation

P1. A Three Dimensional Quadrupolar Mass Analyzer.
Charles S. Harden and Peter E. Wagner---------- 246

P2. Tandem Quadrupole for Use at Extremely Low Pressures (Deep Space).
Wilson M. Brubaker---------- 254

Paper No. Page No.

P3. The Time-Focusing Principle: A Double-Focusing Design for Time-of-Flight Mass Spectrometers.
J. M. B. Bakker---------- 256

P4. Problems Associated with the Resolution of Organic Ions in a Time-of-Flight (TOF) Mass Spectrometer.
M. A. Grayson and C. J. Wolf---------- 257

P5. The Motion of Charged Particles Between Concentric Cylinders and Some Applications.
M. Baril, L. Bolduc, and M. de Celles---------- 259

P6. The Plasma Chromatograph-Mass Spectrometer as a Qualitative Organic Analysis Instrument.
F. W. Karasek and M. J. Cohen---------- 262

P7. Trace Gas Analysis.
David B. Hughes and T. D. Nowlin---------- 266

Analysis of Airborne Particulates
by Mass Spectrometry

Q1.* The Application of Mass Spectrometric Thermal Analysis to Airborne Particulates.
Henry L. Friedman

Q2.* Spark-Source Mass Spectrometer Investigation of Coal Particles and Coal Ash.
T. Kessler, A. G. Sharkey, Jr., and R. A. Friedel---------- 271

Q3.* Elemental Analysis of Air Particulates Using Spark Source Mass Spectrography.
E. R. Blosser and R. J. Thompson---------- 273

Q4.* Ion Probe Analysis of Small Particles.
Michael A. Bayard---------- 274

Q5.* Secondary Ion Imaging Microanalysis of Airborne Particulates.
R. Lewis and P. Deschamps

Q6.* Sputter-Ion Source Mass Spectrometric Analysis of Particulates.
Frank G. Satkiewicz---------- 276

Q7. MS Identification and Measurement of Polynuclear Aromatic Hydrocarbons in Air Pollutants.
R. F. Pottie, R. C. Lao, and J. L. Monkman---------- 287

Instrumentation (concluded);
Ion-Molecule Reactions

R1. Ion Source for Magnetic Mass Spectrometer to be Used in Space.
W. M. Brubaker, D. Burnham, and G. D. Perkins

R2. An Improved Two-Stage Mass Spectrometer for Isotopic Ratio Measurements.
John D. Stein and Fred O. Halliday---------- 291

R3. Uses of Channel Electron Multipliers in Mass Spectrometers.
J. P. Carrico, M. C. Johnson, W. G. Wolber, and K. C. Schmidt----- 299

R4. An AC Operated, Cold Electron Emitter Mass Spectrometer Ion Source.
P. C. McLeod, J. F. Sprouse, K. M. Jackson, R. E. Ware, and M. K. Testerman---------- 307

R5. Absolute Gas Phase Acidity and the Determination of Free Energies of Hydration of Gaseous Anions.
L. Brewster Young, E. Lee-Duff, and D. K. Boehme---------- 314

R6. The Theoretical Relationship Between Ion Mobility and Mass.
David I. Carroll and E. A. Mason---------- 315

Paper No. Page No.

R7. An Experimental Mass-Mobility Relation for Ions in Air at Atmospheric Pressure.
Wallace D. Kilpatrick---------- 320

R8. Strength of Hydrogen Bonding to Negative Ions from Measurements of Gaseous Ionic Equilibria.
R. Yamdagni, J. D. Payzant, and P. Kebarle

R9. Reversible Reactions of Gaseous Ions. IV. The Methane-Water System.
S. L. Bennett and F. H. Field

R10. Ion-Molecule Reactions in High Pressure CH_4-CD_4 Mixtures.
Shuang-Ling Chong and J. L. Franklin---------- 327

R11. Relative Rates and Their Dependence on Kinetic Energy for Ion-Molecule Reactions in Ammonia, Water and Hydrogen Sulfide.
W. T. Huntress

Analytical; Geochemical

S1. Quantitative Analysis of N Compounds.
Thomas Aczel and H. E. Lumpkin---------- 329

S2. An Approach to Optimal Pattern Coefficients from a Calibration Mixture.
T. R. Edwards and G. L. Settle

S3. A Study of Methane Gas - Iron Surface Reactions Using a Mass Spectrometer.
J. Sayer and D. V. Keller, Jr.

S4. Laser--Time-of-Flight Mass Spectrometer Studies of Sorbed Species and Surface Reactions.
A. G. Sharkey, Jr., A. F. Logar, Jr., and R. G. Lett---------- 331

S5. The Determination of Inorganic Pollutants in Water by Spark Source Mass Spectrometry.
R. Brown and P. G. T. Vossen

S6. Gas Chromatographic-Mass Spectrometric Identification of Indigenous Organic Matter of the Murchison Meteorite.
J. M. Gibert, S. A. Wikstrom, and J. Oro---------- 334

S7. Mass Spectral Analysis of Organic Compounds in the Murchison Meteorite.
J. G. Lawless, M. Romiez, K. Kvenvolden, K. Pering, E. Peterson, J. Flores, C. Folsome, and C. Ponnamperuma---------- 341

S8. The Use of Mass Spectrometry in the Identification of Organic Compounds in Arid Soils from Antarctica and the Mohave Desert. Carotenoid Pigments.
H. G. Boettger, A. J. Bauman, A. M. Kelly, and H. Yokoyama--------

Ion-Molecule Reactions

T1. Temperature and Energy Dependence of Ion-Molecule Reactions of Polar Compounds.
S. E. Buttrill, Jr.---------- 349

T2. Ion Cyclotron Resonance Studies of Ionic Reactions in Perfluorocarbons.
Timothy Su and Larry Kevan---------- 353

T3. The Pulsed Ion Cyclotron Technique.
R. T. McIver and Max A. Haney---------- 355

T4. Study of S_N2 Reactions of Negative Ions by Pulsed ICR Spectroscopy.
Max A. Haney and R. T. McIver---------- 356

T5. Study of Ion-Molecule Collision Complexes Using Ion Cyclotron Resonance.
John R. Eyler---------- 357

T6. Ion-Molecule Reactions in Binary Alkene Mixtures.
G. C. Goode, R. M. O'Malley, C. J. Drewery, A. J. Ferrer-Correia, R. I. Massey, and K. R. Jennings

Rotational Effects on the Formation of CH_3^+ from CH_4 in the Threshold Region. A1

H. M. ROSENSTOCK, K. E. McCULLOH, V. H. DIBELER, and J. A. WALKER,
Institute for Materials Research, National Bureau of Standards, Washington, D.C. 20234

Chupka, several years ago, drew attention to the importance of rotational energy effects in interpreting the onset energy of CH_3^+ from CH_4 in photoionization. He assumed, in effect, that the total rotational energy of the parent ion was available for dissociation. A more realistic model of the process is one which takes into account the conservation of angular momentum about the axis of decomposition leading to $CH_3^+ + H$. This model leads to a different rotational tailing of the ion yield curve and also a slightly different extrapolation procedure to give 0°K results. The model is compared to experimental results at several temperatures for the photoionization of both CH_4 and CD_4. Attention is drawn to the anomalous behavior of the CH_2^+ threshold.

Photoionization Studies of Some Diatomic Interhalogens, V. H. DIBELER, J. A. WALKER, and K. E. McCULLOH, Institute for Materials Research, National Bureau of Standards, Washington, D. C. 20234 A3

Mass spectra and molecular ionization thresholds are reported for ClF, ICl, and IBr. Abundances of atomic ions formed by dissociative ionization and by ion-pair processes are tabulated relative to the molecular ion abundance at about 21.22 eV. Although all dissociative ion species are energetically possible, some are unobserved and empirical qualitative relationships between ion abundance and atomic ionization energies and electron affinities are noted. Threshold measurements carried out at and below ambient room temperature indicate ionization of molecules in the ground and in vibrationally-excited states. Unambiguous identification of the 0, 0 transition for molecular ionization is obtained from observed effects of temperature on features near threshold of the ion-yield curve.

Cyclic and Acyclic C_3H_3 and C_3H_4 Neutrals and Cations

A5

F. P. Lossing, Division of Chemistry, NRC Laboratories, Ottawa, Canada.

Recent photon impact studies of ionization and dissociation thresholds for allene, propyne, and derivatives[1] have been supplemented by monoenergetic electron impact measurements on cyclopropene and on propargyl ($HC{\equiv}CCH_2$) radical. The thresholds for formation of $C_3H_3^+$ fragment ion, which is prominent in the mass spectra of many hydrocarbons, are in excellent agreement at a value of $\Delta H_f(C_3H_3^+) = 256 \pm 2$ kcal/mole. This is about 25 kcal/mole lower than is currently found for $\Delta H_f(CH{\equiv}CCH_2^+)$, from the ionization potential of propargyl radical, and must refer to cyclo-$C_3H_3^+$. Formation of this symmetrical cyclopropenyl cation in the dissociative ionization of hydrocarbons appears to involve remarkably facile rearrangement reactions.

[1] A. C. Parr and F. A. Elder. J. Chem. Phys. 49, 2659 (1968).

ACCURATE THRESHOLD POTENTIALS WITH A QUADRUPOLE MASS SPECTROMETER

by

Thomas C. Ehlert
Chemistry Department
Marquette University
Milwaukee, Wis. 53233

ABSTRACT

A rather simple and inexpensive method of removing most of the ambiquity from the determination of ionization and appearance potentials with a conventional electron impact ion source is described. Equations are presented which show that when unknown and reference ion currents are adjusted experimentally or mathematically to compensate for sample dependent parameters such as multiplier gain the data and plotted as log (ion current) vs. ionizing voltage, the result should be parallel curves which are separated by the threshold potential difference. The development shows the relation to the extrapolated voltage difference method and offers some insight into the semi-log method developed by Lossing et al. Results from intercomparisons of knowns indicate an uncertainty of only 0.1 eV may be achieved.

INTRODUCTION

It is well known that the curvature near the threshold of an electron impact ionization efficiency (IE) curve is largely the result of the quasi-Maxwellian distribution of thermal electron energies plus the voltage drop along the exposed length of filament. In high sensitivity instruments one volt or more may be dropped across the length of filament from which electrons may enter the ion source so IE thresholds tend to be rather long curves. Locating the onset under these conditions requires, as one person put it, an almost intuitive feeling for the data. Some of the ambiguity can be removed through mathematical manipulations such as the energy distribution difference (EDD) method described by Winters, et al.[1] or the extrapolated voltage difference (EVD) method described by Warren[2]. In our experience, however, the EDD method requires data freer of perturbations than ordinarily attainable. Similarly, close to the threshold the noise and exponential form makes measurement of the separation between unknown and reference IE curves difficult. Still, one ideally would like to measure separations very close to the thresholds, i.e. in the exponential regions. One way to do this is by using a detection system which responds to log (ion current) so the exponential region can be displayed linearly or nearly so. Then, by x-y recording of log (ion current) as the ionizing voltage is scanned, preferably automatically, and by using noise filtering on the detection system output one can easily accumulate an infinite number of data points in a very convenient form. Lossing, et al.[3] have previously described a semi-log plot method which though empirical gives generally reliable results.[4] It requires that the 50 eV ion current of the unknown be normalized to that of the reference because it usually follows that in the threshold region the log (ion current) vs. ionizing voltage curves are parallel and separated in the energy direction by the threshold potential difference. No theoretical justification for the normalization procedure has been offered nor is it clear what to do when the curves fail to become parallel. It has been pointed out by Nicholson[5] that normalization has no significance and, in fact, misleads because of all the processes contributing to the 50 eV current only simple or dissociative ionization, as the case might be, remains as the threshold is approached. Honig[6] obtained a relation between the rate of ion formation by electrons from a thermionic emitter at temperature T and accelerating voltage V by assuming the probability of ionization P(E) to be proportional to the square of the total electron energy, E, in excess of the threshold value V_c. He showed the slope of log (ion current) vs. $V = 2/3kT$ where $V = V_c$, suggesting that curve separations should be measured as the voltages at which the curves attain this slope. In other words, normalization is not required. If, as seems more likely, P(E) varies as the first power of the excess energy the "critical slope" becomes 1/2kT. For convenience the argument followed in the latter case is repeated here.

The rate of ion formation at V, $N_i(V)$, due to the thermal spread is given by equation 1.

$$N_i(V) = \int_{u=o}^{u=\infty} P(E)\, dN_e(U) \qquad 1.$$

where P(E) has the form

$$P(E) = c_i(E-Vc_i) \qquad \text{if } E \geq Vc_i \qquad 2a.$$

$$P(E) = o \qquad \text{if } E \leq Vc_i \qquad 2b.$$

c_i being a sample-dependent constant and where $dN_e(U)$ is the Maxwell-Boltzmann distribution function, i.e. the number of electrons with thermal energies between U and U + dU emitted from the filament per unit time,

$$dN_e(U) = c_1\, U \exp\left(-\frac{U}{kT}\right) dU \qquad 3.$$

In Eq. 3. c_1 is a sample-independent constant. Integrating Eq. 1. at a constant temperature and noting the limits imposed by Eq. 2a and 2b gives

$$N_i(V) = c_2c_i(V-V_{c_i}) + 2kT) \qquad \text{if } V \geq V_{c_i} \qquad 4.$$

and

$$N_i(V) = c_2c_i(V_{c_i}-V + 2kT) \exp\left(-\frac{V_{c_i}-V}{kT}\right) \text{ if } V \leq V_{c_i} \qquad 5.$$

The region of interest here is that represented by Equation 5. To equate $N_i(V)$ to what one actually measures - the detector output $I_i(V)$ - requires accounting for a non-unity precursor density in the ion source, source collection losses, and analyzer and detector discrimination:

$$I_i(V) = G_i\tau_i n_i c_s N_i(V) \qquad 6.$$

where G_i is the detector gain, τ_i the analyzer transmission efficiency,[7] n_i the number density of precursor molecules, and c_s the source collection efficiency. Using Eq. 6 to eliminate $N_i(V)$ Eq. 5 becomes

$$I_i(V) = c_3c_i(V_{c_i}-V + 2kT) \exp\left(-\frac{V_{c_i}-V}{kT}\right) \qquad 7.$$

where c_3 combines all sample-independent constants and c_i combines all sample-dependent constants given in Eq. 6 with c_i. Equation 7 shows that if one experimentally or mathematically adjusts the unknown's sample constant to equal that of the reference sample, i.e. $c_i' = c_j'$, then the I vs. V curves will be identical for corresponding values of V_{c_i}-V. This is the basis for the EVD method. To avoid the asymptotic approach to I = 0 one may plot the data as

$$\ln I_i(V) = \ln c_3 + \ln c_i' + \ln (V_{c_i}-V + 2kT) - \frac{V_{c_i}-V}{kT} \qquad 8.$$

Again, when c_i' is set equal to c_j' the plots of $\ln I_i(V)$ and $\ln I_j(V)$ will be parallel and separated, at a given value of lnI, by $V_{c_i}-V_{c_j}$. This is the basis for the method used here and is an alternative to Honig's approach. Since the plot of $\ln I_i(V)$ vs. V in this region has a slowly varying slope and since differing values of the sample-dependent constant merely shift the curve in the lnI direction it is clear that the "normalization" required, experimentally or mathematically, assures that the $V_{c_i}-V_{c_j}$ separation is measured between corresponding portions of the reference and unknown curves. Although no expression has been developed which describes the current voltage relation from threshold to 50 eV or higher, this analysis suggests that the normalization procedure in the Lossing method amounts to equating the reference and unknown sample constants. Implicit in this development are the assumptions that autoionization, Franck-Condon factors and internal energy content do not grossly affect the threshold behavior.

Preliminary work here indicates that inclusion of a filament voltage drop effect in the equations will not alter the conclusions drawn above.

EXPERIMENTAL

To apply this method a simple capacitor discharge circuit was constructed for scanning the ionizing voltage at about 2 v min^{-1}. Next the 10^5 ohm input resistor of the Keithley 416 picoammeter, used to amplify the secondary electron multiplier output of the mass spectrometer,[9,10] was replaced with a 2N930 transistor as shown in Fig. 1. As shown this NPN device is used as a diode with the collector lead unconnected. The approximate form of the P-N junction equation[10] shown mathematically describes its response characteristics. The response of the

detection system was checked with a calibrated picoammeter supply and found to be logarithmic from 10^{-6} A to 10^{-12} A. Below 10^{-12} A a predictable deviation occurs as the exponential term in the function equation $I/I_0 = \exp(qV/kT)-1$ becomes comparable to unity. This does not preclude recording data below 10^{-12} A since as an instrumental effect it would appear on all curves. The range of logarithmic response should be extendable by chilling the junction; however, this apparently has not been attempted.[11] After focusing on the ion of interest the voltage scan was initiated and with x-y recording an infinite number of log (ion current) vs. ionizing voltage points were obtained within a few volts of the threshold. Curves for other calibrating substances, introduced through a leak valve, were recorded in the same manner except that the precursor partial pressure in the ion source and/or the transmission efficiency (n_i and τ_i in Eq. 6, respectively) were adjusted so the curves were parallel to that of the first species. The x-axis zero position of the recorder was offset by 10 v while retaining the calibrated 1.00 v in^{-1} sensitivity over the full 10 volt range on this axis. A constant 20 microamperes trap current was automatically maintained at all times. The MnF_2^+ and MnF^+ currents were derived from MnF_2 vaporized from an effusion cell at a constant temperature ± 2°K. At this level the current through the filament did not vary detectably during the voltage scan. Should such changes occur, as required by the trap current regulator, the ionizing voltage scale would be non-linear due to the changing volt drop across the filament.[12]

RESULTS

When the average separations between the calibrant curves in the lower half of Fig. 2 were measured and compared to the differences in the reported ionization potentials (all known to 0.01 eV or better[4]) the average deviation found was 0.08 eV. That is,

$\Sigma|(V_c)_{Lit.} - (V_c)_{Obs.}|/5 = 0.08$ eV. The calibrant and unknown curves could be reproduced to within better than 0.1 eV upon re-recording. Several days later the entire process was repeated. The $IP(MnF_2)$ and $AP(MnF^+/MnF_2)$ found in the repeat study were only 0.07 and 0.04 eV from the first set of results, respectively. The averages of these two determinations are 11.18 for $IP(MnF_2)$ and 13.29 eV for $AP(MnF^+/MnF_2)$, compared with 11.5 and 14.5 eV ± 0.3 eV obtained earlier by the vanishing current method.[13] This reproducibility indicates an uncertainty of 0.1 eV or less for IP measurements from systematic and random effects. Until further tests are performed on ions from dissociative processes an accurate assessment of the method's reliability will be difficult. There are reasons to suspect this method would be less satisfactory for large polyatomic molecules or for fragmentation processes requiring large activation energies.[14] Our data on IP(MnF) and $AP(MnF^+/MnF_2)$ give $D^o(MnF-F) = 4.8 \pm 0.2$ eV which compares well to the thermochemical result 5.1 ± 0.2 eV,[13] however.

The left side of Fig. 3 reveals the chief instrumental problem, the non-logarithmic response mentioned above.

CONCLUSION

The method discussed above, related to the EVD and the semi-log methods, appears to afford a simple yet accurate means of removing most of the ambiguity from electron impact ionization threshold measurements with little or no alternation of the instrument itself. Details of the threshold behavior are not revealed. In fact, the method is based on assumptions that the form of the IE curve with a volt or two of the threshold is essentially the same for all species to be studied.

ACKNOWLEDGEMENTS

The author is very grateful for the most helpful comments of Dr. F. P. Lossing, for the financial support of the U.S. Army Research Office-Durham, and for technical assistance by the Keithley Instrument Co.

REFERENCES

1. R. E. Winters, J. H. Collins, and W. L. Courchene, J. Chem. Phys., 45, 1931 (1966).

2. J. W. Warren, Nature, 165, 810 (1950).

3. F. P. Lossing, A. W. Tickner and W. A. Bryce, J. Chem. Phys., 19, 1254 (1951).

4. J. L. Franklin, J. G. Dillard, H. M. Rosenstock, J. T. Herron, K. Draxl and F. H. Field, "Ionization Potentials, Appearance Potentials and Heats of Formation of Gaseous Positive Ions", Nat. Stand. Ref. Data Ser., Nat. Bur. Stand. (U.S.), 26, 289 pages (June 1969).

5. A. J. C. Nicholson, J. Chem. Phys., 29, 1312 (1958).

6. R. E. Honig, J. Chem. Phys., 16, 105 (1948).

7. T. C. Ehlert, J. Phys. E., 3, 237 (1970).

8. Quad 250, Electronic Associates Inc., Palo Alto, Calif., modified for trap current regulation and adapted for molecular beam studies, see ref. 9.

9. T. C. Ehlert, J. Inorg. Nucl. Chem., 30, 3112 (1968).

10. M. Sachs, "Solid State Theory," McGraw-Hill Book Co., New York (1963).

11. R. Nowak, Keithley Instrument Co. private communication.

12. J. D. Waldron and K. Wood, Mass Spectrometry, Inst. of Petroleum, London 1953.

13. R. A. Kent, T. C. Ehlert, and J. L. Margrave, J. Amer. Chem. Soc., 86, 5090 (1964).

14. A. L. Wahrhaftig "Mass Spectrometry," R. I. Reed ed., Academic Press, p. 137, (1965).

Automatic Semi-Log Recording Of Electron Impact Appearance Potentials

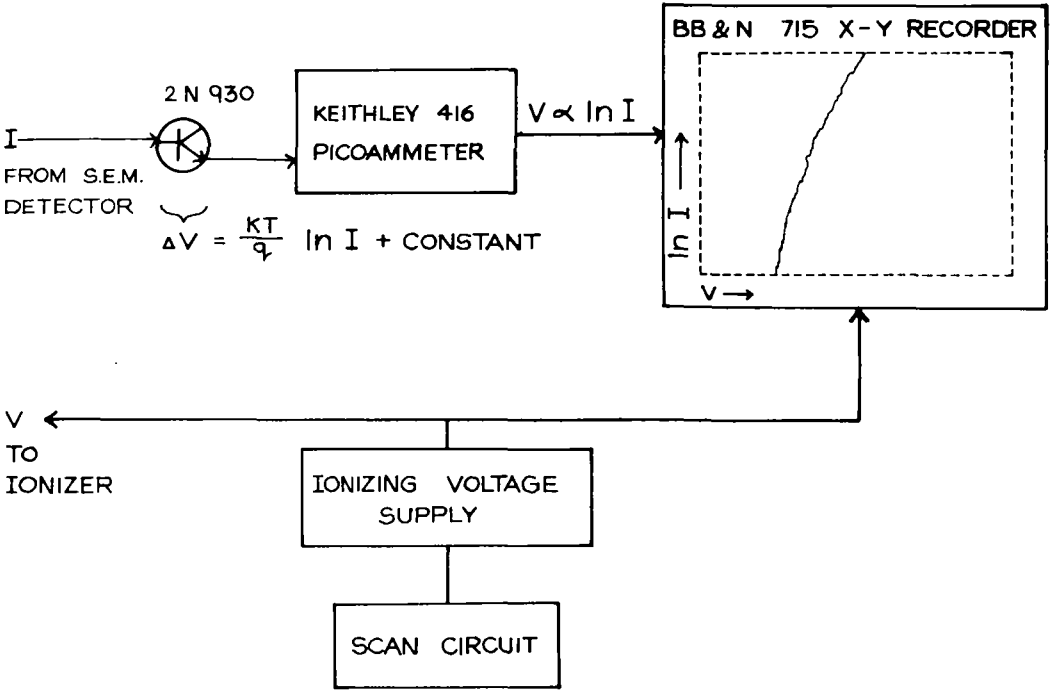

Figure 1.

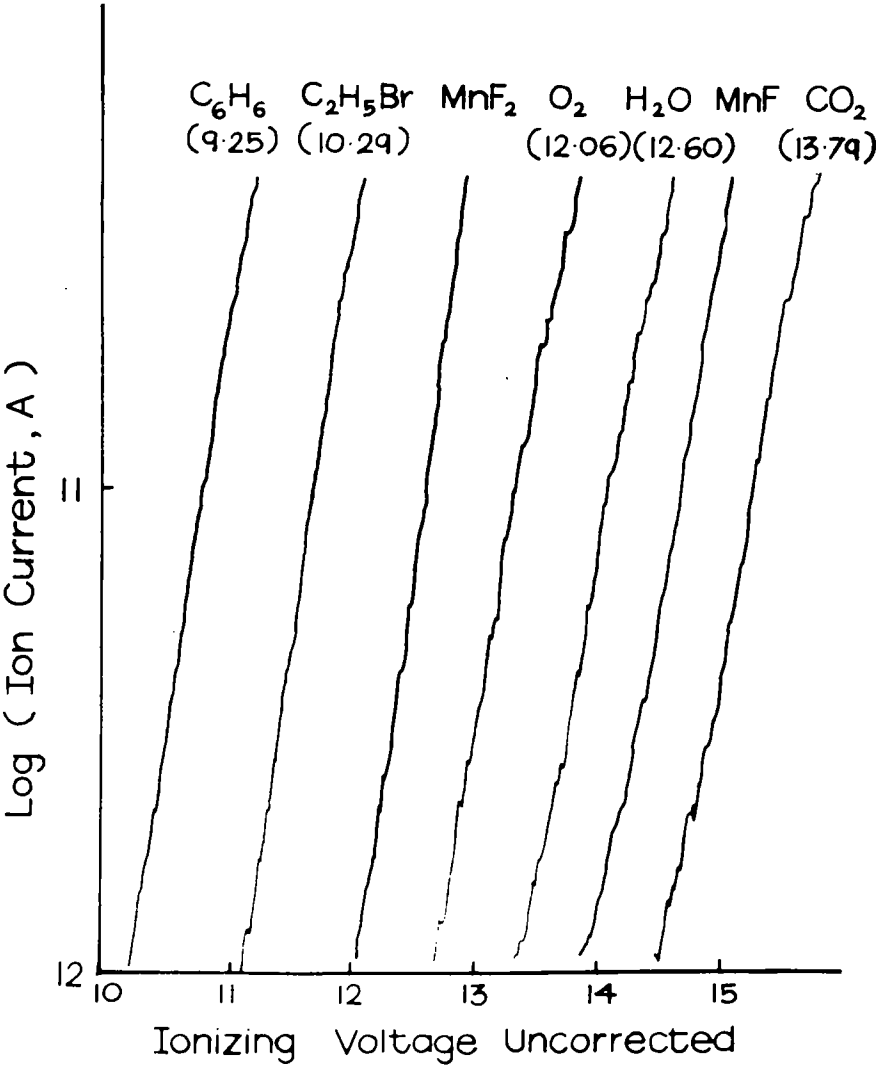

Figure 2. Results on several calibrants and unknowns

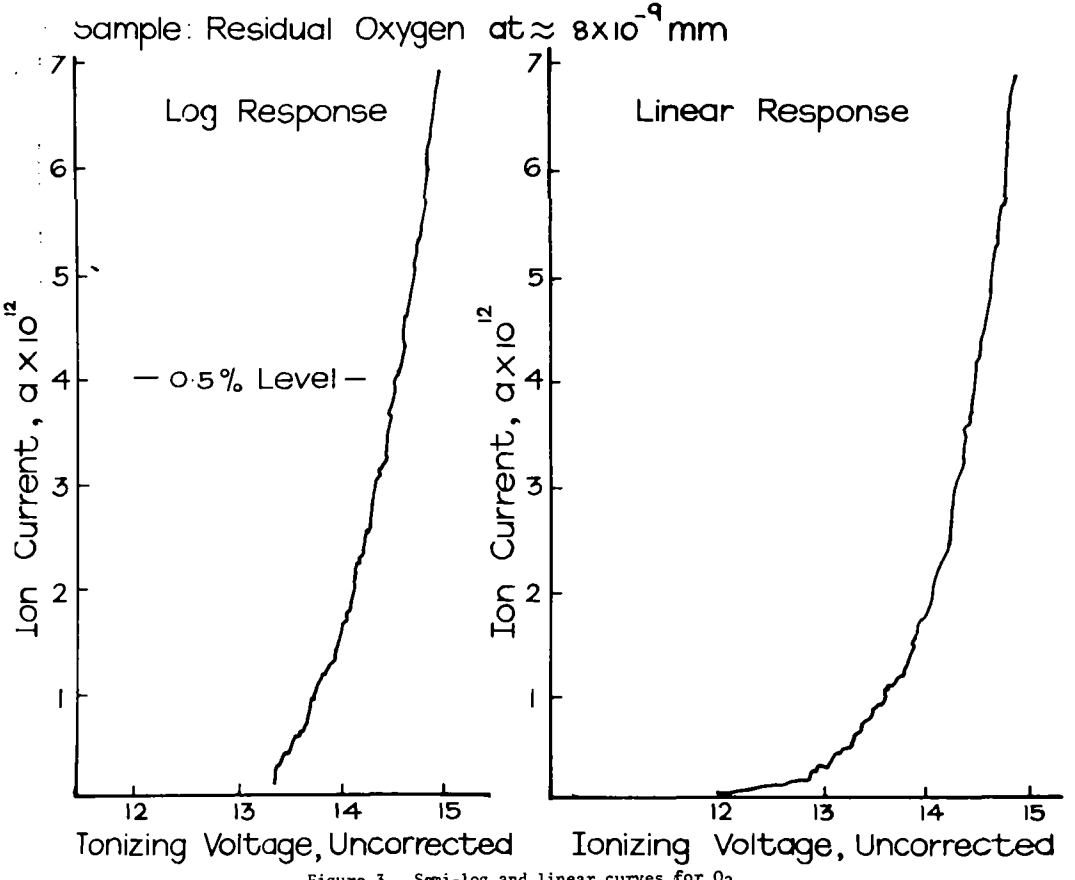

Figure 3. Semi-log and linear curves for O_2

Using Model Ionization Efficiency Curves to Evaluate the Methods for Determining Appearance Potentials. J. L. OCCOLOWITZ and B. CERIMELE, Lilly Research Laboratories, Indianapolis, Indiana 46206

Ionization efficiency curves for normal and metastable fragment ions are computed for model systems described by the Quasi-Equilibrium Theory of mass spectra. The calculations take into account different kinetic situations, the energy distribution of the ionizing electrons and its change with ionizing potential, and the vibrational energy distribution of the precursor molecules. Using the model curves as "experimental" data appearance potentials are found using Warren's method, Morrison's second derivative method, the method of semi-logarithmic plots, and the energy compensation method. The utility of each of these methods is evaluated by comparing the "experimental" results with the true appearance potentials for the model systems.

To be submitted for publication.

REFORMULATION OF THE QUASI-EQUILIBRIUM THEORY OF IONIC FRAGMENTATION* A9

Cornelius E. Klots
Health Physics Division, Oak Ridge National Laboratory, Oak Ridge, Tennessee 37830

Essentially any attempt to calculate the rate with which some ensemble of excited species decomposes will involve treating this rate as a function of some small number of characteristic parameters. By entertaining more and more detailed groupings of these parameters, such a formulation can be made more fine-grained and presumably more accurate, but also less general. On the other hand, the smallest number of parameters which might safely be considered would comprise the conserved quantities of motion. A decomposition rate for such an ensemble can then be obtained from micro-canonical ensemble theory. Indeed, for such an ensemble the equilibrium rate constant is the only unique rate constant. Thus, quasi-equilibrium rate theory assumes quite naturally a central position between generality and detail.

The essence of quasi-equilibrium theory has been most often formulated within the constructs of the transition state. Attendant to such formulations are the usual assumptions of transition state theory regarding reaction coordinates and transmission coefficients. A quasi-equilibrium formulation which avoids these assumptions would be attractive.

The details of such a formulation, together with an application to the fragmentation processes of the methane positive ion, are presented elsewhere.[1] It will suffice here to note that this reformulation invokes microscopic reversibility to connect the fragmentation with the cross-sections for the reverse process. It is also noteworthy that this reformulation in effect puts the ideas of phase-space theory[2] on an absolute time scale. It is often asserted that phase-space theory represents a radical departure from transition state theory. In view of the above remarks, we would prefer to emphasize the kinship.

Of especial interest are the metastable decompositions of the methane ion and its deuterated analogs. The usual transition state formulation does not lend itself readily to a satisfactory interpretation of them. Tunneling through centrifugal barriers on the other hand leads to a reasonably good correlation between the observed[3] and predicted abundances. The correspondence is displayed in the figure. An attempt to place this correlation on an absolute scale requires additional assumptions, but succeeds nevertheless to within a factor of two. Note that metastable D atom ejection from CD_4^+ occurs readily, contrary to the

usual mass dependence of tunneling. This is explained in a paper to appear soon.[4] The usual mass effect does not arise in tunneling through centrifugal barriers. Thus some generality for the tunneling mechanism is suggested.

---

*Research sponsored by the U. S. Atomic Energy Commission under contract with Union Carbide Corporation.

[1] C. E. Klots, J. Phys. Chem. (in press).

[2] J. C. Light, Discussions Faraday Soc. 44, 14 (1967).

[3] Ch. Ottinger, Z. Naturforschg. 20a, 1232 (1965).

[4] C. E. Klots, Chem. Phys. Letters (in press).

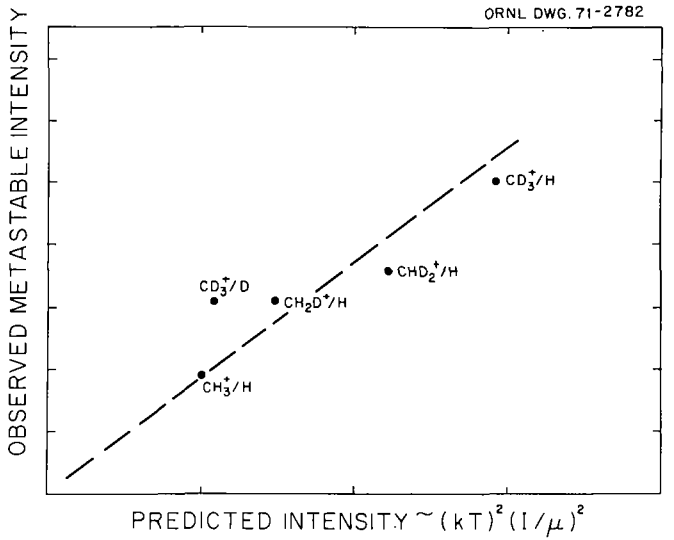

Figure 1. Correlation between predicted and measured abundances of metastable hydrogen atom ejection from methane ions.

ENERGY DEPOSITION FUNCTIONS IN MASS SPECTROMETRY

G. G. Meisels, C. T. Chen, B. G. Giessner, and R. H. Emmel
Department of Chemistry
University of Houston
Houston, Texas 77004

ABSTRACT

Methods for the evaluation of internal energy distribution functions resulting in ions from impact of energetic electrons are examined and their shortcomings are analyzed. An approach to the calculation of energy deposition functions based on the Bethe-Born treatment of collisions is presented. It requires photoelectron spectra and photoionization cross sections as input data. Distribution functions are calculated for methane, ethane, and ethylene, and are evaluated by folding them into known breakdown curves. The resultant ion distributions are in good agreement with experimental fragmentation patterns for 70 eV electrons.

INTRODUCTION

The statistical or quasi-equilibrium theory of mass spectra[1] assumes that ions are formed with a range of excitation energies on initial electron impact, and that this energy is rapidly degraded into vibrational energy of the ground electronic state of the ion. The subsequent fragmentation is then described in terms of first order rate theory. Primary emphasis in the development of this model since its original introduction has been on the correct description of first order rate constants, and good approximations to actual state density counting are now available.[2-13] This aspect of the theory is therefore well able to calculate breakdown curves[14,15] and shows good agreement with such data obtained by charge exchange or photoionization.[11-13] The second major factor affecting the calculation of mass spectra produced by 70 eV electrons, the internal energy distribution function, has received considerably less attention. A variety of approximations have been employed to estimate this quantity since the direct evaluation is extremely difficult and time consuming.[16] Unfortunately, the assumptions underlying the use of the indirect methods may well be invalid.[12] In this communication we show that energy deposition functions can be derived from the well known Bethe-Born treatment of atomic collisions, discuss the restrictions of this approach, and evaluate it for simple molecules.

ENERGY DEPOSITION FUNCTIONS FROM THE OPTICAL APPROXIMATION

It is convenient to begin by reviewing the basis of this approximation[17-19] which is an immediate consequence of the Bethe-Born theory of collisions,[17] in essence a quantum mechanical impact parameter treatment. It is an application of perturbation theory and rests on the assumption that the incident projectile can be described as a plane wave. This condition is met as long as the Born approximation is valid. For sufficiently large values of the kinetic energy T of the incident electron it leads to the following relationship for the total cross section $\sigma_{n,t}$ for the excitation of an atom from the ground state to an excited or ionized state t_n:

$$\lim_{T\to\infty} \sigma_{n,t} = 4\pi a_o^2 R^2/T \cdot (f_n/E_n)\ln(4Tc_n/R) \qquad (I)$$

where a_o is the Bohr radius, R is the Rydberg energy, E_n the excitation energy of the state n above the ground state, f_n the optical (dipole) oscillator strength, and c_n represents a constant of the order of magnitude of unity. In the ionization continuum, f_n is to be replaced by df_n/dE_n.

A similar relationship can be derived by correlating the collision process with radiation theory.[20,21] This approach, the Weizsaecker-Williams method of virtual quanta, analyzes the time-dependent perturbing field of the impinging electron or other charged particle using classical mechanics. Transformation to the frequency domain yields a distribution function of harmonic waves whose intensities and frequencies are defined by the collision process. The effect of these frequencies is then analyzed on the assumption that they add incoherently. Again, the chief assumption is that the perturbation is small.

The basic equation (I) can readily be converted to a probability function $P(E_n)$ that an ion pair formed on passage of highly energetic electrons is created by an energy loss E_n. The fraction of states produced at E_n which ionizes is given by η_n, the ionization efficiency; the product $f_n\eta_n$ varies as the ionization cross section σ_n. Equation (I) can therefore be rewritten in terms of this experimental observable and after normalization:

$$P(E_n) = (\sigma_n/E_n)/(\int_{IP}^{E_{max}} (\sigma_n/E_n)dE_n) \qquad (II)$$

Equation II will be valid for high values of T except for the approximation contained in the assumption that c is independent of E_n.

The familiar Bethe-Born treatment or the Weizsaecker-Williams method thus provide a means of calculating the probability distribution of energy loss as a function of energy. When this process leads to ionization, the energy loss by the incident electron cannot be associated uniquely with a given excited state, but will be divided between the kinetic energy of the ejected electron and the ionization energy.

It is possible to estimate the energy partitioning from photoelectron spectra taken with incident photon energy $E_n = h\nu$ with certain limitations. This will not give correct results for systems where multiple ionization is important because in such processes the energy difference between E_n and the energy remaining with the multiply charged ion may be divided between two or more electrons.

LIMITATIONS AND APPLICATIONS

The optical approximation ideally restricts calculation of energy deposition functions by this method to impacting electron energies in excess of ca. 5 kV for hydrocarbons and other low-Z atom containing molecules. At the same time, however, ionization cross sections and photoelectron or ESCA spectra would have to be known over a very large range of energies. Even then, the folding of these properties weighted by 1/E would not give the entirely correct result because of the limitations imposed by multiple ionization. Ionization cross sections at high photon energies would be overestimated because individual acts would lead to the formation of several ions.

Fortunately, the electron energy range of interest in mass spectrometry (i.e. 50 to 100 eV) is in the region where, for many species, multiple ionization is not an important contributor to total ionization. Most of the interaction occurs with valence electrons, and the optical approximation would therefore only have to be approximately valid for low energy transitions. There is some evidence that the Born approximation gives an adequate description of major processes at energies greater than 70 eV,[22] and particularly at a few hundred eV.[23-25] Moreover, the mass spectra of simple molecules do not change materially at electron energies up to several hundred eV.[26]

Therefore, it is only necessary to know photoionization cross sections over a limited energy range; they are available up to ca. 25 eV from the work of Schoen[27] and that of Metzger and Cook;[28] the data are not in very good agreement with each other, but the former is generally considered more reliable and will therefore be employed in our further discussion.

Photoelectron spectra are typically available only at one or at the most two selected photon energies dictated by the availability of resonance lines, with the 21.21 eV line of helium most frequently employed.[29] It is therefore necessary to assume that changes in incident photon energy cause only a shift in the energy axis of the photoelectron spectrum, and that it is merely truncated at E_n when that energy is less than that of the resonance line used in the determination. Some changes in relative transition probabilities have been reported,[30,31] but generally these are relatively small, or affect primarily higher energy transitions.[31,32] This assumption should not introduce a serious error.

Photoelectron spectra, however, also discriminate against ions resulting from autoionizing states. Derivative electron impact spectra[33] and photoionization mass spectrometry[34] suggest that such processes may be quite important, and photoelectron coincidence mass spectrometry indicate that both parent and fragment ions may result.[35] This presents the possibility of a severe complication even though the relative importance of such processes is not known at present.

The application of this approach to ethane is shown in Figure 1. The photoelectron spectrum (solid circles)[29] is folded numerically by a point by point multiplication and addition procedure[36] into the energy loss function for ethane, and the resultant energy deposition function is shown as the solid curve. The deposition function is qualitatively consistent with the observation of McLafferty et.al.[37] that the use of photoelectron spectra alone overemphasizes high energy processes when comparison is made to 70 eV mass spectra. The general character of the photoelectron spectrum is, however, retained.

EVALUATION

The energy deposition functions can therefore be evaluated approximately by folding them into breakdown graphs[14,15] and comparing the resultant mass spectra with those reported from analytical mass spectrometers.[38] A difficulty is apparent in that mass spectra obtained with various instruments differ substantially from each other. Among the reasons for this discrepancy are instrumental mass discrimination, particularly important for Dempster type instruments, and ion source temperature. Photoionization cross sections, photoelectron spectra, and breakdown graphs are usually reported for

near-thermal molecules, while in mass spectrometry temperatures are usually ca. 520°K. We have therefore compared the mass spectra calculated by our apriori approach with two of those in the literature. Comparison with spectra obtained with sector type instruments is more meaningful because of the lesser discrimination and the probably lower temperature of the measurements.

The results of such calculations and comparisons are shown in Tables I - III. The agreement between calculated and experimental fragmentation patterns is essentially within experimental error when the optical approximation is used for the calculation of energy deposition functions. The direct use of photoelectron spectra leads to a considerable overestimate of the probability of higher energy processes. This is to be expected since there is no apriori validity for the assumption that the intensity distribution of photoelectron spectra reflects the internal energy distribution of the ion formed on impact of 70 volt electrons.[12,16]

Little advantage is obtained from the use of the optical approximation for ethylene. This is directly a consequence of the dominant formation of parent ion in an energy band just below the threshold of fragmentation. The cause of the relatively poor fit may be the contribution of autoionization porcesses which do not manifest themselves in photoelectron spectra.

CONCLUSION

Energy deposition functions even for the impact of 50 to 100 V electrons can be estimated by an application of the Bethe-Born theory of collisions using photoionization cross sections and photoelectron spectra. This approach gives better agreement when applied to the prediction of mass spectra than any of the other commonly employed ones, but will fail if the mass spectrum is greatly influenced by double ionization processes, autoionization, and generally by high-energy states.

ACKNOWLEDGEMENTS

This investigation was supported in part by the United States Atomic Energy Commission under Contract AT-(40-1)-3606 and by the Robert A. Welch Foundation of Houston, Texas. The computer facilities employed in this research were those of the Common Research Computer Facility of the Texas Medical Center, supported in part by USPHS, grant no. RR 00254, and by the Robert A. Welch Foundation and made available to us as a grantee of that Foundation. We are sincerely grateful for this assistance.

LITERATURE CITED

1. H. M. Rosenstock, M. B. Wallenstein, A. L. Wahrhaftig and H. Eyring, Proc. Natl. Acad. Sciences U.S. 38, 667 (1952).
2. M. Vestal, A. L. Wahrhaftig and W. H. Johnston, J. Chem. Phys. 37, 1276 (1962).
3. E. W. Schlag and R. A. Sondmark, J. Chem. Phys. 37, 168 (1962).
4. S. H. Lin and H. Eyring, J. Chem. Phys. 39, 1577 (1963).
5. P. C. Haarhoff, Mol. Phys. 7, 337 (1963).
6. E. Thiele, J. Chem. Phys. 39, 3258 (1963).
7. G. Z. Whitten and B. S. Rabinovitch, J. Chem. Phys. 38, 2466 (1963).
8. K. A. Wilde, J. Chem. Phys. 41, 448 (1964).
9. W. Forst, Z. Prasil, and P. St. Laurent, J. Chem. Phys. 46, 3736 (1967).
10. J. C. Tou, J. Phys. Chem. 71, 2721 (1967).
11. H. M. Rosenstock, Adv. in Mass Spectrom. IV, 523 (1968).
12. M. Vestal, in "Fundamental Processes in Radiation Chemistry", P. Ausloos, Ed., J. Wiley - Interscience, New York (1968) Chapter 2.
13. H. M. Rosenstock and M. Krauss, in "Advances in Mass Spectrometry", 2, 251 (1962).
14. E. Pettersson and E. Lindholm, Arkiv för Fysik 24, 49 (1963).
15. H. von Koch, Arkiv Fysik 28, 559 (1965).
16. H. Ehrhardt, F. Linder, and T. Tekaat, "Advances in Mass Spectrometry", London, Pergamon Press, 4, 705 (1968); ibid. 5, (in press).
17. H. V. Bethe, Ann. Physik 5, 325 (1930).
18. W. F. Miller and R. L. Platzman, Proc. Phys. Soc. (London) A70, 299 (1957).
19. R. L. Platzman, The Vortex 23, 372 (1962).
20. E. J. Williams, Rev. Modern Phys. 17, 217 (1945).
21. J. D. Jackson, "Classical Electrodynamics", J. Wiley and Sons, New York (1963).
22. D. R. Bates, A. Fundaminsky, J. W. Leech, and H. S. W. Massey, Trans. Roy. Soc. (London) A243, 117 (1950).
23. J. A. Simpson and S. R. Mielczarek, J. Chem. Phys. 39, 1606 (1963).
24. J. K. Rice and A. Kuppermann, J. Chem. Phys. 48, 945 (1968).
25. E. N. Lassettre, J. Chem. Phys. 53, 3801 (1970), and A. Skerbele and E. N. Lassettre, J. Chem. Phys. 53, 3806 (1970).
26. J. T. Tate, P. T. Smith, A. L. Vaughan, Phys. Rev. 48, 525 (1935).

27. R. I. Schoen, J. Chem. Phys. 37, 2032 (1962).
28. P. H. Metzger and G. R. Cook, J. Chem. Phys. 41, 462 (1964).
29. A. D. Baker, C. Baker, C. R. Brundle, and D. W. Turner, Int. J. Mass Spectrom. and Ion Phys. 1, 285 (1968).
30. J. E. Collin and P. Natalis, Int. J. Mass Spectrom and Ion Phys. 2, 231 (1969).
31. C. R. Brundle, M. B. Robin, and H. Basch, J. Chem. Phys. 53, 2196 (1970).
32. L. L. Lohr, Jr. and M. B. Robin, J. Am. Chem. Soc. 92, 7241 (1970).
33. J. W. McGowan, M. A. Fineman, E. M. Clarke and H. P. Hanson, Phys. Rev. 167, 52 (1968), and J. W. McGowan, E. M. Clarke, H. P. Hanson, and R. F. Stebbings, Phys. Rev. Let. 13, 620 (1964).
34. W. A. Chupka, M. E. Russell, and K. Rafaey, J. Chem. Phys. 48, 1518 (1968).
35. B. Brehm, presented at the 5th Trienniel International Meeting on Mass Spectrometry Brussels, Belgium (1970).
36. B. G. Giessner and G. G. Meisels, J. Chem. Phys. (accepted for publication).
37. F. W. McLafferty, T. Wachs, C. Lifshitz, G. Innorta, P. Irving, J. Am. Chem. Soc. 92, 6867 (1970).
38. Catalog of Mass Spectral Data, American Petroleum Institute Project 44, Texas A & M College, College Station, Texas 1964.

TABLE I

COMPARISON OF ESTIMATED ENERGY DEPOSTION FUNCTIONS WITH FRAGMENTATION PATTERN FOR ETHANE

Ion	$C_2H_6^+$	$C_2H_4^+$	$C_2H_5^+$	CH_3^+	others
AP,eV	11.52	12.08	12.65	13.6	
After weighting by breakdown curve					
Photoelectron spectrum	9.7	37.4	8.6	4.1	40.2
Optical approximation	12.5	42.0	9.0	3.5	33.0
Experimental					
API spectrum Number 61; Westinghouse L.V.; temperature not specified	14.6	47.4	11.8	1.0	25.2
API spectrum Number 2; CEC 21-102; 250°C	11.8	45.1	9.3	2.3	31.5

TABLE II

COMPARISON OF ESTIMATED ENERGY DEPOSITION FUNCTIONS WITH FRAGMENTATION PATTERNS FOR METHANE

Ion	CH_4^+	CH_3^+	CH_2^+	others
AP,eV	12.65	14.24	15.16	
From Photoelectron Spectrum	39.9%	57.6%	2.5%	
From Optical Approximation	52.2	45.9	1.9	
API spectrum Number 60; Westinghouse L.V., temperature not specified	53.1	40.3	3.9	1.9
API spectrum Number 1; CEC 21-102; 250°C	46.0	39.5	7.4	7.1

TABLE III

COMPARISON OF ESTIMATED ENERGY DEPOSITION FUNCTION WITH FRAGMENTATION PATTERN FOR ETHYLENE

Ion	$C_2H_4^+$	$C_2H_2^+$	$C_2H_3^+$	others
AP,eV	10.51	12.96	13.37	
From Photoelectron Spectrum	44.3%	19.8%	36.0%	
From Optical Approximation	48.7	19.0	32.3	
Experimental				
API spectrum Number 65; Westinghouse L.V.; temperature not specified	44.0	22.89	25.8	9.41%
API spectrum Number 23; CEC 21-102; 250°C	38.1	23.7	24.7	13.5

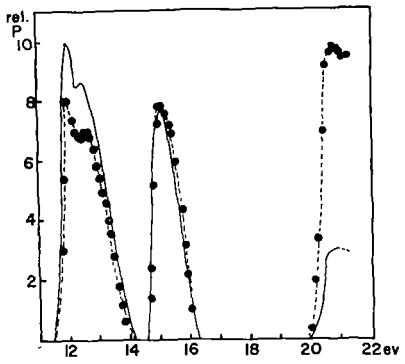

Figure 1. Approximate photoelectron spectrum (points) and energy deposition function (solid line) for ethane; normalized at maximum.

STEREOCHEMICAL REQUIREMENTS FOR INTRAMOLECULAR REARRANGEMENTS IN TRIMETHYLSILYL AND TRIMETHYLSILYLPHOSPHATE DERIVATIVES. B2

D. J. HARVEY, M. G. HORNING AND PAUL VOUROS

Institute for Lipid Research, Baylor College of Medicine
Houston, Texas 77025

Abstract

The mass spectra of the TMS derivatives of alkane diols and sugar phosphates exhibit a large number of rearrangement ions. Migrations have been observed for hydrogen, trimethylsilyl and trimethylsilylphosphate groups. Rearrangement ions involving migration of as many as three groups in sugar phosphates and glycerophosphates have been observed. Preparation of derivatives containing both TMS and D-9-TMS groups on selected positions provided further information about the origin of the interacting groups. Little is known about the stereochemical requirements for the formation of these rearrangement ions. Studies conducted with molecules of rigid or semi-rigid conformation (e.g., trimethylsilyl derivatives of steroid diols and steroid phosphates) indicate a high degree of stereochemical dependence.

The full papers will be published in J. Organic Mass Spectrometry (May or June 1971) and Tetrahedron (a 1971 issue).

B3

INTERACTION OF A SILYL CENTER WITH DISTANT PHENYL GROUPS IN ORGANOSILICON COMPOUNDS

William P. Weber
Department of Chemistry
University of Southern California
Los Angeles, California 90007

The first compound we would like to consider is 1-phenyl-2-trimethylsilyl ethane. The spectrum is extremely simple--there are only four major ions. In addition to the parent ion at mass 178, there are two important ions formed by simple cleavage of a group from the quarternary silyl center. These are the trimethyl siliconium ion at mass 73 and the P-15 siliconium ion formed by loss of a methyl group from the parent at mass 163. The final major ion is the dimethylphenylsiliconium ion at mass 135. This ion is formed by migration of the electron rich phenyl group from carbon to the siliconium ion center with simultaneous loss of ethylene. Observation of a metastable ion at mass 111.5 and deuterium labeling work support this rearrangement. A similar rearrangement of trimethylsilylbenzyl ethers has been reported by C. Djerassi--only in this case formaldehyde is lost rather than ethylene as the neutral species.

The second compound we would like to consider is 1-phenyl-3-trimethylsilyl propane. In this compound, a significantly different type of interaction of the silyl center with the remote phenyl ring is observed.

In addition to the parent ion, two ions formed by simple cleavage of groups from the quarternary silyl center are important, namely the trimethylsiliconium ion at mass 73 and the parent minus a methyl group at mass 177. Interaction of the P-15 siliconium ion with the remote phenyl group with simultaneous loss of C_3H_6 leads to the dimethylphenylsiliconium ion at mass 135. However, this is not the most important interaction of the silyl center with the remote phenyl group. The ion at mass 164 is formed by transfer of the intact trimethylsilyl group of the parent ion to the phenyl ring with simultaneous loss of ethylene. This rearrangement is similar to one observed by S. Meyerson in alkyl aromatic compounds, in which a gamma hydrogen is specifically transferred to the benzene ring with simultaneous loss of ethylene. Similarities in the type of specific rearrangement which trimethylsilyl groups and hydrogen atoms will undergo in the mass spectrometer have been previously noted. For instance, in the mass spectrum of methyl-4-trimethylsilyl butyrate a specific transfer of the trimethyl silyl group from the gamma carbon to the carbonyl oxygen with simultaneous loss of ethylene is observed. This rearrangement is analogous to the specific transfer of a gamma hydrogen to the carbonyl oxygen of ketones--better known as the McLafferty rearrangement.

The transfer of a trimethyl silyl group from a saturated carbon to an unsaturated carbon of a phenyl ring in the mass spectrum of 1-phenyl-3-trimethylsilyl propane was substantiated both by deuterium labeling and by the observation of a metastable ion--both the 3,3-dideuterio and the 1-deuterio compounds were examined.

Other ions of note in the mass spectra of this compound are the tropylium ion at mass 91 and the 1-trimethylsilyl ethyl cation at mass 101. This last ion is often important in the mass spectra of organosilicon compounds.

In the mass spectra of 1-phenyl-4-trimethylsilyl butane in which the silyl center and the phenyl ring are separated by four carbon atoms, no interaction is observed.

The third compound we will discuss is beta-trimethylsilyl styrene.

In addition to a parent ion and a P-15 siliconium formed by loss of a methyl group from the quarternary silyl center two major ions arise by interaction of the silyl center with the remote phenyl group. The dimethylphenylsiliconium ion at mass 135 is formed by interaction of the P-15 ion with the phenyl ring with simultaneous loss of acetylene as the neutral species. The ion at mass 145 is also formed from the P-15 ion as indicated by the observation of an appropriate metastable peak. It is

formed by loss of methane from the P-15 ion. This loss of methane involves loss of a methyl group from the siliconium ion center and one hydrogen from the styryl system.

A tempting possibility was that this involved specific loss of the *alpha hydrogen to form an aromatic 2π-electron system--the silacyclo*propenium ion. However, labeling experiments indicate that the hydrogen atom lost from the styryl system is lost in a completely random fashion. The mass spectra of 1-phenyl-1-deuterio-2-trimethylsilyl ethylene, 1-phenyl-2-deuterio-2-trimethylsilyl ethylene, 1-pentadeuterio phenyl-2-trimethyl ethylene and finally 1-(2',4',6' trideuterio phenyl)-2-trimethylsilyl ethylene were all consistent with the complete loss of identity of the seven hydrogens of the styryl systems prior to loss of one of them with a methyl group from the siliconium ion center as methane. We feel this is consistent with an electrophilic attack of the siliconium ion center on the phenyl ring followed by loss of methane to form an idenyl siliconium ion.

Finally, in the mass spectra of 1-phenyl-2-trimethylsilyl acetylene, no interaction of the silyl center and the phenyl group is observed. This is reasonable in the light of the rigid linear geometrical requirement of the acetylenic bond.

A full report of these results will be published in the Journal of Organic Chemistry.

Abstract

Don C. DeJongh, Martha L. Gay, and Laurence R. Dusold
Department of Chemistry, Wayne State University, Detroit, Michigan 48202

A. Mass Spectra of Aryl Dimethyl Phosphates - In the 20 eV mass spectrum of phenyl dimethyl phosphate (1), the base peak is the molecular ion at m/e 204 ($C_8H_{11}O_4P$). The only intense fragment ions are found at m/e 90 (69%, C_7H_6) and m/e 107 (46%, C_7H_7O). These are shifted to m/e 216, 121, and 104 in the mass spectrum of p-cresyl dimethyl phosphate. The fragment ions result from rearrangement, i.e., C_7H_6 contains seven carbons whereas in 1 there are only six carbons bonded together. This rearrangement has been studied by high resolution, deuterium labeling, and metastable defocusing.

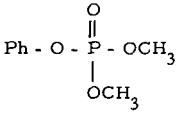

(1)

B. MO Calculations Applied to Free Energy Relationships - A modified Pople and Beveridge CNDO method and program has been used to calculate electronic energies of ions. For example, the energies of $PhCO^{\oplus}$ and of 12 substituted benzophenones, $Ph - CO - C_6H_4 - Y^{\ddagger}$, have been calculated. When log E/E_o, where $E = \frac{\text{energy of } PhCO^{\oplus}}{\text{energy of } PhCOC_6H_4Y^{\ddagger}}$, is plotted versus the Hammett sigma constants, a straight line with a standard deviation of 0.036 log units is obtained. Implications of this result were discussed.

Hydrogen Exchange in a Six-Membered Ring Transition State: Evidence for a Stepwise McLafferty Rearrangement

P. Vouros*, P. R. Briggs and T. W. Shannon

Dow Chemical Company, Wayland, Mass. 01778

Abstract

The mass spectra of 2-methyl-5-chloro-3N-ethylbenzothiazolium iodide and its N-ethyl-d_2, d_3 and d_5 counterparts have been examined. These compounds eliminate HI thermally from the salt to form 5-chloro-3-ethyl-2-methylene benzothiazoline, which under electron impact loses C_2H_4 via a McLafferty rearrangement. The labelled compounds show losses of isotopically mixed ethylenes with increasing deuterium incorporation in the ($M-C_2H_4$) ion as the electron energy is decreased. The data may be explained by a stepwise McLafferty rearrangement in which the intermediate formed has sufficient lifetime for reversible hydrogen migration to occur.

*Institute for Lipid Research, Baylor College of Medicine, Houston, Texas

In Press J. Org. Mass Spec.

B6

The Internuclear Distance Through Which Bifunctional Interaction Can Occur in an Ion Radical. C. C. FENSELAU and C. H. ROBINSON, Department of Pharmacology and Experimental Therapeutics, Johns Hopkins University School of Medicine, Baltimore, Maryland 21205.

We have used the steroid molecule as a rigid template to determine how far apart two functional groups can be moved before detectable interaction ceases. A number of steroid diols in which both hydroxyl hydrogens had been exchanged with deuterium, were examined for loss of D_2O on electron impact. Those compounds which lost D_2O are all 1,2- or 1,3-diols, and with one exception, show strong intramolecular hydrogen bonding in infrared measurements of solutions. We conclude that intramolecular interactions of functional groups will occur on electron impact only when the atoms involved can be brought to within approximately normal bonding distances.

STEROIDAL DIOL	LOSS OF D_2O	CLOSEST DISTANCE	HYDROGEN BONDING (IR)
3β,17β-DIHYDROXY-5α-ANDROSTANE	No	10.8 Å	No
3α,12α-DIHYDROXY-5β-PREGNAN-20-ONE	No	4.9	No
3β,6β-DIHYDROXY-5α-CHOLESTANE	No	4.7	No
3α,5β-DIHYDROXY-5β-CHOLESTANE	No	3.5	No
16α,17β-DIHYDROXY-4-ANDROSTEN-3-ONE	Yes	3.2	No
3β,4β-DIHYDROXY-5α-CHOLESTANE	Yes	2.4	Yes
EXO,EXO-2,3-DIHYDROXYBICYCLO[2,2,1]HEPTANE	Yes	2.0	Yes
3β,5β-DIHYDROXY-5β-CHOLESTANE	Yes	1.6	Yes

This report will be published elsewhere in more detailed form.

Determination of Fragmentation Pathways of [[(1-ethyl-3-methyl-5-pyrazolyl)-amino]methylene] malonic acid, diethylester by High-Resolution Mass Spectrometry and Metastable Ion Defocusing.

Phillip T. Funke and Allen I. Cohen
The Squibb Institute for Medical Research
New Brunswick, New Jersey 08903

Compound I is thermally converted at 150°C. to 1-ethyl-3-methyl-4-hydroxyl-1H-pyrazolo-[3,4b] pyridine-5-carboxylic acid ethyl ester, compound II, with the concurrent liberation of ethanol. Under electron

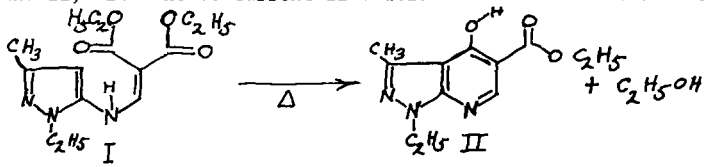

impact, I (cf. Figure 1) also loses ethanol to form an m/e 249 ion whose composition agrees with that of II (cf. Figure 2). The fragmentation pattern of I below m/e 249 is strikingly similar to that of II, although the intensities relative to the m/e 249 ion are diminished. It is the purpose of this study to establish, through metastable ion defocusing and deuterium labelling, the pathways of the conversion of I to II under electron impact.

That the conversion can occur under electron impact is substantiated from the observed metastable ion at m/e 210.2, corresponding to the M^+ going to the m/e 249 ion. Additionally, all the mass spectra obtained from the introduction of I through direct insertion probe at source temperatures of 60°to 140°C. were identical. Low voltage ionization (15 ev nominal) spectra of I and II were equivalent to their 70 ev spectra, with the exception of the m/e 177 ion of I, which occurs by a pathway not available to II. The chemical ionization spectrum of I at 60°C. has a metastable peak at m/e 211 agreeing with the conversion of MH^+ to the m/e 250 ion (cf. Figure 3). The C.I. spectrum of II also showed a MH^+ -46 ion (cf. Figure 4).

The spectra of compounds I and II are extremely rich in metastable ions. The major fragmentation pathways of compounds I and II have been established by means of metastable ion defocusing employing the variable accelerating potential method.[1] The results, summarized in Figures 1 and 2, demonstrate that the pathways are identical and occur by the loss of small neutral molecules.

To further establish the elimination of ethanol from I, the N-monodeuterated derivative was prepared by dissolving the sample in CH_3OD and exchanging the N-H proton. The mass spectrum showed that C_2H_5OD was eliminated to give the m/e 249 ion. As reported by Fenselau and Robinson[2], proton transfer and elimination of small molecules are expected if the groups are within bonding distances. It had been previously established for I, from NMR and IR studies, that the amide proton is intramolecularly H-bonded to the carbonyl group. A second

pathway gave rise to a small m/e 251 ion through the loss of C_2H_5O. Other small-fragment ions, containing deuterium, originate from the m/e 251 ion. Under electron impact, the following mechanism is invoked. If

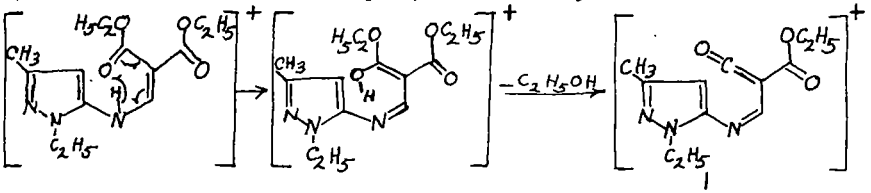

oxygen scrambling occurs, then the elimination could occur by the following mechanism. Differentiation of the

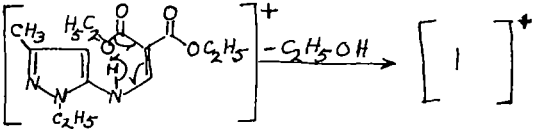

two mechanisms would require ^{18}O labelling. Ring closure would then proceed by a second proton transfer, i.e.

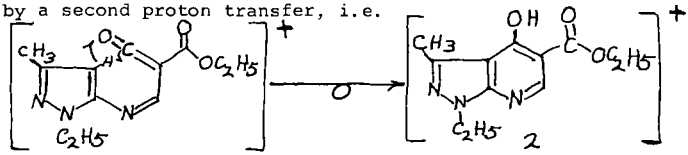

to yield ion 2, corresponding to the M of II. Although it has been demonstrated that the fragmentation of I proceeds through the ion 2, fragmentation could also occur through ion 1. It would be necessary to study the metastable ion energy distribution at an energy resolution greater than attainable with our instrument to establish the extent to which fragmentation may occur through ion 1. Indeed, even at low-energy resolution, differences in metastable ion intensities were observed.

In conclusion, it has been demonstrated that ion 2 is one of the intermediate ions in the fragmentation of I and that the thermal rearrangement of I can also occur in an analogous manner.

EXPERIMENTAL

The mass spectra were obtained on an AEI MS-902 equipped with an analog tape and a manually operated metastable ion defocusing unit. High-resolution data were processed using Squibb programs, on an IBM 1800 or PDP-11. The chemical ionization spectra were obtained on AEI MS-902 equipped with an SRI source using methane at 1 torr or isobutane at 1 torr.

ACKNOWLEDGMENT

We wish to thank Drs. R. C. Dougherty and H. M. Fales who kindly ran the chemical ionization spectra. We would also like to thank Dr. H. Höhn of Squibb Regensburg, Germany, for these compounds.

REFERENCES

1a. K. R. Jennings, J. Chem. Phys. 43,4176 (1965).

b. M. Barber and R. M. Elliott, ASTM E-14 Conference on Mass Spectrometry, Montreal, Canada, May 1964.

2. C.C. Fenselau and C.H. Robinson, ASMS Conference on Mass Spectrometry Atlanta, Georgia, May, 1971.

3. M. S. Puar, B. T. Keeler and A. I. Cohen, J. Org. Chem., 36,219 (1971).

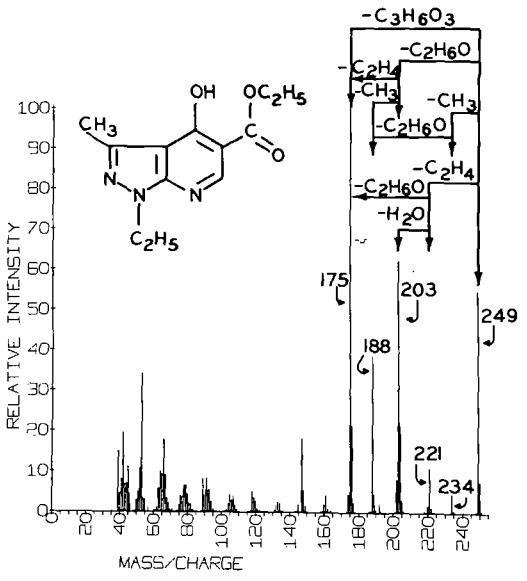

Figure 2. Electron Impact Mass Spectrum of II; Fragmentation Pathways Determined by Metastable Ion Defocusing

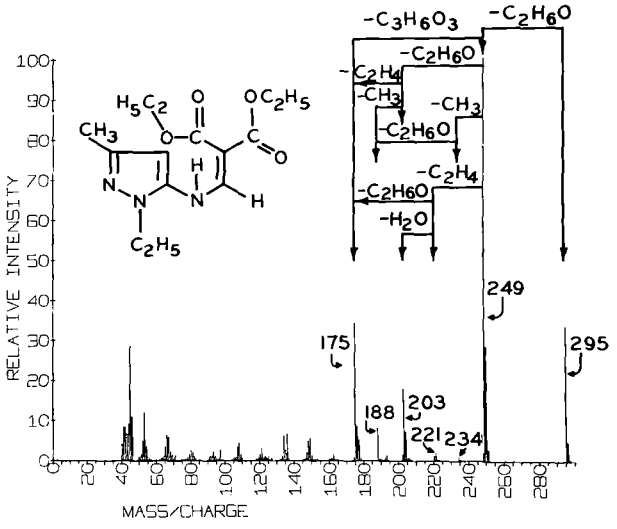

Figure 1. Electron Impact Mass Spectrum of I; Fragmentation Pathways Determined by Metastable Ion Defocusing

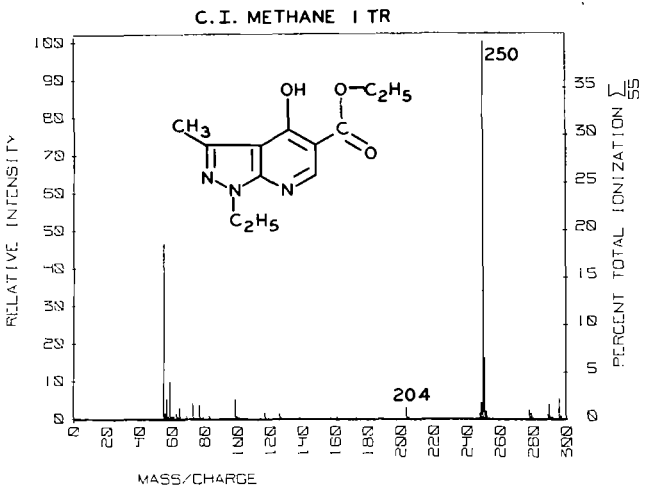

Figure 4. Chemical Ionization Mass Spectrum of II

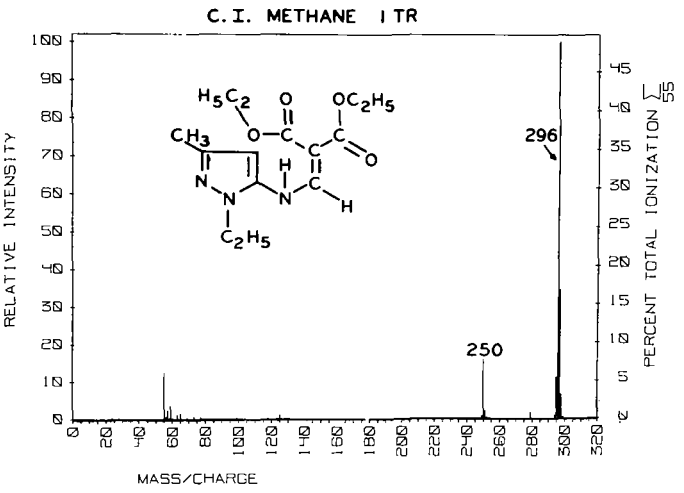

Figure 3. Chemical Ionization Mass Spectrum of I

Mass Spectroscopy of the Dicyanomethylene Derivatives of Long Chain Molecules*

J. Throck Watson & B. J. Sweetman, Department of Pharmacology, Vanderbilt University, Nashville, Tenn. and R. E. Wolff, Institut de Chimie, University of Strasbourg, Strasbourg, France.

The methyl ether of the dicyanomethylene (DCM) derivative of carboxylic acids (1) produce mass spectra which are characterized by an abundant series of fragment ions extending uniformly to the molecular ion as shown in Figure 1. An important feature of this spectrum is the high abundance (nearly 2% total ionization) of the homologous series of ions generated by loss of alkyl fragments from the main carbon chain. The M-15 ion does not belong to this series in that it derives mainly from elimination of the methyl of the methoxyl group. The other ions, especially the series starting at m/e 135 and increasing in m/e by 14 a.m.u., 149, 163, etc. seem to be formed by a different and poorly-understood mechanism. The mass shifts resulting from deuterium labelling at specific positions on the carbon chain of the octadecanoic acid derivatives are tabulated below. Substitution in the α position would be expected to shift m/e 135 to

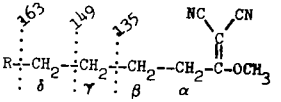

d_2-α position	d_2-β position	d_2-γ position	d_2-δ position
expected	expected	expected	expected
135→137	135→137	135→135	149→149
149→151	149→151	149→151	163→165
found	found	found	found
135→136	135→137	135→135	149→149
149→150	149→149 !	149→151	163→164 !

to 137 and 149 to 151; however, both ions shift by only 1 a.m.u. suggesting that one of the α hydrogen atoms is abstracted prior to production of the ions of m/e 135 and 149. This phenomenon is similar to that observed in the fragmentation of the esters of carboxylic acids (2,3). When the β carbon is substituted by two deuterium atoms, the ion having m/e 149 does not shift at all suggesting that the entire methylene unit at position 3 may be expelled in the formation of this ion. Labelling of C-4 gave the expected results, however, labelling at C-5 produced only a partial mass shift suggesting another mechanism of hydrogen transfer prior to fragmentation.

The DCM derivative of a carboxylic acid is prepared from the acid chloride ($SOCl_2$), which is then reacted with a mixture of 1.5 moles with $CH_2(CN)_2$ and 1.1 moles of pyridine at room temperature for 3-4 hours. The crude condensation product, presumably in its enol form, is reacted with CH_2N_2 to give the methyl ether of the DCM derivative of

* To be submitted to J. Org. Mass Spectrometry.

the starting acid (see structural formula in Fig. 1).

The unique mass spectra of these derivatives may have practical utility in several areas. Use of the C-30 DCM or higher analogs as calibration compounds may be limited by volatility. This compound is readily volatilized at 80° from a direct insertion probe, but only analogs below C_{26} have been successfully analyzed by GLC. The utility of the DCM derivatives in the recognition of branch points in long chain acids has been reported (1). Additional analytical uses of the DCM derivative are under investigation.

References

1. R. E. Wolff, J. T. Watson, and B. J. Sweetman: Tetrahedron Letters, 31, 2719, 1970.
2. N. Dinh-Nguyen, R. Ryhage, S. Stallberg-Stenhagen and E. Stenhagen: Arkiv. for Kemi, 18, 393, 1960.
3. G. Spiteller, M. Spiteller-Friedman and R. Houriet: Monatshefte, 97, 121, 1966.

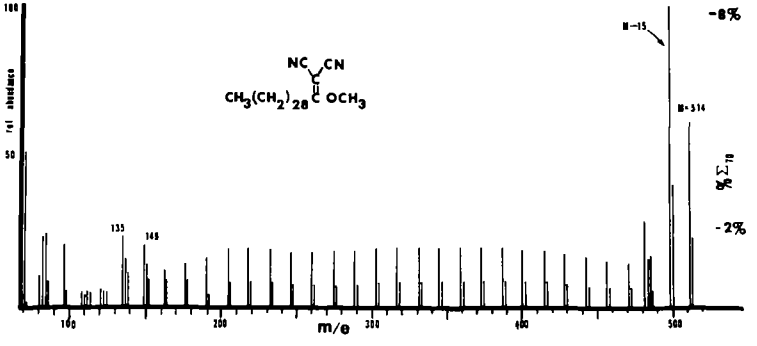

THE MASS SPECTRA OF p-METHYLPHENYLTHIAALKANES

NORMAN G. FOSTER and ROBERT W. HIGGINS*
Department of Chemistry, Texas Woman's University
Denton, Texas 76204

ABSTRACT

The mass spectra of p-methylphenylthiaalkanes present the opportunity to study charge competition in two important fragmentation processes in electron impact of molecules. The molecular ion may fragment by a path to produce ejection of a neutral olefin and the formation of the p-methylphenylthiol rearrangement ion. In competition with this process is the possible formation of a tropylium ion by alpha cleavage at the ring between the C-S bond. This is normally not favored. Simple cleavage or hydrogen abstraction can also occur. With a p-methyl group substituted on the phenyl ring "ortho" effects should not appear, or interfere with fragmentation studies. Mass spectral data at 70 ev and selected low ionization voltage data are presented for seven members, some highly branched, of this series. Metastable ion data are presented supporting the fragmentation routes observed. Energetics of the major decomposition reactions are discussed with emphasis upon the probable charge location and its contribution to the net spectra observed.

Mass spectral data will be submitted to API-44 Data Center.

*Deceased.

B11

Photoionization and Electron Impact Studies on Linear Olefins and Their Stereochemical Derivatives*

B. M. Johnson and J. W. Taylor**
Department of Chemistry
University of Wisconsin
Madison, Wisconsin 53706

A comparison between photon and electron impact fragmentation of the linear ocetenes and decenes has been made using the continuous radiation from the synchrotron as the photon source. There are subtle but real differences in the spectra for the individual positional isomers and some regularity in the spectra of the geometrical isomers. Using a photon source, it was possible to study the fragmentations without the influence of thermal rearrangements caused by the heated filament. The photon data do not show any strong retention of position or geometry but do suggest that the energy transfer process for photon and electron impact are different.

In order to provide structural identity of a particular olefin, stereo-specific derivatives have been prepared using hexafluoroacetone. The alteration of the fragmentation patterns of these derivatives do permit characterization of the position and possibly the stereochemistry of the olefinic bond.

(A full manuscript will be submitted to Analytical Chemistry.)

* This research supported by AFOSR Grant No. 69-1725. The synchrotron-storage ring is operated under funding from the Air Force Office of Scientific Research.

** Address correspondence to this author.

ENERGY PARTITION IN ORGANIC IONS*

R. G. Cooks
Department of Chemistry, Kansas State University, Manhattan, Kansas 66502

K. R. Jennings and S. Jones
Department of Chemistry, The University, Sheffield, England

Partition of the available energy of the activated complex to internal and translational energy (ϵ_k) of the products of a gaseous ionic reaction has been studied for a series of reactions with large activation energies for the reverse reactions (ϵ_o^r). The question of energy partition in organic ions is one on which little experimental evidence is available, nevertheless extreme views have been held regarding the fate of the energy, ϵ_o^r. It has sometimes been assumed to be statistically partitioned between internal and kinetic energy and sometimes assumed to be channeled entirely into kinetic energy of the products. Correlations[1,2] between product ion stability and ϵ_k for a given reaction in a series of aromatic compounds speak for a simple relationship between ϵ_k and ϵ_o^r but the present more complete study does not bear this out.

The reaction chosen for study was the simple four-centered elimination of HCN from the O-methyl ethers of a series of substituted benzaldoximes. The product ion shows the same behavior as does the corresponding anisole molecular ion and is assumed to have the same structure[3]. Moderately large kinetic energy release occurred throughout the series.

In order to determine energy partition the quantity $\epsilon_{excess} = \Delta H_f$ (oxime ether) + $AP(M^+ - HCN) - \Delta H_f$(anisole) - IP(anisole) - ΔH_f(HCN), was determined. In cases where ϵ_o^r is appreciable, $\epsilon_{excess} \gtrsim \epsilon_o^r$ at threshold. The kinetic energy imparted to the ionic fragment was measured from the metastable peak width using the defocusing technique and a narrow monitor (β) slit. The results are summarized in Table 1, which also includes values for the forward activation energy (ϵ_o^f).

Table 1.

Substituent:	pNO$_2$	pCN	H	pMe	pCl	pMeO
ϵ_k(ion)	0·20	0·21	0·37	0·30	0·42	0·54
ϵ_o^f	1·41	2·04	1·66	1·82	1·88	0·54
ϵ_{excess}	1·58	2·11	1·80	1·97	2·02	0·91
% kinetic	14·9	12·0	25·7	18·6	24·8	71·0
$M^+ - HCN/M^+$: (x 10^2)	0·5	12	22	18	14	1·5

In spite of the assumptions involved in this treatment (not detailed here), it is evident that non-statistical energy partition does occur. Furthermore, given that there are no gross mechanistic differences across the series, the relationship between ϵ_k and ϵ_o^r is not simple. Certainly neither the whole of ϵ_o^r, nor a constant fraction, appears as ϵ_k. Nevertheless, there is a trend towards increasing ϵ_k with increasing product ion stability, and the position of the activated complex on the reaction co-ordinate may determine the effectiveness with which energy is channeled away from the stretching bonds and into the rest of the molecule or ion.

---

*This work is to be submitted for publication in the Journal of the American Chemical Society.

REFERENCES

1. M. M. Bursey and F. W. McLafferty, J. Am. Chem. Soc. 88, 5023 (1966).

2. B. Davis and D. H. Williams, Chem. Commun. 412 (1970).

3. R. G. Cooks and A. G. Varvoglis, Org. Mass Spectrom., in press.

FIELD-IONIZATION MASS SPECTROMETRY OF ORGANOSILICON COMPOUNDS

C3

J. E. Coutant and R. J. Robinson

Dow Corning Corporation
Midland, Michigan 48640

Early experiments with field ionization (FI) mass spectrometry showed great promise for this technique in many applications. However, instrumental problems connected with the high voltage necessary to produce the ionizing field gradient still remain, and as a result other techniques such as chemical ionization are becoming more popular for producing "simplified mass spectra" and "increased molecular ion strength." These other methods, though, do not offer what we feel is the main advantage of field ionization--the ability to study extremely fast unimolecular decomposition processes of organic and organosilicon ions in the gas phase.

Most organosilicon compounds exhibit high rate constants for a number of unimolecular decompositions, including both direct bond rupture and rearrangement processes. On the time scale of electron impact spectra, most decompositions occur in the ion source, resulting in the detection of only the product daughter ions to the exclusion of the precursor parent ions and metastable ions. Field ionization allows us to decrease the time scale into the range of 10^{-13} seconds and obtain important structural information.

The instrument used in this work was an AEI MS-12 single-focusing mass spectrometer. The combined FI/EI ion source uses commercially-available razor blades, Schick's Krona-Chrome®, as the field emitter. These blades proved to be both durable and sensitive enough that good FI spectra, using the glc/mass spectrometer, could be obtained even at scan speeds of 3 sec/decade.

Early in our work we were puzzled by the appearance of discontinuities in some of the fast metastable peaks as shown in Figure 1. These skew metastable peaks appear to be similar to the displaced skew fragment ion peaks recently reported by Tou[1] and to the metastable plateau peaks reported by Beckey[2]. In both reported cases these peaks are attributed to a constant field region in the Atlas CH_4 ion source. Figure 2 shows the voltage profile for our FI source, and as illustrated, our source geometry does not allow for such a constant field region. The common factor in all these examples, however, is the high acceleration experienced by the ion going from the emitter anode to the cathode slit, followed by deceleration in traveling from the cathode slit to a focusing plate (labeled the ion exit slit on Figure 2). This slit is usually at a potential value slightly less than that of the emitter anode. These drastic changes in acceleration appear to affect the ion residence time in such a way that a larger relative number of decompositions can take place in this region and give rise to these peaks. When the apparent mass of such a peak is related to the voltage of the ion exit slit, we obtain a good agreement between the calculated voltage and the measured voltage on the ion exit slit. This is an instrumental artifact that one should be aware of when interpreting FI spectra from instruments with similar voltage profiles in the source.

In a survey of some silicon and organosilicon compounds, some interesting trends were observed. The results obtained from a series of linear methylsiloxanes were as follows. In all cases, the molecular ion was not observed in the EI spectra. The FI spectra always showed a molecular ion, although its relative strength decreases with chain length. The peak due to the loss of methyl from the molecular ion is always largest. The molecular ion peak and the M-CH_3 peak are the only significant peaks observed in the FI spectra. Similar results were obtained for a series of cyclic methylsiloxanes. For the 1,3,5,7-tetrasilaadamantanes, we have reported[3] the skeletal rearrangement giving the loss of a methyl involving one of the bridgehead carbons in the EI spectra. The FI spectra of these compounds show only the molecular ion and the metastable corresponding to the loss of the substituent X on silicon in the cases where X = H, Cl, and CH_3.

Figure 1

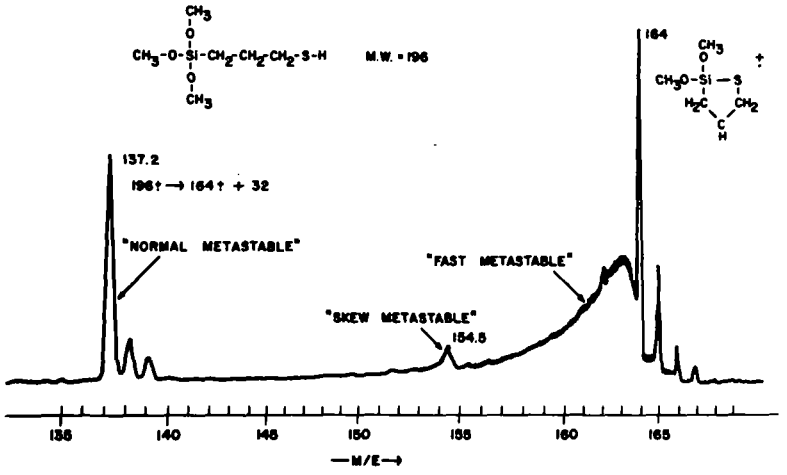

Figure 2

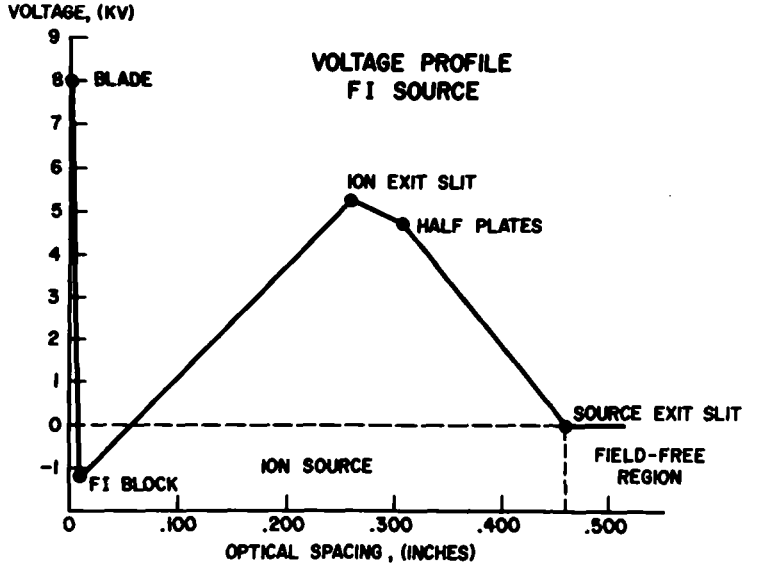

Our biggest application of FI is for structure determination[4] and the identification of ion decomposition pathways. A good example of this has been our work with γ-functional silanes. The EI spectra of 3-chloropropyltrimethoxysilane exhibits no molecular ion and has chlorine-containing peaks at masses 155 and 157. This would correspond to the loss of 43 and 41 mass units from the molecular ion. Figure 3 shows a proposed mechanism. We felt that the chlorine was transferring back to the silicon atom while the alkyl portion lost or gained a hydrogen atom to give a loss of C_3H_5 or C_3H_7. However, there were no metastable ions to support such one-step, concerted mechanisms. When we ran the FI spectra of this compound, we did obtain metastables to support both processes. In addition, the FI spectra showed a small molecular ion but no 155 or 157 rearrangement peaks, as would be expected. The effect of the methoxy group on these rearrangements was studied by a series of 3-chloropropylmethyl-methoxysilanes. The decrease in the intensities of both the EI 155 and 157 peaks, and of the FI metastables, paralleled the decrease in the number of methoxy groups.

Figure 3

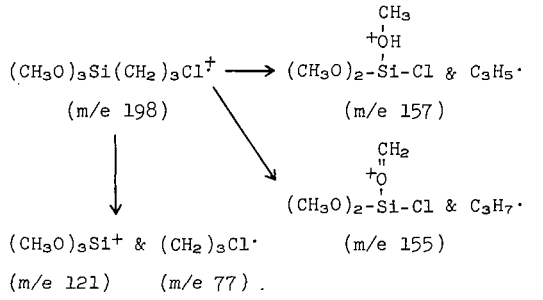

The EI spectra of 3-mercaptopropyltrimethoxysilane also does not exhibit a molecular ion. It has its base peak at mass 164 with several other unexplained lower mass peaks. The peak at 164 is the loss of 32 mass units from the molecular ion, and we believed it to be the result of a rearrangement with the loss of methanol as shown in Figure 4. This cyclic ion would then lose CH_3O and C_3H_5 to give rise to other peaks. Again there was no metastable ion to confirm this rearrangement in the EI spectrum. Figure 1 shows a portion of the FI spectrum of this compound. As can be seen, both the fast and normal metastable for this process are present as well as the rearrangement peak at mass 164. In addition, this compound showed a strong molecular ion and a peak at mass 121 corresponding to the cleavage of the mercaptopropyl group.

Figure 4

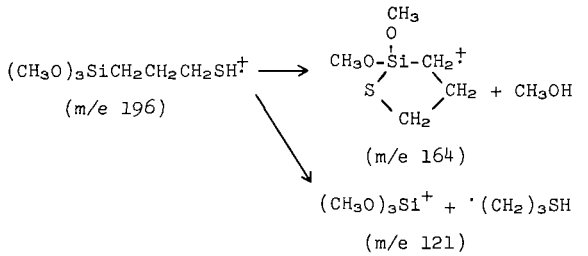

The appearance of the peak at 164 and the shape of the fast metastable was hard to explain initially. The 164 peak really should not be present, especially at its large relative abundance. The shape of the fast metastable tail does agree though with what has been suggested[5] for a slower decomposition process such as a rearrangement. The only explanation consistent with our observations was that two distinct processes were taking

place--one on the surface of the blade and the other in the gas phase near the blade surface. In a time study over the period of a half an hour or so, the relative intensity of both the 164, the rearrangement peak, and the 121 peak increased while the molecular ion and metastable intensity remained constant. This supports the proposal that two decomposition processes are occurring and also points out the care that must be exercised when using relative FI intensities.

These examples are some of many that underline our particular reason for the use of FI mass spectrometry and point out again the great wealth of structural information uniquely obtainable from this method.

References

1. J. C. Tou, J. Phys. Chem., 74 (26), 4596 (1971).

2. H. D. Beckey, H. Hey, K. Levsen, and G. Tenschert, Int. J. Mass Spectry. Ion Phys., 2, 101 (1969).

3. R. S. Gohlke and R. J. Robinson, Org. Mass Spectrom., 3, 967 (1970).

4. E. M. Chait and F. G. Kitson, Org. Mass Spectrom., 3, 533 (1970).

5. A. L. Burlingame, A. M. Falick, G. W. Wood, Peter Schultze, and W. J. Richter, ASMS 18th Annual Conf. on Mass Spectrometry & Allied Topics, San Francisco, June, 1970.

COMPUTER MODEL OF A FIELD ION SOURCE

J.P. Pfeifer, A.M. Falick and A.L. Burlingame

Space Sciences Laboratory
University of California
Berkeley, California 94720

Field ionization (FI) sources in mass spectrometers are generally regarded as having low sensitivities compared to conventional electron impact sources. A comparison of the total ion current emission with the ion current actually entering the mass analyzer suggests that this low efficiency is due primarily to ion optical problems within the source. In fact, it has been shown that the fraction of the ions produced which leave the source is perhaps two orders of magnitude smaller in an FI source than in a typical EB source (1). Thus an improved knowledge of the potential distribution and ion trajectories within the source should afford an excellent opportunity to improve the design of FI sources as well as providing additional insight into the physical processes which occur within the source. The work described below represents an initial attempt at understanding some of the characteristics of a specific FI source.

Various mathematical and analog procedures have been developed over a period of many years for the mapping of electrostatic fields (2), but each has certain limitations and disadvantages. Methods involving an exact solution to the Laplace equation are generally restricted to rather simple geometrical configurations; approximate methods, such as the electrolytic tank or the more accurate resistor network (4) involve specialized apparatus.

The relaxation method (2) which was used in the present work is a numerical solution of Laplace's equation. The problem of laborious calculation was largely alleviated through the use of a computer. The calculations may be performed in either two or three dimensions and, given sufficient computer time, can be carried to any desired degree of accuracy.

The Laplace equation (Eq. 1) describes the electrostatic potential U at any point in a charge-free space when the boundary conditions are properly specified.

$$\nabla^2 U = \frac{\partial^2 U}{\partial x^2} + \frac{\partial^2 U}{\partial y^2} + \frac{\partial^2 U}{\partial z^2} = 0 \qquad (1)$$

The approximate form of this equation (in two dimensions) which was used in the computations was:

$$U(x,y) = A \cdot U'(x,y) + \frac{1}{4}\{U(x+\Delta x,y) + U(x-\Delta x,y) + U(x,y+\Delta y) + U(x,y-\Delta y)\} \qquad (2)$$

where U'(x,y) is the value of U(x,y) from the previous iteration and A is a constant chosen to give the most rapid convergence.

In order to use the Laplace equation it is necessary to have a charge-free space surrounded by well-defined boundaries. In order to check whether the former condition was valid, the average number of ions present in the source under normal conditions was determined. This number was only of the order of 100, indicating that space charge should not be a significant problem.

Most of the results to be described were obtained by using a matrix of dimensions 71 x 111, which provides an effective matrix size of 142 x 111 for geometries having bi-lateral symmetry. The matrix size was chosen both to fit the available computer memory and to give a sufficiently precise result without requiring excessive amounts of computer time. The computations were performed on an XDS Sigma 7 computer with 16K core. Each matrix calculation required about ten minutes.

Even with a matrix containing some 15,000 points, the spatial resolution was far too small to distinguish any features of the blade shape. In fact, to provide sufficient resolution to accurately characterize the emitter edge would require about 10^{12} elements and of course an impossibly large amount of computer time. This problem was overcome by successively enlarging a small section of the potential map until sufficient resolution was achieved. In the work described here the maximum resolution obtained was from 10 to 100 Å.

The enlargement procedure introduces errors in at least two ways: first, boundary conditions for each successive enlargement must be interpolated from values in the previous map. In addition, an appropriate approximation to the blade shape must be made

in the early enlargements in which the blade dimensions are very much smaller than the resolution. A successive approximation procedure was used to determine the best boundary values to be used for the blade in these cases. Fig. 1 shows a typical series of successive enlargements. The area surrounded by the dashed line in (a) was enlarged to give map (b), and so on. Map (e) is linearly enlarged over map (a) by a factor of 10^4.

The magnitude of the errors introduced in these and other possible ways was determined by calculating potential maps for two test cases for which analytic solutions were available. The first test configuration consisted of two coaxial cylinders of radii 0.4 mm and 700 Å. An initial map and four enlargements were made, giving a resolution of about 15 Å in the final enlargement. In all maps the errors were less than 2%.

The second test configuration consisted of a hyperbolic blade of radius 4000 Å suspended 0.25 mm above a flat plane. The results were compared with the exact conformal transformation calculation carried out by Brailsford and Robertson (5). In the initial map and each of the four enlargements the errors were less than 1%.

Results

All of the results below are based on the geometry of a specific source, the DuPont (CEC) 21-110 FI source. Some of the important dimensions of this source are shown in Fig. 2. The normal source voltages are: blade, 8 kV; first slit, -1 kV; and second slit, 4 kV. The third slit was held at ground potential. The blade edge shape was assumed to be a 10° wedge terminating in a cylindrical edge of radius 1000 Å, which was derived from electron microscope measurements of Brailsford and Robertson (5) on an actual razor blade. In addition, some calculations were performed using a hyperbolic edge shape of the same radius. The results for these two shapes were not greatly different.

A rough ion path calculation showed that ions coming off the blade at more than about a 10° angle failed to pass through the first two slits. This means that the effective emitting area of the blade is not more than about 10^{-6} cm^2 if surface irregularities are ignored.

Fig. 3 is a plot of equipotential lines in a portion of the source. Equipotentials are drawn at voltage increments equal to 10% of the blade voltage. An enlargement by a factor of 10 of the area around the blade edge and first slit is shown in Fig. 4. This region is where so-called fast metastable ions are formed. The dashed lines show schematically the paths of ions formed at the blade edge. The time of flight for an ion of mass 100 from the blade edge to the upper plane of the first slit is 2×10^{-9} sec. During this time the ions pass through a potential drop of about 9000 volts so that ions formed by unimolecular decomposition during this part of the flight will have a significantly lower energy than normal ions of the same mass.

The sharply curved equipotential lines around the blade have a strong focusing effect. This was noted by Brailsford (3), who calculated ion paths for the case of a perpendicular edge suspended above a flat plate. The focusing effect can be rationalized in the following way. The ions leave the blade edge with an initial velocity which is perpendicular to the surface. The equipotential lines which it must cross have decreasing curvature. Therefore the force on the ions, which is always perpendicular to the equipotential lines, will be less divergent than the ion velocity vectors. Since the ions are being strongly accelerated in this region, their trajectories will tend to line up with the accelerating force, thereby producing a less divergent beam.

The effect of the presence of the first slit (which is held at about -1000 volts) on the pattern of equipotential lines can be readily seen in Fig. 3. As the first slit is approached the curvature of the center portion of these lines begins to increase again because the blade field penetrates the slit. The ions are still being accelerated in this region, but they now experience a divergent force because of the increasing curvature.

As the ions pass through the slit, they cross a saddle point. The second slit is kept at a high positive potential, about half of the blade voltage, so that once the minimum inside the first slit has been crossed, the ions are retarded again until they pass through the second slit. The reverse curvature of the field lines at the bottom of the first slit will thus also have a defocusing effect.

Several different cathode (first slit) shapes were tried and it was found that in general a thicker slit had better focusing properties than a thinner one. This effect has in fact been noted experimentally by Derrick (6). The effect is readily understood in terms of the foregoing analysis. The penetration of the blade field into a thick first slit is less than with a thinner slit. The resulting flatter equipotential lines in the first slit entrance reduce the defocusing in this region. However, the concomitant increase in the equipotential curvature in the lower part of the slit will have the opposite effect, but because the field gradient is so much larger in the former case than in the latter, the overall effect is beneficial.

The equipotential lines in most of the region between the first and second slits are virtually flat. Since the ions are being decelerated, the y-component of their velocities is being considerably reduced while the lateral component is essentially unchanged, causing the ion trajectories to diverge in this region. The second slit is positive with respect to both the first and third slits (the third slit is at ground potential) so that it has a focusing effect on the ion beam in the same way as a normal electrostatic single slit lens.

Typically, ion flight times to the second slit are about 3.6×10^{-8} sec. for an ion of mass 100.

So far the surface structure of the blade has not been mentioned. It is well known that during the conditioning process a forest of whiskers is grown on the blade edge. Derrick and Robertson and others have published some excellent electron micrographs of these growth (6,7), and Beckey (8,9) has pointed out that fragmentation patterns observed for n-hexane require a field of about 6×10^7 V/cm, so that the assumption of a smooth blade edge is clearly incorrect. In order to examine this question more closely, a model was constructed with an irregularly shaped tip whose dimensions were based on the microphotographs of actual blade edges (Fig. 5). In examining the equipotentials surrounding this blade edge it is clear that the effect of the irregularities is negligible beyond a few thousand angstroms. The effect on the ion paths is not as clear-cut, but generally their average distribution does not appear to be greatly different from the smooth blade case.

In summary, it seems clear that further work on the analysis of FI source characteristics will be useful in increasing sensitivity, as well as providing the necessary measurements for the study of the kinetics of unimolecular decompositions by means of fast metastables.

The authors wish to thank R.W. Olsen and P.J. Derrick for some helpful suggestions and to acknowledge financial support from the National Aeronautics and Space Administration.

References

1. P.A. Blenkinsop, B.E. Job, D.F. Brailsford, C.M. Cross and A.J.B. Robertson, Int. J. Mass Spect. Ion Phys. 1, 421 (1968).
2. E. Weber, Electromagnetic Fields: Theory and Applications, Vol. I, J. Wiley & Sons, New York, 1950.
3. D.F. Brailsford, J. Phys. D: Appl. Phys. 3, 196 (1970).
4. G. Liebman, Nature 146, 149 (1949).
5. D.F. Brailsford and A.J.B. Robertson, Int. J. Mass Spect. Ion Phys. 1, 75 (1968).
6. P.J. Derrick, Ph.D. thesis, University of London, 1969.
7. P. Derrick and A.J.B. Robertson, Int. J. Mass Spect. Ion Phys. 3, 409 (1969).
8. H.G. Metzingen and H.D. Beckey, Z. Phys. Chem. N.F. 52, 1 (1967).
9. H.D. Beckey and J. Dahmen, Z. Naturf. 20a, 141 (1966).

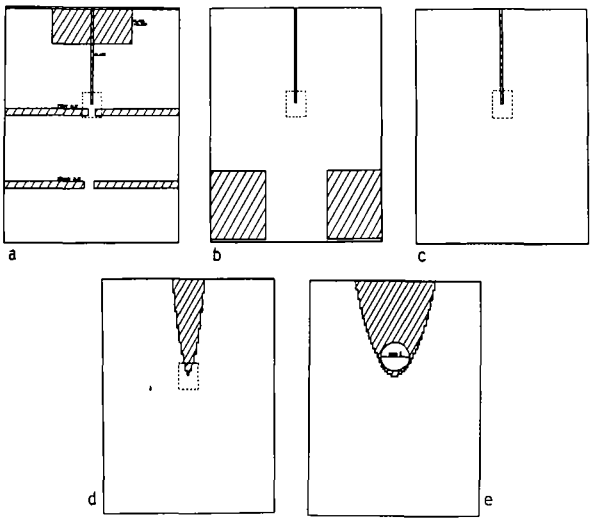

Fig. 1. A series of successive enlargements.

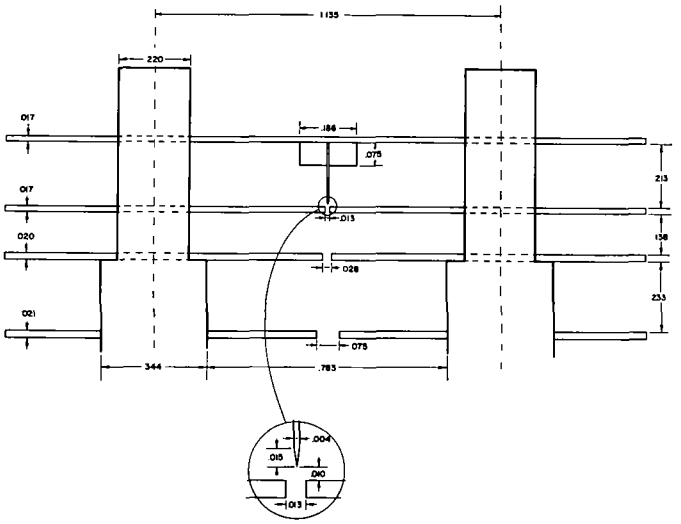

Fig. 2. Dimensions of the FI source used as a basis for the calculations.

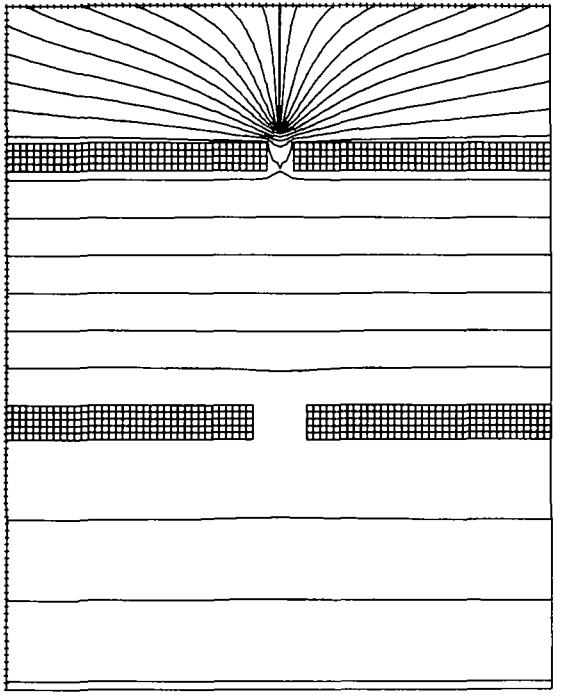

Fig. 3. Equipotential lines calculated for a portion of the source.

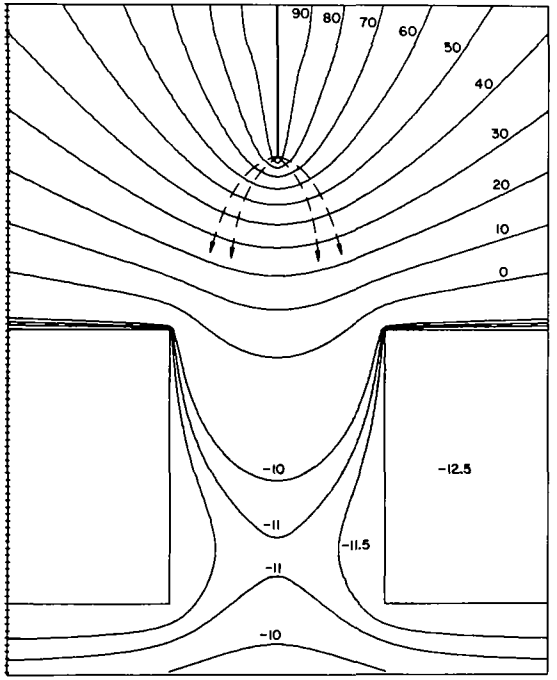

Fig. 4. Enlargement of blade/first slit region of source. Equipotential values are given as percent of blade voltage.

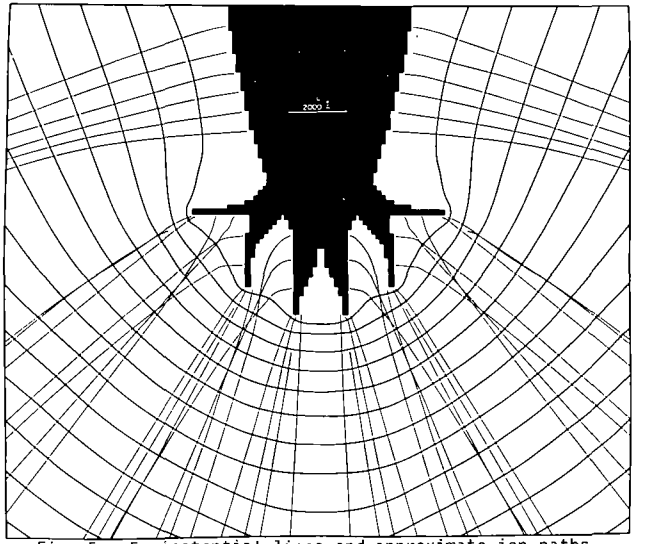

Fig. 5. Equipotential lines and approximate ion paths calculated for an irregularly shaped blade edge.

Mass spectral evidence for the conversion of benzenephosphonic acid to its cyclic, trimeric, anhydride and of benzenephosphonous acid to phenylphosphine. RICHARD H. WILEY, Hunter College of the City University of New York, 695 Park Avenue, New York, New York 10021

Mass spectral evidence for the conversion of benzenephosphonic acid to its cyclic, trimeric anhydride and of benzenephosphonous acid to phenylphosphine has been obtained. At low sample temperatures (85°) the phosphonic acid shows peaks for the molecular ion at 158 amu and for characteristic degradation fragments at 141($C_6H_5PO_2H$), 94(C_6H_6O), 78-7(C_6H_6,C_6H_5), 65(H_3PO_2,C_5H_5), 51(C_4H_3), 47(PO) and 39(C_3H_3) amu. Above 120° and after a pressure surge indicative of dehydration, a peak at 420 for the cyclic, trimeric anhydride $(C_6H_5PO_2)_3$ is observed along with fragment peaks at 373, 357, 343, 327, 280, 262, 233, 216, and 199 amu for which structural assignments are made. The phosphonous acid, at 75°, shows peaks for the molecular ion at 142 amu and for fragments at 124 (C_6H_5PO), 111-107($C_6H_5PH_{\pm 2}H$), 94(C_6H_6O), 78-7(C_6H_6,C_6H_5), 65(H_3PO_2,C_5H_5), 51(C_4H_3), 47(PO), and 39(C_3H_3) amu. The phenylphosphine is apparently formed by intramolecular rearrangement rather than by disproportionation as the latter requires the formation of relatively more of the phosphonic acid than is observed amongst the peaks of mass over 142 amu. Accurate mass measurements and metastable broad peaks confirm the postulated fragmentation processes.

The full report will appear in Organic Mass Spectrometry.

MASS SPECTRAL INFORMATION
A REPORT FROM THE MASS SPECTROMETRY DATA CENTRE

R G Ridley and W M Scott
A.W.R.E., Aldermaston, Berkshire, England

Introduction

Early in 1965 the need for a data and information centre on mass spectrometry was realised by a number of individual mass spectroscopists. As a result of their approaches to the UK government, a study of the requirements for such a centre was initiated by the UK Office for Scientific and Technical Information (OSTI) with an Advisory Committee of representatives from industry, government and universities under the chairmanship of Mr A Quayle, Shell Research Ltd. Following this initial study, the Mass Spectrometry Data Centre (MSDC) was established at A.W.R.E. in 1966 with financial support from OSTI. More recently, the Centre has been jointly supported by OSTI and the Department of Trade and Industry.

Since its inception, the aim of the Centre has been to serve all mass spectrometry users on a world-wide basis. Every effort has been made to coordinate activities and cooperate with other mass spectrometry groups in the USA, France, Germany, Japan etc., and thus avoid duplication of effort. As a result of informal discussions between the representatives of these various national mass spectrometry groups, an International Advisory Committee was established in Berlin in 1967. This committee provides continuing guidance to the Data Centre, discussions having been held at previous ASTM meetings in Pittsburg, Dallas and San Francisco, at the international meetings in Kyoto and Brussels, and another is planned for this meeting. Subjects discussed have included field ionization spectra, "quality" mass spectra, mass spectral data sheets, abbreviated spectral indexes and computer problems.

MSDC has been engaged in three major fields of endeavour, viz:

1. The provision of a current awareness literature service, i.e. a monthly guide to the literature on mass spectrometry and allied topics.

2. The collection and dissemination of mass spectral data, and

3. Compound identification by matching of low resolution mass spectra.

This paper summarises the Data Centre's progress to date in these fields. Criticism of existing services, or suggestions for any additional services that the Centre might provide, will be welcomed.

Current Awareness Service - the Mass Spectrometry Bulletin

Since applications of mass spectrometry are found in a wide variety of disciplines, e.g. chemistry, physics, geology, biology, metallurgy etc., the mass spectroscopist has a particularly difficult task in covering the literature adequately. Prior to 1963, the bibliographies of mass spectrometry information provided annually by ASTM-E14 and by AEI were useful guides to the literature. In 1963-65 Dr Cuthbert, Secretary of the UK Mass Spectrometry Discussion Group, organised a task force to improve literature coverage, by providing a 3 - 6 monthly titles list. Full use of individual lists of ~ 500 titles was limited, however, because of the absence of subject organisation and detailed indexing.

MSDC set out to provide a more complete current awareness service and a provisional layout of the Mass Spectrometry Bulletin was prepared in May 1966. Production began in November, 1966 and has continued monthly since then.

The Bulletin contains references selected from over 250 current journals, reports, abstract journals, patents lists and 5 computer-based retrieval systems. The main entries are divided into eight subject sections: Instrumentation, Isotope Analysis, Chemical Analysis, Organic Chemistry, Atomic and Molecular Processes, Surface Phenomena, Thermodynamics, and Other Applications.

Each reference includes the full title (translated into English where appropriate), authors' names, complete journal reference and selected descriptors which supplement information in the title of the article. As an additional aid, where more than six peaks of mass spectral data have been reported, the reference is preceded by an asterisk. Articles are indexed in at least two out of six indexes, viz. subject,

compound, compounds and ions, materials, elements and authors, which are designed to facilitate both computer and manual retrieval.

The current average retrieval rate is ~ 500 articles/month, or more than 6000/year, and more than 3000 compounds are indexed annually, by name, molecular weight, molecular formula, classification and reference number. From November 1966 - March 1971, over 23,000 articles have been included in the Bulletin and ~ 12,000 compounds indexed.

Distribution of the Mass Spectrometry Bulletin is effected through Her Majesty's Stationery Office. A truly world-wide distribution has been achieved, as indicated in Table 1.

The Mass Spectrometry Bulletin on Magnetic Tape

Since November 1966, computer methods have been used to provide monthly printouts for reproduction, and the annual cumulative indexes have been similarly produced. As subject and compound classifications are coded numerically, simple methods of retrieval are possible here, while the main entry, i.e. title, source, author etc. should be readily adaptable to suit existing natural language retrieval programs. The Bulletin is available on IBM-compatible magnetic tape and can be used for computer retrieval.

Retrospective retrieval from the Mass Spectrometry Bulletin tapes has been successfully demonstrated recently by Professor Biemann's group at MIT[1] using an IBM 1800 computer. This promises to be an extremely useful technique for laboratories with small dedicated computers. The Centre will be pleased to supply information about the availability of the Mass Spectrometry Bulletin on magnetic tape and to provide a tape for experimental trials.

New-Look Bulletin

From January 1971, the Bulletin has been produced by a computer-controlled photo-typesetting technique, and appears in a new and more compact format for easier reading.

Mass Spectral Data

1. Data Sheets

The total number of mass spectra generally available is relatively small. The total in the API[2] and TPC[3] collections is ~ 2400, each spectrum being recorded under strict operating conditions. The ASTM-E14 Committee[4] devised an extremely valuable system for the contribution and circulation of 'Uncertified' spectral data, where this strict control of operating conditions was not possible. The ASTM-E14 and the Dow Chemical Co.[5] 'Uncertified' collections together totalled ~ 3870 spectra.

At the International Advisory Committee in Berlin, 1967, MSDC was invited to continue the collection and distribution of 'Uncertified' spectra on behalf of the various national mass spectrometry groups. Requests for data are issued world-wide, and a truly encouraging response has been obtained from individuals and companies in the 31 countries marked by an asterisk in Table 1. Approximately 6000 spectra have been contributed as tabulated data, and most of these are recent spectral data which have not appeared in the earlier collections.

From the tabulated data processed within the Centre, computer print-out is obtained for reproduction as a data sheet. The structural formula is added to the compound name, molecular formula, instrument operating conditions etc. From MSDC spectrum number 3001 onwards, a computer drawn bar graph has been added to the tabulated m/e and relative intensity values, for rapid visual pattern recognition.

4,500 data sheets were produced by June 1971. Two spectra of the same compound have only been included where there have been differences in operating conditions or in the spectra. The data sheets have been distributed to 192 laboratories, in 15 different countries. Cumulated indexes, ordered on molecular weight, are available.

2. Data Tapes

Increasing use of computers in mass spectrometry has made it essential for spectral data to be produced in machine-readable form. The Centre now provides the MSDC collection of 4000 spectra on magnetic tape, produced on IBM 360 equipment, in a wide variety of specifications. The information is on the tape in a fixed format.

In addition, the Centre has also assembled, with considerable contributions from Dr Boettger, Jet Propulsion Laboratory, Pasadena; Prof. Biemann, MIT; ICI Ltd., (Dyestuffs Division) and Dr Zwolinsky, Thermodynamics Research Centre, a tape containing 6628 spectra from the ASTM-E14, API, TRC and DOW collections in the same format as the MSDC spectra, making a total of 10,628 complete mass spectra.

3. Abbreviated Spectra - 8 Peak Index

The value to the mass spectroscopist of an index based on the few most abundant ions in a spectrum has been demonstrated by the pioneering efforts of the ASTM-E14 Committee (STP 356 and AMD 11 publications)[6], and the Compilation of Mass Spectra produced by Drs Cornu and Massot[7]. ICI (Dyestuffs Division) have completed a similar index, including their own spectral data and data taken from the literature, mostly using the Mass Spectrometry Bulletin. Their generous offer to make this index available world-wide through MSDC led to the publication in January 1971 of the 8 Peak Index of Mass Spectral Data[8] which contains abbreviated data from 17,124 spectra, in three tables, indexed by molecular weight, molecular formula, and by ion m/e values. The index is a valuable entry to the data sheet collections and to the literature. A "how to use" guide to the index is shown in Fig. 2.

4. 8 Peak Index on Magnetic Tape

By further agreement with ICI, this collection of 17,124 abbreviated spectra has now been made available on magnetic tape. Details of the data format and tape options may be had from MSDC on request.

Computer Matching of Low Resolution Mass Spectra

The Centre has been engaged in the study of computer matching of low resolution mass spectral data for compound identification[9]. A variety of methods have been studied of comparing the recorded mass spectrum of an unknown compound against a library file of known spectra using MSDC tapes of more than 9000 spectra. The very successful results have been published recently[10].

These matching methods have recently been applied to a limited number of GC-MS analyses of natural product mixtures. Comparing the "n" largest peaks in ranges of "m" atomic mass units is a particularly convenient way to allow for differences in spectra obtained under widely different operating conditions.

Comparison of the "n" largest peaks in the complete spectrum has also been shown to be of value, and often identification can still be made when "n" is reduced to as low as 6. These results indicate the value of combining matching routines with the abbreviated (8 peak) data file of 17,124 spectra.

Matching programs for an IBM 360/50 computer are currently available from the Centre.

Summary

MSDC's endeavours over the period 1966 - June 1971 have resulted in the following list of items being made available to the mass spectroscopist (see Table 1).

The activities of the Centre have been possible only because of the considerable efforts of individual mass spectroscopists world-wide. We take this opportunity of thanking all those who have contributed new information and data. While the Centre continually strives to make these contributions available to all users, the completion of the cycle requires widespread use of this information and data back in the individual laboratory. It is hoped that this progress report will further this aim.

31 March 1971

TABLE 1

World-wide Distribution of the Mass Spectrometry Bulletin

(Contributions of mass spectral data have been received from the countries marked *)

Algeria	*Finland	New Zealand
*Argentina	*France	Norway
*Austria	*Germany	*Poland
*Australia	*Greece	Portugal
*Belgium	Hungary	Roumania
*Brazil	*India	*South Africa
*B.W.I.	Iraq	*Spain
*Canada	Israel	*Sweden
*China	*Italy	*Switzerland
*Czechoslovakia	*Jamaica	*U.K.
*Denmark	*Japan	*U.S.A.
*East Germany	*Mexico	*U.S.S.R.
*Eire	*Netherlands	*West Germany
		Yugoslavia

TABLE 2

Mass Spectrometry Bulletin	-	Nov. 1966 - to date
Mass Spectrometry Bulletin on Magnetic Tape	-	" " " "
MSDC Data Sheets	-	1-4500 spectra
MSDC Spectral Data on Magnetic Tape	-	1-4000 "
ASTM-E14, DOW, API and TRC spectra on magnetic tape	-	6628 spectra
8 Peak Index of Mass Spectra	-	17,124 abbreviated spectra.

REFERENCES

1. A User Oriented Computer Searchable Library of Mass Spectrometric Literature References, H S Hertz, D A Evans and K Biemann, Org. Mass Spec., 4, 453 (1970).

2. American Petroleum Institute, Research Project 44,
Catalog of "Selected Mass Spectral Data"
Chemical Thermodynamics Properties Centre, A and M College of Texas.

3. Manufacturing Chemists Association Research Project,
Chemical Thermodynamics Properties Centre, A and M College of Texas.

4. Uncertified Mass Spectra, Subcommittee IV,
ASTM Committee E14.

5. Dow Chemical Co., Uncertified Mass Spectral Data,
distributed through ASTM Committee E14.

6. Index of Mass Spectral Data STP 356,
ASTM Philadelphia, Pa., 1963.

   Index of Mass Spectral Data AMD 11,
ASTM Philadelphia, Pa., 1969.

7. Compilation of Mass Spectral Data, A Cornu and R Massot,
Heyden and Son Ltd., London, 1966.

   First Supplement to Compilation of Mass Spectral Data,
A Cornu and R Massot, Heyden and Son Ltd., London, 1967.

8. 8 Peak Index of Mass Spectra,
Mass Spectrometry Data Centre, A.W.R.E., Aldermaston, England, 1971.

9. Compound Identification by Computer Matching of Mass Spectra,
B Knock, D E Wright, W Kelly and R G Ridley,
ASTM E14 Meeting, Dallas, May 1969.

10. Compound Identification by Computer Matching of Low Resolution Mass Spectra,
B Knock, I C Smith, D E Wright, R G Ridley, W Kelly.
Anal. Chem., 42, 1516 (1970).

COMPUTER RECOGNITION OF METASTABLE IONS

A. M. Duffield, W. E. Reynolds, D. A. Anderson, R. A. Stillman, Jr.
and C. E. Carroll

Department of Genetics, Stanford University School of Medicine
Stanford, California 94305

Interpretation of mass spectra by suitably programmed computers has been the focus of an interdisciplinary research effort at Stanford University for several years.[1] As part of the continuing study of computer interpretation of mass spectra we wished to use metastable ion data in a routine manner to extend the scope of machine analysis of mass spectra. Thus the practical problem arose for the routine identification of metastable ions present in mass spectra. We have enlisted the aid of the computer to scan the record of a mass spectrum, help identify the metastable ions, and then list these values for later use. The computer provides as a final output the parent daughter-ion relationships of the fragments present in the mass spectrum.

The equipment, Figure 1, used in this study consisted of a CH-4 mass spectrometer attached to a logarithmic transfer recorder. The virtues of this system for the identification of metastable ions has been reported.[2] The logarithmic signal is then transferred via an interface consisting of a PDP-11 computer to a time-shared IBM 360-50 computer.

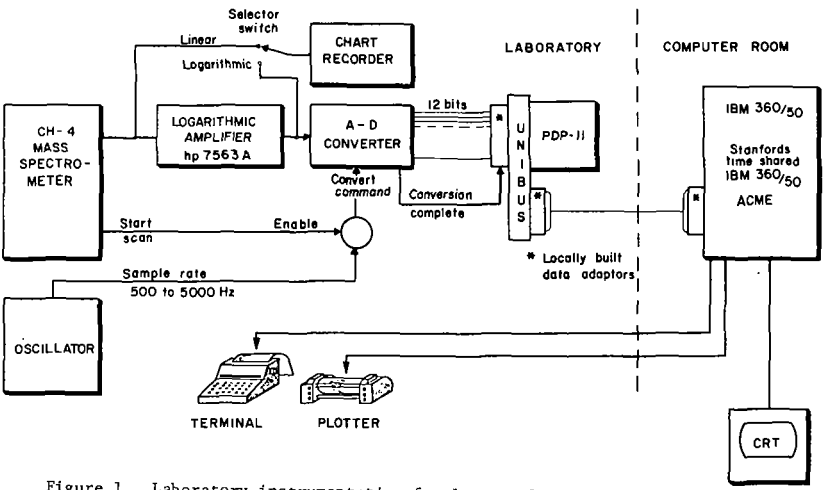

Figure 1. Laboratory instrumentation for low resolution mass spectrometry.

This method of digitizing information that has passed through a logarithmic amplifier tends to preserve the accuracy of the low level signals. It has been shown[3] that the loss in precision due to the integral bit discrimination of the analog-to-digital converter causes an uncertainty that remains a constant percentage of the signal amplitude.

In this application, metastable ion analysis, the PDP-11 does virtually no data processing. It serves simply as a buffer and synchronizer between the laboratory data and the time-shared 360/50. In general we like to be able to transmit raw data during developmental and initial operating phases directly into the large computer. There we have more freedom and greater systems assistance in developing logical algorithms for data processing programs. When the method of data reduction becomes well established we find the economy in reliability by now coding as much of the data processing as possible in the PDP-11. In addition, with data links between the small and large time-shared computer, we can use the text handling facilities of the IBM 360/50 to aid in writing the PDP-11 programs and storing them for operational uses.

In Figure 2 is shown a section (from mass 36 to 59) of a logarithmic spectrum of n-hexane containing several obvious metastable ions. Notice that this data is logarithmic and is an exact reproduction of the data as it entered the IBM 360/50 computer. The vertical tick marks underneath indicates the positions of the integer mass peaks as found by the standard low resolution data processing program. This program has specifically ignored the metastable peaks.

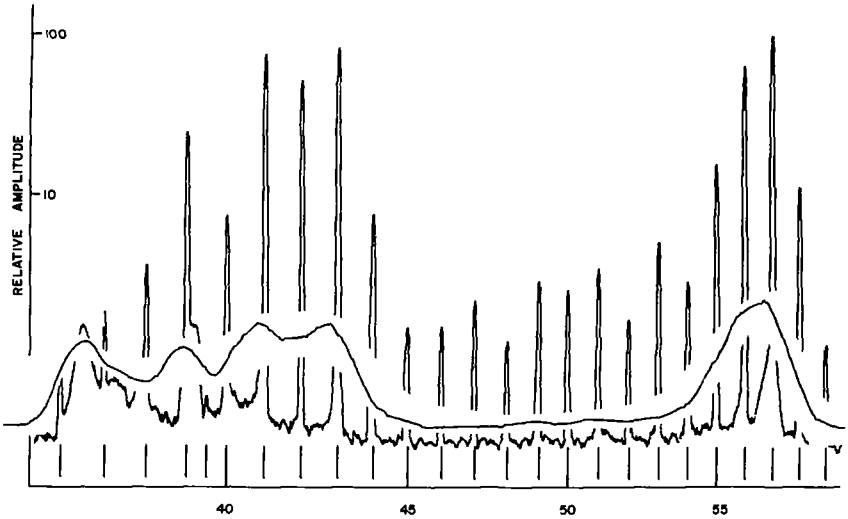

Figure 2. Section of n-hexane (logarithmic amplitude) showing an overlay of the metastable ion positions calculated by computer program.

The purpose of our research was to take the same data base and to develop a corollary program or procedure which would ignore the mass peaks and identify only the metastable ions. The first step in this data processing mode is to subtract the normal peak at each found mass position. Figure 3 shows the area bordering mass 37 in the spectrum of n-hexane before and after normal integer peak subtraction and before any smoothing was attempted on the residual data.

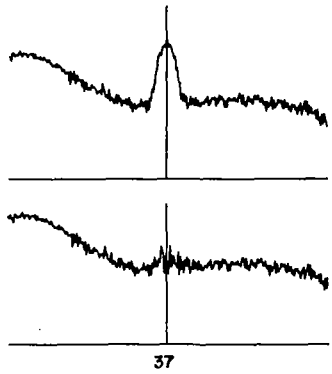

Figure 3. Data profile around mass 37 of n-hexane before (upper) and after (lower) normal peak subtraction.

Figure 4. Effect obtained when normal peak subtraction at mass 37 of n-hexane is slightly offset on the mass scale.

Three problems are involved in subtracting a normal integer peak from the raw data. These are:

a. The model of the peak to subtract. What should be the value in the time stream to subtract from the original?

b. How much to subtract? The residual metastable ion is only 0.1 to 1% of the integer peak abundance.

c. Just where on the mass scale to subtract the desired amplitude of the normal peak.

To the first problem we felt that the best model of a peak is defined within the spectrum itself-or at least a spectrum run under identical conditions. We chose six of the more abundant integer peaks in the spectrum of n-hexane (used as a routine calibration gas with the CH-4 mass spectrometer in our laboratory) as representative of peak shape for that day. These peaks are abstracted from the reference run, linearized, summed and then normalized to a height of one. This peak profile then becomes the model to subtract from all subsequent spectral peaks. All averaging and subsequent subtractions are done point by point in the linear domain, i.e., a logarithmic to linear conversion is made before these operations are attempted. For presentation purposes of these illustrations a linear to log reconversion has been made.

A "peak width" for the purposes of the following discussion is considered to be approximately the width of this model peak at the half height level.

Care is maintained that the data taken for the model peak is over a wide enough range to insure that trace dispersions are represented. A width of about four peak widths either side of the center appears to be necessary. At these distances the contributions from the neighboring peaks are evident. Selection of model peaks that do not have large neighbors and prior subtraction in the adjacent positions are helpful techniques in obtaining a truly representative model.

The second derivative of the residual after peak subtraction proved to be the criterion for how much amplitude to remove. In all cases of smoothing or finding derivatives we have used the methods described by Savitsky.[4] In determining the second derivative at the point of subtraction we considered an area which is about five peak widths distance on either side of the subtracted peak. A second derivative is determined by suitable smoothing over this area. If too much peak amplitude is subtracted, creating a valley, there will result a positive second derivative. Conversely, if not enough peak amplitude is removed a negative second derivative will result. Our method is to estimate an initial amount of the peak to be subtracted and then by an iterative procedure subtract that quantity of the model peak, calculate the second derivative and improve the subtraction estimate. Iteration continues until the second derivative attains a satisfactory low level.

Finally it was found that if the peak model to be subtracted does not precisely center over the normal integer peak the subtraction will result in a characteristic S curve (Figure 4). In this case a measure of this and a qualitative indication of what should be adjusted may be found in the first derivative. This is calculated over an area of approximately one-half a peak width at the point of subtraction. The magnitude of the derivative will indicate if there is a mismatch and the sign of the derivative will determine the direction of mismatch. If displacement does occur the model peak is off-set to the right or left in the course of iteration.

After the completion of "peak subtraction" the residual spectrum has a very noisy appearance. Very slight differences between the model and the peak in each location will give rise to both positive and negative "noise" spikes. A combination smoothing and metastable peak enhancement is then done by using an approximate model of a metastable peak as the coefficients in the algorithm described by Savitsky.[4] This actually amounts to a cross correlation of an expected peak's shape with the spectral data and does greatly enhance the amplitude at the location of a metastable while being insensitive to normal mass peaks and the still narrower noise spikes.

The overlay line in Figure 2 illustrates the result when the metastable ions recognized by the program from n-hexane are superimposed upon the logarithmic scan. The metastable ions at mass 36.6 (m/e 86 → m/e 56) and 39.1 (m/e 43 → m/e 41) are clearly identified. The asymmetry of the low mass edge of the m/e 57 peak is more subtle. The program was able to recognize this as a metastable ion corresponding to the transition m/e 86 → m/e 71. The two metastable ions located by the program in the vicinity of mass 41 and 43 represent extremely dubious metastable ion identifica-

tions. This defines the most serious obstacle faced by our program in this phase of development, namely to distinguish whether metastable ions are present under intense normal ions. This is a variation on the classic recognition problem. The human can still make far more complex decisions quickly in certain areas and the recognition of metastable ions is mass spectrometry is evidently one.

As a by-product of this research we decided to fuse the advantages of the human mind (for metastable peak recognition) and the computer (for arithmetic calculations). This method involved the display of a spectrum on a CRT and following human recognition of the metastable ions (with a light pen) the computer calculated the metastable transitions corresponding to the nominated metastable ion masses. Figure 5 is a section of the spectrum of estradiol on the CRT display.

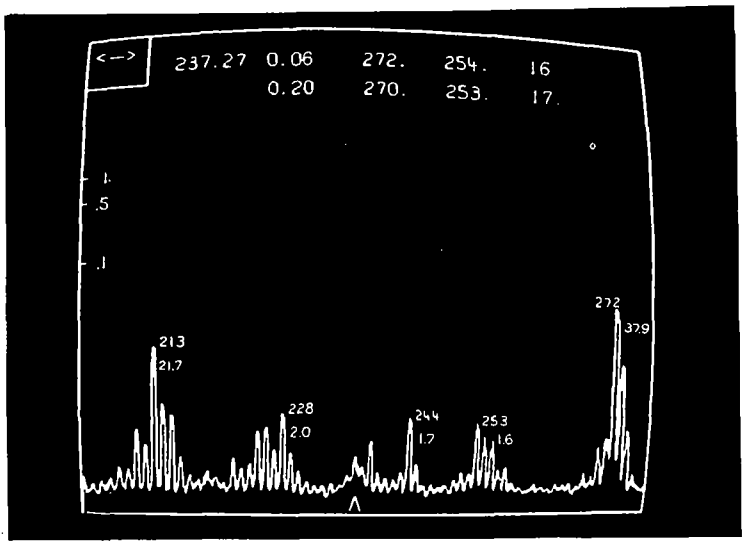

Figure 5. CRT display of a section of a logarithmic scan of estradiol.

The computer program used the raw logarithmic data and determined the mass positions and amplitudes of all the peaks present. The user may direct (using a light pen) the computer to display any portion of the spectrum upon the CRT screen. The user may indicate with the light pen any peak which is then labeled with its mass and relative amplitude. (See for instance peaks 215, 228, 244, 253 and 272.

The operater may also indicate at the base of the spectrum a probable metastable peak. In this case the computer will mark the position with an inverted "V" and search the already known list of masses for a possible parent-daughter pair.

The user was previously asked for the minimum amplitude peak to consider as a parent or daughter and is usually set at 1% or 0.5% relative abundance. Then the actual inequality of the considered cases is computed. If this is below another given tolerance, usually 0.2 amu, the parent daughter pair are displayed for consideration. In the automatic search method, all such matches are listed. In the CRT mode of presentation, each possibility is shown, and succeeding possibilities are shown upon request. All displayed matches are also typed at the teletypewriter for a permanent record. Figure 6 is an example of the hard copy.

The observed metastable mass positions are

237.2	219.0	191.1	166.9	130.9	127.1	108.8

The following neutral species were disallowed

3 4 5 6 7 8 9 10 11 12 13 14 19 20 21 22 23 24 25

Matching pairs of obs. metastable peaks: **ESTRADIOL**
Tolerance is 0.15
Minimum amplitude allowed is 1.00

OBS META	(AMP %)	META OBS VS CALC	PARENT	(AMP%)	DAUGHTER	(AMP%)	LOSS
237.20	(6.00)	0.01	272.0	(37.9)	254.0	(1.1)	18
219.00	(5.20)	0.12	272.0	(37.9)	244.0	(1.7)	28
191.10	(5.20)	-.02	272.0	(37.9)	228.0	(2.0)	44
166.90	(5.50)	0.10	272.0	(37.9)	213.0	(12.7)	59
130.90	(5.00)	-.11	133.0	(7.8)	132.0	(1.8)	1
130.90	(5.00)	-.00	226.0	(1.4)	172.0	(9.6)	54
130.90	(5.00)	-.01	198.0	(1.1)	161.0	(2.0)	37
127.10	(7.00)	-.09	272.0	(37.9)	186.0	(5.3)	86
127.10	(7.00)	0.07	131.0	(3.5)	129.0	(1.5)	2
127.10	(7.00)	0.06	199.0	(2.5)	159.0	(8.8)	40
127.10	(7.00)	0.09	129.0	(1.5)	128.0	(1.8)	1
108.80	(6.50)	0.04	272.0	(37.9)	172.0	(9.6)	100
108.80	(6.50)	-.10	160.0	(12.0)	132.0	(1.8)	28

Figure 6. Hard copy of the parent-daughter ions corresponding to the observed metastable ions in estradiol.

The computer program for this parent-daughter identification from a given apparent metastable position and a list of found m/e peaks in that spectrum, is being made available through the facilities of the American Society of Mass Spectrometry. A copy of this disclosure, in the form of an ALGOL procedure for communication of algorithms, is available from the ASMS Committee III, "Computer and Data Processing", Dr. M. C. Hamming, Continental Oil Co., P. O. Drawer 1267, Ponca City, Oklahoma, 7460 , or by writing directly to this laboratory.

Acknowledgment. This research was supported by the National Aeronautics and Space Administration Grant NGR 05-020-004.

REFERENCES

1. A. Buchs, A. B. Delfino, A. M. Duffield, C. Djerassi, B. G. Buchanan, E. A. Feigenbaum and J. Lederberg, Helv. Chim. Acta, 53, 1394 (1970).

2. R. T. Aplin, H. Budzikiewicz, H. S. Horn and J. Lederberg, Anal. Chem., 37, 776 (1965).

3. W. E. Reynolds, "Use of a Logarithmic Amplifier in Data Processing of Analog Signals", Stanford University Technical Report, IRL 1017, April 1965.

4. H. A. Savitzky and M. J. E. Golay, Anal. Chem., 36, 1627 (1964).

Further Aspects of the Naive Analysis of Structure

D. H. Robertson
Pioneering Research Laboratory
U. S. Army Natick Laboratories
Natick, Massachusetts 01760
and
R. I. Reed
Department of Chemistry
University of Glasgow
Glasgow, Scotland, U.K.

Application of rudimentary set theory[1] was originally made for the purpose of giving clues to the solution of problems of data reduction and processing in the area of mass spectrometry, especially within the confines of calculations which could be performed on a small laboratory computer system. For this purpose, analogies have been taken from the field of information theory, which theory may be considered as a branch of probability theory that is concerned with the likelihood of transmission of messages when the information comprising the messages are subject to varying probabilities of transmission failure.

Two approaches to the classification of mass spectral data are presented, both of which utilize the basic concepts of the theory of sets and have theoretical as well as practical interest.

The first is concerned with probabilities per se; an expression of the form

$$-\eta = \sum_{i=1}^{n} p_i \log p_i \qquad (1)$$

is used to calculate a series of η values which express relative weight factors supporting the probability of the occurrence of a specific collection of events.

From the standpoint of information theory, the expression -p log p is defined as the entropy of the experiment; that is, the probability that the information transmitted by the sender is received by the receiver. This function is designated as η and is called the Khinchine entropy function.

Entropy of the experiment is without dimensions and may be considered as analogous with entropy as it is customarily defined in statistical mechanics. It is the equivalence of ordinary entropy divided by the Boltzman constant. Within the framework of consideration for this discussion, the events are the ions appearing in a given mass spectrum. For these initial calculations, the probabilities represent the ratios of individual ion currents to total ion currents. This is generally equivalent to relative intensity of each ion divided by the total ion current represented as a sum of ion intensities.

In this equation, i is the index of message units corresponding to individual ions and p is the individual probability for each ion in the spectrum.

If only one event has a probability of unity and all others are zero, the value of the entire function is zero; if all probabilities are zero, the value of the entire function is zero; if all probabilities are equal, the function η will have a maximum value. There lies in the continuum between zero and maximum value, a collection of η values which have diagnostic nature for alkanes, alkenes and alkynes.

e.g.

Compound	Khinchine Function
n-butane	0.926614
2-methylpropene	0.812125
t-2-butene	1.041750
3-methyl-1,2-butadiene	1.215960
1,3,5-hexatriene	1.339620
1,5-hexadiyne	1.605300
3-heptyne	1.379110

The second approach is concerned with comparison of spectra for the purpose of determining their likeness with known spectra in a data file. A suitable analogy is the superimposition of two nearly-identical planar figures. The selection of a probability model for the experiment is made which allows this superimposition in a mathematical way that is amenable to programming on a mini computer system.

For the initial model, the following equation was utilized

$$J(1,2) = \frac{c}{N}\sum_{i=1}(p_{1i} - p_i) \log_e \frac{p_{1i}}{p_i} + \frac{c}{N}\sum_{i=1}(p_{2i} - p_i) \log_e \frac{p_{2i}}{p_i} \qquad (2)$$

For random samples 1 and 2, the N values represent the total number of observations for each species (in this case the total ion current for the compound 1 or 2); p_{1i} and p_{2i} represent the probabilities of the i^{th} ion in samples 1 and 2; p_i is defined as $1/2(p_{1i} - p_{2i})$. Resulting J values reflect differences between any two spectra being compared. If the two spectra are identical, J would have a value of zero. Differences among spectra are calculated for a group of hydrocarbons, using the straight chained hydrocarbon as the template upon which comparison is based in each case, i.e., n-pentane serves as template for members of the unsaturated C-5 cyclo systems.

Reference Compound for the Series is Hexane

Comparison Compound	Divergence(J)
n-hex-1-ene	4.2269
2-methylpent-2-ene	7.7805
cyclohexane	10.0238
3-hexyne	11.8302
2-methylpentene	12.5054
1-hexyne	18.7163
2-hexyne	25.8092

In a second case a group of compound pairs is subjected to comparison, thereby showing the sensitivity of the divergence calculation in elucidating structural differences, especially among hetero-atom systems.

Compound Pair	Average Divergence
2-methylpent-1-ene vs. 3-methylpent-1-ene	0.95724
cyclohexane vs. hex-1-ene	1.11170
2,3-dimethylpentane vs. 2,4-dimethylpentane	1.46830
n-heptane vs. 2,4-dimethylpentane	2.6120
2-thiapentane vs. 3-thiapentane	10.2372
1-butanol vs. 2-butanol	17.4428

The general idea with which one is concerned is that of set reduction with the aid of Khinchine entropy functions and divergence values as indices for degree of difference categories; the individual categories constitute subsets from the universal set of all compounds whose mass spectra are available. Once these values are established for a complete series of known compounds, they may be used to determine unknown structure.

The expanded manuscript will be submitted for publication to Analytical Chemistry.

References

1. Reed, R. I., Rev. Port. Quim., 10, 129(1968).

Computer Analysis of Mass Spectral Information

Kain-Sze Kwok, R. Venkataraghavan,
and F. W. McLafferty

Department of Chemistry, Cornell University
Ithaca, New York 14850

This is a brief progress report on a system for computer-aided analysis of low-resolution mass spectral data for compound identification and structural analysis utilizing spectra-structure correlations and a file of 10,000 reference spectra. The general objectives of this system are: (1) to identify the compound if the spectrum is present in the reference file, (2) to find compounds in the file with the most closely related structural characteristics, and (3) to identify directly particular structural features.

Three general approaches have been taken for the computer-aided analysis of mass spectral data. The first method takes the data and predicts the possible molecular ion and molecular formula using the well-established rules.[1,2] The second method involves the usage of learning machine techniques to recognize specific structural features.[3] The third method uses file searching techniques to match the spectrum of the unknown compound with the reference spectrum of a known compound.[4]

Results and Discussion:

A reference file containing around 10,000 spectra has been generated by combining the data from Abrahamsson-Wiley tape and M.S.D.C. tape. The file contains the following information.

1. Compound name, molecular formula, molecular weight, 2 most intense peaks.
2. Wiswesser line notation for the molecular formula.
3. Ion-series data:[1] Sum of intensities of particular significant series (e.g., 15,29,43....) and centroid of the series.
4. Neutral loss data:[1] Masses and intensities of particular significant neutrals lost from M^{+}.
5. Characteristic ions data: Masses and intensities of other significant ions.

This condensed file containing chemically significant spectral information along with the structural formula represented by the Wiswesser line formula notation is used for both the learning machine approach and file searching operations.

Learning Machine Approach:

Application of learning machines to interpret mass spectral data has been reported by Isenhour and his co-workers.[3] In our approach the training set utilizes the condensed mass spectral data instead of the original spectrum. Training vectors were first obtained using the Aldermaston M.S.D.C. compound classification code to recognize the presence or absence of particular structural features in the molecule. Various aspects of feature selection to obtain the best response using the minimal amount of information have been investigated. Success in this has led to our present work on spectral pattern recognition based on complete and fragment Wiswesser line formula notation. This appears to be a very powerful method capable of performing a substantial part of the procedure now done by the human interpreter, and, in particular cases, providing even more structural information than is now possible.

File Searching Method:

For our computerized file searching the unknown spectrum is first condensed employing the same procedure used for reference data, and match factors are calculated for each data class. The ion series match factor indicates whether or not the reference and unknown belong to the same class of compounds. The neutral loss match factor indicates the similarity of more specific structural features and functional groups. The match factor from the characteristic ions data involves the remaining significant ions of the spectrum. Finally an overall index derived from all the match factors is computed indicating how closely the two spectra resemble each other; a high overall index indicates that the compounds are nearly identical. However, even if the compound spectrum is not present in the library, reference spectra with high individual match factors can indicate particular structural possibilities. Figs. 1 and 2 show typical results of the searching operation using unknown spectra not in the reference file.

Figure 1. Search using spectrum of 1-phenylpentane.

Compound Name	M.W.	Neutral-Loss		Series	Charac-Ion		Class	Match
1-Phenylpentane	148	9/18	(1.000)	0.933	2/7	(0.571)	0.939	0.922
(1-Methylbutyl)benzene	148	7/18	(0.778)	0.714	3/7	(0.858)	0.755	0.769
Methyl p-Tolyl Ketone	134	8/18	(0.889)	0.760	0/0	(0.000)	0.890	0.746
ar-Methylacetophenone	134	8/18	(0.889)	0.676	0/9	(0.000)	0.895	0.725
alpha-Phellandrene	136	6/17	(0.706)	0.764	1/6	(0.333)	0.916	0.700
1-Phenyl-3-methylbutane	148	7/18	(0.778)	0.589	2/7	(0.571)	0.689	0.694
p-Methylacetophenone	136	7/18	(0.778)	0.795	0/8	(0.000)	0.820	0.690
2-Phenyl-3-methylbutane	148	6/18	(0.667)	0.663	2/6	(0.667)	0.801	0.683
tert-Butylbenzene	134	6/18	(0.667)	0.747	1/7	(0.286)	0.884	0.667
3-Phenylpentane	148	5/18	(0.556)	0.843	2/7	(0.571)	0.853	0.667

Figure 2. Search using spectrum of 2-t-butyl-p-cresol.

Compound Name	M.W.	Neutral-Loss		Series	Charac-Ion		Class	Match
2-tert-Butyl-m-cresol	164	8/18	(0.889)	0.899	4/12	(0.667)	0.904	0.866
6-tert-Butyl-o-cresol	164	8/18	(0.889)	0.894	4/12	(0.667)	0.899	0.864
4-tert-Butyl-o-cresol	164	7/18	(0.778)	0.814	3/10	(0.600)	0.881	0.778
p-tert-Butylanisole	164	7/18	(0.778)	0.774	3/11	(0.546)	0.862	0.759
p-(1,1-Dimethylpropyl) phenol	164	5/18	(0.556)	0.857	2/12	(0.333)	0.870	0.754
6-tert-Butyl-m-cresol	164	8/18	(0.889)	0.368	4/12	(0.667)	0.517	0.685
alpha-Terpinolene	136	6/18	(0.667)	0.606	2/12	(0.333)	0.870	0.635

In Fig. 1 monosubstituted benzenes and aromatic ketones were selected; the class index, ion-series match factor and neutral loss match factor are fairly high for all compounds in the list as one might expect. An examination of the characteristic-ion column shows zero values for all of the ketones, thus indicating that the unknown is an aromatic hydrocarbon. The high overall match of the compound at the top of the list indicates that it and the unknown are nearly identical, which is true in this particular case.

For the search shown in Fig. 2 a spectrum of the compound used was not present in the reference file. As can be seen all of the compounds of highest overall match are isomers of the compound. The two structurally dissimilar compounds, p-(1,1-dimethylpropyl)phenol and α-terpinolene have low neutral loss match factors and low characteristic ion match factors. The low class index and ion series match factor for the structurally similar compound, 6-t-butyl-m-cresol, is due to the fact that the spectrum in the file does not include peaks below m/e 70.

Conclusion:

Preliminary results from this investigation has shown that a condensed file containing chemically and spectroscopically significant information will not only help in identifying a compound unambiguously if its spectrum is present in the reference file, but also will help select spectra with structural similarities. Spectral pattern recognition based on the Wiswesser line formula notation appears to be especially promising.

References:

1. R. Venkataraghavan, F. W. McLafferty and G. E. Van Lear, Org. Mass Spectrom., 2, 1 (1969).
2. A. Buchs, A. B. Delfino, A. M. Duffield, C. Djerassi, B. G. Buchanan, E. A. Feigenbaum, and J. Lederberg, Helv. Chim. Acta, 53, 1394 (1970).
3. P. C. Jurs, B. R. Kowalski and T. L. Isenhour, Anal. Chem., 41, 21 (1969).
4. H. S. Hertz, R. A. Hites, and K. Biemann, Anal. Chem., 43, 681 (1971) and references cited therein.

D7

COMPUTER TECHNIQUES FOR IDENTIFYING LOW RESOLUTION MASS SPECTRA

Stanley L. Grotch
Jet Propulsion Laboratory
Pasadena, California 91103

Several identification algorithms have been implemented into computer programs which have been tested using 125 different low resolution mass spectra obtained from five different sources (1-5). These spectra have been compared against a library of 6880 known spectra (substantially the same library as used by Knock, et. al. (6).)

In all of the techniques used here, each unknown spectrum is compared against the known spectral library stored on magnetic tape. As the search proceeds, a record is maintained of the ten compounds in the library yielding the minimum value of a selected criterion for each unknown. These "top 10" known spectra are summarized at the conclusion of the search. All programs can accommodate up to 30 unknowns on each pass through the library. Each complete search package consists of approximately 500 FORTRAN IV statements and was tested using an IBM 360/44 computer.

One set of programs used as a disagreement criterion the sum of the absolute values of the differences in peak height when peak height was encoded to either 2, 8 or 10^4 levels at each nominal mass. Another program employed the maximum coincidence of the top N peaks. The choice of the absolute difference criterion coupled with peak height encoded to a few bits results in several beneficial effects: (1) very high search speeds can be achieved by packing many channels into each computer word and utilizing essentially parallel processing, (2) computer memory requirements are reduced, (3) the quantity of data to be entered into the computer for both unknown and library is reduced, significantly reducing data input/output time. Typically, for one bit encoding, using the IBM 360/44, a complete search of the library required about 15-20 sec. For up to five unknowns per pass, the rate limiting process is the tape reading speed entering the library into core.

For each criterion of disagreement, two modes of searching were employed: (1) unrestricted search (all members of the library were compared), (2) filtered search (only library members satisfying certain spectral preconditions were considered): (a) the mass corresponding to the maximum intensity peak (base peak) of the unknown must be among the 5 highest peaks of the library member, and vice versa; (b) the molecular weight of the library member must be greater than an arbitrary specified fraction (generally, 0.7) of the mass of the highest unknown peak with an intensity greater than 0.5% of the total ion current.

The recognition performance of a particular matching procedure is measured here in terms of compound "confusion". For a given unknown, the "confusion" is defined as the number of different library compounds found which yield a value of the disagreement criterion which is less than or equal to that of the correct answer. In essence, the confusion is the number of different compounds which must be considered in order to include the correct compound.

The results of the recognition performance of the various methods of encoding are summarized in Table I for both the unrestricted and the restricted search. The results are presented in terms of the percentage of unknowns correctly identified within a given confusion for peak height encoding of 1, 3, and 32 bits, as well as the maximum coincidence of the most intense 20 peaks in both unknown and library.

These results indicate that the maximum coincidence criterion was significantly poorer in recognition performance than the other techniques which were found to increase in reliability as the number of levels increased. However, even the two level system attained very high reliability. Since computer requirements and economic costs are likely to be minimal for this case, it might suffice for many applications.

A detailed account of these results will be published in "Analytical Chemistry."

Table I. Comparison of One Bit, Three Bit, 32 Bit and Top 20 Results

Confusion = C_o	1 Bit	3 Bits	32 Bits	Top 20 vs Top 20
	***** Unrestricted Search *****			
	% of Compounds With Confusion ≤ C_o			
0	64.8	73.6	80.8	48.0
1	76.0	84.0	88.0	54.2
5	82.4	91.2	96.0	71.2
10	86.4	93.6	97.6	77.6
	***** Restricted Search *****			
Confusion = C_o				
0	70.4	80.8	84.0	60.0
1	79.2	88.0	94.4	71.2
5	96.0	97.6	98.4	85.6
10	99.2	100.0	99.2	92.0

REFERENCES

1. Silverstein, R. M., Bassler, G. C., "Spectrometric Identification of Organic Compounds", 2nd Ed., Wiley and Sons, New York (1967).

2. Baker, A. J., Eglinton, G., Preston, F. J., Cairns T., "More Spectroscopic Problems in Organic Chemistry," Heyden & Son, Ltd, London, 1967.

3. Biemann, K., MIT, Personal Communication, June, 1970.

4. Boettger, H., JPL, Personal Communication, Oct., 1970.

5. Mass Spectrometry Data Centre, Aldermaston, England.

6. B. A. Knock, et. al., Anal. Chem. 42, 1516 (1970).

This paper presents the results of one phase of research carried out at the Jet Propulsion Laboratory, California Institute of Technology, under Contract No. NAS 7-100, sponsored by the National Aeronautics and Space Administration.

D8

Investigation into Intensity Measurements with Automated Data Acquisition Systems

W.J. McMurray and S.R. Lipsky
Yale University School of Medicine
New Haven, Connecticut 06510

Abstract:

A description of the modifications to the IBM-1800 data acquisition system which permits it to be utilized by the mass spectrometer and Fast Fourier Transform N.M.R. spectrometer was discussed. The data acquisition program and the data processing programs for the intensity measurements were described. Rather than scanning the entire spectrum, repeated scans of a limited mass range were employed. The resulting data was sorted by mass and intensity and the abundances and standard deviations in the abundances were calculated for all peaks of interest. Preliminary results on model compounds were reported which showed the presently attained precision and accuracy. These experiments were conducted to determine what level of isotope enrichment can be reliably detected with the present system.

IONIZATION OF He BY ELECTRON IMPACT: MEASUREMENTS OF THE TRIPLE DIFFERENTIAL CROSS SECTION

H. Ehrhardt, K. H. Hesselbacher, K. Jung, K. Willmann*

Department of Physics
University Trier-Kaiserslautern
Kaiserslautern, Germany

In the last fifty years a large number of publications have appeared on the experimental determination of ionization cross sections by electron impact. In the main the different authors have investigated total cross sections as a function of the electron impact energy by measuring the ion production for single and multiple ionization. These data are of considerable interest for the description of plasmas which are not in thermodynamic equilibrium.

By analyzing the electrons instead of the ions produced there is a variety of differential cross sections that one can measure and compare with theoretical results before integration over all scattering parameters[1]. Each integration has an averaging effect, i.e. much detailed information about the process is lost. For this reason, contrary to total cross sections, differential cross sections are much more sensitive to each approximation made in the calculation and to the model considered as a starting point.

The most detailed data about ionizing transitions by electron impact are obtained by studying the triple differential cross section. This cross section is a function of the impact energy E_o of the incident electrons, the energy E_a of one of the two outgoing ionization electrons, the scattering angles θ_a, θ_b of these two particles and the angle ϕ between the two scattering planes defined in the process:

$$d^3\sigma = d^3\sigma(E_o, E_a, \theta_a, \theta_b, \phi)$$

E_o or E_a can be replaced by the energy E_b of the second ionization electron given by the energy conservation law:

$$E_o = E_a + E_b + IP$$

IP is the ionization potential of the target (the atom and the ion produced are assumed to be in their ground state). In measuring the triple differential cross section the kinematic of the collision process is completely defined and the measured signal can be compared with theoretical results without any integrations.

In our laboratory we have investigated the triple differential cross section for helium in an electron spectrometer capable of analyzing both ionization electrons with respect to their energy and scattering angle[2)3)]. The analyzed electrons are detected by multipliers and the pulses produced are counted in coincidence. Measuring the coincidence rate as a function of one scattering parameter keeping constant all

other parameters yields a curve corresponding the intersection of a hyperplane with the hypersurface in a six dimensional space defined by the triple differential cross section. In our experiment the variable parameter is the scattering angle of the slow (ejected) ionization electrons. Measurements are made for E_o = 256.5eV, 80.5eV, 50eV, 41eV, and 30.5eV.

The obtained coincidence cross sections show a strong angular correlation between the two outgoing electrons. There are two well defined maxima in the angular distribution separated by two minima. The cross section is a minimum for processes in which both ionization electrons are moving in the same or in opposite directions. The maxima appear as a forward — and a backward-peak which we refer to as the binary encounter — and recoil peak respectively. For ionizing processes contributing to the recoil peak both electrons are detected on the same side with respect to the direction of the incoming electron beam, i.e. the recoil of the ion produced is a maximum. In ionizing collisions contributing to the binary encounter peak the momentum transferred to the remaining ion is a minimum and to the first approximation only two particles, namely the inelastically scattered and the ejected electron, take part in the collision.

The angular position of the binary encounter peak as well as the relative intensity in the recoil peak and the total coincidence rate are functions of the detector angle of the fast (scattered) electrons and the amount of the excess energy shared by each ionization electron. The obtained coincidence cross section cannot be described in a satisfactory manner by computations based on different Born approximations, not even for impact energies ten times higher than the ionization potential of the target, although total cross sections are reasonably well described at this energy range.

For small primary energies (E_o = 50eV, 41eV, and 30.5eV) there is a strong angular correlation between the two outgoing electrons too. However, whereas for E_o = 256.5eV (in accordance with the reflection model [4]) the recoil peak is never higher than the binary encounter peak and both peaks are almost on an axis, this is no longer true for small electron impact energies [5]. The expected symmetry axis is bent in a backward direction and the recoil peak is larger than the binary encounter peak. The bent axis can be attributed qualitatively to the coulomb interaction between the two continuum electrons, however, until now there is no explanation for the overwhelming backward intensity of the triple differential cross section. In conclusion we can say that for impact energies greater than about 200eV a modified Born approximation (correlation term in the continuum wave functions) can perhaps yield a satisfactory agreement with the experiment but for small electron energies the ionization process by electron impact is not understood at all.

* Presently at St. Francis Xavier University, Antigonish, Nova Scotia

1) H. Ehrhardt, K. H. Hesselbacher, K. Jung, K. Willmann,
In Case Studies in Atomic Collisions, Edited by E. W. McDaniel and M. R. C. McDowell (in press)

2) H. Ehrhardt, M. Schulz, T. Tekaat, K. Willmann,
Phys. Rev. Letters 22, 89, (1969)

3) H. Ehrhardt, K. H. Hesselbacher, K. Jung, T. Tekaat, K. Willmann,
Z. Phys. (to be published)

4) L. Vriens, Physica 45, 400, (1969)

5) H. Ehrhardt, K. H. Hesselbacher, K. Jung, M. Schulz, K. Willmann,
J. Phys. B (to be published)

Measurement and Interpretation of Ionization Potentials of Molecules*)

by Burkhard Brehm

Fakultät für Physik der Universität Freiburg/Br., Germany

The interpretation of molecular photoelectron spectra is usually made according to the following scheme. The electronic band systems are correlated with the orbitals of the molecule by a) comparing the calculated molecular orbital energies with the observed energies of the band systems and by b) comparing the predicted bonding character of the orbitals with the general shape of the vibrational structure in the photoelectron spectrum. If possible, an analysis of the details of the vibrational structure is made using the Franck-Condon principle and the molecular vibrational and rotational constants obtained from spectroscopic data. Only for a number of diatomic molecules can the vibrational structure be completely analysed[2,3]; for polyatomic molecules a quantitative evaluation of the vibrational structure has been made only for a few cases[4].

The identification of the electronic states of the ions found in the photoelectron spectra is based upon the assumption that the ionization processes observed are those processes in which one electron is emitted from a specific occupied molecular orbital without a significant perturbation of the orbitals of the other electrons and upon Koopmans' theorem: The orbital energy of an electron ε_i is equal to the energy necessary to ionize this electron E_o^i. Clearly the ionization energy of Koopmans' theorem is a vertical ionization energy, because the orbital energy of the electrons is calculated with the nuclei in the equilibrium position of the neutral molecule.

$$\varepsilon_i = E_o^i = -(V_2^i - V_1)\big|_{\vec{q}=\vec{q}_o}$$

Here $\vec{q}$ is the vector of the nuclear coordinates of the molecule, $\vec{q}_o$ is the equilibrium position of the nuclei and V_2^i and V_1 are the potential functions for the ion and the molecule respectively.

A quantitative test of Koopmans' theorem would require very accurate molecular orbital calculations, which are close to the Hartre-Fock limit and a quantitative way to extract vertical ionization potentials (IP's) out of the observed photoelectron spectra. Even in such a comparison, however, deviations are expected, because the orbitals of the other electrons are changed due to the presence (or absence) of the electron to be ionized and due to changes in the energy of the correlation of the electronic motion, which is neglected in the Hartree-Fock approximation[5].

*) Contrary to the original intentions of the author the topic of this paper will be limited to the measurement and interpretation of vertical IP's, because problems and methods of measuring adiabatic IP's have recently been discussed in detail by Guyon and Berkowitz[1].

In spite of these shortcomings Koopmans' theorem has proved to be a very powerful tool for the identification of electronic band systems in photoelectron spectra and the following generalisation may also prove to be useful:

$$\varepsilon_i(\vec{q}) = -(V_2^i(\vec{q}) - V_1(\vec{q})) \quad \text{for } \vec{q} \sim \vec{q}_o.$$

Taking the one electron orbital energy ε_i as a function of the internuclear coordinates $\vec{q}$ it should be equal to the negative of the (vertical) energy difference between the potential function of the nuclear motion for the electronic state of the ion $V_2^i(\vec{q})$ and of the molecule $V_1(\vec{q})$. Even though this relation cannot be expected to hold over a large range of internuclear coordinates, it should be a reasonable approximation for the vicinity of the molecular equilibrium position $\vec{q}_o$.

In observed photoelectron spectra the largest band or, if the vibrational structure is not resolved, the peak of a band system corresponding to one electronic state of the ion has been taken as the vertical IP[6], even though there seem to be only qualitative arguments for this choice. As will now be shown, the vertical ionization energy E_o^i can be more directly connected to the "center of gravity" of the band system, if the Franck-Condon principle*) is assumed to be valid. In this case the relative contribution of different vibrational transitions to the electronic transition is given by the Franck-Condon factors:

$$F_{v''}^{v'} = |\langle \varphi_{v'}; \psi_{v''} \rangle|^2$$

Here the $\{\psi_{v''}\}$ are the orthogonal, normalized vibrational wave functions for the molecule

$$T\psi_{v''} + V_1(\vec{q})\ \psi_{v''} = E_{1,v''}\ \psi_{v''}, \quad \langle \psi_i; \psi_k \rangle = \delta_{ik}$$

and the $\{\varphi_{v'}\}$ are the vibrational wave functions for the ion

$$T\varphi_{v'} + V_2^i(\vec{q})\ \varphi_{v'} = E_{2,v'}\varphi_{v'}, \quad \langle \varphi_i; \varphi_k \rangle = \delta_{ik}$$

T is the operator of the kinetic energy, $V_1(\vec{q})$ and $V_2^i(\vec{q})$ are the potential functions for the molecular and ion electronic state respectively and v" and v' stand for all the vibrational quantum numbers. $E_{1,v''}$ and $E_{2,v'}$ are the total energies of the molecule or ion except for the rotational energies, which will be neglected in this paper. A direct consequence of the completeness and orthogonality of the $\{\varphi_{v'}\}$ and $\{\psi_{v''}\}$ is

$$\sum_{v'} F_{v''}^{v'} = \sum_{v''} F_{v''}^{v'} = 1 \text{ and in particular } \sum_{v'} F_o^{v'} = 1,$$

which has been used to normalize the band system. These sums as well as the following must include the dissoziation continua due to the completeness requirement for the function system $\{\varphi_{v'}\}$. For the average energy of the transitions from one vibrational state of the molecule v" to all vibrational states v' of the ion in a particular electronic state one gets:

*) Aside from the Franck Condon principle it is required that the photoionization does not strongly on the energy of the ionized electron.

$$\sum_{v'} F_{v''}^{v'}(E_{2,v'} - E_{1,v''}) = \sum_{v'}(E_{2,v'} - E_{1,v''}) \langle\psi_{v''};\varphi_{v'}\rangle\langle\varphi_{v'};\psi_{v''}\rangle$$

$$= \sum_{v'} \langle\psi_{v''};\varphi_{v'}\rangle\langle\varphi_{v'}|E_{2,v'} - E_{1,v''}|\psi_{v''}\rangle$$

$$= \sum_{v'} \langle\psi_{v''};\varphi_{v'}\rangle\langle\varphi_{v'}|T + V_2^i(\vec{q}) - T - V_1(\vec{q})|\psi_{v''}\rangle$$

$$= \sum_{v'} \langle\psi_{v''};\varphi_{v'}\rangle\langle\varphi_{v'}|V_2^i(\vec{q}) - V_1(\vec{q})|\psi_{v''}\rangle = \langle\psi_{v''}|V_2^i(\vec{q}) - V_1(\vec{q})|\psi_{v''}\rangle$$

Since in photoelectron spectroscopy very often most of the molecules are in their vibrational (and electronic) ground state, v" = 0, one gets for this particular case:

$$\bar{E}_i = \sum_{v'} F_o^{v'}(E_{2,v'} - E_{1,o}) = \langle\psi_o|V_2^i(\vec{q}) - V_1(\vec{q})|\psi_o\rangle$$

This relation can be used as a new definition of the vertical ionization potential. The potential difference can be obtained from the extended version of Koopmans' theorem, given above and vibrational ground state wave functions ψ_o be obtained for the many molecules for which the geometry, the vibrational frequencies and the anharmonicities are well known. On the other hand the sum on the left side of this relation can directly be obtained from the photoelectron spectra even in cases where the vibrational structure is not resolved. $\bar{E}_i$ is the center of gravity of the band system in the photoelectron spectrum.

The next sum rule yields:

$$\sum_{v'} F_{v''}^{v'}(E_{2,v'} - E_{1,v''})^2 = \langle\psi_{v''}|[V_2^i(\vec{q}) - V_1(\vec{q})]^2|\psi_{v''}\rangle$$

and in the special case with v" = 0:

$$\sum_{v'} F_o^{v'}(E_{2,v'} - E_{1,o})^2 = \langle\psi_o|[V_2^i - V_1]^2|\psi_o\rangle$$

$$\Delta_i^2 = \sum_{v'} F_o^{v'}(E_{2,v'} - E_{1,o} - \bar{E}_i)^2 = \langle\psi_o|[V_2^i - V_1]^2|\psi_o\rangle - \bar{E}_i^2$$

This relation can be taken as a quantitative definition of the "vibrational width Δ_i" of the electronic transition and, as $\bar{E}_i$, it can be directly evaluated from the photoelectron spectra as well as from molecular orbital calculations.

Other sum rules involving higher powers of the energy differences can be obtained in the same way, but they do not appear to have a simple meaning so they will not be given here. They all have in common that the only property of the ion which influences these numbers is the shape of the ionic potential function in the vicinity of the molecular equilibrium geometry $\vec{q}_o$. So the shape of the potential functions of the ion and of the molecule and the vibrational wave function of the molecule completely determine the general shape of the vibrational structure of the transition. The vibrational fine structure depends, of course, on the rest of the ionic potential functions.

In particular the adiabatic IP's are not directly connected with the molecular orbital energies, but for classes of related molecules a correlation between the vibrational width Δ and the difference between the vertical and the

adiabatic ionization potentials may exist which would give a very useful estimate for the adiabatic IP from $\bar{E}_1$ and Δ_1.

The convergence of these sums and expectation values can best be discussed after separating the potential functions into two parts: $V(\vec{q}) = V_{el}(\vec{q}) + V_n(\vec{q})$. Here V_{el} is the electronic energy, which is finite for all $\vec{q}$. $V_n(\vec{q})$ is the nuclear repulsion; it is the same for all states of the molecule and molecular ion so that its singularities cancel in the expression $V_2^1 - V_1$. This shows that the two sum rules for $\bar{E}_1$ and $\Delta^2 + \bar{E}_1$ given here converge. For sum rules with higher powers of the energy difference convergence problems may arise from the fact that the operators of the kinetic energy T and of the potential energy V do not commute. A treatment of the nuclear rotation must take the coupling between the nuclear and electronic angular momenta into account a coupling which changes its type for very small and large internuclear distances. These problems and their connection with the angular distribution of the photoelectrons are beyond the scope of this paper.

The meaning of the two numbers $\bar{E}_1$ and Δ_1 defined above can be illustrated by the following simple calculation for diatomic molecules: If q_o is the average value of the internuclear distance in the molecular ground state

$$q_o = \langle \psi_o | q | \psi_o \rangle$$

the potential difference $V_2^1(q) - V_1(q) = \delta V(q)$ and $(\delta V(q))^2$ can be developed around q_o.

$$\delta V(q) = E_o^1 + K(q - q_o) + \kappa(q - q_o)^2 + \ldots\ldots$$

$$(\delta V(q))^2 = (E_o^1)^2 + 2 E_o^1 K(q-q_o) + K^2(q-q_o)^2 + 2 E_o^1 \kappa(q-q_o)^2$$

Neglecting all terms of third and higher powers in $(q - q_o)$ one gets for $\bar{E}_1$ and Δ_1^2

$$\bar{E}_1 = E_o^1 + \kappa(\overline{q^2} - q_o^2) \quad (\sim E_o^1)$$

$$\Delta_1^2 = K^2(\overline{q^2} - q_o^2)$$

This shows that $\bar{E}_1$ is equal to the classical vertical energy difference E_o^1 except for a correction term which has the order of magnitude of the difference between the zero point energies. Δ_1 is equal to the product of the force in the upper state at the equilibrium distance of the lower state and the width $(\overline{q^2} - q_o^2)^{1/2}$ of the lower state wave function. Direct consequences can be drawn from this for isotopic molecules like H_2, D_2 and HD: $\bar{E}_1$ depends on the reduced mass μ only through the correction term, which is proportional to the square root of μ. Δ_1 on the other hand is proportional to the fourth root of μ. These relations have not been tested so far. For harmonic potentials and for Morse potentials analytic expressions can be obtained for $\bar{E}_1$ and Δ_1^2 as a function of the potential parameters.

Another interesting question arises due to the fact that the molecules in a gas sample at room temperature are not all in their lowest vibrational and

rotational state. The effect of rotational excitation can be estimated by taking for ψ_0 in the expectation values the wave function for an average rotational energy corresponding to the temperature T. No centrifugal terms appear, however, in the expression for $V_2^1 - V_1$ because these centrifugal terms must be assumed to cancel in order to be consistent with the set of assumptions made above. If $B_{v'',J}(T)$ is the normalized Boltzmann distribution including the degeneracy factors, the experimental determination of the average energy $\overline{E_i(T)}$ and the mean square deviation $\Delta_i^2(T)$ are given by

$$\overline{E_i(T)} = \sum_{v'',J} B_{v'',J}(T) \sum_{v'} F^{v'}_{v'',J}(E^J_{2,v'} - E^J_{1,v''})$$

$$= \sum_{v'',J} B_{v'',J}(T) < \psi_{v'',J} | V_2^1 - V_1 | \psi_{v'',J} >$$

$$\Delta_i^2(T) = \sum_{v'',J} B_{v'',J}(T) < \psi_{v'',J} | (V_2^1 - V_1)^2 | \psi_{v'',J} >$$

Now $\Theta(\vec{q},T) = \sum_{v'',J} B_{v'',J}(T) |\psi_{v'',J}(\vec{q})|^2$ is the probability density of finding the nuclei at the relative position $\vec{q}$ averaged over an ensemble of molecules at the temperature T. $\Theta(\vec{q},0) = |\psi_0(\vec{q})|^2$. This distribution of internuclear positions at a temperature T as compared to T = 0 is changed in two ways the average internuclear distance is increased due to the centrifugal forces and the anharmonicity of the potential function and the area of internuclear coordinates in which $\Theta(\vec{q},T)$ is substantially different from zero is increased. This has the following effects on $\bar{E}_i(T)$ and $\Delta_i^2(T)$: $\bar{E}_i(T)$ decreases with increasing T if the potential function in the ion state $V_2^i(\vec{q})$ decreases towards larger internuclear distances in the vicinity of the molecular equilibrium position $\vec{q}_0$. This is the case if the electron ionized is bonding. For the ionization of a antibonding electron $\bar{E}_i(T)$ should increase with the temperature. $\Delta_i^2(T)$ should always increase with T, but this increase should be larger in the case of the ionization of a bonding electron. For particular molecules formulae for $\bar{E}_i(T)$ and $\Delta_i^2(T)$ as a function of T can be obtained for temperatures for which the thermal excitation is small compared to dissociation energies.

The sum rules given above have so far only been used to evaluate the photoelectron spectra of a few diatomic and triatomic molecules. For some diatomic molecules (H_2, N_2, O_2) Δ_i^2 and the difference between $\bar{E}_i$ and the adiabatic IP's have also been calculated from the potential functions. The agreement between these theoretical and the experimental numbers has always been good, if good potential functions were available. It is hoped that the sum rules given above will prove to be useful even though deviations from the Franck-Condon-principle and from Koopmans' theorem may in some cases hamper their use. For polyatomic molecules the sum rules should help to give the evaluation of photoelectron spectra a more quantitative basis.

References

1) P.M. Guyon, J. Berkowitz, J.Chem.Phys. 54, 1814 (1971)
see also: B. Brehm, Adv. Mass Spectrometry 5 (1971)
Int.Conf. Mass Spectrometry, Brussels 1970

2) R. Spohr, E. von Puttkamer, Z.für Naturforschung 22a, 705 (1967)

3) D.W. Turner, Proc.Roy.Soc. A 307, 15 (1968)

4) R. Botter, H.M. Rosenstock, Adv. Mass Spec. 4, 579 (1968)
Int.Conf. Mass Spectrometry, Berlin 1967

5) R.G. Parr: "The Quantum Theory of Molecular Electronic Structure."
P. 32, W.A. Benjamin, Inc., New York, Amsterdam 1963

6) D.W. Turner, C. Baker, A.D. Baker, C.R. Brundle: "Molecular Photoelectron Spectroscopy." P. 9, Wiley-Interscience, John Wiley & Sons Ltd., London, New York, Sydney, Toronto 1970

F1

A Multipurpose Computer Interface for High Resolution Mass Spectrometry.

R. P. PAGE and A. V. NOWAK, Atlantic Richfield Company, Harvey Technical Center, Harvey, Illinois 60426

A computer interface for real time acquisition of either electron multiplier signals, or signals from a photoplate reader is described. Although integrated into a non-dedicated laboratory computer system centered around an IBM 1800 computer with 32K of core memory and 3 disk packs, the interface is not dependent on a particular computer (within speed and memory requirements) and, in fact, the general design philosophy is such that subsystems or components may be substituted depending on the requirements of a particular spectrometer or computer. External logic circuitry encodes and switches amplitude and timing information into a single digital channel so that these data can be stored in the correct sequence. This is very economical of computer time and storage and permits all other laboratory instruments, on the system, to be operated simultaneously with the spectrometer. A crystal controlled oscillator and frequency divider trigger a high speed 14 bit plus a sign analog-to-digital converter with a sample and hold amplifier at rates from 312 to 80,000 samples per second for acquisition of electron multiplier signals. For the photoplate reader, triggering is provided at 0.5 micron intervals by a shaft encoder.

F2

THE APPLICATION OF A GC-MS-COMPUTER SYSTEM AND VARIOUS INTERPRETIVE PROGRAMS TO PROBLEMS IN NATURAL PRODUCTS CHEMISTRY

J.E. Biller, H.S. Hertz and K. Biemann

Department of Chemistry
Massachusetts Institute of Technology
Cambridge, Massachusetts 02139

As previously described,[1] the Gas Chromatograph-Low Resolution Mass Spectrometer-Computer System developed in this laboratory is designed for continuously scanning and recording approximately 400 spectra obtained from a GC effluent. Data is acquired during the up-scan portion of each 4 sec. cycle of the magnetic field. Peak centers and intensity data are determined in real time and the partially reduced data is transferred to disk during the collapse of the magnetic field. Background threshold is continuously updated by the software as the data is acquired. In this way the loss of sensitivity usually associated with arbitrarily set thresholds involved in hardware peak detection is avoided by more fully using the capabilities of the computer.

Presently the system consists of a Perkin-Elmer 990 gas chromatograph, an Hitachi-Perkin-Elmer RMU-6L single focusing mass spectrometer, and an IBM 1800 Data Acquisition and Control System using interface hardware and software developed in this laboratory. The 1800 is configured with 32K of core memory, a 3-drive 1810 disk system, two magnetic tape drives, high speed digital and analog input and output capabilities, a line printer, a console typewriter, and a digital plotter. An analog tape system has been interfaced to the computer and to the various low resolution instruments in the laboratory. This provides the capability for data to be acquired and saved for subsequent digitization and processing by the computer at a later time. Finally, the most recent addition is an oscilloscope-microfilming system designed in-house and to be described in this paper.

Improvements in the scanner circuitry to allow a more repetitive computer-controlled scan function and major changes in the software system have permitted faster and more efficient use of the facilities by the laboratory chemist. These faster programs have resulted in the increased use of the GC-MS-Computer system for problems in areas such as lunar crust analysis, carbohydrate chemistry, peptide sequencing, raw opium analysis (discussed below), analysis of drug abuse problems, geochemical analyses, and various other fields of organic and biochemical interest. With the large amounts of data now generated, it was realized that the limiting factor was the relatively slow speed of the output devices required to present the data to the chemist. Furthermore, it is desirable to make all of the data (not just the spectra) readily available to the chemist without requiring him to return to the computer for each additional piece of information. To meet these goals, a new and faster method of outputting data was sought. The microfilm system described below has efficiently solved these problems.

The microfilming system consists of a Tektronix 611 storage oscilloscope, a Bolex 16mm H16M5 Cine camera with a 10 mm Switar lens, and a single-framing control mechanism manufactured by Industrial Camera Company, Epsom, N.H. The plotting and filming are totally controlled by the computer via analog and digital output features. The computer can process and film a GC-MS run of 400 spectra in under 10 min. (including the time-to-mass conversion step). The film is immediately developed using a Kodak Prostar Processor and is thus available to the chemist within a few minutes after filming is completed. The end result is a finished microfilm in a cartridge which can be viewed on the microfilm readers in this laboratory or in any modern library.

With such overwhelming volumes of data, the chemist has more need for interpretive programs to aid in the data analysis. Although programs are available for selecting the significant masses in a GC run,[2] it was found that with the rapid filming system, it is simpler and more advantageous to present all of the available data. Hence, not only spectra, but also mass chromatograms,[2] and more recently homologous series chromatograms[3] are filmed. Each mass and homologous series chromatogram is presented with the total ionization curve overplotted as a dashed line, so that one can easily determine the GC peak in which a feature is significant.

As a specific example of the use of the above techniques, as well as some of the other interpretive programs available in this laboratory, some results of an investigation of raw opium from various geographic origins using the GC-MS-Computer system described above are discussed. Figure 1A shows the total ionization plot obtained from a neutral extract of a sample of Turkish opium. Figure 1B shows the corresponding homologous series chromatogram for the series m/e = 60, 74, 88, ..., etc. (molecular ions of aliphatic esters and their McLafferty rearrangement). As opposed to mass

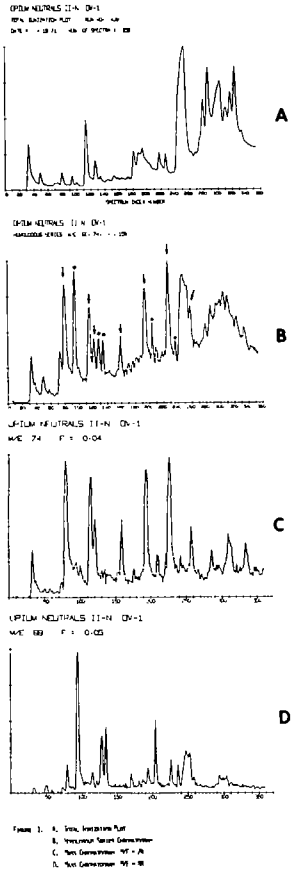

Figure 1. A. Total Ionization Plot
B. Fragmentogram Search Determination
C. Mass Determination m/e = 74
D. Mass Determination m/e = 88

REFERENCE INDEX NUMBER # 1090

ANALYSIS OF MIXED DRUGS BY MASS SPECTROMETRY
PART 3. ANALYSIS OF ANTIPYRINES. (2).
MASS SPECTRA OF MIXED ANTIPYRITES IN VARIOUS
PHARMACEUTICAL PREPARATIONS (JAPANESE)
TATEMATSU A.
GOTO I.
J. PHARM. SOC. JAPAN V.85 P.631 1965

SUBJECTS

BIOLOGICAL	720
COMPOUND IDENTIFICATION	1300
QUANTITATIVE ANALYSIS OF ORGANIC MIXTURES	6520
MASS SPECTRA	4440
LOW RESOLVING POWER DATA	4200

LITERATURE REFERENCE NUMBER= 1090
MOLECULAR WEIGHT 188 +
2,3-DIMETHYL-1-PHENYL-5-
PYRAZOLONE (ANTIPYRINE)
98D 133 135
C 11 H 12 N 2 O 1

Figure 2. Literature Search Output

ANTIPYRINE 4 22 71

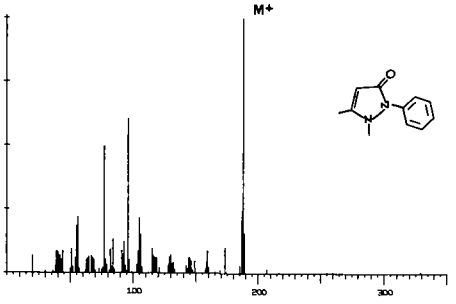

Figure 3. Mass Spectrum of Antipyrine

chromatograms, which plot one m/e value vs. scan index number, homologous series chromatograms plot the sum of the intensities of ions differing by 14 mass units vs. scan index numbers. Hence 14 homologous series chromatograms cover any range. Figure 1C shows the mass chromatogram for m/e = 74, which accounts for many of the peaks in Figure 1B (those denoted with arrows). Analysis of the spectra associated with these peaks indicated that they represent a homologous series of even carbon methyl esters, starting with C_{16} at scan number 81. The "doublet" at scans 115 and 121 correspond to two C_{18} methyl esters, the former being unsaturated. The remaining peaks in Figure 1B (denoted by asterisks) are accounted for in the next mass chromatogram in this homologous series. Figure 1D shows the mass chromatogram for m/e = 88. The spectra corresponding to these peaks fall into two categories. Those peaks which correspond to the asterisks in Figure 1B are a series of even carbon ethyl esters, starting with C_{16} at scan number 95. The "doublet" at C_{18} again corresponds to the unsaturated and saturated esters, respectively. These compounds were identified from analysis of the spectra and the presence of M-45 ions clearly eliminated the possibility of α-methyl methyl esters (which also would show an m/e = 88 ion). The second series of peaks in the m/e = 88 mass chromatogram are from the methyl ester GC peaks discussed above and represent the isotope peak for m/e = 87, the second most intense ion in fatty acid methyl ester spectra.

Another interesting sample of opium, obtained from a different area in Asia, showed chemical and gas chromatographic properties quite different from the other samples analyzed. The gas chromatogram indicated an overwhelming preponderance of one compound, not found in any of the other samples. Comparison of the spectrum of this compound to the computerized collection of 8000 spectra[4] yielded no finds. The absence of even a similar compound in the collection suggested that the compound in question was quite uncommon. High resolution analysis of the total opium extract gave the composition $C_{11}H_{12}N_2O$ for the apparent molecular ion at m/e = 188. Using this formula as input to the computerized literature search routine,[5] three references were obtained. The article shown in Figure 2, the most intriguing of these references, and of immediate interest because it deals with drugs was examined first. The unknown spectrum (Figure 3) agreed with the spectrum of Antipyrine shown in the article. Antipyrine, as its name implies, is an antipyretic agent still used outside the United States but rarely prescribed in this country due to its adverse and cumulative side effects. The presence of such a large amount of this synthetic drug in raw opium is an obvious attempt at cutting. Its presence in the opium was subsequently unambiguously confirmed by comparison of the gas chromatographic and mass spectrometric data with those obtained on an authentic sample of Antipyrine.

From the examples presented one can see the advantages of presenting as much data as possible to the chemist immediately, thus eliminating the constant need for access to the computer (including the time lost waiting for the computer) for each additional piece of information. With previous data output methods the time involved in presenting this amount of data was prohibitive and therefore the chemist had to choose which data he wanted before having adequate information on which to base this decision. With the microfilm system described in this paper, the chemist obtains all the spectra plus the results of various interpretive aids (i.e. mass and homologous series chromatograms) in less time than previously required for the printing of just the spectra. Furthermore, with the literature and spectra data bases as well as other computerized interpretive techniques now more readily available to him, the chemist can more efficiently use the data rather than spending his time deciding which data to obtain.

References

1. R.A. Hites and K. Biemann, Anal. Chem., 40, 1217 (1968).

2. R.A. Hites and K. Biemann, Anal. Chem., 42, 855 (1970).

3. R.C. Murphy, Ph.D. Thesis, Massachusetts Institute of Technology, September 1970.

4. H.S. Hertz, R.A. Hites and K. Biemann, Anal. Chem., 43, 681 (1971).

5. H.S. Hertz, D.A. Evans and K. Biemann, Org. Mass Spectrom., 4, 453 (1970).

A COMBINED HIGH AND LOW RESOLUTION DATA SYSTEM FOR GC-MS APPLICATIONS

P. Powers and M.J. Wallington
AEI Scientific Apparatus Limited
Manchester, England.

INTRODUCTION

The evolution of mass spectrometers specifically designed both for high and low resolution GC, has led to a requirement for an appropriate data system to accept and process the wide variety of information available. Five of the most important features for such a system are the ease of operation, the provision of adequate spectrum storage, the ability to change from high resolution to low or vice versa in a short period of time, the ability to start collecting data for a spectrum soon after the previous one, and the provision of comprehensive background subtraction facilities. This paper describes the DS30 Data System which was designed for this work and illustrates its use in two specific analyses.

Figure 1 shows schematically the hardware configuration of the DS30 System. It is designed so that it may be extended to accommodate other techniques such as electron spectroscopy or inorganic spark source mass spectroscopy as well as to provide multi-mass spectrometer access; software for these other techniques can be stored on the disk at the same time as the DS30 software. Signals from up to four mass spectrometers can be fed sequentially either on line or by way of an intermediate analogue magnetic tape recorder to the computer itself. The standard peripherals connected to the system are a teletype, high speed reader and punch, and disk store. This disk store can have a storage capacity of between 64K and 256K words. With the latter, there is sufficient storage for over 300 spectra, each of 100 peaks. Under GC conditions where repetitive scanning may yield many background spectra containing few peaks, total spectral storage capacity is, of course, much higher. Additional peripherals available include a digital plotter, fast printer and digital tape for dumping of output reports in IBM compatible form.

OPERATION

From the user's viewpoint operation is extremely simple. A total of 16 fundamental commands (see Figure 2) is provided, most of which are applicable to both high and low resolution. Once a command has been given the system prompts the operator for the remaining required information. Indeed at places like the initial command mode, where a number of alternatives exist, it can reproduce all the available choices.

The symbol L.← indicates that the data system is in the mode to accept commands for low resolution operation. An example is shown in Figure 2. Typing the RETURN key at that point caused the data system to reproduce all the basic command information shown there. These commands provide for:

Acceptance of data from the mass spectrometer,
Calibration of the mass spectrometer with a reference compound,
Conversion of peak times to exact mass,
Subtraction of background spectra,
Printing reports of mass, intensity and elemental composition,
Plotting the spectra on a plotter, line printer or teletype,
Setting up the system and the interface,
Reporting detailed information on scans already obtained,
Scan data deletion and reference data handling,
System utility programs.

An examination of the command TUNE in more detail shows the adaptability of the system to different instrumental conditions, see Figure 3. After the command TUNE has been typed in, with the data system in the low resolution command mode, a back arrow is automatically printed. If operator prompting is required the teletype RETURN key is hit whereupon a complete list of all available TUNE commands is printed. Two letter commands can now be typed and the response obtained by pressing the SLASH (/) key. For example typing RF/ causes the system to respond with L so showing that the system is in the low resolution mode; by typing H followed by the RETURN key the resolution mode will be changed from low to high. Thus the operation of changing from low to high resolution mode or vice versa takes

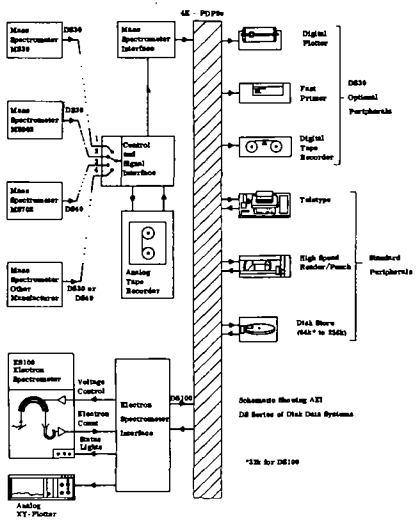

FIGURE 1

```
L.←
TYPE: FOR
MRUN  MASS SPEC RUN
CALB  REFERENCE CALIBRATION
IDEN  MASS IDENTIFICATION
SUBT  BACKGROUND SUBTRACTION
QUAN  QUANTITATIVE SPECTRUM
ATOM  ATOMIC COMPOSITION
PLOT  PLOTTED SPECTRUM
HIST  HISTOGRAM
TUNE  INTERFACE AND PROGRAM TUNING
LIST  DIRECTORY AND DATA LISTS
DELT  SCAN DATA DELETION
FILE  REFERENCE FILE HANDLER
USE   DISC STORAGE USAGE
EXIT  SERF EXIT
BACK  SCAN DATA BACKUP
RENT  SCAN DATA RE-ENTRY
```

FIGURE 2

```
L.←TUNE

←_
SL=SCAN LENGTH
PW=PEAK WIDTH
MT=MULTIPLET THRESHOLD
HR=HRP REFERENCE TOL.
MR=MISSED REFS.
HE=HRP EXCEPTION TOL.
LD=LRP DEFECT TOL.
LI=LRP INTENSITY TOL.
LM=LRP MATCH TOL.
HG=HRP GO REPORT
LG=LRP GO REPORT
RF=RESOLUTION FLAG
SI=SUBTRACTION INTENSITY
SR=SUBTRACTION RATIO
GM=HIST. GO MASS
GS=HIST. GO SCALE
IT=INTERFACE TIMING
IN=INTERFACE NOISE
IG=INTERFACE GAIN

-RF/L    H
-MR/3
-HG/F,T,M,PT,IN,%N,%I,RP      M,%N
-LG/N,%R,NN,HM
-SI/1
-LI/ .0348
-_

H.←
```

FIGURE 3

```
L.-Q
NAME:-STEROID.3
UPDATE RUN TITLES?-N


QUANTITATIVE REPORT

DEVICE: T
TYPE: G
INTENSITY LOWER LIMIT:10
MASS LIMITS: UPPER-300 LOWER-108
STEROID . 3

NO. PEAKS:  114
BASE PEAK INT.:   1117
TOTAL ION CURRENT:   14191
MASS LIMITS: UPPER- 429 LOWER-  28
NO. HALF MASSES:

  NOMINAL     % INT.
    MASS       BASE

    281       18.6
    275       13.6
    274       67.8   <--
    259       13.6
    233       25.6
    218       14.9
    217       12.3
    208       28.2
    207      100.    <--
    203       13.5
    164       10.2
    161       19.5
    149       22.7
    148       17.9
    147       18.7
    135       10.4
    133       18.2
    123       11.9
    122       19.3
    121       13.8
    110       16.8
    109       54.6
    108       25.8
    107       12.5
LIMIT OF DATA
```

FIGURE 4

```
L.-SUBT
SAMP NAME:-STEROID.3
BACK NAME:-STEROID.2


SUBT NAME:-STER3M2


NORM MASS: 207
MASS RANGE - UPPER: 300
LOWER: 50

STER3M2 .0
 SAMP/BACK NORMALIZATION: 103%
 SAMP/BACK T.I.C: 257%
 NEGATIVE PEAKS: 13
```

FIGURE 5

```
L.-HIST
NAME:-STER3M2
UPDATE RUN TITLES?-N

HISTOGRAM REPORT

DEVICE: T
TYPE: S
MASS LIMITS: UPPER- 298
LOWER- 150
SCALE: 5
GAIN:
STER3M2 .0
```

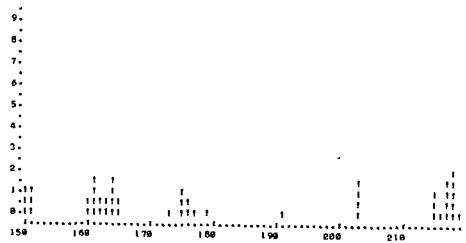

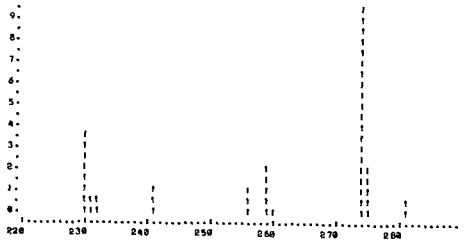

FIGURE 6

only a matter of seconds. In a similar manner many other parameters, such as the number of permissable missed references in the calibration procedure (MR/), can be examined and if necessary reset.

It is also possible for the operator to choose what information is to be printed. The choice can be selected at the time the report is requested or to save time on repetitive reports, a group of codes can be pre-set in the TUNE program allowing the operator to specify the information to be printed under the so-called 'GO' report. There is a set of GO parameters for both high and low resolution. The parameters for the high resolution 'GO' report are selected by typing HG/ and the system responds with a series of codes which indicate in this case (see Figure 3) that the report to be printed for high resolution would be formatted (paginated), include centroid times, exact masses, numbers of points in the peak, absolute intensity, intensities relative to the non-reference base peak, intensities relative to total ionisation, and reference peaks. The underlined user entry at this point indicates that a change to this list was made to make the report simply contain a list of exact masses and intensities relative to the non-reference base peak. Notice that this report is now unformatted. Similarly, the low resolution 'GO' report is set to contain masses, intensities relative to the base peak, an indication that the masses are to be printed as nominal masses rather than as measured mass and to print out any half masses detected.

EXAMPLES OF THE USE OF DS30

The facility for rapid, accurate subtraction of background spectra and indeed of other spectra of any sort from any given spectrum is very important for any data system being used with GC.

An example of the facilities now available with the DS30 is illustrated by the analysis of a sample of a C_{19} steroidal ketone on an MS30 Mass Spectrometer. The sample was run at 1000 resolution with 60 ng injected onto the column. Scans were made at 1 sec/decade on both the peak and the background and the results were processed by the data system. Taking into account the separator efficiency, column conditions and scan speed the amount of sample consumed over one decade was one nanogram.

Figure 4 shows the use of the 'GO' report to obtain a fingerprint spectrum from the composite spectrum which includes the background. The main intent here was to examine the relative intensities of the sample base peak and the column bleed peak at mass 207. Because of the small sample size the 207 peak, which is due to the silicone stationary phase, was the base peak of the resultant spectrum; in contrast the parent ion at mass 274 was 67.8%. Figure 5 shows how the data system was set up to perform the background subtraction. The command SUBT was entered and the names of the sample and background spectra entered via the teletype; a name was then entered for the spectrum to be created from the subtraction process. The data system then requested a normalisation mass. Here the operator specifies a mass number which comes only from the background spectrum and which can therefore be used to allow the background spectrum as a whole to be normalised such that the peak in question is of the same intensity in both spectra. This ensures that on subtraction the peaks of the background will be properly subtracted from the composite spectrum and that a minimum of residual background peaks will be obtained.

Finally the operator can specify the mass range over which this process of subtraction is to be carried out. The data system responds with the name of the compound file and with some parameters connected with the subtraction process. Parameters are built into the system (pre-set under TUNE) which allow the operator to prevent the subtraction process from proceeding if the ratio of peak heights of the normalising mass in the two spectra is outside the user-specified range or indeed if the ratio of total ion current in the two spectra is widely different. Any peaks which go negative on subtraction are retained as such and can be printed out if required. In the summary only the total number of negative peaks is printed out for guidance of the operator.

Figure 6 shows the resultant subtracted spectrum as presented using the histogram output available on either the line printer or the teletype. In this case the output has been produced on the teletype. Notice that mass 274 is now the base peak, that the peaks at mass 207 and 208 have now been eliminated, and 281 is now reduced in intensity.

An example of the need for quick turn-round between consecutive spectra which also exemplifies the use of the subtraction facility, is the separation of GC multiplets. Figure 7 shows the output from a chromatograph of a mixture of amyl acetate, which is eluted first, followed by methyl amyl ketone. This mixture was run through the MS30 GC system and scans taken on the left hand edge of the doublet (to give a spectrum essentially of amyl acetate) and on the shoulder. The reset time of the data system between the two scans was approximately five seconds. The scans themselves were 3 sec/decade at 1000 resolution and the results after subtraction are shown in Figure 8. The upper trace shows the histogram output of part of the scan made on the shoulder of the doublet i.e., a scan made up of amyl acetate and methyl amyl ketone as a mixture. The scan at the bottom of the figure represents the same part of the resultant spectrum after subtraction in which the characteristic spectrum of methyl amyl ketone is dominant. Notice particularly that the typical peaks of amyl acetate are absent from this spectrum. The peaks in the plot of the two spectra have been magnified by a factor of 10 from mass 80 and above.

MONITOR TRACE FROM 0.1µl MIXTURE OF AMYL ACETATE AND METHYL AMYL KETONE
10% SILICONE OIL COLUMN AT 125°

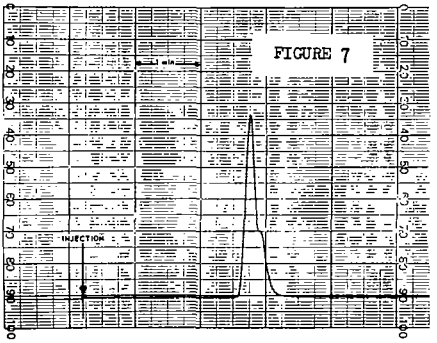

FIGURE 7

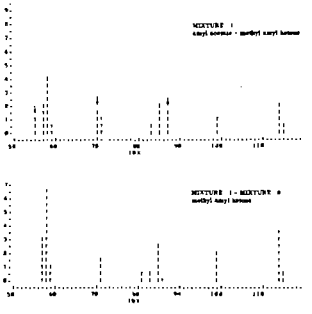

FIGURE 8

F4

A Time-Shared Computer System for the Mass Spectrometry Laboratory.[1,2]

R. N. Stillwell, J. G. Leferink, N. R. Earle,

and L. S. Washco

Institute for Lipid Research, Baylor College
of Medicine, Houston, Texas 77025

A small computer (DEC PDP 8/I, 4K) is used as a time-shared message switching and data preprocessing unit interfaced[3] to an IBM 360/50 computer, which itself operates in a time-shared environment. A photoplate comparator, an LKB 9000 low resolution mass spectrometer, an incremental plotter, teletype terminals, and a dataphone are in turn interfaced to the PDP 8/I. All hardware functions, including the comparator shaft encoder, the LKB mass marker, and a hardware peak detector connected to the analog output of the LKB, are interfaced to the program interrupt facility of the PDP 8/I. About 2.2K of core in the PDP 8/I is used for buffers, which are allocated as needed in 64-word segments. The PDP 8/I program is concerned only with the allocation, deallocation, filling, emptying, and switching of buffers. The 360/50 program, which runs under the Baylor teleprocessing system, transfers data between the PDP 8/I and disk storage, and can also invoke certain applications programs (e.g. plot generation). Other programs can be executed independently from remote 360/50 terminals as teleprocessing programs or as batch programs by remote job entry.

[1] This work was supported by NIH grants GM 13901 and RR 00259.

[2] The cooperation and assistance of Dr. Allan H. Levy and Bill Hobbs, of the Institute of Computer Science is gratefully acknowledged.

[3] From circuit diagrams kindly supplied by Mr. Lee Hundley of the ACME group, Stanford University.

Mass Spectrometric Characterization of Aminocyclitol Antibiotics

F5

KENNETH L. RINEHART, JR., PHILLIP SCHAEFER, and J. CARTER COOK

Department of Chemistry
University of Illinois, Urbana, Ill. 61801

CARL P. SCHAFFNER and ALLAN KERSHNER

Institute of Microbiology
Rutgers University, New Brunswick, N.J. 08903

Although the aminocyclitol antibiotics are relatively non-volatile their trimethylsilyl derivatives pass through a gas chromatograph[1] and can be studied by the combined gc-ms procedure. Other useful mass spectrometric techniques for studying the aminocyclitol antibiotics include high resolution and metastable defocusing. All of these procedures have been employed in studying the neomycins, the gentamicins, and compounds related to them; applications will be described. Of particular note is the assignment of structure from its mass spectrum alone to a new component of the medically important gentamicin complex,[2] gentamicin C_{2a}, isolated by countercurrent distribution.

[1] K. Tsuji and J. H. Robertson, Anal. Chem., 41, 1332 (1969).

[2] D. J. Cooper, H. M. Marigliano, M. D. Yudis, and T. Traubel, J. Infect. Dis., 119, 342 (1969).

F6

A Gas Chromatographic-Mass Spectrometric Investigation of the Alkaloids Found in Single Seeds of *Ormosia paraensis* and *O. tovarensis*

WOODFIN V. LIGON, JR., and KENNETH L. RINEHART, JR.

Department of Chemistry
University of Illinois, Urbana, Ill. 61801

Crude basic extracts obtained from single seeds of *Ormosia paraensis* and *O. tovarensis* have been examined using the combined techniques of gas chromatography and mass spectrometry. The alkaloids isoangustifoline, angustifoline, lupanine, ormosanine, dasycarpine, costulamine (or dihydroormojanine), ormosajine, ormojanine, and 13-hydroxylupanine have been found to be present in both species. The alkaloids were identified by comparison of retention times and mass spectra with those of pure samples. Although dihydroormojanine, costulamine, and dasycarpine cannot be resolved on the gas chromatographic column used, by employing a technique of rapid repetitive scanning of the parent ion region followed by plotting of the intensities of the individual parent ions versus time, the overlapping peaks have been deconvoluted to show that both species contain costulamine or dihydroormojanine ($P^{\cdot+}$ = 315) as well as dasycarpine ($P^{\cdot+}$ = 317).

F7

Gas Chromatography and Mass Spectrometry of the *Erythrina* Alkaloids and Their Trimethylsilyl Derivatives

DAVID S. MILLINGTON and KENNETH L. RINEHART, JR.

Department of Chemistry
University of Illinois, Urbana, Ill. 61801

Using a gas chromatograph in tandem with a low-resolution mass spectrometer, a method has been developed for the routine analysis of *Erythrina* alkaloids.[1] The crude alkaloid mixtures are first treated with bis(trimethylsilyl)acetamide to afford volatile derivatives of the hydroxylic components and then injected onto a glass column (6' x 2mm I.D.) containing 3% OV-17 on Gaschrom Q. The gc-ms system is operated on-line with a computer, the mass spectrometer scanning continuously at one second per decade over a preselected mass range, with each spectrum recorded on magnetic tape. Desired spectra are printed by an electrostatic recorder in bar-graph form, after the computer has subtracted background ions and corrected the spectra for changes in total ionization during the scan. The mass spectral fragmentations of the trimethylsilyl derivatives yield valuable information on their structures and six new alkaloids, two from *E. folkersii* and four from *E. mexicana*, have been identified. Isolation and further studies on these compounds have confirmed the structures deduced from their mass spectra.

[1] R. K. Hill, in "The Alkaloids," Vol. 9, R. H. F. Manske and H. L. Holmes, eds., Academic Press, New York, 1967, p. 483.

THE MASS SPECTRA OF TRIMETHYLSILYL DERIVATIVES OF SOME 6-ACID SUBSTITUTED PTERIDINES

F8

Jim Serum and Pat Haug

Department of Chemistry, Rice University, Houston, Texas 77001

Toshiyuki Urushibara and Hugh S. Forrest

Department of Zoology, University of Texas, Austin, Texas 78712

INTRODUCTION

In the last two years considerable interest has been shown in the mass spectra of pteridines.[1-2] Most of the naturally occurring species have an amino group in the 2-position and a hydroxy group in the 4-position (I), although series of 2,4,7-trihydroxy species (II) have also recently been found to occur naturally. In the 2-amino - 4-hydroxy series, fragmentation is characterized by successive loss of carbon monoxide and hydrogen cyanide. The dimethylpteridine of course loses methyl cyanide. Correspondingly, in the trihydroxy series, one sees loss of HOCN to give m/e 137, followed by loss of carbon monoxide to give m/e 109 which can either lose hydrogen cyanide to go to m/e 82 or another carbon monoxide to go to m/e 81. The propyl substituted pteridine does not give a large molecular ion, as a result of the loss of ethylene via a six membered intermediate.

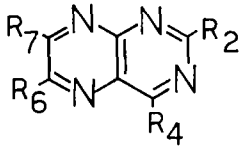

TMS = $Si(CH_3)_3$

I. $R_2 = NH_2$; $R_4 = OH$ 2-Amino-4-hydroxy pteridine series

II. $R_2 = R_4 = R_7 = OH$ 2,4,7-Trihydroxypteridine series

III. $R_2 = NHTMS$; $R_4 = OTMS$; $R_6 = SO_3TMS$; $R_7 = H$

IV. $R_2 = R_4 = OTMS$; $R_6 = SO_3TMS$; $R_7 = H$

V. $R_2 = NHTMS$; $R_4 = OTMS$; $R_6 = CH_2OPO_3(TMS)_2$; $R_7 = H$

VI. $R_2 = NHTMS$; $R_4 = OTMS$; $R_6 = -CH(TMSO)-CH(OTMS)-CH_2O\,PO_3(TMS)_2$; $R_7 = H$

DISCUSSION

Because most of the larger compounds with acid substituents could not be vaporized at temperatures under 350° above which they decomposed, we undertook the trimethyl silylation of these compounds by reacting in a capillary about 20 ug of pteridine, 10 ul BSA (N,O-bis(trimethylsilyl)acetamide) and 1 ul TMCS (trimethylchlorosilane) at 60° for 15 minutes. These derivatives could be volatilized at temperatures ranging from 150° - 275°. GCMS were possible on a 3% SE column, 10' long by 1/4" at 230° with retention

times ranging from 3-20 minutes.

The mass spectra of the trimethylsilyl derivatives of the 2-amino-4-hydroxy and 2,4,7-trihydroxy- compounds exhibited large molecular ions as well as fragments at M-15, m/e 147 [$(CH_3)_2Si = \overset{+}{O}Si(CH_3)_3$]; m/e 75 [$H\overset{+}{O} = Si(CH_3)_2$]; and m/e 73 [$Si(CH_3)_3]^+$.

Unfortunately, in a series of four acids recently studied, none of the unsilylated derivatives could be volatilized. The mass spectra of the silylated compounds were obtained at a source temperature of 300^0 and an ionizing current of 100 μ amps. Considerable difficulty was encountered in obtaining the spectra of these compounds. A number of spectra at lower temperatures showed no molecular ions. No molecular ion for 2-amino-4-hydroxy-6-hydroxymethyl phosphate (V) has been detected, although if the right conditions could be found it is expected that a molecular ion would be detected.

The mass spectrum of the trimethylsilyl derivative of 2-amino-4-hydroxypteridine-6-sulfuric acid (III) shows a clear molecular ion corresponding to mass 459 and 2,4-dihydroxypteridine 6-sulfuric acid (IV) shows a molecular ion at m/e 460. The loss of the elements of HSO_2TMS yielded ions at mass 321 and 322 respectively. This species in the case of the dihydroxy compound (IV) shows further loss of a trimethylsilyl radical to yield a 249 ion. The corresponding fragmentation was not observed for the 2-amino-4-hydroxy compound (III). The ions at m/e 233 and 234 correspond to the loss of CH_3, TMS, and HSO_2TMS from the molecular ion. 2-Amino-4-hydroxy-6-(1', 2', 3'- D-erythro-trihydroxypropyl)-pteridine-3'-phosphate (VI) gave a clear molecular ion at m/e 765 and showed characteristic peaks at m/e 314 corresponding to $PO_4(TMS)_3$ and m/e 299 formed by the loss of an additional methyl radical. Although compound V gave no molecular ion, peaks at m/e 314 and 299 were dominant in its spectrum. Previous investigators have reported the observation of m/e 315 ions in mass spectra of trimethylsilyl-phosphate derivatives.[3,4,5] Recently, the molecular ion of $(TMS)_3\ PO_4(M^+ = 314)$ was reported to lose a methyl radical to give an ion at mass 299 as the base peak.[6] The probability that the 314 ion is not an artifact in our compounds is supported by the loss of 314 mass units from the molecular ion of IV to give the m/e 451 ion and the absence of a m/e 315 may be due to the lack of a rearrangeable hydrogen.

Compound VI exhibited simple cleavage between the two hydroxy substituents yielding ions at m/e 357 (charge retention on side chain) and m/e 408 (charge retention on ring fragment).

We are currently attempting to obtain methyl or acetate derivatives of the pteridine with the hope that these will yield more information.

ACKNOWLEDGEMENTS

The financial support of The Robert A. Welch Foundation is gratefully acknowledged. The CEC 21-110 B mass spectrometer was provided by funds from National Institute of Health and National Science Foundation.

REFERENCES

(1) P. Haug, Anal. Biochem, 37, 285 (1970).

(2) P. Haug, Org. Mass Spectrom., 3, 1365 (1970).

(3) J. H. Duncan, W. J. Lennarz, and C. Fenselau, Biochem, 10, 927 (1971).

(4) M. Zinbo, and W. R. Sherman, J. Amer. Chem. Soc., 92, 2105 (1970).

(5) J. A. McCloskey, A. M. Lawson, K. Tsuboyama, P. M. Krueger, and R. N. Stillwell, J. Amer. Chem. Soc., 90, 4182 (1968).

(6) W. C. Butts and W. T. Rainey, Jr., Anal. Chem., 43, 538 (1971).

INFRARED AND ULTRAVIOLET SPECTROSCOPIC STUDIES OF MOLECULAR IONS TRAPPED IN INERT SOLID MATRICES

G1

Dolphus E. Milligan and Marilyn E. Jacox
National Bureau of Standards, Washington, D. C. 20234

During the past twelve years, we have applied the matrix isolation technique to the study of the infrared and ultraviolet spectra of free radicals and other highly reactive reaction intermediates. These investigations have proved to be exceptionally fruitful; spectroscopic data have been obtained for over sixty diatomic and small polyatomic free radicals, and, in favorable circumstances, the data thus obtained have permitted inferences regarding the structure of these species, as well as computation of the vibrational contribution to the thermodynamic properties. About two years ago, we found that it is also possible to stabilize sufficient concentrations of charged species in the inert, nonionic environment of the rare-gas matrix for direct observation of their infrared and ultraviolet spectra. In turn, these data also have permitted inferences regarding the structures and vibrational contributions to the thermodynamic properties of these small molecular ions. Heretofore, data regarding the electronic and vibrational energy levels of charged species have been largely inaccessible. Of course, the spectra of various charged species in ionic crystal lattices and in polar solvents have often been studied. However, in these environments the energy levels are likely to be significantly perturbed. Only a few small positively charged species, including CO_2^+ and N_2O^+, have been amenable to gas-phase spectroscopic investigation. Prior to the matrix studies, virtually no spectroscopic data were available for negatively charged species in an inert, nonionic environment.

The matrix isolation technique involves the preparation of a mixture of the molecule of interest with a large excess of an inert diluent, followed by the freezing of this mixture onto a sample observation window at a temperature sufficiently low that molecular diffusion is inhibited and individual molecules are surrounded by matrix atoms or molecules. Generally a matrix material such as a rare gas or nitrogen is chosen, both because of its rigidity at cryogenic temperatures and because of its transparency in the infrared and ultraviolet spectral regions. The matrix material used for all of the experiments to receive subsequent discussion is argon. In experiments utilizing rare-gas matrices, the vibrational fundamentals generally appear within 5 or at most 10 cm^{-1} of the gas-phase band origins. The origin of an electronic transition may be shifted as much as a few hundred cm^{-1} from the gas-phase value, but the upper-state vibrational spacings, like those for the ground state, generally correspond closely with the gas-phase values. Because of the very low temperature, between 4 and 20°K, absorptions arising from thermally excited energy levels do not appear. Very little rotational structure is detectable; in an argon matrix, only the lowest rotational levels of a few simple hydride molecules have been observed. The structural information which can be derived from rotational separations is lost. However, because the infrared absorptions typically have half-widths less than about 5 cm^{-1}, it is often possible to resolve isotopic separations. Indeed, studies of the behavior of vibrational absorptions upon isotopic substitution are the key to the definitive identification of both free radicals and molecular ions in matrix-isolation experiments.

In many of our experiments, the molecule of interest is subjected to vacuum-ultraviolet photolysis, leading to photoionization or to the detachment of an atom or a molecule. If a molecule is detached, it cannot diffuse away, and, depending on the activation energy for recombination, may either remain trapped in a site adjacent to the reactive fragment or recombine to re-form the initial species. On the other hand, electrons or atoms may diffuse away from the site of their photoproduction, leaving a positively charged species or a molecular fragment trapped in the matrix. These electrons or atoms may interact with still other molecules trapped in the matrix, leading to the production of negatively charged species or of free radicals. Because the sample is exposed to the photolyzing radiation over an extended period of time, secondary photoprocesses generally also play an important role.

In other experiments, an atomic beam of an alkali metal is codeposited with the gas mixture of the molecule of interest in a large excess of argon. A number of molecules, including NO, NO_2, and SO_2, undergo strong charge-transfer interaction with the alkali metal atoms in the argon lattice, leading to the direct production of negatively charged species in sufficient concentration for spectroscopic study. Other molecules show only a weak charge-transfer interaction with alkali metal atoms, and negatively charged species result on exposure of the sample to radiation effective in photoionizing the alkali metal atoms.

For several years, a band system with origin near 5200 Å which appeared on trapping the products of a discharge through methane or the products of the vaporization of graphite in a rare-gas matrix was ascribed to the Swan system of triplet C_2. This assignment was, however, open to serious question; the absorption band separation was about

200 cm^{-1} greater, and the emission band separation about 150 cm^{-1} greater, than the separations observed for the gas-phase transition. Furthermore, subsequent to the initial assignment, gas-phase studies demonstrated that the ground state of C_2 is a singlet state some 610 cm^{-1} below the lower state of the triplet Swan transition. In an attempt to clarify the assignment, Milligan, Jacox, and Abouaf-Marguin[1] studied the infrared and visible-ultraviolet spectra of the products of the vacuum-ultraviolet photolysis of acetylene in an argon matrix. The appearance of prominent absorptions due to both the Phillips and the Mulliken systems of singlet C_2 demonstrated that the lowest singlet state remains the ground state in rare-gas matrices. However, the 5200-Å band system also appeared. Furthermore, studies on isotopically enriched acetylene samples demonstrated that this band system must arise from a species of formula C_2. It was suggested that, because vibronic interaction between the lowest singlet and triplet states is strongly forbidden, some triplet C_2 might possibly be stabilized in the matrix.

Subsequently, Herzberg and Lagerqvist[2] reported the detection in the spectra of transient products of a flash discharge through gaseous methane of a new band system with origin near 5400 Å and with upper- and lower-state vibrational spacings closely similar to those of the 5200-Å band system of the matrix experiments. Isotopic studies confirmed that this new band system was contributed by a species of formula C_2. Since it was not possible to find a pair of low-lying electronic states of C_2 which could account for the observed bands, Herzberg and Lagerqvist considered the possibility that the band system could be contributed by a charged species of formula C_2. Assignment to C_2^- was especially suitable. Furthermore, the electron affinity of C_2 was known to be appreciable, and supplementary mass-spectrometric studies demonstrated the presence of a significant concentration of C_2^- in the system. The only difficulty appeared to be the failure to detect a spin splitting. However, the high-J lines were significantly broadened.

The correspondence between the vibrational spacings of this new gas-phase transition and those of the matrix experiments suggested a new series of experiments in which a small concentration of an alkali metal was added to the $Ar:C_2H_2$ sample.[3] Upon vacuum-ultraviolet photolysis of the resulting deposit, the intensities of the singlet C_2 absorptions were markedly diminished, and the intensity of the 5200-Å band system was dramatically enhanced. Although the 5200-Å band system could be completely destroyed in the absence of an alkali metal by exposing the sample to 2000-3000-Å radiation, in the presence of an alkali metal the intensity of the band system was unchanged even upon prolonged exposure of the sample to radiation in this wavelength range. These results may be explained by noting that the alkali metal provides a source of photoelectrons which are captured by C_2, producing C_2^-. In the absence of a supplementary photoelectron source, exposure of the sample to 2000-3000-Å radiation results in photoelectron detachment from C_2^-, whereas in the presence of an alkali metal, a steady-state concentration of C_2^- is maintained. Recently, Frosch[4] has identified both the fluorescence emission corresponding to the Swan bands of C_2 and the C_2^- emission bands in $Ar:C_2H_2$ samples which have been exposed to x rays. All of these data have pointed to the conclusion that the 5200-Å band system is indeed contributed by C_2^- and that charged species may be trapped in rare-gas matrices in sufficient concentration for direct spectroscopic detection. Furthermore, the demonstration that the alkali metal atoms are a suitable source of photoelectrons for matrix-isolation experiments has provided a technique useful for the stabilization of still other negatively charged species.

In studies of the vacuum-ultraviolet photolysis of NO_2 in an argon matrix[5], a prominent, unexplained product absorption appeared at 1244 cm^{-1}. Following the discovery that charged species may be stabilized in an argon matrix, we noted that the energy provided by the photolysis lamp was in excess of 9.8 eV, the ionization potential of NO_2. Thus, we came to suspect that photoionization and electron capture processes might also occur in this system. Further experiments showed that the 1244-cm^{-1} peak also appeared in $Ar:NO_2$ samples which had been subjected to electron bombardment, as well as in $Ar:NO_2$ samples which were codeposited with an atomic beam of an alkali metal. In the alkali-metal experiments, the absorption tentatively attributed to NO_2^- appeared in the initial deposit, suggesting the occurrence of strong charge-transfer interaction between the alkali metal atoms and NO_2. Isotopic substitution studies confirmed the assignment of the 1244-cm^{-1} absorption to the antisymmetric stretching absorption of NO_2^- and indicated that the valence angle of this species is close to 115°, the valence angle found for NO_2^- in an ionic crystal lattice. However, the absorption frequency is decreased by 31 cm^{-1} in going from a KBr lattice[6] to the inert, nonionic environment of the argon matrix. In the presence of an alkali metal, other absorptions also appear somewhat to the red of the 1244-cm^{-1} absorption of isolated NO_2^-. These absorptions may be assigned to $M^+\cdots NO_2^-$ and $M_2^+\cdots NO_2^-$ ion pairs.[7]

Similarly, $Ar:SO_2$ samples which are codeposited with an alkali metal show new absorptions near 496, 985, and 1042 cm^{-1} which isotopic substitution studies have demonstrated to be contributed by the three vibrational fundamentals of SO_2^-, produced by strong charge-transfer interaction between the alkali metal and SO_2.[8] Consistent with the relatively small electron affinity of SO_2, no absorptions due to isolated SO_2^- have been

identified; all of the SO_2^- absorptions are somewhat dependent on the alkali metal used in the experiment. When cesium is used, the isotopic data can be fitted to a three-constant vibrational potential function with no frequency deviating by more than 1 cm^{-1} (the experimental error typical of the observations) for a valence angle of $110^o \pm 5^o$, without taking into account the participation of Cs^+ in the vibrations. Simple molecular orbital theory predicts that the addition of an electron to SO_2 should lead to a decrease in the valence angle and to a weakening of the S-O bonds. Whereas the valence angle of ground-state SO_2 is 119.5^o, that found for SO_2^- is approximately 110^o. The S-O stretching force constant, an approximate measure of the strength of the S-O bonds, decreases from a value of 10.2×10^2 N m^{-1} for SO_2 to a value of 6.4×10^2 N m^{-1} for SO_2^-.

In studies of the vacuum-ultraviolet photolysis of samples of approximately 1% HCl in an argon matrix, a prominent absorption appeared at 696 cm^{-1} and a weaker peak at 956 cm^{-1}, corresponding exactly in both position and contour with absorptions reported by Noble and Pimentel[9] in studies of the infrared spectra of Ar:HCl samples which were co-deposited with Ar:Cl_2 samples that had been passed through a glow discharge. These absorptions were most prominent in in experiment in which the Cl_2 discharge was only 3 cm from the cold sample window. Isotopic data were consistent with a linear, centrosymmetric molecule possessing two chlorine atoms and one hydrogen atom. The possibility that the species was the $ClHCl^-$ anion, rather than the ClHCl free radical postulated by Noble and Pimentel, was suggested both by the conditions under which the highest yield was obtained and by the similarity between the spectrum and that reported for the $ClHCl^-$ anion in a relatively symmetric crystal environment. When an Ar:HCl sample was codeposited with an atomic beam of an alkali metal,[10] a pattern of new absorptions appeared in the 700-1000-cm^{-1} spectral range, and, upon exposure of the sample to the radiation of a medium-pressure mercury arc, very prominent absorptions appeared at 696 and at 956 cm^{-1}, once again with contours identical to those observed in the discharge experiments. It was concluded that these two absorptions are indeed contributed by the $ClHCl^-$ anion, formed both by the interaction of Cl^- with HCl and by dissociative electron attachment to $(HCl)_2$ aggregates in the argon matrix. Recently, the corresponding vibrational absorptions of $BrHBr^-$ have also been identified at 728 and at 892 cm^{-1} in parallel studies of the vacuum-ultraviolet photolysis of relatively concentrated samples of HBr in an argon matrix and in studies of the interaction of alkali metals with HBr in an argon matrix.[11] A detailed study of the new absorptions characteristic of unirradiated deposits of HBr together with an alkali metal in an argon matrix indicates that strong charge-transfer interaction leads to the formation of $M^+ \cdots XHX^-$ ion pairs in the initial deposit, and that the mercury-arc radiation facilitates the migration or reorientation of M^+ in the argon lattice, resulting in the appearance of relatively sharp absorptions due to XHX^- anions unperturbed by the presence of a nearby cation.

When chloroform isolated in an argon or a nitrogen matrix is subjected to photolysis by 1216-Å radiation, a very prominent absorption due to CCl_3 appears.[12,13] In the argon-matrix experiments, other unidentified product absorptions are also present. Since the ionization potential of CCl_3 is 8.8 eV and that of $HCCl_2$, a minor product in this system, is 9.3 eV, well below the 10.2-eV output of the hydrogen discharge lamp, photoionization of these two radicals is possible. Simple molecular orbital theory predicts that CCl_3^+ and $HCCl_2^+$ should be planar, with C-Cl bonds somewhat stronger than those characteristic of the neutral radicals. A prominent absorption at 1037 cm^{-1} has the expected position, carbon-13 shift, and chlorine-isotopic splitting for the degenerate stretching fundamental of CCl_3^+ with planar threefold symmetry.

If indeed this absorption is contributed by CCl_3^+, one might expect electron capture processes also to occur, leading to the stabilization of negatively charged species which preserve the overall charge neutrality of the sample. Thus, experiments in which Ar:$HCCl_3$ samples were codeposited with an atomic beam of an alkali metal were suggested. Although the infrared spectrum of the resulting sample was identical to that characteristic of Ar:$HCCl_3$ samples deposited without the alkali metal, upon exposure of samples containing an alkali metal to mercury-arc radiation five prominent new absorptions appeared, with contours and positions identical to those of the remaining unexplained absorptions in the vacuum-ultraviolet photolysis experiments. Four of these absorptions, at approximately 840, 1270, 2500, and 2720 cm^{-1}, behaved appropriately in isotopic substitution experiments for assignment to $HCCl_2^-$. The fifth, at 705 cm^{-1}, must be assigned to another product. Tentatively, it has been suggested that this product may be $HCCl_3^-$, known from gas-phase studies to have only a very shallow potential minimum.

In experiments in which Ar:$HCCl_3$ samples were photolyzed by the 1067-Å argon resonance line, the CCl_3 absorption did not appear, but two absorptions previously assigned to $HCCl_2$ were moderately prominent. Instead of the 1037-cm^{-1} peak, there appeared an absorption at 1038 cm^{-1} with a chlorine-isotopic splitting characteristic of a molecule possessing only two chlorine atoms. This absorption, as well as another peak at 1290 cm^{-1}, shifted greatly in experiments on $DCCl_3$, requiring the presence of a hydrogen atom in the molecule. The assignment of these two peaks to the two nontotally symmetric fundamentals of $HCCl_2^+$ has received further support from studies on carbon-13 enriched chlo-

roform samples.

In gas-phase studies of the interaction between low-energy electrons and chloroform, Cl^- is detected, and it is inferred that $HCCl_2$ is also produced. Thus, the influence of the rigid lattice must be considered in the matrix experiments to account for the stabilization of an appreciable concentration of $HCCl_3^-$, rather than of $HCCl_2$. It is believed that electrostatic interactions between Cl^- and $HCCl_2$ trapped in adjacent sites in the lattice inhibit diffusion of Cl^-. Since Cl atoms should be much less strongly polarizable than $HCCl_2$ radicals, the decomposition of $HCCl_3^-$ into Cl + $HCCl_2^-$, with subsequent diffusion of the Cl atom, would be expected to be less strongly inhibited by the argon lattice.

Studies of the interaction of low-energy electrons with matrix-isolated $HCCl_2F$ and $HCClF_2$ have also been conducted, but analysis of the data is not yet complete. In both of these systems, several absorptions which can be assigned to each of two negatively charged product species have been obtained. There is reason to believe that one of these species is the parent molecule, bearing a negative charge, and that the other negatively charged species is derived from this first species by detachment of a chlorine atom.

Upon codeposition of an alkali metal atomic beam with NO in an argon matrix, a new absorption appears between 1350 and 1375 cm^{-1}, depending on the alkali metal used in the experiment.[7] Isotopic studies are consistent with the presence of a single nitrogen atom and a single oxygen atom in the species responsible for this absorption. It is suggested that the absorption results from the NO^- stretching vibration of $M^+\cdots NO^-$ or $M_2^+\cdots NO^-$ formed by strong charge-transfer interaction between the alkali metal and NO in the argon matrix. Further support for this assignment is obtained from the recent determination of a value of 1355 cm^{-1} for the first vibrational separation of NO^- in the gas-phase studies by Spence and Schulz[14] of the elastic scattering of low-energy electrons from NO.

When N_2O is codeposited with an atomic beam of an alkali metal in an argon matrix,[7] the infrared spectrum of the resulting deposit is found to be unperturbed by the presence of the alkali metal. In the absence of the alkali metal, irradiation of the sample by the full light of a medium-pressure mercury arc leaves the infrared spectrum of the sample unchanged. However, after a short period of irradiation of a sample containing an alkali metal a new absorption appears at 1205 cm^{-1}, and a diminution in the N_2O absorptions is noted. Upon prolonged irradiation of the sample, the 1205-cm^{-1} absorption disappears, the N_2O absorptions are greatly reduced in intensity, and absorptions due to $(NO)_2$ become prominent. Isotopic substitution studies require that the 1205-cm^{-1} absorption be assigned to an O-N-O antisymmetric stretching vibration. The gas-phase studies of the interaction of low-energy electrons with N_2O indicate that dissociative attachment, producing $N_2 + O^-$, occurs. Thus, it seems likely that the 1205-cm^{-1} absorption may be contributed by a product of the reaction of O^- with N_2O. The three most stable resonance structures for N_2O all have a residual positive charge on the central nitrogen atom, suggesting that O^- could attack N_2O at the central position, leading to an $O_2N{=}N^-$ structure.

In supplementary experiments, a small concentration of NO was added to the Ar:N_2O sample, which was codeposited with a sodium atomic beam. The $Na^+\cdots NO^-$ absorption appeared in the initial sample, and on irradiation of the sample with the full light of a medium-pressure mercury arc this absorption and those of N_2O diminished in intensity. Not only the 1205-cm^{-1} absorption but also the absorptions of isolated NO_2^- and of $Na^+\cdots NO_2^-$ grew in. These results also suggest the production of O^-, which may react with isolated NO to produce isolated NO_2^-. The decrease in the intensity of the $Na^+\cdots NO^-$ absorption may result from the reaction of this species with O atoms, produced by photoelectron detachment from O^-, to yield $Na^+\cdots NO_2^-$.

In summary, considerable data have been amassed supporting the infrared and, for C_2^-, the ultraviolet spectroscopic identification of a number of small molecular ions. Whereas the techniques employed in these experiments do not permit the direct detection of the electric charge, under favorable circumstances the isotopic data provide definite information concerning the chemical formula of the molecule, as well as semiquantitative data regarding its structure. When the spectrum of the corresponding neutral species is known, the presence of an auxiliary electron source strongly supports the assignment of the new absorptions to the anion. In the chloroform photolysis experiments, it has also been possible to identify positively charged product species. Accessibility of windowless discharge sources is expected to permit the observation of still other positively charged species in the near future.

It must be emphasized that the cage effect places fundamental restrictions on the matrix experiments. Molecules cannot diffuse through rare-gas matrices at the temperatures employed (4 and 14°K), but the lighter atoms and electrons can undergo at least limited diffusion. Cage recombination processes and inhibition of certain decomposition processes because of polarization effects do occur. Although a number of the ionic

species here considered have been observed to undergo photodetachment in experiments in which they were produced without the use of an alkali metal, the technique is inherently unsuited to the determination of accurate electron affinities.

Despite these limitations, the matrix isolation technique provides an extremely powerful tool for the stabilization of charged species in sufficient concentration for direct observation of their infrared and ultraviolet absorption spectra, often inaccessible from other types of experiment. Such spectra are of fundamental interest. Data derived from them may, under favorable circumstances, lead to the determination of an approximate structure for the molecule. Force constants obtained on analysis of infrared data for the various isotopically substituted species also provide information regarding the strengths of the various chemical bonds. In turn, this information can be used to test the implications of molecular orbital theory for molecules with either a deficiency or an excess of electrons in their valence shells.

References

1. D. E. Milligan, M. E. Jacox, and L. Abouaf-Marguin, J. Chem. Phys. 46, 4562 (1967).

2. G. Herzberg and A. Lagerqvist, Can. J. Phys. 46, 2363 (1968).

3. D. E. Milligan and M. E. Jacox, J. Chem. Phys. 51, 1952 (1969).

4. R. P. Frosch, J. Chem. Phys. 54, 2660 (1971).

5. D. E. Milligan, M. E. Jacox, and W. A. Guillory, J. Chem. Phys. 52, 3864 (1970).

6. R. Kato and J. Rolfe, J. Chem. Phys. 47, 1901 (1967).

7. D. E. Milligan and M. E. Jacox, "Matrix-Isolation Study of the Interaction of Electrons and Alkali Metal Atoms with Various Nitrogen Oxides. Infrared Spectra of the Species NO^-, NO_2^-, and $N_2O_2^-$" (submitted to J. Chem. Phys.).

8. D. E. Milligan and M. E. Jacox, J. Chem. Phys. 55, (1971).

9. P. N. Noble and G. C. Pimentel, J. Chem. Phys. 49, 3165 (1968).

10. D. E. Milligan and M. E. Jacox, J. Chem. Phys. 53, 2034 (1970).

11. D. E. Milligan and M. E. Jacox, "Infrared Spectrum of the $BrHBr^-$ Ion Isolated in an Argon Matrix" (submitted to J. Chem. Phys.).

12. E. E. Rogers, S. Abramowitz, M. E. Jacox, and D. E. Milligan, J. Chem. Phys. 52, 2198 (1970).

13. M. E. Jacox and D. E. Milligan, J. Chem. Phys. 54, (1971).

14. D. Spence and G. J. Schulz, Phys. Rev. A 3, (1971).

G3

Measurement of Rate Constants and Their Dependence on Ion Kinetic Energy by Ion Cyclotron Resonance. Jean H. Futrell, University of Utah, Salt Lake City, Utah 84112.

Recent advances in the technique of ion cyclotron resonance include the direct measurement with moderate precision of all the parameters requried for the determination of rate constants for ion-molecule reactions. Further, ion motion under the customary experimental conditions is now well understood and a formal description of ICR power absorption both in presence and absence of reactive collisions is available. Ion kinetic energy and spread of kinetic energy from the interaction with applied static and oscillating fields have been analyzed analytically and, in some cases, experimentally. Consequently it is now possible to carry our kinetic experiments by ICR with precision comparable to that of other techniques; in addition certain measurements are readily accomplished by ICR which are difficult or impossible by other methods. These new techniques and analytical results will be described and several examples illustrating the character and precision of measurements now possible by ICR will be presented.

INSTRUMENTATION AND TECHNIQUES FOR SCREENING PHSYOLOGICAL FLUIDS FOR TRACE METABOLITES. H1

JOHN ROBOZ, LASZLO SARKOZI, ALEXANDER RUHIG, and FERENC HUTTERER, Department of Chemistry
The Mount Sinai Hospital, New York, N.Y. 10029.

There has been an increasing interest in the so-called "metabolic profiles", involving the single-analysis determination of a large number of low molecular weight components in blood serum, urine, and other physiological fluids. The objectives of this work were to develop routine, automatic methods to measure changes in levels of metabolites of known structure, detect unsuspected metabolites and identify them, and, if an unknown turned out to be of significance, add it to the components that are routinely analyzed.

Instrumentation. The analytical system consists of a gas chromatograph, a high resolution mass spectrometer, an automatic microdensitometer, and a dedicated computer, each properly interfaced with the other for on-line operation, and equipped with a number of accessories to provide an almost completely automatic operation.

The gas chromatograph is a Hewlett-Packard, Model 6720 standard dual-column instrument, equipped with three-level temperature programming, flame ionization detector, and conventional electrometer. A special 1:10 effluent splitter enables one to direct either all effluents into the mass spectrometer, or divert one-tenths of the total for simultaneous flame ionization detector. The gas chromatograph is interfaced with the mass spectrometer through a one-stage jet type helium separator and an isolation valve; separate valving is provided to adjust the rate of helium removal.

The mass spectrometer, JEOL, Model JMS 01SC, is a double-focusing high resolution instrument of the Mattauch-Herzog design, using a conventional electron impact ion source. In addition to the GC/MS interface, separate inlets are provided for the mass calibrant (perfluorokarosene), gases and volatile liquids, and solids or separately trapped GC fractions. For low resolution work electrical detection (via electron multiplier) is provided. This is interfaced with the computer for on-line operation. For high resolution work standard photoplate detection is used. Photoplates are analyzed with an automatic densitometer (JEOL, Model JMD-2C) which, in turn, is interfaced with the computer for on-line operation. Magnetic scanning and computer operation for low resolution, and photoplate shifting for high resolution can be automatically initiated by the rising GC peak as detected on a total ion monitor. The output of the total ion monitor and the GC flame detector are displayed on a 2-pen potentiometer recorder.

The computer system consists of a JEOL, Model JEC-6 computer with a magnetic memory core of 4096 words, 16 bits, binary word construction, two-channel A/D converter, binary 8 bits digital value, sequential comparison, external magnetic drum memory with 8,192 words capacity, teletypewriter (50 ch/min), tape puncher, photo reader, and digital plotter.

Sample Preparation. Ethyl alcohol (4 ml) is first added to blood serum (1 ml) to remove proteins, the separated liquid is next freeze dried or vacuum evaporated. In the "derivative extraction" method, low molecular weight constituents are silylated in a relatively nonspecific manner so that components of widely different structure can be analyzed in a single run. At the same time, compounds that do not form derivatives are separated and a considerable sample concentration is achieved. The dry residue is treated with 250 µl of silylating reagent (2 parts hexamethyldisilazene, 1 part trimethylchlorosilane, 10 parts pyridine), and after a few minutes at room temperature the mixture is heated at 120°C for 5 min. Other physiologic fluids can be processed by essentially the same methodology. (To date, urine, amniotic fluid, and cerebrospinal fluid were tried in our laboratory.). For special "group type" analysis, or additional concentration of selected components, one may, of course, include solvent extraction, column chromatography, or enzymatic decomposition of the original sample. Most of these processes can be automatized without much difficulty.

Analytical Procedures. Gas chromatography conditions are summarized in Table 1, mass spectrometric conditions are summarized in Table 2. These conditions are quite standard and appear to work well for initial screening of serum samples, which is the primary objective of the present investigation. For more specific analysis, conditions may, of course, be changed, e.g., different temperature programming.

Peak identification is facilitated either by fragmentation patterns (low resolution, on-line computer), or high precision mass determination (high resolution, automatic densitometer, computer output of elemental compositions and element map).

Results. Normal serum samples yielded as many as 45-50 GC peaks (detected by both the flame detector of the GC and the total ion monitor of the MS) of various intensities, including such expected components as glucose and cholesterol. The first pathological serum tested was that of an 8-years old boy with a speech defect. Several peaks suggesting diagnostical significance were detected. One peak, present in a quantity of at least an order of magnitude higher than that in normal serum, was identified by high resolution mass spectrometry as alanine. The M-15 peak ($C_8H_{20}NO_2Si_2$) with an observed mass of 218.1025 (0.6 mmu away from calculated mass) was clearly detectable on the photoplates. High resolution measurements on other fragments confirmed the identification. Further proof was obtained with low resolution measurements where even the molecular ion could be detected. Increased concentration of serum alanine has been found in histidinemia, but further studies are needed to ascertain the diagnosis. Considering the present method as a tool for screening, a single run on the serum provided ample evidence for abnormality thus calling attention for more specific testing to follow.

Initial data suggest the applicability of the technique to disorders involving carbohydrate metabolism, organic acids in urine and plasma, and screening for drug abuse.

ACKNOWLEDGEMENT: This work was supported by a grant from the Edanros Foundation.

TABLE 1

Gas Chromatography Conditions

6 ft., 4 mm ID. glass column, filled with 3% GC-grade SE-30 on Chromosorb W, HP, 100/120 mesh. Helium carrier gas 30-45 ml/min flow rate. The sample (2-10μ l) is flash evaporated at 280°C. Temperature programming: isothermal at 80°C for 4 min, increase to 260°C at 4°/min, isothermal for 20 min, recycle. Effluent is split; one-tenths enter flame detector (kept at 300°C), rest enters helium separator (kept at 280°C).

TABLE 2

Mass Spectrometry Conditions

Ion Source: Ionization voltage: 23.5 or 75 V, ionization current: 200μ A, chamber temperature: 280°C, acceleration voltage: 7.6 kV.

Mass Range: 12-400 or 12-800

Low Resolution: Resolution: 2000; scan rate: 5 or 10 sec; electron multiplier: 2.0 kV; oscillograph paper: 10 cm/sec.

High Resolution: Resolution: 20,000; exposure (photoplate): $> 1 \times 10^{-10}$ coul; 50 lines on photoplate; PFK mass standard.

Applications of Mass Spectrometry to Clinical Problems. Utilization of a GC-MS-Small Computer System for Metabolite Identification.

S.P. Markey and J.R. Plattner

B.F. Stolinsky Research Laboratory
Department of Pediatrics
University of Colorado Medical Center
Denver, Colorado 80220

Abstract:

The description of a small computer data system for use with low resolution magnetic deflection mass spectrometers has been recently described.[1] The application of this system to problems of clinical interest is being pursued by our laboratory.

One area of intense interest is drug and drug metabolite identification. The analyses were performed on urine because of its availability and high drug concentration, but it is not always the most appropriate sample. Analysis of other physiological fluids such as blood and stomach washings can provide important information.[2]

Sample preparation is limited to simple extractions. Since drugs are usually weak acids or weak bases, urine is extracted at high (11) and low (2) pH with methylene dichloride. The extracts are brought to dryness under nitrogen and the residue redissolved in methanol for analysis by gc-ms alone.

The gas chromatograph is programmed from 30° to 300° C in 16 minutes which is the largest temperature range and longest period of analysis commensurate with the need for rapid analysis. A general purpose 6 ft. OV 17 column is used.

Some compounds such as acetylsalicylic acid decompose during gas chromatography. Direct probe ms analysis was attempted for identification of these compounds. Such identifications are ambiguous so lower ionizing voltage was proposed as a method of simplifying the spectrum. Other techniques such as chemical or charge transfer ionization could also be useful in this respect.[3] Spectra obtained at low ionizing voltage were found to be less complicated, but libraries of compounds run under these conditions would have to be available to help interpret such spectra.

The results of applying these techniques for emergency toxicology and drug metabolism studies will be published elsewhere. In conclusion this is a method which is useful for emergency toxicological analysis or drug metabolism studies. Similar methods are currently being used at this laboratory for early diagnosis of inborn errors of metabolism by organic acid analysis.

References:

1. J.R. Plattner and S.P. Markey, Org. Mass Spectr., in press (1971).
2. H.M. Fales, N. Law, G.W.A. Milne, and V. Aandahl. Nineteenth Ann. Conf. on Mass Spectrometry and Allied Topics. Atlanta, Ga. (1971).
3. H.M. Fales, G.W.A. Milne, and T. Axenrod, Anal. Chem., 42, 1432 (1970).

ANALYSIS OF MIXTURES OF AMINO ACID AND PEPTIDE DERIVATIVES BY MICROMOLECULAR DISTILLATION IN A MASS SPECTROMETER

R. D. Grigsby, J. S. Bird, and K. E. Bird

Department of Biochemistry and Biophysics
Texas A&M University
College Station, Texas 77843

The concept of micromolecular distillation was first introduced at the ASMS meeting in San Francisco last year[1]. At that time it was shown that a sample could be subjected to molecular distillation conditions in the ion source of the instrument by using the direct-probe inlet system.

Micromolecular distillation data are acquired by distilling the sample to dryness while the temperature of the probe is increased linearly with time. A plot of individual mass peaks *vs.* temperature gives elimination curves similar to those obtained by macro-scale molecular distillation[2,3]. The heights of the curves are proportional to the relative abundances for the individual components and the areas under the curves to the amounts of the components present. The technique is related to mass-spectrometric thermal analysis[4], to the integrated-ion current method of quantitative analysis[5,6], and to a quantitative method of molecular distillation in the ion source at constant temperature[7].

An improved empirical equation is now being used to analyze the data. The equation is given by

$$I = A \frac{e^{-B/T}}{1 + e^{C(T-D)}}$$

where I is the height of an elimination curve, A, B, C, and D are empirical parameters, and T is absolute temperature. The parameters are evaluated by a computerized least-squares analysis of the data[8,9].

Once A, B, C, and D are evaluated, three quantities of importance are obtained from the computer output. These are: T(Im) the temperature at which the curve "peaks out"; Im, the maximum height of the curve; and Ar, the area under the curve. From T(Im) and the rate of temperature increase, the time, t(Im) corresponding to the maximum height can be calculated.

Micromolecular distillation has been extended to allow analysis of mixtures of amino acid and peptide derivatives. The analysis of samples containing 3 and 5 amino acid derivatives each plus another sample containing three dipeptide derivatives will be described below. All samples were run on a CEC21-110B mass spectrometer operated under low-resolution conditions. The fast-scanning circuit of the magnetic chassis was modified to allow mass peaks to be displayed with the usual relationship to distance between the peaks ($\sqrt{M}=a_1+a_2d$). An all-glass probe, described previously[1], was used in the distillation.

Four elimination curves for acetylproline in a mixture with acetylhydroxyproline and acetyltryptophan are shown in Figure 1. Note that the curves peak out together at a T(Im) of ~ 373° K. Elimination curves for acetylhydroxyproline and acetyltyrptophan are similar except that different values for the T(Im)'s were obtained (~413° K and ~450° K, respectively). At a program rate of ~5°/min the values of t(Im) for the three components were 11.7±0.3 min, 18.4±0.4 min, and 24.5±0.1 min, respectively, clearly showing that the 3 families of curves arise from separate components.

Mixtures containing the trifluoroacetyl derivatives of amino acids have also been analyzed. These show a behavior similar to that for the acetyl derivatives except for the values of T(Im). For example, the curve for trifluoroacetylvaline peaks at a temperature about 30° lower than does the acetylvaline curve. A similar difference exists for the trifluoroacetyl- and acetylphenylalanine curves, showing the greater volatility for the trifluoroacetyl derivatives. The higher volatility can be a disadvantage, however, because the distillation of mixtures containing trifluoroacetylglycine must be started below room temperature. Otherwise, significant amounts of the derivative are lost in the vacuum lock of the instrument.

Calculation of the relative intensities for components subjected to micromolecular distillation can be illustrated with results obtained for permethylated N-acetylalanylleucine distilled from a mixture obtained during a permethylation reaction[10]. See table given below. Relative intensities can be calculated either

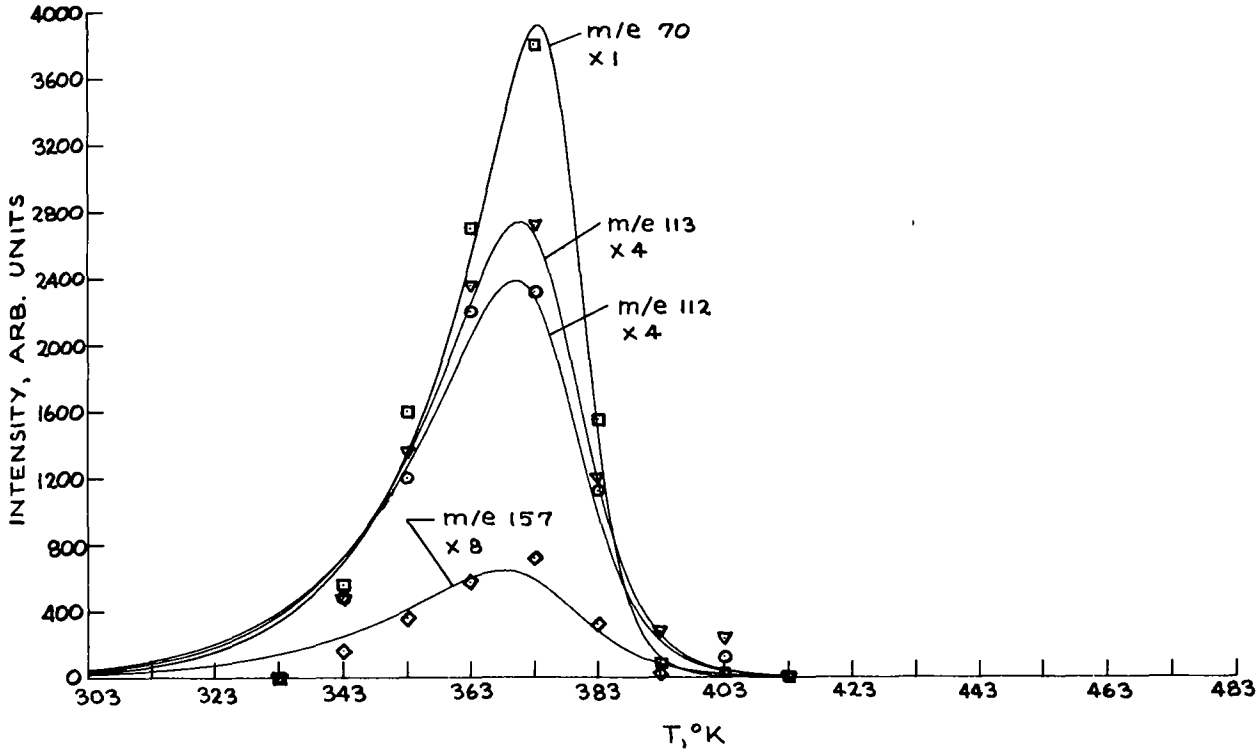

FIGURE 1. ELIMINATION CURVES FOR ACETYLPROLINE IN A MIXTURE WITH ACETYLHYDROXYPROLINE AND ACETYLTRYPTOPHAN

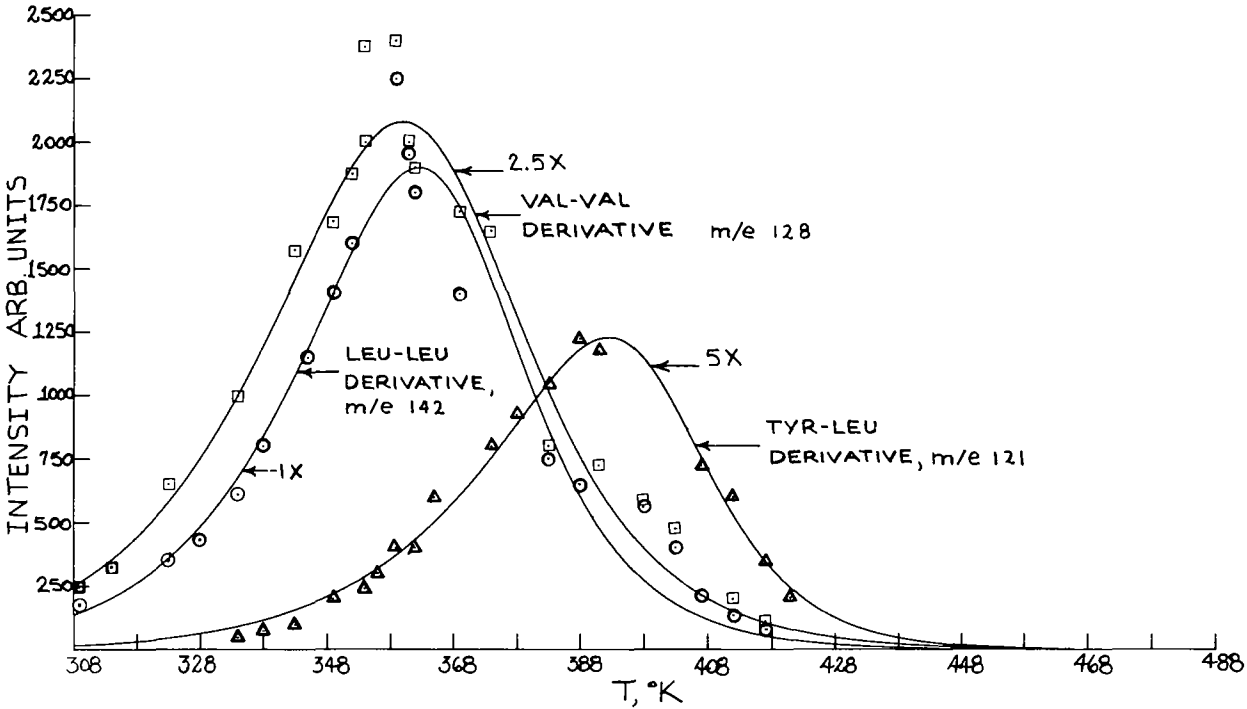

FIGURE 2. SINGLE ELIMINATION CURVES FOR PERMETHYLATED N-ACETYL DERIVATIVES OF VALYLVALINE, LEUCYLLEUCINE, AND TYROSYLLEUCINE IN A THREE-COMPONENT MIXTURE

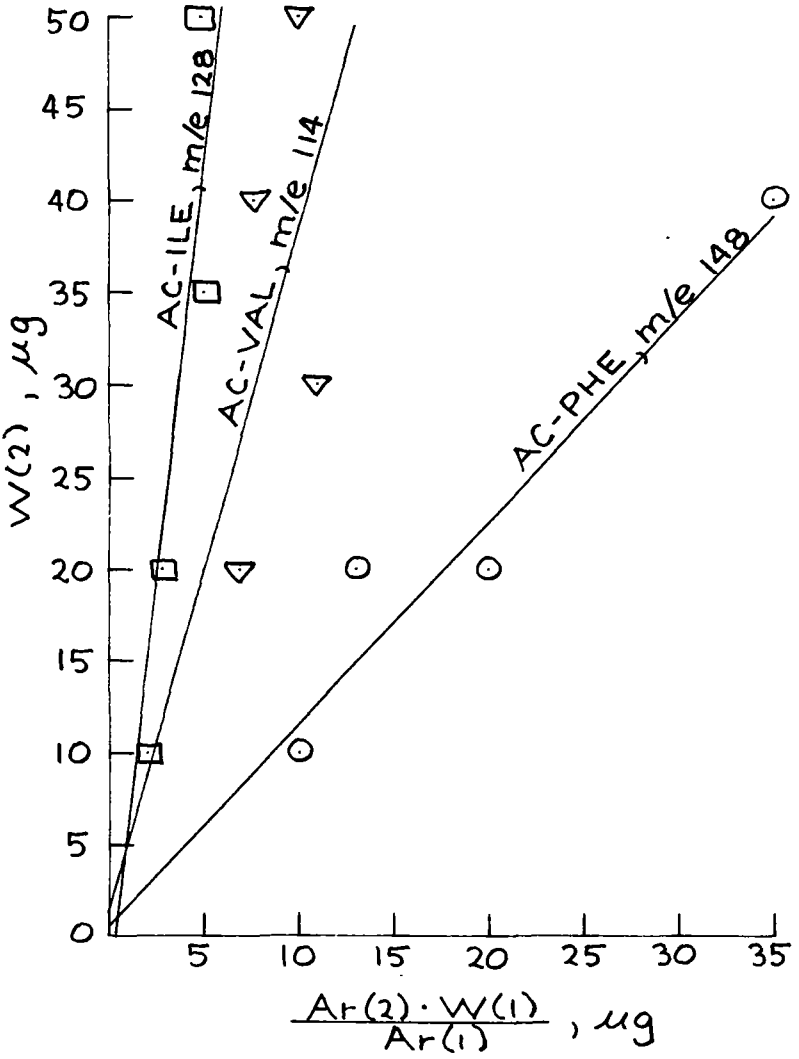

FIGURE 3. STANDARD PLOT FOR DETERMINING ACETYLVALINE, ACETYL-ISOLEUCINE, AND ACETYLPHENYL-ALANINE IN SIX-COMPONENT MIXTURE

from Im or Ar and the values will be the same within error limits, as seen from columns 6 and 7. In column 8 are given the relative intensities for the standard compound run under isothermal conditions. These values should be compared with those given in the two previous columns. In most cases the relative intensities calculated from elimination curves will agree with those obtained by isothermal distillation within ±20%.

Micromolecular Distillation of N-Acetyl-Ala-Leu-OMe

Mass	T(Im), °K	t(Im), min	Im	Ar	RelI(Im)	RelI(Ar)	RelI(Std)
100	359.1	8.6	5555	86787	288	308	251
128	360.9	8.9	1387	19026	72	68	58
226	359.9	8.7	668	9880	35	35	36
241	359.4	8.7	1800	27870	93	99	101
255	358.0	8.5	178	3268	9	12	10
258	359.6	8.7	1244	18723	65	67	64
283	361.2	9.0	1321	16687	69	59	72
286	354.9	7.9	149	3049	8	11	8
	Ave. 8.6±0.3						

The relative intensities given in the table are calculated from the equation[1]

$$\text{Rel I} = \frac{100n}{2} \cdot I_i / \Sigma I_I$$

Here, n is the number of masses used in the calculation. This method of expressing intensity shares the same advantage as per cent ionization in that the intensity of any one peak is not related to a base peak and thus is not subject to the error resulting from the measurement of that peak. By multiplying per cent ionization values by n/2 the average intensity is forced to have a value of 50. Thus most intensities fall in a range from 0 to 100 and do not have to be expressed by small decimal fractions.

Three elimination curves for a three-component mixture of the permethylated N-acetyl derivatives of valylvaline, leucylleucine, and tyrosylleucine are shown in Figure 2. The curve for the tyrosylleucine derivative peaks at ~393° K and is easily separable from the curves for the other two components. On the other hand, the valylvaline and leucylleucine derivatives do not give curves that are significantly different; i.e., both peak at about 361-363° K. Very little difference would be expected, however, because the compounds only differ by two methylene groups.

The quantitative aspect of micromolecular distillation can be illustrated with results from a six-component mixture containing acetophenone azine and the acetyl derivatives of valine, isoleucine, phenylalanine, tryptophan, and proline. The acetophenone azine was added as an internal standard.

Graphs for determining the amino acids in the mixture are shown in Figures 3 and 4. The points were obtained by plotting the weights of the amino acid *vs.* an expression depending on the areas under the elimination curves and the weight of the internal standard. The corresponding equation[1] is

$$W(2) = K \frac{Ar(2) \cdot W(1)}{Ar(1)}$$

where W(2) is the weight of the amino acid (or derivative), Ar(1) the area under an elimination curve for the internal standard, Ar(2) the area under a curve for the amino acid derivative, and W(1) the weight of the internal standard added to the sample.

The error in the determinations for Ac-Val, Ac-Ile, and Ac-Phe is relatively high as compared to that for Ac-Tryp and Ac-Pro. Part of the reason for the difference is that the sensitivity (area under the elimination curve ÷ the amount of the component present) for the analytical peaks is lower for the first three amino acid derivatives as compared to the latter two compounds. Other sources of error also contribute to the data scatter but will be reduced as the technique becomes more refined.

In summary, the technique described here can be used to obtain both qualitative and quantitative information for samples introduced with a probe-inlet system. It is not intended to replace the GC-MS combination, which is obviously very successful. Instead, the method is being developed for samples not having sufficient volatility

for introduction through a chromatograph. Such samples would include mixtures of oligopeptides, dinucleotides, phospholipids, and numerous others.

REFERENCES

1. R. D. Grigsby, R. H. Cole, W. G. Fox, and G. M. Gable, Eighteenth Annual Conference on Mass Spectrometry and Allied Topics, San Francisco, June (1970) Paper No. K8.
2. G. Burrows, "Molecular Distillation," Oxford University Press, London, 1960.
3. N. D. Embree, Ind. Eng. Chem., *29*, 968 (1937).
4. H. G. Langer, R. S. Gohlke, and D. H. Smith, Anal. Chem., *37*, 433 (1965).
5. M. G. Allcock, R. Belcher, J. R. Majer, and R. Perry, Anal. Chem., *41*, 776 (1970).
6. B. R. Kowalski, T. L. Isenhour, and R. E. Sievers, Anal. Chem., *41*, 998 (1969).
7. R. A. Hites, Anal. Chem., *42*, 1736 (1970).
8. S. D. Christian, J. Chem. Educ., *42*, 604 (1965).
9. L. G. Sillén, Acta Chem. Scand., *18*, 1085 (1964).
10. D. W. Thomas, FEBS Letters, *5*, 53 (1969).

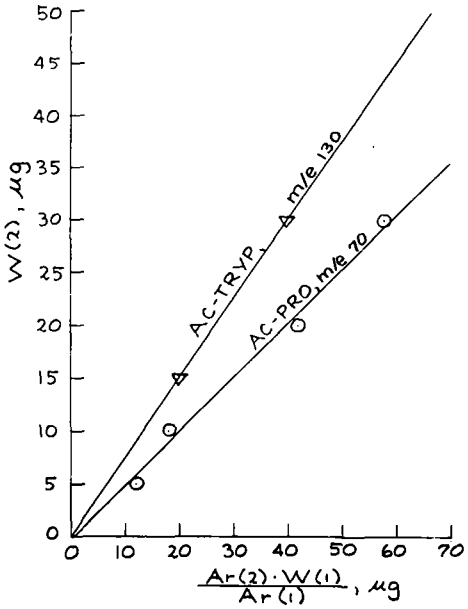

FIGURE 4. STANDARD PLOT FOR DETERMINING ACETYLTRYPTOPHAN AND ACETYLPROLINE IN SIX-COMPONENT MIXTURE

The Quantitative Sequential Degradation of Proteolytic Peptide Mixtures Using Mass Spectrometry

R. E. Lovins, T. Fairwell, C. Cabaniss, and T. Sun

Department of Biochemistry

University of Georgia

Athens, Georgia 30601

Using techniques described earlier[1], the determination of the N-terminal sequence of mixtures of peptides resulting from the proteolytic digestion of a protein is described. The method involves the use of the Edman reaction (phenylisothiocyanate or methylisothiocyanate) and mass spectrometry to quantitatively identify (using ^{15}N isotope dilution) the thiohydantoin mixture produced at each step of the reaction. The use of varying proteolytic digestion rates to produce mixtures of peptides containing nonequimolar concentrations of peptides is discussed together with the use of low ionizing voltages for the simplified identification of the thiohydantoin mixtures. The method has been applied to the identification of the N-terminal sequence of a peptide mixture derived from the tryptic hydrolysis of a protein using varying rates of hydrolysis to produce a mixture composed of nonequimolar amounts of peptides.

Acknowledgment - This work was supported in part by Grant # GB27555 from the National Science Foundation. Robert E. Lovins is NIH Career Development Awardee.

References

[1] T. Fairwell, W. T. Barnes, F. F. Richards and R. E. Lovins, Biochemistry 9, 2260 (1970)

The Use of Chemical Ionization Mass Spectrometry in Biomedical Problems. H6

G. W. A. Milne and H. M. Fales
Laboratory of Chemistry, National Heart and Lung Institute, National Institutes of Health
Bethesda, Maryland 20014.

In the Edman degradation of proteins, phenyl isothiocyanate reacts with the amino-terminal amino acid of a protein. This amino acid is cleaved off and can be isolated as its phenylthiohydantoin derivative, identification of which provides information as to the sequence of the protein. Identification of PTH-amino acids can be done by TLC or by GLC but both methods have shortcomings. Electron impact mass spectrometry has been used for this purpose but the extensive fragmentation of the molecular ions of PTH-amino acids can create difficulties. Chemical ionization (CI) mass spectrometry has been used with great success in this problem because almost all the PTH-amino acids give isobutane CI mass spectra which consist of only a quasimolecular (QM^+) ion at m/e (M + 1).

Sperm whale myoglobin was degraded by the Edman method and each PTH-amino acid released was identified by CI mass spectrometry. The purity of the released PTH-amino acid decreased as the degradation proceeded into the protein and the necessary quantification was achieved by admixture of the sample with a standard amount of the appropriate pentadeutero-PTH-amino acid. Twenty six steps in the degradation were accomplished with ease, giving the correct sequence.

The CI mass spectra of a series of plasticizers have been measured. These molecules, generally esters of di- and tricarboxylic acids, all fail to give molecular ions in their electron impact mass spectra but all give QM^+ ions in their isobutane CI mass spectra. Such fragmentation of QM^+ ions as is observed can be readily rationalized according to the rules of acid catalysis and a study of these spectra has shown that diethyl maleate and diethyl fumarate give quite different CI mass spectra, as might be expected. Similarly, phthalates give CI mass spectra which are very different from those of the corresponding iso- or terephthalates. Plasticizers are found frequently in human serum and this method permits their ready identification in such biological fluids.

This work will be published in Analytical Biochemistry and Analytical Chemistry.

Mass Spectral Structural Elucidation Techniques for Biological Compounds

Piet A. Leclercq, Patricia A. White, and Dominic M. Desiderio

Institute for Lipid Research and Department of Biochemistry
Baylor College of Medicine, Houston, Texas 77025

INTRODUCTION

The development of techniques for the structural elucidation of compounds extracted from biological sources has been a major effort in our laboratory for several years. Generally, these compounds must be derivatized in order to obtain interpretable mass spectra. One of the main thrusts of our research program is the development of derivatization techniques on the microgram level.

Permethylation has been found useful for oligopeptides,[1-7] polyene macrolides[8] and oligosaccharides.[9] This can be extended to compounds such as prostaglandins, steroids, nucleosides, etc.

The method often has definite advantages over other methods for structural analysis of these compounds. Derivatization can be performed and mass spectra obtained on 20 μg of material within 2 to 5 hours. Chemical ionization (CI) mass spectrometry has an increased sensitivity compared to electron impact (EI), in conjunction with the production of a "cleaner" mass spectrum containing only those fragments arising from major fragmentation pathways.[10,11]

Sometimes mass spectrometry is the only method available for structural analysis. This can be exemplified for protected peptides where ultrasensitive "wet" chemical sequencing methods are not applicable. Whenever the N-terminus of a peptide is blocked, neither hydantoyl nor dansyl derivatives can be formed. Whenever the C-terminus is blocked, enzymes such as carboxypeptidase A cannot hydrolyze the peptide bonds.[5]

On the other hand, there are restrictions imposed by mass spectrometry. These include the requirements of volatility and purity of the sample, and the molecular weight must be less than 2000 mass units.

DERIVATIZATION

The molecules found in this type of research have a very large number of replaceable hydrogens and/or a large molecular weight. We found that the trimethylsilyl, trifluoroacetyl, and even the acetyl derivatives were not useful. Therefore, we were forced to choose the smallest chemical derivative - the methyl group.

Up to now, the permethylation technique has been used on the milligram level employing methyl iodide plus a catalyst.[1-4,9] The most commonly employed catalyst is the methylsulfinylmethide carbanion.[2-8,9] Gallop, et.al.[12] reported the first application of these techniques on the microgram level. However, their use of large excesses of reagents would lead to the formation of non-volatile (N and S containing) salts and other degradation products.

Using oligopeptides as a model, we have systematically investigated the stoichiometry of this reaction. By varying the concentrations of the reactants over the range 0:1:1 to 300:300:1, we found that the optimum ratio of carbanion:methyl iodide:peptide is 10:10:1 equivalents.[6,7]

It is necessary to acetylate any free amino groups in order to avoid quaternization during the permethylation reaction. An excess of methanol:acetic anhydride (4:1) is employed. Normally, we apply these derivatization techniques to 50 μg of material.

RESULTS

As an illustration of areas of applicability, EI and CI mass spectra of representatives of different classes of compounds will be discussed.

PCA-Pro-Tyr-His-NH_2[13]. This particular tetrapeptide contains some of the most "difficult" amino acids to sequence by conventional techniques. In addition, the N-terminus is blocked. Only recently was a PCAase found. The C-terminus is blocked by a carboxamide group. The following proline residue inhibits many enzymes. Chemically, histidine is readily quaternized.

The mass spectrum of the permethyl derivative shows a molecular ion plus all possible sequence peaks, including the loss of the various side chains.[5]

Met-Gly-Met-Met. Up to now, methionine had to be desulfurized before methylation due to the ease with which sulfur is oxidized. In those cases where this was not done, a mass spectrum was obtained with sequence peaks up to, but not including nor beyond the methionine residue. Dehydroalanine and cyclopropane derivatives were formed in the permethylation reaction. In the mass spectrum of this tetrapeptide, derivatized according to our procedure, all sequence peaks except the molecular ion were found.[7] This peptide is an excellent test of this procedure due to the presence of the N-terminal methionine and the C-terminal dipeptide Met-Met.

TRF. The structural elucidation of the thyrotropic releasing factor (TRF=PCA-His-

Pro-NH_2) has been reported.[14,15] As an addendum to this structural proof and as an illustration of the use of chemical ionization mass spectrometry for these types of molecules, the CI mass spectrum of TRF was obtained on the NIH MS9.[11] This CI spectrum was obtained on an underivatized tripeptide and abundant sequence peaks were found.

Scotophobin. This pentadecapeptide has been extracted from rats who have been trained to have a fear of the dark.[16] This extracted peptide, when injected into the brain of an untrained rat, induced the same fear of the dark. This is one of the first examples of the transfer of a learned behavior from one animal to another. No wet chemical method of sequence analysis was applicable to this particular peptide due to the extremely low amounts of total available precious material. (300 μg originally; after amino acid analyses - 35 μg.) The choice of mass spectrometry was the only option left.

Because the permethylation technique was in the very early stages of development, we formed the trifluoroacetyl derivative instead. The EI mass spectrum of the derivatized scotophobin did not yield any molecular ion nor any fragments containing more than two or three residues. However, we found that enough overlapping di- and tripeptide fragments were found to yield a unique pentadecapeptide sequence A.[17,18]

A. Ser - Asx - Asn - Asn - Glx - Gln - Gly - Lys - Ser - Ala - Glx - Gln - Gly - Gly - Tyr - NH_2

Actually, sequence A was not unique in the fact that at positions 2, 5, and 11, ambiguities existed due to the possible loss of ammonia from Asn or Gln.

Peptide B was synthesized by Dr. Boris Weinstein, University of Washington, and was found to have 2% biological activity.

B. Ser - Asp - Asn - Asn - Glu - Gln - Gly - Lys - Ser - Ala - Glu - Gln - Gly - Gly - Tyr - NH_2

The peramidated form of scotophobin - sequence C - was synthesized by Dr. Wolfgang Parr, University of Houston, and was found to possess 10% biological activity. By referring to a paper by Sneath,[19] this implies that one amino acid was incorrect, showing a factor of ten decrease in the biological activity.

C. Ser - Asn - Asn - Asn - Gln - Gln - Gly - Lys - Ser - Ala - Gln - Gln - Gly - Gly - Tyr - NH_2

This fact left us with three possible peptides to synthesize, namely, a carboxylic group in residue 2, 5, or 11. After synthesis of the first of these three possibilities,

sequence D was found to possess 100% biological activity.

D. Ser - Asp - Asn - Asn - Gln - Gln - Gly - Lys - Ser - Ala - Gln - Gln - Gly - Gly - Tyr - NH_2

The remaining two peptides are currently being synthesized.

Filipin. In order to illustrate the diversity of the usefulness of this general technique, the polyene macrolide filipin was permethylated. The mass spectrum of O-permethyl filipin shows an abundant molecular ion at m/e 780 plus all eight possible losses of methanol from the macrocylic ring.[8] The driving force behind these losses of methanol seems to be the formation of a totally conjugated macrocyclic lactone ring. These mass spectrometric and chemical techniques are being extended to other polyene macrolides including candicidin and amphotericin B.

Prostaglandins. This type of compound is under investigation in our laboratory due to the wide range of physiological action and the very great biological activity of nanograms of substance. As an example of the application of the described techniques to prostaglandins, the chemical ionization mass spectrum of underivatized PGA_1 was obtained.[20] The adduct ions at M + 1, M + 29, and M + 41 were observed. Water was lost from M + 1, M + 29, and M + 41. Two molecules of water were lost from M + 1.

The O-methylation techniques are being applied to this family of compounds.

SUMMARY

This research is based on the following three points:

1. To further basic mass spectrometry, including EI and CI methods,
2. To employ chemical derivatives on extremely low amounts of sample and on a diversity of compounds,
3. To interface with the biological community to elucidate the structure of hypothalamic releasing factors, memory transfer molecules, prostaglandins, polyene macrolides, and other types of compounds.[21,22]

Acknowledgements. We wish to acknowledge the collaboration of Dr. Klaus Hägele and the technical assistance of Mr. Ken Lyman, Miss Pamela Crain, and Miss Carol Weise. Financial assistance from NIH (GM 13901, 69-2161, 02055, RR 259, RR 254) and the Robert A. Welch Foundation (Q 125) is greatly appreciated.

References

1. B. C. Das, S. D. Géro, and E. Lederer, Biochem. Biophys. Res. Commun., 29, 211 (1967).

2. E. Vilkas and E. Lederer, Tetrahedron Lett., 26, 3089 (1968).

3. D. W. Thomas, Biochem. Biophys. Res. Commun., 33, 483 (1968).

4. M. L. Polan, W. J. McMurray, S. R. Lipsky, and S. Lande, Biochem. Biophys. Res. Commun., 38, 1127 (1970).

5. P. A. White and D. M. Desiderio, Anal. Lett., 4, 141 (1971).

6. P. A. Leclercq and D. M. Desiderio, Anal. Lett., in press.

7. P. A. Leclercq and D. M. Desiderio, J. Amer. Chem. Soc., submitted for publication.

8. P. A. White and D. M. Desiderio, Anal. Lett., 3, 499 (1970).

9. H. Björndal, C. G. Hellerqvist, B. Lindberg, and S. Svensson, Angew. Chem. internat. Edit., 9, 610 (1970).

10. W. R. Gray, L. H. Wojcik, and J. H. Futrell, Biochem. Biophys. Res. Commun., 41, 1111 (1970).

11. D. M. Desiderio, R. Burgus, T. F. Dunn, W. Vale, R. Guillemin, and D. N. Ward, Org. Mass Spectrom., 5, 221 (1971).

12. J. Lenard and P. M. Gallop, Anal. Biochem., 34, 286 (1970).

13. PCA is the abbreviation for 2-pyrrolidone-5-carboxylic acid.

14. R. Burgus, T. F. Dunn, D. M. Desiderio, D. N. Ward, W. Vale and R. Guillemin, Nature, 226, 321 (1970).

15. R. Burgus, T. F. Dunn, D. M. Desiderio, D. N. Ward, W. Vale, R. Guillemin, A. M. Felix, D. Gillessen, and R. O. Studer, *Endocrinology*, 86, 573 (1970).

16. G. Ungar, L. Galvan, and R. H. Clark, Nature, 217, 1259 (1968).

17. D. M. Desiderio, G. Ungar, and W. Parr, Chem. Commun. (No. 158), in press.

18. G. Ungar, D. M. Desiderio, and W. Parr, Nature, submitted for publication.

19. P. H. A. Sneath, J. Theoret. Biol., 12, 157 (1966).

20. D. M. Desiderio and K. Hägele, Tetrahedron Lett., submitted for publication.

21. D. M. Desiderio in "Proceedings of the Second American Peptide Symposium," S. Lande, Ed., Gordon and Breach, New York, N.Y., in press.

22. D. M. Desiderio, in "New Chemistry of Peptides," N. Kharasch, Ed., Intra-Science Research Foundation, Santa Monica, Calif., in press.

H9

Mass Spectral Studies of Natural Products.

Cardenolides and Bufadienolides.

Peter Brown, Yoshiaki Kamano and George R. Pettit,
Department of Chemistry, Arizona State University,
Tempe, Arizona, 85281, U.S.A.

Abstract:-

A comprehensive investigation of the behavior of the bufadienolides [1] (toad venoms), e.g., bufalin, on electron impact has been undertaken for the first time. Free as well as derivatized bufadienolides have been examined, using both high and low resolution and metastable defocussing techniques.

From the molecular formulae of the various characteristic ions, it has been possible to differentiate between (i) ions containing the relatively unsaturated 2-pyrone ring; and (ii) those arising from more saturated portions of the molecule. On this basis, "structural ion types" have been proposed to account for diagnostic ion peaks in terms of the substitution pattern of the particular compound. Using this approach, the prognosis for structure elucidation of other bufadienolides, or the related cardenolides, [2] by high resolution mass spectrometry appears good.

Detailed accounts of this work will be submitted to Organic Mass Spectrometry.

References:-

1. F.M. Dean, "Naturally Occurring Oxygen Ring Compounds", Butterworth and Co. Ltd., London, England, 1963, pp. 93-99.

2. T. Reichstein, Naturwiss., 3, 53 (1967).

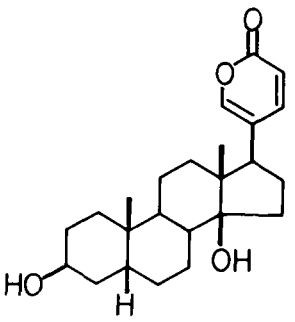

Bufalin 386

$C_{24}H_{34}O_4$

APPLICATION OF AN ISOTOPE MS20 MASS SPECTROMETER IN CLINICAL RESEARCH FOR THE MEASUREMENT OF ^{15}N AND HEAVY WATER

D. Halliday
Clinical Research Centre
Medical Research Council
Middlesex, England.

and

L.E. Moore and G.J. Chew
AEI Scientific Apparatus Limited
Manchester, England.

INTRODUCTION

The production of more sensitive isotope ratio mass spectrometers means that it is now economically feasible to study protein metabolism in human subjects using ^{15}N-labelled amino acids. This is a preliminary report on work currently being carried out at the Clinical Research Centre, Harrow, using an AEI Isotope MS20 instrument.

The Isotope MS20 is a small, low-cost instrument employing a 180° magnetic analyser fitted with double collector systems on each of two radii, 5cm and 2cm. Each ion current is amplified by an electrometer amplifier, the outputs of which are applied to a Kelvin-Varley potential divider and ratio recorder to obtain the ratio of the two ion currents directly. The gaseous samples are admitted via an all-metal dual viscous inlet system enabling the direct comparison of a sample and a standard of known isotopic composition to be made.

The ratios $^{15}N/^{14}N$ and $^{18}O/^{16}O$ at natural levels in nitrogen or carbon dioxide respectively can be determined with a reproducibility of 0.01%. The ratio HD^+/H_2^+ at natural levels can be determined with a reproducibility of 0.1%.

APPLICATIONS

In a normal subject at rest the energy cost of metabolism is about 1 kcal (4 kJ) per minute. A small fraction of this energy is used for the work of breathing, the contractions of the heart, etc., but the great majority is used for biochemical reactions which go on continuously in the body: of these reactions the turnover of some 300 g per day of tissue protein is probably the major factor in determining resting energy requirements. Some obese patients have remarkably low energy requirements, so the hypothesis to be tested is that these low requirements arise because the turnover of tissue protein is greatly reduced. There are two reasons for testing this theory. One is that, if it is true, it would explain why some overweight patients find it almost impossible to lose weight even on a strictly controlled diet. The other is that we do not know the effect on health of diminishing the rate of protein turnover, on which there are two opposing views: one is that a high turn-over rate is a beneficial situation, because old protein is constantly being replaced by new (and presumably better) protein, while the other view is that the process of ageing depends on the transcription errors which occur when protein is replicated, so a high turnover rate simply leads to acceleration of ageing rate.

The measurement of protein turnover rate in man is possible but difficult (see Waterlow 1970, Nutrition Reviews 28.115). Under ideal conditions the free aminoacid pool, from which all body protein is made, should be uniformly labelled by an infusion of ^{15}N aminoacid. In practice we have used a simpler, but theoretically less satisfactory technique of pulse labelling with a single dose of 100 mg. of ^{15}N glycine. With the pulse labelling technique it is not possible to calculate absolute rates of turnover, because the specific activity of the protein precursor is constantly changing with time, but if turnover rates in a given patient alter in response to a change in diet this should be reflected in the amount of isotopically labelled nitrogen which is excreted in the first few days after giving the labelled aminoacid, provided that the size of the metabolic pool is not greatly altered between one experiment and the next.

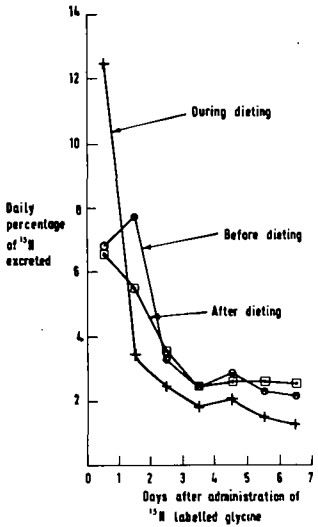

FIGURE 1

Results of Three Experiments
On One Patient

FIGURE 2

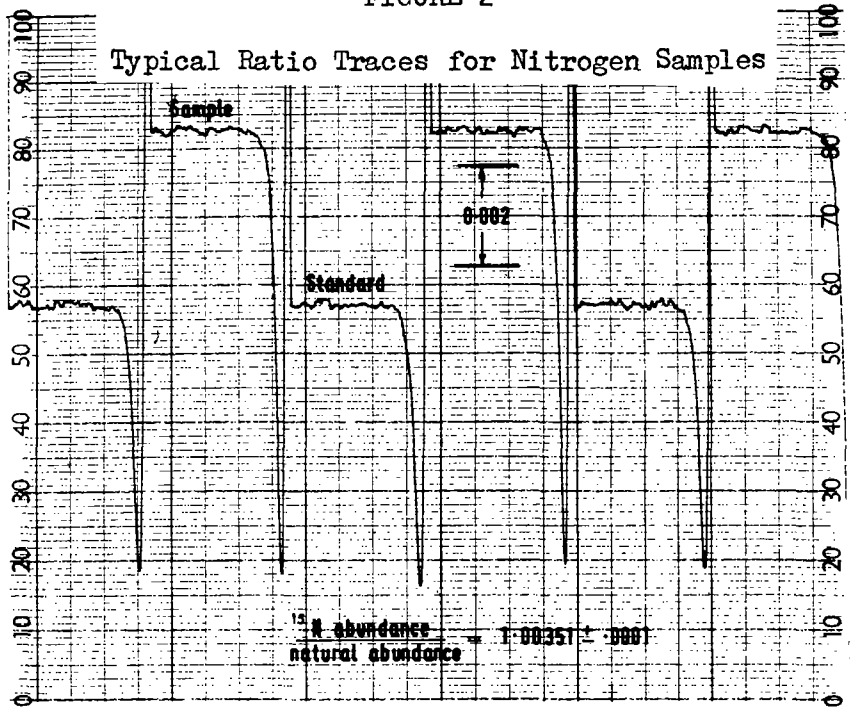

In the case of obese patients who are on a reducing diet it is obviously not justifiable to assume that pool sizes remain constant while body weight is changing, so it is necessary that there should be a measurement of "lean body mass" at the time of each isotope study. This can be achieved if total body water is measured by dilution of deuterium oxide in natural body water, since the lean body mass is approximately 74% water.

RESULTS

Preliminary results of a study on a patient before, during and after a period of weight reduction are shown in Figure 1. In each case 100 mg of ^{15}N glycine and 10 ml of D_2O were given by mouth at 0900 hours after an overnight fast, and no protein was given until 1700 hours on that day. Blood and urine samples were taken 2, 5 and 8 hours after giving the isotopes. In the first and third experiment the diet supplied 2200 kcal per day and during the second experiment only 850 kcal per day, but the protein content of all the diets was 60-90 g per day. The design and purpose of the study was explained to the subject who gave consent.

The results in Figure 1 were calculated from the measured total nitrogen and the measured ^{15}N abundance as in the following example:

^{15}N ingested - 17.7 mg
Total urine nitrogen (day 1, first half) - 2600 mg
^{15}N abundance - 1.06427 times natural level
Atom percent excess ^{15}N - 0.0232%
Percentage of original ^{15}N excreted during day 1 (first half)

$$= \frac{0.000232 \times 2600}{17.7} \times 100 = 3.4\%$$

It would be unwise at this stage to attempt a quantitative interpretation of the results shown in Figure 1, but two points clearly emerge. One is that on the low calorie diet a larger fraction of the labelled nitrogen was excreted on the first day, and a smaller fraction on subsequent days, than was the case when the calorie intake was adequate before or after the period of weight reduction. On the hypothesis of diminished protein turnover this is what would be predicted: with decreased turnover less labelled aminoacid would be incorporated, and hence more would be excreted, on the first day. Thereafter the reverse would apply: since less was incorporated in tissue protein on the first day the specific activity of body protein would be less, and hence as this protein was catabolised less isotope would be available for excretion on subsequent days. It must be emphasised, however, that these preliminary results are merely compatible with the hypothesis, but they do not prove it. To obtain proof it will be necessary to make measurement of tissue protein specific activity, and this work is being undertaken in parallel studies in experimental animals.

The other point which emerged, which is perhaps more relevant to this paper, is that in urine samples after a dose of 100 mg. of ^{15}N glycine to an adult the isotope abundance accuracy required is well within the range measurable with this mass spectrometer. A change in the ordinate in Figure 1 of $\pm$ 0.1% corresponds to a change in isotopic abundance of 0.2%. Figure 2 shows the trace obtained from a nitrogen sample differing by 0.3% in ratio from the standard. The 0.2% accuracy required is indicated and it is clear that the instrument accuracy would permit the tests to be conducted with the ^{15}N enriched sample reduced by a factor of twenty or more.

The technique for the measurement of body water is still under review. The level of accuracy required is not nearly so high as for ^{15}N analyses, because a normal adult has about 50 litres of body water, and an estimate accurate to 250 ml. is perfectly adequate for all clinical purposes. An instrumental error of 0.5% is therefore tolerable for D_2O, whereas it would be completely unacceptable for ^{15}N. We have used the batch inlet system heated to 120°C, admitted samples as water vapour, and measured the ratio of mass 18 and mass 19 peaks. It is possible to achieve the required 0.5% accuracy by this method, but only at the expense of rather long preconditioning with standards enriched to the same extent as the samples. The alternative method is to use the short radius collector system and measure the mass 2:3 ratio in hydrogen derived from water samples. This is a well-known and proven method and is being adopted for future tests.

THE MASS SPECTRA, ENERGY RELATIONSHIPS AND FRAGMENTATION MECHANISMS OF METALLOCENES*

H. J. Svec, G. A. Junk, G. D. Flesch

Institute for Atomic Research and Department of Chemistry
Iowa State University, Ames, Iowa

In the Dec. 15, 1951 issue of Nature, Kealy and Pauson announced the preparation of dicyclopentadienyl iron by means of a reaction between cyclopentadienyl magnesium bromide and ferric chloride in anhydrous ether. Another report, this time in the Feb. 1952 issue of J. Chem. Soc. by Miller, Tebboth and Tremaine described the preparation of the same iron-containing compound by passing cyclopentadiene over specially prepared iron powder containing a small amount of Al_2O_3 at 300°C. Later in 1952 Wilkinson, Rosenblum, Whiting and Woodward determined its now well-known structure, which is shown in Fig. 1. The two Cp rings are parallel and 3.25Å apart with the carbon atoms in a staggered configuration and the iron midway between the two rings. The adjective "sandwich" was first applied to this structure by Dunitz and Orgel in 1953. It was shown by Rosenblum, Whiting and Woodward in 1952 that the molecule behaves as an aromatic system undergoing typical aromatic reactions, for example Friedel-Crafts acylations. Hence they coined the name "ferrocene" which was later generalized to "metallocenes". Thus started a new kind of organometallic chemistry. Today we will discuss the mass spectra of ferrocene, nickelocene, ruthenocene and some mono-substituted derivatives of ferrocene.

Fragmentation. The first important mass spectrometric study of metallocenes was that of Friedman, Irsa and Wilkinson (1955) which involved several MCp_2 compounds. They found that the fragmentation of these compounds resembled that of simple three-atom molecules such as CO_2, H_2O, N_2O etc. There is a prominent parent ion, a somewhat less prominent MCp^+ and a relatively prominent M^+. Only minor fragmentation of the Cp rings occurs. Our fragmentation data for ferrocene, nickelocene and ruthenocene are shown in Fig. 2 for 50 eV electrons. These data are in good agreement with those of Friedman and others. The stability of the molecular ion is indicated by the rather large relative abundance of MCp_2^{++}. The stability of the Cp rings is evident from the low abundances of ions containing residues from ruptured Cp rings, the one exception being $Ni(C_3H_3)^+$. Ions containing C_3H_3 residues are the most abundant of such fragment ions and we presume that the C_3H_3 moieties are cyclic. You can appreciate the 3-atom-molecule character of these spectra when you consider that for 50 eV electrons the principal ions MCp_2^+, MCp^+ and M^+ constitute 94% of the total ions from ferrocene, 88% from nickelocene, and 91% from ruthenocene. In the ensuing discussion we will emphasize these principal ions.

Energetics. The ionization and appearance potentials of these principal ions have been determined using the extrapolated difference technique and automatically recorded ionization efficiency data. Values obtained are shown in Fig. 3. These values are similar in a relative sense to those of others, except that they are several tenths of an eV lower. This probably results from the fact that we normalized all IE data at about 1.5 eV above the initial onset of the IE curves. As reported here in another symposium last year, this results in all such normalized IE curves being superimposable after translation along the electron energy axis. Please note that with this procedure only the foot of each IE curve is used to establish the IP or AP of an ion. All tests with rare gases and materials with well established IP's indicate that this produces better results than any other we have used during many years.

These data (first and second rows) indicate that the molecule ion is very stable since 6-7 eV of excitation above the IP is needed to remove the first Cp ring. However, a comparison of the data in the second and third rows implies a very low value for the dissociation energy of the second Cp group. These conclusions agree with those of previous investigators.

Now this result is contrary to our intuitive feelings and also contrary to any expectations based on bonding theory. Thus we have the

*Work was performed in the Ames Laboratory of the U. S. Atomic Energy Commission.

dilemma concerning "what are the real dissociation energies"? The low abundance of M^+ relative to MCp^+ in the 50 eV spectra suggests that the strength of the bonds between the two Cp groups and the metal should be more nearly equal and thus the inaccuracy concerns 4, 5 or 6 eV.

What possibilities for errors exist in appearance potential measurements? One is that the AP values for MCp^+ are too high. This may be true because of kinetic energy associated with the fragments, excitation energy in the fragments or the usual discrepancies associated with "vertical vs adiabatic" effects in electron bombardment measurements. The latter are too small, generally only 0.1 to 0.3 eV, to be considered as a serious source of the 4 to 6 eV discrepancy. We have measured the kinetic energy of the fragment ions as just above and up to 10 volts above their onset potentials using the method of Clampitt and Dunning, and we have been unable to detect any kinetic energy in the fragment ions different from that of the parent ion. The noise of the measurements was ~0.01 eV. Thus we conclude that there is no kinetic energy effect on these bond dissociation energies. In addition, the shape of the IE curves for both MCp_2^+ and MCp^+ are identical in the region between onset and 1.5 volts above onset, (the normalized curves are superimposable). Because of this, we feel that excitation energies, if they exist, affect these ions similarly and thus their effect upon the AP determinations should tend to cancel.

An alternative reason for the apparent low dissociation energy of the second M-Cp bond is that the AP value for M^+ is too low. On the basis of the usual conclusions about electron impact values for AP's, the idea of a low value is unexpected. However, a careful study of the IE curves shown in Fig. 4 indicates that the conclusions deduced from the IE curve for Fe^+ are erroneous. In this figure, the three plots for the ferrocene IE data were obtained by normalizing the recorded curves in such a way that the ion currents at 50 eV, 26 eV and AP + 2.0 eV produced the same recorder deflection.

The 50 eV normalizations show a long tail on the Fe^+ IE curve. The central region of these curves are roughly similar and the voltage separation suggests that the ionization process leading to most of the Fe^+ ions requires extra excitation of ~7 eV. This conclusion is in agreement with that qualitatively indicated by the mass spectrum of ferrocene at 50 eV.

When the normalization voltage is taken at a value closer to that of the ionization potential, (middle of the figure) this voltage difference decreases considerably and in the central region is < 3 eV. Finally, when the normalization is based on the 2.0 eV interval above the AP all three curves have the same shape and the curves for $FeCp^+$ and Fe^+ are almost superimposed. The difference between the $FeCp^+$ and Fe^+ curves this time is < 0.1 eV. Now, what we have been doing is examining these IE data for possible higher energy processes. It is clear that the Fe^+ IE curve does indicate the existence of a high energy process. When the deconvolution techniques we've described at the last two meetings of the society are applied to the Fe^+ IE data, we find that there are two processes leading to Fe^+. The lower energy process produces Fe^+ and $C_{10}H_{10}$, which we believe is Cp_2, and the higher energy process produces Fe^+ and 2 Cp. The relative abundances of these processes at 26 eV are 60 and 200 for the low and the high energy processes respectively. A comparison of the direct AP measurements and the deconvolution results for both ferrocene and nickelocene is given in Fig. 5.

There is further evidence to support our identifications of these processes. Hedaya and coworkers have shown that one of the products of the flash vacuum pyrolysis of nickelocene is $C_{10}H_{10}$. This was identified as 9, 10 dihydrofulvalene. Presumably this is the same Cp_2 which is seen in the mass spectra of ferrocene and ruthenocene, as well as nickelocene. From the ferrocene IE data the IP of Cp_2 is calculated to be 7.90 eV. This compares with a value of 7.75 eV found for the IP of 9, 10 dihydrofulvalene. Therefore the neutral fragment associated with Fe^+ at the lower AP value is probably Cp_2. It is unfortunate that our neutral fragment instrument has been undergoing some more development and is currently not usable because we'd very much like to have been able to report the direct observation of this neutral compound and its measured IP to you.

For further support we've looked for metastable transitions which would support our premise. Not only were these observable but they were

abundant enough so that appearance potentials could be measured. These data, again for ferrocene and nickelocene, are shown in Fig. 6. Note that the dissociation energy for the second-leaving Cp group is in excellent agreement with the value shown for the deconvolution experiments in the previous figure.

Fragmentation Mechanisms. We feel the use of metastable transitions and the deconvolution of primary IE data have clarified the interpretation of the fragmentation of metallocene molecules when they interact with electrons. On the basis of this evidence the simple mechanism shown for ferrocene in Fig. 7 is proposed. With minor variations it applies to other simple metallocenes. As shown above, the low energy process leading to Fe^+ requires a rearrangement of the two Cp's to form Cp_2. In order to achieve this, two carbon atoms of the Cp rings must come close enough to establish some kind of C-C bond. If the C-C distance is to be 1.6Å, the Cp-Fe-Cp angle must be ~120°. Calculations by Ballhausen and Dahl for protonated ferrocene, $HFeCp_2^+$, show that < 0.1 eV of excitation energy is required to make this angle 135°. On this basis, the production of Cp_2 proposed here is expected to have a low activation energy.

On the basis of the IE data and fragmentation mechanisms, the ionic dissociation energies for ferrocene, nickelocene and ruthenocene have been calculated. These are summarized in Fig. 8. The dissociation energies of the first M-Cp bonds were obtained from AP values for the primary or fast ionization processes. Those for the second M-Cp bonds were obtained from both deconvoluted primary ion IE data and IE data for metastable processes. As you see, the values for these two dissociation energies are quite reasonable and are more in keeping with both intuitive and theoretical expectations.

What are the Implications? If the fragmentation of these simple, essentially three-unit, molecules can be misunderstood for so many years and contribute their share to the mistrust of dissociation energies derived from appearance potential data, what confidence can be placed in any dissociation energy based upon AP values? The answer to this question is an old one and depends upon how well an investigator identifies the reactions leading to the observed appearance potentials. The problem here is the same that the calorimetrist has, namely that of knowing what system is being studied. We have been interested in this kind of ion source chemistry for a number of years and as a result have developed two unique instruments, a simultaneous positive-negative ion mass spectrometer and more recently a neutral fragment mass spectrometer to aid in the studies. The developments have allowed us to attempt to observe directly all of the products of dissociative ionization. Hopefully the energetics of even the neutral fragments will be determinable more routinely in the future. Only after one knows more about the true nature of the reactions taking place in ion sources will values for thermochemical properties derived from IE data merit the same kind of respect afforded calorimetric values.

We've just shown examples of how AP data from electron bombardment experiments can be interpreted, or misinterpreted. Often the long tails at the foot of the IE curves are attributed to excess kinetic energy or excited states in the product ions. However, from this and other studies we have made on inorganic and carbonyl systems over the years, we consider these tails to be more often the sum of product-ion yields from two or more chemically different processes than any other reason. Although this idea is illustrated by our metallocene data let us demonstrate it in more general terms, because we feel it is a common phenomenon. Figure 9 shows a simple reaction in which molecule ABC ionizes to form B^+ by two different processes. These processes have AP's different by an amount equal to the dissociation energy of the rearranged AC.

If B^+ is produced solely by reaction I, but the reaction is misidentified as reaction II, the dissociation energy calculated from AP values will be low by an amount equal to the dissociation energy of AC. If B^+ is produced only by reaction II but the reaction is mis-identified as I, the calculated dissociation energy will be too high. In either case, the IE curve would appear to have a normal shape. Correct identification of the process involved may require some independent information about the product neutrals and/or their dissociation energies. Thus you see it is important to know about the neutral fragments.

If B^+ is generated principally by reaction I, but II also occurs, the effects of reaction II will not be easily discernable in the IE data.

The IE curve shape will appear to be almost normal and the problem of identification will be the same as for the previous case. The effects of reaction II are detectable only by deconvolution of the IE data for the primary ions using the total ionization efficiency data as a reference.

If B^+ is generated principally by reaction II but I also occurs, the observed effect will be an enhanced tail on the IE curve, similar to that we showed earlier for the 50 eV normalization of Fe^+ data from ferrocene. Interpretation of this tail for Fe^+ required further data manipulation and more refined experiments. For some systems it may be impossible to come up with a reasonable interpretation.

If B^+ is produced equally by reactions I and II, the tail will be more sweeping and constitutes the major portion of an IE curve. Such curves are observed frequently in real experiments for low mass fragments which have multiple precursors. However, these IE data are amenable to deconvolution techniques which may allow for reasonable interpretations.

When one considers complex molecules with many possible rearrangements, it is quite easy to come up with fragmentation mechanisms whereby some ions are produced by 3, 4 or more pathways, each of which may have a different energy requirement. It is no wonder then that low mass fragment ions from complex molecules exhibit great tailing in the associated IE curves.

Extension of Metallocene Work. We have shown that deconvolution of fragment ion IE curves aid in interpreting IE data for the simple metalloences, and IE data for metastable transitions corroborated the mechanisms proposed. Are these same techniques useful for more complex molecules? We have studied the substituted ferrocenes shown in Fig. 10 to test this possible extension.

First a survey of the IP's, mass spectra, metastable transitions and IE curves of the more abundant fragment ions of these substituted ferrocenes were made. The numbers on this figure indicate the range of ionization potentials of the parent molecules. A naïve view of the reason for this observed variation in IP's is to consider the ionization of these molecules to be the result of the removal of a non-bonding electron from an orbital associated with the metal atom. Thus the ease with wich such an electron would be removed should be affected by the electron density associated with the metal. Those ligands which are strong electron donors would therefore increase the electron density around Fe making it easier to remove an electron and thus reducing the ionization potential. Strong electron acceptors on the other hand would reverse these effects and the IP's should increase. The data in this figure appear to support this view. Note that the IP's vary above and below the value shown earlier for ferrocene, the lowest value involving a good electron donor, $-OCH_3$, and the highest value involving the strong electron acceptor, $-CN$.

Fragmentation of these molecules in the mass spectrometer ion source leads to spectra whose complexity is also related to the substituting ligand. An example is the spectrum shown in Fig. 11 for the compound in which an acetyl group replaces a hydrogen on one of the Cp rings. It is clear that the fragmentation is much more complex than that for ferrocene. Extensive bond-breaking of the substituent group occurs. When the substituting group is aromatic the mass spectrum resembles more that of a hydrocarbon than the simple metallocene spectrum we spoke of earlier.

Another factor affecting the mass spectrum is the ability of various groups to take part in rearrangement processes. When a functional group of the substituent can form a stable bond with the metal atom, rearrangement ions make a significant contribution to the population of the total ions. In some cases these rearrangement ion currents may be the most intense in the spectrum. For example, this is true of hydroxy substituted ferrocenes such as $CpFeC_5H_4CH_2OH$, where the base peak in the spectrum us $CpFeOH^+$.

A consistent fragmentation mechanism for a variety of substituted ferrocenes can be deduced from these general observations. This mechanism is shown in Fig. 12. The solid arrows indicate transition pathways confirmed by observed metastable transitions while the dashed lines indicate proposed pathways for which no metastable transitions were observed. It is quite plain that many multi-energy pathways are present. It is significant to note that those ions which were products of reactions indicated by two or more metastable transitions generally exhibit broad sweeping

tails in their ionization efficiency curves. Determining dissociation energies for such molecules using present techniques is certainly going to be a horrendous task unless computer techniques can be applied.

Summary. In summary, we have established the fragmentation mechanisms for simple metallocenes using deconvolution and metastable ionization efficiency data. The low value for the ionic dissociation energy concerning the second-leaving Cp group has been corrected to a more reasonable value which is approximately 5 eV for the MCp_2 metallocenes. From these and other studies made on the chromyl oxyhalides and the hexacarbonyls of chromium, molybdenum and tungsten we conclude that the tails of fragment ion ionization efficiency curves are the result of multiple fragmentation pathways having various energy requirements. The data can however be deconvoluted and produce reasonable information about the molecules.

In closing I would like to call your attention to a review of the metallocene mass spectral literature written by G. A. Junk and H. J. Svec which appears as a chapter in a book entitled, "Recent Topics in Mass Spectrometry" edited by R. I. Reed and published by Gordon and Breach, London, 1971. This contains an extensive literature review covering all accessible published papers through 1969.

References

L. Friedman, A. P. Irsa and G. Wilkinson, J. Am. Chem. Soc., 77 3689 (1966).

R. Clampitt and W. J. Dunning, J. Sci. Instrum., 44 336 (1967).

C. J. Ballhausen and J. P. Dahl, Acta Chem. Scand., 15 1333 (1961).

A. Wilkinson, M. Rosenblum, M. C. Whiting and R. B. Woodward, J. Am. Chem. Soc., 74, 2125 (1952).

R. B. Woodward, M. Rosenblum and M. C. Whiting, J. Am. Chem. Soc., 74, 3458 (1952).

J. D. Dunitz and L. E. Orgel, Nature, 171 121 (1953).

E. Hedaya, D. W. McNeil, P. Schizzel and D. J. McAdoo, J. Am. Chem. Soc., 90 5284 (1968).

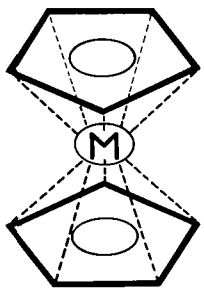

Figure 1.

FRAGMENTATION OF METALLOCENES[a]

	Fe	Ni	Ru
MCp_2^+	100	100	100
$MCp(C_3H_3)^+$	<<1	<1	<1
$M(C_3H_3)_2^+$	<1	2	1
MCp^+	19	62	29
$M(C_3H_3)^+$	2	13	5
MCp_2^{++}	5	8	9
M^+	10	12	3

[a] 50 eV electrons

Figure 2

APPEARANCE POTENTIALS (eV)
(EXTRAP. DIFFS.)

	Fe	Ni	Ru
$MCp_2 \rightarrow MCp_2^+$	6.77 ± 0.02	6.51 ± 0.04	7.53 ± 0.02
$MCp_2 \rightarrow MCp^+ + Cp$	13.89 ± 0.07	12.63 ± 0.05	14.58 ± 0.04
$MCp_2 \rightarrow M^+ + 2Cp$	13.94 ± 0.08	13.26 ± 0.10	16.2 ± 0.3
$MCp_2 \rightarrow M^{++} + Cp_2^+$	18.18 ± 0.05	--	--
IP(M) Spectroscopic	7.90	7.63	7.36

Figure 3

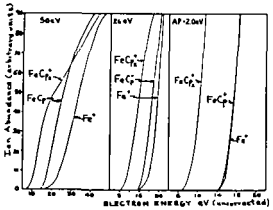

Figure 4

APPEARANCE POTENTIALS OF METASTABLE TRANSITIONS (eV)*

	Fe	Ni
$MCp_2^+ \rightarrow MCp^+ + Cp$	14.0	13.0
$MCp_2^+ \rightarrow M^+ + Cp_2$	14.4	13.4
$MCp_2^+ \rightarrow M^+ + Cp_2^*$	13.7	13.3
$MCp^+ \rightarrow M^+ + Cp$	19.2	17.7

* Uncertainties : 0.2 to : 0.5 eV

Figure 6

IONIC DISSOCIATION ENERGIES (eV)

	Metallocenes		
	Fe	Ni	Ru
MCp^+-Cp	7.1	6.1	7.0
M^+-Cp (Deconv.)	4.0	4.8	5.2
M^+-Cp (AP Metastable)	5.2	4.7	--

Figure 8

SUBSTITUTED FERROCENES

$C_5H_5FeC_5H_4R$

R		R	
$-OCH_3$	(6.5)	$-CH_2OH$	(7.0)
$-CH_2NHCH_3$	(6.6)	$-COCH_3$	(7.3)
$-pC_6H_4CH_3$	(6.8)	-CN	(7.5)
$-oC_6H_3(CH_3)_2$	(6.9)	-CHO	
$-CONHCH_3$	(6.9)	-COOH	
$-pC_6H_4Cl$	(7.0)	$-CN(OH)CH_3$	
$-mC_6H_4Cl$	(7.0)	$-CH=CH_2$	

Figure 10

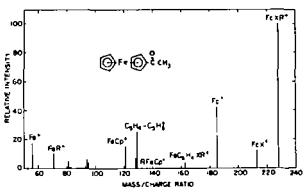

Figure 11. Representative mass spectra(70 eV) of monosubstituted metal complexes($CpMC_5H_4XR$). The bar diagram shown here is for $CpFeC_5H_4COCH_3$.

COMPARISON OF AP VALUES BY EXTRAPOLATED DIFFERENCE METHOD AND DECONVOLUTION

	Fe		Ni		Ru	
	Extrap. Diff.	Deconv.	Extrap. Diff.	Deconv.	Extrap. Diff.	Deconv.
MCp_2^+	6.77	6.8	6.51	6.5	7.53	7.5
MCp^+	13.89	14.0	12.63	13.0	14.58	14.8
M^+(I)	13.98	14.0	13.76	13.0	16.2	16.5
M^+(II)	--	18.2	--	17.8	--	20.0

Figure 5

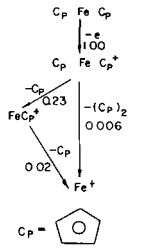

FRAGMENTATION SCHEME FOR FERROCENE
ELECTRON ENERGY(1P+18eV)

Figure 7

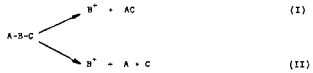

Figure 9

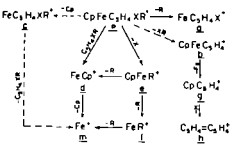

Figure 12. Partial fragmentation scheme for $CpFeC_5H_4XR^+$ where X=O,R=CH_3; X=CH_2, R=OH and $CH_2NC_5H_{10}$; X= CO, R=CH_3, OH, $NHCH_3$, C_6H_5, $C_6H_4OCH_3$ and OCH_3. Metastables were observed only for solid arrow reactions.

Mass Spectral Studies of Substituted Metal Carbonyl Compounds

F. E. Saalfeld, M. V. McDowell and J. J. DeCorpo
Naval Research Laboratory
Washington, D. C. 20390

The mass spectra obtained at NRL of a large number of metal carbonyl compounds, $RM(CO)_x(L)_y$ (R = Cl_3Si, F_3Si, $(CH_3)_3Si$, $F_2Si(CH_3)_2$, H, tris(dimethylamino)phosphine; M = Co, Mn, Fe, Mo, Cr, W; L = PF_3) have been reviewed. The studies reported included positive ion spectra and ionization studies for all of the compounds, negative ion spectra and ionization studies and neutral fragment identification for some of the compounds. From these data, some of the bond energies and heats of formation of these carbonyl compounds have been ascertained and several of their important fragmentation mechanisms delineated.

For most of the compounds studied, an appreciable temperature dependence of the spectra was observed. In addition, in one compound, $[(CH_3)_3SiFe(CO)_4]_2$, a gas-phase reaction between the compound and CO occurred, forming a new compound when the substance was introduced into the mass spectrometer via a heated, direct-insertion probe. These observations emphasize the caution which must be taken in the mass spectral studies of organometallic compounds.

Mass spectral fragmentation patterns, when presented in a ratio of

$$ML_x^+/RML_{x-1}^+,$$

can be interpreted in a manner which supports an intramolecular interaction between the substituent and other ligands in the molecule. This same interpretation can be employed, together with metastable transition data, to give support to the geometrical position of the ligand relative to the substituent.

The relative values of the ionization potentials of various carbonyls investigated appear to indicate the degree of backbonding from the metal to the substituent in the molecule and the heats of formation of a series of cobalt compounds, $RCo(CO)_x(PF_3)_{4-x}$ suggest that the nature of the RCo-CO and RCo-PF_3 bonds is similar.

Much of the information summarized in this talk has been published in the following references:

1. F. E. Saalfeld, M. V. McDowell, S. K. Gondall, and A. G. MacDiarmid, J. Amer. Chem. Soc. 90, 3684 (1968).

2. F. E. Saalfeld, M. V. McDowell, S. K. Gondall, and A. G. MacDiarmid, Inorg. Chem. 7, 1465 (1968).

3. F. E. Saalfeld, M. V. McDowell, A. P. Hagen, and A. G. MacDiarmid, Inorg. Chem. 7, 1665 (1968).

4. F. E. Saalfeld, M. V. McDowell, and A. G. MacDiarmid, Proc. Kyoto Internat. Conf. on Mass Spectroscopy, K. Ogata and T. Hagakawa, editors, University Park Press, Baltimore, Md., 1970, p. 1073.

5. A. G. MacDiarmid, et al., Pure and Applied Chem. 19, 431 (1969).

6. A. D. Berry, et al., J. Amer. Chem. Soc. 92, 1940 (1970).

7. F. E. Saalfeld, M. V. McDowell, and A. G. MacDiarmid, J. Amer. Chem. Soc. 92, 2324 (1970).

8. F. E. Saalfeld, M. V. McDowell, A. G. MacDiarmid, and R. E. Highsmith, J. Amer. Chem. Soc., in press.

J1

Deuterium Labelling as a Mechanistic Probe in Chemical Ionization Mass Spectrometry. CATHERINE FENSELAU, J. H. DUNCAN, and H. M. FALES, The Department of Pharmacology and Experimental Therapeutics, the Johns Hopkins University School of Medicine; and The National Heart and Lung Institute, National Institutes of Health.

In the chemical ionization mass spectrum of heptanal the most intense peak corresponds to ions formed by loss of water from the M+1 species. We undertook to delineate the origin of the hydrogen atoms eliminated in H_2O by the use of deuterium isotope labels, and in a more general sense, to contribute to the mechanistic understanding of chemical ionization decomposition, an area where few isotope labeling studies have been made. Measurements were obtained on deuterium labeled compounds including heptanal -2-d_2, -3-d_2, -4-d_2, -5-d_2, -6-d_2, and -7-d_1. Our data leads us to conclude that in the quasimolecular ion of heptanal the identity of the ionizing proton is not maintained, but that it is randomized with hydrogen atoms in the alkyl chain. Our observation suggests that when deuterium labels are used in chemical ionization studies, careful attention must be paid to the possibility of such randomization.

Per Cent Deuterium Atoms Lost in Elimination of Water From M+1

	E.I.	methane C.I.	isobutane C.I.
2-d_2-heptanal	0 %	3 %	9 %
3-d_2-heptanal	60 %	41 %	45 %
4-d_2-heptanal	57 %	38 %	40 %
5-d_2-heptanal	33 %	25 %	26 %
6-d_2-heptanal	36 %	42 %	42 %
7-d_1-heptanal (x3)	15 %	26 %	25 %
total	201 %	175 %	187 %

Values are averages of three scans made at 80° source temperature and 1 torr pressure. The values are calculated on the basis that the two hydrogen atoms lost as water equal 200%. The values are corrected for contributions from isotopic carbon and for incomplete labeling. Uncertainty is estimated at $\pm$ 2% for the E.I. values and $\pm$ 4% for the C.I. values.

This report will be published elsewhere in more detailed form.

J2

Chemical Ionization Mass Spectra of Pesticides
(Supported in part by the National Science Foundation, Grant No. GD-20231)

Noel Einolf, John Michnowicz, and Burnaby Munson
Department of Chemistry
University of Delaware
Newark, Delaware 19711

The electron (EI) and field (FI) ionization mass spectra of several pesticides have been reported previously[1]. We will discuss the conventional methane chemical ionization (CI) and high pressure charge exchange (CE) mass spectra of a few pesticides for comparison. In general, the CI and CE mass spectra are intermediate in extent of fragmentation between the very simple FI and complex EI spectra.

The spectra were obtained on a CEC 21-110B mass spectrometer which has been modified for high pressure operation[2]. The pressures were 0.5-1.0 torr; the source temperatures were the minimum necessary to give abundant spectra for direct introduction and were different for each compound. We are grateful to Joe Damico for providing us with the FDA standard samples for analysis.

Table I shows the methane CI spectra of two diphenyltrichloroethanes, DDT and the structurally similar Methoxychlor. The ions have been assigned according to species and the sum of all the chlorinated isotopes is indicated for each compound. In addition to the protonated and ethyl addition ions, the only fragment ions correspond to the loss of HCl, C_6H_5X, and $CHCl_3$ from the protonated molecular ions. These fragmentations probably result from protonation of the aliphatic Cl, the aromatic ring, and the aliphatic carbon atoms.

CH_4 CI Spectra of $XC_6H_4\text{-}\overset{CCl_3}{\overset{|}{C}}H\text{-}C_6H_4X$ — Table I

Species	% Additive Ionization	
	DDT (p,p'X=Cl)	METHOXYCHLOR (p,p'X=OCH_3)
$(MW + C_2H_5)^+$	0.8	1.1
$(MW + H)^+$	5.6	13.4
$(MW + H\text{-}HCl)^+$	31	36
$(MW + H\text{-}C_6H_5X)^+$	57	31
$(MW + H\text{-}CHCl_3)^+$	2.5	1.8

Table II shows the methane CI spectra of two carbamates in which structures have been assigned to each ionic species. The abundances of the decomposition ions are very different for these two compounds, but the differences can be explained easily by comparison with the spectra of other esters[3]. Sevin is an aromatic ester and should give the protonated alcohol as the major ion. No protonated acid ions are expected because of the lack of an easily transferrable hydrogen from the alcohol group. CIPC is an aliphatic ester and would be expected to give the protonated acid and alkyl displacement ions characteristic of aliphatic esters. No ions are formed which require dissociative protonation of the nitrogen.

CH_4 CI Spectra of Carbamates, RNHCOOR' — Table II

Species	% Additive Ionization	
	CIPC 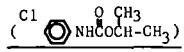	Sevin, Carbaryl 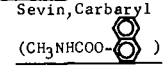
$(MW + C_3H_5)^+$	–	0.2
$(MW + C_2H_5)^+$	–	2.7
$(MW + H)^+$	32	12
$(RNHC(OH)_2)^+$	35	–
$RNHC{\equiv}O^+$	.5	16
$R'OH_2^+$	–	45
$RNH\overset{+}{C}(OH)(OC_2H_5)$	15	–

One of the major problems in high pressure charge exchange was the presence of hydrogen containing ions in the spectra of the reagent gases which gave $(M+1)^+$ ions in the spectra of the additives. By scrupulously removing the water from the gases, we were able to reduce the $(M+1)^+$ abundance to trivially small amounts of the total ionization.

Most of the gases which we tried gave predominantly dissociative charge transfer spectra and in order to obtain abundant molecular ions we used NO as the charge exchange reagent gas. The predominant ion under our conditions was NO^+, whose recombination energy is about 9 ev[4].

The diphenyltrichloroethane, Methoxychlor, shows only molecular ions and fragments corresponding to the loss of CCl_3 from the molecular ions.

Tables III and IV show the charge exchange spectra of the two carbamates obtained with NO and a comparison of these charge exchange spectra with the previously reported FI and EI spectra[1]. Although the same ions are produced, there are striking differences in the abundances of these ions depending on the mode of formation. These differences between CE and the other techniques will be investigated further by studying spectra with different charge exchange reagents.

Mass Spectra of CIPC, 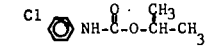 Table III

% Ionization

Species	EI	CE(NO)	FI
M^+	4	65	48
$RCO_2H_2^+$	-	3	--
RCO_2H^+	3	3	--
$RNCO^+$	8	-	7
RNH_2^+	9	9	Tr
$C_3H_7^+$	16	8	--

Mass Spectra of SEVIN, 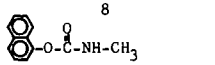 Table IV

% Ionization

m/e	EI	CE(NO)	FI	Species
201	1.5	8	21	MW^+
144	28	68	33	
116	13.5	.2	--	
57	8.5	.1	40	$(CH_3\text{-}N{=}C{=}O)^+$

References:

1. J. N. Damico, R. P. Barron, and J. A. Sphon, Int. J. Mass. Spec. and Ion Physics, 2, 161 (1969).
2. John Michnowicz and Burnaby Munson, Org. Mass. Spectr., 4, 481 (1970); the more recent modifications will be reported later.
3. M. S. B. Munson and F. H. Field, J. Am. Chem. Soc., 88, 4337 (1966).
4. G. K. Lavrovskaya, M. I. Markin, and V. L. Tal'roze, Kinetika i Kataliz, 2, 21 (1961) (Eng. translation).

APPLICATIONS OF CHEMICAL IONIZATION MASS SPECTROMETRY

G. P. Arsenault and J. J. Dolhun

Department of Chemistry
Massachusetts Institute of Technology
Cambridge, Massachusetts 02139

Details of a GC-MS system with a combined EI-CI source were reported earlier (1,2). Since that time, the system has been modified by replacing the combined source with two sources, one EI and one CI. A line drawing of the two-source system is shown in Figure 1, and this paper describes briefly the operation and applications of such a system.

The two-source GC-MS system may be operated in any one of the following four possible modes: (1) EI; (2) CI; (3) alternate EI and CI; and (4) simultaneous EI-CI. Whatever mode of operation is used the path and rate of flow of the GC effluent are the same. The GC effluent enters the CI source which is operated at 0.5 torr pressure. The effluent then leaves this source through the electron entrance or the ion exit apertures. The vacuum envelope immediately surrounding the CI source and in which the EI source is located is maintained at 4×10^{-4} torr. The system is differentially pumped and the pressure in the quadrupole mass filter is 3×10^{-5} torr.

Operation in the EI mode only requires the CI source to be off while the EI source is on. Direct introduction of the GC effluent in the EI source thus takes place since the CI source is merely a flow restrictor between GC and MS under these conditions. The EI source is off while the CI source is on if the system is operated in the CI mode only. The carrier gas for gas chromatography is then the reactant gas for chemical ionization (1,2,3). The alternate mode of operation is accomplished simply by switching rapidly and repeatedly between electron impact and chemical ionization. Finally both sources are on in the simultaneous mode of operation. The mass spectra obtained are thus mixed spectra, i.e. EI + CI, because there is only one quadrupole mass filter and one electron multiplier detector in the system.

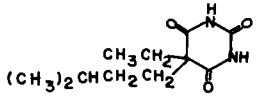

(I)

Figure 2 shows an unretouched reproduction (with the exception of the explanatory labels and numerals) of three consecutive scans of amobarbital (I) taken with the GC-MS system operated in the alternate mode. The total time which elapsed from the start of the first to the end of the third scan was 9 sec. The number of complete EI and CI mass spectra of a GC peak which may be obtained when the GC-MS system is operated in the alternate mode is naturally dependent on the width of the peak. Figure 3 shows an unretouched reproduction (the numerals are added) of a scan of amobarbital (I) taken with the GC-MS system operated in the simultaneous mode. The scan time was 3 sec. The EI and CI features of the simultaneous EI-CI mass spectrum (Figure 3) may be obtained by examining the individual mass spectra shown in Figure 2. Alternate or simultaneous EI-CI mass spectrometry of gas chromatographic effluents is the subject of a separate publication (4).

The advantages of two sources, one for EI and one for CI (Figure 1), over the single, combined EI-CI source are numerous and best discussed in terms of the drawbacks of the combined EI-CI source which are absent in the two-source system. The drawbacks of a combined EI-CI source are: (a) The sensitivity in the EI mode of operation is poor when compared to the sensitivity of a conventional EI source (5); (b) operation of the GC-MS system in the EI mode of ionization requires a splitter or a separator in the GC-MS interface or a drastic reduction in carrier gas flow rate to keep the pressure in the ion source within the limits necessary to obtain electron impact ionization only; (c) two separate injections are necessary to obtain

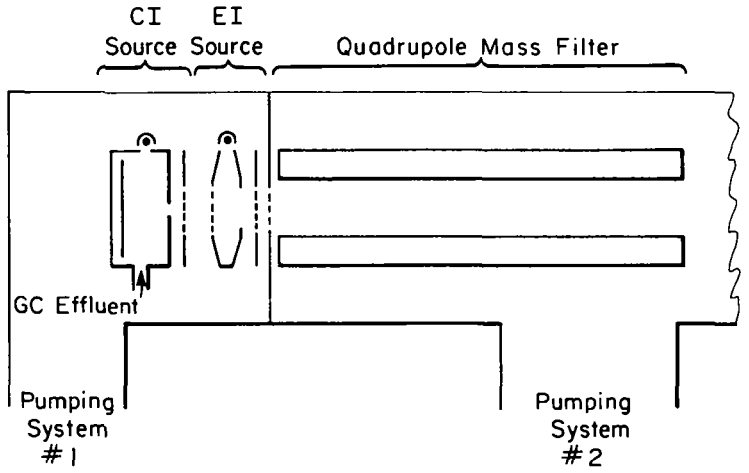

Figure 1. Line drawing -- no scale intended -- of GC-MS system with one CI and one EI source; the mass spectrometer component of the GC-MS system is the QUAD 300 made by Electronic Associates, Inc.

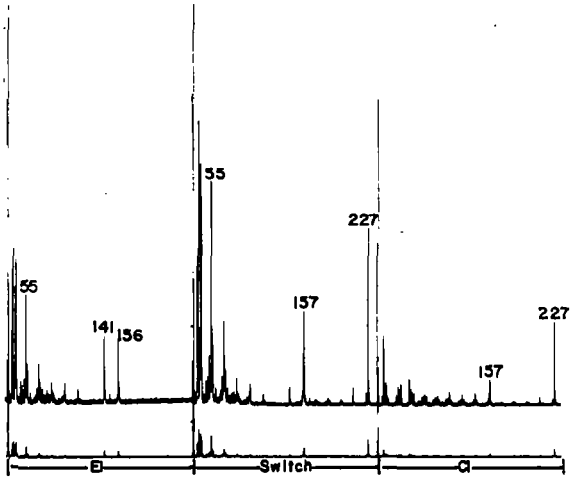

Figure 2. Alternate EI and CI mass spectrometry of GC effluent: oscillographic record of three successive scans of amobarbital (I); carrier-reactant gas: methane.

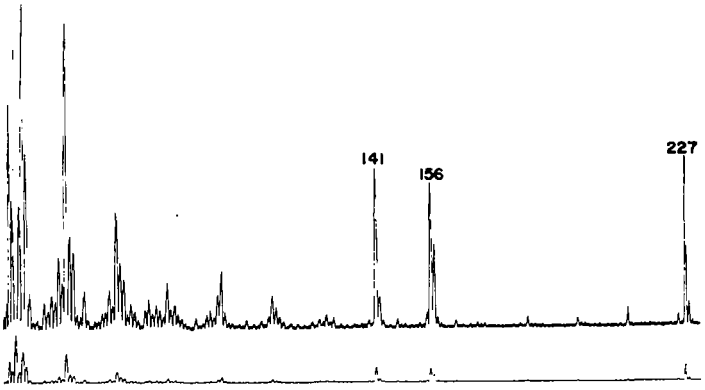

Figure 3. Simultaneous EI-CI mass spectrometry of GC effluent: oscillographic record of a scan of amobarbital (I); carrier-reactant gas: methane.

both EI and CI mass spectra of GC effluent, resulting in considerable labor necessary to collate and interpret the data from a gas chromatogram of any degree of complexity.

In conclusion, three points need to be made: (a) The two-source system could readily be modified for the direct introduction of solids into the CI source; (b) the two-source system described herein is equivalent to a single source with two chambers, one for CI and one EI; (c) while the two-source system was developed around a quadrupole mass filter it is equally applicable to magnetic deflection instruments.

Acknowledgement: The authors are indebted to B. Evans of Electronic Associates, Inc., for his cooperation, to members of the M.I.T. Mass Spectrometry Laboratory directed by Professor K. Biemann for their enthusiastic support and to the National Institutes of Health for financial support (Grant RR 00317 from Biotechnology Resources Branch, Division of Research Resources) and for a traineeship to J. J. D. (Grant No. GM 01523).

REFERENCES

1. G.P. Arsenault and J.J. Dolhun, Eighteenth Annual Conference on Mass Spectrometry, San Francisco, California, June 1970, p.B423.

2. G.P. Arsenault, J.J. Dolhun and K. Biemann, Chem. Communications, 1542 (1970).

3. D.M. Schoengold and B. Munson, Anal. Chem., 42, 1811 (1970).

4. G.P. Arsenault, J.J. Dolhun and K. Biemann, Paper submitted to Anal. Chem.

5. G.P. Arsenault, "Chemical Ionization Mass Spectrometry" in G.R. Waller (Ed.), Biochemical Applications of Mass Spectrometry, Wiley-Interscience, New York, in press, 1971.

NEGATIVE CHEMICAL IONIZATION MASS SPECTROMETRY

Ralph C. Dougherty, John Dalton and J. David Roberts

Department of Chemistry
Florida State University
Tallahassee, Florida 32306

Negative ions beams fully as intense as positive ion beams may be easily obtained under chemical ionization conditions. This is because the high pressure in the ion source thermally degrades the electron beam so there is always an abundance of electrons with energies in the 0-10ev range. With a spectrum of electron energies available all of the major primary anion forming processes[1], electron capture, disassociative electron capture and ion pair formation from molecular excited states will occur. The intensity of the primary ion beam is clearly related to the cross sections for the resonance capture processes and for this reason we have principally used halocarbons as reagent gases in negative chemical ionization experiments.

The high pressure negative ion spectrum of methylene chloride shows the following ions, $Cl^{\ominus}$, $H_2O{:}Cl^{\ominus}$, $HCl_2^{\ominus}$, $Cl_3^{\ominus}$, $Cl{:}CH_2Cl_2^{\ominus}$, $H_2Cl{:}CH_2Cl_2^{\ominus}$, $Cl{:}(CH_2Cl_2)_2^{\ominus}$, and $HCl_2{:}(CH_2Cl_2)_2^{\ominus}$. The intensities of these ions vary smoothly with temperature and pressure. At ~1 torr and 200°C, $Cl^{\ominus}$, $HCl_2^{\ominus}$ and $Cl{:}CH_2Cl_2^{\ominus}$ dominate the mass spectrum. In the presence of small quantities of a substrate, anion attachment and other reactions occur. The specific attachments are very sensitive to the nature of the functional groups present. The spectra are always simple. Table I lists the anions observed for a series of simple molecules in the presence of methylene chloride at ~1 torr and 200°C.

Table I

Negative Ion Chemical Ionization Spectra with Methylene Chloride (1 torr, 200°C).

substrate	Ions observed (relative intensity > 1%) exclusive of the CH_2Cl_2 spectrum
2-octanol	$[M + Cl]^{\ominus}$
n-nonglamine	$[M + HCl_2]^{\ominus}$
benzoic acid	$[M + Cl]^{\ominus}$, $[2M - H]^{\ominus}$
2-octanone	$[M + Cl]^{\ominus}$
benzophenone	$[M]^{\ominus\ominus}$, $[M + HCl]^{\ominus\ominus}$
p-nitrotoluene	$[M]^{\ominus\ominus}$, $[M + O]^{\ominus}$, $[M + Cl]^{\ominus}$, $[M + HCl]^{\ominus\ominus}$

	$[M + ClO]^{\ominus}$, $[2M]^{-\cdot}$
aldrin	$[M - H_3Cl_2]^-$, $[M - H_2Cl]^{\ominus}$, $[M - H]^{\ominus}$, $[M + Cl]^{\ominus}$, $[M + ClO]^{\ominus}$, $[M + HCl_2]^{\ominus}$ $[M + ClCO_2]^{\ominus}$

The simplicity of the spectra, their relatively high sensitivity and the selectivity of the reagent toward different functional groups make negative chemical ionization spectra with methylene chloride an attractive candidate for development as a technique in analytical mass spectroscopy.

High pressure anion spectra also have considerable potential in complex problems in mechanistic organic chemistry. By use of a series of difference reagent gases it is possible to examine the equilibrium heats of association of a large number of anion-molecule pairs by using temperature studies at constant pressure following the leads of Field[2] and Kebarle.[3] These heats must be directly related to the stabilities of the solvent-free nucleophilic substitution complexes. We have determined a large number of heats of association and find that both steric effects in S_N2 reactions and nucleophilicity effects are primarily due to anion-solvent interactions and not to anion-substrate interactions. The methyl chloride-methyl iodide cycle illustrates this point. The literature value

		$-\Delta H_o$(kcal/m)
$CH_3I + Cl^{\ominus}$	$CH_3ICl^{\ominus}$	7.8
$CH_3Cl + I^{\ominus}$	$CH_3ClI^{\ominus}$	9.8
$CH_3I + Cl^{\ominus}$	$CH_3Cl + I^{\ominus}$	1.7

for the final equilibrium is -10.5 kcal/m.[4] The possibility that these heats reflect the stabilities of frontside association ions and not psuedo-Jahn-Teller distorted S_N2 transition states can be eliminated on the basis that 1-bromoadamantane gives no simple halide association ions under conditions which give intense simple halide association ions from other monohalides.

1. C.E. Melton, "Mass Spectrometry of Organic Ions," F.W. McLafferty, ed., Academic Press, New York, 1963 p. 163.
2. F.H. Field, J. Amer. Chem. Soc., 91, 2827 (1969).
3. P. Kebarle, S.K. Searles, A. Zolla, J. Scarborough and M. Ashadi, ibid., 89, 6394 (1967).
4. J.L. Franklin, J.G. Dillard, H.M. Rosenstock, J.T. Herron, K. Draxl and F.H. Field, "Ionization Potentials, Appearance Potentials and Heats of Formation of Gaseous Positive Ions", NSRDS-NBS26, U.S. G.P.O., Washington, 1969.

APPLICATIONS OF CHEMICAL IONIZATION MASS SPECTROMETRY

Rodger L. Foltz

BATTELLE
Columbus Laboratories
Columbus, Ohio 43201

One of the attractive features of chemical ionization mass spectrometry (CIMS) is its compatibility with gas chromatography. Because of its ability to handle higher flow rates, a chemical ionization ion source can be directly coupled to a gas chromatograph without requiring the use of a separator.[1] In this mode of operation the carrier gas used in the gas chromatograph also serves as the reactant gas in the chemical ionization mass spectrometer.

Figure 1 shows a block diagram of the system we have utilized for the past year. It includes a gas chromatograph directly coupled to a quadrupole mass spectrometer modified for chemical ionization.

Normal operation of the GC-CIMS system consists of selecting the desired carrier/reactant gas by opening the appropriate valve and adjusting the gas flow rate to give the optimum ion source pressure. For methane this pressure corresponds to about 1 torr as measured by a thermocouple gauge. Since there is no restriction between the gas chromatograph and the mass spectrometer the pressure in the gas chromatograph column is below one atmosphere. Both 1/8" packed columns and capillary columns have been used under these conditions. In the case of 1/8" packed columns the retention times experienced are comparable to those obtained using a flow rate of 30 ml/min in a conventional gas chromatograph.

For a general purpose GC-MS system it is desirable to be able to obtain both chemical ionization and electron impact mass spectra since often the two techniques provide complementary structural information. If helium or nitrogen is used as the reactant gas under chemical ionization conditions the sample molecules are ionized by a charge exchange process which should result in mass spectra similar to those obtained under electron impact conditions. Therefore, it should be possible to obtain either proton-exchange, chemical ionization spectra or electron impact-like spectra by simply changing the carrier/reactant gas.[2]

In order to determine whether electron impact and helium chemical ionization conditions give similar mass spectra, various compounds were examined using the two methods of ionization. Figures 2 and 3 represent two rather typical examples. The electron impact mass spectra were obtained using a standard AEI MS-9 and the helium chemical ionization spectra were obtained using a Finnigan 1015 quadrupole mass spectrometer equipped with an SRIC model QS-15 chemical ionization source. The differences between the relative intensities of the fragment ions in the electron impact mass spectra and the helium chemical ionization mass spectra are not appreciably greater than one typically encounters in comparing mass spectra obtained on different instruments and under different operating conditions. However, we did find that compounds having a high proton affinity often give intense M + 1 peaks under the helium chemical ionization conditions. For example, note the intense m/e 197 peak in the CI_{He} spectrum of the diketopiperazine (Figure 3). We concluded that the enhanced M + 1 peaks result from self-protonation due to the relatively high sample pressure in the chemical ionization source. We subsequently found that certain compounds give intense M + 1 peaks even in the absence of a reactant gas. This behavior is apparently characteristic of the relatively "closed" or "tight" ion sources used in chemical ionization mass spectrometers. Figures 4 and 5 compare electron impact spectra obtained on two compounds using both "closed" and "open" ion sources. In both cases the M + 1 peak shows a much greater relative intensity in the EI spectrum obtained using the "closed" source. It should be emphasized that these are the most extreme examples that we have encountered and that most compounds do not exhibit this behavior. Furthermore, the fragmentation patterns obtained when the spectra are normalized to the same peak are similar and very different from the fragmentation patterns obtained under normal chemical ionization conditions using methane as the reactant gas.

We are now routinely running GC-MS samples by alternately using methane and helium as the carrier/reactant gases and are finding the technique extremely useful.

---

(1) G. P. Arsenault, J. J. Dolhum, and K. Biemann, Chem. Comm., 1542 (1970).

(2) D. M. Schoengold and B. Munson, Anal. Chem., 42, 1811 (1970).

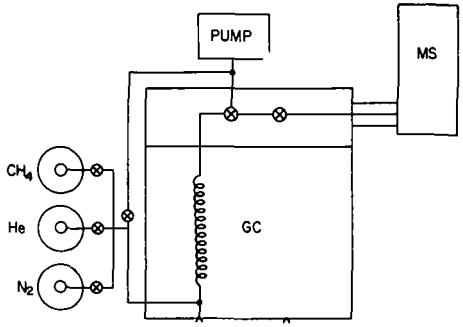

Fig. I. GAS CHROMATOGRAPH - CHEMICAL IONIZATION - MASS SPECTROMETER SYSTEM

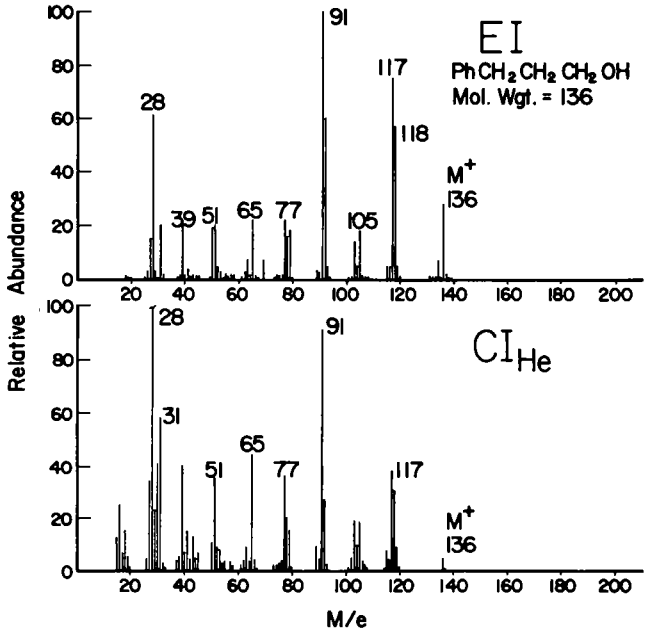

Fig. 2. MASS SPECTRA OF 3-PHENYL-1-PROPANOL

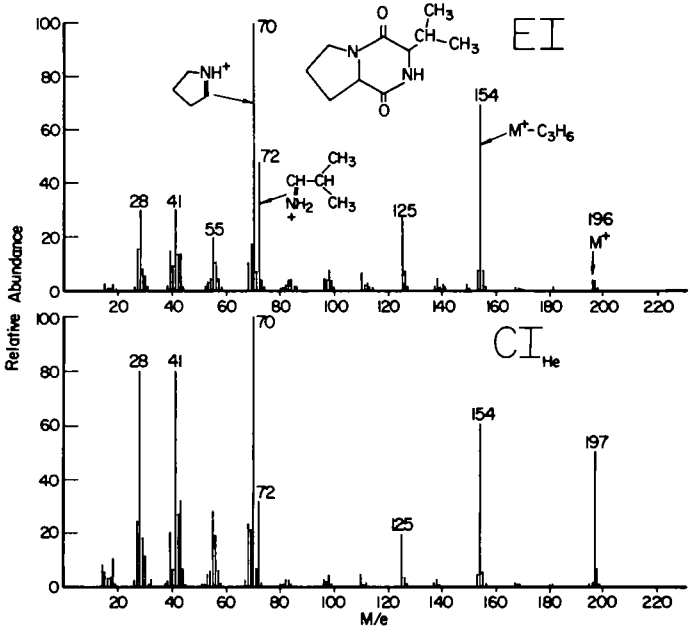

Fig.3. MASS SPECTRA OF THE DIKETOPIPERAZINE FROM PROLINE AND VALINE

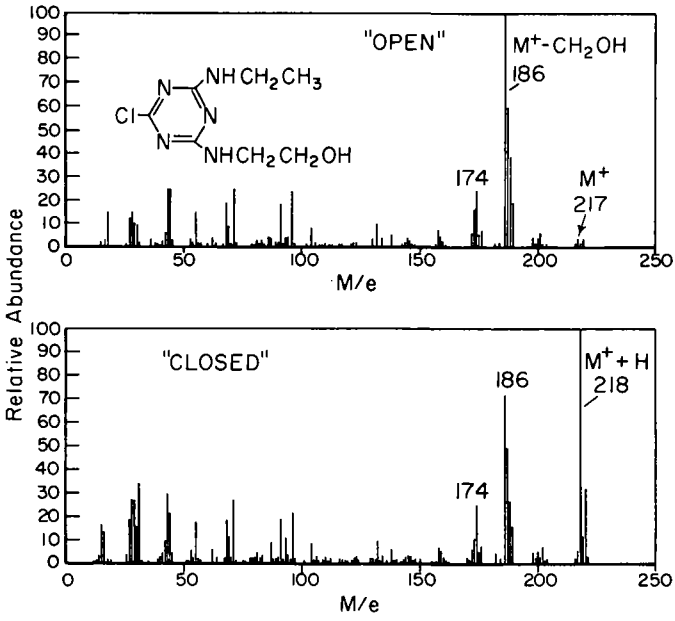

Fig. 4. EI MASS SPECTRA OBTAINED WITH "OPEN" AND "CLOSED" ION SOURCES

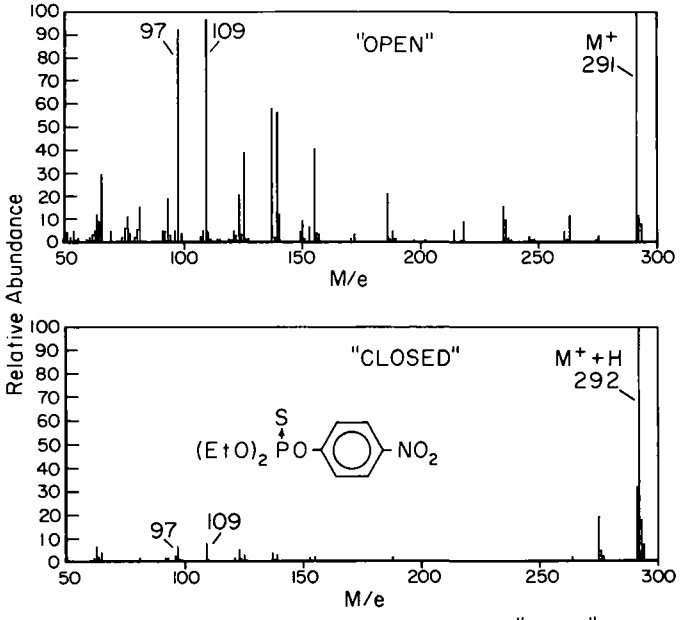

Fig. 5. EI-MS OF PARATHION OBTAINED WITH "OPEN" AND "CLOSED" ION SOURCES

THE APPLICATION OF CHEMICAL IONIZATION MASS SPECTROMETRY TO THE IDENTIFICATION OF DRUGS IN BODY FLUIDS

David P. Beggs, Ralph C. Dougherty, William H. Johnston
Scientific Research Instruments Corporation
Baltimore, Maryland 21207

ABSTRACT

The use of a GLC - chemical ionization mass spectrometer system for the analysis of drugs in body fluids is discussed. The use of hydrogen as the GLC carrier gas and the reagent gas provides improved sensitivity.

The prevalence of the MW+1 or MW-1 peaks in hydrogen chemical ionization spectra provides easy identification of drugs in body fluid extracts. Positive identification of any drug may be obtained by comparison of the simple fragmentation pattern with a standard compound or spectrum.

INTRODUCTION

Recently Fales and Milne[1,2] have demonstrated the need for a fast, efficient, and reliable method to determine the drug contents in body fluids of severe drug overdose patients. This work deals with the application of a GLC - Chemical Ionization Mass Spectrometer system to this problem.

The requirement for an interface or separator between the GLC and the MS was eliminated by using the Chemical Ionization reagent gas as the GC carrier. The samples passed through a 3% OV-17 column into an SRIC Chemical Ionization Quadrupole System. Standardization using pure drug samples was accomplished by direct probe insertion into the chemical ionization system.

Chemical ionization mass spectrometry provides increased sensitivity and specificity for drug analyses. The spectra are simple, and include, in most cases, large peaks corresponding to the molecular weight plus or minus one amu (proton acceptance or hydride ion loss). In many instances, with certain reagent gases, only one peak is present in the entire chemical ionization spectrum. An effort was made to determine the optimum combination carrier-reagent gas to provide "fingerprint spectra".

RESULTS AND DISCUSSION

The effect of reagent upon fragmentation of the sample is shown in Table I. In each case ionization of the sample occurs by proton transfer and these spectra reflect the differences in the proton affinities of isobutene, methane and hydrogen. As the difference in proton affinities between the reagent gas and the sample gas increases, the amount of fragmentation increases. The use of hydrogen provides a sufficient amount of fragmentation while retaining a significant amount of MW+1 peak. One compound, aspirin, did not give an intense M+1 peak but it did produce an easily identified spectra with ions representing the lossof H_2O, CH_3CO and CH_3COOH.

Most of the drugs studied were barbiturates but some other common prescription drugs and some non-prescription, drugs, were also analyzed. All of the drugs studied to date produced simple spectra with at least three fragment peaks and in most cases a strong ion at MW-1, MW, or MW+1. The drugs which were not derivatives of barbituric acid usually gave ions at MW+1, MW, and MW-1 while derivatives of barbituric acid gave ions mainly at MW+1. This is attributed to the relatively strong nucleophilic nature of the barbituric acid derivatives.

To effectively demonstrate the use of this technique in the identification of drugs in body fluids, many synthetic mixtures of drugs in aqueous solution were prepared. These solutions were extracted with chloroform. Aliquot samples were injected into the GLC. Monitor of the GLC effluent was accomplished via the total ion monitor of the quadrupole. Repetitive scans were made over each GLC peak. Identification of the GLC peaks was accomplished by determining the MW+1 peak. If more than one drug with the same molecular weight may be present, identification is made by comparison of the simple fragmentation patterns. In this manner positive identification of each drug in a mixture can be made. Analysis of other constituents of the mixture, including impurities, may be easily accomplished if a standard reference sample or chemical ionization spectrum is available.

No significant change in the spectra of samples was found between 100μ and 1000μ of reagent gas pressure. The optimum operating pressure for this system was 350μ of H_2. At hydrogen pressures above 900μ, extended use of the filament resulted in an abnormally large amount of deposition of the rhenium onto the surrounding surfaces. Variation of the repeller between O and +20 volts produced no significant change. Increasing the repeller above +20 volts resulted in an increase of the relative intensity of the fragment peaks, corresponding to an increase in the excess energy accompanying the ionization process. The sensitivity of this system was found to be 1 to 10 nanograms depending upon the nature of the drug to be analyzed.

CONCLUSION

Several advantages of this system are apparent. A minimum of sample is lost in its transfer from the GLC to the ionization region. This is due to the elimination of the separator and the direct, line of sight connection. The use of hydrogen as the carrier gas provides improved gas chromatographic resolution which allows the GLC flow rate to be increased. Chemical ionization with hydrogen as the reagent gas provides an intense MW+1 or MW-1 peak for most compounds while initiating sufficient fragmentation to establish a "fingerprint" spectrum.

REFERENCES

1. N.C. Law, Virginia Aandahl, H. M. Fales and G.W.A. Milne, Clinica Chemica Acta, 32, 221 (1971).

2. H.M. Fales, G.W.A. Milne, and T. Axenrod, Analytical Chemistry, 42, 1432 (1971).

TABLE I

CHEMICAL IONIZATION OF SANDOPTAL

Relative Intensities Using Various Reagent Gases

m/e	Isobutane	Methane	Hydrogen
124	-	-	1
149	-	4	1
167	-	2	8
168	-	-	9
169	-	2	16
171	-	-	13
185	-	24	6
208	-	-	13
223	-	-	5
224	-	-	15
225	100	100	100

J8

Isotope effect in the formation of HS^- and DS^- by electron impact on H_2S, HDS and D_2S

Florence FIQUET-FAYARD and Jean-Pierre ZIESEL,
Laboratoire de Collisions Electroniques,
Faculté des Sciences, 91-ORSAY, France

-:-:-:-

We have studied the formation of HS^- by dissociative attachment in H_2S. This process is typical of dissociative attachment, with a very small survival probability for the transitory negative ion. We measured the shape of the ionization curve, the total ionization cross section and the isotope effect. The experimental procedure will be described in a paper submitted to the Journal of Chemical Physics.

The threshold of the ionization curve occurs at 1.45 ± 0.1 eV, the maximum at 2.2 eV. The curve ends at 3.4 eV.

The total cross-section at the maximum is

$$\sigma(HS^-/H_2S) = 1.8\ 10^{-18}\ cm^2$$

The isotope effects are :

$$\sigma_1/\sigma_4 = 25 \pm 4$$
$$\sigma_1/\sigma_2 = 14 \pm 5$$
$$\sigma_1/\sigma_3 = 1.26 \pm 0.03$$

where the relative cross sections are defined "per bond" and not "per molecule" :

$H_2S + e$	——	$HS^- + H$	$2\sigma_1$
$HDS + e$	——	$HS^- + D$	σ_2
$HDS + e$	——	$DS^- + H$	σ_3
$D_2S + e$	——	$DS^- + D$	$2\sigma_4$

The asymptotic appearance potential for HS^- can be calculated exactly since the dissociation energy has been measured by Dibeler and Liston[1].

$$D_0(HS - H) = 3.87 \pm 0.02\ eV$$

while the electron affinity has been measured by Steiner[2]

$$EA(HS) = 2.296\ eV$$

We find a value of 1.57 Volt for the asymptotic appearance potential.

The remarkable feature is that the asymptotic appearance potential is identical to the threshold, within the error limits. This implies that the H_2S^- potential curve crosses its dissociation asymptote inside the Franck-Condon region.

We use our results to calculate the complexe energy of the H_2S^- potential curve :

$$V_f(R) - i\,\Gamma_a(R)/2,$$

where Γ_a is the total autoionization width of the resonant state, and R is the distance between HS^- and H.

...

The procedure consist in a parametrization of $V_f(R)$ and $\Gamma_a(R)$. Then we use the O'Malley formula[3] to calculate the isotope effect and the ionization curve. We adjust the parameters to reproduce the experimental results. Several parametric expressions have been used for $V_f(R)$. $\Gamma_a(R)$ is written as $B\left(\frac{R_c - R}{R_o}\right)^{\beta}$, where B and β are parameters, R_o is the equilibrium distance, and R_c is the distance at which the H_2S^- potential curve crosses the H_2S potential curve.

The results will be described fully in the full paper. They are consistent with the assumption of an s-wave resonance ($\beta = 0.5$) and of a small dip in the potential curve (about 0.15 eV).

-:-:-:-:-:-

(1) V.H. DIBELER and S.K. LISTON ; J. Chem. Phys. 49, 482 (1968)

(2) B. STEINER ; J. Chem. Phys. 48, 5097 (1968)

(3) T.F. O'MALLEY ; Phys. Rev. 150, 14 (1966)

Formation of O^- from N_2O at Temperatures Above 2000 K*

J.M. Madson, J.H. Mullen and L.N. Medgyesi-Mitschang
McDonnell Douglas Research Laboratories
McDonnell Douglas Corp., St. Louis, Mo. 63166

The deleterious effect of shock-ionized flow fields on communication and navigation systems may be reduced by electrophilic molecule injection. The assessment of the ability of each molecule for reducing the electron concentration requires detailed high temperature kinetics of the resulting electron-molecule and/or electron-ion reactions. High temperature environments for studying these reactions can be achieved with a plasma. An experimental system employing a high temperature flowing plasma has been developed for studying electron attachment reactions at gas temperatures from 2000 to 3000 K.[1] The system described here has been used to investigate negative ion formation in Br_2, SF_6, and N_2O.[2] The present discussion is limited to negative ions resulting from the reaction of N_2O with an argon plasma.

The overall experimental system is shown schematically in Fig. 1. The system consists of four sections: (a) discharge chamber, (b) reaction channel, (c) expansion-extraction chamber, and (d) mass analysis chamber. An rf induction plasma generated in the discharge chamber is isentropically expanded into the reaction channel. The flow velocity becomes sonic as the plasma enters the reaction channel. While in the channel the flowing plasma reacts with target gas molecules (in this case N_2O) which have been supersonically injected as indicated in Fig. 1. At the end of the reaction channel the flowing plasma undergoes a free jet expansion into the expansion-extraction chamber. This rapid expansion preserves the product species of the reactions occurring in the channel. The centerline core of the expansion plume is sampled with a conical extractor and analyzed with a quadrupole mass spectrometer. Discharge chamber conditions may be varied from 10 to 760 Torr with input power levels up to 100 kW. The temperature and pressure of the flowing plasma in the reaction channel are 0.75 and 0.50 of their respective values in the discharge chamber. The transit time of the plasma through the channel is about 10 μsec; therefore, proper mixing of the N_2O with the plasma is of serious concern and has led to the investigation of several injection techniques. Data obtained using two of these techniques are presented here. The first technique is supersonic injection of N_2O through flush mounted injectors. Three injectors having 50 μm orifices spaced 120° around the channel are inserted flush with the inner wall of the reaction channel. The N_2O pressure behind the injector orifice is always greater than twice the channel pressure to ensure that the N_2O is supersonically injected. The N_2O is injected normal to the plasma flow and mixes with the plasma as it traverses the channel. The second injection technique utilizes three conduction-cooled, protruding injection tubes which extend approximately 1/3 of the distance across the channel (0.125 cm in a 0.4 cm diam channel). N_2O is injected subsonically through the tubes into the plasma stream well inside the channel boundary layer.

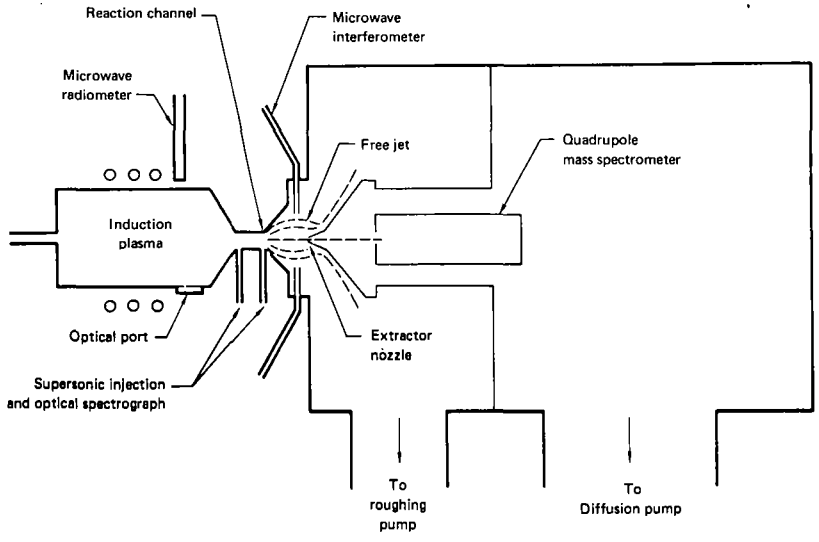

Fig. 1 Schematic drawing of experimental system

*Research supported by Air Force Cambridge Research Laboratories under Contract F-19628-71-C-0024 and by the McDonnell Douglas Independent Research and Development Program.

Figure 2 is a schematic diagram of the ion sampling and detection system. The scale at the top of this figure shows typical operating pressures in various parts of the system. Reversal of the polarity on the lensing and detection elements of the system results in a change in operation from negative ion detection to positive ion detection. In addition, an electron ionization source is used for qualitative identification of neutral gas species.

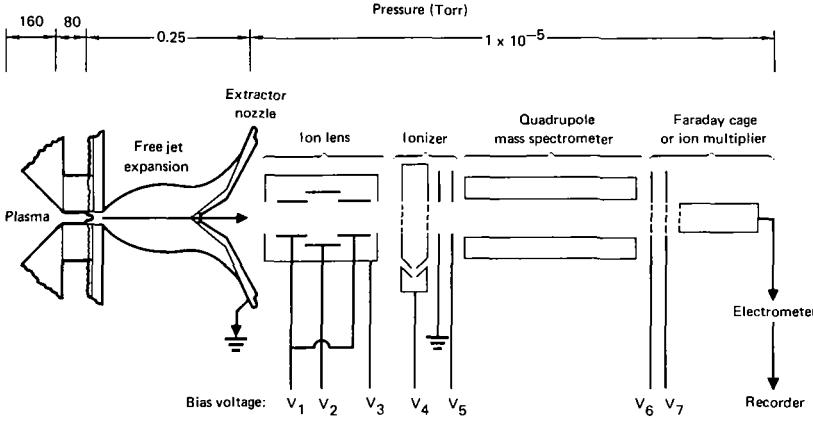

Fig. 2 Mass spectrometer system for analysis of negative ions, positive ions and neutral products of high temperature reactions

Typical O^- signals obtained when N_2O is injected through flush mounted supersonic injectors are shown in Fig. 3. In Fig. 3, the collected O^- current (arbitrary units) is plotted as a function of the mole percent of N_2O injected in the flowing argon plasma.

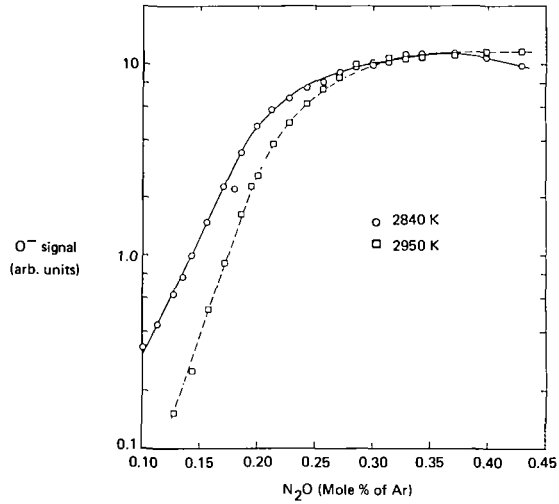

Fig. 3 Negative ion production using flush mounted supersonic injectors

Production of O^- in N_2O results from a dissociative attachment reaction in which an encounter between an electron and a neutral N_2O molecule produces an O^- ion and a neutral N_2 molecule, the reaction proceeding with a characteristic rate constant k_1. The reaction is described by

$$e + N_2O \xrightarrow{k_1} O^- + N_2. \tag{1}$$

O^- ions may be lost by reacting with N_2O in a manner such as

$$O^- + N_2O \xrightarrow{k_2} NO^- + NO \tag{2}$$

or

$$O^- + N_2O \xrightarrow{k_3} O_2^- + N_2. \tag{3}$$

The differential equation which describes the O^- concentration has been solved under the assumptions that electrons and N_2O molecules are lost only to the O^- formation process and that any O^- loss is due to reactions (2) and (3). Solutions for the O^- concentration as a function of the N_2O concentration have been obtained for various values of a parameter "a" which is the product of the rate constant k_1, the initial electron density $[N_e]_o$ and the reacting time T. A comparison between the calculations and experimental data is shown in Fig. 4.

The notations $[N_e]_o$ and $[N_2O]_o$ refer to the initial electron and N_2O number densities at the point where the N_2O is injected. The solid lines represent solutions of the equation describing O^- concentration for various values of "a" = $k_1[N_e]_oT$. The circles represent experimental data points. The reaction time T is governed by the channel length and the gas temperature. Therefore, for fixed channel length and plasma conditions a family of curves can be drawn representing different values of the reaction rate constant k_1. To illustrate the effect of O^- loss, rate constants k_2 and k_3 have been combined and called βk_1. The use of βk_1 to represent a secondary reaction rate constant is not meant to imply that the same functional dependence on physical parameters such as temperature exists for the dissociative attachment rate constant and the secondary ion-molecule reaction rate constant. The curve for $\beta = 0$ represents no loss of O^- through reactions with N_2O molecules. As $O^- - N_2O$ reactions begin to be significant, the O^- signal reaches a maximum and begins to decrease. This feature can be used as an aid in fitting the experimental data to the calculated curves. A dissociative attachment rate constant of about 5×10^{-9} cm^3/molecule sec at about 3000 K is obtained from the data shown in Fig. 4.

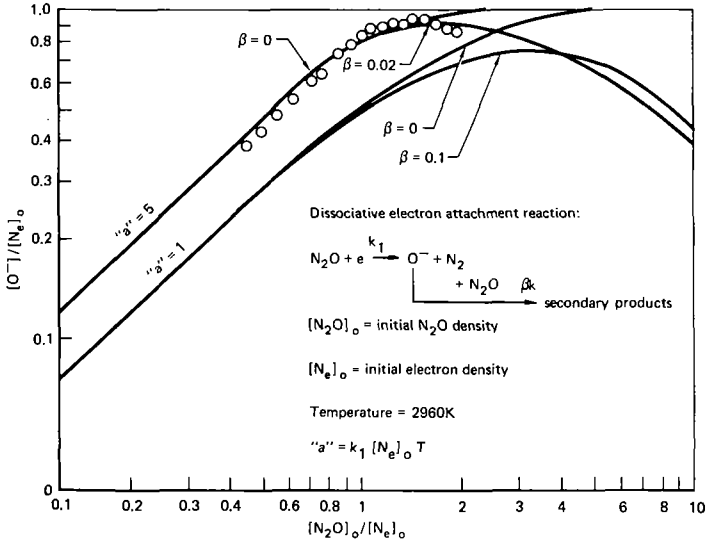

Fig. 4 Comparison of experimental data with theoretically predicted O^- production

Figure 5 shows the negative ion species detected when N_2O is injected into an Ar plasma through injectors protruding into the reaction channel. NO^-, N_2O^-, and O_2^- ions are present in addition to the O^- which was present with the supersonic injectors. Paulson[3] has listed the following set of reactions to explain the formation of these ions;

$$O^- + N_2O \xrightarrow{k_2} NO^- + NO \tag{2}$$

$$O^- + N_2O \xrightarrow{k_3} O_2^- + N_2 \tag{3}$$

$$NO^- + N_2O \xrightarrow{k_4} N_2O^- + NO. \tag{4}$$

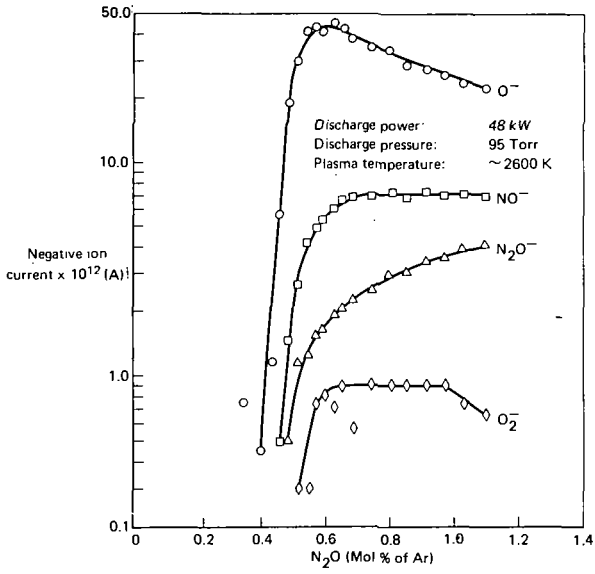

Fig. 5 Negative ion production at 2600 K using three subsonic protruding wall injectors

Figure 6 shows an increase of NO^+, O^+, *and* N_2O^+ *and a rapid decrease in* Ar^+ *as the* N_2O *concentration increases.* The rapid decrease of Ar^+ suggests that it assists the production of the other positive ions, perhaps through a charge exchange mechanism.

Investigation of the channel flow indicated that the protruding injectors create a turbulent condition in the reaction channel flow thus allowing recirculation of the plasma and lengthening of the reacting time in the channel. The production of the additional negative ions shown in Fig. 5 and the positive ions shown in Fig. 6 using the protruding injector technique where these ions were not detectable using supersonic flush mounted injectors may be a result of the turbulence introduced by the injectors.

In conclusion, we have examined O^- production when N_2O is injected into a flowing Ar plasma at temperatures between 2500 and 3000 K. Calculations of O^- production based on a dissociative attachment model have been made which when combined with experimental results yield a rate constant at about 3000 K, of 5 x 10^{-9} cm^3/molecule sec at least two orders of magnitude greater than that obtained at room temperature. Secondary and tertiary reactions occurring when N_2O is injected through protruding injectors indicates an interesting area for further investigation. However, the uncertainties introduced by the turbulent channel flow make this technique less desirable for attachment rate constant measurements.

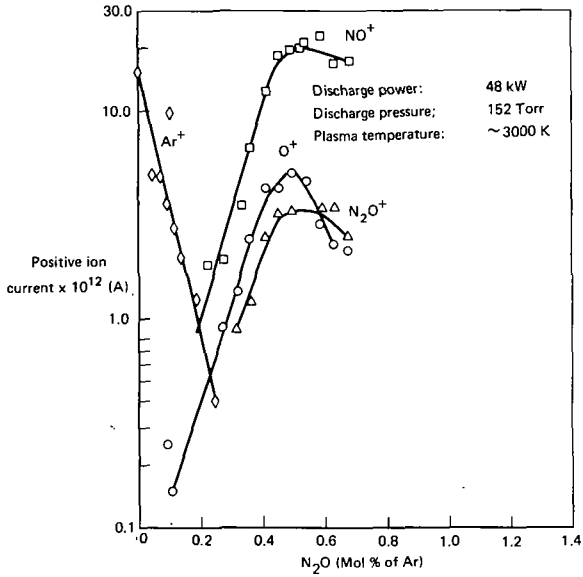

Fig. 6 Positive ion production using subsonic protruding wall injectors

References

1. J.H. Mullen, J.M. Madson, L.N. Medgyesi-Mitschang, T.C. Peng, and P.M. Doane, Rev. Sc. Instr. 41, 1746, (1970).

2. J.M. Madson, J.H. Mullen and T.C. Peng, "Mass Spectrometry of a Chemically Quenched rf Plasma," 18th Annual Conference on Mass Spectrometry and Allied Topics, San Francisco, Calif., June (1970).

3. J.F. Paulson, J. Chem. Phys. 52, 959 (1970).

Reactions of Some Solvated Alkoxy Anions*

J10

E.G. Jones and T.O. Tiernan, Aerospace Research Laboratories
Chemistry Research Laboratory, W-PAFB, Ohio 45433

The reactions of alkoxy anions with alcohols have been extensively studied[1,2]. The order of alcohol acidity in the gas phase, determined by measuring the rates of the forward and reverse reactions, differs from that obtained by solution experiments. To investigate this difference and to obtain information concerning the effects of ion solvation on reaction, we have studied reactions of anions of the form $HOHOR^-$ and R_1OHOR^- with a series of small alcohols. These ions were formed in water-alcohol mixtures in the first stage of a tandem mass spectrometer and were allowed to react with the neutral alcohols in a separate collision chamber.

The principal reaction of alkoxy anions with alcohols is a proton abstraction; however, after solvation we observe three major reactions. In addition to proton abstraction there is a solvent exchange for HOH and also for HOR in the anion. The normalized product distributions are shown in Tables I and II for some typical cases. In general there is a reduction in the basicity of the anions on solvation, as indicated by the relatively lesser importance of the proton abstraction path. This effect is most clearly seen in the reactions of the hydroxide ion. It will abstract a proton from all of the neutrals in Table I; however, after solvation with a water molecule it abstracts a proton only from propanol and butanol, the more acidic alcohols.

Extensive H-D scrambling in the hydroxyl positions was observed after labelling either the reactant ion or neutral. Since the largest product anions are formed preferentially we conclude that these solvent interchange reactions occur via a long-lived collision complex which decomposes according to the stability of the product fragments.

TABLE I
Reactions of Solvated Anions Observed in the Tandem Mass Spectrometer at 0.3eVK.E.

Neutral	Ion	Normalized Product Distribution		
		Proton Abstraction	Exchange HOH	Exchange ROH
HOH	$HOHOH^-$	0	50	50
MeOH	$HOHOH^-$	0	50	50
	$HOHOMe^-$	0	89	11
	$HOHOEt^-$	0	96	4
	$HOHOPr^-$	0	100	0
EtOH	$HOHOH^-$	0	50	50
	$HOHOMe^-$	0	76	24
	$HOHOEt^-$	0	--	--
PrOH	$HOHOH^-$	24	38	38
	$HOHOMe^-$	6	75	19
	$HOHOEt^-$	5	83	12
BuOH	$HOHOH^-$	37	32	32
	$HOHOMe^-$	13	69	18
	$HOHOEt^-$	11	76	13
	$HOHOPr^-$	6	85	9

TABLE II
Reactions of $EtOHOMe^-$ Observed in the Tandem Mass Spectrometer at 0.3eVK.E.

Neutral	Normalized Product Distribution	
	Exchange MeOH	Exchange EtOH
PrOH	65	35
BuOH	63	37

References:

1. T.O. Tiernan and B.M. Hughes: Seventeenth Annual Conference on Mass Spectrometry and Allied Topics, Dallas, Texas, 1969

2. J. Brauman and L.K. Blair, J. Amer. Chem. Soc. 90, 6561 (1968): ibid. 92,5987 (1970)

* A more extensive account of this work will be submitted for publication in the Journal of the American Chemical Society.

Some Negative Ion Reactions with Water*

John F. Paulson
Air Force Cambridge Research Laboratories (AFSC)
L. G. Hanscom Field, Bedford, Mass. 01730

A longitudinal double mass spectrometer system has been used to study the reactions

$$H^- + H_2O \rightarrow OH^- + H_2 \qquad (1)$$

$$O^- + H_2O \rightarrow OH^- + OH \qquad (2)$$

together with the corresponding reactions of their isotopic reactant variants (D^-, D_2O) in the interaction energy range from 0.3 to 50 eV. In the case of reaction (1) the cross section at 1 eV is about 30×10^{-16} cm^2 and at 8 eV is about 1×10^{-16} cm^2. Cross sections for the reactant pairs $H^- + H_2O$, $H^- + D_2O$, $D^- + H_2O$, $D^- + D_2O$ at 1 eV interaction energy give rate constants decreasing from 4 to 2×10^{-9} cm^3 sec^{-1} in the order given. Principally because of uncertainties in relative ion collection efficiencies, the measured cross sections are in general lower limits. True cross sections may be as much as a factor of 2.5 times larger than those measured. Allowing for this uncertainty, the present results are in fair agreement with those from some ion source experiments[1] on $D^- + D_2O$ but differ appreciably with those from other such experiments,[2] giving both lower cross sections and qualitatively different isotope effects.

Reaction (2) is endothermic by about 0.35 eV and shows a cross section increasing sharply to about 20×10^{-16} cm^2 at 1 eV before falling off to 2×10^{-16} cm^2 at 15 eV. Both retarding potential and time-of-flight analyses of the product ions show fast and slow components, which may be identified respectively with the forward and backward scattered OH^- product (in the barycentric system) of this endothermic reaction. Calculations of the energy transferred into internal modes of the products, based on the TOF spectra, give essentially identical values for both the forward and backward scattered product ion components, a result which is a consequence of the nearly identical masses of the ionic and neutral products. The use of $^{18}O^- + H_2{}^{16}O$ shows that the "fast" ion product is $^{18}OH^-$ and the "slow" ion product is $^{16}OH^-$. The kinematic necessity for forward and backward scattered products in an endothermic process above threshold may therefore be identified in this case with hydrogen atom transfer and proton transfer chemical mechanisms, respectively.

References

1. J. F. Paulson, Advan. Chem. Ser. 58, 28 (1966).
2. J. A. D. Stockdale, R. N. Compton, and P. W. Reinhardt, Phys. Rev. 184, 81 (1969).

*To be submitted to the Journal of Chemical Physics

ELECTRON IMPACT FRAGMENTATION MECHANISMS OF SOME HALORUTHENOCENES

K1

by

Arun K. Bhattacharya* and Lee D. Smithson
Air Force Materials Laboratory
Wright-Patterson Air Force Base, Ohio 45433

Fragmentation mechanisms have been studied for some chloro, bromo and iodo derivatives of ruthenocene. In an earlier communication we discussed the mass spectra of polychlorinated ferrocenes.[1] These di-π-cyclopentadienyl compounds have a unique sandwich type structure. The two symmetric five-membered rings in ferrocene have a staggered configuration whereas for ruthenocene they have an eclipsed configuration. The barrier of rotation of the rings about the metal to ring axis is very small, which accounts for the facile cleavage of the ring to metal bond on electron impact.

The nine compounds incorporated for discussion in this paper are as follows:

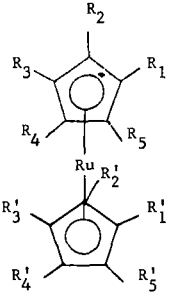

Unassigned R's = H

(I)
(II) R_1 = Cl
(III) R_1, R'_1 = Cl
(IV) R_1, R_2, R'_1 = Cl
(V) R_1 = Br
(VI) R_1, R'_1 = Br
(VII) R_1, R_2, R'_1 = Br
(VIII) R_1 = I
(IX) R_1, R'_1 = I

One of the striking features of the mass spectra of these compounds is the complex cluster of peaks due to the seven naturally occurring isotopes of ruthenium and the isotopes of the halogens. The relative intensities of each cluster were predicted by a statistical method.[2] Normalized isotopic patterns have been drawn on the basis of these calculations. The principal patterns utilized in this paper are shown in Figures 1 and 2.

Fragmentation patterns have been proposed based on considerations of predicted isotopic patterns, exact mass measurements and metastable peaks. The molecular ion is the most intense peak in the mass spectra of all compounds except for iodoruthenocene (VIII). This can be easily explained on the well established fact that the C-I bond is relatively weak as compared to that of the C-Br, C-Cl and C-H bonds. It is conceivable that there is a shifting of electron density from the cyclopentadienyl ligands to the metal atom as the mass increases from iron to ruthenium, with the result that the C-C bond of the cyclopentadienyl ring becomes weaker than the metal to ligand bond. We have observed noticeable cleavage of the skeletal carbon bonds in the cyclopentadienyl rings of these compounds in addition to the usual metal to ring rupture as in ferrocenes.[1] This conforms with earlier work on metallocenes.[3,4]

Some of the fragmentation patterns have been shown in Figures 3-5.

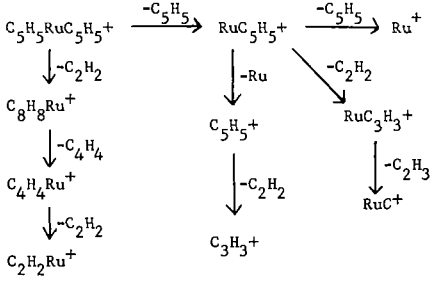

Figure 3. Fragmentation Pattern for Ruthenocene

*Miami University, Air Force Contract

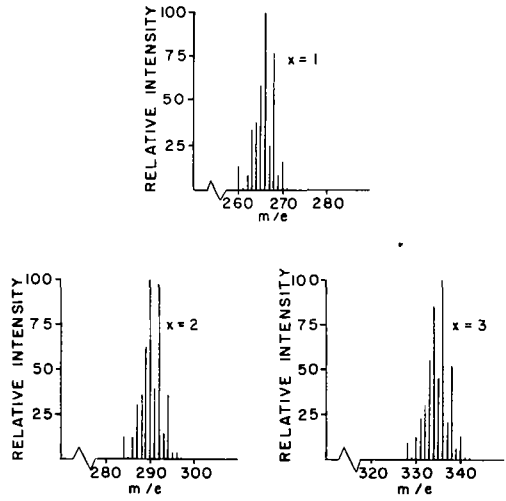

Figure 1. Predicted Isotopic Cluster for the Molecular Ion of $RuC_{10}H_{10-x}Cl_x$

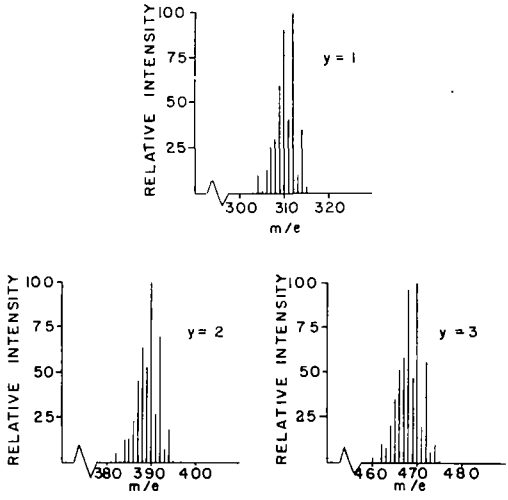

Figure 2. Predicted Isotopic Cluster for the Molecular Ion of $RuC_{10}H_{10-y}Br_y$

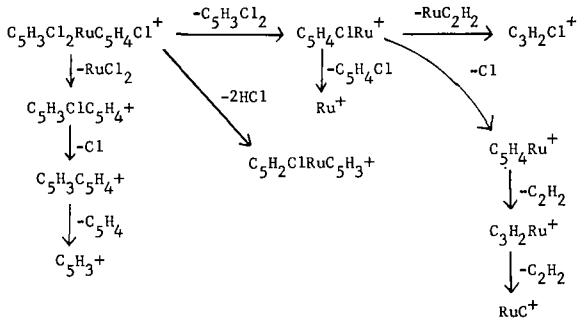

Figure 4. Fragmentation Pattern for 1,2,1'-Trichlororuthenocene

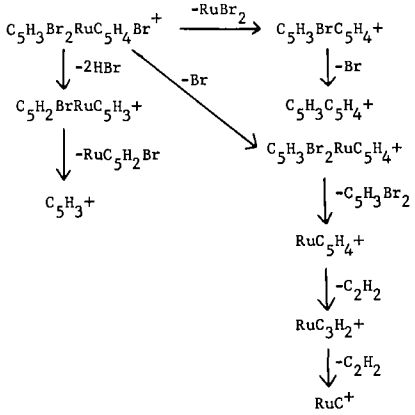

Figure 5. Fragmentation Pattern for 1,2,1'-Tribromoruthenocene

The details of the fragmentation mechanisms will be submitted for publication in Analytical Chemistry.

REFERENCES

1. L. D. Smithson, A. K. Bhattacharya and F. L. Hedberg, Org. Mass Spectrom, 4, 383 (1970)

2. A. K. Bhattacharya, AFML-TR-71-35, Wright-Patterson Air Force Base, Ohio

3. L. Friedman, A. P. Irsa and G. Wilkinson, J. Am. Chem. Soc., 77, 3689 (1955)

4. J. Müller and L. D'Or, J. Organometal. Chem., 10, 313 (1967)

K2

Pyrolysis Studies and Molecular Beam Mass Spectra of 1,2-Dimethoxytetramethyldisilane; 1,1,2,2-Tetramethoxydimethyldisilane and Hexamethoxydisilane. SARA J. STECK, DePaul University, Chicago, Ill. 60614, JOHN L. MARGRAVE and RONALD P. STEIGER, Rice University, Houston, Texas 77001

ABSTRACT

The following compounds (I) 1,2-dimethoxytetramethyldisilane, (II) 1,1,2,2-tetramethoxydimethyldisilane and (III) hexamethoxydisilane were studied in a 60° sector magnetic instrument. Metastable ions with intensities up to nearly 10 percent of the principle peaks indicate that the major ion decomposition pathways are (1) the loss of a methyl group followed by loss of formaldehyde or (2) loss of formaldehyde from the P/2 ion. Pyrolysis studies of the three compounds showed thermal decomposition of (I) to $Si(OCH_3)_2(CH_3)_2$, $Si(CH_3)_2$, and $[Si(CH_3)_2]_2$; (II) to $Si(OCH_3)_3CH_3$ and CH_3SiOCH_3; and (III) to $Si(OCH_3)_4$ and $Si(OCH_3)_2$. Also information about the thermal and ion decompositions of the monosilane producats was obtained.

Positive and Negative Ion Mass Spectra of Some Organomercurials* K3

Stuart C. Cohen

Department of Chemistry, Syracuse University, Syracuse, New York 13210

Organomercurials generally show a basic simplicity in fragmentation under electron impact;

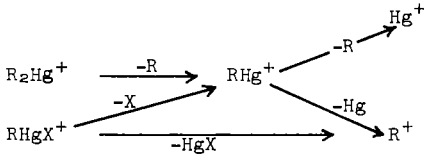

with the organogroup ion, R^+, having the highest intensity. For C_6Cl_5HgCl, however, $C_6Cl_4^+$ was the most intense ion, and the following fragmentations were supported by metastable peaks:

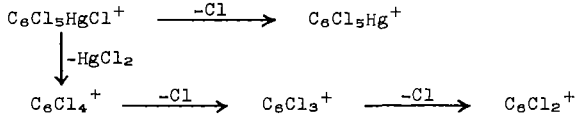

A comparison of the clastograms of C_6Cl_6 and C_6Cl_5HgCl indicate that for the latter compound, $C_6Cl_4^+$ is being formed at the expense of $C_6Cl_5HgCl^+$ rather than $C_6Cl_5^+$; the route expected for the normal fragmentation being:

$$C_6Cl_5Hg^+ \xrightarrow{-Hg} C_6Cl_5^+ \xrightarrow{-Cl} C_6Cl_4^+.$$

The relative appearance potentials, A.P.($C_6Cl_4^+$) - A.P.($C_6Cl_5^+$), for the ions derived from C_6Cl_6 and C_6Cl_5HgCl indicate different processes for formation of $C_6Cl_4^+$ from the two compounds.

C_2Cl_3HgCl behaves in a similar fashion, with $C_2Cl_2^+$ being the most intense ion, formed by loss of $HgCl_2$ from the parent ion. For $(C_2Cl_3)_2Hg$, loss of C_2Cl_2 from the parent ion is supported by a metastable peak. Clastogram data indicates that in this case, $C_2Cl_2^+$, again the strongest ion, is being formed at the expense of $C_2Cl_4Hg^+$ rather than $(C_2Cl_3)_2Hg^+$.

$$\underline{\text{i.e.}}, \quad (C_2Cl_3)_2Hg^+ \xrightarrow{-C_2Cl_2} C_2Cl_4Hg^+ \xrightarrow{-HgCl_2} C_2Cl_2^+$$

The ion, $C_2Cl_4Hg^+$, is thought to be of the same nature as the parent ion $C_2Cl_3HgCl^+$. The relative appearance potential, A.P.($C_2Cl_4Hg^+$) - A.P. ($C_2Cl_3HgCl^+$), value of 0.8 ± 0.4 e.v. (18 ± 9 kcal mole^{-1}) shows good agreement with the value (25 ± 18 kcal mole^{-1}) calculated from the bond energies involved in the formation of $C_2Cl_4Hg^+$

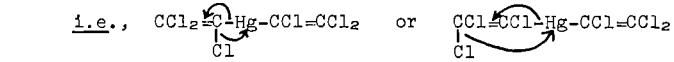

In the mass spectra of $(C_6F_5)_2Hg$ and C_6F_5HgX (X = Cl, Br), the organo ions from C_6F_5HgX have greater intensity, relative to $C_6F_5^+$ (the most intense ion), than those from $(C_6F_5)_2Hg$. This indicates the possibility of HgFX elimination from $C_6F_5HgX^+$, producing $C_6F_4^+$, etc. with higher intensities.

Negative ions were observed from the pentafluorophenyl and trichlorovinylmercurials. $(C_6F_5)_2Hg$ gave the parent anion, formed by secondary electron capture, and $C_6F_5^-$, $C_6F_4^-$, F^-. C_6F_5HgX gave $C_6F_5X^-$ as the most intense negative ion, formed in an analogous fashion to $C_6F_5X^+$:

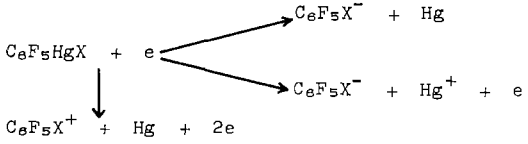

Several organomercury anions were observed for C_2Cl_3HgCl and $(C_2Cl_3)_2Hg$ including $C_4Cl_5Hg^-$, $C_2Cl_4Hg^-$ and $C_2Cl_3Hg^-$. The most interesting observation was that of $HgCl_2^-$, formed by dissociative electron capture from C_2Cl_3HgCl and probably, by ion-pair formation from both mercurials.

The mass spectra of $(CH_3)_2C=C(HgCl)_2$ and $CH_3CH(HgCl)_2$ gave $Hg_2Cl_2^+$, Hg_2Cl^+ and Hg_2^+, in addition to the normal fragmentation. Relative appearance potential measurements for these ions indicate that Hg_2Cl^+ and Hg_2^+ arise by different mechanisms for the two compounds. Thus, for $(CH_3)_2C=C(HgCl)_2$:

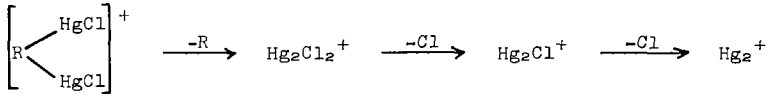

whereas lower energy processes occur for $CH_3CH(HgCl)_2$:

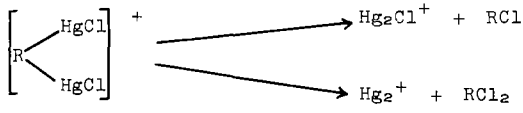

---

* Published, in part, Chem. Comm., 226 (1970), Inorg. Nucl. Chem. Letters, 6, 757 (1970), J. Chem. Soc., (A) 632 (1971). To be published, in part, J. Chem. Soc., (A).

Mass Spectra of Organometallic Acetylenes of Group IV and V Elements

M. L. Bazinet, W. G. Yeomans* and C. Merritt, Jr.
Pioneering Research Laboratory
U. S. Army Natick Laboratories
Natick, Massachusetts 01760

Although there are presently a fair number of laboratories actively involved in the analysis of Group IV organometallic derivatives, relatively little experimental work has been reported until recently on the mass spectrometry of any but tri- or tetraalkyl type derivatives of these elements.

In this work we report on the spectral comparison of six triphenyl silicon or germanium compounds containing a diphenyl phosphine group. These acetylides were analyzed on a CEC 21-110 mass spectrometer, operated at 70 e.V., and equipped with means for electric sector decoupling, for metastable examination. The analyses were made by sampling with the direct solids insertion probe.

The generalized formula for the types of Group IV element acetylides that were analyzed is shown in the lower right hand corner of Figure 1. These are triphenyl silicon or germanium acetylides where the R group is diphenyl phosphine which is either non-coordinated or coordinated on the phosphorus atom with oxygen or sulfur.

The left hand side of Figure 1 illustrates a typical fragmentation diagram for this class of organometallic compounds. The one shown here is for the silicon acetylide with a non-coordinated phosphorus atom. The mass of the principal ion fragments observed in the spectrum and the ion abundance are indicated by the numbers shown below the structural representation of each ion. Ion abundance is expressed as the percentage of total ionization.

The molecular ion decomposition paths are indicated with arrows; when the pathway is supported by the appearance of a metastable ion, an asterisk is shown beside the arrow.

The molecular ion seen in the top center at mass 468 is the most abundant ion in the spectrum of triphenylsilyl, diphenylphosphine acetylide. Rupture of the silicon-carbon bond produces the next largest peak at mass 259, which is the triphenylsilyl ion. Breaking the carbon-phosphorus bond gives an intense ion at mass 283. Further cleavage of phenyl groups accounts for most of the remaining ions.

Fragmentation of the compound in which oxygen is coordinated with the phosphorus atom is quite similar to the non-coordinated compound. The molecular ion is the most abundant ion and the next most abundant is mass 283, corresponding to the loss of the phosphine oxide group. A series of ions from successive loss of phenyl groups appears to be quite characteristic for the compounds of the series we have studied.

Fragmentation of the sulfur coordinated silicon acetylide indicates that the increased electronegativity of the sulfur atom in the phosphine-sulfide group appears to weaken the carbon-silicon and the carbon-phosphorus bonds. The triphenyl silicon ion at mass 259 is the most abundant ion in the spectrum. Loss of the phosphine group by scission at the carbon-phosphorus bond yields an intense ion at mass 283, and loss of sulfur gives a relatively abundant ion at mass 468.

The increased decomposition of the molecular ion results in its being the second most intense ion. A shift of a phenyl group from silicon to carbon and the loss of the diphenyl silicon group gives a rearrangement ion at mass 286.

In general, the fragmentation of the germanium compounds appears to be quite similar to that of corresponding silicon compounds. However, the decomposition of the molecular ions is greater, and a greater number of ion types are produced. In the non-coordinated compound the molecular ion at m/e 514 is only moderately intense. The most

* Present address: Chemistry Dept., Massachusetts Institute of Technology

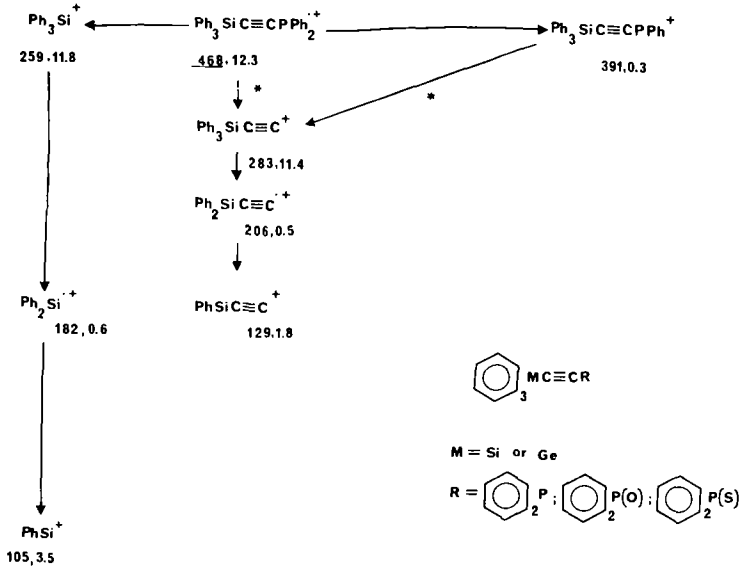

Figure 1

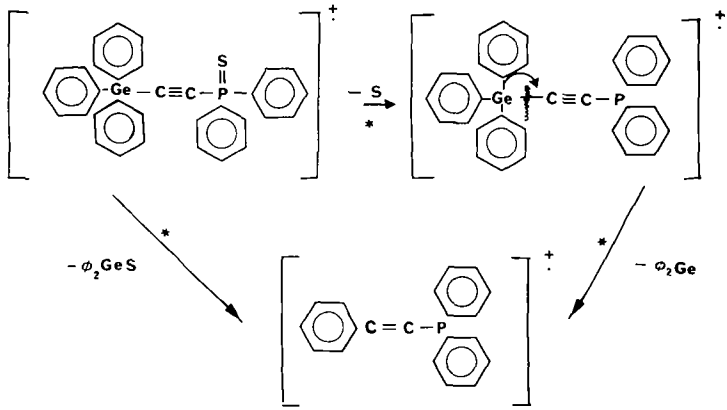

Figure 2

abundant ion in the spectrum arises from cleavage of the Ge-C bond, resulting in the formation of the triphenyl germanium ion at m/e 305. This cleavage also provides an ion of low abundance at m/e 209 when the charge resides on the acetylene containing portion of the molecule.

Splitting of the carbon-phosphorus bond gives rise to an ion at m/e 329 when the charge resides with the acetylene containing portion of the molecule, and to m/e 185 when the charge remains on the phosphorus atom.

As with the silicon compounds, the loss of phenyl groups accounts for most of the remaining ions. The decomposition pathway leading to the series of phenyl phosphonium ions is relatively predominant in the germanium compounds. These ions are relatively abundant in all the germanium containing compounds.

When oxygen is coordinated with the phosphorus atom of the germanium acetylide, the most abundant ion is m/e 453, corresponding to the loss of a phenyl group from the moderately intense molecular ion.

Fragmentation of the sulfur coordinated germanium compound is extensive. The most intense ion is the triphenyl germyl ion at m/e 305, for which four pathways exist, all substantiated by observed metastable transitions. The molecular ion is the second most abundant ion in the spectrum. Rupture of the carbon-phosphorus bond of the molecular ion produces a moderately abundant peak at m/e 329.

Loss of sulfur gives an ion at m/e 514 and loss of the sulfur along with a phenyl group provides two possible ions at mass 437, where the phenyl group can be lost from either the germanium atom or the phosphorus atom. Further decomposition of the mass 437 ion by cleavage at the germanium carbon bond gives an ion at mass 209 if the charge is on the acetylene containing group, and at mass 228 if the charge remains on the germanium containing moiety. Cleavage of mass 437 ion at the carbon-phosphorus bond yields a fairly intense diphenyl phosphonium ion at mass 185. Loss of phenyl groups accounts for most of the remaining ions, except for the rearrangement ion at m/e 286, due to a phenyl shift from Ge to carbon.

The origin of the rearrangement ion at m/e 286 which is seen characteristically in all the spectra, is depicted in Figure 2. This ion is observed in about 1 percent relative abundance in the non-coordinated compounds, 5-6 percent in the phosphine oxide compounds, and from 17 to 21 percent in the phosphine sulfide compounds. Two pathways are found which can be verified by observed metastable ion transitions. In the first, a phenyl group may shift from the germanium atom to the carbon atom which, followed by a loss of sulfur and diphenyl germanium, leads to the rearrangement ion. Another path for its formation is from the mass 514 ion resulting from the loss of sulfur, which then goes through a similar shift of phenyl group from germanium to carbon. The subsequent loss of the diphenyl germyl group produces the rearrangement ion.

The metastable ion spectrum supporting these pathways is shown in Figure 3. The peak corresponding to the rearrangement ion is seen on the left and the two precursors are seen on the right. The more intense peak for the parent ion at mass 546 indicates the principal pathway is through the concerted reaction in which a sulfur atom and a diphenyl germanyl group are lost simultaneously.

In summary, we have studied the spectra of the silicon or germanium phosphino acetylenes and a comparison of their fragmentation behavior made. Typical cleavages are observed which result in the formation of a series of phenylsilyl and phenyl germyl ions, as well as phenyl-phosphorus ions. The parent ion or the parent minus the triphenyl silyl or triphenyl germyl group are generally the most abundant peaks. The effect of coordination of the phosphorus atom with electronegative atoms such as oxygen or sulfur tends to increase the overall fragmentation. The most noteworthy observation has been the discovery of a rearrangement ion which results from a shift of a phenyl group from the Group IV element to the acetylenic carbon atom.

The complete manuscript will be submitted to Organic Mass Spectrometry.

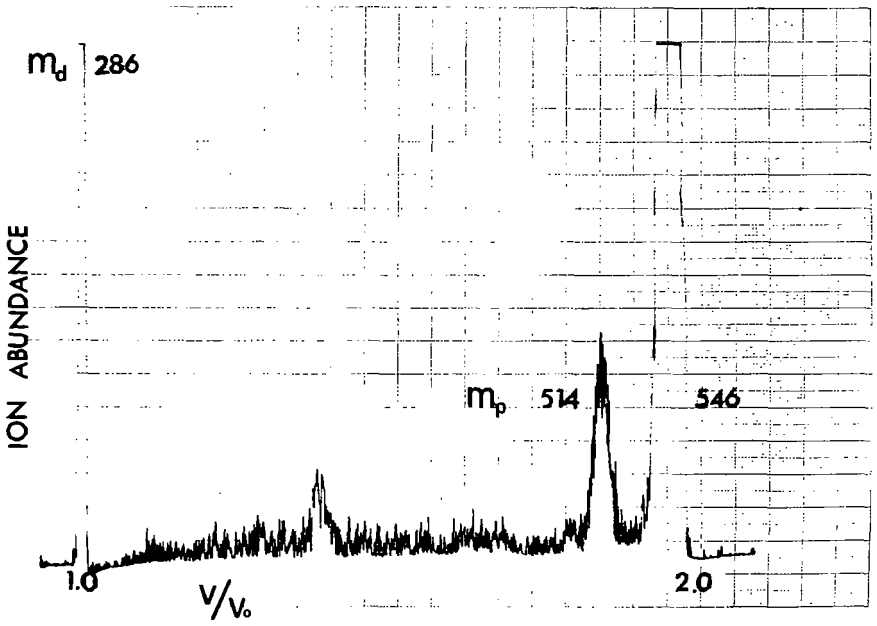

Figure 3

Study of Metastable Decompositions of Doubly-charged Ions by Ion Kinetic Energy Spectroscopy (IKES)

Teodor Ast, John H. Beynon, and Richard M. Caprioli
Purdue University, Lafayette, Indiana 47907

When a doubly-charged ion undergoes metastable decomposition into two singly charged ions: $m_1^{+2} \rightarrow m_2^+ + m_3^+ + T(eV)$, a considerable amount of kinetic energy is released as a consequence of the separation of the charges. As a result, broad dish-topped peaks are observed. The technique of Ion Kinetic Energy Spectroscopy (IKES)[1] can be used very successfully to study these transitions. When the electric sector voltage of a double-focusing mass spectrometer is scanned from the value at which the main beam of stable ions passes through to twice that value, and the ions are collected at the energy-resolving β-slit, dish-topped peaks corresponding to decomposition of doubly-charged ions into two singly charged ions can be observed. The dish-topped peak will be centered at $2m_2E/m_1$, where m_2 is the mass of the heavier of the two decomposition products, whilst E is the voltage at which the main ion beam is transmitted through the electrostatic sector. The width of this peak is a measure of the kinetic energy released in the transition.

However, since more than one transition can be contributing to this peak, accurate measurement of the kinetic energy released is not usually done from the energy spectra. A peak in the energy spectrum can be mass analyzed; thus the daughter ions of all the transitions giving rise to the energy peak can be determined. Once the mass of the daughter ion m_2^+ is determined, the magnetic sector is tuned to allow only ions of that m/e through. If the accelerating voltage is now scanned, keeping the electric sector voltage constant, a dish-topped peak will again be observed, but this time free from any interference. The width of this peak can now be taken as a measure of the kinetic energy released in the transition.[2]

In this study, a group of aromatic hydrocarbons and nitrogen-containing compounds has been selected. Mostly, they were methyl, dimethyl, amino and diamino derivatives of benzene, pyridine and diazines. The selection was made so as to include as many structural isomers as possible.

For each compound, the energy spectrum was plotted, dish-topped peaks mass analyzed and accelerating voltage scans performed. Thus all the transitions of doubly-charged ions into two singly charged ions were identified and the kinetic energy release which accompanied them measured.

The most common m_2^+ fragment lost was 27^+ ($C_2H_3^+$) from hydrocarbon compounds and 28^+ (H_2CN^+) from nitrogen-containing compounds (irrespective of whether it was an amino or ring nitrogen). Other common losses were 15^+ and 17^+, whilst some of the less common losses observed included 1^+, 12^+, 18^+, 26^+, 29^+, 39^+, 41^+ and 42^+.

If it is assumed that all of the kinetic energy released in these transitions is due only to separation of the two charges to infinite distance, the intercharge distance in the decomposing doubly-charged ion can be calculated. This will always be the minimum distance; for if part of the kinetic energy released is contributed from other sources (e.g., internal energy), the intercharge distance will be greater than calculated. The fact that all values for kinetic energy released measured in this study (with very few exceptions) fall into the narrow range between 1.8-3.3 eV suggests that the assumption of charge separation as being the dominant factor is valid.

Results and Discussion

Detailed results for various sets of compounds studied will be published elsewhere. Herein, a few representative examples are presented which ilustrate some general trends observed.

In Table I.A the kinetic energy released and corresponding intercharge distances are shown for the loss of 15^+ from the doubly-charged molecular ion of p-Phenylene-diamine, N-Methyl- p-phenylendiamine and N, N, N', N' - Tetramethyl- p-phenylenediamine. Values for intercharge distances suggest that in each compound the charges are localized as far appart as possible. Values for r increase by 1.3Å, which corresponds to addition of one more bond in each case.

TABLE I.

Compound	Transition	T[eV]	r[Å]
A.			
p-Phenylenediamine (I)	$M^{++} \rightarrow (M - 15)^+ + 15^+$	2.44	5.9
N-Methyl- I	"	2.00	7.2
N, N, N', N' - Tetramethyl - I	"	1.69	8.5
B.			
p-Toluidine	$M^{++} \rightarrow (M - 27)^+ + 27^+$	2.77	5.2
	$M^{++} \rightarrow (M - 28)^+ + 28^+$	3.27	4.4
3,4-Diaminotoluene	$M^{++} \rightarrow (M - 27)^+ + 27^+$	2.77	5.2
	$M^{++} \rightarrow (M - 28)^+ + 28^+$	3.27	4.4

Data for p-Toluidine and 3,4-Diaminotoluene Table I.B. also support the concept of localization of charges on the most distant sites possible in the molecule. Introduction of another amino-group into p-Toluidine does not affect the kinetic energy released since it provides no larger distance for charge localization.

Another example of transitions for which the inter-charge distances show the expected trend is given in Table II.A. The doubly-charged molecular ion in 3,4-Diaminopyridine loses 28^+ with the kinetic energy released corresponding to the charges being 6.9Å apart. If, however, the doubly-charged molecular ion loses neutral HCN first, the resulting ion (82^{+2}) loses 28^+ with kinetic energy released corresponding to a 4.4Å intercharge distance. The difference of 2.5Å is what would be expected, since the structure is two bonds shorter after HCN has been extracted.

TABLE II.

Compound	Transition	T[eV]	r[Å]
A.			
3,4-Diaminopyridine	$109^{++} \rightarrow 81^+ + 28^+$	2.09	6.9
	$82^{++} \rightarrow 54^+ + 28^+$	3.27	4.4
B.			
o-Phenylenediamine	$108^{++} \rightarrow 80^+ + 28^+$	2.60	5.5
m-Phenylenediamine	"	2.63	5.5
p-Phenylenediamine	"	2.73	5.3

Table II. - continued

C.			
2,6-Diaminopyridine	$109^{++} \rightarrow 81^{+} + 28^{+}$	3.08	4.7
2,3-Diaminopyridine	"	2.52	5.7
3,4-Diaminopyridine	"	2.09	6.9

In most sets of structural isomers, the kinetic energy released in corresponding transitions was identical for each isomer. This is exemplified by the transition $108^{++} \rightarrow 80^{+} + 28^{+}$ in o-, m- and p-phenylenediamine (Table II B.)[3]. All three isomers release an equal amount of kinetic energy (within experimental error), which corresponds to identical intercharge distances. The rationalization for this can be the operation of a scrambling mechanism, by which all three 108^{+2} ions acquire the same structure.

In at least one set of isomers with nitrogen in the ring (more of these compounds are now being investigated), the kinetic energy released differs considerably for structural isomers. (Table II. C.) One possible explanation could be that the presence of a nitrogen atom in the ring may prevent operation of the scrambling mechanism.

The tendency of doubly-charged ions to lose neutral hydrogen in various amounts was noted throughout our study. In some cases, this loss of hydrogen caused drastic changes in the amount of kinetic energy released in the corresponding transition. (Table III).

TABLE III.

Compound	Transition	T[eV]	r[Å]
2-Aminopyridine	$94^{++} \rightarrow 66^{+} + 28^{+}$	2.93	4.9
	$92^{++} \rightarrow 64^{+} + 28^{+}$	2.12	6.8
2,6-Diaminopyridine	$109^{++} \rightarrow 81^{+} + 28^{+}$	3.08	4.7
	$107^{++} \rightarrow 79^{+} + 28^{+}$	2.05	7.0
p-Xylene	$106^{++} \rightarrow 91^{+} + 15^{+}$	2.59	5.6
	$104^{++} \rightarrow 89^{+} + 15^{+}$	2.72	5.3
	$102^{++} \rightarrow 87^{+} + 15^{+}$	1.88	7.7

One possible rationalization for the observed phenomenon could be that the ring structure breaks open after several hydrogens have been stripped off. In aminopyridine and diaminopyridine this break occurs after two hydrogens have been lost, whilst in xylene, it occurs only after four hydrogens have been eliminated.

Conclusion

From our experiments, so far, it appears that there are two competing factors involved in regard to charge localization in doubly-charged ions containing hetero-atom(s): loss of 28^{+} (H_2CN^{+}) from nitrogen containing compounds occurs much more readily than 27^{+} ($C_2H_3^{+}$) and tends to suggest that charges prefer to localize on nitrogen; in some cases, intercharge distances obtained are consistent with such assumption. On the other hand, intercharge distances calculated for most of the transitions correspond to structures in which the two charges are localized as far apart as possible, irrespective of the position of nitrogen atom. An added difficulty is the large amount of scrambling observed in doubly-charged ions. These are the main reasons why

assigning definite structures from charge separation data is still uncertain. Nevertheless, some structural correlations can be drawn. The ability to distinguish between the ring and open chain structures is in itself a source of valuable information.

References

1. J. H. Beynon, J. W. Amy and W. E. Baitinger, Chem. Commun. 723 (1969).
2. J. H. Beynon, R. M. Caprioli, W. E. Baitinger and J. W. Amy, Org. Mass Spectrom. 3, 661 (1970).
3. J. H. Beynon, R. M. Caprioli and T. Ast, Org. Mass Spectrom., in press.

ENERGY RELEASE IN METASTABLE TRANSITIONS OF RETRO-DIELS-ALDER REACTIONS

by

Thomas A. Elwood and John H. Beynon
Purdue University, Lafayette, Indiana 47907
and
Peter W. Rabideau
Indiana University-Purdue University at Indianapolis, Indianapolis, Indiana 46205

The kinetic energy released in the metastable transitions of the retro-Diels-Alder reaction for several gaseous, bicyclic ions[1] has been studied. Molecular ions which decompose to form different product ions, but which yield ethylene as the neutral fragment, seem to correlate, in terms of the ion reaction energetics, with ground-state activation energies for the Diels-Alder formation of similar neutral species in solution. The mass spectrometric decompositions of norbornene, [2·2·2]-bicyclo-2-octene and dihydrodibenzobarrelene release ion kinetic energies of 0.056 eV, 0.098 eV and 0.15 eV, respectively; in solution, Diels-Alder reaction of maleic anhydride with cyclopentadiene, cyclohexadiene and anthracene require activation energies of 8.93 kcal/mole, 12.6 kcal/mole and 16.3 kcal/mole, respectively[2]. It is suggested that such correlations may be useful, and that IKES might give estimations of solution parameters, difficult or impossible to obtain by classical techniques.

References

1. S. Meyerson, J. D. McCollum and P. N. Rylander, J. Amer. Chem. Soc., 83, 1401 (1961).
2. J. Sauer, D. Lang and A. Mielert, Angew. Chem., 74, 352 (1962).

METASTABLE TRANSITIONS IN THE MASS SPECTRA OF DEUTERATED ETHYLENES

Irène RAUNEL, Robert HAGEMANN, René BOTTER
Services Isotopes Stables, C.E.N. Saclay, B.P.N°2, 91 GIF S/YVETTE

INTRODUCTION

Metastable transitions provide considerable information, not only about the reaction mechanisms near threshold, but also about the rate constants of the dissociation processes. Thus they are very important to determine the validity of the Quasi Equilibrium Theory [1] in the case of small polyatomic molecules. Such transitions have been studied carefully for small isotopic molecules such as CH_4 and CD_4 [2], C_2H_2 and C_2D_2 [3], C_2H_6 , CH_3-CD_3 and C_2D_6 [4,5]. But no detailed experiments have been performed on the substituted ethylenes. However, these molecules seem very important from the point of veiw of the Q.E.T.

In the case of $C_2H_2^+$, it has been shown that the fragment ion C_2H^+ is formed by predissociation, at least near threshold [6,7,3].

OTTINGER and LIFSHITZ in their publications on CH_3-CD_3 have given intensities of the metastable transitions for the reactions of the ethylene fragment ions and particularly for CH_2-CD_2^+.

However, their results for the competitive loss of the various isotopic hydrogen molecules do not agree.

LIFSHITZ finds that the H_2 loss is the most important reaction, whereas, OTTINGER's result indicate that HD loss is the predominant one. From his metastable studies on CH_3-CD_3 , OTTINGER arrived at the conclusion that the fragment CD_2-CH_2^+ should be only partly rearranged. But, this does not agree with the SCF-CNDO calculations of LORQUET and LORQUET [8]. The calculated activation energy for the isomerisation of $CH_2 = CD_2^+$ through an assymetric form, for example CH_2D-CD^+, has a much lower value(0.8 eV) than the activation energy for the H_2 loss from $C_2H_4^+$ (2.45 eV). Therefore, rearrangement should be much faster than dissociation.

In order to clarify these different points, we have studied the metastable transitions in six of the seven deuterated ethylenes and especially the loss of H_2 from the parent ion. We did not study the cis di-deutero-ethylene. Calculations of the rate constants have also been performed in terms of the Q.E.T.

EXPERIMENTAL

The experiments were performed on a single-focusing, 20 cm-radius, 60°-deflection mass spectrometer. The ionizing electron energy was 50 eV and the ion accelerating voltage 5 kV. The ion source and the analyser were pumped separatly and the tube pressure was always less than 10^{-7} torr. Thus, we did not observe any pressure induced metastable transitions, only pure unimolecular decompositions.

The deuterium substituted ethylenes were prepared in our laboratory. In all cases, the chemical purity was better than 99.9 %. The isotopic purity for C_2D_4 was 98 % . Trans - $C_2H_2D_2$ contained about 8 % C_2H_3D. C_2D_3H and C_2H_3D were not pure mixed with C_2D_4 and C_2H_4 respectively. However the presence of C_2H_4 and C_2D_4 did not disturb the measurement of the metastable transitions because they do not overlap. The geminated $C_2H_2D_2$ was kindly supplied by Dr. DIZABO*.

RESULTS

The observed metastable transitions for C_2H_4 between mass 22 and 25 are given in table 1.

* Dr. DIZABO - Faculté des Sciences, Paris

Table 1

Metastable transition	Apparent mass	Decomposition
29 → 27	25.15	$^{13}CCH_4^+ \rightarrow {}^{13}CCH_2^+ + H_2$
28 → 26	24.14	$C_2H_4^+ \rightarrow C_2H_2^+ + H_2$
27 → 25	23.15	$C_2H_3^+ \rightarrow C_2H^+ + H_2$
25 → 24	23.04	$C_2H^+ \rightarrow C_2^+ + H$

The most important metastable peak corresponds to the loss of H_2 from the parent ion and is 50 times greater than the others.

The mass spectrum of trans-$C_2H_2D_2$ given in figure 1 shows the three metastable peaks corresponding to the competitive reactions :

30 → 28 mass 26.13

30 → 27 mass 24.30

30 → 26 mass 22.53

The isotopic effect is very large (table 2). It is not possible to determine the isotopic

Table 2

Molecule	Reactions		m*	Relative abundances x 10^{-4}		
				loss of H_2	loss of HD	loss of D_2
C_2H_4 (28)	$C_2H_4^+ \rightarrow C_2H_2^+ + H_2$		24.14	3		
C_2H_3D (29)	$C_2H_3D \rightarrow C_2H_2^+ + HD$		23.31		< 0.06	
	$\rightarrow C_2HD^+ + H_2$		25.14	4.5		
$C_2H_2D_2$ (30)	$C_2H_2D_2^+ \rightarrow C_2H_2^+ + D_2$	gem.	22.53			0.01*
	" " "	trans.	"			0.01
	$\rightarrow C_2HD^+ + HD$	gem.	24.30		0.85*	
	" "	trans.	"		0.9	
	$\rightarrow C_2D_2^+ + H_2$	gem.	26.13	7.0*		
	" "	trans.	"	7.4		
C_2D_3H (31)	$C_2D_3H^+ \rightarrow C_2HD^+ + D_2$		22.52			0.1
	$\rightarrow C_2D_2^+ + HD$		25.29		3	
C_2D_4 (32)	$C_2D_4^+ \rightarrow C_2D_2^+ + D_2$		24.50			3.5

purity of $C_2H_2D_2$, especially the C_2H_3D contribution, from the mass spectrum, because the fragmentation of pure $C_2H_2D_2$ is not known a priori. However, the metastable peak 25.14 is due to the loss of H_2 from $C_2H_3D^+$ and, knowing the relative intensity of this metastable reaction, we can thus deduce the contribution of C_2H_3D. This shows that very useful information can be obtained by metastable studies. Two reactions are possible at mass 26.13: $C_2H_2D_2^+ \rightarrow C_2D_2^+ + H_2$ and $C_2H_2D_2^+ \rightarrow C_2H_2D^+ + D$. The contribution of this last reaction must be low since it has not been observed as a metastable in the other substituted ethylenes (C_2D_3H for example).

The isotopic effect concerning the loss of hydrogen from the parent ion, has been studied for all the deuterated ethylenes. The results are summarized in table 2. D_2 loss in

* the absolute values are uncertain

$C_2D_4^+$ is favored, compared to H_2 loss in $C_2H_4^+$. But in all the partly substituted molecules, where two or three competitive reactions can occur, the loss of the lighter fragment is always favored over to the heavier one.

Special mention should be made of $C_2H_2D_2$. We have studied the two stereo isomers, geminated and trans. Both give exactly the same values for the metastable intensities. This point will be discussed below.

DISCUSSION

The identical results obtained for the loss of a hydrogen molecule (table 1) in the two isomers show that a rearrangement has to occur before dissociation. This last reaction has the lowest activation energy for ethylene (2.45 eV). If no scrambling takes place in ethylene before dissociation either of the following two results can be expected :

1. If the hydrogen molecule loss takes place from the two carbon atoms, only HD should be observed, at least for geminated ethylene. For the trans isomer one can reasonably assume that the rotational barrier about the C-C bond is low in the ion and that this isomer is rearranged into a mixture of cis and trans. Thus one would expect a mixture of H_2, HD and D_2 loss.

2. If the hydrogen molecule originated from the same carbon atom, the trans ethylene would give only HD loss and the geminated one only H_2 and D_2 loss.

So we have to assume complete scrambling of hydrogen before dissociation or, as has been stated by VON KOCH [9] and by PRASIL and FORST [10], dissociation from the assymetric form $CH - CH_3^+$. Both hypotheses are in good agreement with the low energy barrier calculated by LORQUET [8] for the equilibrium reaction $CH_2 = CH_2^+ \rightleftharpoons CH_3 - CH^+$, but these results do not agree with those of OTTINGER.

We have also tried to verify the large isotopic effect observed for the competing reactions in partially substituted ethylenes. We have calculated using the C.E.T ;the breakdown pattern and the mass spectra of these molecules (a more detailed report will be published on these calculations).

The calculated breakdown pattern has been compared with the experimental one obtained by charge exchange by SZABO [11].

The convolutions of the calculated and experimental breakdown curves with the photoelectron energy distribution function (obtained with the 584 Å line) have been compared, first, with the mass spectrum obtained by photoionization (using the He resonance line) and, second, to the one obtained by electronic impact at 50 eV. These results are reported in table 3.

Table 3

Comparison of experimental and calculated mass spectra of C_2H_4

m/e	ion	Photoionisation 21.33 eV	Electronic impact 50 eV	Convolution of breakdown curves an photoelectron energy distribution	
				Experimental Bd.	Calculated Bd.
28	$C_2H_4^+$	100	100	100	100
27	$C_2H_3^+$	137	54.5	147	157
26	$C_2H_2^+$	76	52.8	82	96
25	C_2H^+		8.6	2	4
24	C_2^+		2.1		1

The agreement between the calculated spectrum from the experimental breakdowns and the photoionization results is very good. This shows that if the distribution function is well known, as in this case, the convolution of this function with the breakdown curves gives the correct

mass spectrum.

The values obtained with the calculated breakdown curves are in fair agreement with the former results. A better fit could be obtained by a careful adjustment of the vibrational frequencies. The intensities given in the electron bombardment spectrum are very different from those of the photoelectron spectrum.

The same results have been obtained for $C_2H_2D_2$.

The isotope effect of the metastable transitions for the loss of H_2 , HD and D_2 from $C_2H_2D_2$ can be calculated from the rate constants for these reactions. The values have been calculated with an activated complex of the following structure

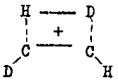

where , the two hydrogen atoms originate from the two carbons. The minimum rate constants ($\sim 10^5$ s^{-1}) are in agreement with the appearance of a metastable peak, but the calculated and the experimental isotopic effects do not agree. The calculated metastable intensities are in the order $HD > H_2 > D_2$.

We have also calculated these rates for the three competitive reactions assuming the following scheme :

$$CH_2 \equiv CH_2^+ \rightleftharpoons CH_3 - C\overset{+}{H} \rightarrow CH \equiv C\overset{+}{H} + H_2$$

where the two hydrogen atoms originate from the same carbon atom of an assymetric form of the parent ion. The rate constants for the isotope effect are in the right order $H_2 > HD > D_2$ but the calculated effect is much smaller than the observed one.

It is not necessary to invoke any special decomposition mechanism, such as predissociation, to explain the mass spectrum of C_2H_4 , however, for the metastable transitions near threshold it might be necessary to take into account tunnelling effects or even predissociation processes to explain the observed isotope effect in the deuterium substituted ethylenes.

REFERENCES

1 ROSENSTOCK H.M., Advances in Mass spectrometry, Vol. 5, pergamon Press

2 DIBELER V.H. and ROSENSTOCK H.M., J. Chem. Phys., 39, 1326 (1963)

3 BOTTER R., HAGEMANN R., KHOMADADI G. and ROSENSTOCK H.M., Recent developments in mass spectroscopy, University of Tokyo Press (1970)

4 LOHLE U. and OTTINGER Ch., J. Chem. Phys., 51, 3097 (1969)

5 LIFSHITZ Ch. and STERNBERG R., I. J. of Mass Spect . and Ion Physics, 2, 303, (1969)

6 FIQUET-FAYARD F., J. Chim. Phys., 64, 320 (1967)

7 YAMACKA H., PHAM DONG and DURUP J. 51, 3465 (1969)
8 LORQUET A.J. and LORQUET J.C. J. Chem. Phys. 49, 4955, (1968)
9 VON KOCH H. Arkiv för Fysik 28, 559 (1965)
10 PRAŠIL Z. and W. FROST J. Phys. Chem. 71, 3166 (1967)
11 SZABO I. Arkiv för Fysik 31, 287 (1966)

ACKNOWLEDGEMENTS

We wish to thank Dr. DIZABO for kindly making the geminated $C_2H_2D_2$ available to us.

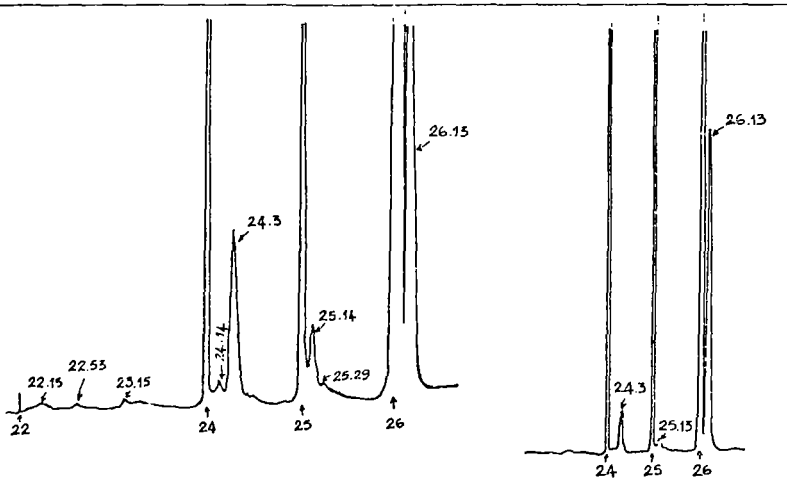

Fig. 1- Mass spectrum of trans - $C_2H_2D_2$ from mass 22 to 26.

L2

PROTON-TRANSFER REACTIONS OF NEGATIVE IONS WITH METHANE AND METHYL COMPOUNDS*

A. di Domenico and J. L. Franklin

Department of Chemistry
Rice University
Houston, Texas 77001

Proton-transfer reactions between a number of negative ions and some CH_3Y-type molecules have been carried out using the high-pressure source of a Bendix time-of-flight mass spectrometer. The primary negative ions (reactants), X^-, used in this study have been ordered according to their decreasing $(D + E_A)$ or driving force values, where D is the dissociation energy for the X-H bond and E_A is the electron affinity of X. If CH_3Y reacts with an ion of driving force $(D_2 + E_{A_2})$ but does not react with one immediately below with driving force $(D_o + E_{A_o})$, the following relationship can be written:

$$(D_o + E_{A_o}) < (D_1 + E_{A_1}) < (D_2 + E_{A_2})$$

where D_1 and E_{A_1} refer to radical CH_2Y. If D_1 is known, E_{A_1} is obtainable and vice versa. The uncertainty with which D_1 and E_{A_1} are found is given by the range $[(D_2 + E_{A_2}) - (D_o + E_{A_o})]$. For example, we have found that $E_A(CH_3) > -29$ kcal/mole and $E_A(CH_2CN) < -34$ kcal/mole. Preliminary results would set the E_A of methyl halides between -45 and -32 kcal/mole but further investigation is required to confirm the above mentioned values. Nitromethane, trimethylamine and methylether are also under study. In this work, X^-: NH_2^-, O^-, F^-, CN^-, S^-, Cl^-, Br^-, I^-, and Y: H, OCH_3, $N(CH_3)_2$, F, Cl, Br, I, CN, NO_2, OD.

*Support by The Robert A. Welch Foundation is gratefully acknowledged.

NEGATIVE ION-MOLECULE REACTIONS IN NON-METAL FLUORIDES

T. C. Rhyne & J. G. Dillard
Chemistry Dept., Va. Tech.
Blacksburg, Virginia 24061

Reactions of AsF_3 and AsF_5 with negative ions produced from the materials and from SF_6 were studied in an RMU-7 Hitachi mass spectrometer which was modified for ion-molecule investigations. (1). These studies have been carried out to learn more about negative ion reactions in inorganic chemical systems and to explore the feasibility of measuring Lewis acidities using fluoride ion transfer processes as a quantitative tool.

Negative ions in the low pressure mass spectrum of AsF_3 include F^- and AsF^- at electron energies around 7-10 ev. No secondary ions were noted at any pressure studied in pure AsF_3. When SF_6 was added to AsF_3 the secondary ion AsF_4^- was observed in the region where SF_6^- and SF_5^- are formed by resonance electron capture. The ionization efficiency curves for SF_6^- and AsF_4^- are superimposable and the pressure dependence of the secondary ion formation is pseudo-first order in AsF_3 and corresponds to the fluoride ion transfer reaction.

$$SF_6^- + AsF_3 \rightarrow AsF_4^- + SF_5 \qquad (1)$$

Reaction Cross sections as a function of repeller potential are given in Table I.

When AsF_5 was introduced into the ion source at high pressure the ions AsF_4^-, AsF_5^-, and AsF_6^- are formed at near 0 eV. Examination of the ionization efficiency curves for AsF_4^-, AsF_5^-, and AsF_6^- reveals that all are formed at the same electron energy. The reaction for the formation of AsF_4^- is the dissociative electron capture process

$$AsF_5 + e^- \rightarrow AsF_4^- + F \qquad (2)$$

Two possibilities exist for the formation of AsF_5^-, either resonance electron capture

$$AsF_5 + e^- \rightarrow AsF_5^- \qquad (3)$$

or charge-transfer ion-molecule reaction

$$AsF_5 + AsF_4^- \rightarrow AsF_5^- + AsF_4 \qquad (4)$$

The AsF_6^- ion may be formed by the reactions

$$AsF_4^- + AsF_5 \rightarrow AsF_6^- + AsF_3 \qquad (5)$$

or

$$AsF_5^- + AsF_5 \rightarrow AsF_6^- + AsF_4 \qquad (6)$$

From a plot of % ion current vs pressure the primary ion AsF_4^- is observed to decrease slightly with an increase in AsF_5 pressure, while both AsF_5^- and AsF_6^- increase with increasing AsF_5 pressure. These results suggest that AsF_5^- is a secondary ion, and since the ionization efficiency curve for AsF_5^- coincides with that of AsF_4^-, the molecular ion AsF_5^- is presumedly formed by charge transfer. At pressures exceeding 0.5μ of AsF_5 the percent ion current of AsF_5^- levels off and proceeds to drop slowly, suggesting that the cross section for charge transfer decreases and that AsF_5^-, formed by charge transfer, is destroyed by some process not operable at lower AsF_5 pressure. Since the initial formation of AsF_5^- is pressure dependent (pseudo-first order) and corresponds to a biomolecular process, reaction 6 would demonstrate pseudo-second order kinetics and would require consecutive bimolecular collisions if this were contributing to the formation of AsF_6^-. This process is not likely since much higher pressures are normally required for such behavior, and no change in slope of the curve for the % ion current of AsF_6^- is observed in the region where AsF_5^- is diminishing. If reaction 6 does contribute to the formation of AsF_6^-, the amount of AsF_6^- formed is insignificant to that resulting from other pathways of formation. AsF_6^- % ion current shows linear pressure dependence over the entire range studied, and the correspondence of the AsF_6^- ionization efficiency curve with that for AsF_4^- identifies reaction (5) as the process for formation of AsF_6^- in pure AsF_5.

When SF_6 was added to AsF_5 at near zero eV. the secondary ion AsF_6^- was observed to increase in abundance while AsF_4^- and AsF_5^- showed no corresponding increases. This behavior suggested that the ion-molecule reaction

$$SF_6^- + AsF_5 \rightarrow AsF_6^- + SF_5 \qquad (7)$$

occurs in mixtures of SF_6 and AsF_5 and that charge transfer between SF_6^- and AsF_5 does not take place. Since the SF_6^- curve is coincident with the curves for all ions containing arsenic, positive identification of reaction 7 to the exclusion of reaction (5) is not possible.

The reaction cross sections for the formation of secondary ions according to the processes discussed above for the arsenic fluorides and in mixtures with SF_6 are presented in Tables I and II. The values tabulated for the formation of AsF_6^- in Table I were calculated after subtracting the contribution to the AsF_6^- ion current due to reaction 5.

Table I

$$SF_6^- + AsF_3 \rightarrow AsF_4^- + SF_5$$
$$SF_6^- + AsF_5 \rightarrow AsF_6^- + SF_5$$

Repeller Voltage	Cross Section (A^2/molecule) Secondary Ion	
(V)	AsF_4^-	AsF_6^-
1.5	100.7	72.4
2.0	84.7	55.8
2.5	78.7	39.6
3.0	73.7	34.7
3.5	69.7	32.7
4.0	65.5	30.4

Table II

$$AsF_4^- + AsF_5 \rightarrow AsF_5^- + AsF_4$$
$$AsF_4^- + AsF_5 \rightarrow AsF_6^- + AsF_3$$

Repeller Voltage	Cross Section (A^2/molecule) Secondary Ion	
(V)	AsF_5^-	AsF_6^-
1.5	138.7	110.5
2.0	105.6	78.2
2.5	97.0	66.8
3.0	87.8	60.5
3.5	85.8	55.4
4.0	84.1	51.1

REFERENCES

1. T. C. Rhyne & J. G. Dillard, Inorg. Chem., 10, 730 (1971).

FRAGMENTATION OF SMALL INORGANIC MOLECULES:

Halides and Pseudohalides

Fred E. Stafford
Department of Chemistry and the Materials Research Center
Northwestern University
Evanston, Illinois 60201

Knowledge of whether or not a molecule will form a parent ion is critical in identifying new molecules by mass spectrometry. In high temperature mass spectrometry, where fragment ions often are masked, it is necessary also to know what fraction of the total ion current is due to the parent ion in order to deduce partial pressures. A specific example is the ion $H_3BO_3^+ (B(OH)_3^+)$ which was observed in small intensities in the H_2O-B_2O_3 system by Meschi, Chupka, and Berkowitz (1960).

Previous work on this problem for small inorganic molecules includes a correlation of the appearance potentials of parent and fragment (Kiser, Dillard, and Dugger, 1968), correlation of the geometry of the molecule and ion for IIA dihalides (Hildenbrand, 1970), and an extensive treatment of halides and oxides (Hastie and Margrave, 1969).

For the small molecules of present interest, it is believed that we are concerned less with how internal energy redistributes itself into a mode that will cause fragmentation, but more with the initial ionization process and the probability of distribution over the various hypersurfaces representing the ionized states. In this case it is expected that a parent ion with a very weak bond is less likely either to be formed, or to hold together long enough for observation, hence removal of an electron from a strongly bonding orbital is likely to cause fragmentation. By the same token, removal of a non-bonding electron or an electron from a double bond is expected not to result in extensive fragmentation.

While it is now possible to predict bond energies or bond stretching force constants with some accuracy, fragmentation poses a more severe problem. The observed fragmentation pattern is the result of competing rate processes. Rather subtle effects might have a large effect in causing a shift from one process to another, especially where either parent or fragment intensity is small. Furthermore, the mass spectrometer is a poor tool for measuring such relative rates since reproducibility from machine to machine can be poor and since the ion source discriminates effectively against ions formed with kinetic energy.

These difficulties notwithstanding, this paper, with emphasis placed on certain three coordinate molecules, will examine two questions:

(1) To what extent is the method of chemical extrapolation useful, i.e.,
   (i) what, if any, are the trends in fragmentation of the halides MX_n?
   (ii) do any of the univalent negative groups CH_3, BH_4, CN, ... OH, OBO, OPO ... behave like a halogen? and
   (iii) do the OR groups (e.g., OH) behave specially because of the possibility that $-M(OR)_2 \longrightarrow -M{=}O + ROR$? D(HO-H), for

instance, is 118 kcal/mole and provides a potentially strong driving force.

While possibly useful, this method of analogy is not as good as hoped. We turn then to

(2) correlation of fragmentation patterns with the molecular orbital patterns as observed by photoelectron spectroscopy.

Chemical Extrapolation.

With predictions for $B(OH)_3$ in mind as a sample case, we look first at fragmentation of some Group III and V MX_3 molecules:

	F	CH_3	OCH_3	Cl	Br	H
B	0.03	~0.01	0.26	0.26	0.27	0.24
Al	0.06	0.07		(~0.31)	0.42	
N	0.38					0.55
P	0.66	~0.31		0.27	0.38	*
As	0.38	0.44		0.37		

*The most intense peak from PH_3 is PH^+.

In this and the following table, the number given is the fraction of the parent and parent-minus-X intensities that is due to the parent, p/[p + (p-X)]. The contribution of the lower mass fragments, unless otherwise noted is ignored for the present.

On the basis of experience in other areas, it is tempting to believe that the OH group might be intermediate in behavior between F and Cl, perhaps closer to the latter; this idea will be tested in the next table. The CH_3 group, where six of the electrons are pinned down by the protons, behaves like the F group in the case of B, but like the Cl in the case of P; other data suggest that cleavage of the M-C bond parallels that of the M-F bond. The methoxy group, which in this case comes off primarily as a group (not eliminating e.g., CH_2O), is fragmented to the same extent as B-Cl. Fluoride follows the rule that "fluoride fragments more" in the case of B and Al, but not in that of P (nor for POF_3 and PSF_3 and will be discussed further under "Correlation with Photoelectron Spectra."

The extent of parent ion formation for some MX compounds, $I(MX^+)/[I(MX^+) + I(M^+)]$, is:

	F	OH	OBO	CN	ReO_4	Cl	Br
Li	~.17**	0.97				0.77	0.69
*(Li	~.17		0.63			0.55	0.50)
*(Na	.03	0.62	0.79	0.24	***	0.38	0.41)
*(K	.002				***	0.15	0.03)

*These last three lines are raw ion intensities, not corrected for possible large contributions from the dimer; compare the first two lines. The latter sometimes are incorrectly quoted as fragmentation patterns.

**Li^+ is formed with appreciable kinetic energy; its intensity is not reproducible.

***Parent is minor peak; M^+ is formed with kinetic energy.

As is often the case, the fluoride fragments most. This may be attributed to the highly ionic nature of the M-F bond. Otherwise, these are woefully few and inconsistent data from which the reader can draw his own educated guess with regard to yet unexplored systems. With respect to the $B(OH)_3$ problem, these are the only data for hydroxyl containing molecules and seem to indicate that they fragment less than the chloride. To our knowledge, data are not available to answer question (1. iii) of the Introduction about the probability of water elimination.

Comparison with Photoelectron Spectra.

As seen above, the chemical extrapolation method, while easy to apply and successful for certain other phenomena, is not sufficiently perceptive when applied to fragmentation. Another question to ask is if the nature and the relative ordering of the ionic energy levels with respect to the minimum energy required for fragmentation can be correlated to the observed fragmentation.

The energies (eV) of the first few most easily ionized orbitals of the MX_3 compounds are (Potts, Lempka, Streets, and Price, 1970):

					"Bonding"		$AP(MX_2^+)$	%
	a_1	e'	a_2'	e''	a	e	$-IP(MX_3^+)$	Parent
BF_3		15.95	16.68	17.2	19.1	20.1	~0.3	3
BCl_3		12.38	11.73	12.65	14.4	15.6	~1	26
BBr_3		11.4	10.68	11.7	13.2	14.3	~1	27
NF_3	13.7	16.0		17.4	19.7		1-1.4	38
PF_3	12.28	15.89	16.29	17.35	18.5	19.3	4	66
PCl_3	10.52	11.71	12.01	12.97	14.2	15.2	1.5	27
PBr_3	10.0	10.7	11.2				1.4	38
AsF_3	13.00	15.24		16.21	17.2	18.2		
$AsCl_3$	10.89	11.75		12.59	13.8	14.6		

The last column in the table gives the difference between the appearance potential of the fragment MX_2^+ and that of the parent; if pair formation, kinetic energy, and other effects are ignored, this becomes the dissociation energy $D(MX_2^+-X)$. These numbers are almost all electron impact results and are culled from various places; in some instances the electron impact IP's are 1/2 to 1 eV lower than the photoelectron value. The last column repeats from the first Table the percentage of total intensity due to the parent.

While there are various changes in the ordering of the orbitals, the dominating feature is the width of the region (next to last column of above Table) in which parent ions are formed but are not sufficiently energetic to dissociate. This very nicely explains the otherwise anomalous PF_3, and is just the correlation suggested by Kiser, Dillard, and Dugger (1968) and quantified by Hastie and Margrave (1969).

According to a simple picture, the main bonding orbitals are the a and e listed in columns 5 and 6 above. Those listed in the first columns, especially the lone pair a_1 are described as "non-bonding." The data in the Table show the oversimplicity of

this description and, further, illustrates the problem with trying to predict fragmentation from the bonding or non-bonding character of the electron removed.

The CH group has the same number of valence electrons as P or N. In CHF_3 the a_1 (CH) orbital is most easily ionized, while in $CHCl_3$ it lies some 5 to 6 eV below those mainly of Cl p character (Potts et al., 1970). As we predicted before seeing this mass spectrum, the most intense ion peak for the former is due to loss of H, while for the latter it is due to loss of Cl.

Conclusion.

Fragmentation poses serious problems in the use of mass spectrometry to deduce the identity and the partial pressures of otherwise unknown (e.g., high temperature) species. In the example of $B(OH)_3$, the resulting range of error in deduced pressure is about a factor of 30 depending on the assumption used. This problem, however, is often ignored. Furthermore, relatively few papers present the mass spectra of the systems studied, making it difficult to survey for trends in fragmentation patterns.

The method of chemical extrapolation, while easy to apply, gives only crude results. The examples shown illustrate that one has to formulate almost as many rules of extrapolation as there are compounds whose mass spectra are now known. With more data the situation may be ameliorated. Indeed, our data for transition metal halides and oxohalides are much better behaved.

Examination of the photoelectron spectra on which are marked lines indicating the minimum energy for dissociation of the ion gives the impression that one could nicely calculate the fragmentation pattern by applying an appropriate weighting factor and taking the areas above and below the line. This is, of course, over simplified. The number, type, and relative spacing of the orbitals is nearly constant in the series considered. We know, however, that relative band intensities change in going from HeI to He II excitation and expect a change for 70 eV electrons. An experiment, such as electron impact with coincidence counting of ions and electrons, is needed to show the contribution of each ionic level to fragment production.

For the purpose of predicting fragmentation patterns, the present results indicate that a calculation, prediction, or measurement of the ordering of energy levels is not sufficient. What is needed are predictions of $D(R^+-X)$ relative to $D(R-X)$, a most difficult situation.

Acknowledgement,

An insightful discussion with Joseph Berkowitz is much appreciated.

A complete manuscript, with full literature citations, is being prepared for publication.

This work was supported by the United States Atomic Energy Commission, Document No. COO-1147-40.

L6

Dissociation Energies of the Molecules Tb_2, Ho_2, Lu_2, TbAu, HoAg, HoAu, and LuAu

K. A. Gingerich, D. L. Cocke, H. C. Finkbeiner, and R. J. Seyse

Department of Chemistry
Texas A&M University
College Station, Texas 77843

The applicability of the Pauling model of a polar bond[1] to intermetallic compounds has been previously noted[2,3]. Its application to interpret the bonding in certain diatomic intermetallic compounds with substantial differences in electronegativities has shown reasonable success[4,5,6]. To further test the applicability of this model, the molecules Tb_2, Ho_2, Lu_2, TbAu, HoAg, HoAu and LuAu have been studied by the Knudsen cell mass spectrometric technique. The experimentally observed dissociation energies of Tb_2, Ho_2, and Lu_2 are used to calculate bond energies of the heteronuclear molecules, and a direct comparison between the calculated and observed bond energies is then possible.

The high temperature mass spectrometer technique has been discussed elsewhere[7,8]. Bond energies were calculated using the third law method, and where a sufficient temperature range was investigated, by the second law method. The lutetium system was studied in a tungsten Knudsen cell while the terbium and holmium systems were both studied using tantalum Knudsen cells. The Knudsen cells and contents were heated by a tungsten resistance heater. Ionic species were identified by their mass to charge ratio (m/e), shutter profile, ionization efficiency curves and where possible, by their isotopic distribution.

Pressure calibrations were made where possible by use of the Au^+/Au_2^+ or Ag^+/Ag_2^+ ratio and the known value of $\Delta G°$ for the dissociation reaction $X_2=2X$, as described by Grimley[8]. Relative multiplier gains were measured using a Faraday cup collector. Ionization cross section data were taken from Mann[9]. Wherever possible, pressure independent reactions were evaluated, where multiplier gains and ionization cross sections may be assumed to compensate one another. Temperatures were measured with an optical pyrometer by means of a black body hole in the bottom of the Knudsen cell. The holmium runs were done using a magnetic focusing ion source, while the other runs all utilized a conventional ion source.

The third law enthalpies, ΔH°_0, were calculated using the relation

$$\Delta H^\circ_0 = -2.303\ RT\log_{10}K_p - T\Delta[(G^\circ_T - H^\circ_0)/T]$$

where K_p, R, and $-\Delta[(G^\circ_T - H^\circ_0)/T]$ represent the equilibrium constant, the gas constant, and the change of the free energy function for the corresponding reaction. Second law enthalpies were calculated from the relation

$$\Delta H^\circ_0 = -Rd\ln K_p/d[1/T]$$

and ΔH°_0 values were obtained by using estimated heat content changes, $\Delta(H^\circ_T - H^\circ_0)$, for the corresponding reaction. Free energy functions, $-(G^\circ_T - H^\circ_0)/T$, used in the calculation of the third-law enthalpies were taken from the literature[10] or calculated by means of statistical thermodynamics, using rigid-rotator, harmonic oscillator approximations from known or estimated molecular parameters.

The experimental results from the holmium-silver and holmium-gold-aluminum systems are given in Table I. The dissociation energy of HoAg

Table I

Summary of reaction enthalpies for the Ho-Ag and Ho-Au-Al System[a]

Reaction	Method	ΔH°_0 kcal mol^{-1}	D°_0(AB) kcal mol^{-1}	AB
$Ho(g)+Ag_2(g)=HoAg(g)+Ag(g)$	3rd law	8.6	29.0[b]	HoAg
	2nd law	13.7	23.9[b]	
$HoAg(g)+Ho(g)=Ho_2(g)+Ag(g)$	3rd law	9.2	19.8[c]	Ho_2
$HoAg(g)=Ho(g)+Ag(g)$	3rd law	28.7	28.7	HoAg
$Ho_2(g)=2Ho(g)$	3rd law	19.0	19.0	Ho_2
$Ho(g)+AlAu(g)=HoAu(g)+Al(g)$	3rd law	17.0	60.0[d]	HoAu
	2nd law	18.4	58.6[d]	

(a) A complete paper has been submitted for publication to the Journal of Physical Chemistry

(b) $D^\circ_0(Ag_2)=37.6$ kcal mol^{-1} used: Drowart, Reference (2)

(c) $D^\circ_0(HoAg)=29.0$ kcal mol^{-1} used: this work

(d) $D^\circ_0(AlAu)=77.0$ kcal mol^{-1} used: Blue and Gingerich, Reference (9)

was obtained from combination of the enthalpy, ΔH°_0, of the pressure independent reaction (1) with the known dissociation energy[2], $D^\circ_0=37.6$ kcal mol^{-1}, of the silver dimer. This dissociation energy for HoAg compares well with that obtained from the pressure dependent reaction (3), where pressure calibration constants were necessarily used.

The third-law enthalpy of reaction (2) in combination with the dissociation, D_0°, of HoAg from the present study yields a dissociation energy, D_0°, of 19.8 kcal mol^{-1} for the Ho_2 molecule. This is in good agreement with the D_0° value obtained for the pressure dependent reaction (4) where pressure constants were again used. The third-law enthalpy, ΔH_0°, for reaction (5) in combination with the known dissociation energy, D_0°=77.0 kcal mol^{-1}, of AlAu[11] gives the dissociation energy, D_0°, for HoAu as 60 kcal mol^{-1}.

The third-law enthalpies for reaction (1) and (5) agree with the corresponding second-law values within experimental error.

Table II shows results from experiments on a terbium-holmium-gold system. The holmium-gold dissociation energy, D_0°, of 62.9 kcal mol^{-1} is

Table II

Summary of Reaction Heats in the Terbium-Holmium-Gold Systems and Terbium-Terbium Dimer System

Reaction	Method	ΔH_0° kcal mol^{-1}	D_0°(AB) kcal mol^{-1}	AB
$TbAu(g)+Au(g)=Tb(g)+Au_2(g)$	3rd law	21.0	74.0[a]	TbAu
$Tb(g)+Au(g)=TbAu(g)$	3rd law	-72.0	72.0	TbAu
$HoAu(g)+Au(g)=Au_2(g)+Ho(g)$	3rd law	9.2	62.2[a]	HoAu
$Tb(g)+Tb(s)=Tb_2(g)$	3rd law	56.0	37.4[b]	Tb_2

(a) $D_0^\circ(Au_2)$=53.0 kcal mol^{-1} used: Blue and Gingerich, Reference (11)

(b) $\Delta H_{v,s}[Tb(s)]$=93.4 kcal mol^{-1} used: Hultgren *et al.*, Reference (10)

in good agreement with that shown on Table I. The terbium dimer and terbium-gold dissociation energies were calculated in an analogous manner to the holmium molecules. The equilibrium constant for the Tb/Tb_2 was about $2X10^7$, resulting in a very weak Tb_2^+ intensity. In order to obtain a readable ion current for the Tb_2^+ species, the capacitor charge method using a Cary 401 vibrating reed electrometer was used. The capacitor was allowed to charge for approximately one minute and the relative ion current was obtained by integrating the trace over the time interval used.

Table III summarizes a lutetium-gold experiment. These results are calculated in a similar manner to those shown on Table I and II.

Table III

Summary of Reaction Heats in the Lu-Au System

Reaction	Method	ΔH° kcal mol^{-1}	ΔD°(AB) kcal mol^{-1}	AB
$Lu_2(g)=2Lu(g)$	3rd law	25.2	25.2	Lu_2
$LuAu(g)=Lu(g)+Au(g)$	3rd law	79.7	79.9	LuAu
	2nd law	77.0	77.0	
$LuAu(g)+Au(g)=Lu(g)+Au_2(g)$	3rd law	26.6	79.6[a]	LuAu

(a) $D^\circ(Au_2)=53.0$ kcal mol^{-1} used: Blue and Gingerich, Reference (11)

The resulting bond energies of the species presented in Tables I, II, and III are summarized in Table IV. The calculated bond energies, using the Pauling model, and the experimentally determined, D°(A-B), bond energies are also presented.

Table IV

Comparison of Experimental Dissociation Energies[a] with those Calculated After the Pauling Model

Molecule (AB)	D°(AB) kcal mol^{-1}	1/2[D(A-A) + D(B-B)] kcal mol^{-1}	D°(AB)[b] calculated kcal mol^{-1}
Tb_2	37		
Ho_2	19		
Lu_2	25		
TbAu	73	45	73
HoAg	29	28	37
HoAu	60	36	64
LuAu	79	39	67

(a) Weighted averages from Tables I-III, rounded off to nearest kcal mol^{-1}

(b) After Pauling model where $D^\circ(AB)=1/2[D(A-A)+D(B-B)]+23[\chi_A-\chi_B]^2$

The calculated dissociation energies assume electronegativities χ[M]=1.3, where M=Tb, Ho, or Lu; χ[Ag]=1.9, and χ[Au]=2.4. The dissociation energies of the terbium-gold and holmium-gold are in fair agreement

to those calculated from the Pauling model. However, the measured dissociation energy of HoAg is lower than calculated and that of LuAu is higher than calculated.

Acknowledgement

The authors wish to thank the National Science Foundation for support of this work under Grant GP-12442.

References

1. L. Pauling, The Nature of the Chemical Bond, 3rd ed. Cornell University Press, Ithaca, N. Y. (1960).

2. J. Drowart, in Phase Stability in Metals and Alloys, P. S. Rudman, J. Stringer and R. I. Jaffee, Eds., McGraw-Hill, New York, (1966) pp. 305-317.

3. M. Ackerman, F. E. Stafford, and G. Verhaegen, J. Chem. Phys. 36, 1560 (1962).

4. G. D. Blue and K. A. Gingerich, "Proc. 16th Ann. Conf. on Mass Spectrometry and Allied Topics," May 1968, Pittsburgh, ASTM-Committee E-14, paper 129, p. 383.

5. K. A. Gingerich and H. C. Finkbeiner, J. Chem. Soc. D, 16, 901 (1969).

6. K. A. Gingerich and H. C. Finkbeiner, J. Chem. Phys. 52, 2956 (1970).

7. J. Drowart and P. Goldfinger, Angew. Chem. 79, 589 (1967); Angew. Chem. Intern. Edn. 6, 581 (1967).

8. R. T. Grimley, in the Characterization of High-Temperature Vapors, J. L. Margrave, ed., John Wiley and Sons, Inc. (1967), pp. 195-243.

9. J. B. Mann, J. Chem. Phys. 46, 1646 (1967).

10. R. Hultgren, R. L. Orr, and K. K. Kelly, Supplement to Selected Values of Thermodynamic Properties of Metals and Alloys, University of California, Berkeley, Calif., Gold (1969), Aluminum (1968), Silver (1968), Holmium (1966), Lutetium (1966), and Terbium (1967).

11. G. D. Blue and K. A. Gingerich, to be published.

MASS SPECTROMETRIC IDENTIFICATION OF GASEOUS InGaO, $InGaO_2$, AND GaAlO*

Fred J. Kohl and Carl A. Stearns
NASA Lewis Research Center
Cleveland, Ohio 44135

ABSTRACT

The Knudsen effusion-mass spectrometric method was used to study the vaporization of the two mixed systems $In+Ga_2O_3$ and $Ga+Al_2O_3$. Relative intensities were measured and metal atoms and the suboxides, M_2O, were found to be the major vapor constituents. M_2O_2 type oxides were minor vapor components. Ionization efficiency curves were measured for all observed ions of interest. Measured appearance potentials were used to identify parent molecular species. The new species InGaO, $InGaO_2$ and GaAlO were established as neutral molecules in the vapor phase. The isomolecular gas phase reaction

$$In_2O(g) + Ga_2O(g) = 2\ InGaO(g)$$

was used to obtain thermodynamic data for the InGaO molecule. Second- and third-law methods were used to calculate the heat of reaction over the temperature range from 973 to 1168 K. The atomization energy of InGaO was determined to be 196±4 kcal $mole^{-1}$.

*A more complete account of this work is given in NASA TN D-6318.

L8

VAPORIZATION OF THE GROUP IVB METAL CARBIDES*

Carl A. Stearns and Fred J. Kohl
NASA Lewis Research Center
Cleveland, Ohio 44135

ABSTRACT

The high temperature vaporization of the metal-carbon systems Ti-C, Zr-C, Hf-C, and Th-C was studied by the Knudsen effusion-mass spectrometric method. For each system the metal dicarbide and tetracarbide molecular species were identified in the gas phase. Ion intensities of the carbides and metals were measured as a function of temperature. Second- and/or third-law methods were used to determine enthalpies for the reactions

$$M(g) + 2C(s) = MC_2(g)$$

$$M(g) + 4C(s) = MC_4(g)$$

Experimentally determined reaction enthalpies were combined with published thermodynamic data to obtain the following dissociation energies in kcal $mole^{-1}$: $D_0^\circ(Ti\text{-}C_2)$ = 136±6, $D_0^\circ(Zr\text{-}C_2)$ = 137±6, $D_0^\circ(Hf\text{-}C_2)$ = 160±7, $D_0^\circ(Th\text{-}C_2)$ = 169±6, $D_0^\circ(C_2\text{-}Ti\text{-}C_2)$ = 291±6, $D_0^\circ(C_2\text{-}Zr\text{-}C_2)$ = 308±7, $D_0^\circ(C_2\text{-}Hf\text{-}C_2)$ = 322±7 and $D_0^\circ(C_2\text{-}Th\text{-}C_2)$ = 335±6. Thermodynamic functions used in the calculations are discussed in terms of assumed molecular structures and electronic contributions to the partition functions. The trends shown by the dissociation energies of the carbides of Group IVB are compared to neighboring groups and discussed in relation to the corresponding oxides and chemical bonding.

*A preliminary account of this work is given in NASA TM X-67844.

L9

VAPOR COMPOSITION AND CHEMICAL REACTIONS OF LASER VAPORIZED CARBON*

R. T. Meyer, A. W. Lynch, J. M. Freese
Sandia Laboratories, Albuquerque, New Mexico 87115

ABSTRACT

The compositions of laser vaporized graphites and carbides have been measured by time resolved mass spectrometry to obtain the C_n abundances vs. laser energy and to establish methods for gas phase C_n titrations. Low energy ($\sim$ 1 cal/cm^2) vaporization of graphite yielded C_1:C_2:C_3 abundances, which agree with Palmer's "best" vapor pressure data[1] if Langmuir vaporization and 4000 K are assumed. Higher incident energies increased the C_3/C_1 ratio and added C_5 and C_7. Laser vaporization of TaC, thought to be a source of C_1 only, yielded both C_1 and C_3, but little or no C_2. The Nb_2C vapor composition varied with apparent changes in the composition of the solid phase. Vapor titrations were performed with pure CH_4, H_2 and O_2. Major products from pyrolytic graphite were C_2H_2 + H_2, C_2H_2, and CO + CO_2, respectively; whereas TaC yielded C_2H_2, very little C_2H_2, and CO + CO_2, respectively. The mass loss from graphite correlated exactly with the sum of CO + CO_2. The results indicate that C_n species can be quantitatively titrated. Specifically, the following reactions appear to dominate: (a) $C_1 + CH_4 \rightarrow C_2H_2 + H_2$; (b) $C_2 + H_2 \rightarrow C_2H + H$, $C_2H + H_2 \rightarrow C_2H_2 + H$; (c) $C_1 + O_2 \rightarrow CO + O$, $C_n(n>1) + O_2 \rightarrow CO + CO_2$.

*This work was supported by the U. S. Atomic Energy Commission.

[1] H. B. Palmer and M. Shelef, in Chemistry and Physics of Carbon (P. L. Walker, Jr., ed.), Vol. 4, pp. 85-135, Marcel Dekker, Inc., New York, 1968.

NEGATIVE ION PRODUCTION FROM CARBON ALLOTROPES

W. K. Stuckey and A. G. Whittaker
Materials Sciences Laboratory
THE AEROSPACE CORPORATION
El Segundo, California

Since the discovery of the formation of the carbon allotrope chaoite at low pressures[1], work has continued on the formation and properties of this form of carbon. A part of this work has involved use of the ion microprobe for analysis of samples[2] prepared in the Aerospace Corporation Materials Sciences Laboratory. The samples were analyzed by x-ray or electron diffraction and by electron probe techniques in most cases. The only non-carbon ions observed were orders of magnitude lower intensity.

The observation of chaoite (white carbon) in the laboratory is evidenced by the characteristic white coloration on the samples. Ion probe studies of the white areas were performed with striking differences in the secondary negative ion spectra of the white areas and other areas of the same sample. In the white areas of the sample, a spectrum of carbon negative ions is observed in which higher molecular weight carbon ions were detected. The spectrum for chaoite is shown by the solid squares in Figure 1, normalized to C_2^-. Secondary ions from chaoite containing materials have been observed up to C_{16}^- with good agreement in the distribution from C_6^- to C_{12}^- for samples prepared by various techniques. The secondary ion spectrum for a-face pyrolytic graphite with 16 KV 0_2^+ is shown by the solid circles in Figure 1. In this spectrum, C_1^- is the most intense ion species. Negative ions from a-face pyrolytic graphite are observed up to C_6^- which is 4 orders of magnitude lower in intensity than C_1^-.

The secondary ion spectra of other carbon forms are also shown in Figure 1. The spectrum of c-face pyrolytic graphite shows a greater tendency toward high molecular weight carbon ions that observed for a-face pyrolytic graphite and is similar to the spectrum of a graphite single crystal. The negative ions observed from a diamond sample show a large contribution in the heavier carbon ions as observed with chaoite. The distribution of the heavier ions is virtually identical for the two forms although the curves are slightly displaced. The distribution is in good agreement with that reported by Honig[3] except for C_1^- where the higher bombarding energy (10-16 KV) used in these experiments results in greater relative amounts of C_1^- than observed in the previous work which employed 500 eV Ar^+. At 16 KV, little change was noted in secondary ion yields from chaoite with O_2^+, Ar^+ or O^- bombardment.

References:

1. A. G. Whittaker and P. L. Kintner, Science 165, 589 (1969).

2. The authors wish to acknowledge the cooperation of Dr. C. A. Anderson of Applied Research Laboratories, Sunland, California, in the studies on the ARL Ion Microprobe Mass Analyzer. Similar results were obtained on a Bell and Howell 27-101A Direct Imaging Mass Analyzer.

3. R. E. Honig, Advances in Mass Spectrometry 2, 25 (1963)

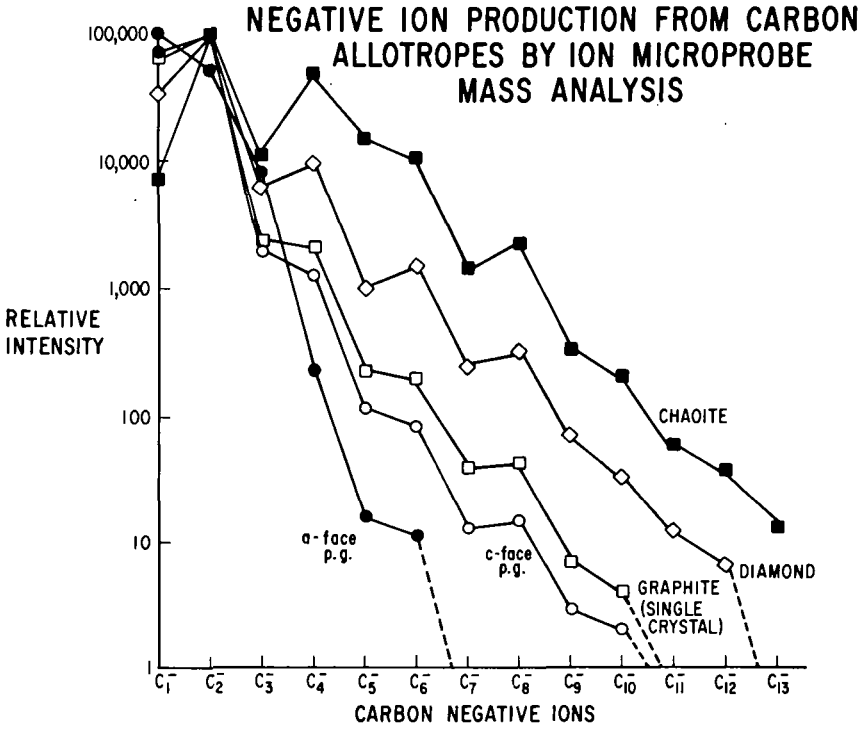
NEGATIVE ION PRODUCTION FROM CARBON ALLOTROPES BY ION MICROPROBE MASS ANALYSIS
100,000
10,000
1,000
100
10
1
RELATIVE INTENSITY
CHAOITE
DIAMOND
GRAPHITE (SINGLE CRYSTAL)
a-face p.g.
c-face p.g.
C_1^- C_2^- C_3^- C_4^- C_5^- C_6^- C_7^- C_8^- C_9^- C_{10}^- C_{11}^- C_{12}^- C_{13}^-
CARBON NEGATIVE IONS

Mass Spectrometric Vaporization of Ilmenite

J. S. OGDEN, C. A. ALEXANDER, AND W. M. PARDUE
Columbus Laboratories, Battelle Memorial Institute, Columbus, Ohio 43201

The vaporization of ilmenite is considered a likely comparison for establishing the similarities or differences between terrestial and lunar environments at the time of solidification. Most terrestial ilmenite is a product of magmatic segregation or it occurs as an accessory mineral in igneous rocks. The transition metal elements of ilmenite should have real potential for determination of conditions of temperature and oxygen pressure during solidification of the lunar surface. The oxygen/metal ratio depend upon the temperature and oxygen pressure at the time of solidification. At the melting point of ilmenite the preferential loss of Fe is easily detected. The ratio Fe/FeO = 420 and TiO_2/TiO = 6 at the melting point under vacuum conditions. The presence of an atmosphere both markedly changes the above ratios and also changes the absolute volatilization rates by orders of magnitude. Preliminary determinations indicate that the relative ratios of $Fe/FeO/TiO/TiO_2$ are clearly indicative of the thermal history of the magmatic ilmenite. A number of thermodynamic values were determined in the course of the investigation; notably of which: D° FeO=108 kcal, D° TiO_2=305 kcal.

Abstract

Ion-Dipole Capture Cross Sections at Low Ion and Rotational Energies; Comparison of Reaction and Capture Cross Sections for NH_3 and H_2O Parent Ion Collisions.
John V. Dugan, Jr., and R. Bruce Canright, Jr., NASA Lewis RC, Cleveland, Ohio

Numerical studies of ion-dipole collisions have been extended to calculating capture cross sections σ_c at ion velocities down to 2.5×10^4 cm sec^{-1} for rotational temperatures T_R of 77 K. The σ_c values are as large as 3500 $Å^2$ at T_R = 77 K and the slope of σ_c vs ion velocity approaches a $v^{-1.6}$ dependence in the range of velocities from 2.5 to 5×10^4 cm sec^{-1}. Comparison of integrated Q_c and monoenergetic σ_c values with reaction cross sections Q_R is made for the polar targets NH_3 and H_2O from thermal to several eV. Generally the σ_c, Q_c and Q_R values are greater than Langevin values but less than the maximum cross section. Conclusions regarding reaction efficiencies and predicted ion energy dependences are discussed in the context of various experimental results.

The details of this study will be published in Chemical Physics Letters.

M2

Reactions of Molecules in Highly Excited Rydberg States Produced by Photon Absorption.* WILLIAM A. CHUPKA and JOSEPH BERKOWITZ, Argonne National Laboratory, Argonne, Illinois 60439

Mass spectrometric studies of photoionization processes show that molecules produced in highly excited Rydberg states by photon absorption can undergo a variety of reactions which produce charged products, e.g., chemi-ionization, Penning ionization, collision-induced ionization, and charge transfer to electronegative molecules. A major advantage of the photon-absorption technique over electron-impact methods is the ability to observe the reactions of specific, identified excited states of energies up to within several millivolts of the ionization limit. The relative probabilities of such reactions of excited rare gas atoms has been studied as a function of the electronic state of the excited atom and of such properties of the reacting partners as dipole moment, electron affinity and electron-capture cross section. The technique has also been used to determine limits to electron affinities. For NO_2 we find $2.2\ eV < EA(NO_2) < 2.5\ eV$.

*Under the auspices of the U.S. Atomic Energy Commission.

REACTION OF NO^+ WITH WATER IN A PHOTOIONIZATION MASS SPECTROMETER* M3

M. J. McAdams and L. I. Bone
Department of Chemistry
East Texas State University
Commerce, Texas 75428

INTRODUCTION

The formation of hydrated protons from the solvation of the NO^+ ion with water is of interest as this process is one of the reactions which must occur in the D region of the earth's ionosphere to account for the abundance of proton hydrates there. The mechanism for this reaction has been studied by Fehsenfeld and Ferguson,[1] Fehsenfeld, Moseman, and Ferguson,[2] Puckett and Teague,[3] and Howard, Rundle and Kaufman.[4] Puckett and coworkers[3] used a stationary afterglow technique, while all other authors used flowing afterglow techniques. We have just constructed a photoionization quadrupole mass spectrometer using krypton resonance radiation which is particularly well suited to reinvestigate this system since we can produce ground electronic state NO^+ with low vibrational energy without ionizing water.

EXPERIMENTAL

The photoionization mass spectrometer used in these experiments consists of a reaction chamber, a krypton resonance lamp, and a C.E.C. 21-440 quadrupole mass analyzer. The reaction chamber which serves as the source of the mass analyzer is field free and has a 1/32" ion exit hole. The entire system is pumped by 6" oil diffusion pump such that the pressure in the mass analyzer region can be maintained below 10^{-5} torr for pressures up to 1 torr in the reaction chamber. The Tobin Bronze reaction chamber is cubical, one centimeter on a side, with lithium fluoride windows in two sides to prevent photoelectron production in the source.

A krypton resonance lamp with a CaF_2 window is used. The design of this lamp has been discussed elsewhere.[5] The lamp emits a single line at 1236 Å (10.03 eV). Since the ionization potential of NO is 9.8 eV whereas the ionization potential of water is 12.6 eV, only NO is ionized and the NO^+ produced is in the ground electronic state.

The reaction mixture is prepared in a conventional glass inlet system equipped with a 2 liter ballast bulb and a Wallace and Tiernan gauge calibrated from 0 to approximately 200 torr. The reaction mixture is bled into the source through a Granville-Phillips manually variable leak. Rough pressure determinations in the reaction chamber are made with a Pirani Gauge between the leak and the reaction chamber. In experiments where rate constants are calculated the pressure in the reaction chamber is calibrated by comparison with reactions with known rate constants. One calibration reaction is the reaction of NO^+ with 2-methyl butane which has been reported by Searles and Sieck[6] using a similar instrument. They report a second order rate constant of 7.8×10^{-9} cm^3/molecule-sec. The other calibration reaction is the reaction of $C_2H_4^+$ from ethylene with ethylene. Of the numerous reported values[7] for this reaction we use a cross section, 62 $Å^2$ as it gives a pressure calibration consistent with the NO-C_5H_{12} reaction.

RESULTS AND DISCUSSION

A graph of the log of percent ionization vs the total pressure for a typical experiment with 0.25 mole fraction of water is shown in Figure 1. From graphs such as

FIGURE I: PRODUCTS FROM THE REACTION OF NO^+

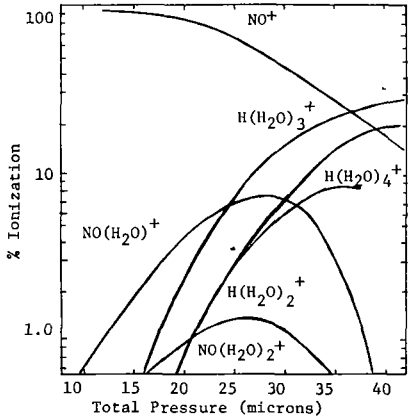

MECHANISM

1) $NO^+ + H_2O + M \rightarrow NO(H_2O)^+ + M$

2) $NO^+ + NO + M \rightleftarrows (NO)_2^+ + M$

3) $(NO)_2^+ + H_2O \rightleftarrows NO(H_2O)^+ + NO$

4) $NO(H_2O)^+ + H_2O + M \rightleftarrows NO(H_2O)_2^+ + M$

5) $NO(H_2O)_2^+ + H_2O + M \rightleftarrows NO(H_2O)_3^+ + M$

6) $NO(H_2O)_3^+ + H_2O \rightarrow HNO_2 + H(H_2O)_3^+$

7) $H(H_2O)_3^+ + H_2O \rightleftarrows H(H_2O)_4^+$

8) $H(H_2O)_4^+ + H_2O \rightleftarrows H(H_2O)_5^+$

9) $H(H_2O)_2^+ + H_2O \rightleftarrows H(H_2O)_3^+$

this for mole fractions of water of 0.125, 0.25 and 0.5 and identical experiments using D_2O, a mechanism which is valid under our experimental conditions is deduced. This mechanism is consistent with that reported by other authors[1-4] except that we observe the production of m/e 37 by reaction 9 which has been reported by Kebarle, et al.,[8] but is not reported by other authors in the NO-H_2O system. We establish the validity of equilibrium steps 7, 8, and 9 by observing the ratios of m/e 91/73/55/37 as a function of the mole fraction of water. The higher hydrates become more abundant at large mole fractions. Rate constants have been calculated but they appear to be consistently too large.

Based on heats of formation of the hydrated proton,[8] tabulated heats of formation,[9] the observation of reactions 5 and 6, and the non-observation of

$$NO(H_2O)_2^+ + H_2O \rightarrow H(H_2O)_2^+ + HNO_2$$

we are able to calculate the heat of formation of the hydrates of NO^+. These are:

$NO(H_2O)^+$ $\quad \Delta H_f^\circ \simeq 161$ kcal/mole

$NO(H_2O)_2^+$ $\quad 90 < \Delta H_f^\circ < 97$ kcal/mole

$NO(H_2O)_3^+$ $\quad 17 < \Delta H_f^\circ < 39$ kcal/mole

We have conducted a series of experiments with H_2O, HOD and D_2O to determine if there is any isotope effect in the hydration of NO^+, i.e., reactions 1, 4, and 5. An equilibrated mixture of H_2O, HOD and D_2O were prepared by mixing equal volumes of H_2O and D_2O. Taking into account the equilibrium constant measured by Friedman and Shiner[10] of 3.75, the H_2O:HOD:D_2O ratio in the mixture is 1:1.94:1. This mixture was reacted with NO^+ in exactly the same manner as before. Inspection of the m/e 48, 49, and 50 peaks, which corresponds to the singly hydrated NO^+, shows a ratio of 1:1.95:1 while the 66:67:68:69:70 ratio which corresponds to the doubly hydrated NO^+, was 1:4:6:4:1 indicating no kinetic isotope effect in the first two hydration steps. The $NO(H_2O)_3^+$ peak was not intense enough to make an isotopic determination, but it appears that any isotope effect in the hydration process is at best very small.

In addition to the above observation we did not observe any isotope effect in the $H(H_2O)_3^+$ peak, or for any of the other proton hydrates. This is surprising since $H(H_2O)_3^+$ is the product of reaction 6 which produces HNO_2. This reaction must involve breaking an O-H bond and therefore should show an isotope effect. Before speculating on the meaning of the non-observation of an isotope effect, a series of experiments were conducted with an equilibrated mixture of H_2O, HOD and D_2O using electron impact. We were able to observe an isotope effect in the production of hydronium ion. This gives us confidence that if there was an isotope effect in reaction 6 we could have observed it.

From the non-observation of the isotope effect in reaction 6, we suggest that the structure of the hydrated NO^+ is

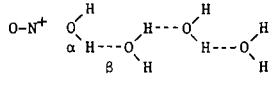

where the dashed line indicates a hydrogen bond. The first water of hydration is attached by electrostatic interaction. Because of the strong inductive effect of the positive ion, the hydrogens on the first water are quite electron deficient and are thus capable of forming a strong hydrogen bond. Additional waters of hydration are added by hydrogen bonding which further delocalizes the charge. This strengthens the β O-H bond while weakening the α O-H bond. When four waters are attached, the α bond breaks and the β bond forms leaving $H(H_2O)_3^+$ and HNO_2. Since the process is perfectly symmetrical, i.e., formally the bond strengths in the reactant and the activated complex are identical for reaction 6, no isotope effect is expected. In addition HNO_2 is properly constituted.

REFERENCES

* Funded by the Robert A. Welch Foundation, to be submitted for publication to J. Chem. Phys.

1. F. C. Fehsenfeld and E. E. Ferguson, J. Geophys. Res., 74, 2217, (1969).
2. F. C. Fehsenfeld, M. Moseman and E. E. Ferguson, Submitted for publication, J. Chem. Phys.
3. L. J. Puckett and M. W. Teague, J. Chem. Phys., 54, 2564, (1971).
4. C. J. Howard, H. W. Rundle and F. Kaufman, Bull. Am. Phys. Soc., 16, 213, (1971).
5. P. Ausloos and S. G. Lias, Radiation Res. Rev., 1, (1968), 75-107.
6. S. K. Searles and L. W. Sieck, J. Chem. Phys., 53, 795, (1970).
7. T. O. Tiernan and J. H. Futrell, J. Phys. Chem., 72, 3080, (1968).
8. P. Kebarle, S. K. Searles, A. Zolla, J. Scarborough, and M. Arshadi, J. Am. Chem. Soc., 89, 6393, (1967).
9. "Ionization Potentials, Appearance Potentials, and the Heats of Formation of Gaseous Positive Ions," National Bureau of Standards Circular 26, U.S. Government Printing Office, Washington, D.C., 1969.
10. L. Friedman and V. J. Shiner Jr., J. Chem. Phys., 44, 4639, (1966).

M5

ION-MOLECULE REACTIONS INVOLVING ALKYL SILICONIUM AND RELATED ALKYL METAL IONS.

PAUL VOUROS, D. J. HARVEY AND M. G. HORNING

Institute for Lipid Research, Baylor College of Medicine,
Houston, Texas 77025

Abstract

The mass spectra of TMS derivatives of various compounds exhibit ions of mass higher than the molecular ion, e.g., M + 73, M + 147. The relative abundance of these ions was observed to be dependent on source pressure, indicating that they were formed via an ion-molecule reaction. Further examination of the spectra indicated that these ions corresponded to the combination of a molecular species and abundant fragment ions. Isotope labeling showed that all the fragment ions concerned contained a positively charged silicon center. Experiments with a dual inlet system confirmed that the ions with masses higher than the molecular ion arose from the simple addition of fragment ions to a neutral molecular species. Differences in the reactivity of various alkyl metal ions were observed.

For more details see: J. Chem. Soc. (D) 1970, p. 898; Analytical Letters 3, 489 (1970); Org. Mass Spectrom. (in press).

INTERMOLECULAR HYDROGEN TRANSFER REACTIONS IN THE MASS SPECTRA OF DIALKYL MALONATES

M6

Mary H. Wilson and James A. McCloskey

Baylor College of Medicine
Houston, Texas 77025

The formation of $(M + H)^+$ ions at low pressures has been observed for many types of compounds, especially alcohols, nitriles, and esters. Few efforts have been made to determine the sources of the transferred hydrogen and to relate structure and reactivity. The alkyl malonates were studied in order to investigate these problems in a system of moderate complexity with a strong tendency to form $(M + H)^+$ ions.

Methyl, ethyl, n-propyl, and i-propyl malonates were exhaustively deuterated; and n-butyl, i-butyl, sec-butyl, n-amyl, and n-octyl were deuterated in selected positions. The ratio $(M + D)^+/[(M + H)^+ + (M + D)^+]$ was obtained for each labelled compound from 12 eV to 20 eV at 170°C on a LKB-9000 gas chromatograph-mass spectrometer.

Fragmentation of n-alkyl malonates leads predominantly to the formation of ions such as a-d which contain labile hydrogen and would be expected to be good proton

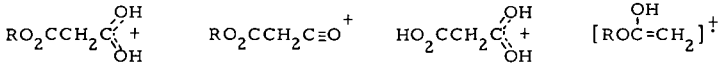

a b c d

donors. Molecular ions are absent for propyl and higher esters. Hydrocarbon ions are prominent in the spectra of malonic esters of secondary and tertiary alcohols and comprise the base peaks in some instances. The origin of the hydrogen rearranged to oxygen in the formation of a, c, and d has been determined from the spectra of deuterated analogs of methyl, ethyl, n-propyl, i-propyl, and n-butyl malonates. Relationships are found between the variations of relative ion abundances and of $(M + D)^+/[(M + H)^+ + (M + D)^+]$ with electron energy for each labelled molecule. On the basis of this data ions a-d may be identified as precursors to $(M + H)^+$ and the most labile hydrogen of each ion is found to be that which is transferred. ICR double

resonance[1] confirms the importance of proton donation and conclusively proves a-d and several minor ions as precursors of $(M + H)^+$. Hydrogen abstraction by M^+ cannot be ruled out but must be a process of minor significance. Chemical ionization with CD_4 suggests that the transferred proton in $(M + H)^+$ may be retained in fragment ions resulting from the decay of this species.

[1] Provided by Dr. Robert Wilcox of Varian Associates, Palo Alto, California

CHEMICAL IONIZATION: ARRIVAL TIME DISTRIBUTIONS OF REACTANT IONS

G. Sroka, C. Chang, and G. G. Meisels

Chemical Physics Program
Department of Chemistry
University of Houston
Houston, Texas 77004

ABSTRACT

A method for the determination of arrival time distributions in high pressure mass spectrometry (0.5 to 3 torr) is described. It employs a pulsed electron gun and time-of-flight analysis of reactant ions using nuclear instrumentation and delayed coincident individual ion detection. Arrival time distributions of CH_5^+ and $C_2H_5^+$ are presented, and mean residence times calculated from the first moments of these curves are shown to be substantially less than those calculated from idealized Langevin drift theory commonly employed to estimate this quantity. The change in the arrival time distribution of methane ion when small concentrations of methane are added to helium is used to evaluate the total rate constant of methane ion reaction with methane as $1.00\pm0.08 \times 10^{-9}$ccsec^{-1}. It is shown that the simple technique employed for rate constant measurement gives excellent reproducibility and an accuracy which is primarily limited by the ability to assess pressure in the reaction region.

INTRODUCTION

Chemical Ionization[1] has become an important tool in analytical chemistry.[2,3] Recently attention has been focussed on the possibility of measuring ion-molecule reaction rate constants under conditions of chemical ionization[4,5] and the approach has been extended to measure ionic equilibria.[6,7,8] Results have not always been in agreement with each other,[4,5] and heats of reaction derived from such measurements[6] are not always consistent with those obtained by other methods.[9]

In order to carry out quantitative determinations of first and second order rate constants it is necessary to know residence time of ions in the source.[4,5] Similarly, residence time is an important parameter in the assessment of the applicability of equilibrium considerations.[7] These times are calculated from idealized ion drift considerations originally developed by Langevin[10] and summarized by McDaniel.[11] However, it is known that such calculated residence times can be in error by as much as an order of magnitude even under idealized drift conditions.[11,12] We have therefore constructed a pulsed high pressure ionization source to measure arrival time distributions directly, and report here on some of the problems associated with residence time calculations for chemical ionization sources.

EXPERIMENTAL

The high pressure ion source was constructed by replacing the source block and draw-out slits of a commercial Varian-MAT CH-4, type AN-4B ion source. The revised block has an electron entrance slit of 0.025 X 2.0 mm, while the electron trap is tightly mounted against the flange using a 1 mm Teflon sheet as an insulator. The single draw-out plate contains an ion exit slit of 0.05 X 5.0 mm, and is located 7.0 mm from the electron beam and 7.6 mm from the rear wall of the chamber. A four inch Edwards pumping system is used to evacuate the region surrounding the ion source, maintaining a pressure of 10^{-3} torr or less at an ion source pressure of 3 torr. The source region is connected to the analyzer only through a skimmer throttling tube approximately 5 mm below the beam defining slit. Pressure in the analyzer section did not exceed 0.05 mtorr.

The gas introduction system consists of two five liter reservoirs and a one liter reservoir. Either of the former and the latter can be opened to the ion chamber via Granville-Phillips metering needle valves. Pressure in the ion source is measured with an MKS Baratron Capacitance Manometer. The sensing side of this manometer is connected to a separate port of the ion source located at right angles to the electron beam and the gas inlet. The pressure gauge was calibrated using a trapped McLeod gauge.

The electron gun was pulsed by unblocking a biased 85 line per cm Tungsten screen (90% transparent) between the Rhenium filament and the entrance slit using a 50 nsec pulse from a Hewlett-Packard Model 214A pulse generator. The trigger pulse from the generator also started the voltage ramp of a time to pulse height converter (W.H. Johnston Labs.). The electron multiplier ion detector output was coupled directly into an amplifier-discriminator and pulse shaper (W.H. Johnston Labs.), whose output terminated the voltage ramp of the time to pulse height converter, creating a pulse

whose height is proportional to flight time. Pulses were sorted on a TMC model 401B 400 channel pulse height analyzer whose output was either recorded on a Hewlett-Packard model 2D-2 X-Y recorder or on a Hewlett-Packard model 500 digital recorder. The experimental arrangement is shown in Figure 1.

The electron pulse width at the screen was measured using a Tektronix model 564 Oscilloscope with 351 and 3T77A Plug-Ins, and showed some broadening to ca. 100 nsec FWHM. Arrival time distributions are also greatly affected by the electron beam spread in the ionization region; this was assessed approximately by evaluating the arrival time distribution of CH_4^+ ion from methane at the lowest pressure where sufficient count rates could be obtained (ca. 1 mtorr); the distribution had a width of ca. 0.5 microseconds at half maximum.

RESULTS AND DISCUSSION

A. RESIDENCE TIMES OF CH_5^+ AND $C_2H_5^+$ ION IN METHANE

The theoretical residence time, t_{theor} is readily calculated from the expression[11]

$$t_{theor} = (L/E)(P/T)\sqrt{\alpha\mu} \cdot 10^{-2} \text{ sec} \qquad (I)$$

where E is the field strength in V/cm, L the drift length of the ion in cm, or approximately the distance between electron beam and ion source exit slit, P the pressure in torr, T the temperature in °K, α the polarizability in atomic units (0.053 nm) and μ the reduced mass, also in atomic units.

There are four limitations associated with the application of this equation to the calculation of residence times in chemical ionization sources.

1. Instrumental factors causing unequal sampling of the arrival time distribution and the dependence of this factor on the diffusion coefficient D or on ion mass.
2. The questionable reliability of equation I even under conditions where ion drift is slow and experimental conditions are well defined. Differences between experimental and calculated diffusion coefficients involving factors up to ten have been reported.[11,12]
3. The effect of details of the transport process such as ion-molecule reactions, charge transfer, proton transfer, and other metathetical reactions on the momentum transfer cross section.
4. Poorly defined experimental conditions such as pressure, electrical fields, etc. These complications will introduce relatively minor, consistent errors which should not affect relative measurements. They can also be overcome by careful source design.

In this paper we are chiefly concerned with the first two problem areas. The idealized drift equations require complete collection of all ions, corresponding to total ionization measurements. The small ion sampling aperture or ion exit slit in chemical ionization sources discriminates against the observation of ions produced at longer residence times. It can be shown,[13] that the fraction of the ions which reach the exit slit plane and pass through the sampling orifice may vary as strongly as 1/Dt. Experimental ion arrival time distributions span nearly an order of magnitude in time. Discrimination should therefore be substantial and residence times should be measured.

The quantity measured in our experiments is an arrival time distribution which includes the transit time through the acceleration and mass analysis regions of the mass spectrometer beyond the ion source exit aperture, as well as the small delays in the electron multiplier and electronics. The totality of these transit times can be evaluated by changing the field strength in the ion source while examining the flight time of a primary ion at low pressures. Since a draw-out field is used and the ion origin is near the back plate, terminal ion energy in the transit region is essentially unaffected by draw-out field in the absence of ion-molecule reactions. The mean residence time $\bar{t}$ should vary as $(V_{draw\text{-}out})^{-1/2}$ if electronic delays are negligible; this is indeed observed and $t_{transit} = 1.58 \cdot \sqrt{m/e}$ µsec as determined at m/e = 16.

Experimentally observed residence time distributions for CH_5^+ and $C_2H_5^+$ ions in methane are shown in Figure 2. Mean arrival times for these ions were calculated at various values of E/P from the first moments of these curves; these in turn yielded $\overline{v_d} = L/\bar{t}$. This formulation is not entirely correct but is thought not to introduce a serious error[14,15] and is employed commonly.[16] Figure 3 demonstrates that drift velocities calculated in this manner are a linear function of E/P as required for low field drift conditions. The calculations of reduced mobility and of the diffusion coefficient D, which can be obtained from the Einstein relation K/D = e/kT (provided that E/P is small) are shown in Table I. Experimental and theoretical diffusion coefficients, calculated from Langevin theory, are in substantial disagreement, confirming the inability to estimate residence times accurately from the simple equation I.

Under a particular set of experimental conditions discrimination towards the

detection of different ionic species is governed entirely by the diffusion coefficient for each ionic species.[11,14] The identity of the observed diffusion coefficients for CH_3^+ and for $C_2H_5^+$ can therefore not easily be ascribed to discrimination and may be the result of differences in the transport mechanism.

B. ION-MOLECULE REACTION RATE CONSTANTS FROM DRIFT EXPERIMENTS

The ability to measure ion intensity directly as a function of reaction time (i.e. ion residence time) provides a rapid, convenient and accurate means of determining rate constants for ion-molecule reactions involving near-thermal ions. The only parameters which need to be known are pressure in the reaction region and arrival time distributions with an accurate time scale. The approach can be used for chemical ionization systems, but also generally for all types of ion-molecule reactions.

The reaction leading from reactant (primary) ion R^+ to product ions X_i^+ can generally be written as

$$R^+ + N \xrightarrow{k_1} \Sigma X_i^+ + Y_j \qquad (1)$$

where N is the reactant neutral and Y the product neutral. The total rate of reaction 1 is $-d[R^+]/dt \approx k_1[R^+][N]$. Since the concentration of N is essentially invariant and much larger than R^+ the reaction is quasi-first order and yields on integration

$$\ln(R^+/R_o^+) = -k_1 t[N] \qquad (II)$$

Here R_o^+ is the initial concentration of reactant ions at zero time. Since the decrease in reactant ion concentration is usually difficult to evaluate accurately, particularly when the pressure of reagent is changed, it has been customary to equate $R_o^+ = \Sigma X_i^+ + R^+$. t is obtained from equation I, but the resultant rate constants are inconsistent between investigators[4,5] and vary with E/P.[5] This can probably be ascribed at least to the change in diffusion coefficient D with ion identity.

When arrival time distributions can be determined, however, R^+ is evaluated directly as a function of t. R_o^+ is still not readily accessible as a function of time, however, at two reactant concentrations N_1 and N_2,

$$\ln(R_1^+/R_2^+) = \ln(R_{o,1}^+/R_{o,2}^+) - k_1 t([N_1]-[N_2]) \qquad (III)$$

As long as the initial ion arrival time distributions differ only in terms of intensity, the logarithmitic term on the right hand side of equation III will be independent of t, and the logarithm of the ratio of reactant ion abundances at two pressures should be a linear function of t with slope $-k_1([N_1]-[N_2])$.

This method does not require knowledge of the ion transit time since this quantity merely offsets the curve laterally. We believe that this technique should be substantially free of the pitfalls of rate evaluations frequently encountered in such measurements.[17]

The applicability of this approach was verified by examining the well known reference reaction

$$CH_4^+ + CH_4 \rightarrow CH_5^+ + CH_3 \qquad (2)$$

Since this reaction is fast, small concentrations of reactant methane gas were introduced into the ion source already containing 1.08 torr helium as a drift or "bath" gas in the manner previously described by Vredenberg et.al.[5] Three representative sets of data plotted according to equation III are shown in Figure 4. Rate constants derived from the least squares fits of such graphs are shown in Table II. The variation of the rate constant with E/P reported elsewhere[5] is not observed, indicating that conditions in our experiment are well defined. The absolute rate constant derived from these measurements is in good agreement with the value $1.09\pm0.09 \times 10^{-9}$ ccsec^{-1} reported by other investigators.[18]

ACKNOWLEDGEMENTS

This investigation was supported in part by the National Science Foundation and by the Robert A. Welch Foundation, of Houston, Texas. We are sincerely grateful for this support. One of the authors wishes to express his gratitude to Professor E. W. McDaniel for a very stimulating and extremely helpful discussion, and permission to visit his laboratory.

LITERATURE CITED

1. M.S.B. Munson and F.H. Field, JACS. 88, 1621 (1966).
2. F.H. Field, Accts. of Chem. Res. 1, 42 (1968).
3. H.M. Fales, G.W.A. Milne and T. Axenrod, Anal. Chem. 42, 1432 (1970).

4. F.H. Field, JACS. 91, 2827 (1969).
5. S. Vredenberg, L. Wojcik, and J. H. Futrell, J. Phys. Chem. 75, 590 (1971).
6. D. P. Beggs and F.H. Field, JACS 93, 1567 (1971).
7. D. P. Beggs and F.H. Field, JACS. 93, 1576 (1971).
8. F.H. Field and D.P. Beggs, JACS. 93, 1585 (1971).
9. P. Kebarle, S. K. Searles, A. Zolla, J. Scarborough, and M. Arshadi, JACS. 89, 6396 (1967).
10. P. Langevin, Ann. Chim. Phys. 5, 245 (1905).
11. E. W. McDaniel, Collision Phenomena In Ionized Gases (John Wiley & Sons, Inc., New York, 1967), Chapter 9.
12. Y. Kaneko, L. R. Merrill and J. B. Hasted, J. Chem. Phys. 45, 3741 (1966).
13. G. G. Meisels; to be published
14. J. T. Moseley, I. R. Gatland, D. W. Martin, and E. W. McDaniel, Phys. Rev. 178, 234 (1969).
15. W. S. Barnes, Phys. of Fluids. 10, 1941 (1967).
16. J. T. Moseley, R. M. Snuggs, D. W. Martin, and E. W. McDaniel, Phys. Rev. 178, 240 (1969).
17. E. W. McDaniel, J. Chem. Phys. 52, 3931 (1970).
18. For a recent summary, see R. P. Clow and J. H. Futrell, Int. J. Mass Spectrom. Ion Phys. 4, 165 (1970).

TABLE I. DIFFUSION PROPERTIES OF CH_5^+ AND $C_2H_5^+$ IONS IN METHANE

ION	E/P ($Vcm^{-1}torr^{-1}$)	$D_{1atm,0°C}$ (cm^2sec^{-1})X 10^2
CH_5^+	15.9	4.51
	13.5	4.46
	12.9	4.46
	10.1	4.42
	7.1	4.68
	Average	4.51 ± 0.07
	Theoretical value	6.98
$C_2H_5^+$	17.2	4.60
	14.1	4.59
	13.7	4.49
	9.3	4.75
	7.6	4.02
	Average	4.49 ± 0.18
	Theoretical value	6.15

TABLE II. REACTION RATE OF CH_4^+ WITH CH_4 IN HELIUM

E/P(He) $Vcm^{-1}torr^{-1}$	k X 10^9 $cm^3mol^{-1}sec^{-1}$
1.25	1.05
2.00	1.00
3.69	1.03
5.12	.89
6.19	.99
9.08	.98
12.5	1.04
	1.00 ± .04

Figure 1. Schematic of experimental arrangement for arrival time measurements.

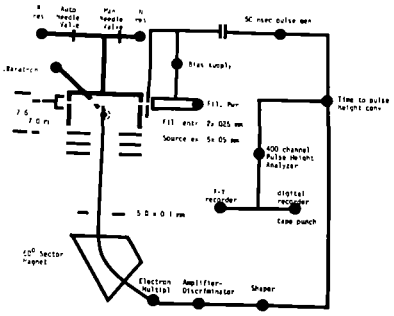

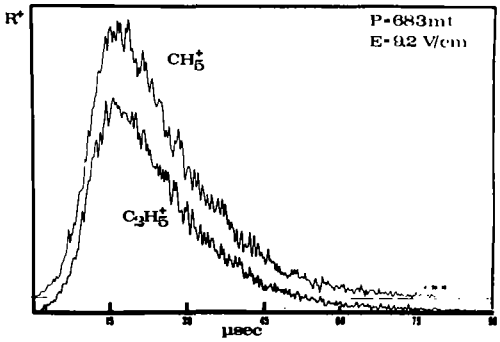

Figure 2. Arrival time distributions of CH_5^+ and $C_2H_5^+$ at a source pressure of 683 millitorr and a field strength of 9.2 V/cm.

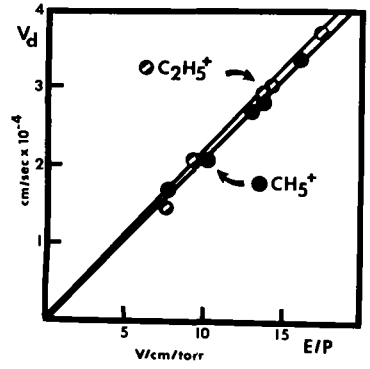

Figure 3. Variation of drift velocity of reactant ions in methane with E/P.

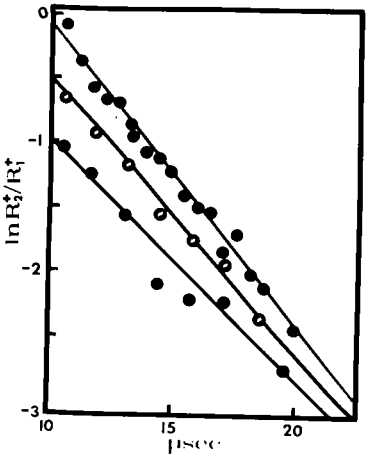

Figure 4. Evaluation of rate constant for reactions of CH_4^+ at three values of E/P(He). Top to bottom:

E/P(He) = 6.19, 5.12, and 1.25 V/cm/torr.
$\Delta P(CH_4)$ = 13.3, 16.6 and 15.1 mtorr.

N1

DIRECT COUPLING OF A GAS CHROMATOGRAPH TO A MASS SPECTROMETER

Pat Haug, James Serum, and William Updegrove

Department of Chemistry, Rice University, Houston, Texas 77001

INTRODUCTION

At the time that we began our attempt to connect a Barber Coleman gas chromatograph directly to a CEC 21-110B high resolution mass spectrometer, the only report in the literature of such a connection without a separator interface utilized a quadrupole mass spectrometer,[1] although a few laboratories had used chemical ionization sources with methane as the carrier gas.[2,3,4] Since that time, Finnigan has commercially announced the direct connection of their quadrupole and DuPont the connection of their 490 sector instrument.

INSTRUMENTATION

For both stability and pressure reduction, helium was run from a gas cylinder tank through about 200' of .02" bore stainless steel capillary tubing, with additionally imposed mechanical restrictions, into a Hamilton injector, adapted for low volume. 300' of .02" bore stainless steel capillary tubing coated with Apiezon L and FFAP were used for the separation. (150' of FFAP followed in series by Apiezon to provide the necessary length to maintain a source background pressure of 5×10^{-5} mm.) A high vacuum, low dead volume, 4 port valco (micropore) valve permitted three modes of operation: 1) coupling of the capillary columns to a mechanical pump for preliminary pump down with simultaneous connection of a packed column to the mass spectrometer through a Bieman-Watson glass separator, 2) direct coupling of the gas chromatograph to the mass spectrometer, and 3) isolation of the gas chromatograph from the mass spectrometer. This system is illustrated in the diagram. The capillary line entered the source housing through the

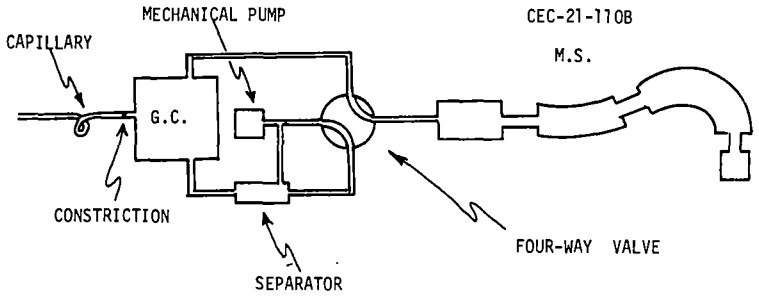

removed shutter assembly flange via an insulated, platinum-plated bus bar welded to the flange. The stainless steel capillary tubing ran into the source block via a ceramic insulator. The helium flow rate was less than 1 ml/min, when 5 lbs. of head pressure was maintained (the source pressure with the gas chromatograph isolated from the mass spectrometer was 1×10^{-6}). Spectra were run at 6 KV to prevent arcing and the unregulated ionizing current mode of operation was utilized. Most spectra were obtained with the electron multiplier set at 100 v/stage and a beam monitor reading of 10^{-10}. Sample sizes of 0.02 μ liter to 0.1 μ liter were adequate.

RESULTS

Hexane and heptane were easily separated from each other and the resultant spectra were identical with the individual compounds, although slight difficulty was experienced in establishing the separating conditions for a mixture of furan, pyrole, and acetonitrile. A fraction of a seep oil from a stream bank near Pataste Arriba in Costa Rica boiling from 90^{0} - 95^{0}C displayed at least four components although the separation was again poor. Although the system worked comparatively well with low molecular weight samples, difficulties were encountered with components consisting of over ten carbons due to the low flow rates dictated by a lack of pumping capacity. The obvious advantage of such a system is that extremely small amounts of sample may be detected and identified with ease.

ACKNOWLEDGEMENTS

The financial support of The Welch Foundation is gratefully acknowledged. The Consolidated Electrodynamics Corporation's high resolution mass spectrometer, Model 21-110B was provided by the National Institute of Health and the National Science Foundation.

REFERENCES

(1) W. S. Updegrove, J. Oro, A. Zlatkis, J. Gas Chromatogr. 3, 359 (1967).

(2) D. M. Schoengold and B. Munson, Anal. Chem. 42, 1811 (1970).

(3) G. Arsenault and J. J. Dolhun, Paper presented at the 18th Conf. on M. S., San Francisco, California, June 1970.

(4) Marvin Vestal, Paper presented at the 18th Conf. on M. S., San Francisco, California, June 1970.

ANALYSIS OF STEROID HORMONES BY A NEW DIRECT GC/MS INTERFACE *

N2

H. M. McNair, C. R. Dobbs, and L. H. Aung
Virginia Polytechnic Institute & State University
Blacksburg, Virginia 24061

D. C. Damoth and A. J. Luchte
Bendix Corporation
Rochester, New York 14603

INTRODUCTION

The successful application of gas chromatography (GC) to the separation of steroids a decade ago[1] has made GC the popular choice for the qualitative and quantitative analysis of these biologically important macromolecules. The analysis of steroids by GC has evolved into the preparation of sophisticated chemical derivatives, the development of selective stationary phases, utilization of all-glass analytical systems, and further optimization of chromatographic detection conditions.

The positive identification of GC peaks poses special problems because the analysis frequently involves only trace quantities of the molecule of interest. The final characterization of the molecular species has depended primarily upon the comparison of the retention times of "unknown" steroid peaks to those of authentic standards. Mass spectrometry (MS), however, offers an unequivocal molecular analysis.

The coupling of the GC and the MS into an operating system for steroid analysis involves problems which, when solved, apply to a broad range of analytical applications. Fortunately, when the GC/MS system is operating properly, data interpretation for biological analyses is easier than is frequently the case in food or petrochemical analysis. This report describes the development of a GC/MS interface system and its application to the separation and analysis of a series of steroid hormones.

EXPERIMENTAL

The direct combination of GC/MS has been accomplished by interface systems developed by several workers[2,3,4,5]. Littlewood[6], Spiteller[7], and Rees[8] have recently reviewed combined GC/MS techniques. The problems of direct interfacing have traditionally included:

a) the time required for MS analysis of an emerging molecular species,
b) enrichment by the analytical system of the molecule of interest, with respect to the carrier gas,
c) retention of molecular or derivative integrity throughout the GC and MS systems and interface, and
d) sensitivity.

We found, further, that temperature, surface contact, and effluent stream dynamics profoundly affected the quality and quantity of the resultant ion beam. The effluent from the GC column is composed predominantly of carrier gas, and we developed a transfer arrangement whereby the total GC effluent of a Bendix Model 2500 gas chromatograph was delivered to the ion source of a Bendix Model MA-2 Time-of-Flight mass spectrometer.

The GC column operates at nearly atmospheric pressure and the MS pumping system must maintain a sufficiently low pressure in the ion flight (analyzer) region to prevent collisional destruction of the ion beam. Thus, a high-efficiency differential pumping system (500 liters/sec. for air) was designed to accommodate the resulting high flow rate (about 20 ml/min.). Utilizing the total GC effluent for MS analysis allows the total ion current monitor to be used as the "GC tracing". The helium (carrier gas) signal is blanked out, allowing the ion source electron beam to be operated at 70 electron volts.

PREPARATION OF SAMPLE MATERIALS AND DERIVATIVE FORMATION

Free steroids were obtained from Supelco, Inc. Trimethylsilyl derivatives were formed by reacting 1 - 2 mg of the crystalline free steroid with 100 microliters of silylating reagent. Each of the steroids analyzed form silyl ethers which were stable

* Trivial names incorporated in this paper include: Etiocholanolone, 3α-hydroxy-5β-androstane-17-one; Dehydroepiandrosterone, 3β-hydroxyandrost-5-ene-17-one; Estrone, estra-1,3,5(10)-triene-3-ol-17-one; Estradiol, estra-1,3,5(10)-triene-3,17β-diol; Estriol, estra-1,3,5,(10)-triene-3,16α,17β-triol; TMS, trimethyl silyl ($-Si(CH_3)_3$).

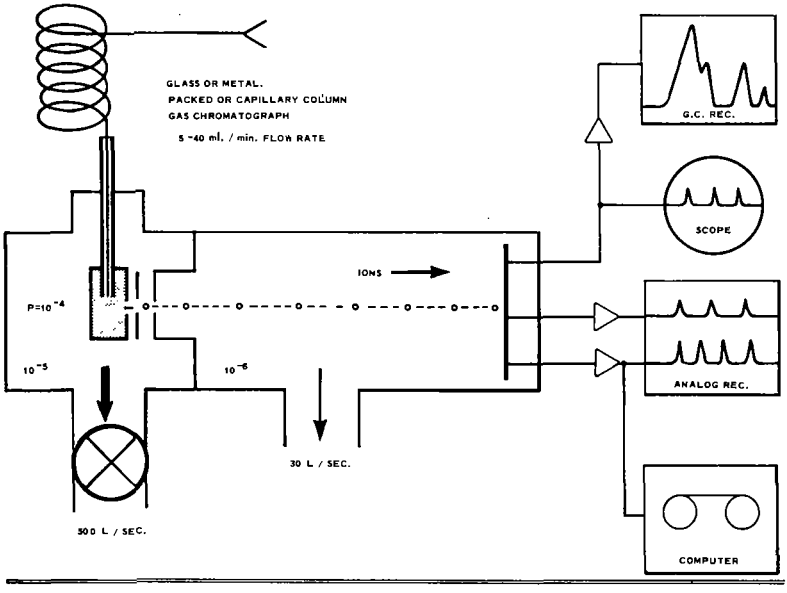

Figure 1. Schematic Diagram of the Direct GC/MS System

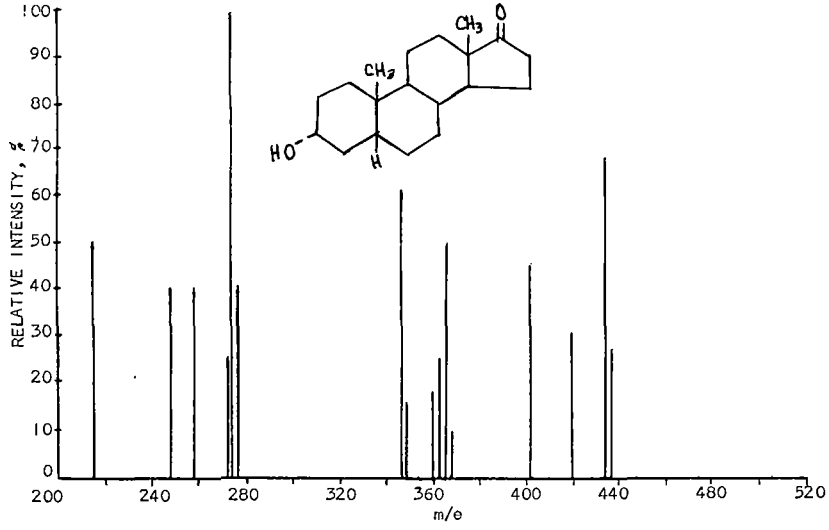

Figure 2. Mass Spectrum of Etiocholanolone as the TMS Derivative

to the experimental chromatographic conditions. The reactions were carried out in 1 ml. conical glass, Teflon-sealed reaction vials (Reacti-Vials, Pierce Chemical Co., Rockford, Ill.); these vials served also as the dispensing containers from which the samples were withdrawn for analysis.

The androgenic steroids (etiocholanolone and dehydroepiandrosterone) were derivatized with bis (trimethyl silyl) trifluoroacetamide (BSTFA) containing 1% trimethylchlorosilane (Regis Chemical Co., Chicago, Ill.); reactions were carried out at room temperature for 20 minutes.

The estrogenic steroids (estrone, estradiol, and estriol) were derivatized with BSTFA, warming to 60° for 5 minutes to effect solution of the steroids, followed by reaction at room temperature for 15 minutes.

The formation of methoxime derivatives of the ketonic steroids has been suggested[9] to avoid the formation of enol-TMS derivatives. This procedure can lead to the formation of isomeric derivatives that vary in retention time. To exclude this possibility, and to demonstrate the sensitivity of this GC/MS system to the analysis of multisilylated derivatives, we have not incorporated the methoxime technique.

There are commercially available derivatives of androgenic and estrogenic steroids, prepared in BSTFA containing 1% trimethylchlorosilane as catalyst and stabilizer (Regis Chemical Co.); these are packaged in acetonitrile in septum-stoppered glass vials under nitrogen, and have been found to be a convenient, stable series of steroid standards.

CHROMATOGRAPHIC ANALYSIS CONDITIONS

The steroid derivatives were separated in a Bendix Model 2500 gas chromatograph (Bendix Corp., Rochester, N.Y.) fitted with twin 4-foot, 1/4" OD glass columns packed with 3% OV-17 and 3% OV-1 (Ohio Valley Specialties Co., Marietta, Ohio) coated on 100/120 mesh Supelcoport (Supelco, Inc., Bellefont, Pa.). The following chromatographic conditions were used: Injection port, 220 C; GC/MS transfer line, 240 C; Helium (carrier gas) flow, 20 ml/min. Temperature programming (androgens): Injection, 200 C; isothermal, 5 min.; program @ 5 C/min. to 230 C; isothermal. Analyzed on OV-17 column. Temperature programming (estrogens): Injection, 220 C; isothermal, 7.5 min.; program @ 5 C/min. to 245 C; isothermal. Analyzed on OV-1 column.

The steroid derivatives were completely separable under the chromatographic conditions described. Mass spectra were obtained by rapid scan (10-25 sec.) of the peaks detected by the total ion current monitor.

The GC/MS interface is composed of an all-glass system. Figure 1 shows a schematic drawing of the interface design. The coiled glass GC column delivers the total column effluent through a heated, foil-insulated glass transfer line directly into the ion source of the Time-of-Flight mass spectrometer. The ion source differential pumping system is the 500 liter/sec. pump (shaded arrow). The 30 liter/sec. analyzer region pump is shown to the bottom right. The ion detector and analytical systems are shown on the right.

RESULTS AND DISCUSSION

Figures 2 - 6 show the bar graphs of relative peak abundance for the series of steroids analyzed by the interface described here. The graphs were calculated from the fast scan recordings obtained from a Honeywell Model 1508 Visicorder (Honeywell Inst., Denver, Colorado), using perfluoro kerosene as the standard.

Figure 2 represents the bar graph obtained from the mass spectrum of the silyl derivative of etiocholanolone. A prominent peak at 434 (the highest m/e observed) corresponds to the disilyl derivative of the parent steroid, corresponding to silyl derivative formation at the 3-α-ol and 17-enol sites. The mono-silyl derivative, which can arise not only as a discreet derivatization product but also as an ion fragment of the larger parent, appears at m/e 362. The "free steroid" peak at m/e 290 is not observed. A major peak at m/e 272 represents the loss of the silyloxy group ($-OSi(CH_3)_3$) from the monosilylated derivative.

Figure 3 shows the bar graph for the silyl derivative of dehydroepiandrosterone, which displays an upper limiting peak at m/e 432, characteristic of the singly-charged disilyl derivative, as well as m/e 360, corresponding to the monosilyl derivative. The "free steroid" peak at m/e 288 is not observed. The major peak at m/e 270 corresponds to the loss of the silyoxy group from the parent-monosilyl derivative.

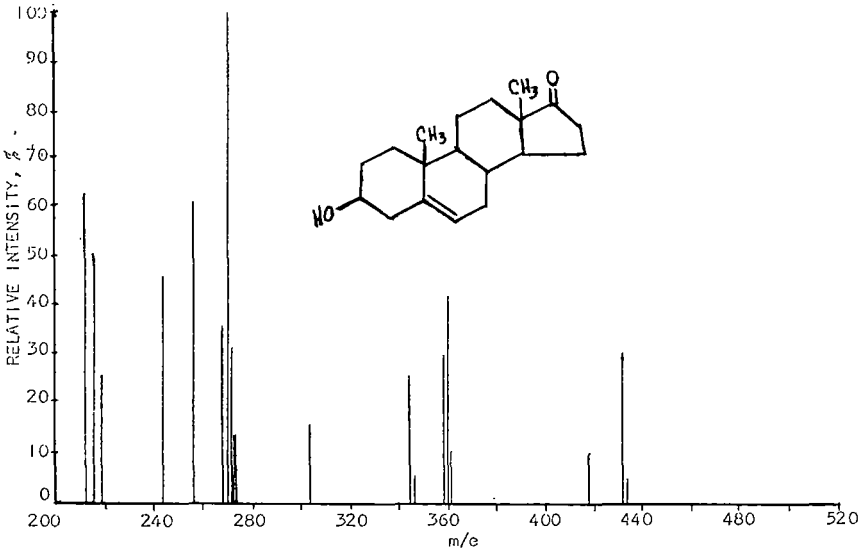

Figure 3. Mass Spectrum of Dehydroepiandrosterone as the TMS Derivative

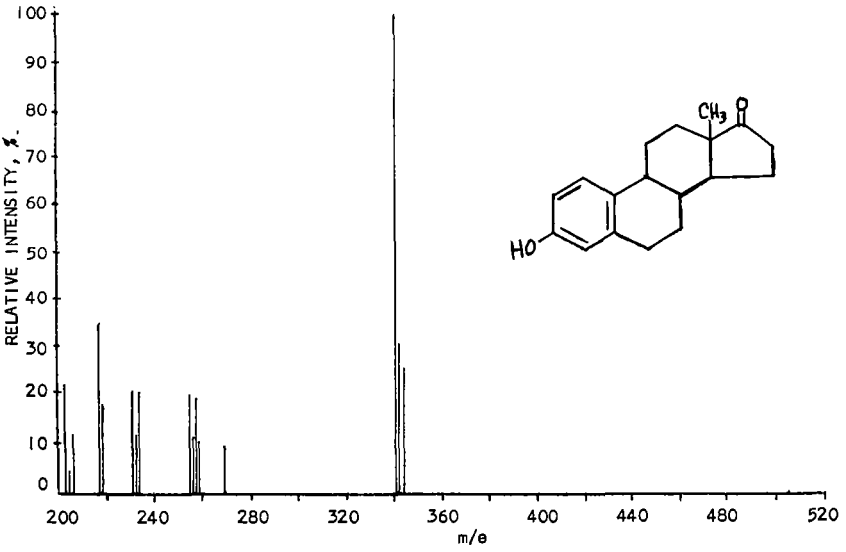

Figure 4. Mass Spectrum of Estrone - TMS

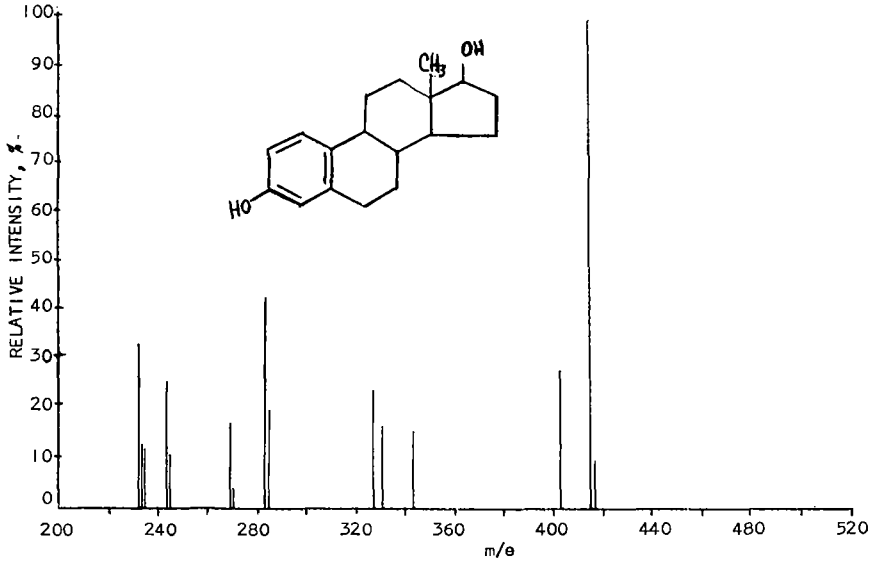

Figure 5. Mass Spectrum of Estradiol - TMS

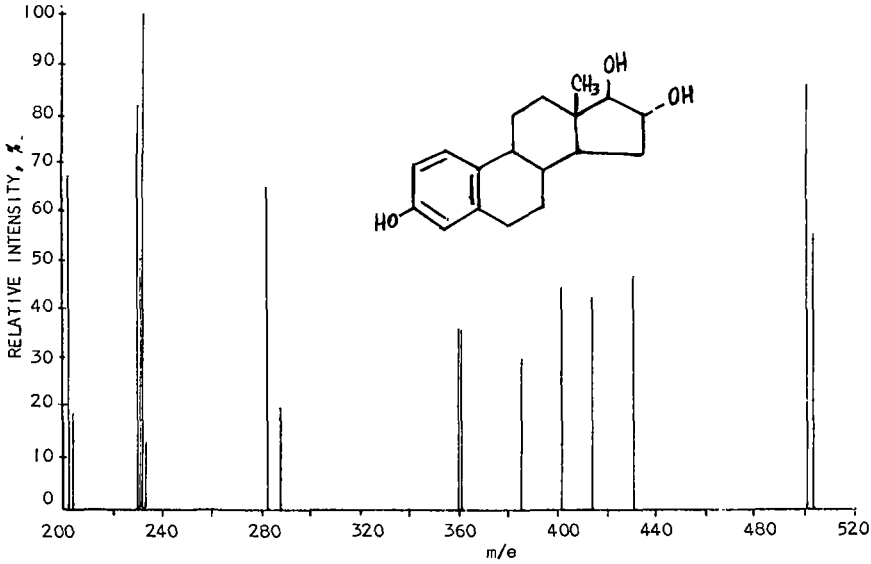

Figure 6. Mass Spectrum of Estriol - TMS

A comparison of the spectra of these closely related molecules reveals several distinct peaks that differ systematically by 2 m/e units. The data are consonant with the theoretical calculations between molecules differing only by one ethylenic linkage.

Figures 4, 5, and 6 display the mass spectra bar graphs obtained from chromatographic separation and analysis of a mixture of 2 micrograms each of the silyl derivatives of the female sex hormones - estrone, estradiol, and estriol.

Figure 4 is the graph for estrone. The m/e observed at 342 corresponds to the monosilyl ether of estrone. No m/e 414 is observed, indicating that the 17-enol-TMS derivative is not formed under these conditions. The "free steroid" peak is present at m/e 270 and there is a prominent m/e 256, corresponding to the loss of a methylene, $-CH_2-$, from the (M-1) ion, or possibly the 13-β-CH_3 group, from the free molecule.

Figure 5 shows the graph for the silyl derivative of estradiol. The highest m/e observed in 416, corresponding to the disilyl derivative (3, 17β-disilyl estradiol). The peak at m/e 344 corresponds to the monosilyl ether derivative, and the free steroid appears at m/e 272.

Figure 6 is the bar graph representation for the silyl derivative of estriol. The highest mass peak occurs at m/e 502, corresponding to the trisilyl derivative, wherein all three hydroxyl groups of the parent steroid are converted to the silyl ethers: 3,16α,17β-trisilyl estriol. The peak at m/e 432 corresponds to either of the three possible disilyl derivatives, quite probably the 3,17β-disilyl estriol molecular ion. A prominent m/e 402 may correspond to the ion resulting from the loss of the 13-β-CH_3 and one of the hydroxyl groups from the parent.

The analysis of these steroid hormones indicates that the high molecular weight silyl derivatives survive the chromatographic conditions from the injection port thru the column and transfer line to the MS ion source. The multi-silyl derivatives can be analyzed intact, as indicated by high m/e peaks identical to the theoretical calculations in each case.

This interface has the further advantage of simplicity; it does not require extra pressure taps or fittings other than those associated with glass GC columns. The overall sensitivity of the system approaches the submicrogram range - full-scale ion current deflection was obtained with 2 micrograms of the silyl derivative of estradiol. The analytical range under the present conditions, extended to 0.6 micrograms, for half-scale deflection of the chemical standard, androstane ($C_{19}H_{32}$). The speed of analysis, including the chromatographic separation and recording of the mass spectra, is just that required for GC analysis alone.

References:

1) W. J. A. Van den Heuvel, C. C. Sweeley, & E. C. Horning, J. Am. Chem. Soc., 82, 3482 (1960)

2) J. C. Holmes and F. A. Morrell, Appl. Spectroscopy 11, 86 (1957)

3) R. S. Gohlke, Anal. Chem. 31, 535 (1959)

4) R. Ryhage, Anal. Chem. 36, 759 (1964)

5) J. T. Watson and K. Biemann, Anal. Chem. 36, 1135 (1964)

6) A. B. Littlewood, Chromatographia 1, 37 (1968)

7) G. Spiteller, In: "Shering Symposium - Berlin 1968" (Ed., G. Raspe), Pergammon Press, 1969, p. 41

8) D. I. Rees, Talanta 16, 903 (1969)

9) E. M. Chambaz, G. Maume, B. Maume, and E. C. Horning, Analyt. Letters 1, 749 (1968)

NEW TECHNIQUES IN GAS CHROMATOGRAPHY - MASS SPECTROMETRY

J.R. Chapman, T.O. Merren and H.J. Limming
AEI Scientific Apparatus Limited
Manchester, England.

The MS30 double beam mass spectrometer was described by Barber et al (1) and some preliminary data were presented to show the feasibility of double beam mass measurement. With this technique, sample and reference are separated, one to each beam, so enabling mass measurement to be carried out at low resolution. In this way, data can be obtained from smaller samples than previously. This paper will describe some applications of the double beam technique to the analysis of small samples introduced via a chromatograph and show how the simultaneous collection of accurate mass and metastable data is particularly useful in structural analysis.

To obtain atomic composition data by conventional single beam methods of mass measurement, a mixture of sample and reference is admitted to the mass spectrometer source and high resolution is needed to separate the sample and reference peaks at the same nominal mass. An example of some MS30 data obtained in this way from one of the components of a mixture of four esters admitted via the chromatograph is shown in Figure 1 and the corresponding total ion current monitor record is shown in Figure 2. The spectrometer resolution was set at 10,000, the mass spectrum was scanned at 10 seconds per decade and the data was acquired and processed by the DS30 Data System. Actually 2 micrograms of the component, methyl stearate, was injected into the column. These results are typical of operation at high resolution, when of the order of a hundred nanograms of sample need to be admitted to the source during the scan to obtain accurate mass data. If the sample quantity injected on the column is reduced much below the microgram level, the smaller number of ions in all but the strongest peaks, prevents their being defined confidently and therefore mass measured.

At a lower resolution, however, say 1000, spectra can be obtained from sample quantities of the order of a few nanograms injected onto the chromatograph. Provided that the sample and reference can be kept separate, mass measurements of unknown components can be made at this very small sample level. With the double beam instrument, they are kept separate very simply by admitting them to two quite separate sources.

Table 1 shows some of the results obtained by the injection of 100 nanograms each of methyl stearate and methyl palmitate onto the GC column. The quantity of sample consumedin the source during the scan time was about 20 nanograms. The double beam mass measurement principle was employed at a scan speed of 10 secs per decade in mass and a resolution of 1000.

	Measured Mass	Calculated Mass	Composition
C16 Ester	270.260	270.256	$C_{17}H_{34}O_2$
	227.203	227.201	$C_{14}H_{27}O_2$
	143.105	143.107	$C_8H_{15}O_2$
C18 Ester	298.285	298.287	$C_{19}H_{38}O_2$
	255.228	255.232	$C_{16}H_{31}O_2$
	143.105	143.107	$C_8H_{15}O_2$

TABLE 1

MS30 Double Beam Mass Measurements on 0.1 Microgram Methyl Esters

CALCULATED MASS	DEV	C12/13	H	O	N	MEASURED MASS	NO. PTS	REL INT
REFERENCE						354.9793	4	.4
REFERENCE						342.9793	6	1.7
REFERENCE						330.9794	6	2.2
REFERENCE						318.9793	6	1.1
REFERENCE						304.9825	5	.6
299.2949	-3.2	19/0	39	2	0	299.2917	8	2.2
299.2904	1.3	18/1	38	2	0			
298.2870	.5	19/0	38	2	0	298.2876	9	10.8
REFERENCE						292.9825	6	1.6
REFERENCE						280.9825	6	3.3
270.2513	.9	16/1	33	2	0	270.2521	3	.2
269.2480	2.7	17/0	33	2	0	269.2507	5	1.1
REFERENCE						268.9825	5	2.3
268.2765	-2.4	18/0	36	1	0	268.2741	4	.2
268.2721	2.1	17/1	35	1	0			
267.2687	.9	18/0	35	1	0	267.2696	5	3.1
256.2357	1.0	15/1	31	2	0	256.2366	5	1.1
255.2323	-1.9	16/0	31	2	0	255.2304	7	5.8
255.2278	2.6	15/1	30	2	0			
REFERENCE						254.9855	4	.7

FIGURE 1

MS30: 2μgm methyl stearate on column.
10 secs/decade at 10,000 resolution.

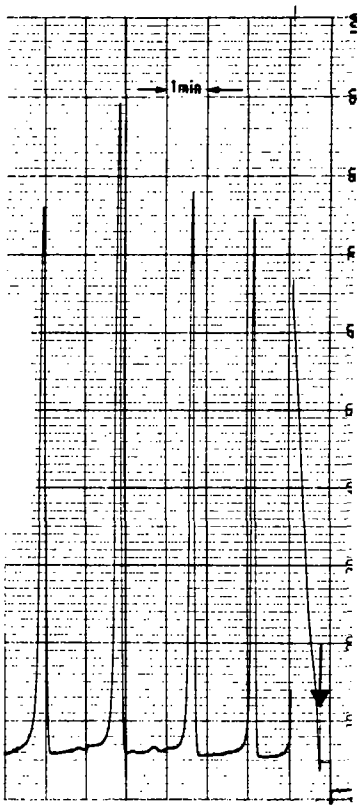

FIGURE 2

MS30:

1 μg each n-C12, 14, 16, 18 esters:

2% OV 1 column

170°→250° at 12° /min

The rms error on the measurements on these peaks, which are all approximately 10% of the base peak intensity, is 14 ppm. The same peaks could have been mass measured even if 10 nanograms or less had been loaded onto the column, although the accuracy then obtainable, would be approximately 30 ppm (accuracy decreases with sample size). With that loading the same peaks would not have been detected at all at a resolution of 10,000.

The double beam method offers many other advantages in addition to being able to carry out accurate mass measurements on small sample quantities, for example, the simultaneous acquisition of metastable and accurate mass data. As is well known, metastable peaks, which are widely used in structural elucidation, are usually less than one percent of the base peak intensity. By conventional single beam methods, separate experiments to obtain high and low resolution spectra are needed and several micrograms of sample are required. However, when collecting mass measurement data by the double beam method, the ultra violet recorder can be run simultaneously so that the trace provides the usual metastable information. A smaller amount of sample is required depending on the level of the metstables being investigated. For metastables at the 0.3% level, about 100 nanograms of sample is required instead of several micrograms.

The following example illustrates the advantage of simultaneously obtaining mass measurement and metastable data by the double beam method in structural elucidation. A mixture of fatty acids, extracted from the remains of a fossilised plesiosaurus, was being analysed after methylation of the carboxyl group. The total ion current monitor record is shown in Figure 3. Comparison of the spectrum obtained on component 2 with standard spectra had failed to establish any match. Although the spectrum contained no obvious parent ion which could be mass measured, the double beam method did provide useful accurate mass data on fragment ions which were seen from the ultra violet chart to be linked by metastables. From the mass measurement data (Table 2) and the metastable data (Table 3) it can be deduced that the fragment at mass 201 which undergoes two successive losses of methanol, contains both a methyl ester and a methyl ether group, as both these groups are known to lose methanol in the mass spectrometer. Similarly, it can be established that the fragment at mass 157 contains just a methyl ether group. The mass measurement data provides supporting evidence for this interpretation by establishing the exact composition of four of the fragments involved. It can be concluded from this data that component 2 is 9, 10 - dimethoxy methyl stearate (I) which would cleave on electron impact across the 9, 10 disubstituted bond according to well documented reactions to give the fragment ions mentioned above.

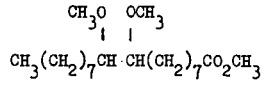

(I)

REFERENCE

(1) M. Barber, J.R. Chapman, B.N. Green, T.O. Merren and A. Riddoch 18th Annual Symposium on Mass Spectrometry, San Francisco, 1970.

Measured Mass	Calculated Mass	Composition
201.148	201.149	$C_{11}H_{21}O_3$
169.124	169.123	$C_{10}H_{17}O_2$
137.096	137.097	$C_9H_{13}O$
157.160	157.159	$C_{10}H_{21}O$

TABLE 2

Mass Measurements Using Double Beam Method on Ester 2 from Fossil Extract

Metastable Mass	Transition
142.1	201 → 169
111.1	169 → 137
99.5	157 → 125

TABLE 3

Metastable Data in Spectrum of Ester 2 from Fossil Extract

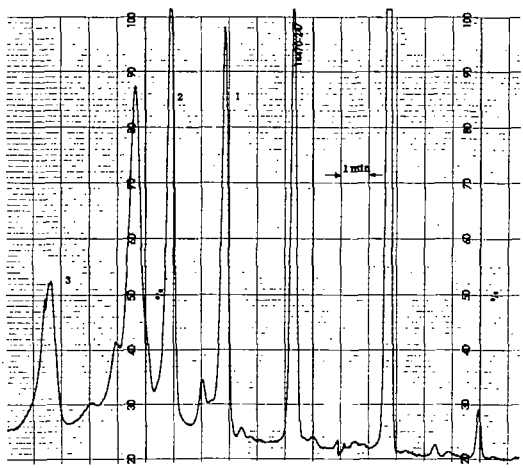

FIGURE 3

MS30 : Fossil extract:

2% OV 1 column 150° → 250° at 4° min $^{-1}$

Combined Molecular Beam - Mass Spectrometer for Analyzing Transient Intermediates in Gaseous Reactions[1]. Myron Kaufman and Charles Kolb, Frick Chemical Laboratories, Princeton University, Princeton, N.J. 08540.

The neutral parent of each ion observed in a mass spectrometer can be identified by measuring its properties in a molecular beam prior to ionization. This novel technique, which we term "molecular beam analysis", is particularly useful for detecting small concentrations of free radical intermediates in gaseous reactions. Although intermediates have been detected by use of ordinary mass spectrometry, the free radical signals are generally obscured by much larger ion currents resulting from dissociative ionization of stable molecules. These interferences have in the past been avoided by careful control of the energy of the ionizing electrons, but only by sacrificing much of the inherent sensitivity of mass spectrometry. In addition, it is difficult to completely eliminate fragmentation when it can result from breaking a very weak bond or a vibrationally excited bond, or when the transient of interest has a high ionization potential.

In molecular beam analysis, the magnetic and electric dipole moments and the velocity distributions of the neutrals are determined. The rough measurement of magnetic dipole moment that can be obtained from deflection by an inhomogeneous (hexapole) magnetic field is sufficient to indicate whether the parent of an ion has a large moment characteristic of a free radical or atom. Transients identified in this manner are: SO, BrO, IO, OH, CH_3, CF_3 and $^3CH_2$, as well as many atoms. Such paramagnetic species have been detected at partial pressures as low as 0.01 micron, in the presence of large interferences at their parent ion. Similarly, deflection in an inhomogeneous electric (quadrupole) field demonstrates whether the parent is polar. The magnitude of this deflection is strongly dependent upon the symmetry of the molecule, which results in either a 1st or a 2nd order Stark effect.

Velocity distributions are particularly informative since, for a molecular beam effusively sampled from a source with a definite translational temperature, they provide a value for the mass of the parent of each ion. These distributions are determined by a time-of-flight method, whereby the beam is pulsed and the spreading of this pulse during free flight to the ionizer is measured. For very weak signals, time-of-flight distributions are extracted, by correlation techniques, from the signal produced by a psuedo-randomly modulated beam.[2] With either method, major distortion of the time-of-flight curve can result if the ions are delayed in the ionizer due to their attraction to the intense electron beam. We have avoided this ion trapping by adding gaseous helium to the ionization chamber, thereby forming helium ions which largely neutralize the electron space charge. Good agreement with time-of-flight distributions calculated from the beam-modified Maxwellian distribution are currently achieved.

We have been utilizing molecular beam analysis to investigate the rates and mechanisms of some of the reactions of atomic fluorine with halogenated methanes. In these experiments, fluorine atoms are generated in a flow reactor by microwave discharge through F_2 or CF_4. Discharged CF_4 produces F (and C_2F_6) in the presence of very little F_2. This is important since F_2 is a very efficient free radical scavenger, and will thus reduce the concentration of such intermediates below our level of detectability. Absolute measurements of the concentrations of F and F_2 are obtained by calibrating the molecular beam analyzer by a gas phase titration with H_2. In the reaction of F with CCl_4 at 298°K, no CCl_3F is

formed in the absence of F_2. This rules out this reaction proceeding by a displacement mechanism at this temperature. Studies of F_2-halogenated methane flames had suggested that this mechanism predominated at flame temperatures.[3] Atomic chlorine is produced in the reaction mixture, most likely as the product of reactions such as,

$$F + CCl_3 \rightarrow CFCl_2 + Cl,$$

which are expected to be very rapid. Our preliminary value for the rate constant of

$$F + CCl_4 \rightarrow CCl_3 + FCl$$

is 2×10^8 cm^3/mole-sec, which is almost 5 orders of magnitude lower than the accepted literature value for this reaction.[4]

1. To be published in Chemical Instrumentation - Volume 2.

2. V. L. Hirschy and J. P. Aldridge, Rev. Sci. Instr. 42, 381 (1971).

3. K. H. Homann and D. I. MacLean, Comb. and Flame 14, 409 (1970).

4. Table of Bimolecular Gas Reactions, NSRDS-NBS9, p. 15 (1967).

Research support from the Office of Naval Research is gratefully acknowledged.

A Combined Gas Chromatograph-Vapor Phase Pyrolysis-Mass Spectrometric Analysis System

C. Merritt, Jr., C. DiPietro and M. L. Bazinet
Pioneering Research Laboratory
U. S. Army Natick Laboratories
Natick, Massachusetts 01760

Although combined gas chromatography/mass spectrometry has become a time honored technique, it is not entirely foolproof, particularly when it is applied to problems involving the identification of unknown components of very complex mixtures.

Nearly a decade ago attempts were made to utilize gas chromatographic patterns resulting from thermolytic dissociation as a substitute for mass spectra as a means of identification. It was soon realized, however, that g.c. retention indices are not sufficiently reliable for qualitative analysis, and many workers returned to the use of the mass spectrometer to aid in the identification of the pyrolysis products. Nevertheless, an analysis of the products of the non-catalytic thermal dissociation of organic molecules provides a great deal of information about their structure.

This paper describes the use of a combined gc - vpp - ms analysis system which has been devised to utilize the information content of both the thermolytic cracking patterns and the mass spectra of various organic compounds to accomplish their identification.

A schematic diagram of the apparatus is shown in Figure 1. A first gas chromatograph is used to separate the components of the sample. This is designated as GC-1. A dual detector system is used to produce a thermal conductivity output or a flame ionization output as the sample may require. The chromatogram obtained from GC-1 provides for quantitative analysis. The vapor phase pyrolysis unit is indicated by enclosure within the dashed line. The details of construction may be obtained in literature from Chemical Data Systems, Inc. When a component is eluted from GC-1, it is trapped in a delay coil and transferred to the thermolytic reactor where it is dissociated under carefully controlled conditions of temperature and carrier gas flow. The resulting products are swept out of the reactor to a second gas chromatograph. Actually, two gas chromatographs are available to analyze the pyrolysis products. A short column, called the small molecule column, is used to measure the amounts of CH_4, C_2H_6, C_2H_4, CO, CO_2, H_2O, NH_3 or H_2S, that may be produced in the reaction. This column is a part of the pyrolyzer unit and may be very useful in establishing the functional group type of the parent compound. Alternatively, the pyrolysis products may be transferred to a second gas chromatograph, called GC-2, which is a part of a complete, combined gc/ms analysis system. The combined gc/ms system may be used to separate and identify all of the pyrolysis products of the parent compound. The total analysis system is designed to be as flexible as possible, with appropriate vents and bypasses, and separate inlets so that all or any of the component systems may be used independently.

Although it would be desirable for the mass spectrum of every organic compound to be unique, and different from every other compound, this situation is unfortunately not always the case. An example is seen in Figure 2 which shows the spectra of two phenolic ingredients from the spice, oregano. They are positional isomers and their mass spectra are essentially identical. Evaluation of the quality of oregano depends on determination of the relative amounts of these two components. The compounds may be distinguished by vapor phase pyrolysis as seen in Figure 3.

Different functional group type compounds can frequently have spectra which are sufficiently similar to cause trouble. The parent ion of long chain alkanols is characteristically very weak or absent from the spectrum and a series of ions corresponding to the decomposition of a parent minus 18 ion, makes the alkanol spectrum resemble the corresponding alkene spectrum very closely. Although the 31 peak may be considered diagnostic for an alcohol, when the amount of component, or the sensitivity is low, or when the 8 or 10 most abundant peaks are being used for identification, alcohol and olefin spectra may be frequently confused.

Such compounds may be distinguished by pyrolysis patterns. Nonanal and nonene

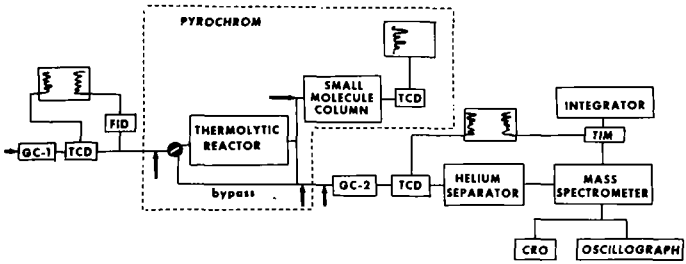

Figure 1

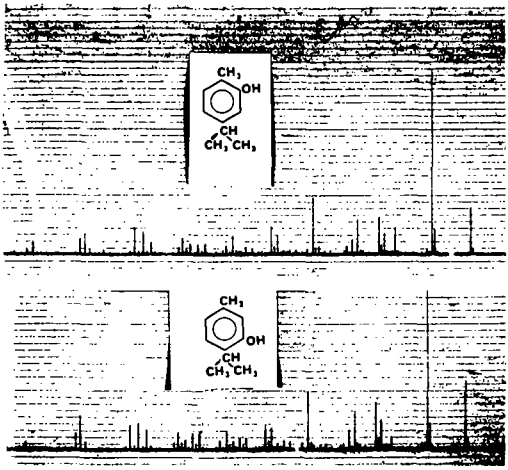

Figure 2

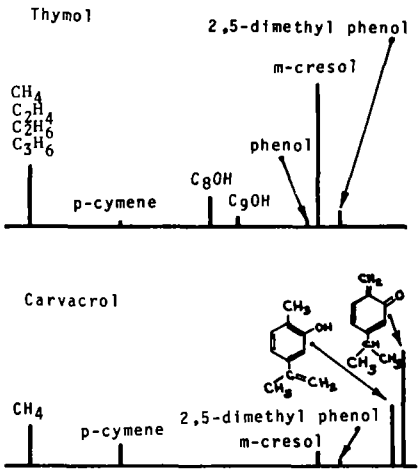

Figure 3

have been studied as examples. The pyrolysis of nonene produces a series of olefins from C_2 - C_9 corresponding to the successive cleavage of all the carbon bonds, and including the parent compound. Nonanol gives gc peaks and spectra for the same series, but, in addition, gc peaks for nonanal as well as the parent compound are observed. The pyrogram for nonanol would have two apparent nonene peaks in it, but the one at longer retention would correspond to the alcohol. The clearly distinguishable nonanal spectrum would in any event be diagnostic.

Trimethylsilyl derivatives are now being increasingly utilized to permit mass spectrometric analysis of non-volatile or slightly volatile compounds. Although the volatility of the compounds is enhanced, the spectra obtained of the derivative compound sometimes present problems in identification. The spectra of the trimethylsilyl amino acids are a typical example.

The typical fragmentation behavior of the TMS amino acids may be summarized as follows:

$$\text{R-CH(NH(TMS))-COOTMS} \xrightarrow{e} \text{TMS}^+ \text{ m/e 73} \quad + \quad \text{M-R}^+ \text{ m/e 218} \quad + \quad \begin{matrix}\text{M-15}\\ \text{M-43}\\ \text{M-117}\end{matrix}$$

The most abundant peaks are those containing the TMS moiety. We see the peaks at mass 73 due to TMS ion and at 218 due to the molecular skeleton less the R group. The peaks are common to all the TMS amino acid spectra. The other predominant ions are formed from loss of methyl or 3 methyls from the TMS group or from loss of 117 due to the carboxy trimethylsilyl group. Although these three peaks are the most useful in the interpretation of the spectrum of a TMS amino acid, the task is frequently very difficult or impossible with mixtures of unknowns, since the molecular ion is usually absent or very weak in the spectrum. Likewise, the ions which do not carry the TMS moiety have very low abundance. The result is that TMS amino acid spectra, particularly of the ones where the R group is alkyl such as alanine, valine and leucine are seemingly identical. We recently had occasion to try to identify some unknown free amino acids isolated from mushrooms and were unable to do so by using the TMS derivative spectra since they all provided only the TMS containing ions.

Vapor phase pyrolysis can clarify this situation. The pyrolysis behavior of TMS amino acids is summarized below:

$$\text{R-CH(NH(TMS))-COOTMS} \xrightarrow{\Delta} \text{RH} \quad + \quad \text{TMS fragments}$$

The essential feature of the thermolytic dissociation of these compounds is that a series of compounds is obtained which is characteristic of the R group. This series is designated here as RH. We also obtained some compounds containing the TMS group, but these have less diagnostic value than the RH series. A few examples of the characterization of some TMS amino acids by their pyrolysis patterns is shown in Table I.

Table I

Components Found in Pyrograms of Certain Amino Acids

A.A.	R	Compounds
glycine	H-	
alanine	CH_3-	CH_4
valine	$(CH_3)_2CH$-	CH_4, C_2H_4, C_3H_6
leucine	$(CH_3)_2$ -CH $-CH_2$	CH_4, C_2H_4, C_3H_6, C_4H_8
iso-leucine	CH_3 CH_2 (CH CH_3) -	CH_4, C_2H_4, C_3H_6, C_4H_8
Ø alanine	$ØCH_2$-	ØH, $ØCH_3$

The complete manuscript will be submitted to the J. of Chromatographic Science.

N7

AN AUTOMATED QUADRUPOLE MASS SPECTROMETER FOR HIGH TEMPERATURE EFFUSION STUDIES

by

Margaret Frisch

IBM Thomas J. Watson Research Center, Yorktown Heights, New York 10598

Abstract

The electronic circuitry of a Finnigan mass spectrometer has been modified for control by an IBM 1800 computer. The automated operation provides new possibilities for exploration, e.g. obtaining time resolved spectra of freshly heated materials for determining the volatility, composition and energetics of surface contaminants.

Ion detection is now performed in a novel approach by counting of the electron multiplier output pulses at rates up to 10 MHz using a bidirecitonal scaler. The scaler is reversed synchronously with the modulation of the molecular beam, resulting in a digital lock-in detector. With this technique data can be obtained at rates up to five times faster than analog phase sensitive methods because of the absence of a time constant.

The interface between the computer and the mass spectrometer contains four 13 bit registers which are addressed by an additional 3 bits. These registers are used for storing the control data required for the automatic operation of the spectrometer.

Register 1 a) Mass range (low, medium or high) is selected via RF relays (2 bits).
b) The counter is remotely programmed for either normal or bidirectional scaling (1 bit).
c) Ion energy (proposed) will be varied from 0 to 10 volts by a 10 bit D/A.

Register 2 The timing interval for gating of the scaler is transmitted in units of the modulation cycles (8191 maximum). The scaler is gated on for an integral number of reference cycles in phase with the leading edge.

Register 3 The mass position is selected at rates up to 100 per second via a 13 bit 0 to 8.191 volt D/A with a precision of 0.01, 0.03 and 0.09 AMU on the low, medium and high mass ranges, respectively.

Register 4 The electron energy is controllable between 0 and 100 volts. The output of a 0 to 10 volt 13 bit D/A is fed to an operational amplifier with a gain of 10.

The relationship between the mass spectrometer, interface, computer and other essential electronics is presented in the accompanying figure.

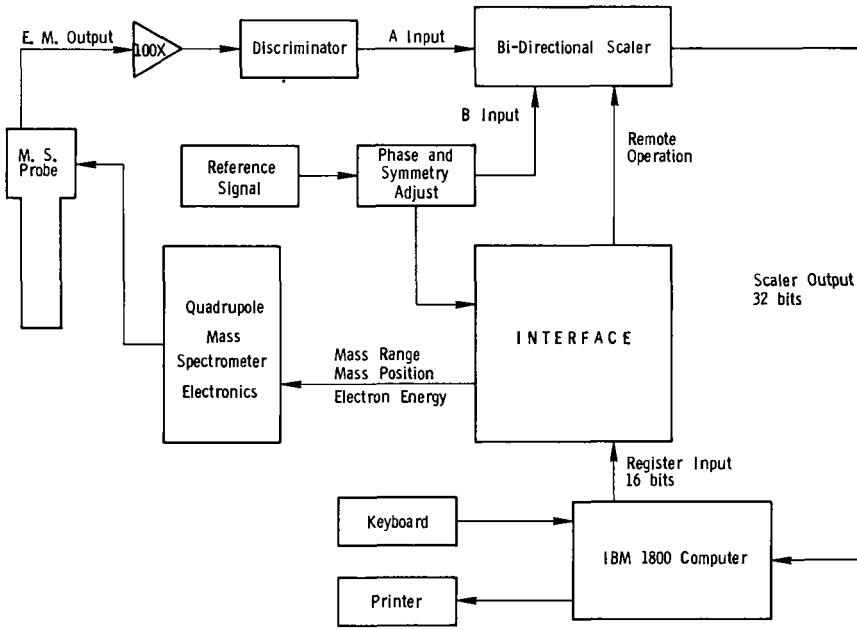
E. M. Output
100X
Discriminator
A Input
Bi-Directional Scaler
B Input
Remote
Operation
M. S.
Probe
Reference
Signal
Phase and
Symmetry
Adjust
Quadrupole
Mass
Spectrometer
Electronics
INTERFACE
Scaler Output
32 bits
Mass Range
Mass Position
Electron Energy
Register Input
16 bits
Keyboard
IBM 1800 Computer
Printer

N8

COMPUTER DETERMINATIONS OF QUADRUPOLE MASS SPECTROMETER PERFORMANCE CHARACTERISTICS IN CYLINDRICAL COORDINATES*

M. Mosharrafa**
Old Dominion University
Norfolk, Virginia 23521

G.M. Wood, Jr.
NASA Langley Research Center
Hampton, Virginia 23365

A B S T R A C T

A generalized computer model of the quadrupole-type mass spectrometer has been developed using the Control Data 6600 system at NASA Langley Research Center. The model is a versatile FORTRAN program capable of generating ion beams of specified cross-sectional density and energy distributions, producing mass scans of the quadrupole field based upon a desired resolution, computing the ion trajectories in cylindrical coordinates, and determining the percent transmission of the specified ion beam. The program is the initial phase of the compilation of a library containing functional realizable models of various types of mass spectrometers. Such models are invaluable for the optimization of the design of a mass spectrometer system for a specialized application, and in understanding the observed peculiarities in mass spectrometer performance.

The program was tested for accuracy by operating the model quadrupole mass spectrometer at various exact focusing conditions[1] and plotting the ion parameters R, $\emptyset$, radial velocity, and angular velocity versus the number of rf cycles experienced by the ion in traversing the quadrupole analyzing field. Maximum truncation errors were limited to .001%.

Studies of the effects of cross-sectional density and energy distributions of the ion beam entering the quadrupole analyzing field were performed. Results showed that non-uniform density distributions contribute to the deterioration of peak shapes and the appearance of the pre and post cursors observed experimentally in some quadrupole mass spectrometers. Those results emphasize the need for a new type of ion source which should be designed for optimum coupling with quadrupole analyzing fields in order to obtain maximum sensitivity and peak shape quality.

A study was undertaken to determine the exit conditions of a mass-filtered ion beam with uniform cross-sectional density distribution and constant axial injection energy at various operating points along the scan line within the stability triangle. Preliminary results indicate that the quadrupole analyzing field affects the ion beam in two ways simultaneously during the scan:

a) It images the ion beam at the exit with successive magnifications and demagnifications as a function of the operating point during the scan.

b) The ion beam is progressively rotated clockwise during passage through the field; the total angle of rotation upon exit is dependent upon the operating point during the scan.

1. R.F. Lever, IBM Journal 26, 1966

* A more detailed account of this work will be submitted for publication in the Journal of Mass Spectrometry & Ion Physics.

** Present address: Automated Medical Systems, Inc.
Minneapolis, Minnesota 55420

A Low Energy Study of Symmetric and Asymmetric Charge-Transfer †

David L. Smith and Jean H. Futrell, Department of Chemistry,
University of Utah, Salt Lake City, Utah 84112.

At high kinetic energies, electron transfer usually occurs over large impact parameters and results in little or no momentum transfer. The general charge-transfer reaction

$$A^+ + B \rightarrow B^+ + A \qquad (1)$$

is classified as symmetric if A and B are identical asymmetric if A and B are not identical. The difference in ionization potentials of A and B is the energy defect of the reaction and is equal to zero for symmetric reactions. Theoretical analysis[1,2] indicates that the mechanism through which charge-transfer takes place is different for the two types of reactions.

It is the objective of this study to assess the significance in the case where A and B are not identical but the energy defect is nearly zero. An ion cyclotron resonance (ICR) mass spectrometer is used to measure the rate constants for the four possible reactions in the Kr/CO system over the energy range from 0.1 eV to 10 eV. This system was chosen because there are no reactions which might compete with charge-transfer and because the recombination energies of CO^+ and $Kr^+ (^2P_{3/2})$ are equal to within 0.01 eV. The experimental rate constants are converted to cross-sections using

$$Q = \frac{k}{v} \qquad (2)$$

where v is the root mean square velocity which is obtained through a detailed analysis of ion motion in the ICR mass spectrometer. Since this study covers the energy range over which ion-induced dipole orbiting collisions become important, it is also of interest to assess the effect of such collisions on the charge-transfer process.

The thermal energy rate constants corresponding to an average ion energy of 0.1 eV measured in this work are given in Table I. The rate constant for the Kr^+/Kr system reported by Jones and Harrison[3] and the Langevin orbiting collision rate constants are also given for comparison. Their value of 15×10^{-10} $cm^3 mol^{-1} sec^{-1}$. This descrepancy probably results from a combination of factors. Because of resolution problems in studying Kr by ICR, it is felt that the present value may be in error by as much as 50 percent. The method used by Jones and Harrison is associated with a wide spread in ion residence time. Because of this, the authors feel that their results refer to reaction of ions with kinetic energies ranging from zero to approximately 1 eV.[4] The energy dependence of this rate constant has been measured in

the present work; the rate constant increases from 8.5×10^{-10} cm^3 mol^{-1} sec^{-1} at 0.1 eV to $17. \times 10^{-10}$ cm^3 mol^{-1} sec^{-1} at 1.0 eV. Thus the discrepancy between the present thermal energy result for this reaction and that of Jones and Harrison may be rationalized in terms of energy spread in the Jones and Harrison experiment. The uncertainty in the rate constants for the other reactions given in Table I is substantially less than for the Kr^+/Kr reaction and is probably within the range of $\pm$ 20 percent. There are no previously available data for comparison for the latter three reactions. The charge-transfer cross-sections obtained in this work may be compared with the Langevin orbiting collision cross-sections. If the probability for charge-transfer in the two symmetric reactions is taken to be 0.5 out to some impact parameter and zero beyond this distance,[5] an effective maximum impact parameter over which charge-transfer takes place can be established. For the Kr^+/Kr system this value is 11 Å and for the CO^+/CO system 8.4 Å for an ion kinetic energy of 0.1 eV. The critical impact paramater necessary for orbiting collisions are 6.1 and 6.0 respectively. The important point is that for an ion kinetic energy of 0.1 eV the maximum impact parameter over which charge-transfer takes place is still greater than the critical impact parameter for orbiting collisions. This treatment cannot be applied to the two asymmetric reactions since the probability of charge-transfer is unknown. The fact that the maximum impact parameter for symmetric charge transfer is substantially greater than the Langevin critical impact parameter does not imply the presence of both a long range and a short range charge-transfer mechanism. The probability of electron transfer as a function of impact parameter rapidly oscillates between zero and one corresponding to a rapid oscillation of the electron between the two nuclei. Thus charge-transfer results from an odd number of oscillations, while an even number of oscillations is observed as no reaction. For the reactions studied here it is presumed that the "final" transfer occurs at long distances whether or not orbiting collisions occur.

It is interesting to compare the cross-sections for the four reactions studied in this work with each other. The cross-section for the two asymmetric reactions are equal and are greater than that of either of the symmetric reactions. That the cross-sections for the two crossed-reactions are equal clearly implies that charge-transfer from the $^2P_{1/2}$ state of Kr^+ is an efficient process, despite the fact that this reaction is 0.7 eV exothermic.

† to be published in J. Chem. Phys.

1. D. R. Bates and N. Lynn, Proc. Ray. Soc. (London), A 253, 141 (1959).

2. E. W. McDaniel, V. Cermak, A. Dalgano, E. E. Ferguson, and L. Friedman, Ion-Molecule Reactions, New York Wiley-Interscience, Chpt. 3, (1970).

3. E. G. Jonesand A. G. Harrison, Int. J. Mass Spec Ion Phys. 5, 167 (1970).

4. E. G. Jones and A. G. Harrison, to be published in Int. J. Mass Spec. and Ion Phys. (1971)

5. D. Rapp and W. E. Francis, J. Chem. Phys. 37, 2631 (1962).

Funding

Aerospace Research Labs F33615-68-C-1022

Air Force Office of Scientific Research 71-1986 A

TABLE I

Reaction	$k \times 10^{-10}$ $cm^3\ mol^{-1}\ sec^{-1}$			$Q \times 10^{-16}$ cm^2			$\frac{k}{k_L}$	$\frac{Q}{Q_L}$
	Present Results	Other Results	Langevin	Present Results	Other Results	Langevin		
1. $Kr^+ + Kr \rightarrow Kr^+ + Kr$	8.3	15[a]	5.6	170	90[b]	114	1.5	1.5
2. $Kr^+ + CO \rightarrow CO^+ + Kr$	13.		7.0	270		143	1.9	1.9
3. $CO^+ + CO \rightarrow CO^+ + CO$	8.5		8.4	105		112	1.0	.9
4. $CO^+ + Kr \rightarrow Kr^+ + CO$	22.		7.9	270		105	2.8	2.5

a. ref 3

b. B. Ziegler, Z. Physik 136, 108 (1953).

Charge Transfer Spectra of C_4H_8 Isomers*

T.O. Tiernan and L.P. Hills
Aerospace Research Laboratories
Wright-Patterson AFB, Ohio 45433

Previous studies in our laboratory were concerned with the structure and reactions of $C_4H_8^+$ ions formed by electron impact on cyclobutane[1]. This work demonstrated quite clearly that some structural isomerization of the cyclobutane parent ions takes place. An interesting feature of the C_4H_8 isomers is that their 70eV mass spectra show pronounced differences, as is evident from the data given in Table I. There are two conceivable explanations for the observed differences;

TABLE I

Major Peaks in the 70eV Mass Spectra of C_4H_8 Isomers

m/e	1-C_4H_8	cis-2-C_4H_8	Trans-2-C_4H_8	iso-C_4H_8	C-C_4H_8	Methyl cyclo-propane
56	39	51	50	67	62	61
55	18	23	23	24	19	--
41	100	100	100	100	89	100
39	35	38	37	40	20	57
29	13	15	19	11	11	--
28	29	23	31	19	100	38
27	31	20	34	16	42	--

a) these may reflect the fact that the molecular ion of each C_4H_8 isomer, from which fragmentation occurs, has its own unique structure; or b) the same parent ion structure or structures may be accessible to all the C_4H_8 isomers prior to fragmentation, and the differences in the spectra would then result from differences in the heats of formation of the various molecular ions in their ground states. Correlations between the energetics of fragmentation processes and their abundance have been widely employed to explain ionic dissociation processes.

Recently, Meisels and coworkers[2] reported measurements of the appearance potentials of ions formed by electron impact on the C_4H_8 isomers and concluded that there are indeed differences in the heats of formation of the $C_4H_8^+$ molecular ions from the various isomers. It was therefore suggested that the isomers essentially lose their identity prior to fragmentation and that the differences in their mass spectra therefore result from a shift in the internal energy distribution which is caused by this inequality of the heats of formation of the parent ions.

The competition between isomerization and dissociation will depend ultimately on the relative magnitudes of the activation energies for the two processes, but no direct information on the barrier for isomerization is available. It is of interest therefore to compare fragmentation of the C_4H_8 isomers with varying internal energy over a wide energy range. This can be accomplished by determining the ion spectra of these isomers produced by charge transfer reactions. In the present study, the charge transfer spectra were determined using an in-line tandem mass spectrometer which has been described earlier[3,4]. All reactions were studied using incident ions of 0.3eV kinetic energy so that the energy transferred in the collision is solely a function of the recombination energy of the reactant ion. Modifications were made to the tandem instrument to permit detection of metastables, that is, delayed decompositions, following charge transfer. These changes involved decoupling of the second stage electric sector and accelerating voltages, and insertion of more precise controls for the accelerating potential, as described in more detail elsewhere[5].

The lower section of Figure 1 shows that the onset of fragmentation of the $C_4H_8^+$ parent ion occurs at the same transferred energy for all the isomers. Following onset, the rates of fragmentation for all isomers increase rapidly, the relative rates being consistent with the order of the heats of formation of $C_4H_8^+$ ions; that is, c-$C_4H_8^+$ has the highest ΔH_f, (250 kcal/mole), while

Figure 1. (lower) Relative intensities of 56^+ ion from C_4H_8 isomers. (upper) Intensities of metastable from decomposition $C_4H_8^+ \rightarrow C_3H_5^+$ for various C_4H_8 isomers.

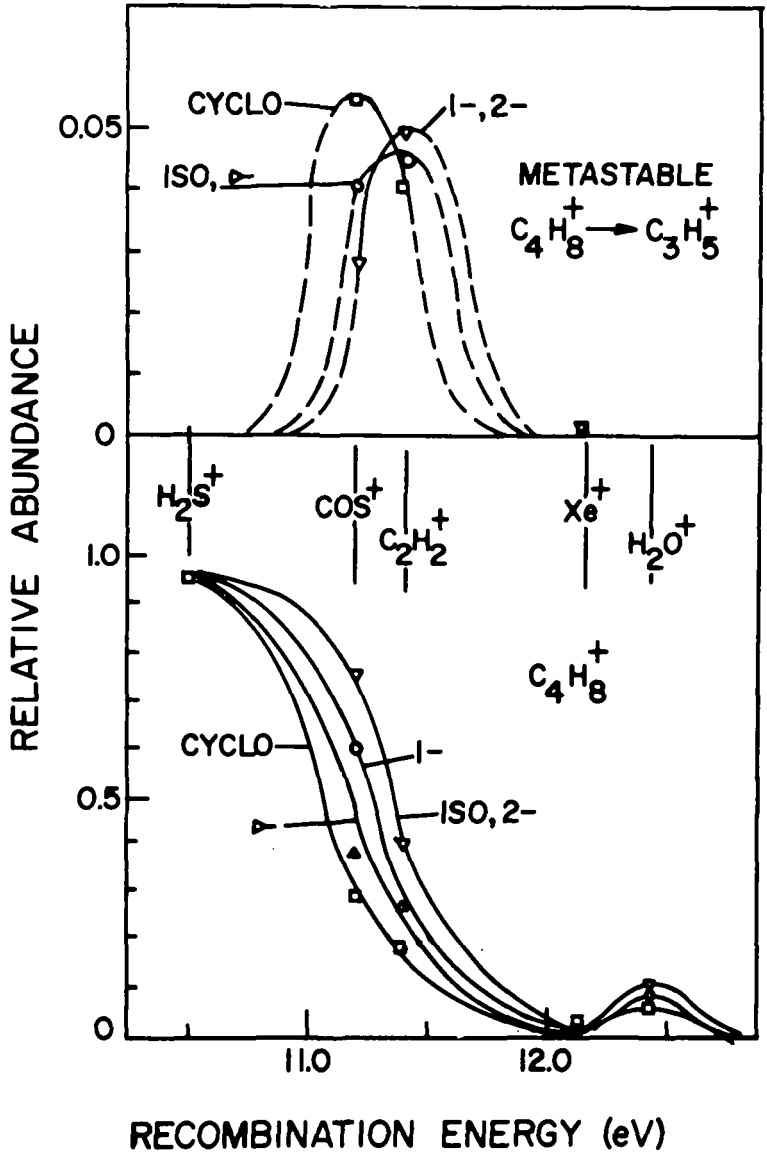

isobutene and butene-2 have the lowest (209 kcal/mole). We are not able to attribute any real significance to the second rise in the parent ion curve when H_2O^+ is used as the reactant ion. Perhaps this is due to the fact that some fraction of the H_2O^+ has a lower recombination energy. Such factors have been discussed in a recent paper from our laboratory[6]. In the upper section of Figure 1, the relative intensities of the metastables observed from the decomposition $C_4H_8^+ \rightarrow C_3H_5^+$ are plotted as a function of energy. The shapes of the curves sketched from this limited data are obviously quite qualitative, but it is clear that the indicated metastable decomposition from cyclobutane maximizes at a lower internal energy than does the corresponding decomposition from the other isomers.

Figures 2 and 3 show the breakdown curves for the major fragment ions from the various C_4H_8 isomers. Of particular interest in Figure 2 is the significantly larger 28^+ fragment from cyclobutane. In other experiments[7] we have shown that this must be due to direct fragmentation of cyclobutane without prior isomerization, a process which occurs via a "loose" transition state. It is also quite interesting, as seen in Figure 3, that the behavior of the 27^+ fragment from methylcyclopropane closely parallels that from cyclobutane rather than the behavior shown for isobutene. This indicates that cleavage of the methyl cyclopropane ion leads to a linear rather than an iso- structure.

Metastable ions were also detected for other delayed decompositions as shown in Table II. In general, the position of these metastables is observed to be consistent with the breakdown curves, that is, their intensities maximize at

TABLE II

Metastable Ions Observed from Charge Transfer to C_4H_8 Isomers.

	Reactant Ion				Relative Abundances	
Reaction	H_2S^+	$C_2H_2^+$	Xe^+	Kr^+	Ar^+	Ne^+
$C_4H_8^+ \rightarrow C_3H_5^+$	0.002	0.05	0.001	--	--	--
$C_4H_8^+ \rightarrow C_2H_4^+$	--	0.001	--	--	--	--
$C_4H_5^+ \rightarrow C_2H_3^+$	--	--	--	--	--	0.003
$C_3H_5^+ \rightarrow C_3H_3^+$	--	--	--	0.006	--	--
$C_2H_4^+ \rightarrow C_2H_2^+$	--	--	--	--	0.004	--

internal energies near the crossing point of the parent and fragment ion curves. Somewhat surprising was the observance of a metastable for the Ne^+ reaction corresponding to the decomposition, $C_4H_5^+ \rightarrow C_2H_3^+ + C_2H_2$. This has not previously been reported as far as we are aware.

In general, the breakdown curves indicate that there is some isomerization of the $C_4H_8^+$ parent ions at lower internal energies, but at higher energies, direct elimination predominates. This is strikingly illustrated by the data in Figure 4, where the product ion ratio is plotted which corresponds to direct loss of CH_3 from $D_2C = CHCH_2CH_3$ as compared to loss of CDH_2. Loss of the latter fragment obviously requires rearrangement prior to fragmentation or consecutive processes. The dotted line in Figure 4 is the ratio expected if complete randomization of the $C_4H_6D_2^+$ ion occurs.

References:

* A more complete account of this work will be submitted for publication in the Journal of Chemical Physics.

1. B.M. Hughes and T.O. Tiernan, J. Chem. Phys., 51, 4373 (1969).

2. G.G. Meisels, J.Y. Park and B.G. Giessner, J. Am. Chem. Soc. 92, 254 (1970).

3. J.H. Futrell and C.D. Miller, Rev. Sci. Instr. 37, 1521 (1966).

4. T.O. Tiernan and R.E. Marcotte, J. Chem. Phys. 53, 2107 (1970).

5. L.P. Hills and T.O. Tiernan, to be published.

6. T.O. Tiernan and C. Lifshitz, "Dissociation of Molecule-Ions Formed by

Figure 2.Relative intensities of 41^+, 39^+ and 28^+ fragments from C_4H_8 isomers.

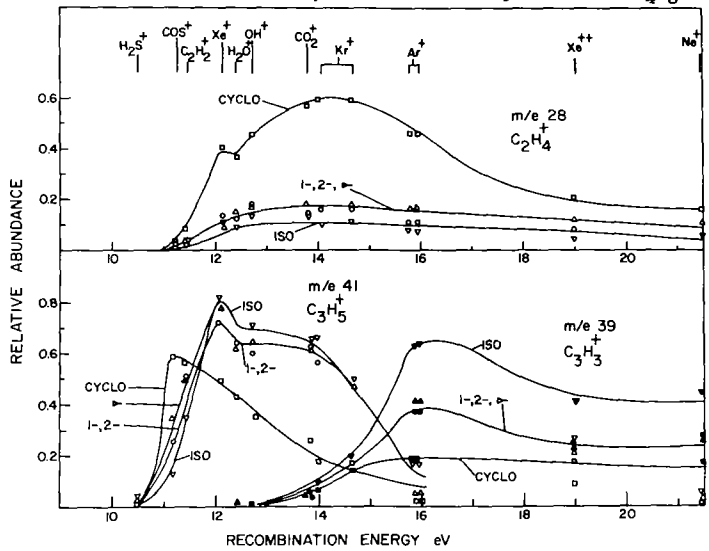

Figure 3. Relative intensities offragments from C_4H_8 isomers.

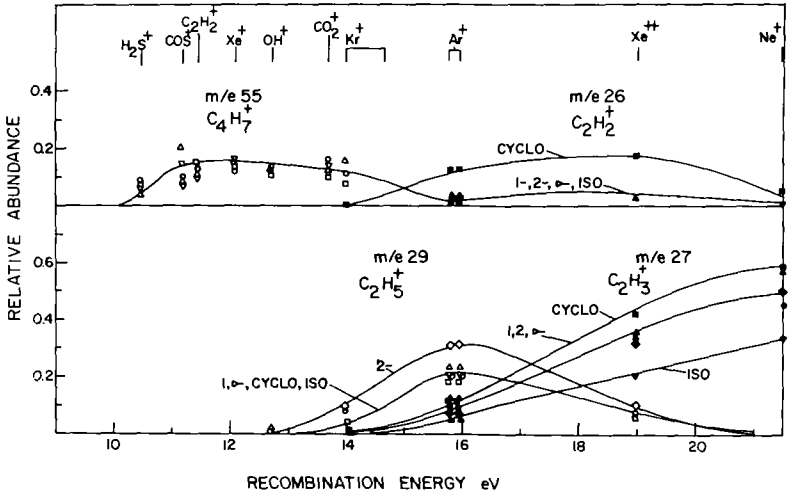

References: (*Continued*)

Charge Exchange Collisions in an In-Line Tandem Mass Spectrometer", Advances in Mass Spectrometry, Vol. V, Institute of Petroleum, London (In Press).

7. C. Lifshitz and T.O. Tiernan, J. Chem. Phys. (to be published)

Figure 4. Ratio of $C_3D_2H_3^+/C_3DH_4^+$ fragments from charge transfer to 1-butene-1,1-d_2

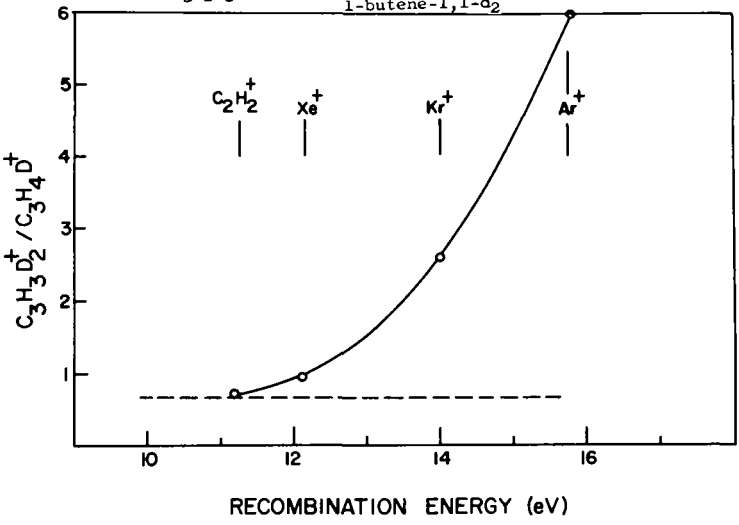

ČERMÁK TYPE STUDIES OF CHARGE EXCHANGE IN A PULSED ELECTRON IMPACT SOURCE*

P. M. Hierl,** J. L. Franklin and D. K. Sen Sharma
Department of Chemistry
Rice University
Houston, Texas 77001

It is shown that the pulsed source of a time-of-flight mass spectrometer can be used successfully to study charge exchange and ion-molecule reactions. Since the source is pulsed, it is possible to display and record both the primary spectrum and the secondary (charge exchange) spectrum simultaneously. Application of the method to acetonitrile is discussed.

*Support by The Robert A. Welch Foundation is gratefully acknowledged.

**Current Address: Department of Chemistry, University of Kansas, Lawrence, Kansas 66044.

A complete paper has been accepted for publication in the International Journal of Mass Spectrometry and Ion Physics.

Single Ion Impact Mass Spectra of Peptide Derivatives.* ROBERT J. BEUHLER and **04** and LEWIS FRIEDMAN, Brookhaven National Laboratory, Upton, New York 11973

We wish to report results of a study of mass spectra generated by single ion-impact processes in the collision chamber of a tandem mass spectrometer. Simple peptide derivatives were chosen for investigation with the object of assessing the utility of the ion impact technique as an analytical tool for the mass spectrometric sequencing of amino acids. The primary ion beams used in this ion impact study were Xe^+, CH_5^+, and aquo-solvated proton and deuteron systems $H_3O^+\cdot(H_2O)_n$ and $D_3O^+\cdot(D_2O)_n$ with n varying from zero to three. In sharp contrast to results obtained with similar systems using electron impact ionization, spectra obtained with highly solvated proton and deuteron beams showed protonated or deuteronated parent ions as the most abundant ions. Fragmentation patterns provided evidence for the structure of the protonated parent ion with the ionizing proton attached to an oxygen atom at the methyl ester terminus of the acetylated peptide methyl esters. There was no evidence for formation of gaseous ammonium ion derivatives by proton attachment to the nitrogen atom in these molecules and no evidence for the protonation of the acetyl oxygen. The analytical capabilities of the tandem mass spectrometer technique will be discussed.

* Research performed under the auspices of the U.S. Atomic Energy Commission.

Determination of the Abundance of Excited States in O^+ Ion Beams Produced by Electron Impact on O_2, CO_2, N_2O, NO_2 and H_2O*

06

B.M. Hughes and T.O. Tiernan
Aerospace Research Laboratories
Wright-Patterson AFB, Ohio 45433

Reactions between O^+ and simple inorganic molecules such as N_2, O_2, and NO have been extensively studied in several laboratories. The O^+/N_2 reaction has received particular emphasis. The effect of translational energy upon reaction of $O^+(^4S)$ with N_2 has been studied by Hasted, et. al.[1] in the temperature region from 77°K to 300°K and at temperatures up to 600°K by Ferguson, et. al.[1]. Giese[2] studied the $O^+ + N_2$ interaction at translational energies from less than 1eV up to about 35eV. The effect of N_2 vibrational energy for this reaction has also been studied by Schmeltekopf et. al.[3]. Theoretical treatments of these systems have been reported by Stubbe[4] and by Kaufman and Koski[4]. One factor that has been studied only briefly for such reactions is the effect of electronic excitation of the O^+ ion. Stebbings et. al.[5] showed that the fraction of O^+ produced in the $O^+(^2D)$ state from electron bombardment of oxygen was dependent upon electron energy. They found that ionization with 50eV electrons produced approximately 30% of the O^+ ion beam in the ^2D state. In addition they determined that the reaction of $O^+(^2D)$ with oxygen is faster by more than one order of magnitude than the reaction of ground state $O^+(^4S)$ ions, although both reactions are exothermic.

We have recently studied reactions of O^+ with N_2 and CO in experiments in which the molecular source of O^+ was varied[6]. These reactions were investigated using the ARL tandem mass spectrometer, described previously[7]. Since these reactions were studied at very low kinetic energy (0.3 ± 0.3eV), only exothermic or very slightly endothermic reactions are energetically possible. Charge transfer from $O^+(^4S)$ to N_2 is endothermic by 1.9eV for thermal ions. Similarly the $O^+(^4S)$ charge transfer reaction with CO is approximately 0.4eV endothermic. On the other hand, charge transfer from both the $O^+(^2D)$ and $O^+(^2P)$ to these two molecules is energetically possible even for thermal ions. Since the lifetimes of these two electronically excited states are very long[8] (~2.1 hours for the ^2D state and ~6.0 seconds for the ^2P state) reactions of these states can be observed in the tandem mass spectrometer. Thus, the reactions with N_2 and CO can serve as detectors of O^+ ions in the incident beam which are in metastable electronically excited states.

Table I shows the results of impacting O^+ from various sources on N_2 and CO.

TABLE I.

Apparent Rate Coefficients for Charge Transfer Reactions of O^+ to N_2 and CO and Fractional Abundances of Excited O^+ Ions from Various Oxygenated Molecules[a]

Source of O^+	$k_{N_2^+}$[b]	Fraction of O^{+*}	k_{CO^+}[b]	Fraction of O^{+*}
O_2	0.14	0.28[c]	0.16	0.28[c]
CO_2	0.019	0.038	0.024	0.041
N_2O	0.22	0.43	0.25	0.43
NO_2	0.17	0.34	0.18	0.31
H_2O	0.48	0.95	0.50	0.86

a. Reactant ions formed by 60eV electron impact on indicated molecules; rate coefficients measured for kinetic energy, E_{lab}~0.3eV.

b. In units of 10^{-9} cm^3/molecule sec.

c. Taken from data of Reference 5.

The rate data reported here were determined relative to the CH_4^+/CH_4 reaction which was used as a standard. The incident ion current is measured directly at the collision chamber in these experiments and secondary products are detected using a multiplier operated in the pulse counting mode. As can be seen from the table, the apparent rate coefficients determined by measuring the total incident ion current, vary by a large factor. The smallest apparent rate coefficient is

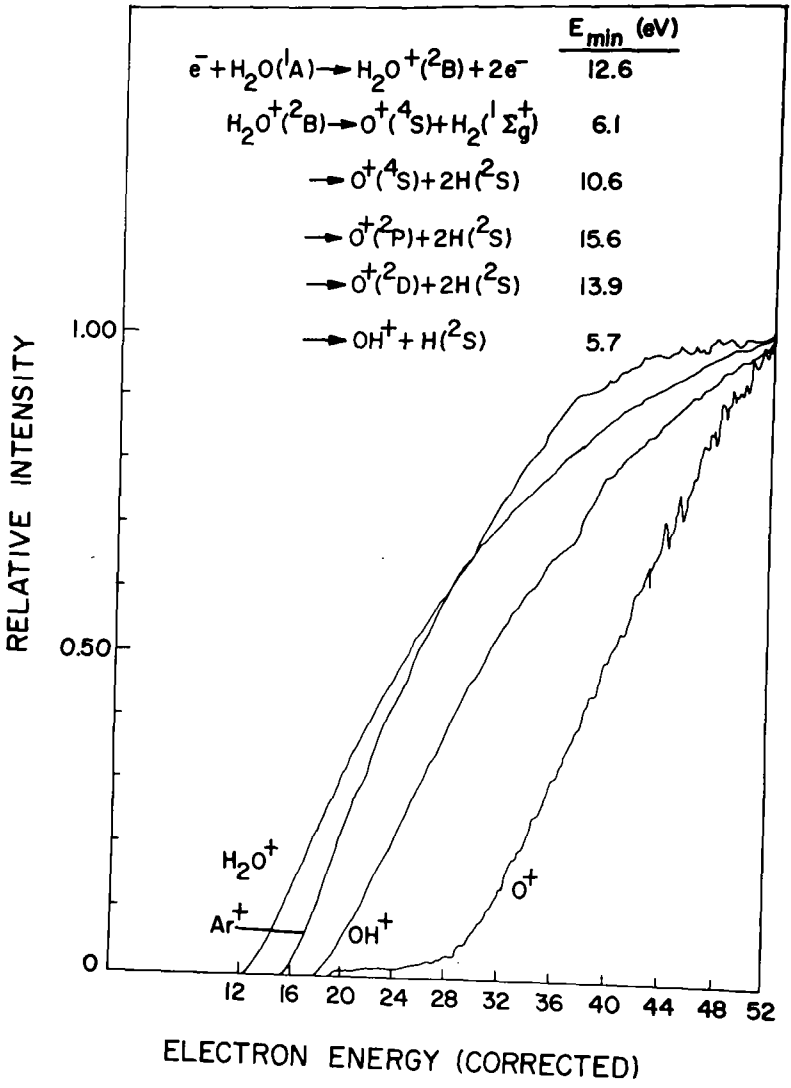

Figure 1. Appearance Potential Curves for the Major Ions in Water with Argon as a Calibrant.

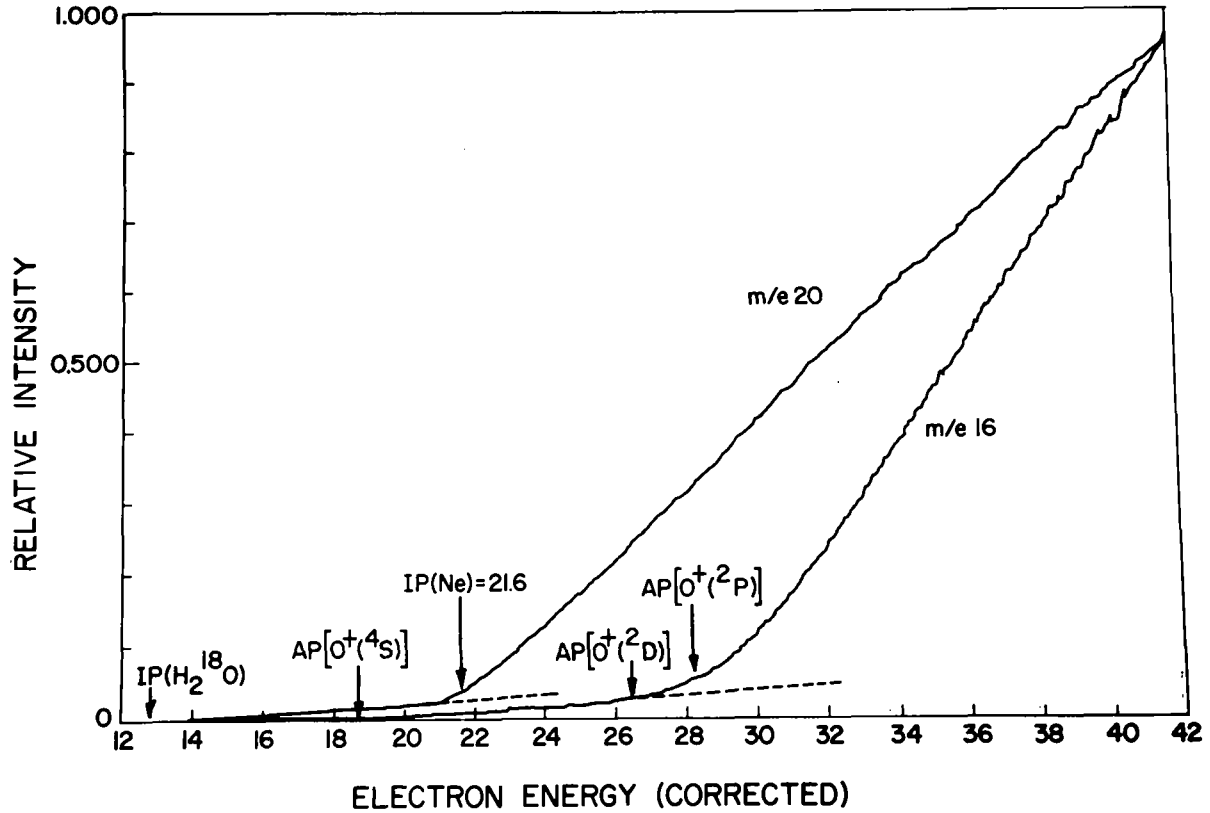

Figure 2. O^+ Appearance Potential Curve in Water with Neon as a Calibrant.

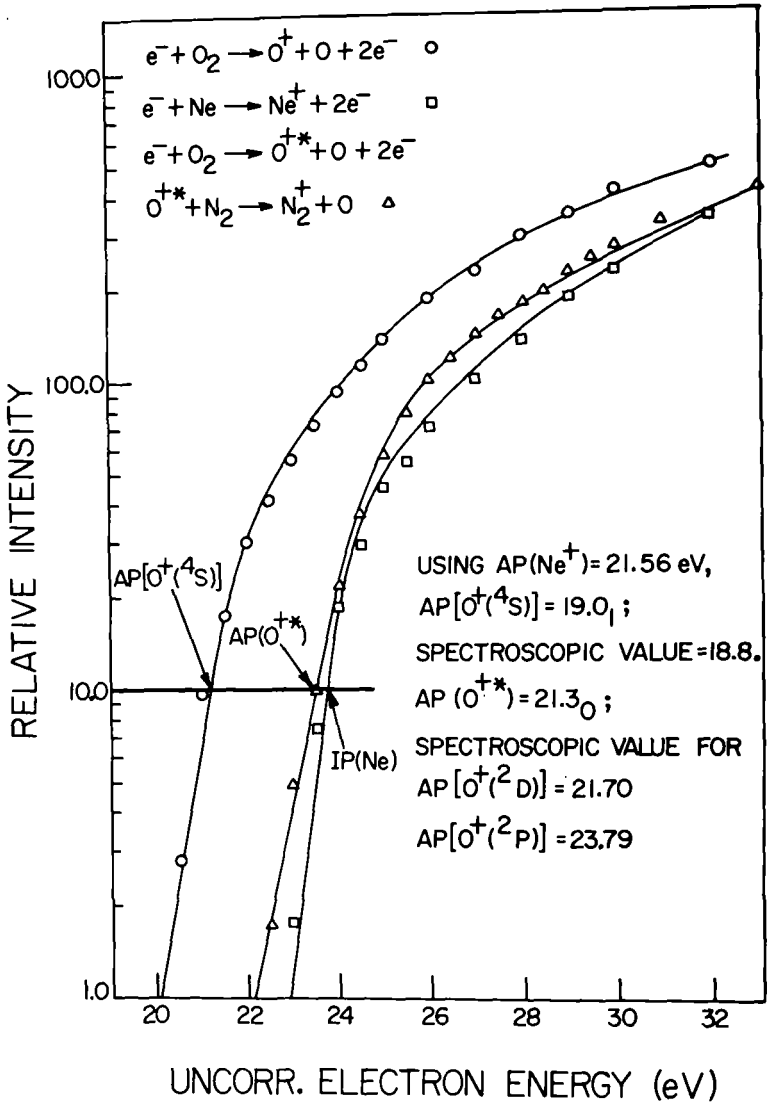

Figure 3. O^+ and O^{+*} Appearance Potential Curves in Oxygen with Neon as a Calibrant.

for O^+ produced from CO_2, indicating that the beam from this source contains the smallest percentage of excited ions. Conversely, the largest fraction of excited O^+ appears to come from H_2O. If the fraction of excited O^+ ions in the beam produced by electron impact on O_2 is taken as 28%, as is reported by Turner, et. al.[5], the fractional abundances of excited ions produced from the other molecules can be determined. This is a reasonable procedure because our experimental conditions and reactant ion transit time are very close to those of Turner, et. al.[5].

It is seen that this procedure indicates that approximately 90% of the O^+ ions produced by electron impact on H_2O are in an excited state. Since this state is several volts above the level of the ground state ion, appearance potential measurements may be used to determine the energy of the excited ions. Figures 1 and 2 show ionization efficiency curves for the major ions in water along with those for Ar or Ne which was needed as a calibrating gas. In both figures, a sharp break in the O^+ curve is evident at approximately 28eV. This is some 10 volts above the minimum energy needed to form $O^+(^4S)$ and H_2 as a neutral product. Figure 2 shows the threshold region on an expanded scale, with the energies labeled corresponding to the processes $e^- + H_2O \rightarrow O^+(^2D) + 2H + 2e^-$ and $e^- + H_2O \rightarrow O^+(^2P) + 2H + 2e^-$. Since the calibrating gas was present in a concentration on the order of 1% of the total water, the long tail observed for m/e 20 is attributed to the $H_2{}^{18}O^+$ parent ion curve superimposed upon the Ne^+ curve.

From the curves shown in Figures 1 and 2, it is very difficult to conclude with any certainty which of the two excited states is produced by electron impact. However, the tail of the excited state curve extends below the energy required to produce the $O^+(^2P)$ state by more than a volt, indicating that at least a large portion of the excited ions are produced in the ^2D state. Figure 3 presents some more definitive data. Here are shown a series of experiments conducted with the tandem mass spectrometer, in which the O^+ and Ne^+ ion currents in an O_2/Ne mixture are plotted as a function of electron energy. In addition, the N_2^+ product from charge exchange of the excited O^+ ion with N_2 is plotted as a function of ionizing electron energy. Using the Ne^+ onset to define the electron energy scale, the $AP(O^+)$ was found to be 19.0eV. This may be compared with a spectroscopic value for the formation of ground state O^+ of 18.8eV. The O^{+*} appearance potential (using the onset of the $O^{+*} + N_2 \rightarrow N_2^+ + O$ reaction as an indicator), was found to be 21.3eV. The spectroscopic value of 21.7eV has been reported for the $O^+(^2D)$ state. These results are in very good agreement with those obtained earlier by Turner et. al.[5], and show that the major portion of the metastable O^{+*} produced from 50eV electron impact on oxygen is in the ^2D state. Presumably, the same excited state is also formed from the other source molecules.

References:

1. (a) D.K. Bohme, P.P. Org, J.B. Hasted and L.R. Magill, Planet. Space Sci. 15, 1777 (1967); (b) M.M. Nakshbondi and J.B. Hasted, ibid., 1781 (1967); (c) E.E. Ferguson, D.K. Bohme, F.C. Fehsenfeld and D.B. Dunkin, J. Chem. Phys. 50, 5039 (1969).

2. C.F. Giese, Advances in Series 58, 20 (1966).

3. A.L. Schmeltekopf, F.C. Fehsenfeld, G.I. Gilman and E.E. Ferguson, Planet. Space Sci. 15, 401 (1967).

4. (a) P. Stubbe, Planet. Space Sci. 17, 1221 (1969); (b) J.J. Kaufman and W.S. Koski, J. Chem. Phys. 50, 1942 (1969).

5. (a) R.F. Stebbings, B.R. Turner and J.A. Rutherford, J. Geophys. Res. 71, 771 (1966); (b) B.R. Turner, J.A. Rutherford and D.M.J. Compton, J. Chem. Phys. 48, 1602 (1968).

6. B.M. Hughes and T.O. Tiernan, J. Chem. Phys. (in press) (1971).

7. J.H. Futrell and C.D. Miller, Rev. Sci. Instr. 37, 1521 (1966).

8. J.W. McGowan, "Excitation-Deexcitation Processes", in "DASA Reaction Rate Handbook" (Defense Atomic Support Agency, Washington, D.C. 1967). Chapter 15.

* A more detailed account of this work will appear in J. Chem. Phys. (1971).

A THREE DIMENSIONAL QUADRUPOLAR MASS ANALYZER

by

Charles S. Harden and Peter E. Wagner*

Research Laboratories
Edgewood Arsenal, MD 21010

In recent years a new mass spectrometer has been developed which is potentially advantageous in the detection of trace quantities of gases in the atmosphere. The device is called a "Three Dimensional Quadrupolar Mass Analyzer" (3DQ). The theory of operation has been fully reported, as have some experimental measurements of some of its operational characteristics[1-5]. The ability of the 3DQ to trap ions depends upon the fact that a charged particle which is subjected to rotationally symmetric, three-dimensional, quadrupole electric fields can be made to execute bounded trajectories.

OPERATION

A cutaway sketch of the device is shown in Figure 1. An electrode system consisting of a shaped ring and two shaped caps is excited with a combination of dc and rf voltages. The ring and caps are hyperboloids of revolution about the z-axis and are tangent to two cones placed tip-to-tip at the center of symmetry. The electrode spacing is described by $R^2 = 2z^2$, where z is the vertical distance from the center of symmetry to either end cap and R is the radius of the ring. Ions are generated in the interior region by means of either of two electron guns which inject ionizing electrons through holes in the electrodes. If the dc and rf voltage amplitudes are properly chosen, ions are caused to execute closed trajectories within the chamber. Periodically, an auxiliary voltage is applied to the upper end cap. This voltage gate withdraws ions through the screen; and, once outside, the ions are accelerated to the active surface of a channel electron multiplier. A positive bias voltage is applied to the grid between the upper end cap and the electron multiplier while the withdrawal voltage is off; thus, positive ions are repelled from the multiplier except during ion withdrawal. The output pulses from the multiplier are amplified and counted or otherwise recorded.

Figure 2 shows a plot of the dc voltage V_d, as a function of the rf voltage amplitude V_a, for which several mass-to-charge ratios will be stable in our device. Voltages are plotted for an rf frequency of 300 kHz and for z_o = 1 cm. The trajectories of an ion of a given m/q are stable inside a bounded region and unstable outside. If the amplitudes of both the rf and dc voltages are changed at a constant ratio the mass scan line passes through regions of stability and instability and the device becomes mass selective. The resolution is increased while sensitivity is decreased as the mass scan line intersects a stability region nearer to the apex.

ELECTRONICS AND TIMING SEQUENCE

If the ionization-withdrawal sequence is made time coherent with the rf driving voltage, it is possible to study the effect of phase of ion injection and withdrawal on the sensitivity of the device, and to make accurate lifetime measurements on trapped ions.

Figure 3 shows schematically the electronic controls used in our instrument. The rf, which oscillates about ground potential, is applied to the ring electrode. The dc voltage is made negative with respect to ground and applied equally to both end caps. The dc is derived from an rf detector circuit whose dc output is proportional to the amplitude of the rf input. The dc to rf voltage ratio is changed by applying a different fraction of the rf amplitude to the detector input. Mass spectra are swept by varying the amplitude of the rf.

A scaler is used to divide the rf by 2^n, with $4 \leq n \leq 12$. The output of this circuit triggers the ionization pulse generator and a delay circuit. The delay circuit the triggers the withdrawal pulse generator. Thus, the ionization-withdrawal events are locked to the rf. Ionizing electrons enter the trap through either the ring or the lower end cap. The electron pulse is turned on by applying a positive pulse to the negatively biased grid. The pulse height, width, and phase of the ionization and withdrawal pulses are adjustable at each pulse generator. The electron multiplier output pulses are amplified and

* Permanent address: Department of Electrical Engineering, The Johns Hopkins University, Baltimore, Maryland

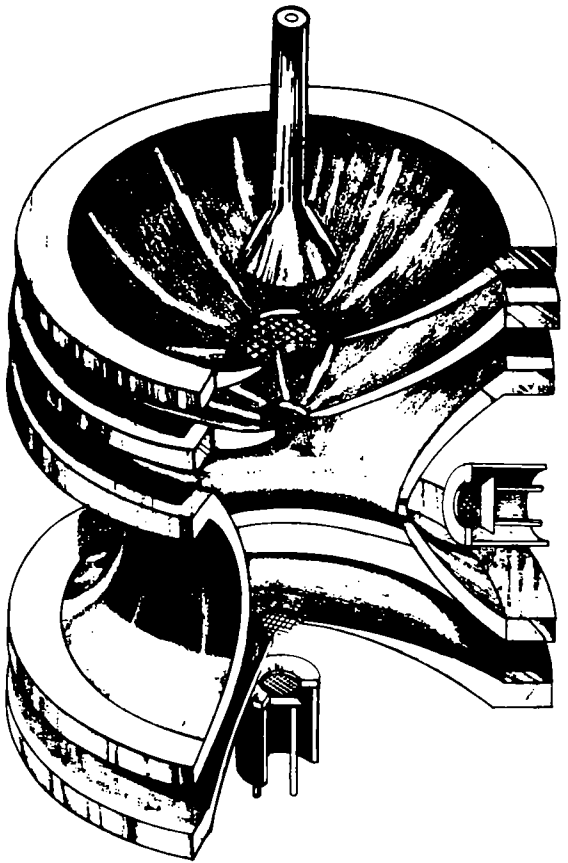

Figure 1: Cutaway Sketch of 3DQ

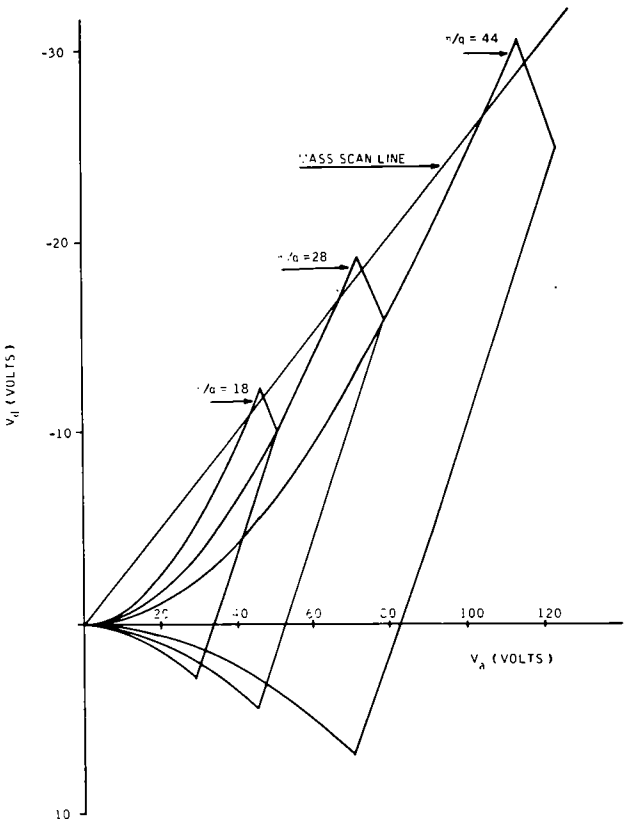

Figure 2: Stability Zones for Several m/q

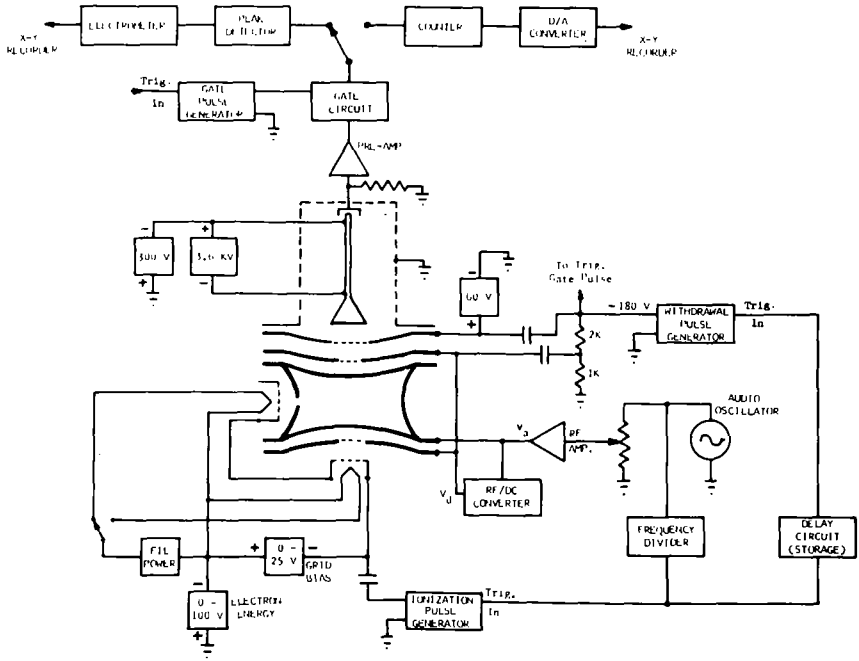

Figure 3: Block Diagram of Electronic Controls

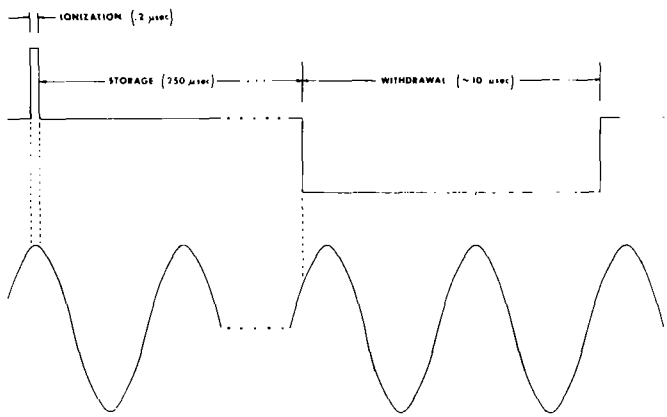

Figure 4: Timing Sequence

applied to a gated peak detector circuit and an electrometer. The gate is open only while the withdrawal voltage is on. For digital data representation, a counter is connected at the output of the gate circuit.

Figure 4 illustrates the timing of the ionization-storage-withdrawal sequence. The dotted lines indicate the phase relationship between the rf and the ionization and withdrawal voltages for which ion trapping is most efficient when the applied frequency is 220 kHz. The storage time is varied by means of the delay circuit; a typical value of 250 μsec is shown.

EXPERIMENTAL RESULTS

We first describe several miscellaneous phenomena which occur consistently but are not completely understood at this time. When the device is first turned on, several minutes - perhaps an hour - pass before any mass-selected ions can be observed. Usually this time is reduced if V_d/V_a is kept small; then V_d/V_a can be increased to a value where mass selection is possible. In other words, the ion trap appears to require a kind of pre-conditioning prior to operation as a mass spectrometer.

A mass peak is nearly always observed to be larger when a spectrum is scanned downward, from high masses to low masses, than when scanned upward. The amplitudes of mass peaks obtained on successive upward scans, however, are found to be more repeatable from scan to scan.

Finally, some long term drift in sensitivity occurs, probably because of drift in ionizing current and/or rf voltage amplitude.

Resolution

The intensity of a mass peak was studied as a function of resolution under varying conditions of the rf frequency, the energy of the ionizing electrons, and the storage time. Resolution is defined as the mass-to-charge ratio of an ion divided by the peak width in atomic mass units measured at half-height. The data were taken by varying the voltage ratio V_d/V_a under the conditions given below.

Frequency	Average Electron Energy	Storage Time
315 kHz	70 ev	250 μsec
220 kHz	60 - 85 ev	250 μsec
220 kHz	70 ev	1000 μsec

The ionization pulse width was 10 μsec in all cases.

Figure 5 shows a plot of peak heights of N_2^+, normalized at an arbitrary resolution of 40, versus resolution measured at half-height. The data have been fitted by the method of least squares to a single empirical curve. The equation thus obtained is:

$$\text{Peak Height} = (3.65 \pm .23) \exp [-(.0322 \pm .0023) \times \text{Resolution}]$$

The fit is quite good and indicates that the slope (V_d/V_a) of the mass scan line completely controls the sensitivity-resolution relationship under the experimental conditions given here. The energy of the ionizing electrons has no effect on the relationship.

Dependence of Sensitivity on V_d/V_a

As stated in the previous section, the sensitivity is strongly dependent on the slope V_d/V_a of the mass scan line. This dependence is in accord with a very simple empirical model for the trapping process. Figure 6 shows a stability zone for a single m/q. The zone is cut along line BC by the mass scan line. The number of ions trapped will be proportional to a quantity which we call the number of stable orbits available for occupancy in the chamber. The model assumes the density of stable orbits (the number per unit area on the stability diagram) to be uniformly distributed and, further, the total number of stable orbits corresponding to a given mass scan line to be proportional to the area A of the zone which lies above the line BC.

The number of ions trapped should be proportional to the integrated area I under a mass peak. When the angle θ between the mass scan line and a line passing through the apex of the zone is small (as is the case for mass-selective operation) the area A is proportional to θ^2; thus since $\theta = \tan^{-1}\phi - \tan^{-1}(V_d/V_a)$, $I \propto [\tan^{-1}\phi - \tan^{-1}(V_d/V_a)]^2$, where ϕ is the dc to rf voltage ratio at the tip of the zone. For the values of $|V_d/V_a - \phi| \ll \phi$

one can show that, $I = K (\tan^{-1}\phi - V_d/V_a)^2$, where K is an adjustable proportionality constant. A least-squares fit to a representative set of data with K and $\tan^{-1}\phi$ allowed to be adjustable, is shown in Figure 7. Although the value of K depends on a number of factors (e.g., ionizing current, ionizing voltage) it is satisfying to note that the empirical value $\tan^{-1}\phi = 0.276$ is close to the theoretical value of 0.272. Other data were fitted similarly, $\tan^{-1}\phi$ ranging from 0.25 to 0.28 and K varying from .3 to 1.7×10^6 mv/amu.

Phase and Width of Withdrawal Pulse

As the location in time of the ion withdrawal pulse is changed with respect to the rf phase, a corresponding change in the intensity of the collected ion current is observed. Studies at a frequency of 220 kHz show that ions are most efficiently withdrawn if the withdrawal pulse is applied when the amplitude of the rf is increasing and has about one-half of its maximum positive value. When the rf frequency is 315 kHz the withdrawal pulse must be applied when the rf amplitude is nearly at its maximum positive value. The output pulses of the electron multiplier are observed to start approximately 2 to 4 μsec after the withdrawal pulse is turned on. This delay is attributed to the time of flight of the ions from inside the trap to the electron multiplier and to the transmission time of the multiplier. Under most conditions all of the ions are withdrawn from the trap in a time less than 5 μsec. A withdrawal pulse wider than about 10 μsec offers no noticeable advantage in the operation of the instrument.

Since the potential of the end caps is negative with respect to the dc level of the rf voltage, one might expect ion withdrawal to be most effective when the rf voltage has its most positive value. The situation is more complicated, however, because half of the trapped ions are below the center of the device and because the time of flight of the ions out of the trap is significant. It is therefore not surprising that at different frequencies (hence different values of the rf voltage) the timing of the most efficient ion withdrawal pulse varies with respect to the rf.

Phase of Ion Production

Theoretical considerations[2] show that ions which will be most efficiently trapped are those produced either in phase with the rf or 180° out of phase. The trapping is expected to be more efficient when the ions are produced in phase with the rf. This phase dependence was examined experimentally in the following way.

A pulse of 0.2 μsec duration was applied to the grid of the electron gun to allow a very short period of ionization in the trap. The ion withdrawal pulse was set for most efficient withdrawal about 250 to 300 μsec later. The entire sequence was repeated after 128 rf periods (~ 580 μsec). The phase of the ionizing pulse was varied over several cycles of the rf. Figure 8 shows the results when electrons entered (a) through the ring electrode and (b) through the bottom end cap. In (a) the electrons are subjected to a dc field with a superimposed rf field and in (b) the electrons experience a dc field only. In both cases the behavior is a theoretically predicted. Peaks in the ion current occur when the ionization pulse is in phase with the rf, and smaller peaks occur when they are 180° out of phase. In (a) the out-of-phase peaks are smaller relative to the in-phase peaks than in (b). This is because of the fact that electrons entering the trap through the ring experience retarding potentials during the negative portion of the rf cycle. consequently, the signal produced during this portion of the rf cycle, which is usually small, becomes even smaller or disappears altogether. The dotted curves represent ions which excape the trap immediately after the ionization pulse is turned off. For this case the detector sensitivity has been reduced by about a factor of 10. These ions are not mass selected. They were collected by moving the gate pulse (which activates the detector) as close as possible to the ionization pulse while leaving the withdrawal pulse (which destabilizes the ions) at the 250 - 300 μsec delay position.

Width of Ion Production Pulse

Unstable ions that have not yet left the trap just after their creation might be expected to degrade the performance of the device by virtue of the destabilizing influence exerted by their space charge on the paths of desired ions. This effect would be manifested in the variation of trapped ion current with width of the ionization pulse.

A plot of N_2^+ peak height vs ionization pulse width is given in Figure 9. A strong oscillation is exhibited with a period equal to that of the rf. As the pulse width is increased the oscillatory structure becomes less pronounced and eventually disappears (presumably when the trap approaches saturation with stored ions). The time scale for the structure to disappear is roughly 500 μsec.

There are two reasons other than the space charge mechanism mentioned above why the

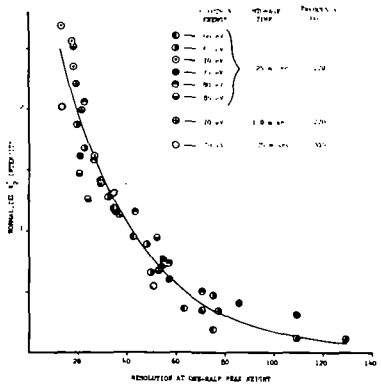

Figure 5: N_2^+ Intensity vs Resolution

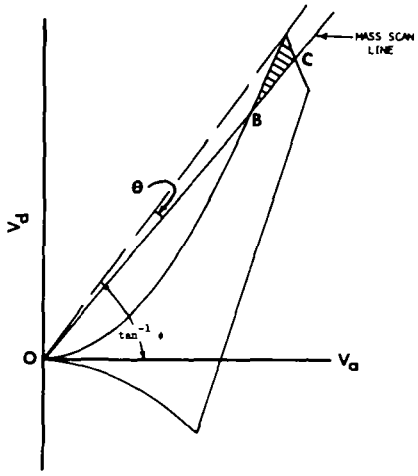

Figure 6: Stability Diagram for Single m/q

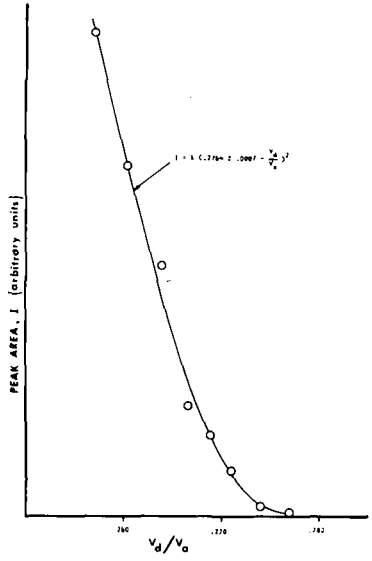

Figure 7: Least-Squares Fit of Data to Empirical Model

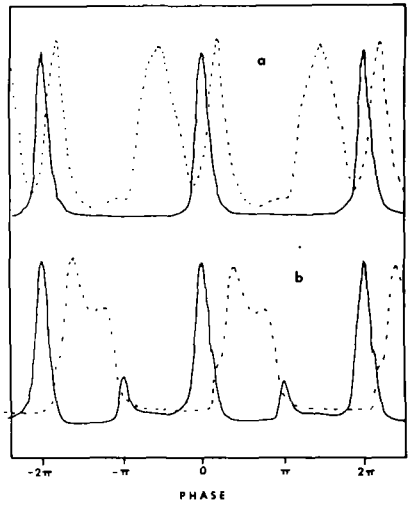

Figure 8: Phase Dependence of Peak Height on Ionization Pulse

peak height might vary with pulse width. First, as is clear from Figure 8, stable ions are only created during a small fraction of the rf cycle. Second, the ionizing efficiency could have varied significantly during the rf cycle for the data of Figure 9, because the side electron was used for this study and the electron energy therefore varied throughout the rf period. Both of these effects, however, should produce a step-shaped curve, more like the integral of Figure 9 than the figure itself. A subsequent study made with the electron gun on the underside of the device showed similar oscillations. It is therefore clear that ion production extending into the region of unfavorable rf phase not only fails to contribute to the stored ion density; it actually destroys stored ions. Estimates of rate constants for ion-neutral and ion-ion collisions indicate times between collisions on the order of 10^{-5} to 10^{-4} sec, which is far too slow to be important; thus we are left only with the space charge mechanism.

Ion Storage Lifetime

If the 3DQ is operated with very short ionization pulses, rate constants for the decay of stored ions can be measured directly by varying the storage time (the time between the ionization pulse and the withdrawal pulse). Other workers[5] have deduced rate constants from build-up curves of ion concentrations during steady state ion production.

In this work, an electron pulse width of 0.2 μsec was used for ionization. After a variable delay time, the stored N_2^+ ions were withdrawn from the trap and the peak heights were measured. The phases of the ionization and withdrawal pulses were set for maximum peak heights.

The mechanisms causing ionic decay are assumed to be ion-ion and ion-neutral collisions. Since most trapped ions should be repelled by the walls of the device, ion-wall collisions are neglected. The ion loss rate equation is

$$\frac{dn}{dt} = - k_1 n^2 - k_2 pn + k_3 p \qquad (1)$$

where n is the number density of ions remaining in the trap at time t, k_1 is the ion-ion collision rate constant, k_2 is the ion-neutral collision rate constant, k_3 is an ion production rate constant, and p is the background pressure. The term $k_3 p$ is included to account for any sources of ionization that do not depend on the pulse of ionizing electrons. Residual ions collected from the vacuum chamber by the trap during the storage period or ions generated by the gun if it were not completely turned off between pulses would contribute to $k_3 p$.

Experimentally, the quantity measured is the trapped ion current, i (given in millivolts of recorder response) rather than n. Since $i \propto n$, we have

$$\frac{di}{dt} = - K_1 i^2 - K_2 i + K_3 . \qquad (2)$$

In Figure 10 is shown a representative set of data for N_2^+ at 10^{-6} Torr. The solid curve is a least-squares fit to equation (2). The values of the K's thus determined are: $K_1 = 1.29 \times 10^{-5}$ $mv^{-1}sec^{-1}$, $K_2 = 1.25 \times 10^{4}$ sec^{-1}, and $K_3 = 2.14 \times 10^{6}$ mv sec^{-1}. Attempts were also made to fit the data with one or more of the K's in (2) assumed to be zero. The best fit resulted in the constants: $K_1' = 0$, $K_2' = 3 \times 10^{4}$ sec^{-1}, and $K_3' = 5.79 \times 10^{6}$ mv sec^{-1}. However, the fit to experiment (indicated by the dashed curve in Figure 10) was clearly inferior to equation (2) with the values of the K's given above.

To convert K_1 and K_3 to k_1 and k_3 requires a knowledge of the scale factor between n and i. The value of k_2 is independent of the scale factor. A rough estimate of n/i (1mv $\sim$ 1 ion/cm^3) gives

$$k_1 \approx 1.29 \times 10^{-5} \text{ cm}^3\text{sec}^{-1}$$
$$k_2 \approx 1.25 \times 10^{10} \text{ Torr}^{-1}\text{sec}^{-1}$$
$$k_3 \approx 2.14 \times 10^{12} \text{ cm}^{-3}\text{Torr}^{-1}\text{sec}^{-1}$$

The value of k_1 agrees with that reported by Dawson, Hedman, and Whetten[5]; our k_2 is about two orders of magnitude larger; out k_3, although it may not be directly comparable to their value, is about three orders of magnitude smaller. These results indicate that ion decay is predominantly due to ion-neutral collisions; however, even at relatively high

pressures, ion-ion collisions seem to play an important role in the initial ion decay. Additional work is planned to determine the accuracy of the rate constants. Curve fitting of other data taken at pressures ranging from 10^{-8} to 10^{-6} Torr, to first, second, and first and second order decay mechanisms yields k_1 values around the 10^{-5} $cm^3 sec^{-1}$ value and k_2 values from about 10^{10} to 10^{12} $Torr^{-1}$ sec^{-1}. Only one value of k_3 has been determined.

REFERENCES

1. Fischer, E. Three Dimensional Stabilization of Charge Carriers in a Quadrupole Field. Z. Phys., 156, 1 (1959).

2. Dawson, P.H. and Whetten, N.R. Ion Storage in Three Dimensional Rotationally Symmetric, Quadrupole Fields. I. Theoretical Treatment. J. Vac. Sci. Technol., 5, 1 (1968).

3. Dawson, P.H. and Whetten, N.R. Ion Storage in Three Dimensional Rotationally Symmetric, Quadrupole Fields. II. A Sensitive Mass Spectrometer. J. Vac. Sci. Technol., 5, 11 (1968).

4. Rettinghaus, G. Determination of Low Partial Pressire With an Ion Cage. Z. Angew. Phys., 22, 321 (1969).

5. Dawson, P.H., Hedman, J.W., and Whetten, N.R. A Simple Mass Spectrometer. Rev. Sci. Instr., 40, 1444 (1969).

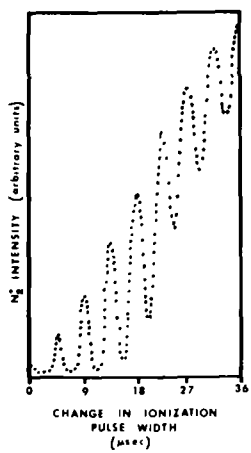

Figure 9: Peak Ht. vs Pulse Width

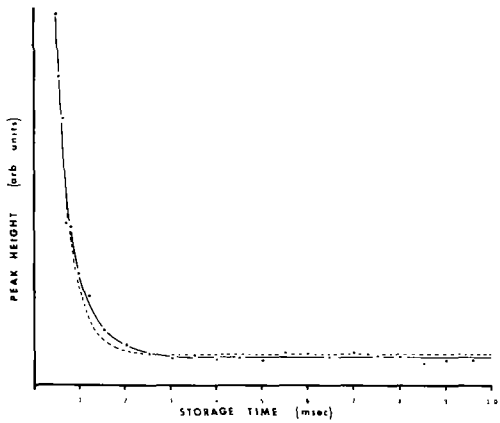

Figure 10: Least-Squares Fit of Equation (2) to Experimental Data

P2

TANDEM QUADRUPOLE FOR USE AT EXTREMELY LOW PRESSURES (DEEP SPACE)*

Wilson M. Brubaker

Analog Technology Corporation
Pasadena, California 91107

Instruments used in deep space are exposed to intense photon bombardment. Some of these photons may pass directly through the quadrupole to the detector, where they induce signals similar to those produced by incident ions.

Experiments made with a quadrupole 10 inches long showed that there is a photon-induced current at a Faraday detector.(1) When the gas in the ion source is hydrogen, this photon-induced signal is about 2×10^{-9} amperes per torr. One manner of suppressing the photon-induced signal is to use a tandem quadrupole with rods of the second section bent into the arc of a circle to separate the mass resolved ions from the photons.(2) Such an instrument has been built.

Apparatus - The figure accompanying depicts the geometry of the tandem quadrupole. Segmented rods provide the delayed dc ramp mode of operation. The contours of the straight rods are hyperbolic; those of the curved ones are round. Internal coupling capacitors transmit ac potentials from the straight to the curved rods, while resistors attached to curved rods maintain their average potential at ground. The ion detector assembly can be placed at the ion exit end of the curved section, as shown, or it can be placed at the end of the straight section, as in the conventional quadrupole.

Theory - The function of the curved rod assembly is to direct the mass resolved ion beams along the arc of a circle, thus separating them from the photon beam, which enters the quadrupole through the ion entrance aperture. The working points for the ions which enter the curved section lie on the q-axis, directly below the apex of the stability diagram. Since this region is quite remote from the boundaries of the stability diagram, the ions are transmitted at high efficiency, and their trajectories are little perturbed by imperfections in the positions of the field-forming surfaces. Similarly, perturbations in the fields owing to the curving of the quadrupole axis are of negligible importance.

The bent rods lie in two planes. This geometry provides an unobstructed path for photons to escape without striking a rod. The inside of the vacuum envelope for the curved section has been blackened to reduce the reflectance of the photons.

Experimental Procedure and Results - Using ion counting at the output of a channeltron multiplier, photons were observed with the instrument assembled as shown in the figure, as well as with the detector at the end of the conventional quadrupole. The passage of ions through the instrument was blocked by the application of a dc potential between the rod pairs of the straight section.

The addition of the curved section attenuates the photon-induced signal by a factor of 2,000 and makes no apparent change in the instrument sensitivity or resolving power.

Conclusions - The addition of a curved quadrupole section to form a tandem quadrupole increases the signal-to-noise ratio by a factor of 45 without degrading the instrument sensitivity or resolving power.

---

(1) Final report, "Quadrupole Mass Filter," Contract No. NASW-1736, by W. M. Brubaker.

(2) U. S. Patent 3,410,997, "Multiple Mass Filter," W. M. Brubaker, November 12, 1968.

*This work was supported in whole by NASA Contract #952835, monitored by C. E. Giffin of JPL.

ABSTRACT*

ION SOURCE FOR MAGNETIC MASS SPECTROMETER TO BE USED IN SPACE**

W. M. Brubaker, D. Burnham, and G. D. Perkins

Analog Technology Corporation
Pasadena, California 91107

A special ion source is being developed for use with a double-focussing, tandem-sector, magnetic mass spectrometer that is intended for possible use in conjunction with a gas chromatograph on a mission to Mars. The combination of the requirements for scanning a wide mass range and using a high and a low energy ionizing electron beam present unusual demands on the stabilization (in space) of the electron beam. The demand for a spare filament further complicated the design. A proposed solution to these constraints is found through the use of an unusually strong magnetic field to collimate the beam. The design of the source and its operating characteristics are discussed.

---

* Article appeared in The Journal of Vacuum Science and Technology, Vol. 8, No. 1, January/February 1971.

** This work was supported in whole by JPL on Contract 952576.

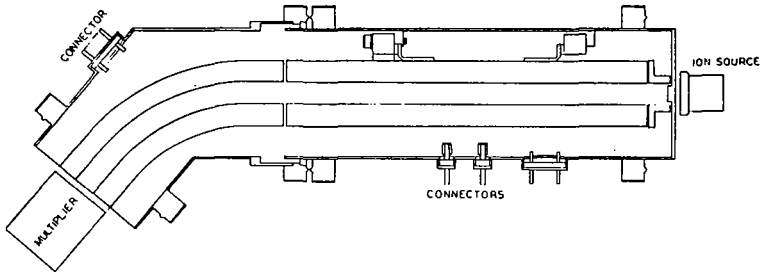

QUADRUPOLE STRUCTURE FOR LUNAR MASS SPECTROMETER

P3

THE TIME-FOCUSING PRINCIPLE: A DOUBLE-FOCUSING DESIGN FOR TIME-OF-FLIGHT MASS SPECTROMETERS*

J. M. B. Bakker,

Shell Research Limited,
Milstead Laboratory of Chemical Enzymology,
Sittingbourne, Kent, England.

One of the major problems in the measurement of the time-of-flight of charged particles is the spread in the time of arrival of particles of equal mass and supposedly equal energy. Thus, if the time-of-flight in a linear field free path of a particle with velocity v_o is T_o, then the time-of-flight of a particle deficient in velocity by an amount Δv will be $T_1 = T_o (1 + \beta + \beta^2 + \beta^3 + \ldots)$ where $\beta = \frac{\Delta v}{v_o}$, the fractional deviation in velocity. Similarly, particles with an excess velocity Δv will have a time-of-flight given by $T_1 = T_o (1 - \beta + \beta^2 - \beta^3 + \ldots)$

The time-focusing principle, a first order theory of which is presented here, makes the time of arrival of charged particles independent of the fractional deviation in velocity β. This is achieved in the following manner: the particles are made to spiral in a radial electric field, in which the particles will describe helical orbits. If the time-of-flight of those particles which have velocity v_o while in orbit is made equal to T_o, then, to a first order approximation, the time-of-flight of particles deficient in velocity by an amount Δv will be $T_h = T_o (1 - \beta - \beta^2 - \beta^3 - \ldots)$. Similarly, particles with an excess velocity Δv will have a time-of-flight given by $T_h = T_o (1 + \beta - \beta^2 + \beta^3 - \ldots)$. This is a direct consequence of the energy focusing properties of radial electric fields and the fact that angular momentum is conserved in such fields. The addition of a helical flight path to a linear flight path will give a total time-of-flight $T = T_1 + T_h = 2T_o$ for particles of the same mass, independent of β, provided that the time-of-flight of v_o-particles is equal over the linear path and the helical path. In other words, this arrangement gives complete time-focusing.

* A more detailed account of this work has been submitted to the International Journal of Mass Spectrometry and Ion Physics.

Problems Associated with the Resolution of Organic Ions in a Time-of-Flight Mass Spectrometer

By: M.A. Grayson and C.J. Wolf
McDonnell Douglas Research Laboratories
McDonnell Douglas Corporation
St. Louis, Missouri 63166

A problem unique to time-of-flight (TOF) mass spectrometry is concerned with differences observed in the resolution of organic and inorganic ions. This problem is illustrated in Fig. 1, where the mass spectrum of the mercury isotopes (Fig. 1a) is compared with that of hexadecane (Fig. 1b). Note that the mercury isotopes (peaks at m/e = 198, 199, 200, 201, 202, and 204) are well resolved while the peaks from hexadecane (m/e = 226 and 227) are poorly resolved even though the two spectra were obtained with identical operating conditions in the TOF mass spectrometer. Since the detector in the TOF mass spectrometer is "line-of-sight" with the ion source, all species, charged and neutral, are recorded. Therefore, a retarding potential was applied to the detector stack to separate primary ions from secondary ions and neutral species.[1] The spectrum obtained from hexadecane with a retarding potential of 800V is shown for comparative purposes in Fig. 1c. Both the neutrals and charged daughter fragments are separated from the primary ions. Obviously, the neutral species and charged daughter fragments, when superimposed upon the parent ion, drastically degrade the resolution of the TOF mass spectrometer.

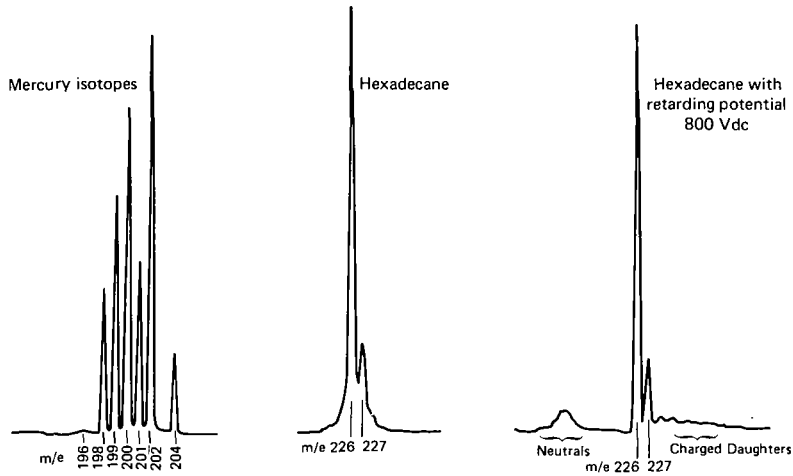

Fig. 1 Comparison of the mass spectra of inorganic and organic ions. The six naturally occurring isotopes of mercury (pressure 1 x 10^{-6} Torr) are shown well resolved in Fig. 1a. The parent ion and (M + 1) ion of hexadecane (pressure 1 x 10^{-6} Torr) shown in Fig. 1b are not well resolved. When a retarding potential of 800Vdc was applied to the detector stack (to separate charged from neutral species) the M and M + 1 ions of hexadecane are well resolved as shown in Fig. 1c.

The neutral species which give rise to the deleterious effects in the TOF mass spectrometer must be formed in the drift tube from the ions in question; otherwise the ions and neutrals would not reach the detector simultaneously. The mechanisms responsible for the formation of both neutrals and charged fragment species were investigated. The relative amounts of neutrals, charged daughters, and primary ions were studied as a function of pressure, nature of the gas in the drift tube, and the molecular weight and number of degrees of freedom in the parent molecule.

The percent neutrals as a function of pressure in the drift tube for six different organic compounds are shown in Fig. 2. For pressures less than 5 x 10^{-6} Torr the neutral fraction for all materials is independent of pressure. However, at higher pressures, i.e., > 5 x 10^{-6} Torr, the neutral fraction increases rapidly with pressure. Additional experiments have shown that the neutral fraction increases in a similar manner as a function of pressure when the gas in the drift tube is either nitrogen or helium. These observations suggest that neutrals are formed by two different mechanisms within the drift tube, one pressure independent and the other pressure dependent.

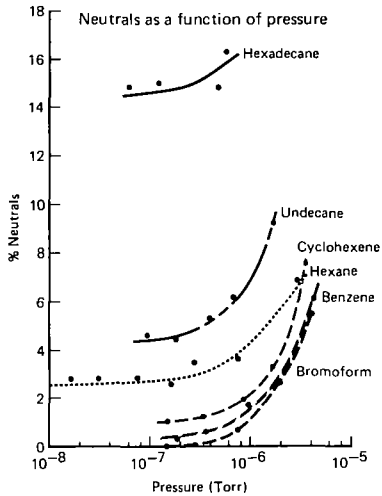

Fig. 2 Percent neutral species arriving at the detector simultaneously with the parent ion as a function of pressure in the drift tube for six organic compounds.

The pressure independent reaction is a unimolecular decomposition of the parent ion to a neutral fragment and a charged daughter. These are commonly called metastable decompositions. Although metastable reactions are well known in mass spectrometry, they are a serious problem in the TOF mass spectrometer because the detector is "line-of-sight" with the source and the detector is unable to distinguish between charged and non-charged species. Within a homologous series, i.e., hexane, undecane, and hexadecane, the pressure independent neutral fraction increases with molecular weight.

This observation is in good qualitative agreement with existing theory for unimolecular decomposition[2] which states that the time for an excited molecule to decompose is proportional to the number of internal degrees of freedom. Thus, the simpler excited ions such as those of hexane will decompose in the ion source prior to extraction into the drift tube of the TOF mass spectrometer while the more complex ions, such as those of hexadecane, will enter the drift tube in the excited state. Hence, complex molecules with many degrees of internal freedom will yield poorly resolved mass spectra unless the neutral and charged daughter fractions are separated from the primary ions of interest.

The pressure dependent reactions are probably collisional induced charge transfer reactions coupled with decomposition to form both a charged and neutral species. This process also occurs in the drift tube since the products arrive at the detector simultaneously with the primary ion. This effect is not restricted to complex molecules with many degrees of freedom as are the metastable decompositions. The effect can, however, be essentially eliminated by operating the TOF at low pressures.

*This work was conducted under the McDonnell Douglas Independent Research and Development Program.

References

1. R.E. Ferguson, K.E. McCulloh, H.M. Rosenstock, J. Chem. Phys. 42, 100 (1964).

2. S.W. Benson, The Foundations of Chemical Kinetics, (McGraw Hill Book Co., New York, 1960)

THE MOTION OF CHARGED PARTICLES BETWEEN CONCENTRIC CYLINDERS AND SOME APPLICATIONS

M. BARIL, L. BOLDUC and M. De CELLES*
C.R.A.M., Département de physique,
Université Laval,
Québec, Canada.

During our work on multipassage magnetic mass spectrometers[1,2] we decided to study the possibility of using the cylindrical condenser as a mirror. Ion optical work[3,4] on this apparatus has been restricted to the calculation of trajectories near the equipotential circle corresponding to the mean energy of the incident particles. Waters[5] has studied the more general problem of oblique entry through the inner electrode but with analog techniques.

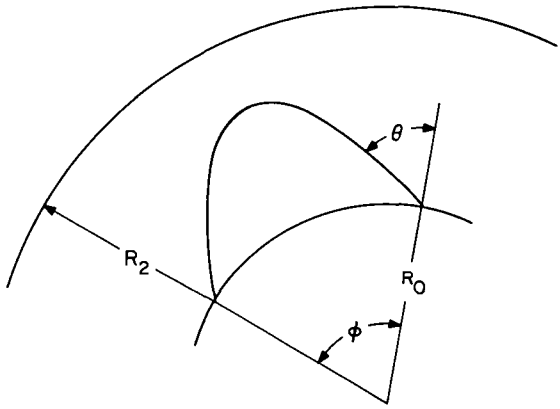

Figure 1

Figure 1 shows one trajectory to be studied. It could be easily shown that the ion optical properties of a beam centered on this trajectory can be calculated if ϕ and its derivatives relative to θ and E (the energy of the particle) are known. ϕ is given by the following integral:

$$\phi = 2 \int_{R_o}^{R_a} \frac{R_o \sin\theta \, dR}{R^2 \sqrt{1 + \frac{1}{X} \ln \frac{R_o}{R} - \frac{R_o^2 \sin^2\theta}{R^2}}}$$

where:

R_a = apogee radius
R_o = inner electrode radius
θ = angle of incidence
$X = E/P_o$
E = total energy of the particle
$P_o = eV/\ln (R_2/R_o)$
V = potential difference between outer and inner electrodes
e = electronic charge
R_2 = outer electrode radius.

* Université du Québec, Québec, Canada.

This integral has no direct analytical solution. De Celles[6] has shown that it could be evaluated by using an infinite series of Dawson integrals:

$$\phi = \sum_{i=0}^{i=\infty} c_i (\theta) F_i (X, D(X))$$

where

$$D(X) = e^{-k^2} \int_0^{k^2} e^{+q^2} dq \quad \text{(Dawson integral)}$$

Bolduc has written a computer program to calculate ϕ and its derivatives. These values are utilized in the transfer matrix between the entry and the exit of the mirror. Initial conditions are: lateral displacement x_i, angular displacement α_i and energy variation $\Delta E/E$ of a definite particle relative to a particle following the main path. Final or exit conditions are noted by the subscript f.

$$\begin{vmatrix} x_f \\ \alpha_f \\ \Delta E/E \ f \end{vmatrix} = \begin{vmatrix} A & B & C \\ a & b & c \\ 0 & 0 & 1 \end{vmatrix} \begin{vmatrix} x_i \\ \alpha_i \\ \Delta E/E \ i \end{vmatrix}$$

Value of A, B, C, a, b, c are function of ϕ and its derivative. Since entry and exit are on the same electrode and thus at the same potential, the relation $Ab - aB = 1$ should be valid. The values for the six elements of the matrix, A B ... are:

$$A = \left(\frac{d\phi}{d\theta} - 1 \right)$$

$$B = -R_o \cos \theta \frac{d\phi}{d\theta}$$

$$C = -R_o \cos \theta \ X \ P_o \frac{d\phi}{dE}$$

$$a = \frac{-1}{R_o \cos \theta} \left(\frac{d\phi}{d\theta} - 2 \right)$$

$$b = \left(\frac{d\phi}{d\theta} - 1 \right)$$

$$c = XP_o \frac{d\phi}{dE}$$

Second order matrix elements have also been calculated.

This ion optical element has three main features which are: reflexion, deflection and dispersion. By an appropriate choice of the parameters, the dispersion can either be reduced to zero or increased, leading respectively to a deflector or to an energy analyser. The complete work will be described in a paper to be submitted to the R.S.I.[7]

References

1. M. Baril and M. Fortin, Proc. of the International Conference on Mass Spectroscopy, Kyoto, 1969.
2. M. Fortin and M. Baril, to be published.
3. A.L. Hugues and V. Rojansky, Phys. Rev. 34, 284 (1929).
4. H. Wollnik, Focusing of Charged Particles, A. Septier ed., vol. II, ch.4.1.

5. W.E. Waters, Diamond Ordnance. Fuze Laboratories, Technical Rep. no. 525 (1957).
6. M. De Celles, Can. Jour. Phys. 48, 2192 (1970).
7. L. Bolduc, M. De Celles, M. Baril, to be published.

THE PLASMA CHROMATOGRAPH-MASS SPECTROMETER AS A QUALITATIVE ORGANIC ANALYSIS INSTRUMENT P6

Francis W. Karasek, University of Waterloo, Waterloo, Ontario
&
Martin J. Cohen, Franklin GNO Corporation, West Palm Beach, Florida

INTRODUCTION

The technique of plasma chromatography permits characterization and analysis of trace constituents in a gaseous mixture at atmospheric pressure. The instrumentation involves a positive and negative ion-molecule reactor coupled with an ion-drift spectrometer. Reactions occur between a generated reactant ion and the trace molecule to be detected. The ion-molecule complexes formed are separated in the ion-drift spectrometer and arrive at the spectrometer detector as ion peaks which are recorded as a plasmagram. Individual peaks can be directed into a quadrupole mass spectrometer for mass identification.

The first publications on plasma chromatography appeared only recently. Karasek(1) described the basic features of the method. Considerations attendant to coupling a gas chromatograph to the system are a subject of a recent paper by Cohen(2). A further paper by the above authors presents a study of the plasmagrams obtained for the compounds 1-octanol and 1-nonanol(3). An experimental correlation of plasmagram time of an ion-molecule complex to its mass has been reported by Karasek(4) and is further described by Kilpatrick(5). This method will be used for interpretation of the results obtained in this study. Cram(6) recently described experiments with the PC in which metal chelates of Al and Cr were identified as ion-molecule complexes with molecular weights as high as 2500 a.m.u. For a more complete description of the instrumentation one is referred to references (1), (2).

This study was undertaken to determine the qualitative aspects of the plasmagrams obtained for a series of compounds of very similar molecular weights but different molecular structures and functional groups. The molecular weights ranged from 122 to 128. These compounds were selected also to provide further data on the ion-drift behavior as a function of molecular weight.

Separation of the ion-molecule complexes formed is brought about by their different mobilities as they move through an inert gas at 760 torr under the influence of an electrical field. The detailed quantitative treatment of the mobility for such ions was given by Langevin in 1905; his equation predicts a polarization mobility limit which begins below a molecular weight of 100 as shown in fig. 1. A plot of a large amount of mobility data taken in the plasma chromatograph-mass spectrometer indicates that this limit does not occur and that mobility actually follows a curve inversely proportional to the 1/3 power of the ion-molecule mass (4,5). Recent work by Carroll and Mason(6) using a more complete form of the equation predicts that the mobility can be expected to follow an experimental curve such as that shown in fig. 1

This experimental and theoretical evidence for the validity of the curve of ion-mobility versus mass provides a basis for interpretation of the times of the plasmagram peaks in terms of mass units and the ion-molecule complex corresponding to that mass. For a given set of operating parameters in a plasma chromatograph the data of fig. 1 can be used for such interpretation.

RESULTS AND DISCUSSION

The data obtained for these compounds are indicated in the positive and negative plasmagrams shown in figs. 2-4. Mass assignments for the individual ion-molecule peaks were made from the correlation curve in fig. 1. Structures consistent with these masses and the most probable ion-molecule reactions creating them were assigned. Exact values for the sample concentrations were not obtained. The estimate that concentrations of organic compounds involved in these plasmagrams fall in the range of 10^{-7} to 10^{-11} molar parts is adequate for the purposes of the qualitative interpretation in these experiments.

The primary reactant ion for formation of the positive ion-molecule complexes is a mixture of the hydrated protons $(H_2O)_2H^+$ and $(H_2O)_3H^+$. The predominating species in any given sample run depends upon the concentration of water vapor reaching the reaction cell from both the sample carrier gas and sample itself. The reactant ions giving rise to the negative plasmagrams are predominantly the $(H_2O)_2O_2^-$ ions.

The positive plasmagrams of benzoic acid, salicylaldehyde and naphthalene indicate the concentrations of the compounds are low, as is shown by the presence of the reactant ion and a single peak of the ion-molecule complex formed. The benzoic acid forms ion-molecule complexes with the $(H_2O)H^+$; the salicylaldehyde and naphthalene, with $(H_2O)_2H^+$.

As either the concentration or reactivity of the organic molecule increases, the reactant ion-peak will decrease and even disappear, with the resultant formation of higher molecular weight ion-molecule complexes containing multiples of the trace molecules. This is shown in fig. 2 for the negative plasmagram of benzoic acid. The appearance of dimers and trimers at higher concentrations is also found to occur in chemi-ionization spectra.

Both salicylaldehyde and benzoic acid show that the molecular negative ion is formed by electron transfer, while the major ion-molecule species appear as different complexes formed with water molecules and the negative oxygen molecule.

The plasmagrams for naphthalene indicated in fig. 3 show a behavior that is exactly opposite to that found for benzoic acid. The positive ion-molecule reactions are the most favored. At a concentration of naphthalene sufficiently high to leave no reactant ion in the positive mode, there are no apparent negative ion-molecule reactions occurring. The negative plasmagram differs little from the reactant ion plasmagram of the blank. This behavior is consistent with that observed in the electron capture detector where hydrocarbons have little sensitivity.

The plasmagrams of these compounds contain a great deal of qualitative information. The patterns are characteristic of the compounds and their concentrations. When the negative plasmagram is obtained at the same time as the positive one, much more information is available. Even isomeric compounds have different characteristic patterns.

The plasmagram one obtains for a given compound is a sensitive function of its concentration. When this concentration is kept sufficiently low to retain a strong reactant ion peak in the plasmagram, the pattern is the simplest, usually consisting of the peak for one ion-molecule complex. Higher concentrations can be discerned by the disappearance of the reactant ion with the formation of more complex, higher molecular weight ion-molecule complexes.

These data strongly suggest that were one to deliver a definite concentration of an organic compound to the plasma chromatograph, perhaps via a chromatographic peak, it would be possible to run reference plasmagrams. These can then be used in the same way that one uses infrared, NMR. or mass spectra to identify an unknown compound by comparison of patterns.

CONCLUSIONS

All of these compounds studied give plasmagrams in both the positive and negative modes. These plasmagrams are not only characteristic of the sample molecules involved, but also provide an indication of reactivity between the reactant ion and sample under positive and negative reactant ion conditions. Further information relative to concentration and molecular weight of the sample molecules is given by their plasmagrams.

Work on a more definitive study of the quantitative aspects of plasma chromatography is in progress. Quite clearly, only the surface of the potential of this method has been explored here. A study of the selectivity and sensitivity possible when one uses different reactant ions for analysis of specific trace compounds promises to broaden the scope of the method considerably.

REFERENCES

1. F. W. Karasek, Res./Dev., 21, 34, March, 1970.
2. M. J. Cohen and F. W. Karasek, J. Chromatog. Sci., 8, 330 (1970).
3. F. W. Karasek, M. J. Cohen and D. I. Carroll, J. Chromatog. Sci., (IN PRESS).
4. F. W. Karasek, Res./Dev., 21, 25, December, 1970.
5. W. D. Kilpatrick, "An Experimental Mass-Mobility Relation for Ions in Air at Atmospheric Pressure", presented at the ASMS Meeting, May 2-7, 1971, Atlanta, Georgia.
6. D. I. Carroll and E. A. Mason, "The Theoretical Relationship Between Ion Mobility and Mass", presented at the ASMS Meeting, May 2-7, 1971, Atlanta, Georgia.

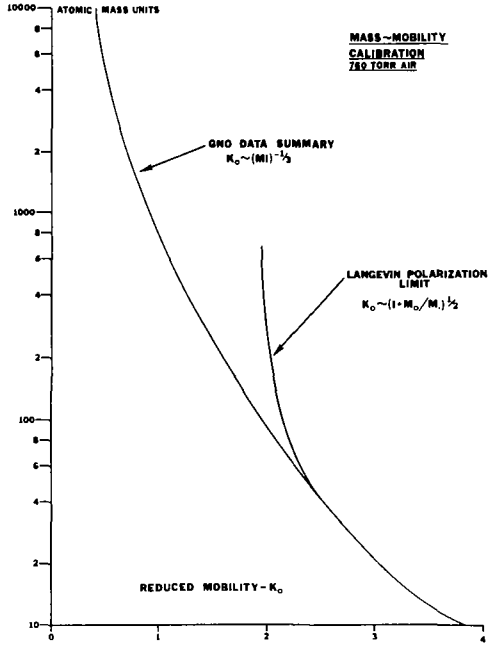

Figure 1. Comparison of the Langevin equation and experimental data in the PC.

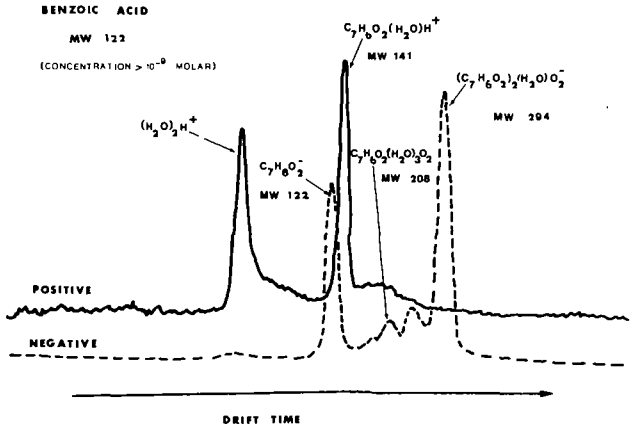

Figure 2. Comparative positive and negative plasmagrams of benzoic acid - high concentration.

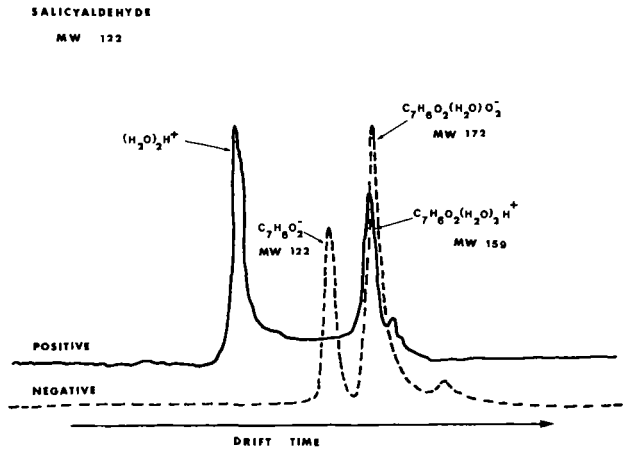

Figure 3. Comparative positive and negative plasmagrams of salicylaldehyde.

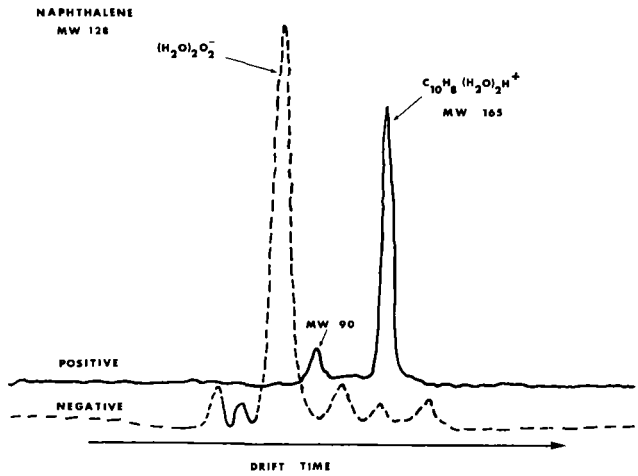

Figure 4. Comparative positive and negative plasmagrams of naphthalene.

TRACE GAS ANALYSIS

by

David B. Hughes, E. I. Du Pont and
T. D. Nowlin, NASA-Langley Research Center
Hampton, Virginia 23365

INTRODUCTION

This paper describes a sampling technique and associated apparatus for trace gas analysis that eliminate some of the difficulties experienced in conventional methods. It is well understood that the outstanding deterrents to a reliable trace analysis are instrument background and elution. The instrument background was nullified using the delta method of computation; that is, sensing the difference between two selected input pressure levels and their corresponding peak heights. Employing an X-Y plotter, total pressure was recorded on the X-axis and partial pressure on the Y-axis. A straight line is formed by increasing the pressure. The value of the slope thus obtained was used in lieu of the conventional peak height measurement. The elution or memory was overcome by using an all metal heated flow system through which new sample is continually flowing.

The analytical mass spectrometer used in this work was the CEC Model 21-104. Except for the addition of the specially designed inlet system, no modifications were required other than stabilizing the more critical electronics with a power line conditioner.

This method of gas analysis also eliminates four other major variables which are detrimental to performance. Therefore, the prominent variations appearing in the conventional batch analysis are as follows:

1. Instrument Background - H_2O, pump oil, CO, etc.
2. Elution - elution of previous sample gases from inlet manifold.
3. Sample Pressure - accuracy of measurement device.
4. Amplifier Noise - determination of exact peak intensity.
5. Amplifier Zero or Baseline Position - exact zero location.
6. Gas Mixture Composition - light molecules flow at greater rate; mixture composition always changing; thus requiring careful programing.

A review of the sequence of events in conventional batch operation further points out possibilities for impaired accuracy.

1. A background scan is run in the same manner as the sample scan.
2. Sample is introduced at least three times to elute and flush away previous gases.

3. The sample is introduced and pressure measured.

4. Valve to the leak is opened and scan is run.

5. The sample scan result is adjusted by subtracting background scan.

DISCUSSION

A more accurate trace analysis could be obtained using a conventional batch inlet manifold by applying the delta method with the expectation of canceling background. This can be accomplished by taking two separate scans of the sample at different pressures. The net height is then computed from the difference of the two peaks. It follows that the net pressure is the difference of the two input pressures. In the system developed by the authors, this procedure was taken one step further. Rather than taking just two points, many scans are run to obtain an infinite number of points yielding a straight line. In actual operation, the X-Y plot is produced by resting on a single peak while increasing the sample pressure.

A diagram of the system is shown in Figure 1. The sample is admitted to the capillary at a flow rate of 0.05 atmospheric cc/second. The gas passes through the check valve, which facilitates changing capillaries for other pressure ranges, to the leak cavity. The leak cavity consists of the volume formed by the "In" and "Out" ports, the pressure transducer housing, and the molecular leak. At full pumping speed, the sample pressure is reduced to about 1 torr. In the leak cavity, the flow must always be viscous in order that the partial pressures of each component in a mixture are an accurate representation of the input sample. Approximately 0.04 percent (1 part in 2500) of the total sample flows through the molecular leak to the ion source. Thus, the great bulk of the sample flows through the leak cavity and out to the pump eluting and flushing trapped gases.

The operating technique requires setting the mass spectrometer to a m/e that represents the trace component. By closing the micrometer valve the sample pressure can be increased in the cavity and the slope of the straight line produced on the X-Y plotter is dependent upon the peak intensity. Since peak height is a linear function of pressure, a deviation from a straight line indicates an error; this in fact provides a continual check of performance. For example, this could be due to drifting off peak, change in emission, or even a change in mol %.

The amplifier noise may be integrated by using a high time constant RC filter at the output of the amplifier. The ion current amplifier zero position only affects the Y-intercept, not the slope value.

Basically, the volume percent of each gas in a mixture is computed by comparison of the tangents of the unknown to a known concentration.

$$\text{Vol. \%} = \frac{10^2 \tan \theta_1 \cdot \Omega_2 \cdot \mu_1 \cdot \alpha}{\tan \theta_2 \cdot \Omega_1 \cdot \mu_2}$$

where:

θ_1 the angle formed by the X-axis and the line for the unknown gas

θ_2 the angle obtained using the known gas

Ω_1 the ion current amplifier input resistance used for the unknown gas

Ω_2 the input resistance used for the known gas

μ_1 the recorder attenuation used for the unknown gas

μ_2 the recorder attenuation used for the known gas

α the relative gas sensitivity factor

A high purity gas is selected to serve as the known quantity. The large dynamic range is obtained by switching amplifier input resistances and recorder attenuations. Gas sensitivity factors are applied when the calibration gas is not the same as the trace gas. Further dynamic range can be obtained through the use of minor isotopes.

To illustrate the principle, the concentration of N_2 in air can be determined by the following: Pure N_2 is admitted to the mass spectrometer and a 45° line, for convenience, is obtained by adjusting recorder parameters since the tangent of this angle is one. A dry air sample is then introduced with the mass spectrometer still resting on the N_2 peak. With the same parameters, a line is drawn at an angle whose tangent is 0.781, the decimal fraction of N_2 in air. Conventionally, we observe a mass peak in the form of arbitrary units or voltage output. The mass peak intensity is gross and must therefore be adjusted to a net value according to the aforementioned variables. Here the only concern is the slope created by an increasing pressure.

EXPERIMENTAL RESULTS

To establish the validity of this method, the percent of Argon in air as well as the Argon isotopes were determined. These were compared to the published values in order that the analytical capability of the system over a wide range of concentrations could be investigated. The sample consisted of dry air. The only sensitivity parameters that were changed during the analysis were the ion current amplifier input resistance and the recorder attenuations. The percent of Argon in air was within one percent of the published value. The limiting accuracy for routine analysis seemed to be the error in measuring the angle. Of course the accuracy is improved in calculating

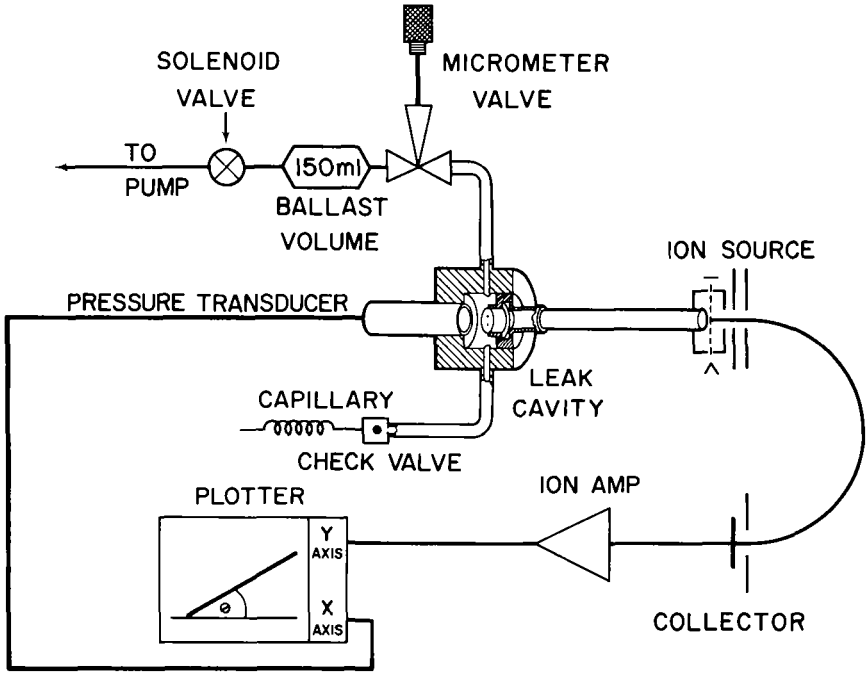
SOLENOID
VALVE
MICROMETER
VALVE
TO
PUMP
150ml
BALLAST
VOLUME
ION SOURCE
PRESSURE TRANSDUCER
LEAK
CAVITY
CAPILLARY
CHECK VALVE
PLOTTER
ION AMP
Y
AXIS
X
AXIS
COLLECTOR

FIGURE 1

the tangent by dividing the total Δy by the total Δx. Determination of the isotopic abundances of Argon in air are shown in the following table:

	ARGON ISOTOPES		
m/e	Nier (Ref. 1)	NBS (Ref. 2)	This Paper
36	0.307	0.35 ± 0.01	0.34 ± 0.01
38	0.060	0.08 ± 0.01	0.08 ± 0.01
40	99.633	99.57 ± 0.03	99.58 ± 0.02

The values for the isotopes obtained for this paper agree quite well with those obtained by Dibeler et al, of NBS. It is felt the accuracies shown here are quite good since the Argon 38 isotope represents approximately 7 ppm concentration in air and especially so when considering that the measurements made by the other investigators were made on pure Argon, two orders of magnitude greater in concentration.

CONCLUSIONS

This method has overcome the difficulties of instrument background and elution often encountered with the use of the conventional batch inlet systems. Individual values of the sample and calibration gas pressures are not used since the slope is substituted for peak height and pressure. However, a large amount of sample is required by this method and unique peaks are desirable. Only samples which can be introduced with a capillary may be analyzed.

The data obtained indicates that samples of gas, such as air, containing ppm trace components can be quantatively analyzed with improved accuracy. In many cases considerable time savings will result from the use of this method. Many component analysis can be performed with a measure of certainty that cannot be obtained with the conventional batch inlet system.

REFERENCES

1. A. O. Nier, Physics Rev. 50, 1041 (1936).
2. Vernon H. Dibeler, Fred L. Mohler, and Robert M. Reese,: Research Paper RP 1799, Vol. 38, June 1947, J. of Research of the National Bureau of Standards.

ACKNOWLEDGEMENT

The authors wish to express their appreciation to Melvin D. Kuhns for assistance in the design of the leak cavity.

Q2

SPARK-SOURCE MASS SPECTROMETER INVESTIGATION OF COAL PARTICLES AND COAL ASH

T. Kessler, A. G. Sharkey, Jr., and R. A. Friedel

Pittsburgh Energy Research Center, Bureau of Mines,
U.S. Department of the Interior, Pittsburgh, Pa. 15213

Samples of a Pittsburgh seam float coal dust and an ash prepared from the same float dust were analyzed by spark-source mass spectrometry. Spark-source mass spectrometry analyses were made on (1) various sizes of coal particles obtained from Pittsburgh seam coal and (2) various sizes of coal particles and a respirable dust* obtained from a mine in the Upper Freeport seam.

Float Coal Dust

A sample of float dust from the Pittsburgh seam was used to determine if coal dust can be analyzed directly. (Float dust is the term given to dust which is less than 74 μ in size and is readily obtainable in mines). A portion of the float dust was ashed in a platinum crucible in a muffle furnace at 500° C.

Thirty-two elements out of 68 detected at trace levels (0.1 to 200 ppm) in the dust and ash from the dust agreed to within a factor of 2 or better in concentration.

Whole Coal

Spark-source analyses were obtained of coal samples without ashing from single mines in the Pittsburgh and Upper Freeport seams. The concentrations of 24 elements determined in the whole coal by spark-source mass spectrometry were compared with published emission values for (the same elements obtained from) coal ashes from the same two seams.[1/] Twenty out of 24 elements determined in the Pittsburgh seam sample and 19 out of the same 24 elements in the Upper Freeport sample agreed within a factor of 5 or less. With the exception of Ga, the elements in disagreement were not the same in these two samples.

Concentration versus Particle Size

Representative samples of raw coal obtained from mines in the Pittsburgh and Upper Freeport seams were used to determine if the concentrations of trace elements change as a function of particle size. The samples were crushed, separated into 4 sizes less than 5 microns and 2 sizes greater than 5 microns, and spark-source mass spectrometry analyses performed.

For the majority of trace elements the concentrations are similar for the particle sizes investigated. The Pittsburgh seam samples have 27 elements with the same concentrations and 11 elements differing by a factor of 3 or less.

The only elements showing differences in concentration for the Pittsburgh seam samples are Be, U, and Pb. The Be concentration is lower in the < 1.0 μ fraction than in the other fractions. The U concentrations are lower in the < 1.0 μ and the 3.3-5.5 μ fractions by factors of 100 and 5, respectively, compared to the -250 μ and -44 μ samples. The Pb concentration in the < 1.0 μ fraction is higher by a factor of 10 compared to the other fractions. The Be, U, and Pb concentrations are as follows:

Fraction, μ	-250	-44	3.3-5.5	< 1.0
	ppm, weight			
Be	5	5	2	0.2
U	50	50	10	0.2
Pb	2	2	2	20.

The only elements showing differences in concentration for the Upper Freeport samples are Be and U. As with the Pittsburgh seam samples, the lowest concentration of Be occurs in the < 1.0 μ fraction. The U concentration is lower in the respirable range fractions (5 microns or less) compared to the larger size fractions; the same trend appears to occur in the Pittsburgh seam samples. The Be and U concentrations are as follows:

* Respirable dust has been defined as particulates that are 5 microns or less in size and are retained in the lungs.

Fraction, μ	-74	> 9.2	5.5-9.2	3.3-5.5	2.0-3.0	1.0-2.0	< 1.0
	ppm, weight						
Be	1	1	1	0.2	0.2	0.5	< 0.1
U	2	5	5	< 1	< 1	< 1	< 1

Respirable Dust

Because the atmosphere in a mine can contain in addition to coal dust other materials such as rock dust ($CaCO_3$), slate, etc., there is the possibility that respirable dust in a mine can have a different composition than coal dust of a similar size.

To determine if there are any differences in composition, samples of (1) respirable mine dust and (2) a coal dust of respirable size and of similar particle size distribution, prepared from a representative sample from the same mine, were analyzed. The respirable dust and coal sample were collected in a mine in the Upper Freeport seam of Allegheny County, Pa.

The elemental compositions of the respirable dust and a similar size coal fraction are very similar. The only major differences are for Ca, Ag, and B. The Ca, Ag, and B values for these samples are as follows:

	Ca	Ag	B
	ppm, weight		
Respirable dust	0.80%[a/]	50	10
Similar size coal fraction	0.33%[a/]	0.5	100

a/ Optical emission results

Calcium and Ag are higher in the respirable dust than in the prepared fraction. The concentration of B is lower in the respirable dust.

This investigation has shown that:

1. The presence of organic material does not interfere with the spark-source determination of certain elements in whole coal.

2. For one sample of Pittsburgh seam coal, the only elements showing a change in concentration with particle size are Be, U, and Pb. Be and U are lowest in the smallest particle size investigated (< 1.0 micron) and Pb is the highest.

3. For one sample of Upper Freeport seam coal, the elements showing a change in concentration with particle size are Be and U. Be and U are lower in the particles less than 5 microns in size compared to particles above 5 microns.

4. For one sample from an Upper Freeport seam mine, concentrations of Ca and Ag are higher and B is lower in a respirable dust than in a coal fraction having the same sizes of particles.

REFERENCE

1. Abernethy, R. A., Peterson, J. J., and Gibson, F. H., BuMines Rept. Inv. 7281 (1969).

Q3

Q 3 IN Elemental Analysis of Air Particulates Using Spark Source Mass Spectrography. E. R. BLOSSER, Battelle Memorial Institute, Columbus, Ohio 43201 and R. J. THOMPSON, National Air Pollution Control Admin., Durham, North Carolina 27701

Air particulates in ambient urban atmospheres have been studied extensively for the benzene-soluble components, and to some extent for selected inorganic constituents. The work reported here utilized spark source mass spectrography to perform nearly complete elemental analyses of particulates from six cities. In addition, cross check data for certain elements were obtained by optical emission spectrography, atomic absorption, wet chemistry, X-ray fluorescence, electron microprobe, gas mass spectrometry, and high resolution mass spectrometry.

To be submitted to Science for publication.

ION PROBE ANALYSIS OF SMALL PARTICLES

Q4

by

Michael A. Bayard

This paper is a preliminary outline of the problems experienced in the analysis of small atmospheric particles with the ion microanalyzer. It is based on a rather limited amount of data; therefore, some points may need refining in the future. Up to now, the electron microprobe has been the most useful tool for general elemental analysis of particles. The electron probe has a sensitivity on the order of 10^{-16} grams. With the electron probe, we have been able, with difficulty, to determine major components of particles as small as 0.1 μm. The ion microanalyzer will have somewhat similar size limitations, but it will give major and minor components of a 0.1 μm particle.

The first effect one notices when small particles are analyzed is a fall-off in intensity as smaller particles are examined. The beam in the ion probe is about 2 μm in diameter, 85-90% of the beam energy can be packed into this 2 μm circle. There is some energy available as far as 25 μm from the center of the beam. With an infinite sample, we see a signal from the periphery, as well as the central 2 μm. When particle size drops below 2 μm, the signal drops roughly as the reciprocal of the particle area. However, because the beam distribution is approximately Gausian, small (less than 1 μm) particles in the center of the beam give greater intensity than would be expected by calculating particle areas. Also, it seems that as particle diameter decreases, there is a slight additional contribution from the sides of a particle; the particle behaves as if it were larger than the measured diameter.

Things now become more complicated. If one can plot the measured area of a particle against intensity, it should, on the surface, be quite easy to note the size of an unknown and, from expected relative intensity, correct for this small size of the particle. Or, alternatively, one could simply ratio the measured intensities and determine the relative amounts of each element and then normalize. There is an effect that will tend to enhance the intensity of some elements. In the positive ion collection mode, negative ions will condense on the substrate. These negatives can be neutralized and then re-ionized by the primary beam and increase the measured intensity of the element. The effect can be quite large--an enhancement of a factor of 3 in some cases. This tends to make quantatative analysis difficult.

Another problem for the analysis of small particles is their survival time. If we are to look in detail for all elements in a sample, we would like to have a few seconds counting time on each isotope. This generally means a minimum of a few hundred seconds to look at each particle. As size decreases, the survival time approaches a few tens of seconds. For particles on the order of 1 μm, there should be no real difficulties. Survival times on the order of 500-1000 seconds with good count rates are possible. As size drops below this, the particle disappears roughly as the reciprocal of the area. There is some enhancement of erosion as the particle drops below 0.5 μm; and at 0.1 μm, we can expect the particle to exist for 5-50 seconds.

The sensitivity to trace elements in a particle is affected by particle size. Down to about 1 μm, we can still expect 1-10 ppm types of numbers. As we go below this size, the sensitivity drops rapidly. We cannot buy more sensitivity by increased count times, since our particle soon disappears. At 0.5 μm, sensitivity for an element that could be seen in a bulk sample at 1 ppm

is about 100 ppm. The condensation effect can increase sensitivity by a factor of 2-3 in a few cases. However, with present techniques, we are in poor shape for good trace analysis of small particles. (The electron probe will yield 5% type sensitivity on 0.5 μm particles).

The last problem to be considered is one of sample handling and mounting. The substrate must be chosen with care. There should be very low solid solution impurities which overlap the elements of interest, and even lower inclusion impurities. If a particle is mounted near an inclusion, both inclusion and particle may be analyzed as one. Another criterion is the surface finish of the substrate. A very good, pit-free surface is desirable so that the particle can be located with the optical microscope in the ion probe. Tantalum or an evaporated gold on glass film are two useful substrates.

Sample handling is usually straightforward. If a filter sample with a large number of particles is to be analyzed, the particles are simply dispersed on the substrate using a clean organic solvent, such as benzene. Sometimes the sample is freeze-dried from benzene to limit reagglomeration as the solvent dries. Single particles can be manipulated using etched tungsten needles. A single 1 μm particle can be mounted and analyzed with the ion probe.

In summary, the ion probe should prove to be a very useful tool for small particle analysis. Its sensitivity is roughly three orders of magnitude better than the electron probe. With considerably more data, it should prove possible to routinely perform quantatative analysis on particles less than 1 μm in diameter.

SPUTTER-ION SOURCE MASS SPECTROMETRIC ANALYSIS OF PARTICULATES

Frank G. Satkiewicz
GCA Corporation, Bedford, Massachusetts 01730

INTRODUCTION

Although the forte of the GCA Ion Microprobe Analytical Mass Spectrometer (IMS 101-B) is in the area of thin film analysis and composition profile studies, interest in air pollution extended to the mass spectrometry department through our Pollution Control Laboratory. One of the first things obtained several years ago was the composition of fly ash from a coal fired power station. Later, several samples of particulates were examined. Since a concerted effort was not made in this area, the results set forth in this paper are exploratory in nature and serve merely as an introduction to the potential capabilities of the IMS 101-B.

PRINCIPLE OF TEST SIGNAL GENERATION AND DETECTION

A source of high energy noble gas ions (in this work 10 KeV Ar^+) generated in a Duoplasmatron is directed at the target of interest whereupon sputtering occurs. From an exchange of momentum +, −, and neutral atomic and polyatomic species are generated. In the IMS 101-B, the + (or −) ions constituting the secondary ion beam is focused onto the entrance slit of a double-focusing mass spectrometer.[1-3] (Normally, a resolution of 700 at half peak intensity is employed.)

By sweeping the magnetic field from 0-10,000 gauss, the charge to mass separated ions impinge on a multiplier coupled to a vibrating reed electrometer and then to an X-Y recorder. In normal operation, it takes about fifteen minutes to obtain a spectrum in the range of 1-240 amu. Depending on the nature of the solid and the primary beam flux density, 0.05 μg - 5 μg of material is consumed in obtaining a spectrum. In this work, the lowest sputtering rates were used for all but a flyash sample.

THE ENERGY WINDOW

In order to properly interpret an ion spectrum obtained by sputtering, due consideration must be given to the nature of the secondary ion energy distributions.

After having observed different spectra from the same material, Poschenrieder and his co-workers made a systematic study of the initial ion energy distributions.[3,4] This was done by reducing the energy bandwidth in the spectrometer and recording the intensities of various ion species with initial ion energy. It was found that in general the distribution for elemental ions is very broad and very narrow for complex polyatomic ions; the distribution for simple polyatomic ions such as XO^+ or XH^+ was found to be intermediary. For a normal setting of a 50 eV bandwidth which can be moved along the distribution curve (accomplished electronically), one can obtain spectra consisting of elemental ions or one which includes both. This is illustrated for silicon monoxide.

Figure 1 is an atomic spectrum showing major intensities (log-linear) of singly and multiply charged Si and O, with far lower intensities of the simple polyatoms of SiO^+ and Si_2^+. By moving the energy window out further, the latter species will be further suppressed. It can now be seen that the detection limit for impurities such as $Sc^{45,+}$, $Fe^{56,+}$, and $Ni^{58,+}$ in SiO depends on the shapes of the respective distribution curves of SiO^+, and Si_2^+. By varying the energy window in the proper manner, the exact nature and degree of interference can be determined. There are many instances

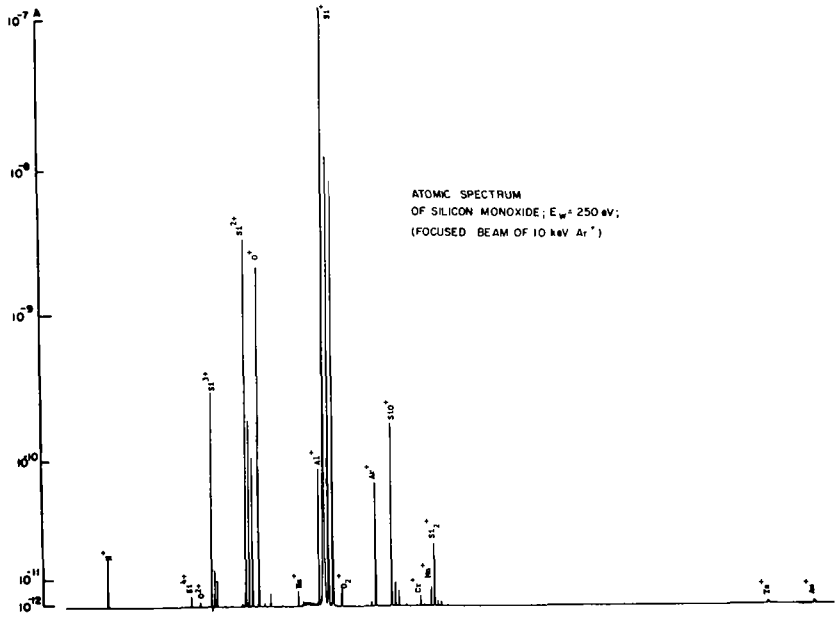

Figures 1 and 2

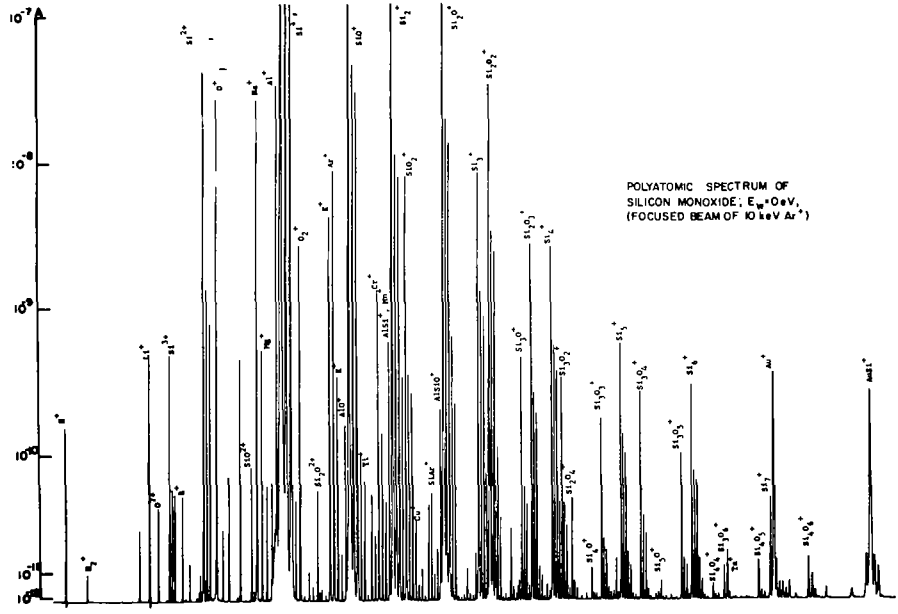

where polyatomic interferences can provide approximately the same isotope ratios as a suspected impurity, so the latter is not sufficient for positive impurity identification.

By moving the window in the neighborhood of 0 eV, a polyatomic spectrum characteristic of silicon monoxide (see Figure 2) is obtained. This is reproducible and provides a way of obtaining insight into the bonding characteristics of the solid. This has been used to evaluate differences in stoichiometry and to establish the nature of solids in thin film form.[5,6]

Thus, the spectrum for SiO_2 shows polyatomic ion intensity distribution differences over SiO, etc., providing the basis for interpreting films of Si contaminated with O_2, SiO films, and SiO_2 polycomponent systems of the latter.

SAMPLE DESCRIPTION AND PREPARATION

The following samples were analyzed:

1. Flyash from a coal-fired power station's precipitator hopper. A small portion was pelletized (no additives or binders) and examined directly. Alternatively, a small amount could have been sprinkled on a pure gold or tantalum substrate.

2,3. Bedford, Massachusetts air particulates (inside GCA laboratory air and air outside the building) were collected by impaction on a tantalum substrate by Dr. P. Lilienfeld. The particulates from approximately one cubic meter of air for each sample formed a round spot about 1/32" diameter. The results for these samples will be discussed in more detail since the idea of obtaining composition data following particulate concentration determination by impaction appears very desirable. The analyses were performed by direct sputtering of the particulates.

4,5. Particulates from unknown sources collected on organic and inorganic filters (provided by Dr. Enrione of NAPCA) were examined by sputtering a small piece of the filters which were placed on tantalum. The defocused beam was directed at each assembly so that approximately equal areas of the sample and substrate were sputtered. Charge-up of the sample was prevented in this way. Alternatively, the charge compensation filament could have been employed.[3]

ANALYSIS PROCEDURE

After placing the sample in the target chamber and pumping down to 4×10^{-7} Torr or less, sputtering is started. If the instrument was adjusted for a previous analysis, a spectrum can be obtained immediately; if not, a peak is located by sweeping the magnet and secondary ion optics parameters varied to provide maximum intensity. By using the defocused beam, the sample can be analyzed at a leisurely pace. It takes fifteen minutes at the normal scan rate to obtain a spectrum (1-240 amu). The results can be qualitatively evaluated at a glance providing the groundwork for changing emphasis in the procedure if necessary. This includes varying the energy window, directing attention to the intensity history of selected species, etc.

A typical spectrum is shown in Figure 3. Note that the intensity axis covers 5-6 orders of magnitude so that matrix and impurity elements are recorded without switching. At an energy window of 100 eV, the spectrum is mainly atomic in nature; peaks followed by (B) are derived from the substrate. In obtaining this spectrum, a uniform

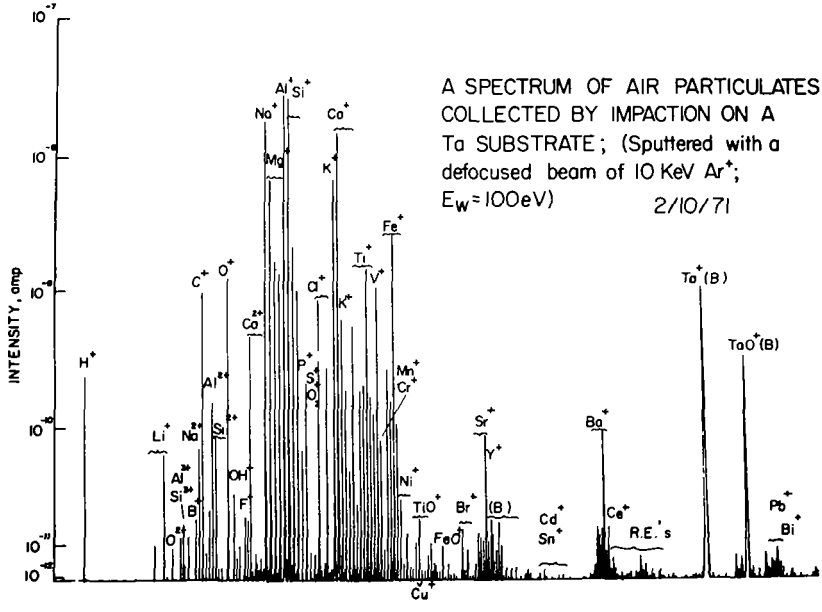

Figures 3 and 4

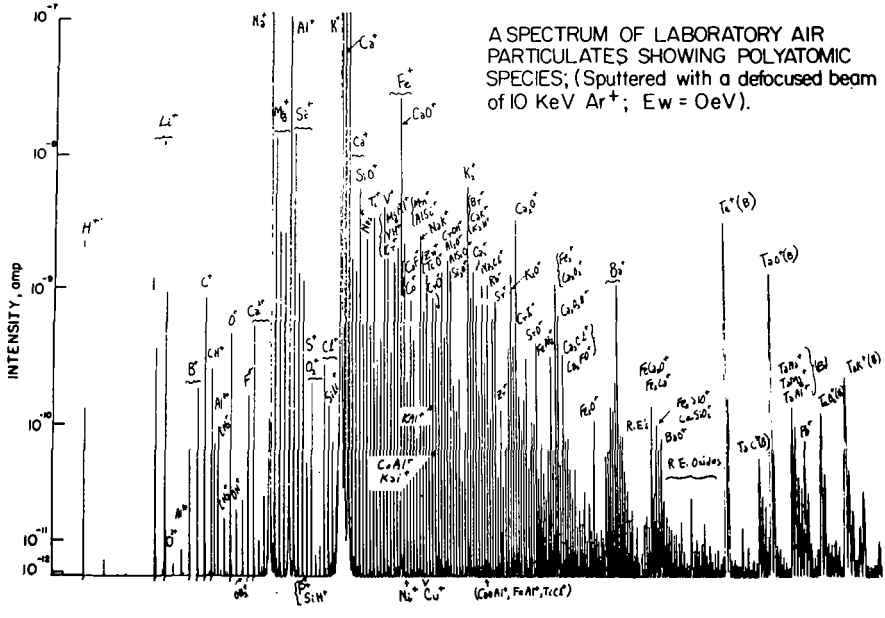

depth element of about 1000Å was removed leaving the bulk of the sample intact. Despite the presence of a strong $C^{12,+}$ peak derived from the organic portion of the particulates, interferences from complex polyatomic ions are negligible at this energy window.

A typical polyatomic spectrum of particulates is shown in Figure 4. Although complicated, a detailed study of the spectrum can result in helping identify the major bonding form in the particulates. In this instance, the predominant bonding is through oxygen although significant amounts of P, S, Cℓ and Br are present. The presence of combination peaks such as $A\ell SiO^{+}$ and $CrTi^{+}$ shows intimate bonding for these elements such as is found in glasses or minerals. Clearly without control of the energy window, a positive approach to the interference problem and trace identification is more complicated.

CALCULATION OF CONCENTRATIONS FROM INTENSITIES

The spectra provide intensities which can be converted to concentrations with the proper choice of sputter-ion yield factors. The problem is not simple and proper discussion of such a subject is beyond the scope of this paper. Ideally, a calibration standard containing approximate but known concentrations of impurities in the bonding form in the particles is desirable. In many instances this can be achieved with relative ease, especially with metallic samples. For example, the sputtering of a series of Cu-Aℓ alloys containing from 0-12 atomic % of aluminum revealed a linear relation with the $A\ell^{+}$ intensity at energy window settings for elemental ion spectra.[7] These results and others in this laboratory suggested that as long as the bonding form of the element in question is the same in the concentration range of interest, the sputter-ion yield will be a constant; accordingly, calibration is an easy task.

For the particulates, calibration samples could be prepared by fusing known quantities of oxides or sulfates of the elements in a glass matrix.[3]

In the absence of specific calibration samples, the ion yield factors obtained from the sputtering of the elements or selected compounds can be used as a first approximation.

Figures 5 and 6 show relative yield factors of the major isotope of many elements. This has been drawn from personal experience and intuition. Elements with triangle identification are educated guesses for the yields.

As can be seen, the highest ion yields are from the noble gases, the alkali metals, and alkaline earths. A general correspondence with atomic volumes of the elements was observed, i.e., the higher the atomic volume, the higher the ion yield. The poorest ion yields are from elements such as As, and Cd. It must be stressed, however, that these are values for Ew=250 eV and for elements. For elements having narrow distribution such as Pt and Au, the intensities at low energy window are significantly higher.

There is also a possibility that in trace amounts the ion yield may be considerably higher than for the element. This is suggested in the result for Rh. This value was obtained from sputtering an NBS doped platinum sample #681. A plot for oxides of many elements would appear somewhat similar since we have observed parallel intensity enhancement in oxygen in many experiments. For example, Figure 7 shows the enhancement of B and Si in B-doped Si when sputtered in increasing oxygen pressure. The use of oxygen for chemically enhancing intensity is good only for those elements

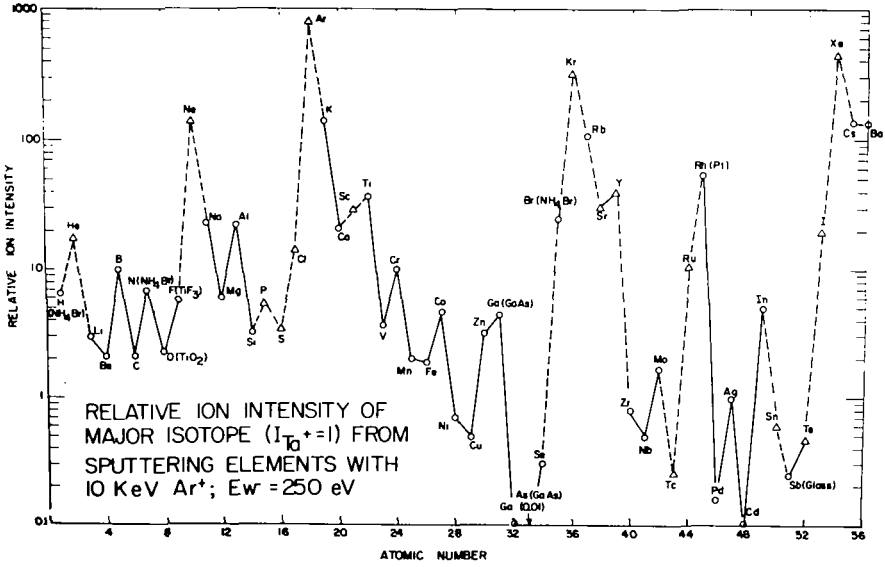

Figures 5 and 6

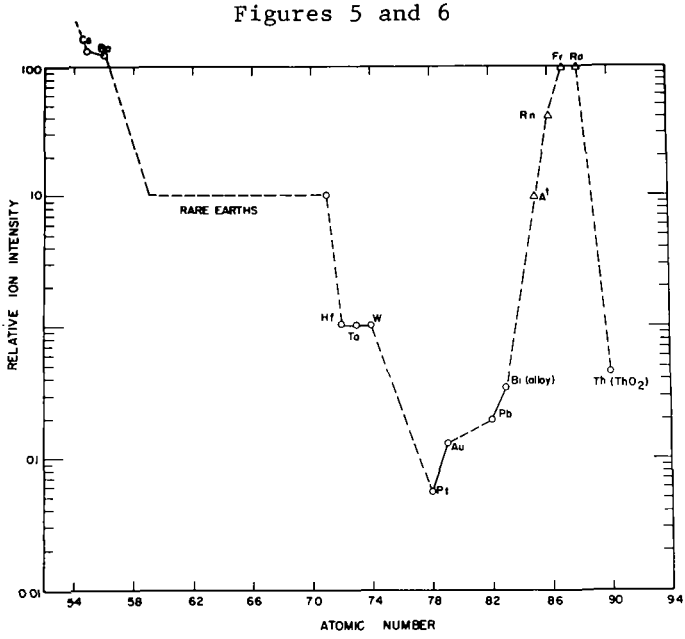

which normally react with O_2; thus, no effect at all is observed sputtering GaAs in the presence of oxygen.

Sputter-ion yield data based on the above considerations were used in the following equation to calculate the atomic fraction, f, of the elements:

$$f_X = \frac{\frac{I_Y^+}{Y_X^+}}{\frac{I_X^+}{Y_X^+} + \frac{I_Z^+}{Y_Z^+} + \cdots \frac{I_A^+}{Y_A^+}} \qquad (1)$$

where I_X^+ is the ion intensity of the major isotope of the element in question, and Y_X^+ is the sputter-ion yield relative to tantalum. The other I's and Y's are for the rest of the peaks associated with the particulates.

The f's were converted to Ppm by weight from:

$$\text{Ppm X(weight)} = 10^6 \left(\frac{m_X}{\bar{m}}\right) f_X \qquad (2)$$

where m_X is the mass of the major isotope of X and $\bar{m}$ is the average mass calculated from:

$$\bar{m} = f_X m_X + f_Z m_Z + \cdots\cdots f_A m_A \qquad (3)$$

RESULTS

Table I shows the composition of Bedford laboratory air particulates. The same sample was analyzed in 1969 and later in 1971. The particulates are mainly O, Mg, Aℓ, Si, Ca and Fe, with significant amounts of C, P, S, V, and Pb. For the above species, the differences noted in concentration are larger than the expected reproducibility and suggest that smaller particles of somewhat different composition may be coating large particles. For any of the elements of interest such as Ca, the intensity variation as a function of time can be observed. This provides a statistical evaluation of the signal and gives an idea about homogeneity of composition.

If collection by impaction is carried out, it should be possible to obtain simultaneously, particulates in selected particle size ranges. Subsequent microprobe analysis would provide information on the composition of these distributions.

Table II shows the elements detected in summary for the samples examined. The origin of the particulates on the filter papers is not known, however, the unusual amounts of species such as Pb and Cu suggest a source probably other than the atmosphere. The last column is derived from data presented by Morgan et al.[8]

The question of how good the results are can be answered in terms of the nature of the sample and its substrate and the instrument parameters used in the analysis. Some of these have already been discussed, such as sputter-ion yield factors. If the latter are unreliable, the data must be qualified, but relative results are quite valuable. However, there is no reason why a good calibration cannot be carried out. The precision of the results depends on the signal strength for a given primary beam density. In sputtering a homogeneous sample with a defocused beam, multiplied signals of 10^{-12}

Dependency of Intensity on Oxygen Partial Pressure; Sputtering of B-Doped Si With 10 KeV Ar^+

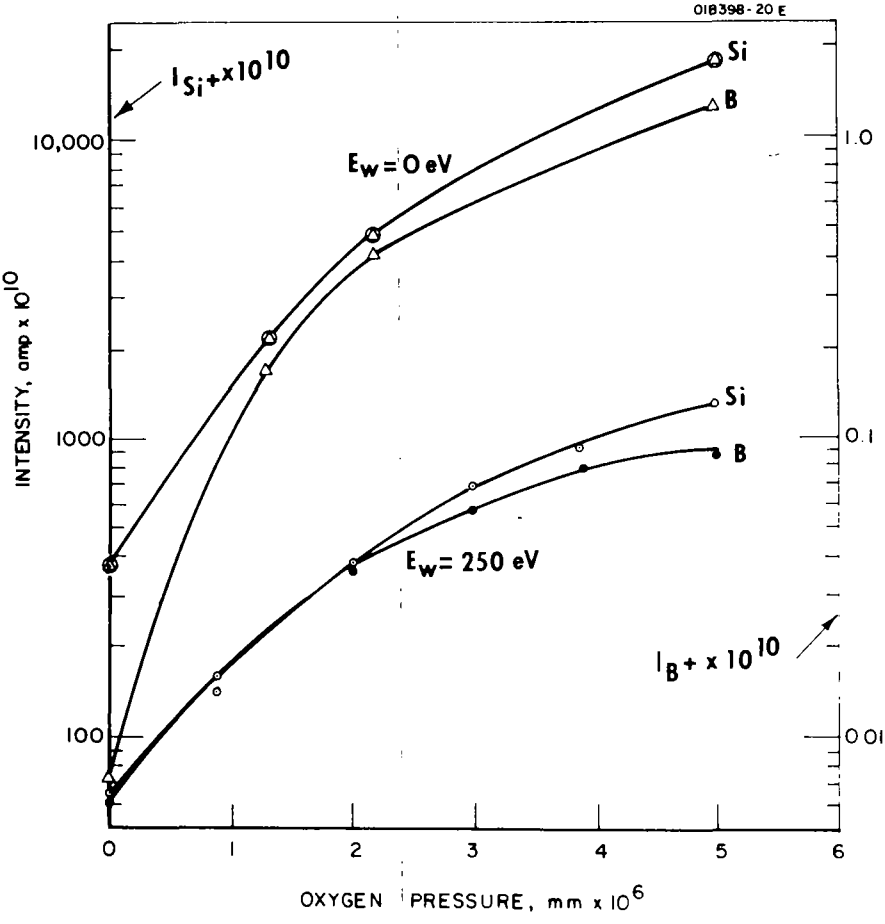

Figure 7

amp can be interpreted as approximately ± 50 percent in a normal scan. The detection limit will average approximately 50 ppm atomic using the atomic energy window setting.

To work in the ppm range requires either focusing the beam or moving the energy window. The latter will be possible only when interferences are excludable and will not be possible in a wide mass range.

The former must be approached with caution. For small amounts of sample without a disbursing matrix, the focused beam may result in a change in reference intensity due to penetration to a substrate; in addition, the sample will be strongly heated with possible preferential removal of volatiles. This would obviate one of the major advantages of sputter-ion source spectrometry. In addition, the use of a homogeneous defocused beam and an extraction diameter that is as large as the beam, secondary ion sampling occurs over a larger and more representative area.

In summary, the analysis of a very small but statistically meaningful, samples can be accomplished for elements in the 10-50 ppm range employing a low primary flux density and in the 0.1-1 ppm range using a focused primary beam.

REFERENCES

(1) "Solids Mass Spectrometer," Herzog, R.F.K., Poschenrieder, W.P., Liebl, H.J., and Barrington, A.E., NASA Contract NASw-839, GCA Technical Report No. 65-7-N, 47 (1965).

(2) "The Ion Microprobe Mass Spectrometer," Barrington, A.E., Herzog, R.F.K., Poschenrieder, W.P., Progress in Nuclear Energy Series IX, Analytical Chemistry, 7, Pergamon Press, New York (1966).

(3) "Mass Spectrometer Analysis of Solid Materials with the Ion-Microprobe Sputter Source," Herzog, R.F.K., Poschenrieder, W.P., Satkiewicz, F.G., NASA Report CR-683 (January, 1967).

(4) "Recent Results Obtained with the Sputtering Ion Source for Solids," Herzog, R.F.K., Poschenrieder, W.P., Ruedenauer, F.G., and Satkiewicz, F.G., Porceedings of the 15th Annual Conference - Mass Spectrometry, Denver (May, 1967).

(5) "Sputter-Ion Source Mass Spectrometer Studies of Thin Films," Satkiewicz, F.G., Technical Report AFAL-TR-69-332 (1970). (Air Force Avionics Laboratory, WPAFB, Ohio).

(6) "Chemical and Microstructural Characterization of Photoconducting Lead Sulfide Films," Smith, D.K., Blount, G.H., Yamada, R.T., Santa Barbara Research Center Technical Report AFML-TR-68-26, (September, 1968). (Wright Patterson Air Force Base, Ohio).

(7) Satkiewicz, F.G., unpublished work.

(8) "Air Pollution Surveillance Systems," Morgan, G.B., Ozolins, G., Tabor, E.C., Science, 170, 289 (1970).

TABLE I

Sputter Ion Source Mass Spectrometer Examination of Laboratory Air Particulates on a Tantalum Substrate (Defocused beam of 10 KeV Ar^+; Ew = 100 eV).

Species, X^+	$I_{X^+} \times 10^{10}$ amp		Parts per million (weight)	
	10/30/69	2/10/71	10/30/69	2/10/71
Li^+	0.6	0.7	800	200
B^+	0.1	0.3	100	40
C^+	3.8	10	29000	10000
O^+	2.2	13	220000	180000
F^+	0.02	0.2	70	80
Na^+	14	190	8400	15000
Mg^+	7.5	70	36000	51000
Al^+	28	300	45000	67000
Si^+	23	280	250000	420000
P^+	0.08	0.7	15000	19000
$S^+ + (O_2^+)$	0.27	2.0	28000	28000
Cl^+	0.9	9	6700	9200
K^+	36	70	6900	1800
Ca^+	80	160	180000	53000
Ti^+	3.2	16	5200	3600
V^+	0.9	11	16000	26000
Cr^+	0.2	0.8	1200	820
Mn^+	0.2	1.6	6000	8600
Fe^+	3.4	28	130000	150000
Ni^+	0.035	0.3	3600	4300
Co^+	0.04	0.05	700	230
$Zn^+ + (TiO^+)$	0.09	0.2	2500	680
Cu^+	0.03	0.1	5000	2200
Br^+	0.015	0.16	300	400
Sr^+	0.12	0.9	130	140
Y^+	0.03	0.1	100	40
$Cd^+ + (Fe_2^+)$	0.01	0.02	13000	3900
Sn^+	0.01	0.01	700	90
Ba^+	0.28	1	350	180
Ce	0.05	0.17	350	140
R.E.'s	0.05	0.2	350	180
Pb^+	0.03	0.09	39000	16000
$Bi^+ + (TaSi^+)$	0.04	0.03	29000	3300

TABLE II

Summary of Particulates Composition; Parts per Million (Weight)

	Brayton Point Flyash	New York City*	Bedford Lab Air	Bedford Outside Air	Particulates on Org.Filt.	Part. Inorg. Filt.	Mean Urban Part.
Li	10	10	500	50			
B	40	140	70	80	150	1000	
C	4000	19000	20000	6000	39000	3400	
O	350000	85000	200000	69000	130000	84000	
F	7	80	75	30	30	100	
Na	40	1400	12000	25000	2800	4900	
Mg	4600	15000	44000	64000	19000	9000	
Aℓ	150000	55000	60000	87000	23000	22000	
Si	340000	400000	350000	510000	150000	660000	
P+(SiH)	700	7300	17000	12000	18000	3000	
S+(O_2)	1000	10700	28000	12000	10000	18000	32000
Cl	ND	16000	8000	3900	480	7000	
K	150	1900	4400	2400	2800	670	
Ca	33000	120000	120000	53000	43000	92000	
Ti	4200	3200	4500	3300	600	800	400
V	730	16000	21000	20000	900	1400	500
Gr	290	1400	1000	480	300	100	150
Mn	310	5500	7500	4900	7300	1700	1000
Fe	130000	260000	140000	130000	84000	27000	15800
Ni	250	2700	4000	3000	1400	200	340
Co	10	100	500	60	70	20	< 5
Cu	100	1900	4000	1300	22000	500	900
Zn+(TiO)	~100	200	1100	700	800		6700
Br	ND	340	350	260	100	1400	
Rb	3	6		9			
Sr	460	300	140	85	150	430	
Y	100	30	70	30	40	20	
Cd+(Fe_2)	< 50	600	8000		16000		20
Sn	< 5	40	400		870		200
Ba	300	230	270	150	270	6200	
Ce	200	100	250	150	240	50	
R.E.s	200	200	270	200	700	60	
Pb	ND	5500	28000	30000	440000	20000	7900

*Sample supplied by Dr. J. Wagman of NAPCA.

Q7

MS Identifaction and Measurement of Polynuclear Aromatic Hydrocarbons In Air Pollutants

by
R.F. Pottie, Division of Chemistry,
National Research Council, Ottawa, Canada
and
R.C. Lao, and J.L. Monkman
Air Pollution Control Division,
Department of Fisheries and Forestry, Ottawa, Canada

Introduction

Despite the importance of polycyclic aromatic hydrocarbons (PAH), which contain five or more rings, as air pollutants, little attention has been given to the mass spectra of individual PAH compounds. Thus we can only find two standard spectra in the literature those for perylene and benzo [a] pyrene (BaP) as compared to the ten or more isomeric compounds of the formulae $C_{20}H_{12}$ or $C_{22}H_{12}$ which are likely to appear in the "benzo [a] pyrene fraction" of air pollutants. (1) We have, therefore, initiated a study to obtain mass spectra for these compounds, and to evaluate the mass spectrometric techniques as an aid to the analysis of PAH in air. The model systems, reported here, included mixtures of BaP, benzo [e] pyrene (BeP) and benzo [k] fluoranthene (BkF). It is usually of most interest to determine BaP, since it is carcinogenic. The chromatographic resolution of BaP to seperate from BkF is incomplete. Also, mutual interferences occur when UV absorption or fluorescence is the analytical method that is used for their measurement. BeP is included, since it is usually found with BaP and BkF in the same eluate fractions from the column chromatography.

Experimental

The mass spectrometer used in this study has been previously described (2). A solid probe was designed and built for the direct introduction of these samples. Mixtures were prepared by weighing individual components and dissolving in cyclohexane, followed by evaporation and transference of the solid to the probe. Sample sizes were less than a microgram for the pure compounds and synthetic mixtures, and quantities were of the order of a nanogram for the partially resolved column fractions from polluted air. Probe temperatures were approximately 100°C, with no changes in spectra occurring over the range 75°-130° C.

Results

Some 20-30 spectra were recorded for each compound with deviations of less than ±5% from the averaged peak height ratios for an individual scan. The averaged spectra for the major peaks are listed in Table 1. Complete spectra will be published elsewhere (3). Fragmentation patterns of all three PAH are very similar, and the relatively intense ions in the region m/e 113-126 attest to the high degree of multiple ionization in these compounds.

The ionization potentials were nearly equal (7.3-7.7 ev) and no trend could be found that would relate resonance energies to carcinogenic activity. A similar lack of correlation has been observed with other physical methods (4).

Although the mass spectra of these three PAH are similar, sufficient differences occur in selected peak ratios to permit their qualitative and quantatative measurement. Some of these are summarized in Table 2, and it can be seen by inspection that only a relatively small number of peaks are required to obtain the composition of mixtures of these compounds.

Thus, a number of mixtures were prepared with known composition. Mass spectra were obtained for the vaporized material and the compositions were calculated by reference to the data in Tables 1 and 2.

Results are shown in Table 3. The average deviation in the percentage compositions obtained from the mass spectra was approximately ±5%. The error in preparing the original mixtures is estimated to be of the order of±1%. The compositions correspond very well within these error limits, and the results are very encouraging in view of the similarities of the spectra.

The technique was tested further by analysing the column chromatographic fractions of air samples collected in urban environments. One such study is summarized in Table 4. The results were entirely consistent with UV absorption and fluorescence analysis of the trapped column fractions.

We intend to pursue these studies by extending them to other PAH that are present in air.

Table 1: MASS SPECTRA OF PAH

m/e	Relative Abundance		
	BaP	BeP	BkF
252	100.00	100.00	100.00
250	19.34	23.95	16.69
226	2.33	2.17	1.90
225	2.27	1.65	1.99
224	3.06	2.94	3.21
126	16.39	14.47	20.56
125	11.46	15.53	12.65
113	8.26	7.95	7.76

Table 2: RATIOS OF SELECTED PEAKS IN THE MASS SPECTRA OF VARIOUS PAH

Compound / Peaks Ratio	BaP	BeP	BkF
250/252	0.1934	0.2395	0.1669
113/126	0.5039	0.5494	0.3774
113/125	0.7207	0.5119	0.6134
125/126	0.6992	1.073	0.6125

Table 3: COMPARISON OF COMPOSITION OF SYNTHETIC MIXTURES WITH THAT OBTAINED BY MASS SPECTROMETRY

Mixture no. / PAH & Composition %	I		II		III		IV		V	
	Known	M.S.	Known	M.S.	Known	M.S.	Known	M.S.	Known	M.S.
BaP	25.13	23.38	50.22	53.67	74.83	78.92	74.42	68.73	51.38	48.62
BeP	-	-	-	-	-	-	25.58	31.27	17.41	18.88
BkF	74.87	76.62	49.78	46.37	25.17	21.08	-	-	31.21	32.50

Table 4: MASS SPECTROSCOPIC ANALYSIS OF ALGAE SAMPLE VII, 1969.

Fraction No. / Composition % / PAH	108-118	123-133	134-150
BaP	72.73	19.47	13.20
BeP	22.07	41.37	4.17
BkF	5.20	40.16	82.63

References

(1) API Table 1020, Atlas of Mass Spectral Data No. 1755

(2) P.E. Knewstubb and A.W. Tickner, J. Chem. Phys., 36, 674 (1962)

(3) To be submitted for publication in International Journal of Environmental Analytical Chemistry

(4) A. Pullman and B. Pullman p.9; E.D. Bergmann p.72 in "The Jerusalem Symposia on Quantum Chemistry and Biochemistry" vol.1 "Physico-Chemical Mechanisms of Carcinogenesis", The Israel Academy of Sciences and Humanities. Jerusalem (1969)

R2

AN IMPROVED TWO-STAGE MASS SPECTROMETER FOR ISOTOPIC RATIO MEASUREMENTS

J. D. Stein, F. O. Halliday
General Electric Company, Vallecitos Nuclear Center
Pleasanton, CA 94566

ABSTRACT

A two-stage magnetic analyzer has been designed and constructed for research in the measurement of heavy element isotopic ratios. The analyzer consists of two symmetric 90° sector, 15-in. radius of curvature, homogeneous field electromagnets with circular field boundaries, normal entry, and fringing field clamps. Construction features and ion optics are described and performance factors given.

INTRODUCTION

When performing isotopic analysis in our laboratory it is often necessary to measure a low abundance isotope adjacent to one that is as much as 10^6 times more abundant. A good example is the analysis of isotopes produced by neutron capture. The major limitation in these analyses is that collisions with either residual gas molecules or the vacuum chamber walls scatter ions from a major peak into the small peak being measured. The ability to detect isotopes of low abundance is called abundance sensitivity, and is defined as the ratio of the detected ions of mass M to those of mass M±1 when only mass M ions are present.

In a spectrometer with a single 15-inch radius magnet operating in the uranium mass region, the abundance sensitivity is approximately 10^4 or 10^5 to one. When two such magnets are run in tandem, the abundance sensitivity ranges from 10^5 to 5×10^6. If an electrostatic lens or prism is added between the final magnet and detector the abundance sensitivity may increase from 10^7 to as high as 10^9.

A number of multistage instruments have been constructed,[1,2] however virtually all of them have used wedge-shaped homogeneous magnetic fields with straight field boundaries and normal beam entry. Since shortly after World War II investigators have discussed improving the focal property of magnetic lenses by giving the magnets appropriate detailed shaping. Most of the improvements in ion optics and magnet design, however, have occurred not in mass spectrometry, but in the development of beam transport systems for high energy particle physics. This article will comment on the possibility of improved ion focusing by homogeneous field magnets and will discuss the design and construction of a three-stage mass spectrometer.

DESIGN CONSIDERATIONS

The general consideration of this mass spectrometer system was that it should be capable of measuring isotopic ratios with a high abundance sensitivity, $\gtrsim 10^7$, without sacrificing high ion transmission. In addition it was desired that the system be designed with sufficient flexibility to allow its use as an engineering instrument for the development and testing of a variety of sources and detectors.

Specifically desired instrumental characteristics were:

1. Analysis of singly charged ions of up to mass 250 with energies of 15 keV.
2. An operating vacuum of 10^{-8} torr or below - to reduce gas scattering.
3. Focusing both in the plane of the magnet and perpendicular to this plane to insure high transmission.
4. Provision for monitoring the beam at each focal point.
5. Minimum fringing field in the source and detector regions.

ION OPTICS

Neglecting fringing fields it is possible to construct a magnetic field shape that will focus ions from a monoenergetic point source to an object point with a large angular acceptance. Figure 1 shows a sketch of such a design with a source to detector distance of $2\sqrt{2}$ times the radius of curvature R. As Figure 2 shows, a conventional magnet with straight pole boundaries is only a first order approximation to this ideal curve. It can be demonstrated that the geometrical aberration shown is a widening of the image equal to $\alpha^2 R$ where α is the half-angle of acceptance[3]. For a 15-inch radius of curvature magnet and an angular divergence of $\mp 1°$, a beam broadening of approximately 0.005 inch occurs.

By approximating the ideal field boundary with circular pole faces, a geometrical aberration is reduced to $\alpha^3 R$ for a 90° magnet. The image broadening of a 15-inch magnet is then reduced to approximately 0.0001 inch.

With most sector magnets, compensation for the fringing field is made by moving the magnet in a direction bisecting the sector angle. This is not possible in a circular pole edge magnet without perturbing its focusing properties. To solve this problem, fringing field clamps were designed for our magnets which force the effective magnetic field limits to correspond to the actual pole edge. These fringing field clmaps or shunts have three other advantages:

1. They significantly reduce the magnetic field strength in the source and detector regions.
2. They shield the beam from stray magnetic fields generated by the coils, allowing a very compact magnet design.
3. Uncompensated fringing fields usually defocus the ion beam in the vertical direction. The clamps reduce this effect.

Figure 3 shows a plan view of the geometry chosen for the two electromagnets constructed for our spectrometer.

PHYSICAL DESCRIPTION

The physical arrangement of this mass spectrometer is shown in Figure 4. It consists of two symmetric 90° sector magnets arranged in the zero dispersion configuration with an electrostatic vertical focusing lens between them. The magnetic analyzers are followed by an electrostatic retardation lens which reflects ions which have lost energy through collisions. After passing through the retardation lens the ions are detected by a Daly-type detector.[4]

A Dietz type single filament source is used.

The retardation lens and the center lens are both simple three element lenses with the outer elements operated at ground potential. The center lens operates at a few hundred volts while the retardation lens operates at a few tens of volts less than the ion accelerating voltage.

Except for the sample lock, the entire vacuum envelope is constructed of OFHC copper and 304 stainless steel with metal gasket seals. A large part of the vacuum envelope consists of modified commercial fittings to allow experimental flexibility. The system is pumped by three 80 liter/sec ion pumps to a base pressure of 6×10^{-9} torr in the beam trajectory region, and normal operating pressure is approximately 5×10^{-8} torr.

The two 90° symmetrical electromagents with 15-inch radii are constructed of 8-inch thick low-carbon steel plates. A maximum magnetic field of 8 kilogauss is obtained across the 0.805-inch gap when the magnets are energized by a 50 ampere 18 volt supply. Figure 5 shows the pole edge region with the fringing field clamp in place. The contouring of the pole edge is to prevent field saturation. Figure 6 shows the fringing field and effective field boundary with and without the field clamps.

At present the system abundance sensitivity is approximately 5×10^5 with only the two magnetic stages operating, and fixed slits set at 0.030-inches. This sensitivity is in reasonable agreement with predicted performance.

REFERENCES

1. F. A. White and T. L. Collins, Applied Spectrometry, 8, 169 (1954).

2. C. R. Lagergren and J. J. Stoffels, Int. J. Mass Spectrom. Ion Phys., 3, 429 (1970).

3. R. Persson, Arkiv för Fysik, 3, 455 (1951).

4. N. R. Daly, Rev. Sci. Instrum., 31, 264 (1960).

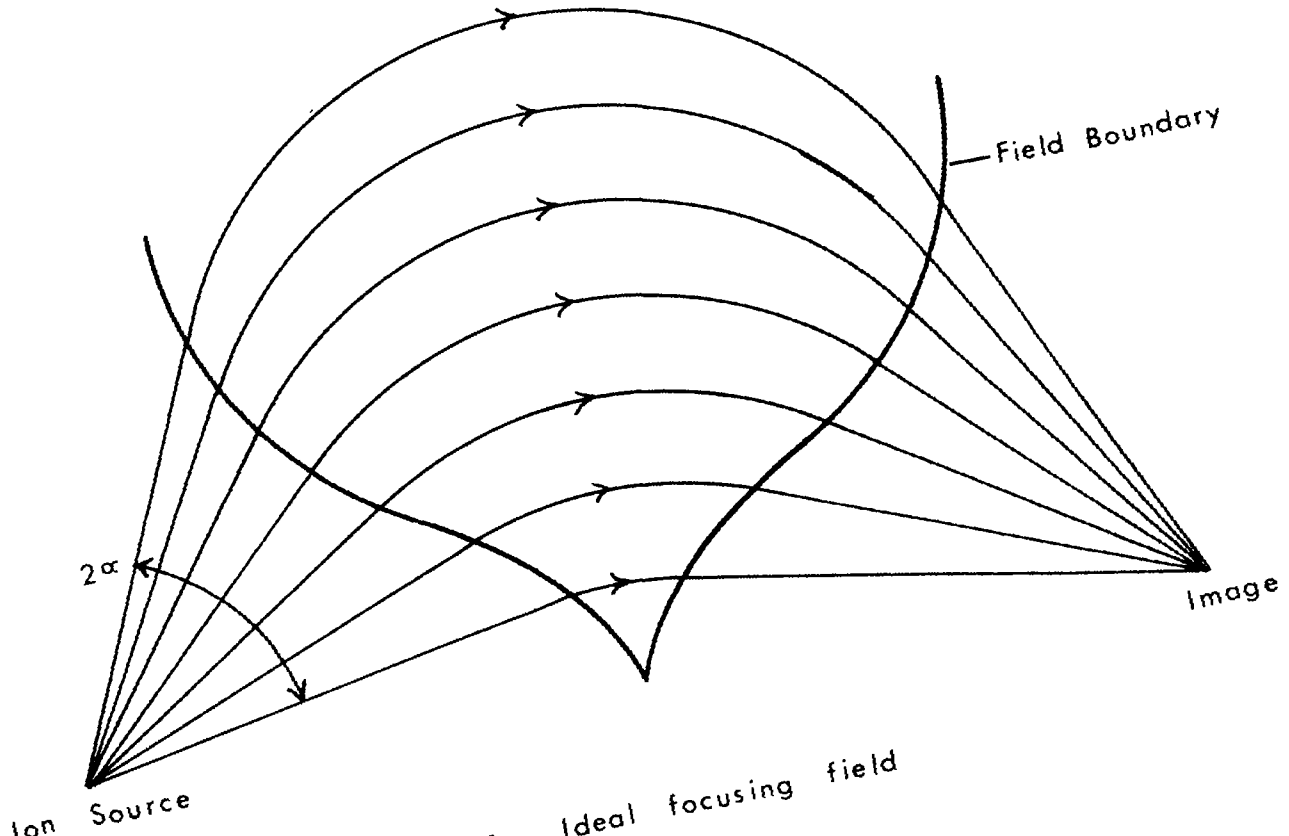

Fig. 1 Ideal focusing field

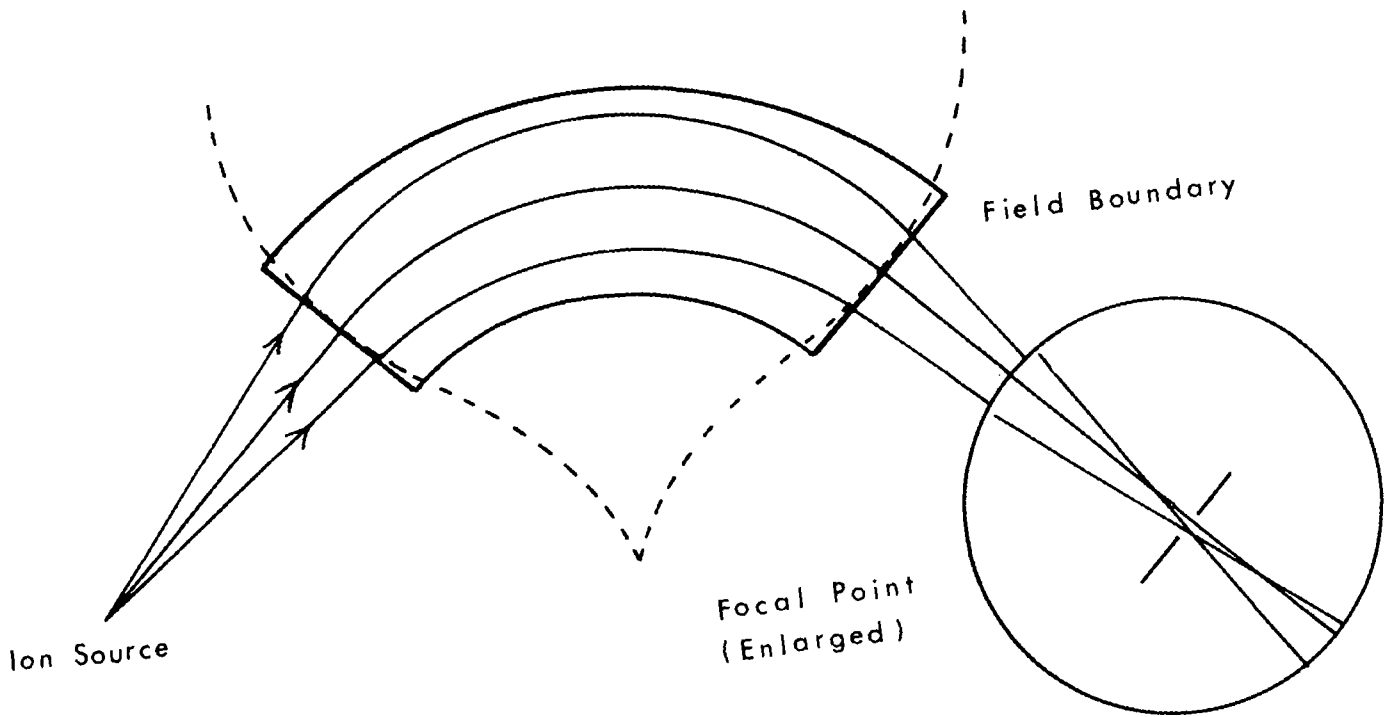

Fig. 2 A linear approximation to the ideal field

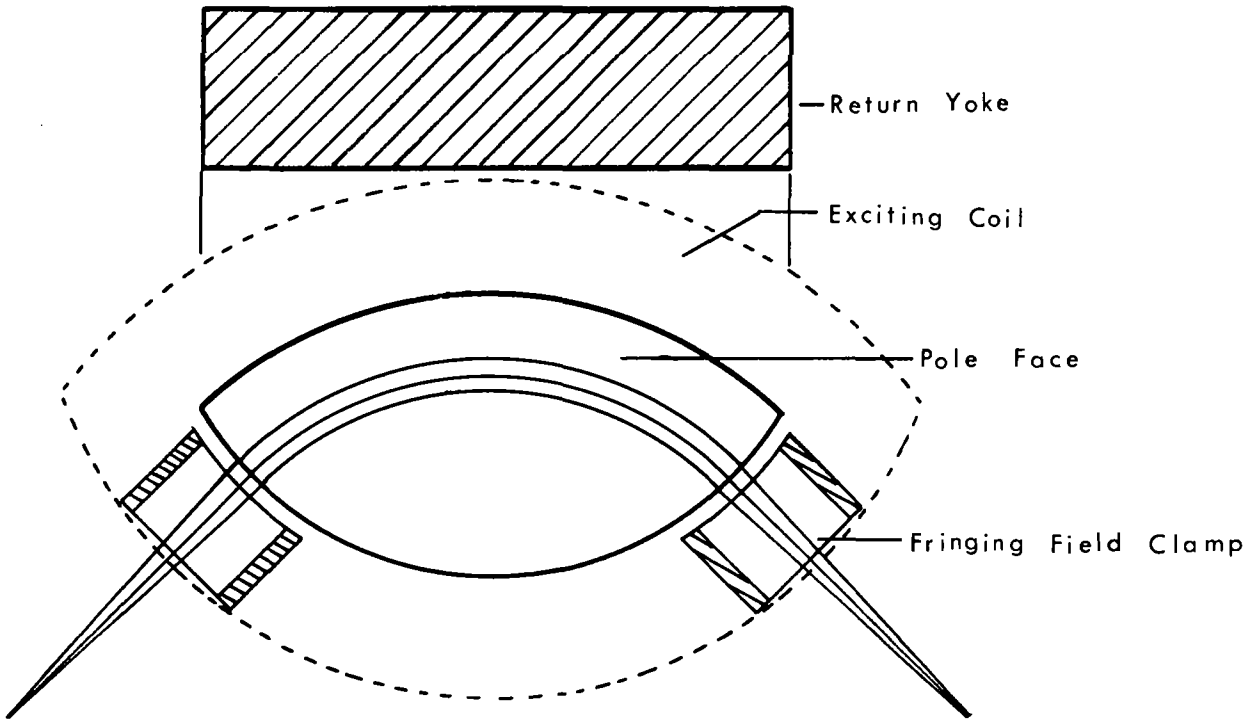

Fig. 3 A cross section of one analysing electromagnet

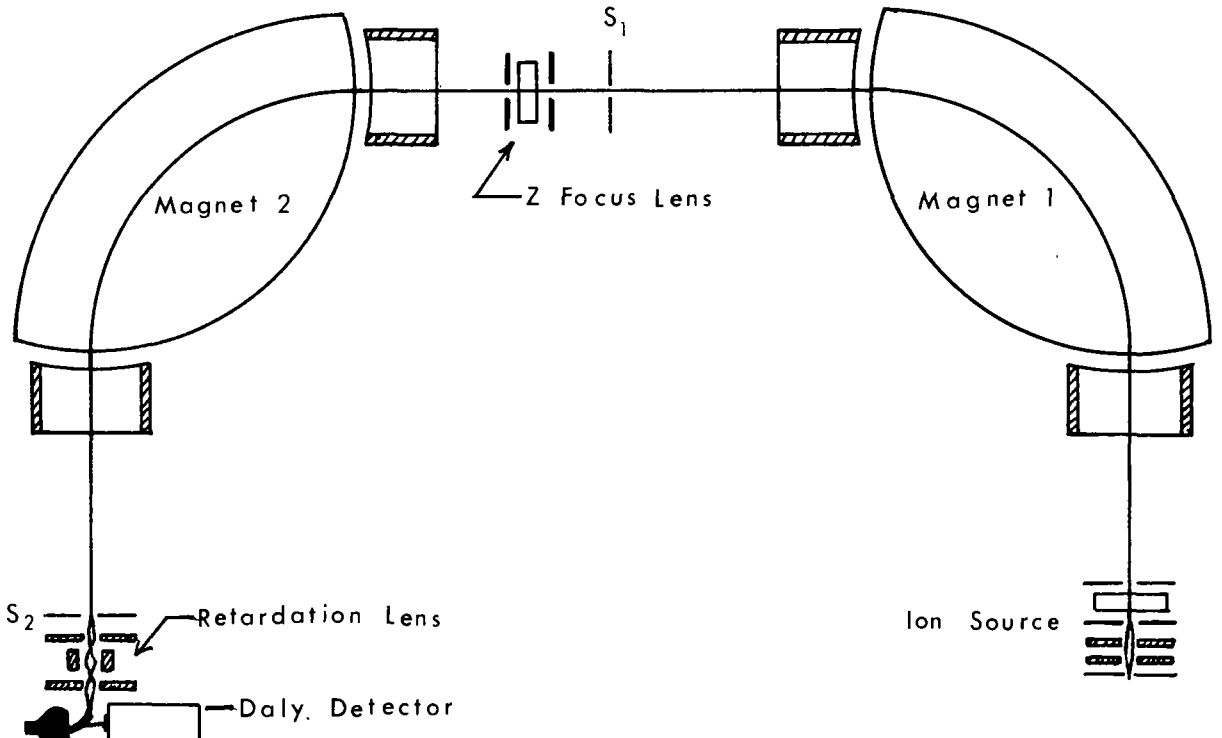

Fig. 4 A schematic diagram of the ion beam trajectory

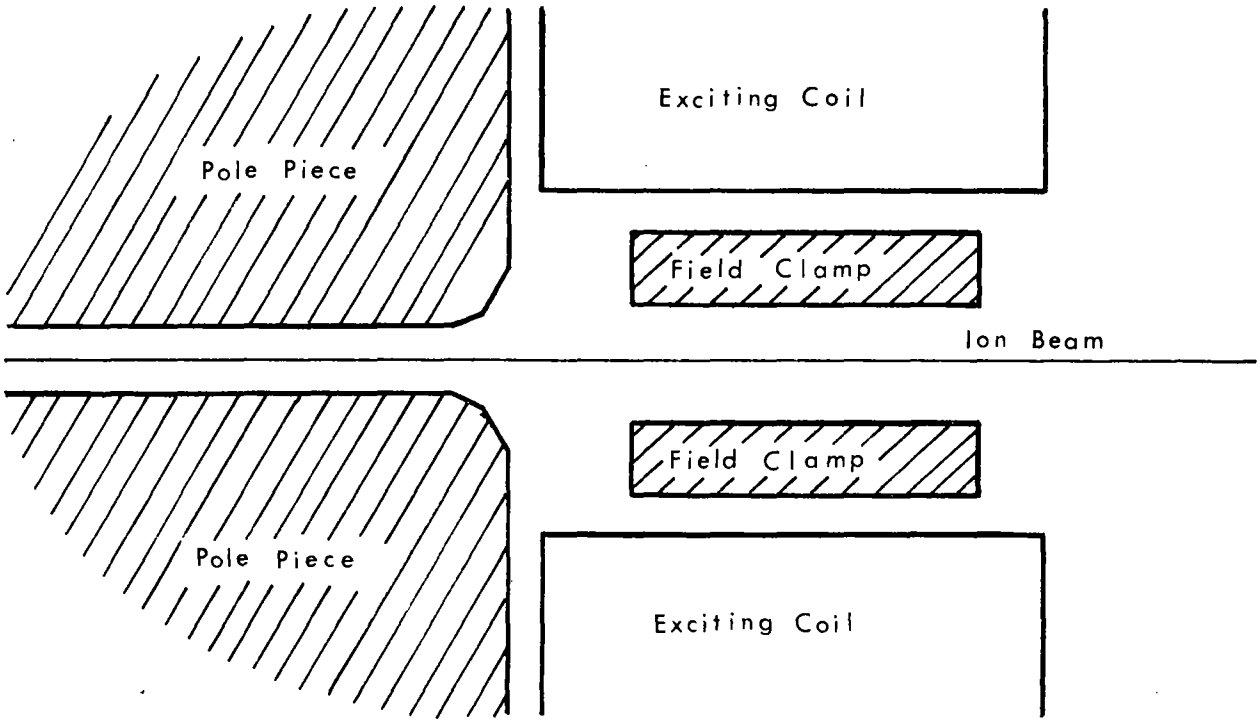

Fig. 5 Pole edge detail

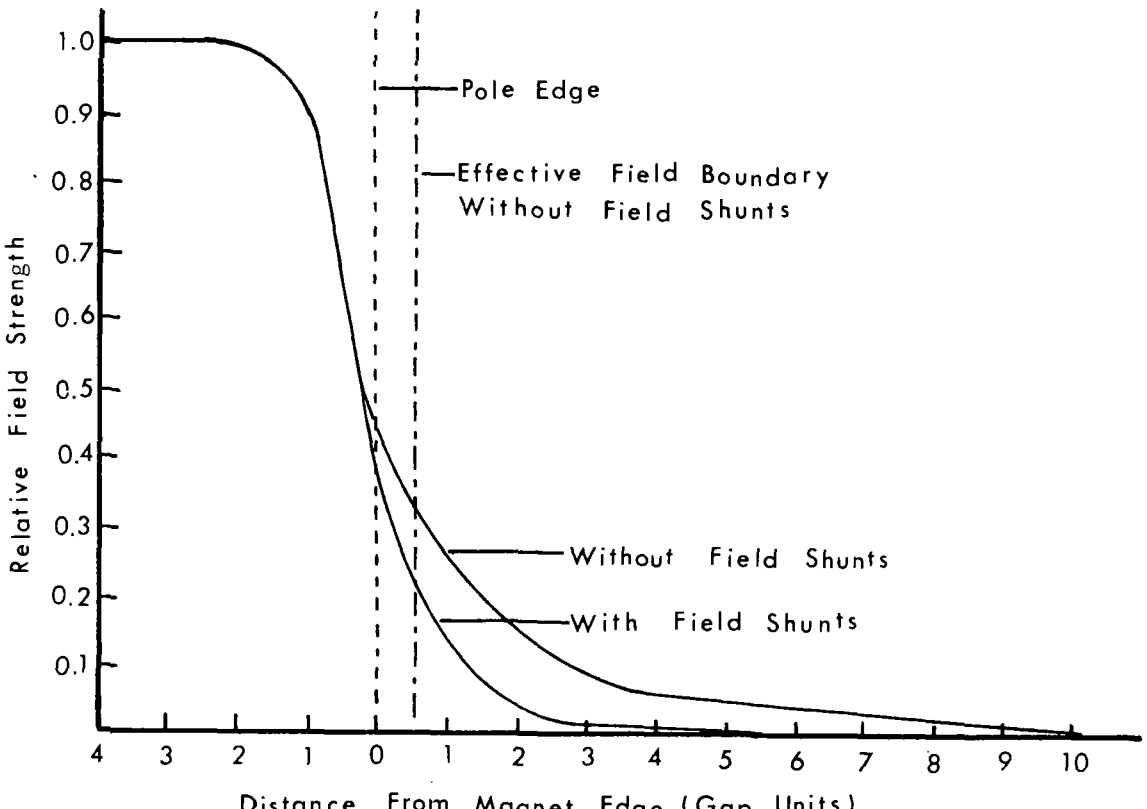

Fig. 6 Magnet Fringing Field

USES OF CHANNEL ELECTRON MULTIPLIERS IN MASS SPECTROMETERS

R3

J. P. Carrico, M. C. Johnson, and W. G. Wolber

Bendix Research Laboratories
Southfield, Michigan 48076

and

K. C. Schmidt

Bendix Electro-Optics Division
Ann Arbor, Michigan 48107

In experiments using a vacuum system, better information is sometimes required on the residual gas background than is provided by an ionization gauge, yet it is not desirable to go to the expense or complication of a commercially available residual gas analyzer (RGA). What we needed was a very simple RGA which would give a rough measurement of residual gases present in the vacuum system and perhaps serve as a leak detector. We considered various existing mass spectrometer principles such as quadrupole, magnetic, and time-of-flight (TOF) and finally decided to use two channel electron multipliers in a simple TOF device. One multiplier served as the source of electrons and the other as the ion detector.

The channel electron multiplier (CEM) possesses a number of features which make its use as a cold cathode electron source and as an ion detector in mass spectrometers attractive. These features include a simple dynode structure, stable dynode surfaces, small size, a variety of configurations, high gain, and a narrow pulse-height distribution.

A channel electron multiplier[1] is a small glass tube which is many diameters long and has a semiconducting, secondary-emitting inner surface. With a few thousand volts applied across the ends of the channel, electrons, ions, and photons (soft x-ray and hard UV) striking the negative end of the channel dislodge electrons from the inner surface. These electrons drift across the channel and at the same time are accelerated along its axis, thereby gaining sufficient energy to release secondary electrons upon colliding with the wall. On the average, more than one secondary is released per incident electron when the field strength is sufficiently large for a given diameter channel. This process is repeated many times until a large electron pulse, containing as many as 10^9 electrons, emerges at the positive end of the channel. The operation of a channel is shown in Fig. 1 where typical trajectories of the electrons in the channel field are indicated. Assuming that the secondary emission coefficient δ obeys the relation $\delta = KE$, where K is a constant and E is the energy of an impacting electron, a simplified expression for the gain of the channel is

$$G = \delta^n = \left(\frac{K}{4} \frac{eV^2 d^2}{V_o L^2} \right)^{\left(\frac{4V_o}{V} \frac{L^2}{d^2} \right)}$$

where n = number of multiplying stages, eV_o = initial energy of a secondary electron, d = channel diameter, V = voltage applied across the channel, and L = channel length. This expression serves to show the general behavior of the gain as a function of the applied voltage and the length-to-diameter ratio. Figure 2 shows the gain as a function of the applied voltages for various L/d ratios. In order to avoid ion feedback at high gain, the channel is curved or bent into a helix.[2] If the gain of the channel is sufficiently large, each input photon or charged particle results in a charge pulse near the channel output end that is large enough to distort the field in this region to the extent that further electron gain is impossible. The result is a narrow pulse-height distribution.[3] Typical pulse-height resolution as a function of channel voltage is shown in Fig. 3 for various accumulated counts.

The foregoing properties of the channel electron multiplier were used in the simple RGA shown schematically in Fig. 4. A channel (CEM 1, Bendix Model 4020), operated in the pulse-saturated mode,[3] was used as an electron source. It was excited by 1850Å photons transmitted by a quartz window from an ultraviolet lamp outside the vacuum. Fig. 5 shows the detector efficiency of the channel; tungsten efficiency is shown for comparison. The geometry was adjusted so that the interval between detected photons was longer than the flight time of the heaviest ions.

Electron pulses emitted by CEM 1 were accelerated to a piece of .005" thick tungsten which was used as electrode 2. The potential on the electron control grid (electrode 1 in Fig. 4) could be varied from 100 to 300V. Positive ions desorbed by electrons striking the tungsten and gas-phase ions were accelerated to the drift tube which was a piece of stainless steel tubing (1.6-cm diameter by 13-cm long). Inside the drift tube, ions separated according to mass-to-charge ratios as in the conventional TOF mass spectrometer.[4] The drift tube potential V_D could be varied from 100 to 500V.

Ions transmitted by the drift tube were detected by an electron multiplier (CEM 2, Bendix Model 4028-A). The output of this channel was fed via an electron multiplier to a 585 Tektronix oscilloscope having a Model 82 dual trace plug-in unit. Pulses having heights of ∿200 mV and widths of 30 nsec were developed. The scope was triggered by the pulse developed at the output end of the first channel and therefore was timed to the production of ions at or near the tungsten target.

Using a bombarding electron current of $\sim 3 \times 10^{-10}$ Amps (about 100 charge pulses per second) and an ion energy of ∿300 eV, resolved peaks of N^+, O^+, H_2O^+, N_2^+, O_2^+ and CO_2^+ were observed when the residual gas was analyzed. The N_2^+ current was $\sim 10^{-16}$ ion Amp when the pressure was 10^{-5} Torr.

The resolution depended on the orientation of the tungsten electrode with respect to the drift tube. The best achievable resolution was estimated to be ∿20 (10% criterion). The effect of the orientation of the tungsten target was attributed to the dependence of the ion transmission efficiency through the drift tube on the location of the ionization region. As shown in Fig. 6, the direction of the source field changes with position. Ions formed in regions where the transverse component of the field is large receive too much transverse momentum to make it through the drift space. As a result, only ions from a restricted portion of the ionization region reach the detector. By rotating the tungsten target, the size of this restricted region and hence, the resolution varies. Additional improvements in resolution should be possible through the use of a second source accelerating region and space focusing.[4]

ACKNOWLEDGMENTS

Assistance in the experimental work by R. Essad, W. Naife, and G. Wassell is gratefully acknowledged. The support of Dr. R. K. Mueller and R. Farrah is sincerely appreciated.

REFERENCES

1) G. W. Goodrich and W. C. Wiley, Rev. Sci. Instr. 33, 761 (1962).

2) D. S. Evans, Rev. Sci. Instr. 36, 375 (1965).

3) K. C. Schmidt and C. F. Hendee, IEEE Transactions on Nuclear Science, NS-13, 100 (1966).

4) W. C. Wiley and I. H. McLaren, Rev. Sci. Instr. 26, 1150 (1955).

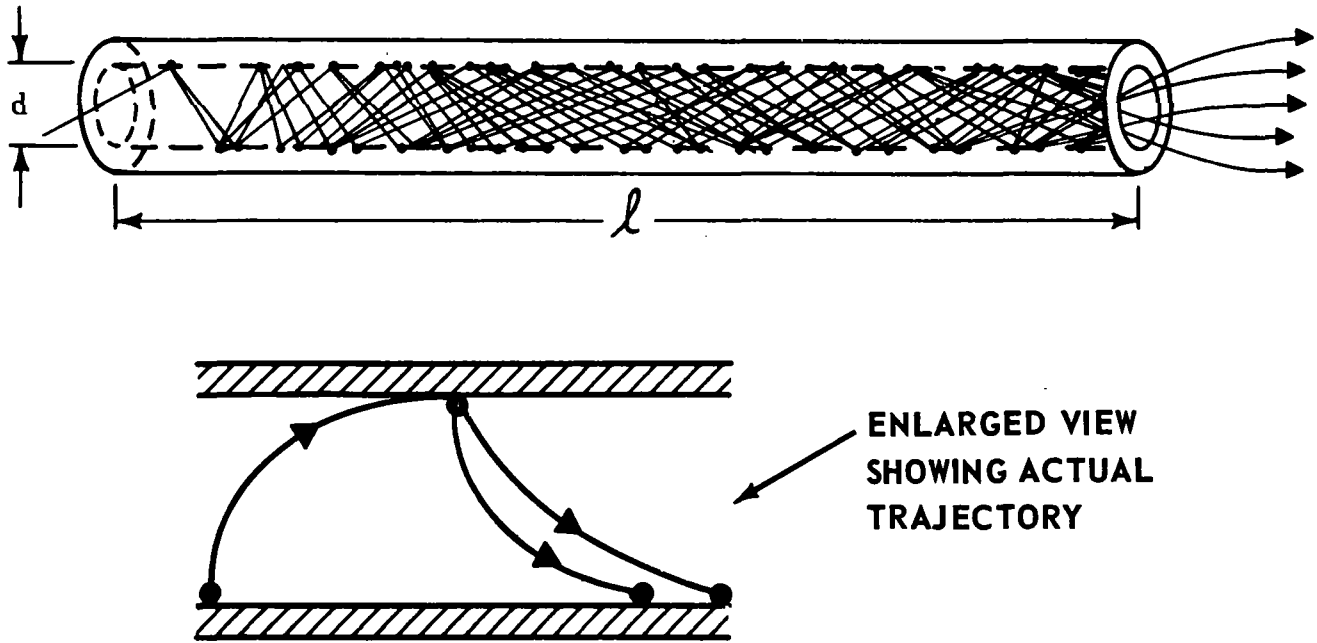

Figure 1 - Channel Electron Multiplier Operation

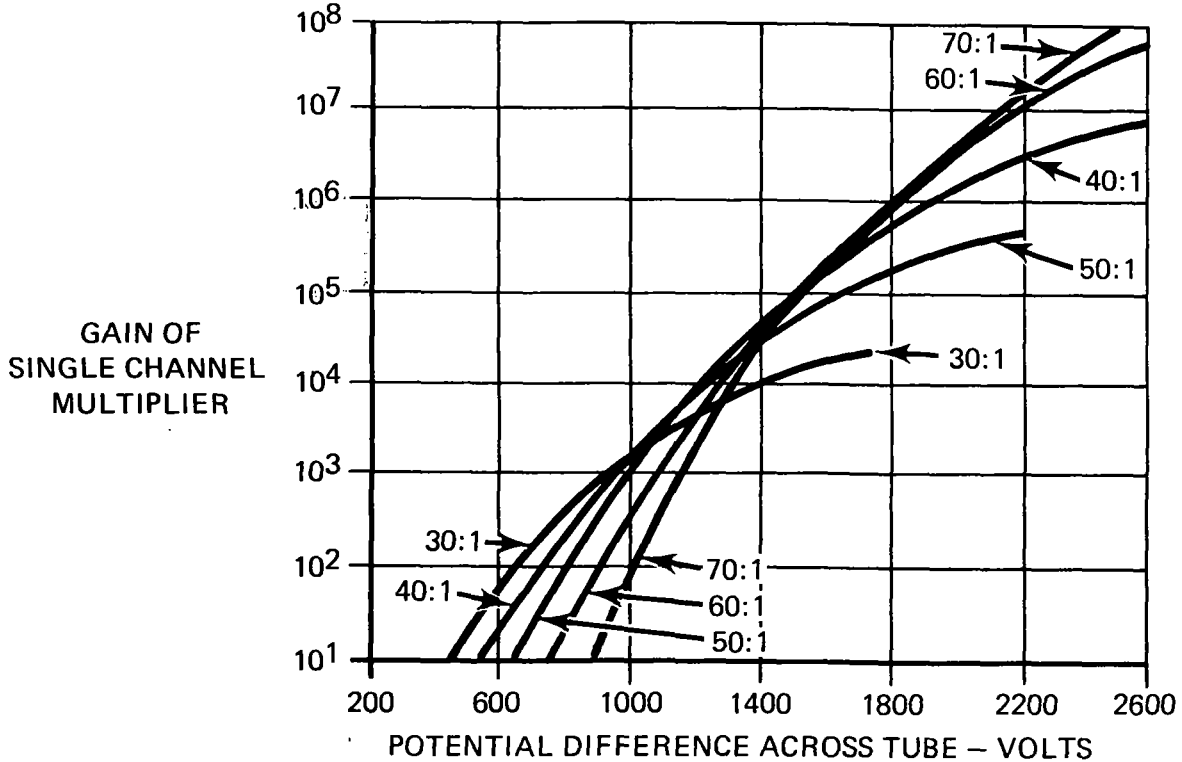

Figure 2 - Gain vs Channel Voltage (L/d as a ratio)

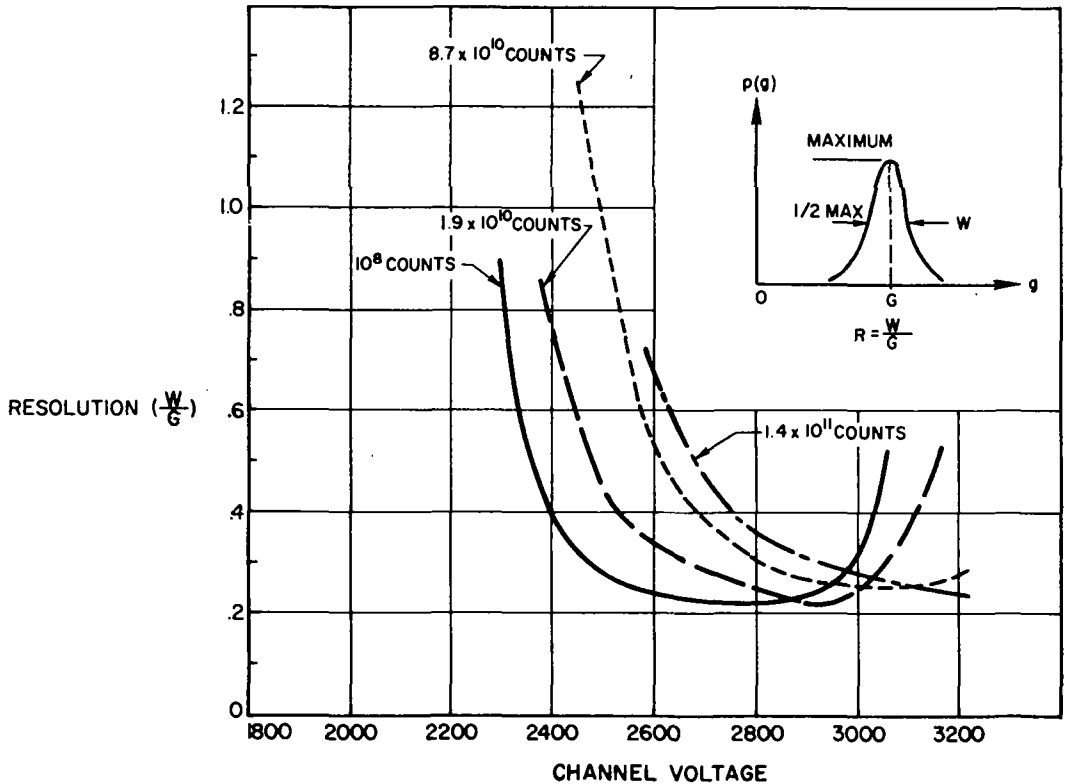

Figure 3 - Pulse Height Resolution vs Channel Voltage
(Accumulated Counts as a Parameter)

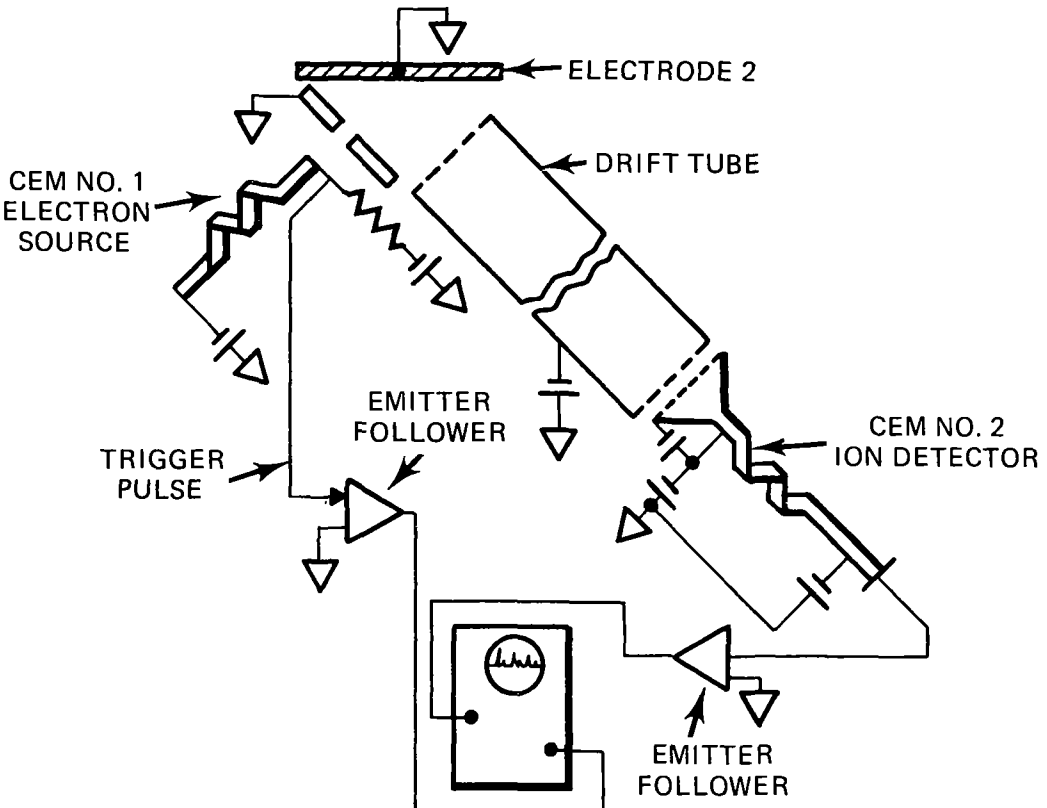

Figure 4 - RGA Apparatus

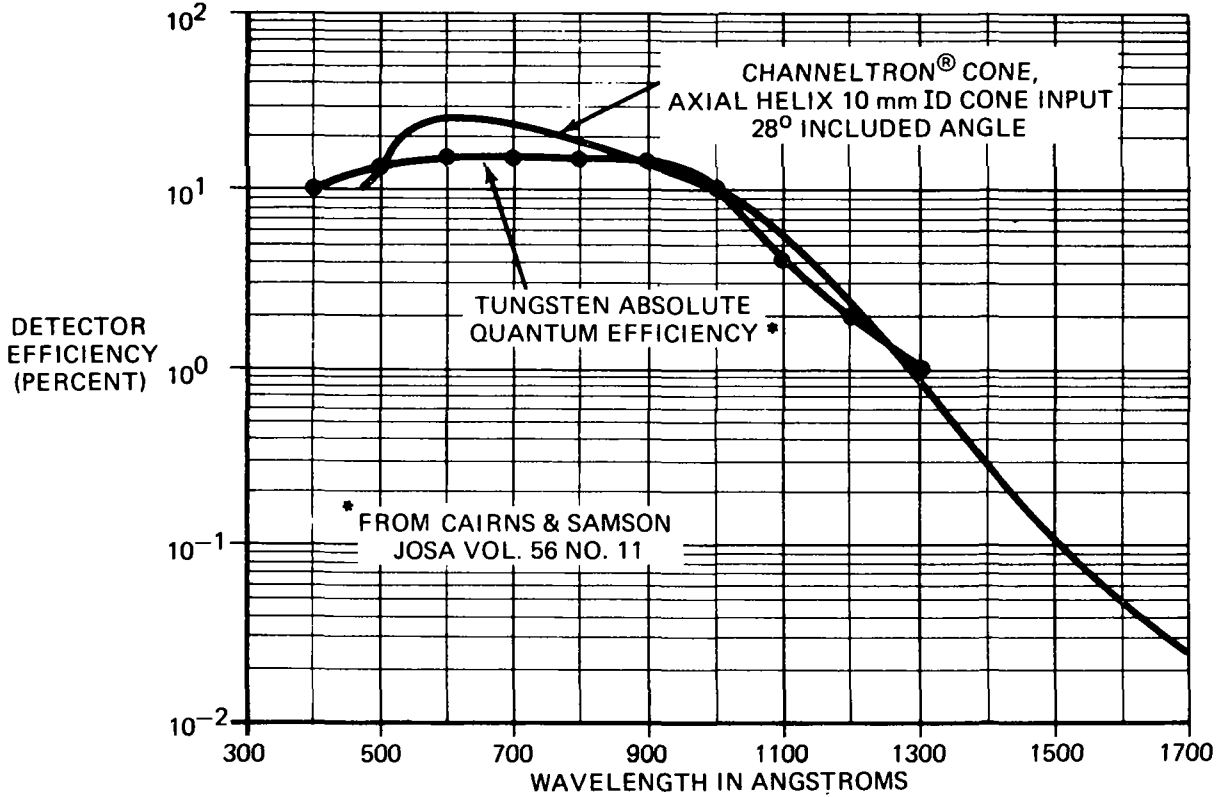

Figure 5 - Detector Photon Efficiency

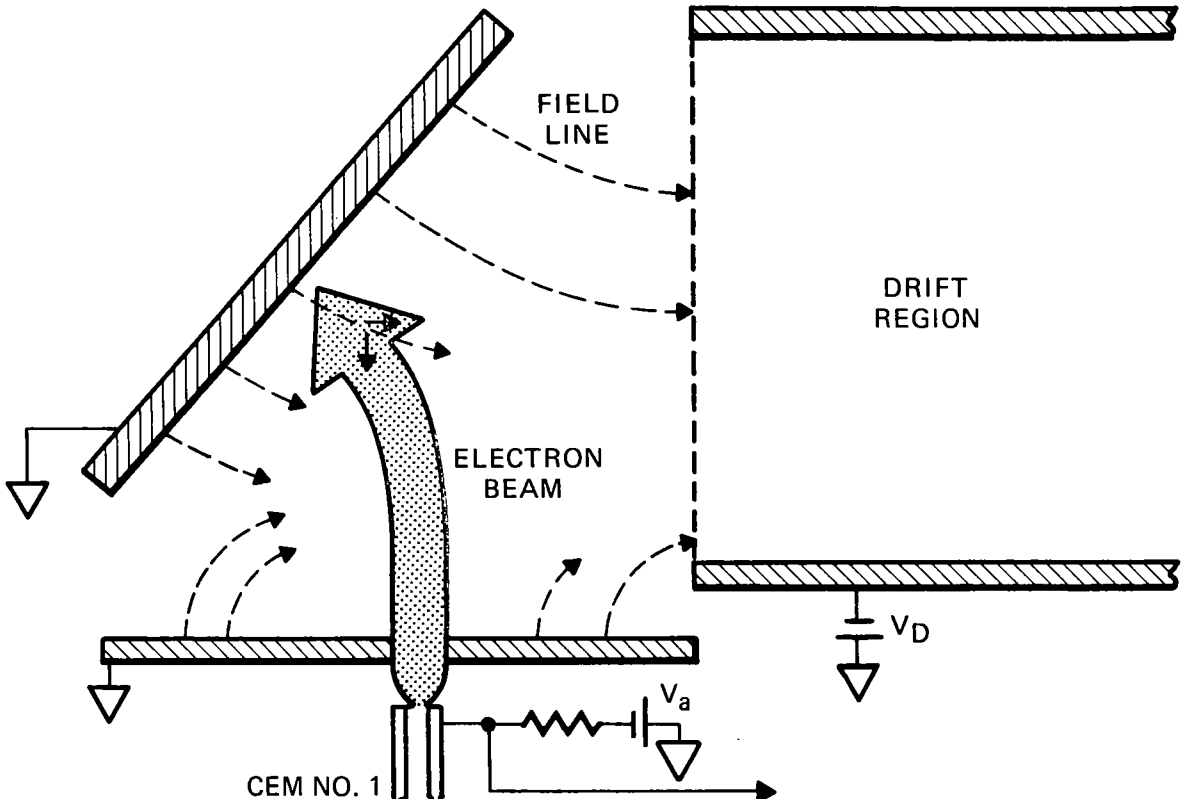

Figure 6 - Enlarged View of Source

"AN AC OPERATED COLD ELECTRON EMITTER MASS SPECTROMETER ION SOURCE" R4

P. C. McLeod, J. F. Sprouse, K. M. Jackson, R. E. Ware, and M. K. Testerman

Department of Electronics and Instrumentation
University of Arkansas Graduate Institute of Technology
Little Rock 72203

An ambient temperature electron emitting device that will produce either a pulsed or an AC modulated electron beam is being investigated. This is a continuation of an investigation of a DC operated cold electron source reported by Sprouse et al[1]. AC operation of the emitter provides higher instantaneous output currents, longer lifetime, and permits emission control of the electron beam. The emitter may be pulsed or modulated directly without the use of grids and exhibits a frequency response of 10^5 Hz or greater at temperatures of -100°C to 150°C.

Figure 1 is a diagram of the cold electron source. This source consists of a short piece of Vycor capillary tubing having typically a 2 millimeter bore. The bore of the capillary contains a thin film of tin oxide applied by vapor deposition techniques. The ends of the capillary are coated with gold to provide ohmic contacts to the tin oxide within the bore. The tin oxide film is disrupted completely around the bore at the point where the bore intersects one end of the capillary. This is done electrically using either a stainless steel or a tungsten probe with approximately 50 to 100 volts DC applied to the probe. Upon application of a voltage from one end of the capillary to the other, electrons will be emitted from the region which has been electrically etched. More recently, mechanical scribing using a 0.001 inch radius diamond tipped phonograph needle has been performed one millimeter down in the bore from the end of the capillary. This was done in an effort to achieve a greater degree of collimation of the electron beam and to cause the higher energy electrons to exit more nearly straight out of the bore, rather than to fan out as they do if the etch is provided at the intersection of the bore and the end of the capillary. If a positive potential is applied to the end of the capillary nearest the etch and the opposite end maintained negative, the electrons will then emit toward the positive potential in an uncollimated divergent beam. If the bias voltage applied to the capillary is reversed so that the end away from the etch is made positive, the electrons will exit through the bore of the capillary in a collimated beam at a much reduced value of current. Obviously, then, if alternating current was applied to the emitter, the source would emit electrons in the forward direction in one half cycle and through the bore in the next half cycle. In the AC mode of operation instantaneous currents in the forward emitting condition as high as 400 microamperes, and currents

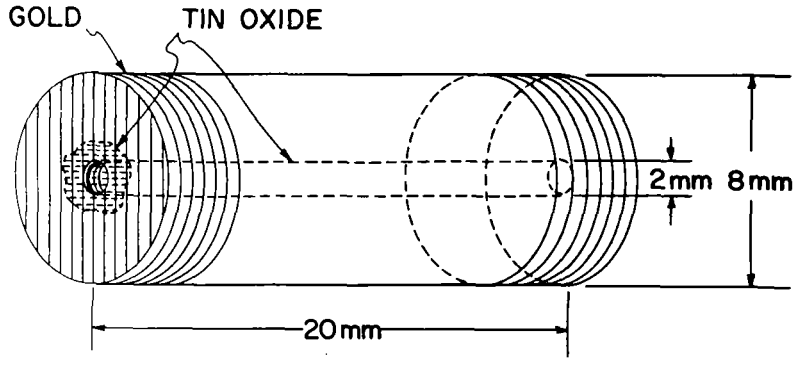

CAPILLARY ELECTRON EMITTER

Figure 1

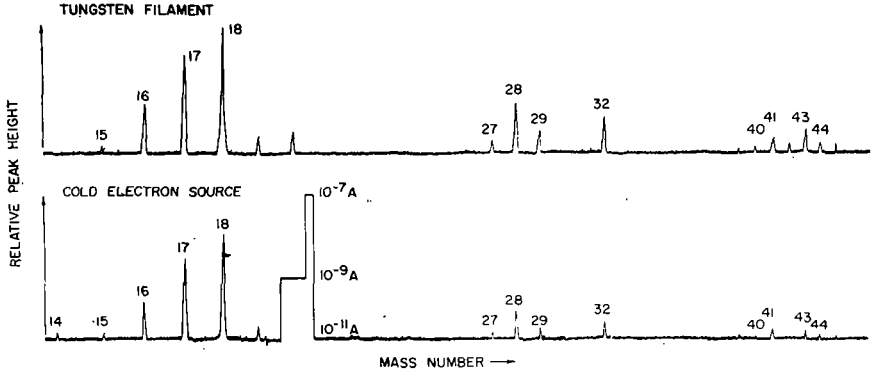

Mass Spectrometer Background

Figure 2

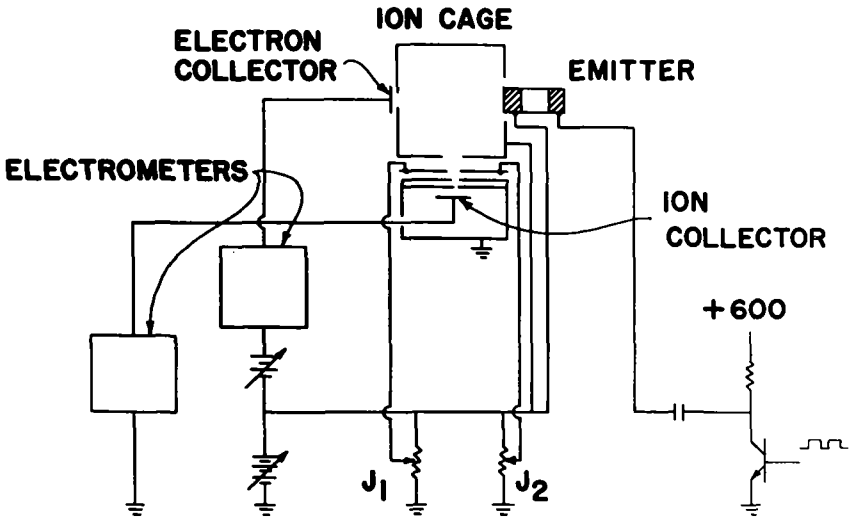

BLOCK DIAGRAM OF COLD ELECTRON TEST STAND

Figure 3

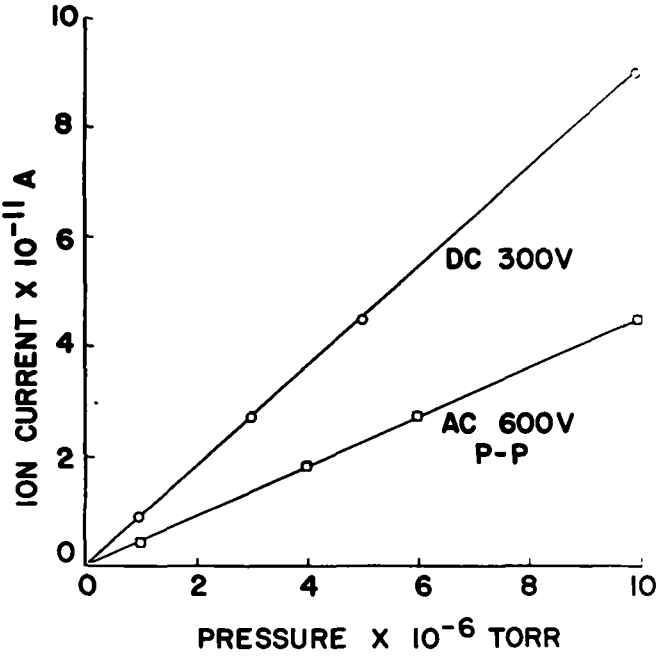

Figure 4

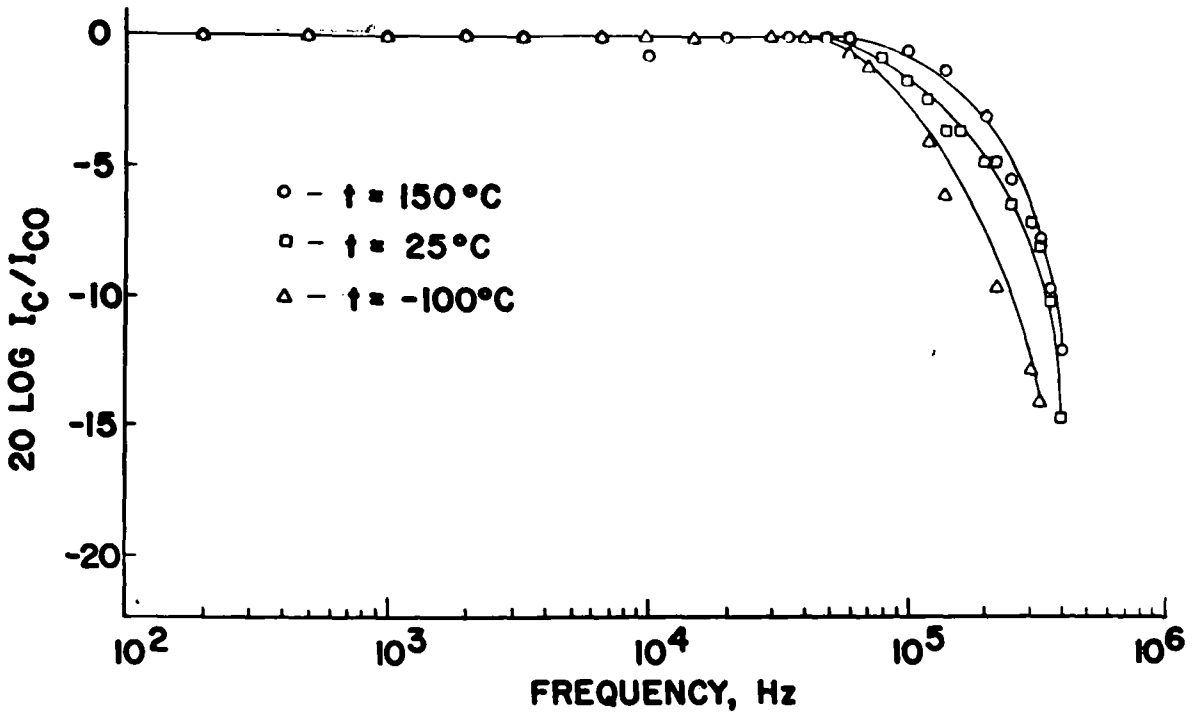

FREQUENCY RESPONSE

Figure 5

through the bore of the capillary as high as 20 microamperes are frequently obtained. The power required to excite the emitter is typically less than 0.5 watt.

Figure 2 is a comparative spectra from a magnetic mass spectrometer showing the background spectrum of the system containing the mass spectrometer, first using a tungsten filament and then a cold electron source. The cold electron source in this case was operated in the DC mode. These spectra are shown here only to indicate that the cold electron source may be used in a mass spectrometer and that it compares favorably with a tungsten filament. At the present time, no spectra have been recorded with a cold source operated in the AC mode. All tests on an ion source using the cold electron emitting device with AC excitation for the ionizing electrons have been performed using total ion collection. There is reason to believe that the AC mode performance in a mass spectrometer would be similar to that of the DC mode.

Figure 3 is a block diagram of the test apparatus employed to determine the magnitude of ions generated by an AC modulated electron beam. The physical design of the ion source shown in this figure is nearly identical to that which was in use when the spectra shown in Figure 2 were recorded.

The ion collector was positioned at the point where the image slit was brought to focus. This provided a measure of the number of ions that would impinge on the entrance slit of the analyzer section of the magnetic sector of a magnetic mass spectrometer if one had been employed. For the test purposes, the forward end of the emitter and the ionization region were maintained at approximately 500 volts and the ions were collected at ground potential.

Figure 4 shows the ion current versus pressure for DC and AC voltage applied to the cold electron source. For this test a 600 volt peak-to-peak symmetrical square wave was applied to the cold source so that the emission entered the ionization region at an excitation voltage of 300 volts during one half cycle and exited through the bore of the capillary during the remaining half cycle. The ion current, measured with a DC electrometer, was approximately one half of the ion current generated with 300 volts applied continuously to the cold source. The frequency of the applied square wave was one kiloHertz. For each of these curves and for all ionization measurements with the cold electron source, the electron emission must be measured and used to correct the ion current because, as the pressure approaches 10^{-5} torr or higher, the electron emission tends to decrease. However, the ratio of the ion current to the emitted electron current varies linearly with pressure. In the DC condition this correction must be performed mathematically or the ratio taken electronically since at this time no research has been performed to accomplish emission control for DC operation. However, for AC operation emission control may be applied.

As stated before, a symmetrical square wave was employed for the AC data shown. If

the waveform had been unsymmetrical so that the emitter was in the forward emitting mode (into the ionization region) longer than the reverse emitting mode, the slope of the AC curve of ion current would be higher but the energy distribution of the electron beam would be unchanged. Therefore, the emission may be controlled by varying the width of the pulse applied to the emitter (at constant frequency) to maintain a constant time average electron emission regardless of pressure.

At the present time this has been performed only manually, but it has been shown that, by varying the symmetry of the applied square wave, the time average electron emission may be maintained constant. Therefore, a linear relation between ion current and pressure may be generated with no additional correction.

Figure 5 shows the frequency response of the electron emitter with sine wave excitation. From this it may be seen that the frequency response is 10^5 Hertz or higher and that the indicated temperature range varies from $-100^{o}C$ to $150^{o}C$. It should be pointed out that the device turns on readily at liquid nitrogen temperatures. In separate tests performed employing a single pulse of very rapid rise time from a pulse generator, the time constant of the electron source measured at 63.2% was found to be slightly less than 1 microsecond. This indicates that the device could be used as a pulsed electron source by pulsing the excitation voltage rather than running the source continuously and applying a gating pulse to a grid.

Figure 6 is a block diagram of a small AC operated ionization gauge employing a cold electron source. The source was driven with a 600 volt peak-to-peak sine wave. The electron collector was put at the opposite end of the capillary for convenience of testing. However, it could be designed into the same end with the ion collector so that it would be unnecessary to have any obstruction except an electrical connection on the end of the capillary away from the ion collector. The performance characteristics of the device are the same as that for the AC curve of ion current in Figure 4 except that the slope of the ion current versus pressure curve is approximately 10^{-3} amperes per torr. If a square wave had been used, the slope of the curve would have been considerably higher since, for sine wave excitation, the emitter has a duty cycle of less than 50% for each half cycle.

At the present state of development, the emission current from the cold source may be expected to decay to approximately 30% of the initial value and then remain stationary. For example, the AC lifetime test reported by Sprouse et al was continued and the emitter was still producing an emission current of 60 microamperes after 25 days, at which time it was removed from the test apparatus. However, for many applications requiring electron beams, such as ionization gauges, full time operation of the electron emitter is employed only because starting from cold causes severe disruption of the conditions within the system, due to outgassing. Since there is very little heat generated at the emitting

region of the cold electron source, the outgassing problem does not exist. Therefore, an ionization gauge employing a cold electron source may be switched on and the pressure determined immediately. If the source is energized only when it is necessary to determine the pressure, the lifetime of the source would be almost indefinite, and greater emission currents would be available. An additional factor would be the absence of continued bombardment of various surfaces by the electrons, thereby maintaining cleaner conditions within the gauge.

This research was supported in part by the University of Texas at Dallas, and the included mass spectra were recorded by Dr. John Hoffman of the University of Texas at Dallas.

Reference

1. J. F. Sprouse, K. M. Jackson, T. A. Raju and M. K. Testerman, Rev. Sci. Instruments, 42; 114 (1971).

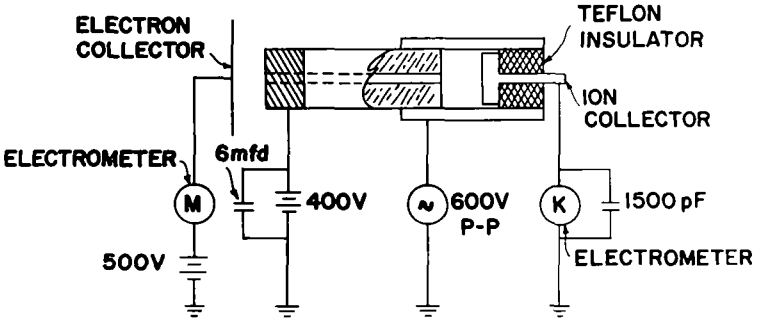

AC OPERATED IONIZATION GAUGE

Figure 6

R5

Absolute Gas Phase Acidity and the Determination of Free Energies of Hydration of Gaseous Anions. L. BREWSTER YOUNG, Mobil Chemical Company, Edison, N. J. 08817, E. LEE-RUFF and D. K. BOHME, York University, Downsview 463, Ontario.

Application of the flowing afterglow technique at 300° K to the study of the kinetics of proton transfer reactions of the type $X^- + YH \rightleftarrows Y^- + XH$ has led to information regarding the energetics of such reactions. This information, together with thermochemical data presently available, allows the determination of absolute acidities for certain Brönsted acids. An absolute pK_a may be defined by analogy with solution work. The relation of absolute pK_a values to solution pK_a values allows the determination of free energies of hydration of anions which are as yet essentially inaccessible to solution studies.

R6

THE THEORETICAL RELATIONSHIP BETWEEN ION MOBILITY AND MASS

D. I. Carroll, Franklin GNO Corporation, West Palm Beach, Florida and
E. A. Mason, Division of Engineering, Brown University, Providence, Rhode Island

INTRODUCTION

In the past few years the Franklin GNO Corporation has applied the principles of gaseous electronics to the motion of stable molecular ions through a nonreactive drift gas to develop a new analytical instrument. This instrument is termed a Plasma Chromatograph™. A combination of a Plasma Chromatograph with a mass spectrometer was described at the last conference in San Francisco by Cohen and Karasek.[1] The Plasma Chromatograph measures the drift time of an ion between two shutter grids. In this paper the Plasma Chromatograph is combined with a quadrupole mass spectrometer. This combined instrument additionally measures the drift time of a mass-identified ion between either of two shutter grids and the mass spectrometer detector. In both instruments the result is to form and drift the ions at atmospheric pressure.

For application as an analytical tool, the measured drift times are shown to be a continuous function of the ion mass and size.

EXPERIMENTAL APPARATUS

The experimental data was taken using the Plasma Chromatograph-Mass Spectrometer combination shown schematically in Figure 1. The procedure is as follows. Primary ions are produced in a carrier gas by a beta-ray source; these primary ions start a sequence of ion-molecule reactions which, within a fraction of a millisecond, yield a few simple molecular ions. These simple molecular ions, in turn, undergo ion-molecule reactions with the trace compound to form the ion or ions measured in the drift tube. Thus, if the carrier gas is nitrogen containing a small amount of water vapor, the primary nitrogen ions start a sequence of reactions yielding $(H_2O)_nH^+$, which react with the trace molecules M to form ions like MH^+, M_2H^+, $M(H_2O)H^+$, etc. The reaction time is normally 10 milliseconds. The ions thus formed in the reaction

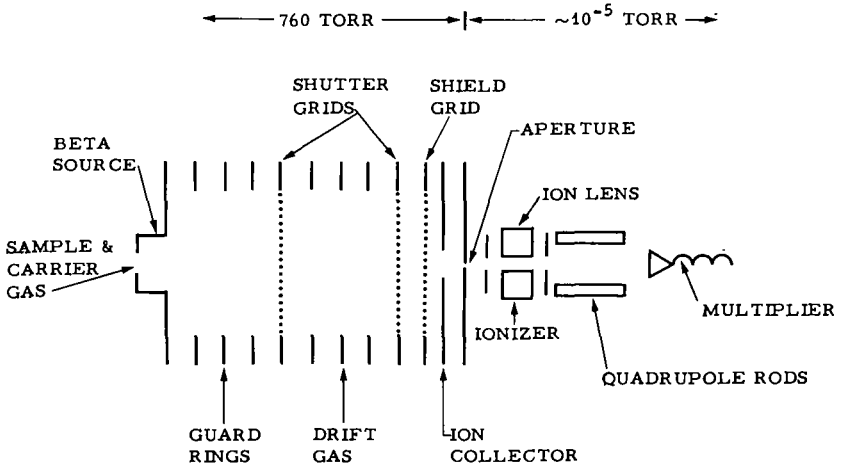

FIGURE 1 PLASMA CHROMATOGRAPH-MASS SPECTROMETER

region are then introduced into the drift region, where they drift through nitrogen at about atmospheric pressure under the influence of an electric field, finally arriving at a detector. The transit times of the ions through the drift region are recorded and are of the order of milliseconds. The signal of the instrument is, thus, ion current as a function of time. The principles of operation are those of electrophoresis in the gaseous rather than the liquid state.

A large flow of nonreactive drift gas is used to clear the drift region of the trace molecules to prevent ion-molecule reactions from continuing during the drift time measurement period.

Either one of the two shutter grids is used to pulse the ions into the drift region. The ions drift from one of the shutter grids to the sampling aperture and are entrained in the gas flow into the mass spectrometer region. This low-pressure region is maintained at 10^{-5} Torr pressure by a high-speed oil diffusion pump. An ion lens focuses the ions from the aperture into the quadrupole rod structure. A standard ionizer is used for calibration only. Provision for optimizing the ion lens and quadrupole rod bias voltages for both positive and negative ion operation is provided. A Channeltron electron multiplier is used as a detector and pulse counting techniques employed.

In typical operation a mass spectrum and drift time spectrum is taken of the total drift cell current. The mass spectrometer is then set to respond to a single ion mass only. The arrival time of that ion is then measured from each grid to the detector. The difference in arrival times is the drift time of the mass-identified ion between the two shutter grids. Since the grid distances and the drift tube temperature and pressure are known, the mobility of the mass-identified ion can be calculated.

MOBILITY THEORY

The drift velocity of an ion through a drift gas, in the presence of an electrical field, is controlled by the very large number of collisions the ion makes with the neutral molecules. The average velocity of the ion through the gas is called the drift velocity, V_d, and is directly proportional to the electric field intensity, E. The proportionality constant, K, is called the ion mobility.

In 1905, Langevin developed a general theory of ion mobility which is shown in modern notation here.[2]

$$K = \frac{3e}{16N}\left[\frac{1}{m} + \frac{1}{M}\right]^{1/2}\left(\frac{2\pi}{kT}\right)^{1/2}\frac{1}{\Omega_D}$$

In this equation N is the neutral density in molecules per cm^3, e is the charge on the ion, M the neutral mass, m the ion mass, and Ω_D the average collision cross section. This relationship between the mobility and the average cross section is essentially exact. The evaluation of the cross section, however, depends upon the nature of the assumed interaction forces between the ion and neutrals.

Early measurements of ion mobility were concerned with simple atomic ions in diatomic gases. Under these conditions, the results are generally well explained by what is known as the "small ion limit" of the mobility equation.

$$K_p = \frac{13.88}{\alpha^{1/2}}\left[\frac{1}{m} + \frac{1}{M}\right]^{1/2}$$

Assuming that the drift gas has no appreciable dipole moment, then the longest range interaction potential is the inverse r^4 polarization. If this is the only interaction force, the polarization limit mobility K_p is proportional to the square root of the sum of the reciprocal masses of the ion and neutral. Thus, K_p reaches a constant value for high values of ion mass.

This has not proved to be the case, however, for the more practical situation considered here, of large complex molecular ions drifted at atmospheric pressure. Under these conditions, the simple small ion limit equation is inadequate.

In 1926, the collision integral was evaluated by Hasse for the more general case of hard sphere repulsion and polarization attraction.[3] Under these conditions the mobility is inversely proportional to the sum of the ion and neutral radii squared. In order to relate this equation to ion mass, the hard sphere assumption that the mass is proportional to the radius cubed must be made. With this assumption, the hard sphere mobility is inversely proportional to the ion mass to the two-thirds power for very large ion mass. A relatively good fit to the experimental data obtained can be made using this rigid sphere interaction model; however, the absolute values of mobility are about twenty percent above those obtained experimentally.

The collision integral has recently been calculated by Mason and Schamp for a much more generalized case which includes both short-range repulsive and attractive terms, as well as the long-range polarization attraction.[4] The assumed interaction potential in this case is:

$$V_{(r)} = \frac{\epsilon}{2}\left[(1+\gamma)\left[\frac{r_m}{r}\right]^{12} - 4\gamma\left[\frac{r_m}{r}\right]^{6} - 3(1-\gamma)\left[\frac{r_m}{r}\right]^{4}\right]$$

In this equation ϵ is the depth of the potential minimum and r_m, its position. The Langevin rigid sphere repulsion has been replaced by an inverse r^{12} and the short-range inverse r^6 attractive term added. γ is a dimensionless constant which is used to weigh the relative importance of the short and long range attraction terms. The mobility equation in the notation of Mason and Schamp is:

$$[K]_1 = \frac{3e}{16N}\left[\frac{1}{m}+\frac{1}{M}\right]^{1/2}\left(\frac{2\pi}{kT}\right)^{1/2}\frac{1}{r_m^{\,2}\,\Omega^{(1,1)*}}$$

Values of $\Omega^{(1,1)*}$ have been tabulated by Mason and Schamp as a function of the parameter T^*, which is the ratio of the thermal energy to the potential well depth of the ion and molecule:

$$T^* = \frac{KT}{\epsilon}$$

The potential well depth ϵ is related to the size parameter r_m by the equation:

$$\epsilon = \frac{e^2\alpha}{3r_m^{\,4}(1-\gamma)}$$

The relationship between r_m and the molecular weight is based on the model of a hard sphere where:

$$r_m = A\left[1+\left(\frac{m}{M}\right)^{1/3}\right]$$

where A is the scaling size for the drift gas of molecular weight M.

COMPARISON OF THEORY AND EXPERIMENTAL DATA

A list of the experimental values of mobility for the mass-identified ions is given in Table I. The sample material and assumed ion is also listed.

In Figure 2 the reciprocal reduced mobility in nitrogen is plotted as a function of ion mass. The solid line is based upon a 12-6-4 interaction potential and the collision integrals calculated by Mason and Schamp.

A scaling value of 2.7 Å for A for nitrogen gas at mass 28 was used with a value of 0.35 for the weighting factor γ. The scaling value of 2.7 Å gives the proper shape and slope to the curve, and the weighting factor gives the correct absolute values.

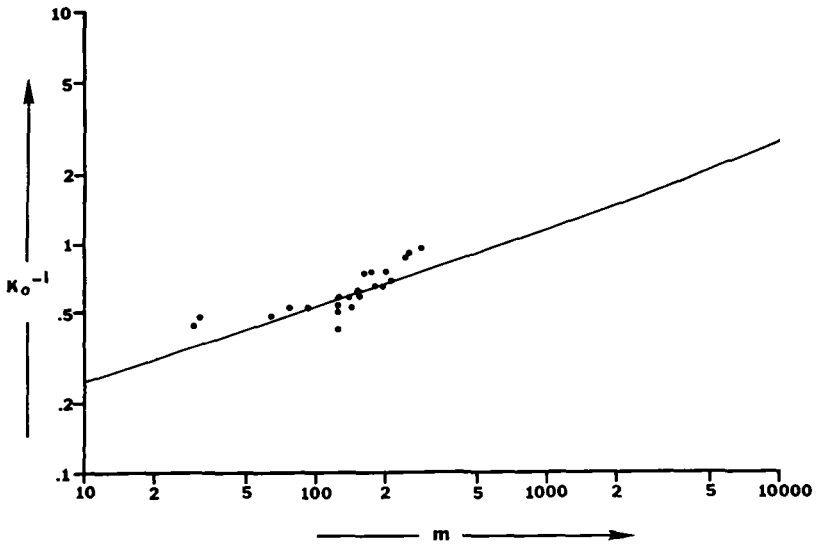

FIGURE 2 RECIPROCAL MOBILITY VERSUS ION MASS

Sample Material	m/e	K_o^{-1}	Ion Interpretation
$CH_3 \cdot C_6H_2(NO_2)_3$	182	0.629	$CH_3 \cdot C_6H_3(NO_2)_2^-$
	198	0.645	$CH_3 \cdot C_6H_3(NO_2)_2O^-$
	227	0.694	$CH_3 \cdot C_6H_2(NO_2)_3^-$
SF_6	146	0.517	SF_6^-
	127	0.496	SF_5^-
$(C_2H_5)_3PO_3$	94	0.504	$(C_2H_5)POH^+$
	124	0.533	$(C_2H_5)_2HPO_2H^+$
	156	0.586	$(C_2H_5)_3PO_2H^+$
	141	0.570	$(C_2H_5)_2HPO_2 \cdot O^-$
$C_9H_{19}OH$	65	0.463	$(CH_3O)_2H^+$
	179	0.735	---
	250	0.855	---
	289	0.943	$(C_9H_{19}OH)_2H^+$
$CH_3 \cdot SO \cdot CH_3$	79	0.508	$(CH_3 \cdot SO \cdot CH_3)H^+$
	157	0.606	$(CH_3 \cdot SO \cdot CH_3)_2H^+$
O_2	32	0.468	O_2^+
	30	0.434	NO^+
I_2	127	0.408	I^-
$C_8H_{17}OH$	131	0.559	$(C_8H_{17}OH)H^+$
	149	0.690	$(C_8H_{17}OH)(H_2O)H^+$
	188	0.730	---
	261	0.893	$(C_8H_{17}OH)_2H^+$

$$K_o = K \frac{273}{T} \cdot \frac{P}{760}$$

TABLE I MOBILITIES OF MASS-IDENTIFIED IONS

The scatter of the data about the average theoretical values is to be expected. This is because the collision integral does not contain the mass of the ion as a parameter, but only essentially its size. A much better correlation should occur if the mobility were plotted as a function of ion size, which is unfortunately not generally known.

Two mass-identified ions have been measured, however, for which the molecular size can be deduced from viscosity data and the measured results compared with the theoretical predictions.

The atomic ion of iodine has a mass of 127 and a size, based upon viscosity data, of 4.2 Å. It would be expected to have a much higher mobility than that of the molecular ion SF_5^- with a mass of 127 and a size of 5.1 Å. The difference predicted theoretically, based upon the 12-6-4 interaction potential, and the scaling factor assumed, is fourteen percent, while the actual measured difference is twelve percent. Thus, the experimental results are in good agreement with the theoretical predictions.

Since the measured ion drift times are a continuous function of the average cross section and, thus, the ion size, the Plasma Chromatograph can serve as a powerful new analytical tool of very high sensitivity. The ion-molecule reaction with the millions of collisions possible at atmospheric pressure accounts for the great sensitivity of the Plasma Chromatograph to trace gases. The reactions may be those normally occurring in the air with trace gases, or selective reactions may be chosen by the introduction of outside reactant gases into the reaction region.

Mass-identified data reported here extends out to mass 300. The 12-6-4 interaction model predicts that the mobility will vary at high values of KT/ϵ on the average, inversely as mass to the four-ninths power. The general result in the limit $KT >> \epsilon$ for an r^{-n} repulsive case is a variation of mobility inversely as M to the $[(2/3)(n - 4)/n]$ power. This gives the two-thirds power variation for the rigid sphere $n = \infty$ and four-ninths for the 12-6-4 model.

An accompanying paper by Kilpatrick shows additional experimental evidence of a continuing variation of mobility out to mass 2000.

REFERENCES

1. F. W. Karasek, M. J. Cohen, D. I. Carroll, "Trace Studies with Ion-Molecule Reactions in the Plasma Chromatograph-Mass Spectrometer Instrument," Proceedings of the 18th Annual Conference on Mass Spectrometry and Allied Topics, June 1970, pB251.

2. E. W. McDaniel, Collision Phenomena in Ionized Gases, App. II, John Wiley and Sons, New York (1964).

3. H. R. Hasse, Phil. Mag. I, 139 (1926).

4. E. A. Mason and H. W. Schamp, Jr., An. Phy. (NY), 4, 233 (1958).

R7

AN EXPERIMENTAL MASS-MOBILITY RELATION FOR IONS IN AIR AT ATMOSPHERIC PRESSURE

W. D. Kilpatrick, Franklin GNO Corporation, West Palm Beach, Florida

The purpose of this report is to relate ion mobility and ion mass in such a way that an accurate measure of mobility will allow a first order identification of ion species. The instrument used for these measurements is a Plasma Chromatograph™[1-3], a device which detects the presence of small concentrations of vapor at atmospheric pressure (760 Torr).

BACKGROUND

The PC method of measurement involves conversion of the trace gas into negative or positive ions by ion-molecule reaction, and then directing them along an electric field. The time interval for an ion pulse to proceed through a fixed distance is related to a characteristic ion mobility. Under clean conditions and for very dilute concentrations (0.01 to 100 ppb), this ion mobility becomes identifiable with mass -- an unconventional mass spectrometer.

The Plasma Chromatograph is somewhat like a time-of-flight spectrometer. But, unlike the time-of-flight spectrometer, the gas impedes ion motion by collisions, so that a constant ion velocity requires a constant electric field. The collisions also limit ion energies to the thermal energy of the drift gas, thus giving transit times of milliseconds instead of customary microseconds for the comparable time-of-flight device.

Gaseous diffusion tends to destroy the ion pulse contours; but because the diffusion rate is different from the total displacement along the field, it is possible to complete ion pulse transits before intolerable resolution sets in. Ion mobility is, therefore, an adequate variable for a general analysis.

Consider the basic equation for ion mobility, K:

$$K = v/E = x/\tau E$$

where v is the drift velocity of the ion when there is an electric gradient E along the path of the cell, and the drift velocity is determined by the transit time τ for ions to travel a fixed length x. In addition, ion mobilities vary inversely with the drift gas density because of the rate of momentum exchange per encounter, so that a reference temperature and pressure are normally used for scaling apparatus and comparing different data. By definition, reduced mobility K_o refers all conditions to 273° Kelvin and 760 Torr which, for a perfect gas, means that:

$$K_o = (x/\tau E) \cdot (P/760) \cdot (273/T)$$

where T is degrees Kelvin, and P is the pressure in Torr of the drift gas. Accordingly, specific transit times for an ion species in a plasmagram are comparable if $\tau \cdot E \cdot T$ = constant, all other conditions remaining the same.

Figure 1 shows a schematic of the measurement arrangement. A carrier gas of bottled air flows at a rate of about 30 ml/min through a molecular sieve where moisture is removed. After the sample is introduced into the carrier stream, they both enter the PC apparatus through a glass inlet. Ions are formed in the ion-molecule reaction chamber and then cross the drift space, become collected, and recorded by an electrometer. The write-out from the electrometer is called a plasmagram, which, therefore, displays the transit time of individual ion pulse peaks. The drift space is maintained at 200°C and is scavenged by dry nitrogen for all measurements. Operating conditions for the following measurements are substantially uniform and are shown in Table I.

DATA

Mobility measurements for twenty-five molecular species have been included, but similar results have been obtained for hundreds of other compounds which were examined over an extended period. For all the different samples measured, the diversity in molecular structure has caused no great dispersion in the data, affirming that ion mobility can form a useful base for identifying ion species. Low concentrations and clean conditions must prevail, however, if significant results are to be obtained.

Table II lists all the materials examined. There are both negative and positive ions, and the range covers from 35 to about 2000 amu. Species include monatomic, aliphatic, aromatic, and complex structures with characteristic groups, such as those of the Lu, Cr, and Mg chelates. Dimers and monomers appear, depending on the sample concentration. Figure 2 displays these data in graph form, which also indicates the continuity of the data.

In Figure 3 the same experimental data are superimposed on an actual transit time scale which applies to these particular measurements. With such a direct transit time calibration, it is possible to interpret plasmagram peaks directly in terms of mass.

Figure 4 shows a plasmagram of DMSO-d. The dominant response is positive--a dimer. All of the reactant positive ion has vanished.

Figure 5 shows iodine, which has a dominant negative ion response. This is a monomer, and some of the reactant is still apparent. Both DMSO and iodine are shown on a 20 msec time base.

Figure 6 shows a complex lutetium chelate, where several ion-molecule reactions are in process. Because of the heavier ions, it has been necessary to increase the time base to 50 msec.

Figure 7 shows a heavy complex fluorocarbon, Freon E-9. Reasons for the "humpback" shape are not clear, but they correspond to fractional complexes, E-1, E-2, etc.

CONCLUSIONS

Under suitable conditions, a simple ion-mobility relationship appears over a large mass range, approximately $10 < \text{amu} < 10,000$.

Comparison of present data with available references gives a general agreement for less than 30 amu, but not for higher values. No ion mobility data have come to my attention for the very high mass region of $200 < \text{amu} < 10,000$, and for all masses there are only limited references to the use of dry nitrogen as a common drift gas.

The experimental data here include many different ion-molecule classes, with the most variation in a small region represented by iodine (127, monatomic), isooctane (114, aliphatic), and vanillin (152, aromatic). Mass determinations from the mobility measurements are within five percent in amu along the mass-mobility curve. A different group was considered where all had similar mass, but were of a cyclic structure: acetophenone (120), salicylaldehyde (122), and benzoic acid (122). They were all measured as dimers, but they agreed again to within five percent amu. Further comparison between classes of materials was obtained from consideration of various biphenylchlorides (188 to 499 amu), where all of the ion mobility data fit well together, and they fit well with the other data along the curve.

To first approximation, there have been no gross departures from the general relationship over a wide range in mass for many different ion species.

ACKNOWLEDGEMENTS

- A group of aromatic compounds with mass about 120 amu was obtained from Dr. F. W. Karasek, University of Waterloo, Waterloo, Ontario, Canada.
- Metallic chelate crystals were donated by Dr. S. P. Cram, University of Florida, Gainesville, Florida.
- Pure samples of biphenylchlorides were acquired through Dr. F. W. Karasek from Dr. O. Hutzinger, National Research Council, Halifax, Nova Scotia, Canada.

REFERENCES

1. *F. W. Karasek, R/D, 21, 3 (March 1970).*

2. M. J. Cohen and F. W. Karasek, J. Chem. Sci., 8, 6 (June 1970).

3. F. W. Karasek, R/D, 21, 12 (Dec 1970).

TABLE I
ALPHA/I OPERATING CONDITIONS

Temperature:	Cell 200 ±5°C Inlet 200°C Sample, variable 26-200°C
Dimensions:	Drift length 8 cm x diameter 10 cm Cell length 28 cm
Gases:	Drift of 300 cc/min, dry nitrogen Carrier of 30 cc/min, dry air System closed to atmosphere Molecular sieve, Linde #3A
Electrical:	Both shutter grids 0.25 msec Scan time 20 - 50 min Time Base 20 - 50 msec Drift gradient 286 V/cm dc electrometer current ~ 2 x 10^{-9} A Source Ni-63 ~ 20 mCi

TABLE II

ATOMIC MASS ~ ION MOBILITY DATA

Negative Ion	amu	K_o
Chlorine	35.5	2.49
Nitrogen Dioxide	46	2.36
2 · Formaldehyde	60	2.06
3 · Formaldehyde	90	1.83
Isooctane	114	1.69
Iodine	127	1.52
Vanillin	152	1.46
Diethylphthalate	222	1.27
BPC-4 (2, 4)	292	1.14
BPC-4 (2, 3, 4, 5)	292	1.13
fod (fragment)	295	1.19
BPC-6	361	1.06
Hexachlorophene	407	.984
BPC-8	430	.976
BPC-10	499	.906
$Cr(tfa)_3$	511	.922
2 · $Mg(tfa)_2$	660	.820
$Lu(fod)_3$	1061	.607
Freon (E-9)	1612	.497
2 · $Lu(fod)_3$	2122	.411

Positive Ion	amu	K_o
2 · Formaldehyde	60	2.07
Dimethylsulfoxide-d	84	1.84
Isooctane	114	1.73
Octanol	130	1.56
Vanillin	152	1.44
2 · Dimethylsulfoxide-d	168	1.47
BPC-1	188	1.34
Benzoanthracene	215	1.21
2 · Acetophenone	240	1.24
2 · Salicylaldehyde	244	1.27
2 · Benzoic Acid	244	1.28
2 · Napthalene	256	1.26
BCP-4 (2, 4)	292	1.14
BCP-8	430	.976
BCP-10	499	.906
2 · $Mg(tfa)_2$	660	.842

Notes:

BPC biphenylchloride
tfa trifluoroacetylacetone
fod heptafluorodimethyloctanedione

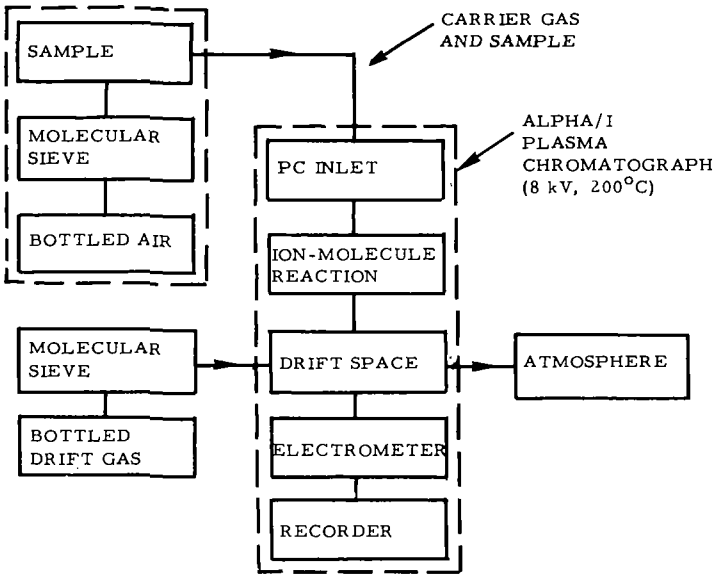

FIGURE 1 MEASUREMENT SCHEMATIC

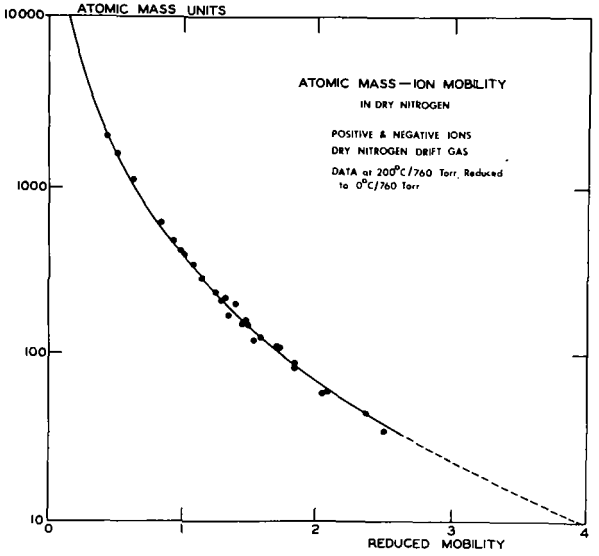

FIGURE 2 ATOMIC MASS--ION MOBILITY

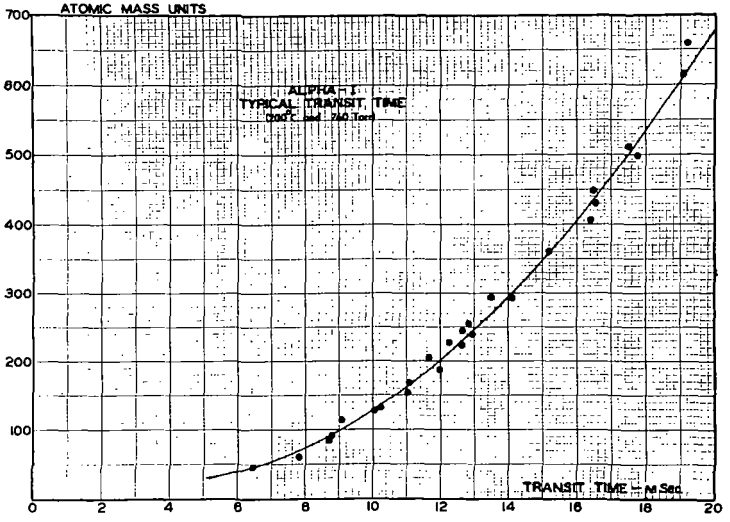

FIGURE 3 TYPICAL TRANSIT TIME, ALPHA/I

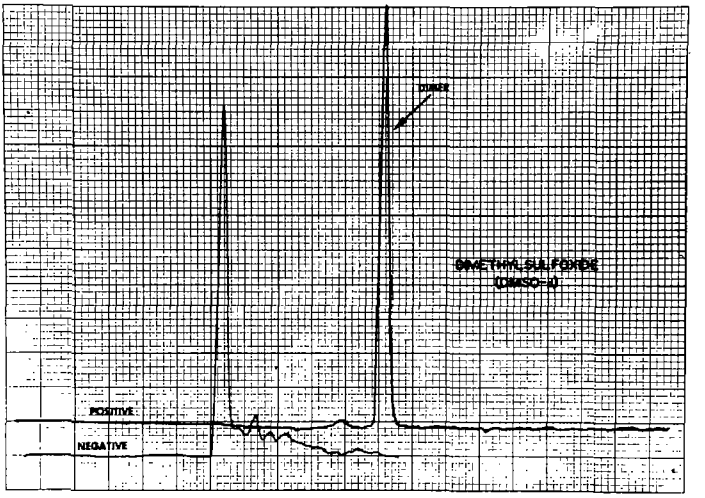

FIGURE 4 DIMETHYLSULFOXIDE PLASMAGRAM

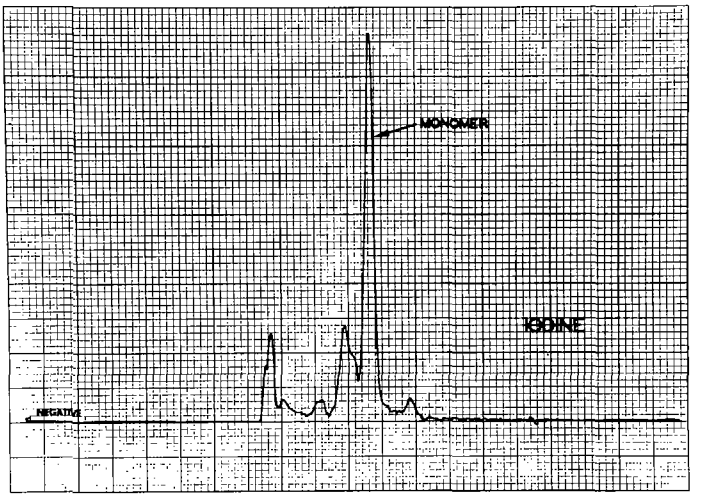

FIGURE 5 IODINE PLASMAGRAM

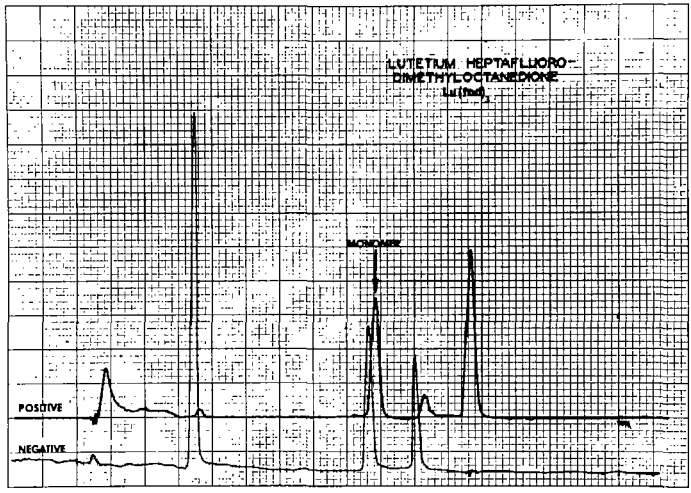

FIGURE 6 LUTETIUM CHELATE PLASMAGRAM

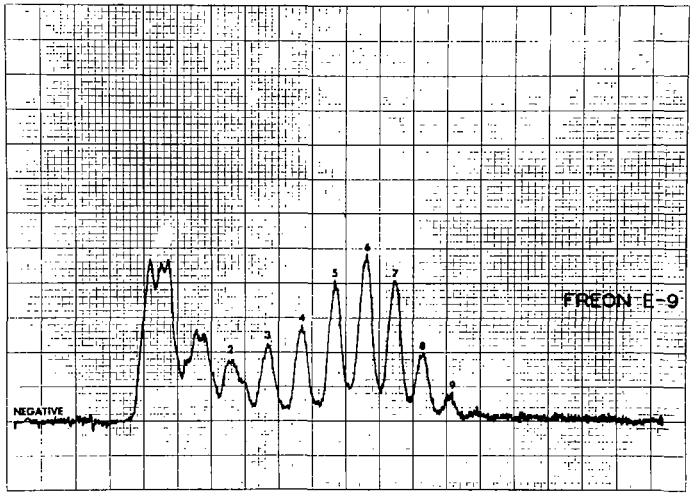

FIGURE 7 FREON F-9 PLASMAGRAM

ION-MOLECULE REACTIONS IN HIGH PRESSURE CH_4-CD_4 MIXTURES*

R10

Shuang-Ling Chong and J. L. Franklin

Department of Chemistry
Rice University
Houston, Texas 77001

Addition of small amounts of CD_4 to methane at 0.25 to 0.5 torr pressure results in the formation of ethyl ions containing various amounts of deuterium. The ratios of the various products correspond to scrambling occurring in reactions of CH_3^+ and CD_3^+ with CH_4 and CD_4. The results are those that would be expected from a long-lived complex of methyl ions with methane. Similarly, CH_4D^+ and CD_4H^+ ions are formed in ratios that are in accord with a mechanism involving the reaction of CH_4^+ and CD_4^+ with CH_4 and CD_4 rather than the reaction of CH_5^+ with CD_4. It is concluded that the latter reaction is quite slow if it occurs. There is consistent indication of an isotope effect which favors the transfer of a proton or a hydrogen over that of a deuterium or deuteron. Similar results were obtained when small amounts of CH_4 were added to CD_4 at high pressures.

*Support by Project SQUID of the Navy is gratefully acknowledged.

A complete paper has been accepted for publication in The Journal of Chemical Physics.

QUANTITATIVE ANALYSIS OF NITROGEN COMPOUNDS

Thomas Aczel and H. E. Lumpkin
Esso Research and Engineering Company
Baytown, Texas

High resolution - low voltage mass spectrometry is used in our laboratories for the semiroutine quantitative determination of the nitrogen compounds present in petroleum and coal products. This analysis is an extension of the method used for the detailed characterization of the hydrocarbons and the aromatic sulfur and oxygen compounds.(1)

We use an Associated Electrical Industries Model MS9 mass spectrometer with a dynamic resolving power of 1 in 10,000. Data acquisition and data handling are computerized.(2)

The procedure used for the analyses of nitrogen compounds involves three main steps: concentration of the nitrogen compounds in a polar fraction by means of a clay-gel separation; identification of the formulas of the components present with the high resolution mass spectrometer; and quantitative analysis, using experimental and extrapolated calibration data. This last step yields at the present quantitative data for up to 720 nitrogen compounds per sample.

The clay-gel separation technique, ASTM D-2007, modified to collect an aromatic fraction, concentrates 80-95 percent of the nitrogen compounds and of the phenols in the polar fraction. It is more selective in this respect than silica gel alone. These conclusions were confirmed by coulometric (Dohrmann) analyses and by the examination of the mass spectra of fractions obtained from several samples. MS data on a typical case are shown below.

Weight Percent of Compound Class in a Coal Liquid

Compound Classes	Saturates	Aromatics	Polars
CH	100.0	96.6	1.5
CHO, CHO_2, CHO_3	0.0	3.4	57.3
CHN, CHNO	0.0	0.0	32.4
Residue	0.0	0.0	8.8

This separation procedure simplifies the mass spectra of the polar fraction. The ^{13}C isotope peaks of the hydrocarbons which interfere with the CHN compounds are essentially eliminated. Less resolving power is thus required for unequivocal identification of the nitrogen compounds. Unseparated samples can still be analyzed, provided that higher resolution power is available. In our case, this higher resolving power is provided, if needed, by a computer program which separates and identifies partially resolved multiplets. Typical multiplets occurring in a polar fraction and in an unseparated sample are shown below.

A. Polar Fraction

Component Mass	Component Formula	R.P. Required for Separation
255.1047	$C_{19}H_{13}N$	8,700
255.1340	$C_{16}{}^{13}CH_{18}O_2$	
255.1704	$C_{17}{}^{13}CH_{22}O$	7,000
255.1984	$C_{18}H_{25}N$	9,000

B. Unseparated Sample

Component Mass	Component Formula	R.P. Required for Separation
147.0684	C_9H_9NO	18,400
147.0764	$C_9{}^{13}CH_{10}O$	
147.1048	$C_{10}H_{13}N$	5,200
147.1128	$C_{10}{}^{13}CH_{14}$	18,400

Use of the above summarized techniques resulted in the identification of a large number of CHN, CHNO, $CHNO_2$, and CHN_2 compounds in samples derived from petroleum or coal. These ranged from one to 6-ring systems, with as many as 20-25 homologs per series. Compounds with one nitrogen atom per molecule were generally the most abundant, followed by the CHNO types. Similarly to what observed for CH, CHS, and CHO compounds, the relative abundances of homologs in a given CHN or CHNO series corresponds to a normal type distribution. A summarized list of nitrogen compounds detected in the polar fraction of a typical crude oil is given on the following page.

Compound Types		Number of Homologs per Series		
Range	Number	Minimum	Maximum	Average
$C_nH_{2n-5}N$ - $C_nH_{2n-35}N$	16	1	21	14
$C_nH_{2n-9}NO$ - $C_nH_{2n-25}NO$	9	1	10	6
$C_nH_{2n-22}N_2$ - $C_nH_{2n-26}N_2$	3	1	7	3
Number of types:	28	Number of individual formulas:		386

Quantitative analysis at low voltages requires a calibration data set containing the parent peak sensitivities of all expected components. Unfortunately very few of these are available for direct calibration, and thus extrapolation techniques are needed for completing the set.

The extrapolation rules used are based on the trends observed with the available data. These trends are summarized below:

- Pyridinic type compounds are less sensitive than the corresponding aromatics, which in turn are less sensitive than pyrrolic types. This effect becomes less pronounced with increasing number of rings per molecule and the consequent decrease in the "importance" of the pyrrolic or pyridinic ring with respect to the rest of the molecule. This effect can be related to ionization potentials. Pyridine has a higher ionization potential than benzene, which has a lower ionization potential than pyrrole. Lower ionization potentials correspond in general to higher low voltage sensitivities.(3)
- The sensitivity increases with aromaticity (number of condensed rings per molecule) and with number of substituents. Again, the substituent effect is less pronounced in the more condensed systems.
- The sensitivity decreases with the length of the sidechains.

Data illustrating some of these trends are shown below:

A. Substitution Effect

Compound Type	No. of Substituents	Avg. Rel. Sensitivity
Pyridines	0	59
	1	116
	2	175
	3	255
Quinolines	0	284
	1	355

Average data are derived from 1 to 7 pure compounds per substitution.

B. Structure Effect

Compound	No. of Rings	Relative Sensitivity
Pyridine	1	59
Benzene	1	148
Pyrrole	1	394
Quinoline	2	284
Naphthalene	2	390
Indole	2	741
Phenanthrene	3	532
Carbazole	3	865

In practice, sensitivities for the pyrrolic and pyridinic nuclei are derived from the curves shown below, in which the ratios of sensitivities between the corresponding pyrrolic and aromatic structures, as well as between the pyridinic and aromatic structures, are plotted against the number of aromatic rings in the structure. These curves yield the sensitivity ratios with respect to the corresponding aromatic nuclei, whose sensitivities are known.(3) These ratios are set to unity for eight-ring structures, in which the effect of the nitrogen atom is assumed to be negligible.

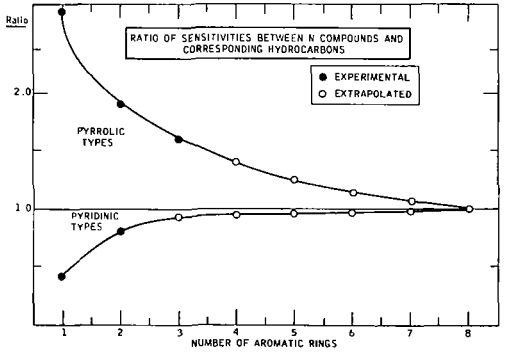

Sensitivity values for homologs are derived in a manner similar to that discussed for the sensitivities of hydrocarbons.[3] In most series, these are assumed to change as the inverse of the molecular weight, and the substitution effect is calculated only for the one- and two-ring systems.

The reliability of this calibration data set has been tested both by comparing the weight percent nitrogen calculated from MS data to conventional values and by adding pure nitrogen compounds to a complex mixture of hydrocarbons. Both types of data indicate that the data set is reasonably accurate. In one case, for example, 38.4 percent nitrogen compounds was added to a nitrogen-free kerosene-type material, and the amount found by MS was 37.0 percent.

At present, quantitative data are obtained for 720 components in 20 CHN and 10 CHNO series, with 24 homologs considered per series. Types included are $C_nH_{2n-3}N$ to $C_nH_{2n-41}N$ and $C_nH_{2n-7}NO$ to $C_nH_{2n-25}NO$. Calculations are performed with an IBM-1802 computer.

Parameters calculated include weight percent of each component and weight percent of each compound type. Values for average molecular weight and weight percent elemental nitrogen and oxygen are given for each compound type and also for the sum of all CHN and CHNO types. The weight percent nitrogen found by this procedure is then compared to the elemental nitrogen found by coulometric (Dohrmann) analysis, and the MS data are renormalized to the conventional nitrogen level if the agreement is not within ten percent. The format of the quantitative analysis is shown below, for a portion of the data.

C Atoms in Sidechains	$C_nH_{2n-13}N$	$C_nH_{2n-15}N$	$C_nH_{2n-17}N$	$C_nH_{2n-19}N$	$C_nH_{2n-11}NO$
0	0.00	0.38	0.08	0.24	0.00
1	0.05	2.48	0.31	0.26	0.00
2	0.53	4.05	0.47	0.20	0.04
3	1.33	3.52	0.24	0.18	0.07
.	.	.	.	.	.
.	.	.	.	.	.
.	.	.	.	.	.
24	0.00	0.00	0.00	0.00	0.00
Total	8.15	13.71	1.39	1.06	0.80
Avg. MW	224.9	204.5	224.5	218.9	213.2
% N	0.50	0.93	0.08	0.06	0.05
% O	0.00	0.00	0.00	0.00	0.06

A major disadvantage of the separation procedure used is that it does not separate pyrrolic and pyridinic types. This separation can be attempted by mass spectrometric means, assuming, for example, that the $C_nH_{2n-5}N$ series is pyridines, the $C_nH_{2n-9}N$ series is indoles, the $C_nH_{2n-11}N$ series is quinolines, the $C_nH_{2n-15}N$ series is carbazoles, and so forth. This approach yields a qualitative distinction between pyrrolic and pyridinic components.

The procedure outlined above yields a reliable quantitative method for the analysis of nitrogen compounds in samples derived from petroleum or coal. It requires only a minimum of separation work and can be performed semiroutinely. It results in a very detailed analysis, determining the relative amounts of as many as 720 components per sample. Its major disadvantage is the lack of accurate separation between pyrrolic and pyridinic types. This difficulty may be overcome by additional separation steps.

---

(1) B. H. Johnson and Thomas Aczel, Anal. Chem. 39, 682 (1967).

(2) Thomas Aczel, D. E. Allan, J. H. Harding and E. A. Knipp, Ibid., 42, 341 (1970).

(3) H. E. Lumpkin and Thomas Aczel, Ibid., 36, 181 (1964).

LASER—TIME-OF-FLIGHT MASS SPECTROMETER STUDIES OF SORBED SPECIES AND SURFACE REACTIONS

A. G. Sharkey, Jr., A. F. Logar, Jr., and Richard G. Lett

Pittsburgh Energy Research Center, Bureau of Mines,
U.S. Department of the Interior, Pittsburgh, Pa. 15213

INTRODUCTION

The purpose of this investigation was to study sorbed species, surface reactions, and pyrolysis products of carbonaceous materials using laser irradiation-mass spectrometric techniques. Four types of samples were investigated: (1) Mildly oxidized coals, (2) sorbents used to remove pollutants from flue gases, (3) airborne particulates collected in an urban area, and (4) coals of three ranks to study products evolved during rapid pyrolysis.

It is well established that even mild oxidation has a marked effect on the properties of coal. Results of several previous investigations have indicated that the initial stages of oxidation involve the hydrogen-rich structures on the surface of the coal.[1] While it has been shown that water vapor, carbon dioxide, and carbon monoxide are major products from the pyrolysis of oxidized coal, little is known about other gaseous products and in particular about gases derived exclusively from surface components. Irradiation with mild laser light provides a means for limiting the vaporization and pyrolysis to surface materials.

Various sorbents for SO_2 and NO_x present in flue gases are being investigated at the Pittsburgh Energy Research Center. Materials investigated include alkalized alumina, copper oxide impregnated on alumina, and trona. To evaluate potential sorbents the sorption-regeneration cycle must be studied in detail. Investigations of gases removed from surfaces of sorbents by mild heating with laser light have assisted in elucidating the chemistry of the cycle and in evaluating potential sorbents.

The physical properties and chemical composition of urban particulate matter have been the subject of much investigation. Mass spectrometric studies of organic material derived from airborne particulates have been reported by the Pittsburgh Energy Research Center (PERC).[2] This investigation and studies by others have shown that only 10-20 percent of the material in particulates has been identified. In the present investigation, rapid pyrolysis of the particulates by laser irradiation in the source region of the Time-of-Flight (TOF) mass spectrometer is being used to study material collected in an urban area.

In studies of the carbonization properties and reactions of coal it is important to know the initial as well as stable products formed during coal carbonization. Using combined laser irradiation-TOF mass spectrometry, Vastola and Pirone[3] and Joy, Ladner, and Pritchard[4] have studied gases from the rapid pyrolysis of several coals. In the present investigation laser-TOF techniques were used to study products from coals of a wide range of rank.

EXPERIMENTAL

For studies of the surfaces of oxidized coals and sorbents, a 10-watt, continuous CO_2 laser with a non-focused beam was used for irradiations. Irradiations were carried out on samples in evacuated tubes and the products were then analyzed by mass spectrometry.

Rapid pyrolysis of the airborne particulates, sorbents, and coal samples was carried out using a pulsed ruby laser with an output of approximately 6 joules. The samples were placed in the source region of the mass spectrometer and irradiated through a window.

RESULTS AND DISCUSSION

Oxidized Coals

Oxidation produced major changes in gaseous products (table 1). Large increases in the concentrations of CO and CO_2 were observed as reported by other investigators. In addition, the concentration of hydrogen and light hydrocarbons to C_4 decreased by factors of 5 to approximately 10. These data, representing products from the pyrolysis of surface components, support the proposals of Howard and others that the hydrogen-

rich structure of the coal is preferentially oxidized. While the temperature of the surface and the depth of material examined by this technique are not known, the major changes in the gas composition indicate that the oxidized layer is the primary contributor to the gas.

Gases from Laser Irradiation of Sorbents

Samples of copper oxide impregnated on alumina were examined after spending by exposure to flue gas containing SO_2 and NO_x and after regeneration in hydrogen. Gases from laser irradiation of samples from the 20th and 75th cycles are shown in table 2. The lower values of SO_2 following regeneration indicate successful regeneration and are consistent with the operating characteristics of the material.

It had been observed that alkalized alumina removed SO_2 from flue gas more efficiently when NO_x was in the gas. Laser irradiation of the surface of spent sorbent revealed for the first time the interaction of NO_x with the alkalized alumina. While traces of NO were obtained in the gas from material exposed to synthetic flue gases without NO_x, approximately 10 times as much NO was obtained from the material exposed to flue gas with NO_x (table 2). The yield of SO_2, indicative of unreacted SO_2 on the surface of the alkalized alumina, is also consistent with other data. Four to five times as much SO_2 was observed in gas from the sample exposed to flue gas without NO_x. These data reflect the higher reaction rate of SO_2 to form sulfate with NO_x present. The concentration of CO_2 was also much higher in gases from the material exposed to flue gas containing NO_x.

Airborne Particulate Matter

A TOF spectrum was recorded for the ruby-laser vaporization of a sample of particulate matter collected in the Pittsburgh area. For this investigation and also the following studies of coal, the samples were pressed into thin, one-half-inch diameter wafers and placed in a stainless steel holder. Spectra were recorded 20 milliseconds after firing the laser. Peaks attributable to SO_2 (masses 64 and 48) were prominent in the spectra. A major peak was also observed at mass 30 and, in a related investigation of particulates by high-resolution mass spectrometry, the composition of the ion was shown to be NO.

Pyrolysis of Coals of Several Ranks

Mass spectra were obtained of the stable products from the pulsed laser irradiation of Anthracite coal, Pittsburgh seam bituminous coal, and North Dakota lignite. Spectra were recorded for a 2-millisecond interval, 20 milliseconds after firing the laser. Good pattern reproducibility was noted for duplicate experiments on the same sample. The total spectral intensity observed for each coal was nearly proportional to the percent volatile matter determined for the coals. The yields of oxygenated compounds, H_2O, CO, and CO_2, show the expected increases, relative to hydrocarbons, as the rank of the coals decreases. Diacetylene is a major product, corresponding to at least 20 percent of the acetylene in several instances. Ethylene and also HCN appear to be present.

Mild laser irradiation of surfaces has provided information concerning surface reactions and the extent of reaction with the bulk material. More intense irradiation and TOF recording of the spectra can be used to examine organic material associated with airborne particulates and dusts.

REFERENCES

1. Howard, H. C., Trans. Am. Inst. Min. Metall. Engrs, 1947, 177, 523-534.

2. Sharkey, A. G., Jr., Shultz, J. L., Kessler, T., and Friedel, R. A., Research/Development, Sept. 1969, 30-32.

3. Vastola, F. J., and Pirone, A. J., Preprints, 151st Am. Chem. Soc. meeting, Petrol. Chem. Div., Pittsburgh, Pa., March 1966.

4. Joy, W. K., Ladner, W. R., and Pritchard, E., Fuel, 1970, 49, 26-38.

Table 1.- Gases from laser irradiation of oxidized Pittsburgh seam hvab coal

Form	-200 Mesh	
Treatment	Control	Oxidized[a]
Analysis[b]	Mol. percent	
H_2	18.2	3.2
C_1	41.5	4.8
$C_2^=$	4.6	1.3
C_2	8.9	0.9
$C_3^=$	5.6	1.1
C_3	4.4	0.3
CO	10.4	35.5
CO_2	6.4	52.9

a/ Heated in air at 150° C for 72 hours.
b/ Air and water free.

Table 2.- Gases from laser irradiation of sorbents

Sorbent	Cu on alumina				Alkalized alumina	
Treatment	20th Spent	20th Regen.	75th Spent	75th Regen.	Flue gas + NO_x	Flue gas without NO_x
Gas	Gas yield[a]					
SO_2	2.13	.83	2.01	.29	.03	.14
CO_2	.06	.13	.23	.17	7.56	.44
NO	-	-	-	-	.23	.02
O_2	.53	.09	.51	.03	.26	.19
N_2	.12	.07	.04	-	.19	.34
H_2	.01	.01	.02	.02	.14	.02
H_2O	.93	.81	3.35	1.74	6.08	3.81

a/ Mm in standard cell; 5-second laser irradiation.

S6

GAS CHROMATOGRAPHIC-MASS SPECTROMETRIC IDENTIFICATION OF INDIGENOUS ORGANIC MATTER OF THE MURCHISON METEORITE

J.M. Gibert, S.A. Wikstrom, and J. Oró
Department of Biophysical Sciences
University of Houston
Houston, Texas 77004

ABSTRACT

The Murchison Meteorite contains significant amounts of complex mixtures, of amino acids, aliphatic and aromatic hydrocarbons, and other solvent extractable organic compounds. The amino acids found include several protein as well as non-protein components. The aliphatic hydrocarbon fraction of low molecular weight has a predominance of branched saturated alkanes. The cyclic and unsaturated series increase in abundance with increasing molecular weight of the hydrocarbons. The benzene fraction contains predominantly alkyl substituted unsaturated rings. On the basis of their unique distribution and identities it appears that these organic compounds are indigenous to the meteorite. The combined technique of gas chromatography and mass spectrometry has proven once more to be an advantageous combination for the separation and identification of such complex mixtures or organic substances.

INTRODUCTION

Interstellar space, initially thought to be essentially empty, can now be imagined as an enormous chemical reactor where a number of simple organic and organogenic compounds have been identified (1). Therefore as star and planet formation occur in the galaxies, these simple organic compounds could eventually be incorporated in planetoidal environments, thus becoming potential precursors of biogenic structures. With increasing evidence for more organic structures in interstellar space, the analysis of extraterrestrial samples for organic compounds receives an added momentum.

Carbon compounds in meteorites have been the subject of extensive studies during the last century. If one thinks of meteorites as being the remains of the primeval matter in the collapsing solar nebula, the study of these bodies certainly can provide very valuable information regarding the stages and mechanisms of evolution within the solar system (e.g. 2,3).

Two types of organic compounds, hydrocarbons and amino acids, have been the subject of extensive analysis. They constitute a most interesting fraction of the solvent extractable organic compounds found in carbonaceous chondrites, a carbon rich type of meteorites.

Extraterrestrial samples are potentially subject to organic contamination while exposed to the earthly biota as has been demonstrated (e.g. 4,5). Consequently it is commonly accepted that recently fallen and freshly collected carbonaceous chondrites, or very well preserved specimens, are the most suitable samples to study.

The fall of the Murchison occurred near Murchison, Victoria, Australia, on September 28, 1969. The specimens analyzed at the University of Houston weighed 10 and 499.7 grams, respectively, and had been collected about two weeks after the fall of the meteorite. They were obtained through the courtesy of Dr. R.S. Clarke, Jr. (Field Museum of Natural History, Chicago, Illinois).

GAS CHROMATOGRAPHIC-MASS SPECTROMETRIC ORGANIC ANALYSIS

A relatively large piece of the Murchison meteorite almost entirely covered with fusion crust, was the primary source of material. It had no visible fractures and a minimum of soil-staining and weathering, giving it a very clean general appearance. Several inside pieces were obtained after removing more than two centimeters of the fusion crust and outer surface from the original specimen. Figure 1 shows three representative gas chromatograms obtained by injection of aliquots of the amino acids N-trifluoroacetyl-O- isopropyl esters (6), aliphatic and aromatic hydrocarbon fractions, into a 150 m. long x 0.5 mm i.d. open tubular stainless steel capillary gas chromatographic column coated with 3% SF-96 connected to an LKB 9000 gas chromatograph-mass spectrometer. This column has an estimated efficiency of 180,000 theoretical plates. The complexity of these three fractions is apparent. Mass spectrometric evidence was obtained for several protein and non-protein amino acids such as alanine, α-aminoisobutyric, glycine, α-aminobutyric, β-alanine, valine, norvaline, proline and glutamic acid. Preliminary evidence for some other 10 amino acids has also been obtained (7,8).

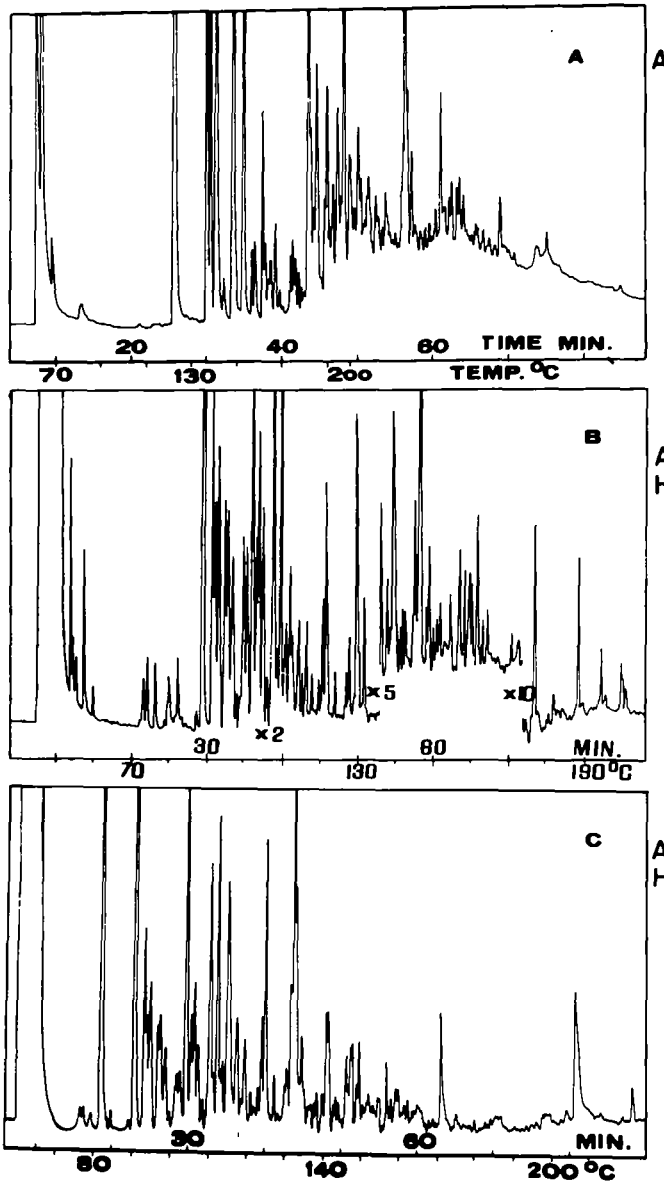
A
AMINO ACIDS
20
40
60
TIME MIN.
70
130
200
TEMP. °C
B
ALIPHATIC
HYDROCARBONS
×5
×10
×2
30
60
MIN.
70
130
190°C
C
AROMATIC
HYDROCARBONS
30
60
MIN.
80
140
200 °C

Some of the spectra recorded are difficult to interpret since these amino acid derivatives lack a parent ion, and some of the spectra corresponding to different isomers are very similar. It is fortunate that in many cases similar isomers have different chromatographic retention times and therefore this brings about very valuable information in establishing the interpretative criteria.

The amino acids found, with the exception of proline and glutamic acid, are predominantly of the aliphatic type. For this type of amino acids the base fragment ion generally corresponds to either the loss of the ester or the alkoxy moeity. The β and γ amino acids behave in slightly different ways.

The most significant fragment ions for some of the amino acids investigated are summarized in Table 1. These fragments are independent of the specific alcohol used for esterification of the acid moeity.

TABLE 1

AMINO ACID	SIGNIFICANT MASS SPECTRAL FRAGMENT IONS FROM n-TFA-O-ALKYL AMINO ACID DERIVATIVES AT 20eV						
	1	2	3	4	5	6	7
PROTEIN							
GLY	127	126	154				
ALA	140	141	57	168			
PRO	166	211	194				
VAL	168	169	55	153	114	196	
LEU	69	182	140	183	171		
ILE	69	182	171	183	114	153	140
GLU	198	180	240	152			
NON-PROTEIN							
SARCOSINE	140	141	184	168			
β-ALA	168	55	139	185	186	141	126
α-Amino-N-Butyric Amino	154	155	140	182			
β-Amino-N-Butyric	140	182	(60)	154	102		
α Amino Isobutyric	154	155	83	85	182	166	114
β-Amino Isobutyric	82	69	168	153	155		
NORVALINE	168	55	169	126	140	114	154
NORLEUCINE	182	69	168	153	155		

Glycine was the major amino acid observed (5.3 μg/g) and the other amino acids were found in amounts of the order of 0.1 μg/g or higher (alanine 3.1 μg/g). Obviously an appreciable number of other amino acids and possibly amines, remain to be identified, as shown by the relatively large number of components of the gas chromatogram (Figure 1) and the complex spectra recorded.

Figure 2 displays two consecutive mass spectra obtained during the actual analysis of the amino acid fraction. These representative spectra labelled Murchison 70/74 NR 25 and 70/74 NR 26 have been identified as α-amino-N-butyric acid and β-alanine, respectively. The spectra of standards are included in the figure for comparison. In the spectrum Murchison 70/74 NR 26 the fragment at 154 originates due to memory effect from the immediately preceeding compound. When complex spectra corresponding to more than one compound, as indicated above are obtained, the use of gas chromatographic retention times of standard compounds add valuable information that extends the usefulness of combined GC-MS as an identification technique (9). However the unavailability of a computer system adds a tremendous burden to the analytical chemist in the identification of such complex mixtures, otherwise impossible to handle by conventional methods of chemical analysis.

Figure 1B depicts a representative gas chromatogram of the pentane fraction. The aliphatic hydrocarbons observed range from C_{10} to relatively high molecular weight components. The most abundant series corresponds to the branched saturated alkanes. They include predominantly monomethylated and dimethylated isomers. Intense ions that correspond to the loss of fragments with m/e 29, 43, 57 and higher values suggest the presence of branching at positions 2, 3, 4 etc., respectively (8,9).

The C_nH_{2n-1}, C_nH_{2n-3} series were also observed but were substantially less abundant. Up to C_{15} some of the C_nH_{2n-1} ions could be assigned to olefins rather than monocyclic alkanes since the m/e doublets corresponding to the fragment ions C_nH_{2n-1} and C_nH_{2n-2}, for n = 5, 6 or higher, characteristic of cyclics, were not abundant. The

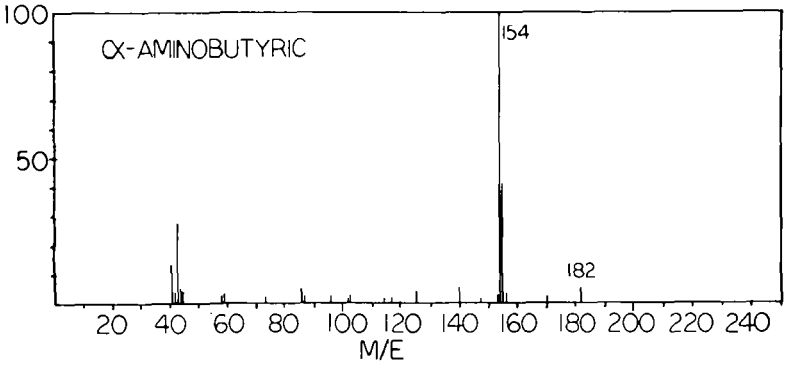
100
50
α-AMINOBUTYRIC
154
182
20 40 60 80 100 120 140 160 180 200 220 240
M/E

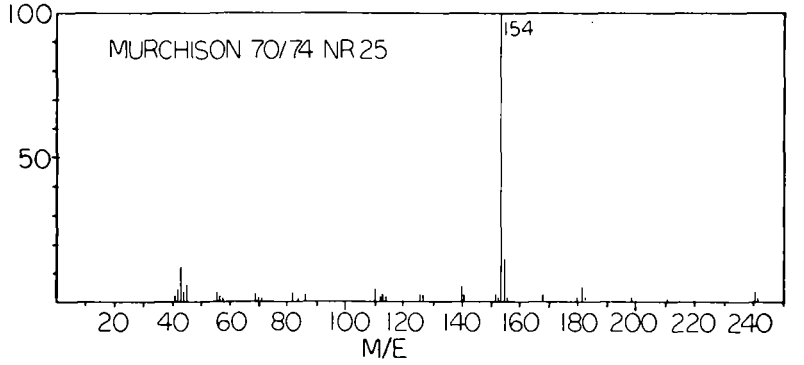
100
50
MURCHISON 70/74 NR 25
154
20 40 60 80 100 120 140 160 180 200 220 240
M/E

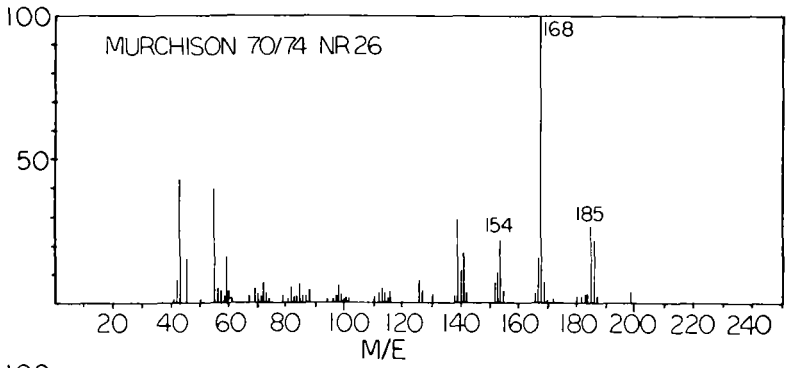
100
50
MURCHISON 70/74 NR 26
168
154
185
20 40 60 80 100 120 140 160 180 200 220 240
M/E

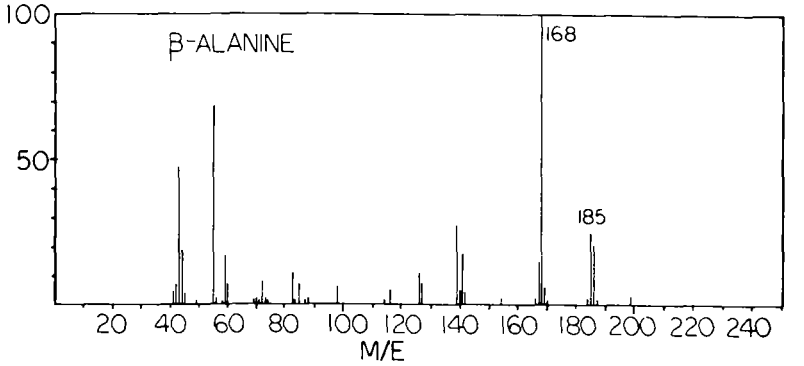
100
50
β-ALANINE
168
185
20 40 60 80 100 120 140 160 180 200 220 240
M/E

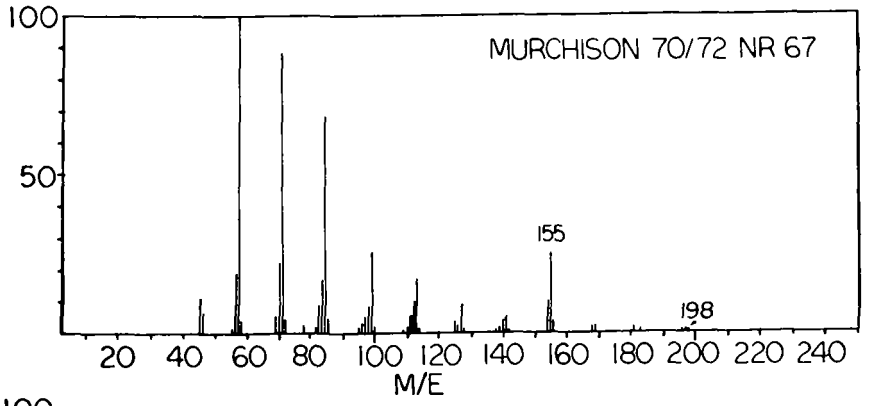
MURCHISON 70/72 NR 67
100
50
155
198
20 40 60 80 100 120 140 160 180 200 220 240
M/E

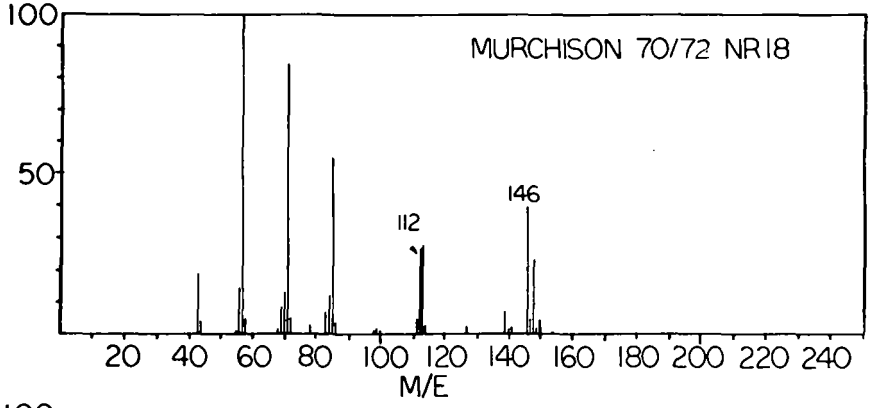
MURCHISON 70/72 NR 18
100
50
112
146
20 40 60 80 100 120 140 160 180 200 220 240
M/E

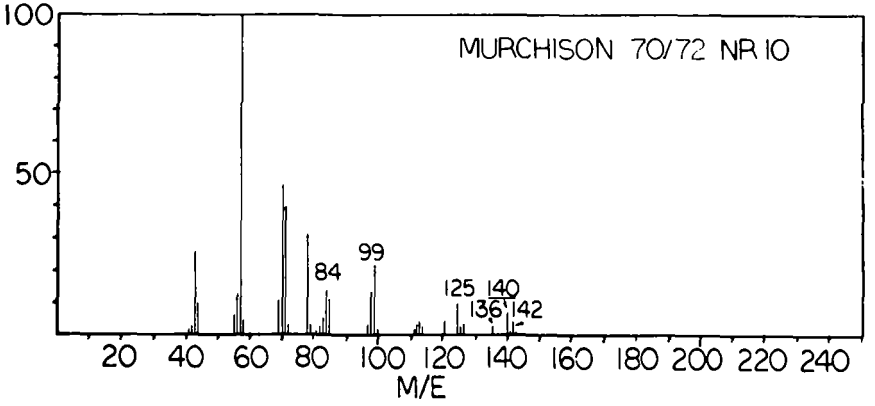
MURCHISON 70/72 NR 10
100
50
84
99
125 140
136 142
20 40 60 80 100 120 140 160 180 200 220 240
M/E

C_nH_{2n}-3 series increased in intensity after the C_{14} region, and suggested bicyclic structures with aliphatic branching.

The top spectrum in Figure 3 is representative of branched alkanes. The higher fragment at m/e 155 corresponds to the loss of 43 units, therefore the most likely position for the methyl group is in the second carbon of the alkane chain. Thus this spectrum can be interpreted as being that of 2-methyl tridecane.

While the bottom spectrum displays ions representative of monocyclic and branched alkanes, the middle spectrum depicts several ions belonging to polycyclics or polyunsaturated compounds.

The bottom spectrum in Figure 3 displays several molecular ions 142, 140, and 136. The molecular ion at 142 corresponds to an aliphatic alkane with some branching at position 2, probably a 2 methyl-C_{10}; 140 most probably corresponds to a cyclohexane since the peaks at 83 and 84 are suggestive of cyclohexanes with aliphatic branching and 136 has at least 3 unsaturations (rings plus double bonds) and since no other ions can be related to it, its structure is difficult to determine.

The middle spectrum of Figure 3 has the molecular ions 146, 148, and 150, which have respectively, 5, 4, and 3 rings plus double bonds. Their identities are indeed difficult to establish.

The aromatic fraction yielded mass spectra with fragmentation patterns corresponding to napthalene, pehanthrene or anthracene, and some spectra with branched aliphatic chains on these aromatic rings were observed. These data together with gas chromatographic retention times indicate the presence of alkyl substituted bicyclic and tricyclic aromatic compounds (8,9).

On the basis of their unique distributions and identities, it appears that the organic fraction of this meteorite is indigenous and of probable extraterrestrial origin. The high complexity of the fraction investigated suggests abiotic types of synthesis.

These and other organic fractions of products with biogenic significance are currently under investigation.

BIBLIOGRAPHY

1. Donn, B., Organic Molecules in Space, in Exobiology, (ed. by C. Ponnamperuma) North Holland, Amsterdam (in press).

2. Oró, J., Investigation of Organo-chemical Evolution, in Current Aspects of Exobiology (ed. G. Mamikunian and M.H. Briggs). Pergamon Press, New York, p. 13 (1965).

3. Oró, J., Stages and Mechanisms of Prebiological Organic Synthesis, in the Origins of Prebiological Systems and of Their Molecular Matrices, (ed. by S.W. Fox). Academic Press, New York, p. 137 (1965).

4. Gibert, J., Flory, D., and Oró, J., Identity of a Common Contaminant of Apollo 11 Lunar Fines and Apollo 12 York Meshes. Nature 229, 33 (1970).

5. Oró, J. and Tornabene, T., Bacterial Contamination of Some Carbonaceous Chondrites. Science 150, 1046 (1965).

6. Gelpi, E., Koenig, W., Gibert, J., and Oró, J., Combined Gas Chromatography-Mass Spectrometry of Amino Acid Derivatives. J. Chromatog. Sci. 7, 604 (1971).

7. Kvenvolden, K., Lawless, J., Pering, K., Peterson, E., Flores, J., Ponnamperuma, C., Kaplan, I.R., and Moore, C., Evidence for Extraterrestrial Amino Acids and Hydrocarbons in the Murchison Meteorite. Nature 228, 923 (1970).

8. Oró, J., Gibert, J., Lichtenstein, H., Wikstrom, S., and Flory, D.A., Amino Acids, Aliphatic and Aromatic Hydrocarbons in the Murchison Meteorite. Nature 230, 105 (1971).

9. Gibert, J.M., Studies in Chemical Evolution, Gas Chromatographic-Mass Spectrometric Determination of Organic and Organogenic Matter in Lunar Samples, Carbonaceous

Chondrites and Terrestrial Samples. Ph.D. Dissertation, University of Houston (1971).

FIGURE CAPTIONS

Figure 1: Gas chromatograms obtained on an LKB 9000 gas chromatograph-mass spectrometer with a 150 m x 0.5 mm stainless steel open tubular capillary column coated with SF-96 operated at 1.41 kg/cm^2 and the temperatures listed below.

A. N-TFA-isopropyl derivatives of the water extracted amino acids. Column isothermal at 70°C for 10 min. and programmed at 3°/min. up to 200°C.

B. Alkanes from the pentane fraction of the benzene-methanol extract. Column isothermal at 50°C for 10 minutes and programmed at 2°/min. up to 200°C.

C. Benzene fraction from benzene-methanol extract. Column isothermal at 65°C for 15 min. and programmed at 2°/min. to 200°C.

Figure 2: Spectra of α-amino-N-butyric acid and β-alanine standards compared with those obtained from the Murchison meteorite. Notice the memory effect for fragment 154 in the spectra 70/74 NR26 of β-alanine which is the base fragment in the preceeding spectra (70/74 NR 25).

Figure 3: Three representative spectra of the alkane fraction soluble in pentane. The top spectrum is representative of branched saturated alkanes, the middle of polycyclic or polyunsaturated and the bottom is a complex spectra where a six membered ring C_{10} alkane appears to be present.

S7

MASS SPECTRAL ANALYSIS OF ORGANIC COMPOUNDS IN THE MURCHISON METEORITE

J. G. Lawless, M. Romiez, K. Kvenvolden,
K. Pering, E. Peterson, J. Flores
C. Folsome, and C. Ponnamperuma
Exobiology Division, Ames Research Center
NASA, Moffett Field, Calif. 94035

The presence of organic compounds in meteorites has often been discounted because their distribution patterns were suggestive of terrestrial contamination (1). Recent work with the Murchison meteorite (2) has suggested that the organic compounds are indigenous and extraterrestrial in origin.

An analysis of the Murray meteorite, another Type II carbonaceous chondrite, was undertaken to substantiate these findings. The combined gas chromatography-mass spectrometry of the N-trifluoroacetyl-D-2-butyl ester derivatives of the amino acids in the Murray was studies. A suite of amino acids similar to those found in the Murchison was observed. The presence of amino acids with nearly equal amounts of D and L isomers, and others which are non-protein in character, suggest that they are indigenous to the Murray meteorite.

An investigation of aqueous and formic acid extracts of the Murchison meteorite by gas chromatography combined with both low and high resolution mass spectrometry has lead to the identification of 4-hydroxy-pyrimidine and two of its methyl isomers as their trimethylsilyl derivatives. No purines or triazines were detected.

This work has been submitted to Science for publication.

References

1. J. M. Hayes, Geochim. Cosmochim. Acta 31, 1395 (1967).
2. K. Kvenvolden, J. Lawless, K. Pering, E. Peterson, J. Flores, C. Ponnamperuma, I.R. Kaplan, and C. Moore, Nature 228, 923 (1970); J. Oro, J. Gibert, S. Wikstrom, and D.A. Flory, Nature 230, 105 (1971); K.A. Kvenvolden, J.G. Lawless, and C. Ponnamperuma, Proc. Natl. Acad. Sci. U.S.A. 68, 486 (1971).

The Use of Mass Spectrometry in the Identification of Organic Compounds in Arid Soils from Antarctica and the Mohave Desert. Carotenoid Pigments. H. G. BOETTGER, A. J. BAUMAN, A. M. KELLY, Jet Propulsion Laboratory, California Institute of Technology, and H. YOKOYAMA, Fruit and Vegetable Laboratory, USDA, Pasadena, Calif.

For a number of years we have been involved in an effort to characterize soils from the arid and hostile regions of the planet Earth which resemble the Martian model as closely as possible. Samples are being collected by R. E. Cameron of our laboratory from places that are either very hot or very cold, but always extremely dry and usually more or less saline. The samples, which may come from the surface or from several feet below the surface and may contain visible remmants of life or be totally devoid of any detectable life forms, are characterized in the usual biological ways, such as type and number of life forms, total organic content, total carbon, nitrogen, salinity and soforth.

Our interest as chemists and mass spectroscopists in these soils is three-fold. First of all, there is very little known about the chemistry of soils in general and hostile ones in particular in relation to the various life forms in it. Secondly, a more detailed knowledge of the chemistry of soils is vital to the question of the search for extraterrestrial life via space probes equipped with analytical-chemical instruments. Thirdly, the problem in itself is an extremely challenging one for the organic-analytical chemist due to the great complexity of the samples.

In order to attack this problem, collaboration is needed by experts from a number of disciplines. The organics have to be isolated from the soil matrix and split into the various chemical classes. These fractions must be further separated into individual compounds which finally have to be identified. Also we have found that many of the classical biochemical techniques for isolation and separation often do not work well with mixtures as complex as soil extracts. Therefore, modification of existing techniques or development of totally new techniques is required.

Very early in this work it was recognized that mass spectrometry, in both the HRMS as well as the LRMS mode, presents a tool of great value. It permits us to check the presence or absence of certain classes of compounds. It lets us follow these compounds through all steps of the isolation and purification procedures. In the end it aids us in, or often solely performs the identification of the separated compounds.

We shall now demonstrate this use of mass spectrometry with one recent phase of our work. This concerns the identification of carotenoid pigments in an algal mat collected in the Mojave Desert near Thermal, California. Figure 1 shows the result of the column chromatographic separation. The sample which is chromatographed was isolated by the latest conventional techniques for the isolation of carotenoids from biological media. In addition to the carotenoid composition listed, each fraction contained a host of other things. This is demonstrated by Fig. 2 which represents a plot of the total ion monitor output versus the probe temperature for fraction 07-3. I might inject at this point that all fractions are analyzed by means of our previously reported Temperature-Programmed-Probe technique. As you can see, we have a variety of substances still present. Wherever the amount of sample permitted, further purification was carried out by TLC and/or crystallization and mass spectra of these samples were used for final characterization. All samples were also digested with deutero-methanol and spectra taken of the residue to aid in the detection and localization of OH and COOH groups. The next two figures show computer plots from HR-spectra of some of the fractions where we had enough sample for purification.

Figure 3 shows from top to bottom the spectrum of authentic Canthaxanthin and fractions 06-7 and 07-3. The latter is Canthaxanthin as confirmed by visual spectra and NMR. 06-7 is most likely a Cis/trans isomer. As can be seen in the "authentic" Canthaxanthin spectrum, we have a series of peaks at M-16 which ELCOMP shows to be an apparent loss of oxygen and is reported as such by a number of investigators. As will be reported elsewhere in detail, we were able to show in all cases where we could obtain samples, that there is no M-Oxygen. The peaks at these masses were proven to be either due to artifacts, such as impurities, etc., or we were unable to duplicate the reported spectra. Figure 4 shows the high mass region of the HRMS listing for fraction 07-3 and represents all the characteristic peaks for carotenoids in general and Canthaxanthin in particular. Figure 5 shows the plotted spectra of some previously unreported Keto-carotenoids from fractions 07-2, 06-4a, and 06-4b. The top one is Echinenone, the next one is 3-Keto-α-Carotene. The third one is probably again a cis/trans isomer.

In the next two figures we have summarized the carotenoid content of the soil sample with positive molecular composition assignments by HRMS and more or less firm structural assignments also mostly carried out by HRMS. Only in case of Canthaxanthin and Echinenone enough sample was available for supporting evidence from NMR, etc. I might add that all this work was carried out with 2.6 mg of "carotenoid" extract which was obtained from 12 Kg of soil and, as mentioned above, still contained large quantities of other materials.

CHROMATOGRAPHIC ELUTION PATTERN (THERMAL SOIL)

FRACTION	%	COMPOSITION
07-3	57.50	$C_{29}H_{40}O_2$, $C_{30}H_{44}O$, $C_{40}H_{52}O_2$, $C_{40}H_{46}O_2$
07-2	6.95	$C_{40}H_{54}O$
35-3	1.78	$C_{40}H_{52}O_2$, $C_{29}H_{40}O_2$
06-8	5.73	$C_{40}H_{52}O_2$
06-7	5.04	$C_{40}H_{52}O_2$
06-4	6.89	$C_{40}H_{54}O$, $C_{40}H_{52}O_2$
20-3	1.63	?
20-2	1.52	$C_{40}H_{52}O_2$
26-5	2.34	$C_{29}H_{40}O_2$, $C_{41}H_{56}O$
26-4	2.30	$C_{40}H_{52}O_2$, $C_{40}H_{54}O$, $C_{40}H_{56}O_4$
26-3	6.08	?
36-2	2.17	$C_{40}H_{56}$, $C_{40}H_{56}O_2$, $C_{41}H_{56}O$

Figure 1

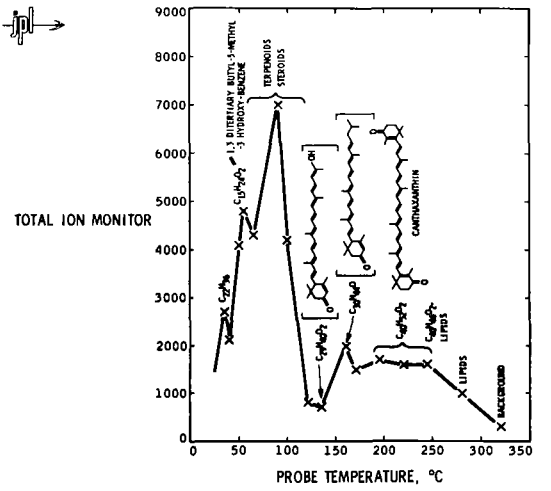

Figure 2

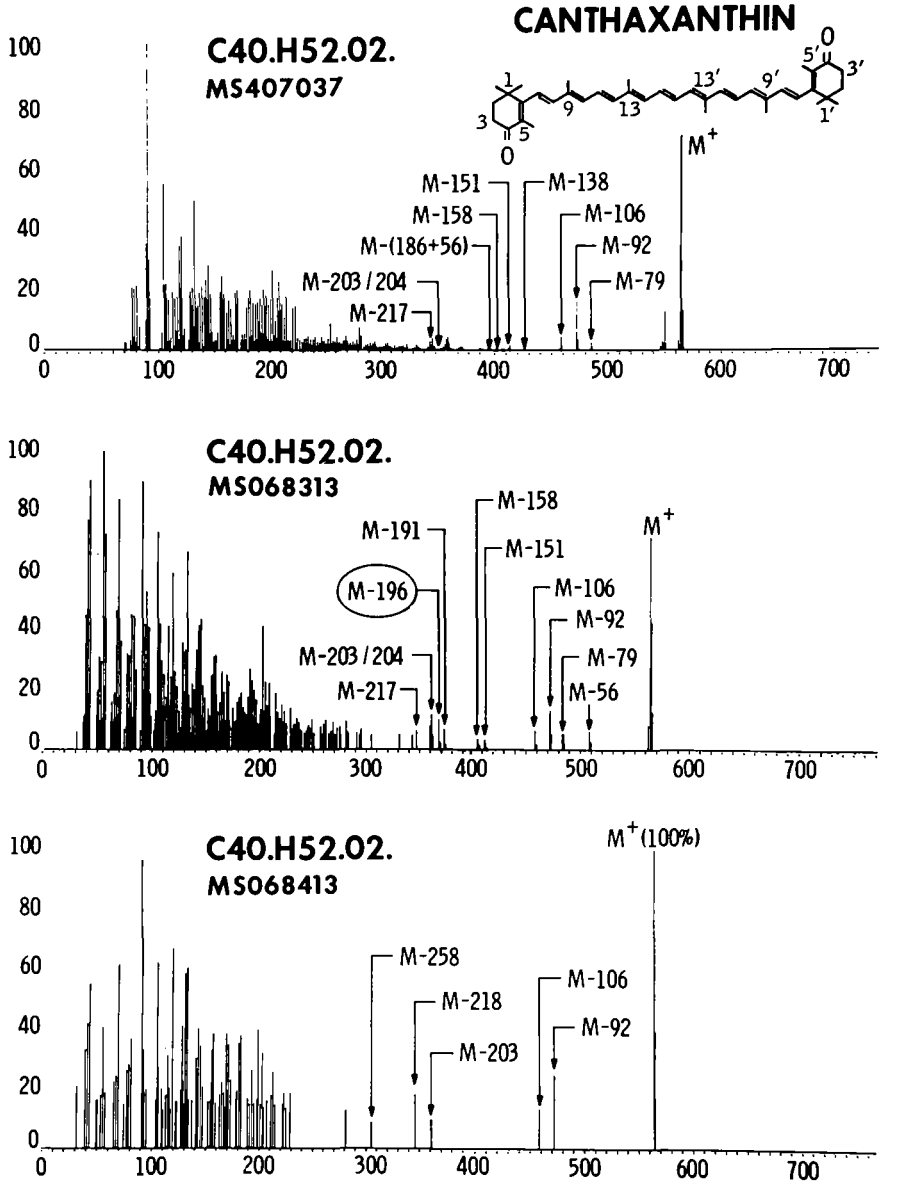
CANTHAXANTHIN
C40.H52.02.
MS407037
M+
M-151
M-138
M-158
M-106
M-(186+56)
M-92
M-203 / 204
M-79
M-217
C40.H52.02.
MS068313
M-158
M-191
M+
M-151
M-196
M-106
M-92
M-203 / 204
M-79
M-217
M-56
C40.H52.02.
MS068413
M+(100%)
M-258
M-218
M-106
M-92
M-203

Figure 3

MASS MEASUREMENT OF MAJOR PEAKS OF FRACTION 07-3

564.3974 = 564.3967	$C_{40}H_{52}O_2$	M^+
549.3765 = 549.3733	$C_{39}H_{49}O_2$	$M - CH_3$
508.3359 = 508.3341	$C_{36}H_{44}O_2$	$M - C_4H_8$
485.3467 = 485.3419	$C_{34}H_{45}O_2$	$M - C_6H_7$
472.3362 = 472.3341	$C_{33}H_{44}O_2$	$M - C_7H_8$
458.3175 = 458.3185	$C_{32}H_{42}O_2$	$M - C_8H_{10}$
412.2770 = 412.2766	$C_{30}H_{36}O$	$M - C_{10}H_{16}O$
(406.2872)* ~ 406.2872	$C_{28}H_{38}O_2$	$M - C_{12}H_{14}$
373.2478 = 373.2531	$C_{27}H_{33}O$	$M - C_{13}H_{19}O$
368.3026 = 368.079	$C_{26}H_{40}O$	$M - C_{14}H_{12}O$
361.2515 = 361.2531	$C_{26}H_{33}O$	$M - C_{14}H_{19}O$
360.2444 = 360.2453	$C_{26}H_{32}O$	$M - C_{14}H_{20}O$
347.2342 = 347.2375	$C_{25}H_{31}O$	$M - C_{15}H_{21}O$

*TOO SMALL FOR PRECISE MEASUREMENT

Figure 4

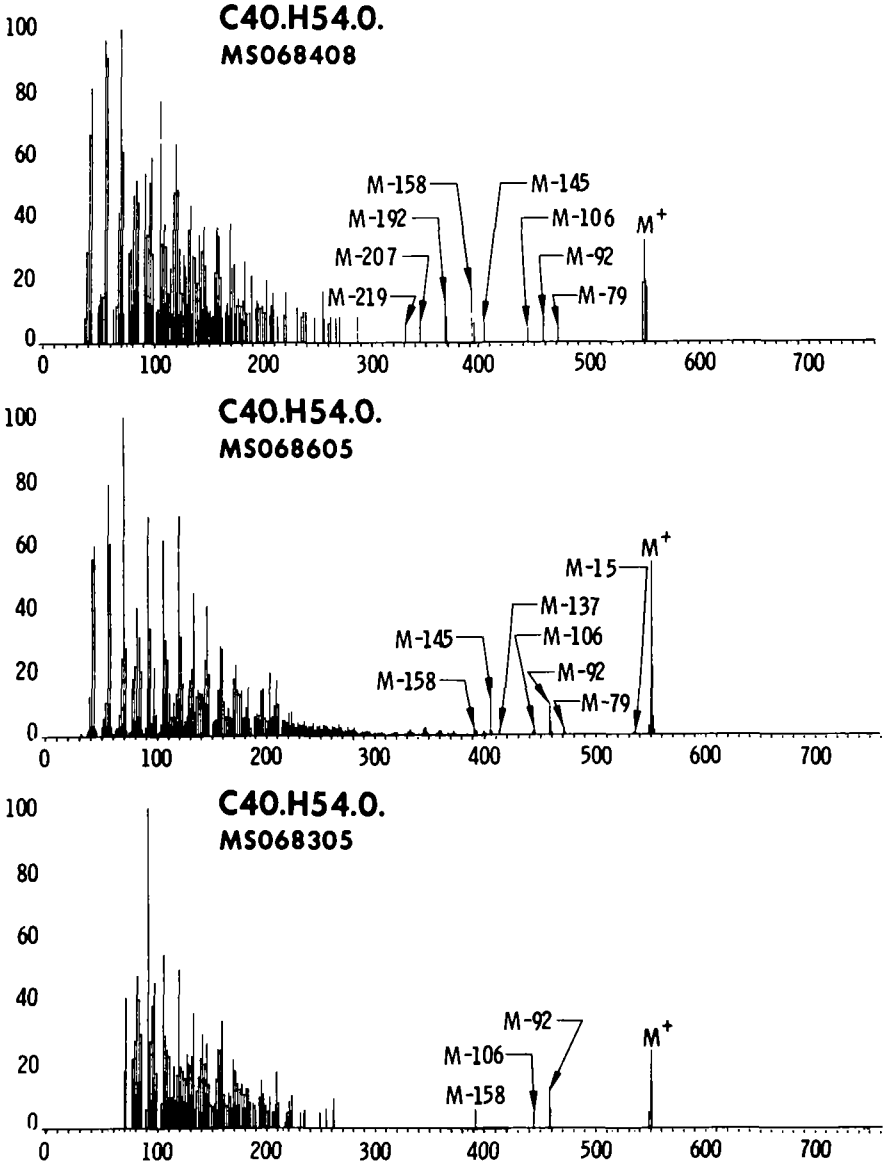
C40.H54.0.
MS068408
M-158
M-145
M-192
M-106
M+
M-207
M-92
M-219
M-79
C40.H54.0.
MS068605
M+
M-15
M-137
M-145
M-106
M-158
M-92
M-79
C40.H54.0.
MS068305
M-92
M+
M-106
M-158

Figure 5

CAROTENOID PIGMENTS IN SURFICIAL ALGAL CRUST COMMUNITIES OF DESERT SOILS

FRACTION NO.	MOL WEIGHT	MOL COMPOSITION	TENTATIVE STRUCTURE
07-3	420.3018	$C_{29}H_{40}O_2$	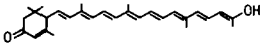
	420.3381	$C_{30}H_{44}O$	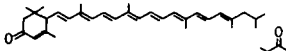
	564.3954	$C_{40}H_{52}O_2$	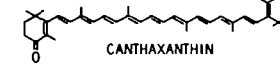 CANTHAXANTHIN
	558.3486	$C_{40}H_{46}O_2$	?
07-2	550.4161	$C_{40}H_{54}O$	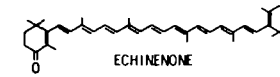 ECHINENONE
35-3	564.3954	$C_{40}H_{52}O_2$	?
	420.3018	$C_{29}H_{40}O_2$	?
06-8	564.3954	$C_{40}H_{52}O_2$	?
06-7	564.3954	$C_{40}H_{52}O_2$	?
06-4	550.4161	$C_{40}H_{54}O$	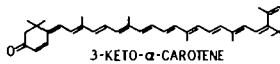 3-KETO-α-CAROTENE
	564.3954	$C_{40}H_{52}O_2$	?

Figure 6

CAROTENOID PIGMENTS IN SURFICIAL ALGAL CRUST COMMUNITIES OF DESERT SOILS (contd)

FRACTION NO.	MOL WEIGHT	MOL COMPOSITION	TENTATIVE STRUCTURE
20-3			TRACES AT 550-564-566
20-2	564.3954	$C_{40}H_{52}O_2$	
26-5	420.3018	$C_{29}H_{40}O_2$	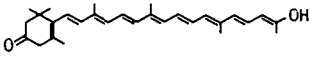
	564.4317	$C_{41}H_{56}O$	?
26-4	564.3954	$C_{40}H_{52}O_2$	?
	550.4161	$C_{40}H_{54}O$	?
	600.4164	$C_{40}H_{56}O_4$	?
26-3			TRACES OF CAROTENOL OR ONE-OL AT M/c = 550 AND 564
36-2	536.4368	$C_{40}H_{56}$	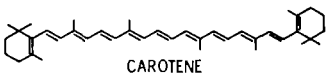 CAROTENE
	568.4266	$C_{40}H_{56}O_2$	?
	564.4317	$C_{41}H_{56}O$	?

Figure 7

TEMPERATURE AND ENERGY DEPENDENCE OF ION-MOLECULE REACTIONS OF POLAR COMPOUNDS

S. E. Buttrill, Jr.

Department of Chemistry, University of Minnesota
Minneapolis, Minnesota 55455

Introduction

The interaction between an ion and a polar molecule may be written as

$$V(r) = -(e^2\alpha/2r^4) - (ep/r^2) \quad (1)$$

where α and p are the angle-averaged polarizability and the dipole moment of the neutral. It is assumed in Eq.(1) that the dipole 'locks in' on the ion giving the maximum ion-neutral attraction. If one assumes that a reaction occurs on every collision in which the ion passes over the centrifugal barrier, then Eq.(1) gives the reaction rate constant as

$$k(E) = 2\pi e\left(\frac{\alpha}{\mu}\right)^{1/2} + \pi ep\left(\frac{2}{E\mu}\right)^{1/2} \quad (2)$$

where μ and E are the reduced mass and relative energy of the ion and neutral.

Experimental

Energy dependence studies were performed by applying a constant rf electric field at the cyclotron frequency of the reactant ion to the source region of a commercial ion cyclotron resonance spectrometer (Figure 1). The time that the ions spend in the source region is $\tau_S = L_S H/cE_S$ and normally the source drift field E_S is adjusted to make τ_S about one tenth of the total time that the ions spend in the cell. Reactant ions are thus accelerated to an average energy of

$$T = e^2E_2^2\tau_S^2/8m$$

before they enter the analyzer region. Both the product ion signal and the total ion current are measured as a function of reactant ion energy. Relative reaction rates are determined from relative product ion signal intensities corrected for small changes in total ion current.

Temperature dependence studies below room temperature were performed by cooling the analyzer vacuum chamber with liquid nitrogen. A jacket of 0.005 inch stainless steel extends from the six inch flange over the entire analyzer can. Using polyurethane foam insulation, liquid nitrogen consumption is about 2 liter/hour and operating temperatures of 140°K are attained after about 3 hours.

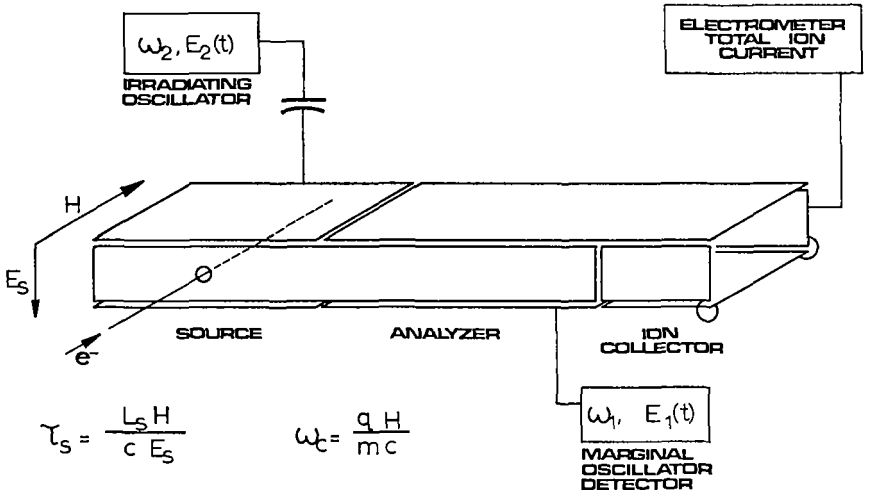

Figure 1: Side view of the flat ICR cell used for the energy dependence studies. Ions are formed by an electron beam in the source and are irradiated for τ_S seconds as they drift into the analyzer.

Results and Discussion

In order to test Eq.(2) relative rates of ion-molecule reactions in methane, HCl, ammonia, methyl fluoride, and hydrogen sulfide were measured as a function of reactant ion energy. The results are shown in Figures 2 and 3. The methane data are in good agreement with the work of Clow and Futrell (1) and the ammonia results agree with those of Huntress, et al (2). These workers used a sophisticated pulse technique to obtain relative reaction rate constants as a function of ion energy. The good agreement with this work confirms that reliable results can be obtained by the simpler technique used in this study. Since methane does not have a dipole moment, the reaction which forms protonated methane should have a rate which is independent of ion energy. In fact the rate constant for this reaction has fallen by 10 percent at an ion energy of 0.5 eV (Figure 2). In contrast the rate constant for the formation of protonated methyl fluoride in methyl fluoride (Figure 3) does not fall to 90 percent of the thermal value until the reactant ion energy reaches 0.9 eV. Detailed analysis of this data is not yet complete but the results indicate that Eq.(2) can not adequately describe the energy dependence of these ion-molecule reactions.

One factor not included in Eq.(2) is the rotational state of the polar molecule. Molecules with high rotational quantum numbers probably would not be able to 'lock in' on the ion and thus would not contribute as much to k(E) as molecules in lower rotational states. In order to examine the effect of the rotational state of the dipole moment on the ion-neutral interaction the total momentum transfer collision frequencies for non-reactive ions in methane, hydrogen sulfide, methyl fluoride, and nitrogen have been measured as a function of neutral gas temperature.

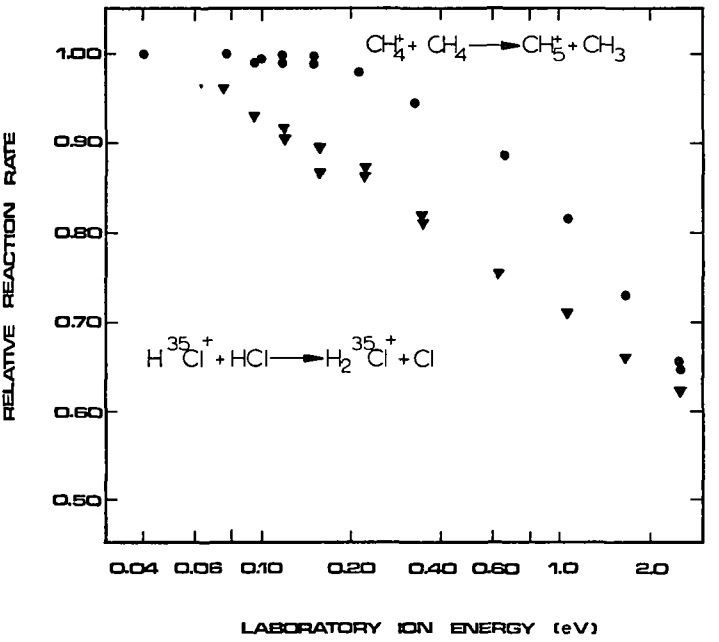

Figure 2: Relative reaction rate vs reactant ion energy for the reactions shown in methane and hydrogen chloride.

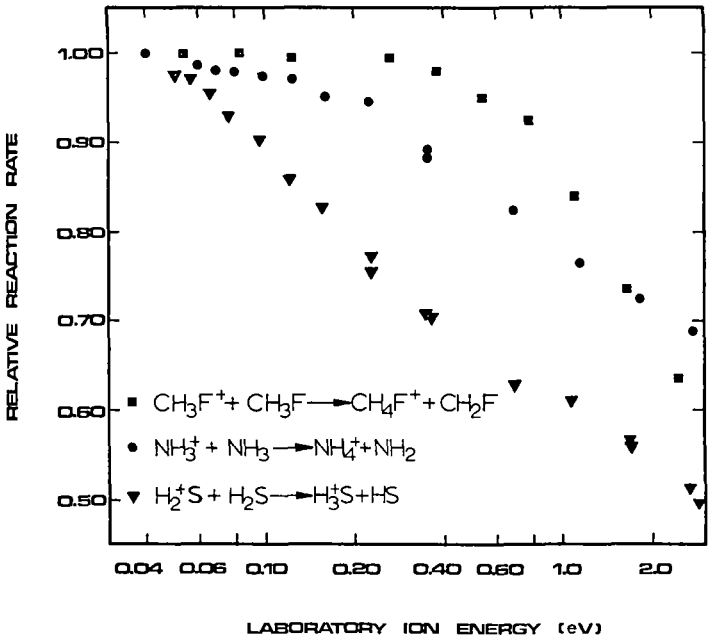

Figure 3: Relative reaction rate vs reactant ion energy for the reactions shown in methyl fluoride, ammonia, and hydrogen sulfide.

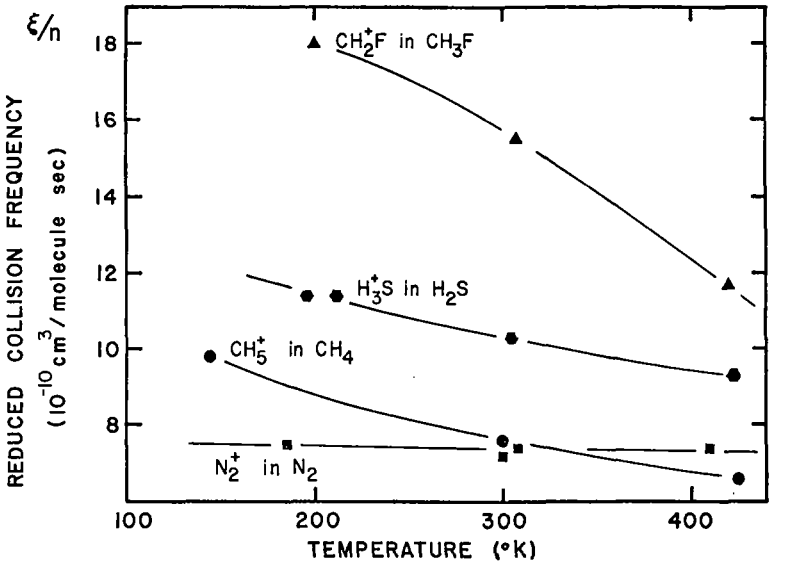

Figure 4: Reduced collision frequencies vs temperature for non-reactive ions in methyl fluoride, hydrogen sulfide, methane, and nitrogen. Relative ion-neutral translational energy is approximately 0.08 eV for all points shown.

The reduced collision frequency of an ion is obtained from the linewidth of the ICR power absorption signal at high pressure. The power absorption is given by

$$A = \frac{e^2 E_1^2}{4m\xi} \frac{\xi^2}{(\omega_1 - \omega_c)^2 + \xi^2}$$

where E_1 is the electric field strength of the observing oscillator and ξ is the momentum transfer collision frequency (3). The experimental results are shown in Figure 4. The pressure and the intensity of E_1 were adjusted to give a relative ion-neutral kinetic energy of approximately 0.08 eV in all experiments.

The temperature dependence of the CH_2F^+ collision frequency in methyl fluoride is the most striking, dropping from 18(-10) cm^3/molec sec at 200°K to 1.2(-10) cm^3/molec sec at 420°K. Since all other parameters are held constant, this effect must be due entirely to the change in the average rotational state of the dipole. The temperature dependence of the CH_5^+ collision frequency was suprising and prompted the experiments in nitrogen. The nitrogen results are in good agreement with data obtained by Huntress at room temperature (4).

Although quantitative comparisons are not possible at this time, these results are in qualitative agreement with the trajectory calculations of Dugan and Magee who found that the calculated collision cross section for HCl decreased with increasing rotational energy (5).

References

1. H. P. Clow and J. H. Futrell, Int. J. Mass Spectrom. Ion Phys., 4, 165 (1970).

2. W. T. Huntress, Jr., M. M. Mosesman, and D. D. Elleman, J. Chem. Phys., 54, 843 (1971).

3. J. L Beauchamp, J. Chem. Phys., 46, 1231 (1967).

4. W. T. Huntress, Jr., J. Chem. Phys., in press.

5. J. V. Dugan, Jr. and J. L. Magee, J. Chem. Phys., 47, 3103 (1967).

Research supported by the Graduate School of the University of Minnesota.

T2

Ion Cyclotron Resonance Studies of Ionic Reactions in Perfluorocarbons

Timothy Su and Larry Kevan
Department of Chemistry
Wayne State University, Detroit, Michigan 48202

Perfluorocarbon ion chemistry differs markedly from that of analogous hydrocarbons. The most interesting feature is that collision induced dissociation (CID) reactions are generally the most predominant reaction type for both perfluoroalkanes and perfluoroalkenes. Also the reaction rate constants are generally a factor of ten or more lower in perfluorocarbons compared to hydrocarbons. We have used ion cyclotron resonance (ICR) mass spectrometry to study the ion chemistry of C_3F_8 and to compare with our previous studies of this system by tandem mass spectrometry.[1] The complementary use of both instruments has led to an interesting comparison of kinetic energy effects on F^- transfer reactions.

By using low drift fields ICR has been used to detect a variety of F^- transfer, F transfer, F_2 transfer and CID reactions in C_2F_6 and C_3F_8. Examples include the following.

No	Reactions	ΔH^o_{rxn}, kcal/mole	dk/dE
1	$CF_3^+ + C_3F_8 \rightarrow i\text{-}C_3F_7^+ + CF_4$	14.9	+
2	$C_2F_5^+ + C_3F_8 \rightarrow i\text{-}C_3F_7^+ + C_2F_6$	7.8	+
3	$i\text{-}C_3F_7^+ + C_3F_8 \rightarrow CF_3^+ + C_2F_4 + C_3F_8$	20.8	+
4	$CF_3^+ + C_2F_6 \rightarrow C_2F_5^+ + CF_4$	7.2	+
5	$CF_2^+ + C_3F_8 \rightarrow CF_3^+ + i\text{-}C_3F_7$	-28.8	-
6	$CF^+ + C_3F_8 \rightarrow CF_3^+ + C_3F_6$	-23.6	-

The heats of reaction are calculated from a recent critical compilation of heats of formation of fluorocarbon species.[1] The dk/dE signs correlate with the thermochemistry. All endothermic reactions, which include all CID reactions, have positive signs and all exothermic reactions have negative signs. The correlation holds for all fluorocarbon reactions we have observed including reactions in C_3F_6, $2\text{-}C_4F_8$ and $cyclo\text{-}C_4F_8$. CID reactions predominate in these other perfluorocarbons also.

The kinetic energy dependence above threshold was studied for reactions 1 to 4 by both tandem and ICR mass spectrometry. In the ICR measurements a second radio frequency field of variable magnitude was applied to the source region of the ICR cell.

The source residence time was measured experimentally. Thus the ion kinetic energy was changed by varying the amplitude of the source radio frequency field. In this way measurements could be made to about 3 eV ion kinetic energy. The ICR measurement of the rate constant, k, vs ion center-of-mass kinetic energy showed that k increased rather sharply up to about 1 eV and then increased more slowly at higher energies for reactions 1, 2 and 4. This is the kinetic energy behavior that would be expected for these endothermic F^- transfer reactions. In striking contrast the tandem measurements on these same reactions show that the rate constant decreases with increasing kinetic energy. This is what one expects for an exothermic reaction. We believe that these apparently discordant results are due to the different time scales for ion detection in the tandem and ICR instruments. Since endothermic reactions are observed at near thermal energies in fluorocarbon systems it is apparent that excited ions are produced by electron impact fragmentation. This has been verified by studying the effect of varying the ionizing electron energy. In the tandem instrument the ion detection time is about 25 μsec while in the ICR instrument the ion detection time is about 3-5 msec. It appears that the excited CF_3^+ and $C_2F_5^+$ ions that participate in F^- transfer reactions are deexcited in the order of 1 msec. Thus the CF_3^+ and $C_2F_5^+$ reactions in the tandem are those of excited ions and are effectively exothermic, while the reactions in the ICR are indeed mainly endothermic.

In contrast to the F transfer reactions the CID reaction 3 shows the same kinetic energy behavior in the tandem and ICR instruments. In both instruments the rate constant increases with ion center-of-mass kinetic energy, reaches a maximum near 2 eV, and then decreases. This is quite reasonable for a reaction that is less than 1 eV endothermic.

1. T. Su, L. Kevan and T. O. Tiernan, J. Chem. Phys. (1971), in press.

This work will be submitted for publication to the Journal of Chemical Physics.

The Pulsed Ion Cyclotron Technique. R. T. McIVER and MAX A. HANEY*, T3
Dept. of Chemistry, Stanford University, California 94305.

A new ion cell and technique for ICR spectroscopy has been developed. All of the advantages of conventional ICR are retained. In addition, the technique permits the accurate determination of rate constants of ion-molecule reactions down to 10^{-13} cc/mol-sec. The ions are formed in a single-chamber cell by a short pulse of the electron feam. They are subsequently trapped within the cell for a known, variable period of time (up to 1 sec at 10^{-5} torr). During the reaction period, the ion motion is not perturbed by the marginal oscillator detector, which is set at a frequency off resonance. At the end of the reaction period, the electrostatic trapping field is pulsed to a higher value. This changes the resonant frequency of the ions and brings those with the desired mass into resonance. At the end of this detection period, all ions are ejected from the cell by inverting the electrostatic trapping field, and the cycle is repeated. The kinetic analysis is very simple and does not involve the approximations inherent in determining rate constants by conventional ICR. The long time for which ions can be trapped in the cell is advantageous in several other ways.

*Present address: National Bureau of Standards, Washington, D.C. 20234.

Study of S_N2 Reactions of Negative Ions by Pulsed ICR Spectroscopy. **T4**

MAX A. HANEY* and R. T. McIVER, Dept. of Chemistry, Stanford University, California 94305.

Rate constants for the class of nucleophilic substitution reactions $Y^- + RX \rightarrow X^- + RY$ have been obtained using the pulsed ion cyclotron technique. All exothermic reactions of this type occur, with rate constants ranging from 6×10^{-10} to 2×10^{-12} cc/mol-sec. The series $Cl^- + RB \rightarrow Br^- + RCl$ was studied to determine if alkyl substituents affect S_N2 reactivity in the same manner as they do in solution. The occurrence of the bromide displacement reaction in 1-bromoadamantane proves that a front-side attack mechanism can operate in the gas phase. Moreover, the effect of some of the other alkyl groups on reactivity is different from that in solution, suggesting that the Walden inversion mechanism may be absent in the gas phase. The series $Y^- + CH_3Cl \rightarrow Cl^- + CH_3Y$ was studied to obtain the order of nucleophillicity of anions in the gas phase. The reactivity of the anions appears to correlate with the negative charge density at the reactive center. This result is in accord with the traditional definition of nucleophilic reactions, although it is usually obscured in solution, where the degree of solvation largely controls reactivity.

*Present address: National Bureau of Standards, Washington, D. C. 20234.

T5

Study of Ion-Molecule Collision Complexes using Ion Cyclotron Resonance. JOHN R. EYLER, Chemistry Dept., Stanford Univ., Stanford, Ca. 94305

Using an ion cyclotron resonance spectrometer equipped with a trapped-ion analyzer cell[1], the kinetics of formation, decomposition, and stabilization of long-lived ion-molecule collision complexes have been investigated. The complexes studied were proton-bound dimer ions, $(2M+1)^+$, produced in simple aldehydes by the following mechanism:

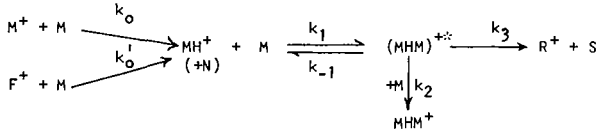

M = HCHO, CH_3CHO, C_2H_5CHO, i-C_3H_7CHO .

For all four systems studied, k_o and k_o' are much greater than k_1 and k_2, and for propanal and 2-methyl propanal, $k_3 = 0$. These two observations make it possible to analyze the much simpler scheme:

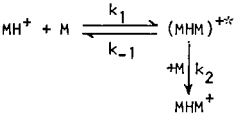

for propanal and 2-methyl propanal.

The exact kinetic equations for this scheme have been solved, and a computer program written which compares calculated values of ion intensity vs. time with those obtained experimentally.

For the propanal system, preliminary results indicate best agreement between observed and calculated curves for $k_1, k_2 \cong 3\text{-}4 \times 10^{-10}$ cc/mol.sec, and $k_{-1} \cong 1\text{-}2 \times 10^4$ sec^{-1}. The lifetime of the collision complex with respect to unimolecular decomposition is the inverse of k_{-1} and is thus found to be $0.5\text{-}1.0 \times 10^{-4}$sec.

[1]R.T. McIver, Rev. Sci. Instrum., 41, 555(1970).

Author Index

Name	Paper No.
Aandahl, V.	H2
Aczel, T.	S1
Alexander, C. A.	L11
Anderson, D. A.	D4
Arsenault, G. P.	J3
Ast, T.	K7
Bakker, J. M. B.	P3
Baril, M.	P5
Bauman, A. J.	S8
Baumel, I.	K11
Bayard, M. A.	Q4
Bazinet, M. L.	N5,K4
Beauchamp, J. L.	G2
Bennett, S. L.	R9
Beggs, D. P.	J6
Berkowitz, J.	A2,A4,M2
Beuhler, R. J.	O4
Beynon, J. H.	K7,K8
Bhattacharya, A. K.	K1
Biemann, K.	F2
Biller, J. E.	F2
Bird, J. S.	H4
Bird, K. E.	H4
Blosser, E. R.	Q3
Blue, G. D.	L5
Boettger, H. G.	S8
Bohme, D. K.	R5
Bolduc, L.	P5
Bone, L. I.	M3
Botter, R.	K11
Brehm, B.	E2
Briggs, P. R.	B5
Brown, P.	H9
Brown, R.	S5
Brubaker, W. M.	P2,R1
Brunnee, C.	K9
Burlingame, A. L.	C4
Burnham, D.	R1
Buttrill, Jr., S. E.	T1
Cabaniss, C.	H5
Canright, Jr., R. B.	M1
Caprioli, R. M.	K7
Carrico, J. P.	R3
Carroll, C. A.	D4
Carroll, D. I.	R6
Cerimele, B.	A7
Chen, C. T.	A10
Chew, G. J.	H10
Chong, S.-L.	R10
Chapman, J. R.	N3
Chupka, W. A.	A2, M2
Cocke, D. L.	L6
Cohen, A. I.	B7
Cohen, M. J.	P6
Cohen, S. C.	K3
Colby, B. N.	H11
Cook, J. C.	F5
Cooks, R. G.	B12
Coutant, J. E.	C3
Dalton, J.	J4
Daly, N. R.	K10
Damoth, D. C.	N2
De Celles, M.	P5
De Corpo, J. J.	I2
De Jongh, D. C.	B4
Deschamps, P.	Q5
Desiderio, D. M.	H8
Dibeler, V. H.	A1,A3
Di Domenico, A.	L2
Dillard, J. G.	L3
Di Pietro, C.	N5
Dobbs, C.	N2
Dolhun, J. J.	J3
Dooley, C. J.	D1
Dougherty, R. C.	J4,J6
Drewery, C. J.	T6
Duffield, A. M.	D4
Dugan, Jr., J. V.	M1
Duncan, J. H.	J1
Earle, N. R.	F4
Edwards, T. R.	S2
Ehlert, T. C.	A6
Ehrhardt, H.	E1
Einolf, N.	J2
Elwood, T. A.	K8
Emmel, R. H.	A10
Eyler, J. R.	T5
Fano, U.	E0
Fairwell, T.	H5
Fales, H. M.	H2,H6,J1,K6
Falick, A. M.	C4
Fehsenfeld, F. C.	L1,O7
Fenselau, C. C.	B6,J1
Ferrer-Correia, A. J.	T6
Field, F. H.	J7,M8,R9
Finkbeiner, H. C.	L6
Fiquet-Fayard, F.	J8
Flesch, G. C.	I1
Flores, J.	S7
Foglia, T. A.	D1
Folsome, C.	S7
Foltz, R. L.	J5
Forrest, H. S.	F8
Foster, N. G.	B10
Fraas, R. E.	I3
Franklin, J. L	L2,O3,R10
Freese, J. M.	L9
Friedel, R. A.	Q2
Friedman, H. L.	Q1
Friedman, L.	O4
Frisch, M. A.	N7
Funke, P. T.	B7
Futrell, J. H.	G3,H7,O1
Gay, M. L.	B4
Gilbert, J. M.	S6
Giessner, B. G.	A10
Gingerich, K. A.	L6
Goode, G. C.	T6
Gray, W.	H7
Grayson, M. A.	P4
Green, M. M.	B1
Grigsby, R. D.	H4
Grotch, S.	D7
Guyon, P. M.	A2
Habfast, K.	K9
Hagemann, R.	K11
Haney, M. A.	T3,T4
Halliday, D.	H10
Halliday, F. O.	R2
Harden, C. S.	P1

Author Index

Name	Paper No.
Harvey, D. J.	B2,M5
Haug, P.	F8,N1
Henis, J. M. S.	G4
Hertz, H. S.	F2
Herzberg, G.	C0
Herzog, R. F.	C2
Hesselbacher, K. H.	E1
Hierl, P. M.	O3
Higgins, R. W.	B10
Hills, L. P.	O2
Horning, M. G.	B2,M5
Hughes, B. M.	O6
Hughes, D. B.	P7
Huntress, W. T.	R11
Hutterer, F.	H1
Itoh, M.	O5
Jackson, K. M.	R4
Jacox, M. E.	G1
Jennings, K. R.	B12,T6
Johnson, B. M.	B11
Johnson, M. C.	R3
Johnston, W. H.	J6
Jones, E. G.	J10
Jones, S.	B12
Jung, K.	E1
Junk, G. A.	I1
Kamano, J.	H9
Kappus, G.	K9
Karasek, F. W.	P6
Kaufman, M.	N4
Kebarle, P.	R8
Keller, Jr., D. V.	S3
Kelly, A. M.	S8
Kempter, V.	M4
Kershner, A.	F5
Kessler, T.	Q2
Kevan, L.	T2
King, R. B.	I4
Kilpatrick, W. D.	R7
Kiser, R. W.	I3
Klemann, L. P.	J7
Klots, C. E.	A9
Kohl, F. J.	L7
Kohn, F. J.	L8
Kolb, C.	N4
Kupperman, A.	N6
Kvenvolden, K.	S7
Kwok, K.	D6
Lanthier, G. F.	I5
Lampe, F. W.	M4
Lao, R. C.	Q7
Laurie, W. A.	B8,M8
Law, N.	H2
Lawless, J. G.	S7
Leclercq, P. A.	H8
Lee-Ruff, E.	R5
Leferink, J. G.	F4
Lett, R. G.	S4
Lewis, R.	Q5
Ligon, Jr., W. V.	F6
Limming, H. J.	N3
Lipsky, S. R.	D8
Logar, Jr., A. F.	S4
Lossing, F. P.	A5
Lovins, R. E.	H5
Luchte, A. J.	N2
Lumpkin, H. E.	S1
Lynch, A. W.	L9
Madson, J. M.	J9
Margrave, J. L.	K2
Markey, S. P.	H3
Mason, E. A.	R6
Massey, R. I.	T6
Maurer, K. H.	K9
McAdams, M. J.	M3
McCloskey, J. A.	M6
McCormick, A.	K10
McCulloh, K. E.	A1,A3
McDowell, M. V.	I2
McGrew, J. G. II	B1
McIver, R. T.	T3,T4
McLafferty, F. W.	D6
McLeod, P. C.	R4
McMurray, W. J.	D8
McNair, H.	N2
Medgyesi-Mitschang, L. N.	J9
Meisels, G. G.	A10,M7
Merren, T. O.	N3
Merritt, Jr., C.	K4,N5
Meyer, R. T.	L9
Michnowicz, J.	J2
Miller, J. M.	I5
Milligan, D. E.	G1
Millington, D. S.	F7
Milne, G. W. A.	H2,H6
Mitani, E.	O5
Monkman, J. L.	Q7
Moore, L. E.	H10
Morrison, G. H.	H11
Mosharrafa, M.	N8
Mullen, J. H.	J9
Munson, B.	J2
Nowak, A. V.	F1
Nowlin, T. D.	P7
Occolowitz, J. L.	A7
Ogden, J. S.	L11
O'Malley, R. M.	T6
Oro, J.	S6
Osman, S.	D1
Page, R. P.	F1
Pardue, W. M.	L11
Paulson, J. E.	J11
Payzant, J. D.	R8
Pering, K.	S7
Perkins, G. D.	R1
Peterson, E.	S7
Pettit, G. R.	H9
Plattner, J. R.	H3
Pfeifer, J. P.	C4
Ponnamperuma, C.	S7
Porter, R. F.	K5
Pottie, R. F.	Q7
Powell, R. E.	K10
Powers, P.	F3
Rabideau, P. W.	K8
Reed, R. I.	D5
Reynolds, W. E.	D4
Rhyne, T. C.	L3
Ridley, R. G.	D3

Author Index

Name	Paper No.
Rinehart, Jr., K. L	F5,F6,F7
Roberts, D.	J4
Robertson, D. H.	D5
Robinson, C. H.	B6
Robinson, R. J.	C3
Roboz, J.	H1
Romiez, M.	S7
Rosenstock, H. M.	A1
Rudenauer, F. G.	C5
Ruhig, A.	H1
Russell, M. E.	A8
Saalfeld, F. E.	I2
Sage, H.	H7
Sarkozi, L	H1
Satkiewicz, F. G.	Q6
Sayer, J.	S3
Schaefer, P.	F5
Schaffner, C. P.	F5
Schmidt, K. C.	R3
Schroder, U.	K9
Schulze, P.	K9
Scott, W. M.	D3
Serum, J.	F8,N1
Settle, G. L.	S2
Seyse, R. J.	L6
Shannon, T. W.	B5
Sharkey, Jr., A. G.	Q2,S4
Sharma, D. K. S.	O3
Smith, D. L.	O1
Smithson, L. D.	K1
Solka, B. H.	A8
Solomon, J. J.	K5
Spohr, R.	A4
Sprouse, J. F.	R4
Sroka, G.	M7
Stafford, F. E.	L4
Stearns, C. A.	L7,L8
Steck, S. J.	K2
Steiger, R. P.	K2
Stein, J. D.	R2
Stillman, Jr., R. A.	D4
Stillwell, R. N.	F4
Stuckey, W.	L10
Su, T.	T2
Sun, T.	H5
Svec, H. J.	I1
Sweetman, B. J.	B9
Taylor, J. W.	B11
Testerman, M. K.	R4
Thompson, R. J.	Q3
Tiernan, T. O.	J10,O2,O6
Ting, K.-L.	K6
Tsuyama, H.	O5
Updegrove, W.	N1
Urushibara, T.	F8
Venkataraghavan, R.	D6
Vossen, P. G. T.	S5
Vouros, P.	B2,B5,M5
Wacks, M. E.	B8
Wagner, P. E.	P1
Walker, J. A.	A1,A3
Wallington, M. J.	F3
Ware, R. E.	R4
Washco, L. S.	F4
Watson, J. T.	B9
Weber, W. P.	B3
White, P. A.	H8
Whitney, T. A.	J7
Whittaker, A. G.	L10
Wikstrom, S. A.	S6
Wiley, R. H.	D2
Willmann, K.	E1
Wilson, M. H.	M6
Wojcik, L.	H7
Wolber, W. G.	R3
Wolf, C. J.	P4
Wolff, R. E.	B9
Wolfgang, R.	M0
Wood, Jr., G. M.	N8
Yamdagni, R.	R8
Yeomans, W. G.	K4
Yokayama, H.	S8
Young, L. B.	R5
Yu, T.-Y.	M4
Ziesel, J.-P.	J8

ASTM COMMITTEES AND ASTM E-14 SUBCOMMITTEES

ASMS Com. II - "Fundamental Aspects", R. S. Berry, Department of Chemistry, University of Chicago, Chicago, Illinois 60637

Joint Com. III -"Computer and Data Processing", M. C. Hamming, Continental Oil Company, P.O. Drawer 1267, Ponca City, Oklahoma 74601

ASTM E-14 Subcom. IV - "Data and Information Problems", P. W. Shearer, Hercules, Inc., Wilmington, Delaware 19899

ASMS Com. V - "New Instruments and Techniques", H. J. Svec, Department of Chemistry, Iowa State University, Ames, Iowa 50010

Joint Com. VI - "Biological Applications", J. A. McCloskey, Institute for Lipid Research, Baylor College of Medicine, Houston, Texas 77025, and J. R. Roboz, Mt. Sinai School of Medicine, New York, New York

ASMS Com. VII - "Study of Solids", A. J. Ahern, 9621 E. Bexhill Drive, Kensington, Maryland 20795

ASMS Com. VIII - "High Resolution Studies", D. C. DeJongh, Wayne State University, Detroit, Michigan 48202

ASMS Com. IX - "Aids to Education", J. G. Dillard, Chemistry Department, Virginia Polytechnic Institute, Blacksburg, Virginia 24061

ASTM E-14 Subcom. X - "Definitions and Terms", G. L. Cook, Laramie Energy Research Center, Box 3395, University Station, Laramie, Wyoming 82070

Joint Com. XI - "Evaluation of Critical Data for Health Sciences", A. J. Sharkey, U. S. Bureau of Mines, 4800 Forbes Avenue, Pittsburgh, Pennsylvania 15213

COMMITTEE II. FUNDAMENTAL ASPECTS

CHAIRMAN, R. S. BERRY

Committee II on Fundamental Aspects met at 5:00 P. M., Monday, May 3, 1971. Professor R. S. Berry, Chairman of the Committee, was unable to attend due to temporary disability and Program Chairman F. H. Field appointed W. A. Chupka to conduct the meeting.

Approximately 50 persons attended the meeting. The major subject of discussion was the suggestion of research areas which are particularly appropriate as subjects of symposia for the 1972 meeting. The subjects proposed together with the number of votes in support and additional comments are given below.

1. Dissociative Attachment of Electrons to Molecules (26 votes)

   This would include both experiment and theory. A review of the status of theoretical developments, rather than a detailed exposition of calculational procedures was judged to be most appropriate in the category of theory. Possible speakers mentioned were G. J. Schulz (Yale University), H. S. Taylor (U. S. C.-Theory), L. G. Christophorou (ORNL), P. J. Chantry (Westinghouse).

2. Photodetachment of Negative Ions (21 votes)

   Suggested as speakers were Linebarger (JILA), some member of the Stanford group working with Baldeschwider, B. Steiner (NBS-Washington). It was suggested that this topic might well be combined with 1 to constitute a more general symposium on negative ions.

3. Electron Spectroscopy (other than analytical applications) (12 votes)

   This subject would include electron spectroscopy of gases and possible of solids and surfaces. In the latter case, the possibility of a symposium jointly sponsored by Committee VII on Solids might be explored.

4. Ion Cyclotron Studies of Ion Molecule Reactions (4 votes)
5. Ions in Flames (3 votes)
6. Electrical Discharges (2 votes)

Joint Committee III - Computer and Data Processing
ASMS Committee and ASTM E-14 Subcommittee

Mynard C. Hamming, Chairman
Continental Oil Company
Research and Development Department
Ponca City, Oklahoma 74601
Phone: (405) 762-3456 Ext. 4741
(405) 764-4190

Purpose and Scope:

To serve as a clearing house to handle the international exchange of computer programs related to mass spectrometry.

Summary of Meeting in Atlanta, 1971

Several indicated that they planned to send computer programs to this committee. Such programs or information about these programs will be made available on a continuing basis throughout the entire year by the Newsletter (a joint effort with Committee XI). As one person attending the meeting expressed it, much can be learned about computer programs by carefully reading existing programs. The desire to collect and examine small computer programs was expressed. A program which took a half day for one person to write may save the same amount of time for another individual. Even "tricks" used in setting up a program may prove useful.

One of the objectives is that technical activities become organized into a modest workshop taking place at the 1972 meeting. Small groups of those with computer knowledge could exchange it directly with others on a person to person basis. This idea is being developed and if your desires are expressed, the program can be more useful to you and others. A number of programs have been collected and the usefulness of the committee in the past was expressed.

Discussions are invited during the year with any of the members on this committee:

E. M. Emery
Colgate-Palmolive Co.
909 River Road
Piscataway, N. J. 08854
Phone: (201) 463-1212 Ext. 375
(201) 264-0754, North Brunswick, N. J.

F. W. Karasek
University of Waterloo
Department of Chemistry
Waterloo, Ontario
Canada
Phone: (519) 744-6111 Ext. 3423

P. R. Kennicott
General Electric Co.
Box 8
Schenectady, N. Y. 12301
Phone: (518) 346-8771 Ext. 6131
(518) 399-4567

J. Rogers Woolson
RCA Laboratories
David Sarnoff Research Center
Princeton, New Jersey 08540
Phone: (609) 452-2700 Ext. 2858

G. R. Sparrow
Analytical Research and Services
3M Company
Central Research Laboratories
P. O. Box 3221
St. Paul, Minnesota 55101

COMMITTEE V, NEW INSTRUMENTS AND TECHNIQUES

AMERICAN SOCIETY FOR MASS SPECTROMETRY

Chairman, Harry J. Svec

Committee V met from 5:00 to 7:00 P.M. in the York Room, Regency Hyatt House, Atlanta, Georgia, May 4, 1971. An over-run crowd (estimated to be ~175) packed into the meeting room in which there were 140 chairs. The meeting began with a short statement by Chairman, H. Svec concerning the objectives of the committee. This committee has had topical programs for many years at which instruments and techniques, once they had become well enough established to become a coherent part of the tools of a mass spectroscopist, were discussed. These discussions have been in the forms of talks, panel discussions, question and answer sessions, and exchanges of ideas by the members attending the committee meetings. Generally, the format has broken down into more or less formal reviews of a topic followed by open exchange of questions about and approaches to problems pertinent to the topic. This topical approach has involved many practical aspects of magnetic deflection instruments, leak detectors, vacuum systems, ion pumps, spark source mass spectrometers, high resolution mass spectrometers, time-of-flight instruments, radio frequency instruments, cyclotron-resonance instruments, quadrupole instruments, the gas chromatograph-mass spectrometer combination and ion probe and imaging instruments.

The topic for the 1971 meeting concerned a review of the gas chromatograph-mass spectrometer combination along lines which would not only benefit the expert but most of all the neophytes. A ~40 minute informal talk was presented by G. A. Junk of the Ames Laboratory USAEC summarizing the subject as it is currently practiced. A comprehensive bibliography covering the literature of the field through 1970 was available to committee members. Mr. Junk's talk was followed by a lively discussion concerned with practical aspects of the subject. The discussion persisted unabated until the chairman cut if off at ~6:45 P.M. in order to summarize what had gone on and take care of any business.

During the summary of the meeting and just prior to adjournment the members were polled concerning whether or not they approved of the format of the Committee V meeting. There was an overwhelming opinion that not only did they approve of the format but those present questioned why more of the ASMS Conference was not devoted to similar meetings. As a result of this ground swell, an ad hoc committee consisting of Leonard Herzog (Nuclide), Frank Preston (Olin), and Donald R. Woods (Ashland Oil) was formed whose charge was to report to the general membership the feelings of the 90-100 people still present at the end of the Committee V meeting. This report was made by Dr. Herzog at the annual business meeting on Wednesday, 5 May, 1971. A transcript of the manuscript version of the report has been submitted to the ASMS Executive Board for their consideration.

A new mailing list consisting of 120 names was collected at the meeting. Several attendees on the list indicated their interest in the business of the meeting and willingness to cooperate in the work of the committee.

The talk given by G. A. Junk was a synopsis of a review which is being prepared for publication in the International J. of Mass Spec. and Ion Physics. Publication is expected in 1971. End of committee report.

COMMITTEE VI: BIOLOGICAL APPLICATIONS

Co-Chairmen: Dr. J. A. McCloskey

Institute for Lipid Research
Baylor College of Medicine
Houston, Texas 77025

Dr. J. Roboz

Automation Development Laboratory
Mount Sinai Medical Center
11 East 100th Street
New York, N.Y. 10029

Committee VI on Biological Applications of Mass Spectrometry is a new Committee created during the 1971 meeting of the ASMS in Atlanta. The topics discussed during the organizational meeting were: name of the committee, subjects with which the Committee should be concerned, and means of dealing with these topics.

The name of the Committee - Biological Applications - was approved.

Scope of the Committee: General area of biomedical applications of mass spectrometry. Emphasis will be placed on GC/MS applications but without restricting activities to this area.

Plans for 1971/1972:

1.) A list of all US government-funded projects involving biomedical applications of mass spectrometry will be prepared and distributed to members of the Committee. In charge: Dr. J. Milne of NIH. To make this list as complete as possible, project titles of non-government funded clinical applications should be communicated to Dr. Milne by members.

2.) The Committee will be involved in questions of GC/MS instrumentation only to the extent of: (a) Special instrumentation needs for clinical applications, (b) Dissemination of information concerning new developments. An effort will be made to continue the GC/MS bibliography compiled by G. Junk and H. Svec. Volunteers are solicited for this work.

3.) An attempt will be made to collect and distribute mass spectra of clinically interesting drugs and metabolites as they become available. (The term "metabolite" is meant to be used in a rather loose sense). In charge: Dr. S.P. Markey, address: JFK 3113 (2741), University of Colorado Medical Gr., 4200 E. 9th Avenue, Denver, Colorado 80220. Spectra should be submitted to Dr. Markey. Next year an attempt will be made to standardize the method of submission. Also, efforts will be made to coordinate this activity with that of the Aldermaston data collection center.

4.) A Newsletter will be initiated and published periodically. Items will include new publications (references) of general interest, availability of new instruments, novel attachments, etc. Contributions are solicited.

5.) A mailing list will be set up. Suggestions for the program in 1972 are requested.

ASMS COMMITTEE VII FOR STUDY OF SOLIDS

1. Purpose and Scope of Committee VII

This committee is charged with concern for all aspects of mass spectrometric analysis of inorganic solids. In practice its scope has been limited to spark source, sputter ion source and laser ion source mass spectrometry. This limited scope merely reflects the interests of most of the people that participate in the work of the committee.

2. Roster of Key Personnel

A. J. Ahearn, Chairman
P. R. Kennicott, Vice-Chairman
R. J. Couzemius, Secretary
P. R. Kennicott, Task Force Leader, Cooperative Testing Studies
H. Farrar, Task Force Leader, Compilation and Evaluation of Relative Sensitivity Coefficients for Spark Source Mass Spectrometry

3. Major Projects 1969-1971

A. Workshop in Pittsburgh Nov. 17-18, 1969
W. M. Hickam, Chairman
B. Workshop in San Francisco June 16, 1970
J. R. Woolston, Chairman
C. Workshop in Pittsburgh Nov. 16-17, 1970
F. D. Leipziger, Chairman
D. Workshop in Atlanta May 5, 1971
W. W. Harrison, Chairman

4. Projects Planned for 1971-1972 and/or Later

A. Autumn Workshop 1971
B. Spring Workshop 1972
C. A detailed study of the ionization processes in electrical discharge ion sources is proposed. The purpose would be to derive the relations between the pertinent properties of trace and matrix elements in a solid sample and the relative numbers of trace ions and matrix ions produced in the discharge.

5. Committee VII Meeting and Workshop on May 5, 1971 in Atlanta during ASMS Annual Conference.

The meeting was opened at 9 AM by presentations of the point of view of the ASMS Board of Directors regarding committee activities in general and workshops specifically. This can be summarized as follows.

The ASMS Board of Directors believes that if an activity, such as an extended committee meeting or workshop, draws a sizeable attendance year after year, this is a clear indication that ASMS should support, and provide for, such functions as a service to its members. At the same time, there is definite concern among ASMS Board Members over a number of problems posed by such activities. The Board feels that one should make certain that such an activity whether held during the Annual Conference or at some other time, have technical content commensurate with the time allotted to it; that it fit in well with, and not duplicate, the remainder of the organized program; and that attendance at outside workshops not affect adversely attendance at the Annual Conference.

To achieve these goals, the Board of Directors suggests that prior to setting up any activity, the Committee Chairman involved should submit to the Vice-President for Programs a specific outline indicating its timing, location, format, technical contents, and any ASMS support required. The Vice-President for Programs will review the proposal and, if necessary, confer with the originator in case there are problems or conflicts. Once approved, the details of setting up the activity remain the full responsibility of the Committee Chairman.

To assess the current workshop needs and desires of Committee VII participants, the following questionnaire was then submitted to those in attendance. The number of responses favoring each choice in the questionnaire is included.

QUESTIONNAIRE - ASMS Committee 7 Workshops

1. What is your preference regarding future workshops?

   19 A workshop during the ASMS Annual Conference

   3 A workshop before or after the ASMS Annual Conference

   8 A two day workshop during this autumn

   14 Both

   1 Neither

2. What is your preference for a workshop during the ASMS Annual Conference?

   36 A one day workshop as in 1970 and 1971

   5 A half day workshop as in 1968 and 1969

   3 Other 0, 2, 5 days

3. What is your preference regarding location of an autumn workshop for 1971?

   5 Pittsburgh as in 1969 and 1970

   20 St. Louis if held during the week of the SAS meeting there in Oct. 18-22

   7 Elsewhere NYC, Santa Barbara, Las Vegas, Washington, D.C.

4. Mark the following conferences that you have attended.

   28 1968 May ASMS Conference in Pittsburgh

   28 1968 November Workshop at National Bureau of Standards

   27 1969 May ASMS Conference in Dallas

   26 1969 November Workshop in Pittsburgh

   22 1970 June ASMS Conference in San Francisco

   23 1970 November Workshop in Pittsburgh

At the end of the day, after the above responses to the questionnaire were presented, an hour long vigorous discussion on Committee VII workshops ensued. A resolution was then passed 35 to 4 favoring the usual autumn workshop in 1971 and the usual spring workshop in 1972. The resolution also suggested that the Vice President for Programs consider a symposium on Mass Spectrometric Analysis of Solids for the ASMS Conference in 1972.

During the week the conviction grew that the workshops were an excellent potential source for formal papers at subsequent ASMS conferences and that a concerted effort should be made to spot exceptional work in progress, to persuade the doers to finish the job and to present formal papers. Conversely, individuals tempted to make formal papers out of inadequate material might be dissuaded.

The major part of the day was devoted to a workshop, organized and conducted by Dr. W. W. Harrison, a summary of which is attached. The attendance at this day long meeting fluctuated from 44 to 70, with 62 people signing the attendance register.

A. J. Ahearn
Presiding Officer and Acting Secretary

WORKSHOP SUMMARY

Topic I. A CLOSER LOOK AT ELECTRICAL DETECTION

Moderator: J. C. Franklin (Union Carbide, Oak Ridge, Tennessee)

The purpose of this session was to examine some of the problems associated with the initial setup of electrical detection systems for spark source mass spectrometry, to provide information concerning the reliability and accuracy of the method, and to point out some applications of the electrical detection technique.

Some parameters for critical tuning of the instrument for isotopic analysis in the peak switching mode were discussed. These parameters included collector slit, focus voltages, and cassette position. Additional improvements in precision were reported due to use of synchronized beam chop and accurate beam monitoring methods. Precisions of less than $\pm 1\%$ were obtained consistently for isotopic analysis.

The accuracy of an automatic spark control was discussed as it applies to control of the spark gap and its effect on analytical precision. The analytical gap was deemed to be most critical for metal samples. A system of monitoring spark gap width by means of an RF probe was described and the results obtained from measuring gap width were presented. In addition, a gadget was displayed that allowed use of micromanipulator and sample vibration simultaneously. This device provided a significant improvement in operating conditions. Additional modifications presented during the session were: (1) a monitor modification that allows use of the ratiometer and ion current to visually locate peak maxima without changing monitor heads, (2) an improved collector slit for more accurate centering of the ion beam, (3) a multichannel scaler that could be synchronized with the mass spectrometer scan and thus provide a more reliable method of adjusting the mass scale from one scan to another.

Several viewpoints were provided concerning scanning methods of electrical detection. All scanning methods were exponential scans of the magnet current. Precision data were presented for uranium, steel and copper samples. The precision at the one ppm level seemed to vary from about 15% to as much as 40%, depending on matrix and impurity. Some discussion was presented of the ion statistics available in the scanning mode.

Comparisons were made of the inherent sensitivity of the photoplate and the electrical detection systems, which was in turn related to time of analysis for the two methods of detection. In addition, the effects and problems of background on the photoplate and in the multiplier were described. Relative sensitivity factors as obtained from photoplate data were compared with relative sensitivity factors obtained by electrical detection.

The point was made several times that although electrical detection has many advantages, there are problems that are less satisfactorily carried out by electrical detection methods. These problems include certain pressed samples, very small samples, and point to plane type samples.

Data were presented that showed that electrical detection can provide analytical data that are very accurate and precise. However, the effect of beam chop, sample position, and multiplier effects, among other parameters, have yet to be fully evaluated.

Topic II. NEWER ROLES FOR SPARK SOURCE MASS SPECTROMETRY

Moderator: D. L. Malm (Bell Telephone Laboratories, Inc., Murray Hill, New Jersey)

In recent years, the capabilities of SSMS have been getting attention from a number of interesting new areas. This session was designed to discuss several of these, particularly environmental problems, and to show the valuable role which SSMS may play in the future.

The application of SSMS to Apollo 12 lunar samples was described, showing greatly improved precision and accuracy by use of an internal standard of Lu. Intensity ratios of the analyte ion to Lu were plotted against concentrations of known geological standards to form working curves against which the lunar "unknowns" were evaluated. Analysis results from SSMS compared favorably with data obtained by neutron activation analysis and isotopic dilution mass spectrometry.

The analysis of human fingernails by SSMS was shown to be of potential use as a clinical diagnostic tool. Excess elements, as from toxilogical problems, may accumulate in the hair and nails where identification can be made. A group of 17 subjects were monitored for over one year and "normal" distributions shown. Chronological profiles with points on a two week or monthly basis showed possible cyclical nature of certain elements. Sample preparation and ashing techniques were also discussed. The evaluation and analytical use of ratios of +2 to +1 ions often eliminated interferences from organic contributions for certain elements.

A major new area of SSMS application is in the field of environmental pollution studies. Problems concerning both airborne particles and water analysis, along with contaminated food sources resulting from man made waste were outlined. It was pointed out that essentially all the elements have been detected in this type of application at one time or another. The high sensitivity and survey capability of SSMS make it well suited as a supplementary technique to methods which are more rapid, accurate, and portable. However, in cases where high sensitivity is the prime requirement, it may be the only approach that will provide the necessary information for survey work.

Sample handling methods were described in relation to air-borne particle analysis. A direct analysis with no chemical, mechanical, or thermal treatment is preferable for elements which are easily lost during these operations. However, even without any treatment, Hg was not detected. For elements less sensitive to the above mentioned operations, an ashing step is used to eliminate interfering spectra that would be caused by organics present in the sample or collection media.

Some SSMS data were compared with chemical, x-ray fluorescence, and optical emission data. The values relative to these techniques ranged from ±0 to ± a factor of 10 or more.

SSMS has also been applied to polluted river and stream water. A sample handling technique was described. Detection sensitivities of one nanogram per milliliter were achieved without preconcentration of the sample. Problems with the analysis of Hg were again encountered.

A successful method for the analysis of Hg at the ppb levels utilizing an isotopic dilution technique was presented. The Hg 196 isotope is added just prior to the acid digestion of samples such as fish flesh, river waters, and sludge. Copper electrodes are left overnight in the mercury containing solutions which causes partial amalgamation to take place. A modified, direct sample insertion probe is employed which permits the analysis of fifteen samples per hour.

The method has also been applied to the analysis of Pb in beverages, Cd in air monitor samples, and Zr in reactor fuel salts.

Topic III. RECENT DEVELOPMENTS IN ION MICROPROBE ANALYSIS

Moderator: J. A. McHugh (General Electric Co., KAPL, Schenectady, N. Y.)

The last topic of the day included discussions on applications of the ARL and CAMECA ion probes to various solids analysis problems, the addition of a sputter ion source to an MS-7 spectrograph, and use of ion scattering as a quantitative surface analysis tool.

The first series of applications and results of ion probe analyses were presented by users of ARL Ion Microprobe Mass Analyzers and included the following: Thin film analysis capability was demonstrated by analysis results from <10 A impurity layers on a vacuum evaporated gold surface. A technique for analyzing single airborne particulates was discussed and a polished Ta mount with a vacuum deposited gold film was described for mounting such particulates. Analysis results for a number of 3 to 6 micron size particulates were presented which demonstrated that the ion probe method provides statistically significant data for a wide variety of elements and elemental concentrations in a short period of time. In most instances, a few seconds integration time is sufficient. Analysis results for some NBS steels and mineral samples of both terrestrial and lunar origin were presented along with a discussion of the quantitative accuracy presently achievable with the ion probe. The accuracy was shown for a number of sample types to be better than 5% over a wide range of elemental concentrations. The chemistry and characteristic nature of surface oxide layers can be deduced from in depth profiling by a combination of inert and reactive gas sputtering. The capability of performing Rb-Sr age dating solely with the ion probe was also presented.

The CAMECA Imaging Ion Analyzer has been applied to a wide variety of material problems, as well as the analysis of airborne particulates. The depth resolution capabilities have proved useful in the study of anti-reflective coatings on glass, ion implanted semiconductors, and surface coatings on semiconductor substrates. Use of negative ion sputtering has worked well in studies on insulators and nonconducting corrosion films.

The discussions departed from ion probe applications to consider certain instrumental innovations. One was a modification of an MS-7 to provide a capability for ion sputtering. A modification of the source chamber with the addition of a differentially pumped primary column and associated sample viewing optics was described.

The new technique of ion scattering spectrometry for surface layer analysis was presented. The method is based on monitoring binary scattering of low energy noble gas ions from surface atoms. The method is primarily sensitive to the first monolayer of atoms and can directly monitor insulating semiconducting and metallic surfaces.

W. W. Harrison, Chairman

J. C. Franklin

D. L. Malm

J. A. McHugh

Committee VIII, High Resolution Studies

Don C. DeJongh, Committee VIII Chairman
335 Chemistry Building
Wayne State University
Detroit, Michigan 48202

When high resolution mass spectrometry was in its period of greatest growth in terms of applications, Committee VIII served as a forum for mass spectrometrists having high resolution mass spectrometers to discuss problems and new techniques. Also, anyone considering buying an instrument could meet users, ask questions, and listen. Has high resolution mass spectrometry become so routine that this function of Committee VIII is no longer valid? I have questioned several people active in the field about the continued existence of Committee VIII.

There is general, but not unanimous, agreement that Committee VIII should continue to function. Meetings should be informal, with free discussion, and with only as much structuring as is required to keep things moving. Some people favor formation of task forces to do specific jobs, whereas others feel that this is impractical with an informal group that meets once a year. There was not much interest in having the Committee discuss specific applications. Other Committees and the papers presented at the meetings do that.

By far the greatest need seems to be related to standardization. There should be standardization of procedures for determining sensitivity; compilation of standards which can be used above m/e 700; standards for negative ion work, field ionization, and chemical ionization; standards to test resolution and mass accuracy at various masses; etc. We could help the general mass spectrometric public by giving them an idea of how much resolution is needed in most applications. When are HR data needed, and when is a complete high resolution mass spectrum necessary. Many users of HR equipment use it only to obtain low resolution data.

Many of these items were discussed at the Committee meeting in Atlanta, May 3, 1971. As a result of this meeting, a number of people have agreed to help propose standards for testing instrumental parameters and overall performance. We will then attempt to get manufacturers to produce and publish test data. Hence, our project for 1971/1972 is to have a paper on this subject ready for general discussion and, hopefully, for action at the 1972 ASMS meeting.

ASMS Committee IX
"Aids to Education"

The committee has as its overall objective:

OBJECTIVE

To disseminate information and aid in providing a better understanding of mass spectrometry and to develop an interest in and enthusiasm for the application of mass spectrometry in all areas of science. The initial steps of a program suggested to attain these objectives is presented below:

1) Establishment of Regional Mass Spectrometry Centers for Instruction and Demonstration.

The committee plans to designate regional centers for mass spectrometry. Through individual volunteers who would be willing to open their laboratories to visitors and tour groups. Some thought has been given to requesting that the volunteers provide some sort of informal training sessions on operation, and use, of the mass spectrometers and interpretation of data.

2) Organization of a Speaker Bureau.

This activity is designed to provide a list of speakers on various aspects of mass spectrometry who would be willing to present talks or a series of talks at small colleges and/or universities.

3) Bibliography of Writings in Mass Spectrometry.

The committee hopes to complete a comprehensive list of materials; books, journals, reports, etc., on mass spectrometry which would be made available to interested parties who want a survey of the mass spec literature. It was thought that this would be particularly valuable to small schools where resource materials may be limited.

4) Educational Articles on Mass Spectrometry.

The committee plans to write a series of articles on different aspects of mass spectrometry for publication in a journal similar to Journal of Chemical Education. The format and level of presentation would be such that any advanced level undergraduate student would be informed and stimulated to learn more about mass spectrometry.

J. G. Dillard, Chairman

Subcommittee X - Definitions and Terms

Minutes of Meeting May 5, 1971, Atlanta, Georgia

The charter of the committee reads as follows:

> Assume responsibility for a long-term, deliberate, and comprehensive study of the words, phrases, terms, numbers, and specific language of mass spectrometry. The primary objective will be the writing of formal standards for publication by ASTM.

Eighteen members attended the meeting to hear reports by:

Glenn L. Cook, Chairman
Subcommittee X
Laramie Energy Research Center
Box 3395, University Station
Laramie, Wyoming 82070

U. "Jerry" McCleary, Chairman
Task Force on Instrumental Definitions
and Terms
E. I. DuPont
1500 S. Shamrock
Monrovia, California 91017

Seymour Meyerson, Chairman
Task Force on Organic Definitions
and Terms
American Oil Co., R. & D. Dept.
2500 New York Ave.
Whiting, Indiana 46394

Dan Oblas, Chairman
Task Force on Inorganic Definitions
and Terms
GTE Lab, Inc.
208-20 Willets Pt. Blvd.
Bayside, N.Y. 11360

Chairman Cook reported that contacts had been made with the principal European mass spectrometry groups by Meyerson and McCleary. In attending the International Conference in Brussels, they assembled a group of 35 spectroscopists who are interested in participating in the work of the committee. This brings the total of those who wish to participate or to be kept informed to over 70. A timetable for the first review of definitions was devised. Six months from this meeting date was suggested as reasonable for circulation of the first list of definitions for review. Cook will combine the lists from the task force chairmen for circulation. Any serious disagreements about definitions will be discussed at the next committee meeting.

Each of the task force chairmen presented a short discussion of the philosophy he expected to use in assembling his list of definitions. Each has a nucleus of working committee members. Others may participate by contacting the chairmen.

After some discussion, it was voted to recommend to the Board of ASMS and to the Executive Committee of ASTM E-14 that Subcommittee X be designated a joint committee of both organizations. It was recognized that some

difficulties might be encountered in complying with ASTM regulations, but it was felt that these could be resolved. Until the recommendation is acted upon, the chairmen of the subcommittees of both groups will be kept informed of the activities of Subcommittee X.

JOINT SUBCOMMITTEE XI: EVALUATION OF CRITICAL DATA FOR ENVIRONMENT AND POLLUTION STUDIES

The major activities of Joint Subcommittee XI are the collection, evaluation, and distribution of mass spectral techniques and data relating to environmental problems and pollution.

Subcommittee XI was organized at the 1970 ASMS Conference in San Francisco and the first formal meeting was held at the 1971 Conference. Approximately 90 laboratories have indicated an interest in the activities of the Subcommittee; 65 laboratories were represented at the Subcommittee meeting in Atlanta. The Subcommittee meeting consisted of two informal presentations on mass spectral data related to the determination of polynuclear aromatic hydrocarbons, discussion of the Newsletter issued by the Subcommittee, and a discussion of possible symposia for the 1972 meeting. The informal presentations were:

Application of Gas Chromatography-Mass Spectrometry to Studies of Polynuclear Aromatics; Auto Exhaust Tars, by Roy A. Pancirov, Esso Research and Engineering Co.

Mass Spectrometry of Polynuclear Aromatic Hydrocarbons; Application to Tobacco Smoke, by James Stauffer, Arthur D. Little, Inc.

Three issues of the Newsletter have been distributed and a fourth issue is contemplated for August 1971. Representatives of eight laboratores indicated they will probably have contributions for the next issue.

Three symposia topics for the 1972 meeting were suggested: Mass Spectral Analysis of Pesticides, Analysis of Oil Spillage, and the Determination of Sulfur Compounds in Exit and Flue Gases.

Activities during 1970-71 consisted of (1) distributing two issues of the Newsletter to approximately 160 laboratories participating in the activities of Subcommittees III and XI, (2) organizing a symposium concerned with the analysis of airborne particulates, and (3) contacting several groups that are collecting mass spectral data, with the aim of establishing a collection of mass spectral data for air, water, and soil pollutants. The Chairman of Subcommittee XI is a member of the JCAMP Committee for the collecting and evaluation of mass spectral data and will continue to assist this group during 1971-72 as part of the activities of Subcommittee XI.

Three activities planned for 1971-72 are:

1. Distribute the Newsletter to disseminate information related to mass spectral techniques and data applicable to environment and pollution studies.

2. Organize a symposium for the 1972 ASMS meeting.

3. Assist groups now actively collecting mass spectral data with the aim of distributing spectral data related to environment and pollution studies.

Dr. Philip Levins, Arthur D. Little, Inc., will serve as Vice-Chairman of the Subcommittee. Theodore Kessler, U.S. Bureau of Mines, will continue to serve as Editor of the Newsletter.

A. G. Sharkey, Jr., Chairman

ASMS Nominating Procedures

Any ASMS member can nominate another member for any office, except President, by submitting to the Secretary before February 15:

1. signature of at least 30 ASMS members endorsing the nomination;

2. signature of the nominee agreeing to hold office if elected;

3. resumé of the candidate.

The Nomination Committee (appointed by the ASMS President) will recommend one candidate per office, and obtain the candidate's consent to serve and a resumé which will be published and distributed to the members before September.

F. E. Saalfeld
Secretary

Benefits of Membership

in

THE AMERICAN SOCIETY FOR MASS SPECTROMETRY

1. The registration fee for ASMS members attending the Annual Conference has been set $10.00 below the nonmember fee.

2. All ASMS members receive the printed collection of Conference papers, regardless of whether or not they attend (in past years, only attendees were sent the collection).

3. The following publishing houses grant price reductions to ASMS members on journal subscriptions and some technical books:

a. Heyden & Son, Ltd.
c/o Dr. Gunter Heyden
Spectrum House
Alderton Crescent
London NW 4, England

"Journal of Organic Mass Spectrometry" - 10% discount on current rates (one year - $18.00; two years - $34.00; three years - $54.00); 20% discount on selected books (ask publisher for recent listing).

b. Elsevier Publishing Company
c/o Dr. Marc Atkins
Jan van Galenstraat 335
P. O. Box 211
Amsterdam, The Netherlands

"International Journal of Mass Spectrometry and Ion Physics" - 20% discount on regular rate of $50/yr (add $5.00 for air freight). There is a possibility that the discount may be extended also to some of their books.

c. University Park Press
115 Chamber of Commerce Bldg.
Baltimore, Maryland 21202

20% discount on "Recent Developments in Mass Spectroscopy" (Proceedings of the 1969 Kyoto Conference), K. Ogata and T. Kayakawa, editors - $46.00 instead of regular price of $57.50.

To obtain these discounts, your order should include the statement "ASMS Member." The subscriptions are for PERSONAL use only.

4. An Employment Register for ASMS Members has been established. Contact J. N. Damico, Food and Drug Administration, BF-145, Washington, D. C. 20204.

F. E. Saalfeld
Secretary

INFORMATION AVAILABLE TO ASMS MEMBERS

In order to keep ASMS members better informed on the activities of their Society, it was decided to publish the following list of items deposited with the Society's Secretary (currently, F. E. Saalfeld, Naval Research Laboratory, Washington, D. C. 20390 U.S.A.):

ASMS Charter
ASMS Seal

"Recent Advances in Mass Spectroscopy," edited by K. Ogata and T. Kayakawa

Vols. 17 and 18 of "Mass Spectroscopy " - the journal of the Mass Spectroscopy Society of Japan

Vol. 6 N 4 Methods Physique d'Analyse GAMS

Abstracts of the 11th, 12th, 15th, 16th, 17th, 18th and 19th meetings of the Annual Conference on Mass Spectrometry and Allied Topics

Proceedings of the 10th ('61), 11th ('62), 12th ('63), 13th ('64), 14th ('65), 15th ('66), 17th ('67), 18th ('69), and 19th ('70) Annual Conference on Mass Spectrometry and Allied Topics (one copy each; not for sale - reference use only)

Any ASMS member having need for the above documents should contact the Secretary for details.

F. E. Saalfeld
Secretary

In an attempt to inform mass spectroscopists of the existence of various organizations concerned with mass spectroscopy throughout the world, the Secretary has collected the following information:

Name of Organization	Benefits of Membership	Dues	Name and address of organization/contact for more information
The American Society for Mass Spectrometry (ASMS)	Yearly Conference; free bound volume of Conference papers; $10.00 lower Conference registration fee; discount rates on several journals and books.	$8.00 (U.S.)/yr.	Dr. F. E. Saalfeld Naval Research Lab., Code 6110, Washington, D. C. 20390 U.S.A.
The Australian Society for Mass Spectrometry	Yearly or bi-yearly Conference; abstract service for all members.	2.00/yr.	Mr. P. T. Greenhalgh The Australian Soc. for Mass Spectrometry 48 Atchison Street St. Leonards Sydney NSA 2065, Australia
Mass Spectroscopy Society of Japan (MSSJ)	Annual Conference in May; all members receive the Society's journal "Mass Spectroscopy" - papers are written in Japanese (with English abstract) or in a European language (including English).	8.00 (U.S.)/yr.	Professor K. Ogata Dept. of Physics, Faculty of Science, Osaka Univ., 1-1 Machikaneyama-cho, Toyonaka, Osaka-fu, Japan
Mass Spectroscopy Group	Advance information about the Group's Annual Conference.	None (Conf. Reg. Fee)	Mr. R. M. Elliott, AEI Scientific Apparatus Ltd., Barton Dock Road, Urmston, Manchester M31 2LD, England
Arbeitegemeinschaft Massenspektroskopie	Lower Conference registration fees	Membership in the German Physical Society plus $1.25 (U.S.)/yr.	Dr. Grutzmacher, Frachbereich Chemie, University Hamburg, 2 Hamburg, Germany

(cont'd)

Name of Organization	Benefits of Membership	Dues	Name and address of organization/contact for more information
Groupement pour l'Avancement des Methodes Physiques d'Analyses (G.A.M.S.)	Free participation in GAMS working groups - M.S. group meets every other month; access to documentation, books, reviews and to a large collection of various types of spectra.	$135/yr (fee is for a firm)	Madame Frere - GAMS 8, 10 rue du Delta 75 Paris 9 é me, France
Time of Flight Symposium	Biennial Conference (1969, 1971. . .)	Conference Registration Fee	Dr. D. Price, Cockcroft Bldg., Univ. of Salford, Dept. of Chem. and Applied Chem., Salford VII M5 4WT Lancashire, England